

# UNDERSTANDING THE MECHANISM OF TRAUMATIC BRAIN INJURY-INDUCED ENERGY METABOLISM

EDITED BY: Guoqiang Xing, Heng-Ye Man and Yumin Zhang  
PUBLISHED IN: Frontiers in Neurology





# frontiers

## Frontiers eBook Copyright Statement

The copyright in the text of individual articles in this eBook is the property of their respective authors or their respective institutions or funders. The copyright in graphics and images within each article may be subject to copyright of other parties. In both cases this is subject to a license granted to Frontiers.

The compilation of articles constituting this eBook is the property of Frontiers.

Each article within this eBook, and the eBook itself, are published under the most recent version of the Creative Commons CC-BY licence.

The version current at the date of publication of this eBook is CC-BY 4.0. If the CC-BY licence is updated, the licence granted by Frontiers is automatically updated to the new version.

When exercising any right under the CC-BY licence, Frontiers must be attributed as the original publisher of the article or eBook, as applicable.

Authors have the responsibility of ensuring that any graphics or other materials which are the property of others may be included in the CC-BY licence, but this should be checked before relying on the CC-BY licence to reproduce those materials. Any copyright notices relating to those materials must be complied with.

Copyright and source acknowledgement notices may not be removed and must be displayed in any copy, derivative work or partial copy which includes the elements in question.

All copyright, and all rights therein, are protected by national and international copyright laws. The above represents a summary only. For further information please read Frontiers' Conditions for Website Use and Copyright Statement, and the applicable CC-BY licence.

ISSN 1664-8714

ISBN 978-2-88971-979-2

DOI 10.3389/978-2-88971-979-2

## About Frontiers

Frontiers is more than just an open-access publisher of scholarly articles: it is a pioneering approach to the world of academia, radically improving the way scholarly research is managed. The grand vision of Frontiers is a world where all people have an equal opportunity to seek, share and generate knowledge. Frontiers provides immediate and permanent online open access to all its publications, but this alone is not enough to realize our grand goals.

## Frontiers Journal Series

The Frontiers Journal Series is a multi-tier and interdisciplinary set of open-access, online journals, promising a paradigm shift from the current review, selection and dissemination processes in academic publishing. All Frontiers journals are driven by researchers for researchers; therefore, they constitute a service to the scholarly community. At the same time, the Frontiers Journal Series operates on a revolutionary invention, the tiered publishing system, initially addressing specific communities of scholars, and gradually climbing up to broader public understanding, thus serving the interests of the lay society, too.

## Dedication to Quality

Each Frontiers article is a landmark of the highest quality, thanks to genuinely collaborative interactions between authors and review editors, who include some of the world's best academicians. Research must be certified by peers before entering a stream of knowledge that may eventually reach the public - and shape society; therefore, Frontiers only applies the most rigorous and unbiased reviews.

Frontiers revolutionizes research publishing by freely delivering the most outstanding research, evaluated with no bias from both the academic and social point of view. By applying the most advanced information technologies, Frontiers is catapulting scholarly publishing into a new generation.

## What are Frontiers Research Topics?

Frontiers Research Topics are very popular trademarks of the Frontiers Journals Series: they are collections of at least ten articles, all centered on a particular subject. With their unique mix of varied contributions from Original Research to Review Articles, Frontiers Research Topics unify the most influential researchers, the latest key findings and historical advances in a hot research area! Find out more on how to host your own Frontiers Research Topic or contribute to one as an author by contacting the Frontiers Editorial Office: [frontiersin.org/about/contact](http://frontiersin.org/about/contact)

# UNDERSTANDING THE MECHANISM OF TRAUMATIC BRAIN INJURY-INDUCED ENERGY METABOLISM

Topic Editors:

**Guoqiang Xing**, Affiliated Hospital of North Sichuan Medical College, China

**Heng-Ye Man**, Boston University, United States

**Yumin Zhang**, Uniformed Services University of the Health Sciences, United States

**Citation:** Xing, G., Man, H.-Y., Zhang, Y., eds. (2022). Understanding the Mechanism of Traumatic Brain Injury-induced Energy Metabolism. Lausanne: Frontiers Media SA. doi: 10.3389/978-2-88971-979-2

# Table of Contents

- 04** *Consequences of the dynamic triple peak impact factor in Traumatic Brain Injury as Measured With Numerical Simulation*  
Hans von Holst and Xiaogai Li
- 12** *Mathematical Models of Blast-Induced TBI: Current Status, Challenges, and Prospects*  
Raj K. Gupta and Andrzej Przekwas
- 33** *Metabolic Crisis in Severely Head-Injured Patients: Is Ischemia Just the Tip of the Iceberg?*  
Emilie Carre, Michael Ogier, Henry Boret, Ambroise Montcriol, Lionel Bourdon and Jean-Jacques Risso
- 39** *Synaptic Activity and Bioenergy Homeostasis: Implications in Brain Trauma and Neurodegenerative Diseases*  
Natasha Khatri and Heng-Ye Man
- 50** *Impact of Repeated Stress on Traumatic Brain Injury-Induced Mitochondrial Electron Transport Chain Expression and Behavioral Responses in Rats*  
Guoqiang Xing, Erin S. Barry, Brandi Benford, Neil E. Grunberg, He Li, William D. Watson and Pushpa Sharma
- 63** *Culturing Layer-Specific Neocortical Neurons as a Cell Replacement Therapy Following Traumatic Brain Injury*  
Nathan Peter Cramer, Mitali Chatterjee, Fritz Walter Lischka and Sharon L. Juliano
- 71** *Temporal Dynamics of Cerebral Blood Flow, Cortical Damage, Apoptosis, Astrocyte–Vasculature Interaction and Astrogliosis in the Pericontusional Region After Traumatic Brain Injury*  
Sonia Villapol, Kimberly R. Byrnes and Aviva J. Symes
- 80** *Differential Expression of Brain Cannabinoid Receptors Between Repeatedly Stressed Males and Females May Play a Role in Age and Gender-Related Difference in Traumatic Brain Injury: Implications From Animal Studies*  
Guoqiang Xing, Janis Carlton, Xiaolong Jiang, Jillian Wen, Min Jia and He Li
- 92** *Divergent Temporal Expression of Hyaluronan Metabolizing Enzymes and Receptors With Craniotomy vs. Controlled-Cortical Impact Injury in Rat Brain: A Pilot Study*  
Guoqiang Xing, Ming Ren and Ajay Verma
- 101** *Mitochondrial Gene Expression Profiles and Metabolic Pathways in the Amygdala Associated With Exaggerated Fear in an Animal Model of PTSD*  
He Li, Xin Li, Stanley E. Smerin, Lei Zhang, Min Jia, Guoqiang Xing, Yan A. Su, Jillian Wen, David Benedek and Robert Ursano
- 116** *Efficacy and Safety of Panax notoginseng Saponin Therapy for Acute Intracerebral Hemorrhage, Meta-Analysis, and Mini Review of Potential Mechanisms of Action*  
Dongying Xu, Ping Huang, Zhaosheng Yu, Daniel H. Xing, Shuai Ouyang and Guoqiang Xing





# Consequences of the *dynamic triple peak impact factor* in traumatic brain injury as measured with numerical simulation

Hans von Holst<sup>1,2\*</sup> and Xiaogai Li<sup>2†</sup>

<sup>1</sup> Section of Neurosurgery, Division of Clinical Neuroscience, Karolinska Institutet, Stockholm, Sweden

<sup>2</sup> Division of Neuronic Engineering, School of Technology and Health, Royal Institute of Technology (KTH), Stockholm, Sweden

## Edited by:

Guoqiang Xing, Lotus Biotech.com, USA

## Reviewed by:

Sonia Villapol, Uniformed Services University, USA

Amade Bregy, University of Miami, USA

## \*Correspondence:

Hans von Holst, Department of Neurosurgery, Karolinska University Hospital, SE-171 76 Stockholm, Sweden.

e-mail: hans.vonholst@karolinska.se

## †Present address:

Xiaogai Li, Royal Institute of Technology, Alfred Nobels Allé 10, SE-141 52 Huddinge, Sweden.  
e-mail: xiaogai@kth.se

There is a lack of knowledge about the direct neuromechanical consequences in traumatic brain injury (TBI) at the scene of accident. In this study we use a finite element model of the human head to study the dynamic response of the brain during the first milliseconds after the impact with velocities of 10, 6, and 2 meters/second (m/s), respectively. The numerical simulation was focused on the external kinetic energy transfer, intracranial pressure (ICP), strain energy density and first principal strain level, and their respective impacts to the brain tissue. We show that the oblique impacts of 10 and 6 m/s resulted in substantial high peaks for the ICP, strain energy density, and first principal strain levels, however, with different patterns and time frames. Also, the 2 m/s impact showed almost no increase in the above mentioned investigated parameters. More importantly, we show that there clearly exists a dynamic triple peak impact factor to the brain tissue immediately after the impact regardless of injury severity associated with different impact velocities. The dynamic triple peak impacts occurred in a sequential manner first showing strain energy density and ICP and then followed by first principal strain. This should open up a new dimension to better understand the complex mechanisms underlying TBI. Thus, it is suggested that the combination of the dynamic triple peak impacts to the brain tissue may interfere with the cerebral metabolism relative to the impact severity thereby having the potential to differentiate between severe and moderate TBI from mild TBI.

**Keywords:** traumatic brain injury, kinetic energy transfer, finite element modeling, intracranial pressure, strain energy density and first principal strain, dynamic triple peak impact

## INTRODUCTION

During the last three decades there has been a substantial increased experience and knowledge about the consequences of traumatic brain injury (TBI) with regard to the neurochemical cascades of events following the kinetic energy transfer into the brain tissue (Narayan et al., 1995). However, there is a lack of knowledge when it comes to the neuromechanical pattern and its consequences.

The awareness of primary prevention of TBI in all categories has improved among the general population resulting in a reduced number of TBI. The same holds true also for the more specific prevention of secondary injuries in the acute neurosurgical treatment. However, despite the numerous publications there is still a lot to be desired when it comes to the neuromechanical cascades immediately after TBI at the scene of accident where the experience is limited. An increased knowledge about the immediate mechanical consequences within milliseconds should have a strong potential to further improve not only primary but also the secondary prevention at the neurosurgical treatment.

The improved computer capacity and the introduction of the neuroengineering field makes it possible to use advanced numerical simulations aiming at better understanding the consequences of TBI and which has been a topic under many previous

investigations (Ward et al., 1980, 1997; Anderson et al., 1999; Willinger and Baumgartner, 2003; Zhang et al., 2004; Viano et al., 2005; Balestreri et al., 2006; Kleiven, 2007; Nyein et al., 2010). Various injury predictors have been proposed from numerical modeling or *in vivo* experiments. The first principal strain has been shown to correlate closely with diffuse axonal injuries (Bain and Meaney, 2000; Viano et al., 2005) as well as hemorrhage (Kleiven, 2007). The pressure was suggested to be associated with concussion (Ward et al., 1980) while strain energy density was found to correlate with contusion (Kleiven, 2007). Other predictors include, however not limited to global total energy (Willinger and Baumgartner, 2003) and shear stress (Anderson et al., 1999; Zhang et al., 2004). Thus, assuming that the human brain model is well validated the numerical analysis has an outstanding potential to further improve the existing knowledge about the direct neuromechanical consequences during the following milliseconds after the accident (von Holst and Li, 2013) and also when the patient is under neurosurgical treatment (von Holst et al., 2012). The present study proposes that the immediate consequence of an impact should be looked upon as an effect specifically from the three parameters kinetic energy, intracranial pressure (ICP), and strain level in a sequential manner thereby influencing the brain tissue at different times following the accident.

Thus, the aim of the present study was

- to evaluate the immediate consequences of kinetic energy transfer to the brain tissue focusing on the ICP, strain energy density, and first principal strain level by using the numerical simulation of finite element (FE) model and
- to estimate the kinetic energy impact level which could potentially separate the severe and moderate TBI from mild TBI focusing on the ICP, strain energy density, and first principal strain level.

## MATERIALS AND METHODS

### THE FINITE ELEMENT HEAD MODEL

A previously developed and validated numerical model of the human head was used and which includes the scalp, skull, brain, the meninges, and cerebrospinal fluid (CSF) (Kleiven, 2002). A simplified neck, including the extension of the brain stem to the spinal cord and dura mater was also modeled. To cope with large elastic deformations, a hyper-viscoelastic constitutive law was used for the brain tissue. The model has been validated against ICP and brain motion, more detailed information about the model and validations can be found in previous publications (Kleiven and von Holst, 2002; Kleiven, 2006, 2007). The skull bone was modeled as a three-layered structure including inner and outer compact bone and porous bone. During an impact loading, the mechanical parameters of the skull bone are expected to have a strong influence on the dynamic response of the brain. The choice of skull bone parameters in this study was consistent with a previous study (Fahlstedt et al., 2012) and was found to be justified.

### SIMULATION OF IMPACT

The loading conditions of the impact were based on a real accident to the right frontal lobe in a TBI patient due to a fall. A Computer Tomography (CT) scan on admission to the hospital showed a 3 cm large subdural hematoma on the right side including subarachnoid hemorrhage and multiple contusions in frontal, parietal, and temporal lobes from the medical record, swelling was observed at the right eye and this information was used to estimate the angle and area of impact in the model (Figure 1, lower row). The head model was placed at a very small distance from the impact surface. With a starting point from a non-injured simulation condition the model simulated three falling accidents with an initial velocity of 2, 6, and 10 meters/second (m/s), respectively, to represent minor, medium, and more severe injuries. The external kinetic energy levels were calculated to 227.3, 81.8, and 9.1 J for the 10, 6, and 2 m/s impacts, respectively according to the kinetic energy theorem  $E = 1/2 * m * v^2$  where  $E$  is kinetic energy,  $m$  is the mass of the head model, and  $v$  is the initial velocity. The impact ground was simulated as concrete with a Young's modulus of 30 GPa.

### ESTIMATION OF THE ICP AND STRAIN LEVEL

In reality, brain tissue can be seen as a continuum consisting of an infinite number of tissue points. According to the FE theory, FE modeling is a powerful tool to estimate the complex mechanical response of a continuum by dividing it into a finite number of elements (Belytschko et al., 2000). The results obtained at an element

are a reasonable approximation to the brain tissue represented by that element. In total the FE head model used in this study consists of around 24,000 elements.

At the time of the simulated impact to the head ICP is defined as the hydrostatic pressure obtained in each of the FEs. For one-dimensional problem, the strain level represents the relative change in length and can be defined as  $(L - L_0)/L_0$ , where  $L_0$  is the original length and  $L$  is the length after stretching. For three-dimensional situation, however, a scalar is not enough to represent the complex deformation pattern. Instead a tensor field is needed (i.e., strain tensor) to describe the deformation state. Based on the strain tensor, various scalar indexes can be derived, of which the first principal strain represents the maximum stretching at a tissue point.

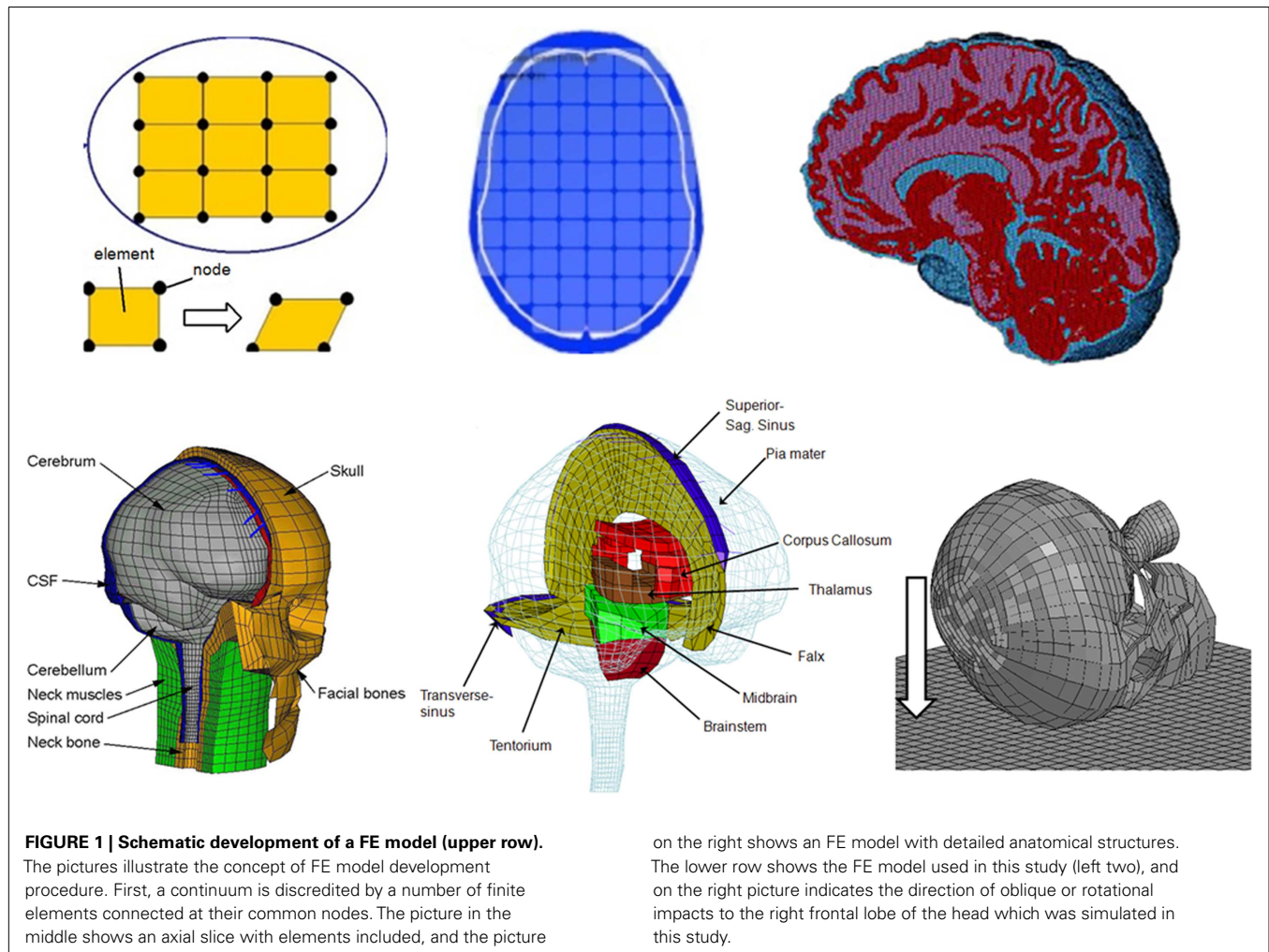
When the head is subjected to an impact, the external kinetic energy transferred to the brain causes deformation of nervous tissue and stores the energy in the form of elastic strain energy. This is then translated all the way down to the protein structures at the molecular scale. From the FE model, the kinetic energy transferred to the whole brain can be obtained in the form of strain energy density defined as the strain energy per unit volume of the brain tissue.

## RESULTS

The general pattern of the numerical simulation from the three impacts of 10, 6, and 2 m/s was quite different with regard to the head and brain tissue response when comparing the ICP with that of strain energy density and first principal strain as evaluated from the axial, sagittal, and coronal sequences (Figures 2–5). Also, the external kinetic energy levels during the oblique impacts to the head were calculated to 227.3, 81.8, and 9.1 J for the 10, 6, and 2 m/s impacts, respectively.

Following the 10 m/s impact the ICP level was highest in the right frontal lobe at the site of impact area where it reached over 1162 kPa. Then the ICP decreased successively with the distance from the impact site reaching a negative pressure on the opposite side. The patterns of the predicted pressure response within the cranial cavity showed distinct pressure gradients across the entire brain. The pressure varies from a positive pressure close to the impact point to reach a maximum magnitude of negative pressure at the opposite side of the impact which indicated a coup and countercoup pressure phenomenon. The same pattern was found also following the 6 m/s impact, however with a pressure peak reaching about 825 kPa at the impact site. In contrast, the peak pressure following 2 m/s impact reached only 221 kPa at the same area. Moreover, the highest peak pressure came earlier in the two higher impacts. Thus, in the 10 m/s impact the ICP increase started already after 1.0 ms and reached the highest peak at 1.8 ms before normalized after 4.2 ms. The same pattern was true also for the 6 m/s impact although the ICP increase started at 1.8 ms. In contrast, following 2 m/s impact the highest peak pressure of about 400 kPa was found after 4.2 ms (Figures 2–4).

The increased strain levels following 10 m/s impact reached a peak over 35% after 4.8 ms (Figures 2–4, upper rows). For the 6 m/s impact, the strain level in most brain tissue remained lower than 28%, and the peak value was found in time frame of 6.8 and 10.0 ms. The highest strain level occurred later compared to the 10 m/s impact. Following the 2 m/s impact there was a slight and local increase found after 4.8 ms during only a short time



(Figures 2–4). Compared to the ICP gradient generated across the brain, the strain level had a different response pattern. Initially, the strain level on the cortical surface and brain stem was high before gradually moving to the central region of the brain especially at the tissue close to falx and tentorium which is stiffer compared to the surrounding brain tissue.

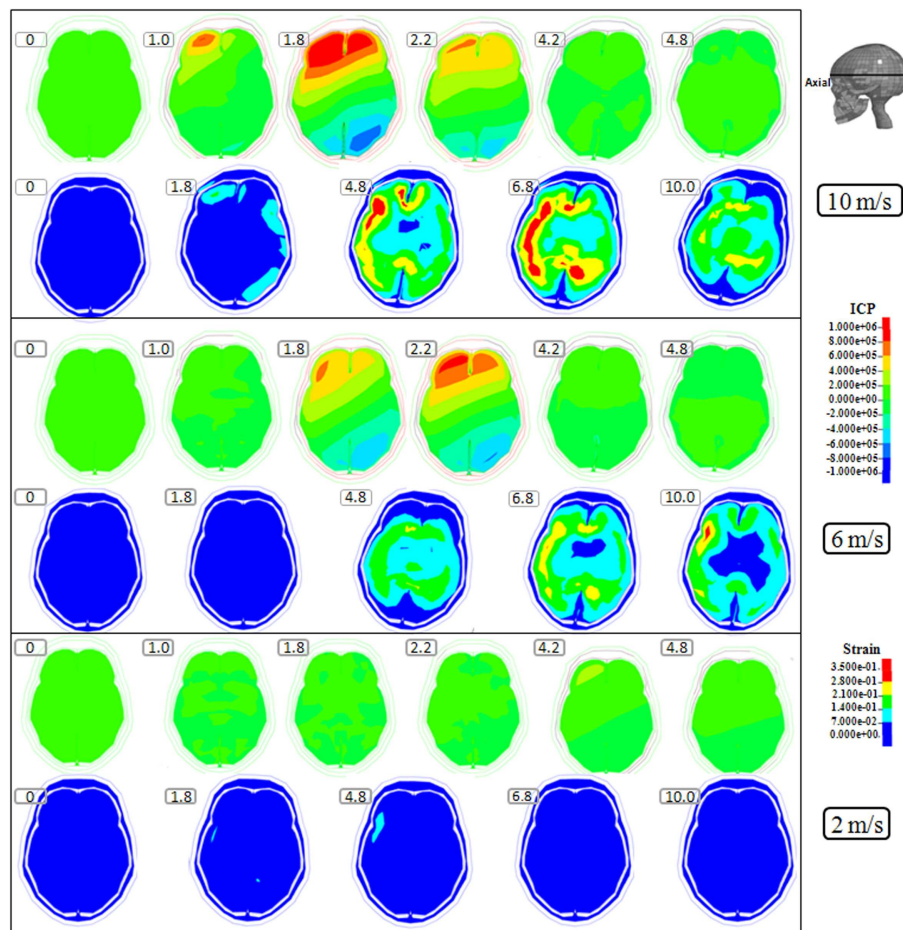
Thus, the kinetic energy transfer resulted in the dynamic triple peak impact consisting of a rapid increased ICP level for a short period while the increased strain level was delayed and more long-standing (Figure 5). To further analyze quantitatively the time frame of the dynamic triple peak impact, the time-history curve for one element at the right frontal brain tissue was plotted which shows that the time for the highest peak values were similar for ICP and strain energy density reaching their peaks in correlation to the impact intensity. The curves were filtered using an SAE 180 low-pass filter. The location of the element in the brain model used for analysis is indicated in the white area (Figure 5, left). All the peaks occur earlier for the more severe injuries due to the higher impact velocities which needs shorter time to reach an impact peak. Of interest is to integrate the strain energy density curve with time thereby representing the total energy density received at this point during the impact. Thus, the results were calculated as

$5.81 \times 10^4$ ,  $2.76 \times 10^4$ , and  $2.14 \times 10^3$  respectively for each of the three impacts. Further, the ICP level had returned to normal when the strain level reached the peak value. As the first principal strain level increase was delayed and prolonged, the brain tissue encountered a dynamic triple peak impacts with the highest impact for 10 m/s followed by the 6 m/s and with the lowest impacts in all categories following 2 m/s (Figure 5).

## DISCUSSION

The present numerical simulation study shows for the first time that the kinetic energy transfer in fact results in a dynamic triple peak impact event during the first milliseconds after the accident to the head. Consequently, this may have a profound effect on the cerebral metabolism. An FE model of the human head has been investigated in numerous studies aiming at better understanding the complex mechanisms of TBI. From the FE model simulations, spatial and temporal distribution of the mechanically response parameters can be determined mainly in terms of ICP, strain energy density, first principal strain level. If one parameter or a combination of several parameters obtained from the FE model is correlated with the site and severity of the injuries, the result can be used to better understand the consequences of the





**FIGURE 2 | Representative axial slice of ICP and first principal strain captured at different time points during the impact for velocities of 10 m/s (two upper rows), 6 m/s (two middle rows), and 2 m/s (two lower**

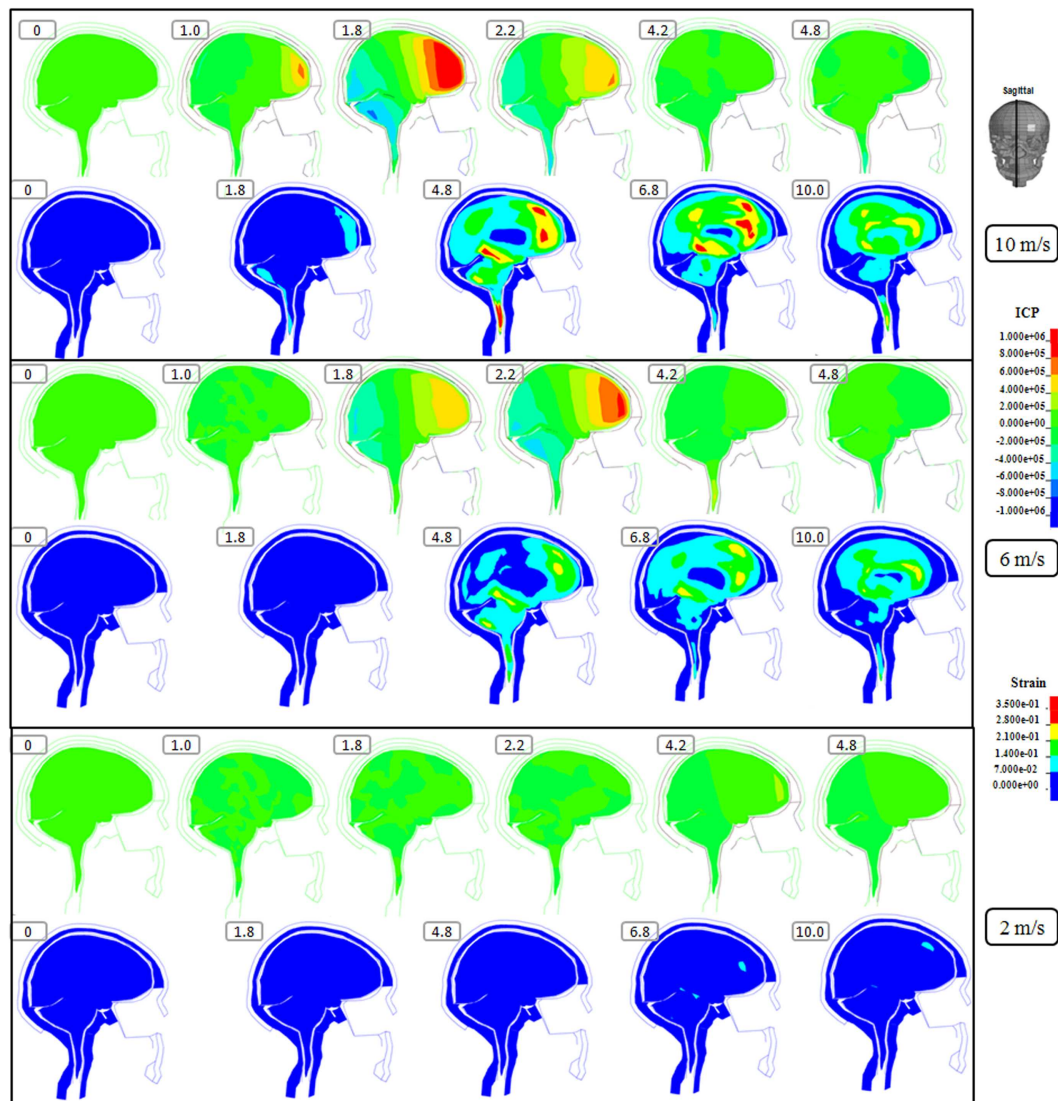
**rows).** The location of the axial slice is indicated in the figure. The numbers included in the figure represent the time after the impact with unit of millisecond.

dynamic triple peak impact shown in the present study. Also, such a combined evaluation of several parameters should be used as an injury prediction of TBI consequences. Many predictors have been proposed in the literature based on either numerical simulations or *in vivo* experiments. Among them are ICP (Ward et al., 1980; Kleiven, 2007), strain energy density (Kleiven, 2007), first principal strain (Viano et al., 2005; Kleiven, 2007), global total energy (Willinger and Baumgartner, 2003), and shear stress (Anderson et al., 1999; Zhang et al., 2004). In this study, we focused on the three widely used parameters ICP, strain energy density, and first principal strain.

The kinetic energy transfer of 227.3, 81.8, and 9.1 J defined for the three impact scenarios in this study should have a profound effect on the cerebral metabolism. Earlier analytical and animal studies proposed a peak ICP threshold of 235 kPa for fatal or serious head injuries and 173 kPa for moderate head injury (Ward et al., 1980). From a clinical perspective it has been shown that high ICP is strongly associated with fatal outcome in patients with TBI (Balestreri et al., 2006). Thus, in contrast to clinically increased ICP, which is developed at a static or semi-static event, our simulation

shows a substantially increased ICP developed during dynamic impacts and lasting for several milliseconds. The pressure reached a maximum positive value at the impact site while a maximum magnitude of negative pressure at the opposite side of the impact which indicated a coup and countercoup pressure phenomenon. Although countercoup injury is widely recognized both in clinics and experiments, the mechanisms is still controversial nowadays (Post and Hoshizaki, 2012). Also, the difference in increased ICP is substantial between 10 and 6 m/s impacts compared to that of 2 m/s impacts. Based on our results it is tentative to suggest a possible separation of severe and moderate TBI following 10 and 6 m/s impact from that of mild TBI following 2 m/s impacts. The increased ICP developed during dynamic events may very well influence the cerebral metabolism in such a way that it makes the brain tissue more sensitive to the secondary increased ICP often found during the clinical treatment of TBI.

It has been suggested that a threshold of strain energy density at  $2.1 \text{ kJ/m}^3$  indicated a 50% chance of concussion similar to that found in a range of about  $0.8\text{--}1.9 \text{ kJ/m}^3$  (Ward et al., 1997). In the present study the strain energy density reached a peak value



**FIGURE 3 | Representative sagittal slice of ICP and first principal strain captured at different time points during the impact for velocity of 10 m/s (two upper rows), 6 m/s (two middle rows), and 2 m/s (two lower rows).**

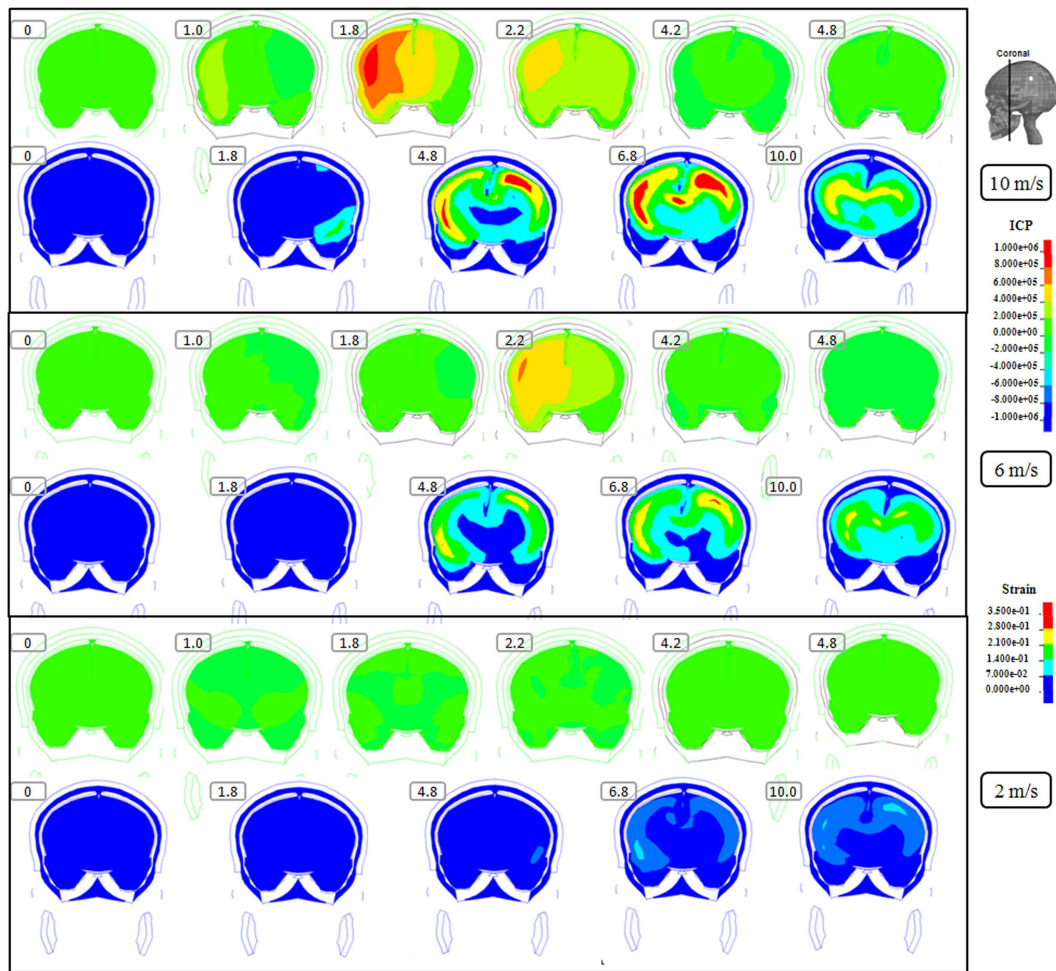
The location of the sagittal slice is indicated in the figure. The numbers included in the figure represent the time after the impact with unit of millisecond.

of about 33 and 18 kJ/m<sup>3</sup> following 10 and 6 m/s impacts, respectively, while the 2 m/s impact reached a peak of only 2 kJ/m<sup>3</sup>. In line with our suggestion from the dynamically increased ICP also the strain energy density may stress the cerebral metabolism in the deformed brain tissue which is then more sensitive to the secondary injuries developed within the nearest days after the impact. Also, the calculated area under the strain energy density curve may support clarify the dysfunction of the cerebral metabolism in future experiments.

An increased first principal strain level of 21% has been shown to result in a 50% probability to cause mild TBI (Kleiven, 2007). This is similar to the values demonstrated from *in vivo* axonal stretching experiments that a strain level of approximately 21% will elicit electrophysiological changes while a strain level of

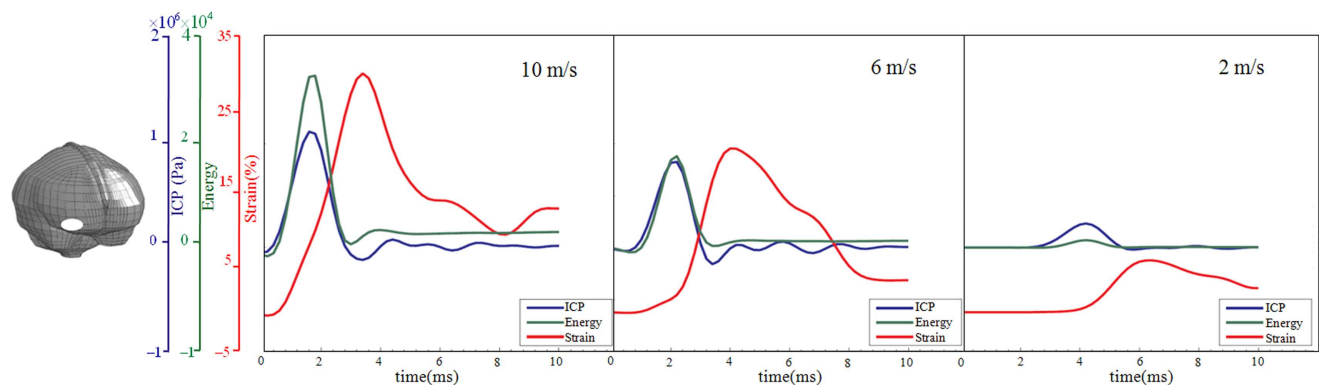
approximately 34% will cause morphological signs of damage to the white matter (Bain and Meaney, 2000). In our present study the first principal strain level increased to over 30 and 20% for 10 and 6 m/s impacts, respectively. This may very well result in an electrophysiological dysfunction which may jeopardize the cerebral metabolism in the brain tissue both at the time of impact but also later on.

The kinetic energy transfer of 227.3, 81.8, and 9.1 J defined for the three velocity impact scenarios in this study should be highlighted as this may be beyond the energy forces that can be tolerated in some of the normal cellular metabolism. Since the nervous tissue contains a substantial amount of protein structures, it is of clinical interest to evaluate whether or not the kinetic energy transferred to brain tissue during an impact has



**FIGURE 4 | Representative coronal slice of ICP and first principal strain captured at different time points during the impact for velocity of 10 m/s (two upper rows), 6 m/s (two middle rows), and 2 m/s (two lower rows).**

The location of the coronal slice is indicated in the figure. The numbers included in the figure represent the time after the impact with unit of millisecond.



**FIGURE 5 | Time-history curve of ICP, strain energy density, and first principal strain at one element in the right frontal lobe (white area) with the maximum peak ICP value as illustrated in the figure. x Axis**

represents the time after impact, and y axis represents the values of ICP (blue), strain energy density (green), and first principal strain (red). From left to right are the results for the impact velocities of 10, 6, and 2 m/s impact.



the potential to unfold the native proteins. As suggested from earlier experimental data a high pressure may induce unfolding of the protein structures as the pressure exerts a destabilizing effect on the folded protein structures (Hummer et al., 1998; Hillson et al., 1999). Upon unfolding the protein structures developed a swelling process as has been shown in a previous experimental study (Jha et al., 2009). As shown from our previous studies (von Holst and Li, 2013), when severe enough, the external kinetic energy may unfold native proteins after severe and moderate TBI. The unfolded protein structures with a larger number of hydrophilic amino acids residues exposed to the aqueous environment within the nervous tissue tend to attract more water molecules and, hence, initiating the cytotoxic brain tissue edema often seen in TBI patients.

The triple peak impact is illustrated for one element at the frontal lobe close to the impact site elements at other parts of the brain is expected to have also experienced an impact peak sequential, however, may have different magnitude ratios at different locations of the brain. Disturbance of cerebral metabolism following TBI have been reported in both animal models and in clinical measurements including but not limited to elevated extracellular glutamate and lactate and decreased glucose (Alves et al., 2005), increased glycolysis and or/decreased oxidative metabolism (Casey et al., 2008). Thus, these provide clear evidence that there is a metabolic disturbance following TBI. However, the exact mechanisms how each of the impact peaks affects the cerebral metabolisms remain unclear and they need further experimental investigations.

An accurate reconstruction of real accident demands information regarding the accident impact ground material properties, impact velocity and angle etc. Due to the lack of the information, the impact location and angle in the model was estimated from the medical image where swelling was observed at the right frontal lobe. The impact ground is assumed to be with similar stiffness as concrete. However, in reality the impact ground may be different. Therefore, the simulation results presented in this study should be interpreted with caution since the conclusions are limited by

the specific modeling conditions and impact parameters. Nevertheless, the dynamic triple peak during an impact presented in this study is expected to remain valid for slightly different global mechanical loads. Future investigations could include a larger number of trauma patients with accident report at the scene of accident and their medical reports. From numerical simulations the intracranial response during various loading conditions could be predicted and this should provide more insight into the relative importance of different impact peaks in a certain type of brain injury.

There has been a substantial interest to better clarify the precise mechanisms of brain injury aiming at improving the clinical treatment of patients with TBI. However, this has not yet been fully established (Yang et al., 2011; Post and Hoshizaki, 2012). It has been widely recognized that there are limitations with using only single parameters related to TBI. In this study, rather than suggesting another predictor, we propose that the external kinetic energy transferred to the head during an accident may result in at least three sequential impacts to the brain tissue defined as the immediate dynamic triple peak impact factor which occurred in a sequential manner first showing strain energy density and ICP and then followed by first principal strain. The denominator in common for the three parameters is the impact it has on influencing different cerebral metabolic situations after the accident. Even if it will not alter the cerebral metabolism at the time of accident, it is tentatively suggested that the dynamic triple peak impact factor influences the cerebral metabolism in such a way that it is more sensitive to the neurochemical cascades often found after a short time in patient with severe and moderate TBI. Thus, it is evident that the immediate and dynamic triple peak impact factor presented in this study can be looked upon as a forerunner thereby making the cerebral metabolism in the injured area more vulnerable to secondary dysfunctions.

## ACKNOWLEDGMENTS

The present study was supported by research funds from the Royal Institute of Technology, Stockholm, Sweden.

## REFERENCES

- Alves, O. L., Bullock, R., Clausen, T., Reinert, M., and Reeves, T. M. (2005). Concurrent monitoring of cerebral electrophysiology and metabolism after traumatic brain injury: an experimental and clinical study. *J. Neurotrauma* 22, 733–749.
- Anderson, R., Brown, C., Blumbergs, P., Scott, G., Finney, J., Jones, J. N., et al. (1999). "Mechanisms of axonal injury: an experimental and numerical study of a sheep model of head impact," in *IRCOBI conference Proceedings* (Sitges), 107–120.
- Bain, A., and Meaney, D. (2000). Tissue-level thresholds for axonal damage in an experimental model of central nervous system white matter injury. *J. Biomech. Eng.* 122, 615–622.
- Balestreri, M., Czosnyka, M., Hutchinson, P., Steiner, L., Hiler, M., Smielewski, P., et al. (2006). Impact of intracranial pressure and cerebral perfusion pressure on severe disability and mortality after head injury. *Neurocrit. Care* 4, 8–13.
- Belytschko, T., Liu, W., and Moran, B. (2000). *Nonlinear Finite Elements for Continua and Structures*, Vol. 26. New York: Wiley.
- Casey, P. A., McKenna, M. C., Fiskum, G., Saraswati, M., and Robertson, C. L. (2008). Early and sustained alterations in cerebral metabolism after traumatic brain injury in immature rats. *J. Neurotrauma* 25, 603–614.
- Fahlstedt, M., Baeck, K., Halldin, P., Vander Sloten, J., Goffin, J., Depreitere, B., et al. (2012). "Influence of impact velocity and angle in a detailed reconstruction of a bicycle accident," in *2012 IRCOBI Conference Proceedings* (Dublin), 787–799.
- Hillson, N., Onuchic, J., and Garcá, A. (1999). Pressure-induced protein-folding/unfolding kinetics. *Proc. Natl. Acad. Sci. U.S.A.* 96, 14848–14853.
- Hummer, G., Garde, S., Garcá, A., Paulaitis, M., and Pratt, L. (1998). The pressure dependence of hydrophobic interactions is consistent with the observed pressure denaturation of proteins. *Proc. Natl. Acad. Sci. U.S.A.* 95, 1552–1555.
- Jha, S., Dhar, D., Krishnamoorthy, G., and Udgaonkar, J. (2009). Continuous dissolution of structure during the unfolding of a small protein. *Proc. Natl. Acad. Sci. U.S.A.* 106, 11113–11118.
- Kleiven, S. (2002). *Finite Element Modeling of the Human Head*. Ph.D. thesis, Stockholm: Royal Institute of Technology.
- Kleiven, S. (2006). Evaluation of head injury criteria using a finite element model validated against experiments on localized brain motion, intracerebral acceleration, and intracranial pressure. *Int. J. Crashworthiness* 11, 65–79.
- Kleiven, S. (2007). Predictors for traumatic brain injuries evaluated through accident reconstructions. *Stapp Car Crash J.* 51, 81–114.
- Kleiven, S., and von Holst, H. (2002). Consequences of head size following trauma to the human head. *J. Biomech.* 35, 153–160.
- Narayan, R., Wilberger, J., and Povlishock, J. (1995). *Neurotrauma*.

- McGraw Hill: Health Professions Division.
- Nyein, M., Jason, A., Yu, L., Pita, C., Joannopoulos, J., Moore, D., et al. (2010). In silico investigation of intracranial blast mitigation with relevance to military traumatic brain injury. *Proc. Natl. Acad. Sci. U.S.A.* 107, 20703–20708.
- Post, A., and Hoshizaki, T. (2012). Mechanisms of brain impact injuries and their prediction: a review. *Trauma* 14, 327–349.
- Viano, D., Casson, I., Pellman, E., Zhang, L., King, A., and Yang, K. (2005). Concussion in professional football: brain responses by finite element analysis: part 9. *Neurosurgery* 57, 891–916.
- von Holst, H., and Li, X. (2013). Numerical impact simulation of gradually increased kinetic energy transfer has the potential to break up folded protein structures resulting in cytotoxic brain tissue edema. *J. Neurotrauma*. doi:10.1089/neu.2012.2730. [Epub ahead of print].
- von Holst, H., Li, X., and Kleiven, S. (2012). Increased strain levels and water content in brain tissue after decompressive craniotomy. *Acta Neurochir.* 154, 1583–1593.
- Ward, C., Chan, M., and Nahum, A. (1980). Intracranial pressure—a brain injury criterion. *Stapp Car Crash J.* 801304, 163–185.
- Ward, C., Chan, M., and Nahum, A. (1997). In vivo thresholds for mechanical injury to the blood-brain barrier. *Stapp Car Crash J.* 973335, 277–291.
- Willinger, R., and Baumgartner, D. (2003). Human head tolerance limits to specific injury mechanisms. *Int. J. Crashworthiness* 8, 605–617.
- Yang, K., Mao, H., Wagner, C., Zhu, F., Chou, C., and King, A. (2011). Modeling of the brain for injury prevention. *Stud. Mechanobiol. Tissue Eng. Biomater.* 3, 69–120.
- Zhang, L., Yang, K., and King, A. (2004). A proposed injury threshold for mild traumatic brain injury. *J. Biomech. Eng.* 126, 226–236.
- Conflict of Interest Statement:** The authors declare that the research was conducted in the absence of any commercial or financial relationships that could be construed as a potential conflict of interest.
- Received: 04 January 2013; accepted: 26 February 2013; published online: 12 March 2013.
- Citation: von Holst H and Li X (2013) Consequences of the dynamic triple peak impact factor in traumatic brain injury as measured with numerical simulation. *Front. Neurol.* 4:23. doi: 10.3389/fneur.2013.00023
- This article was submitted to *Frontiers in Neurotrauma*, a specialty of *Frontiers in Neurology*.
- Copyright © 2013 von Holst and Li. This is an open-access article distributed under the terms of the Creative Commons Attribution License, which permits use, distribution and reproduction in other forums, provided the original authors and source are credited and subject to any copyright notices concerning any third-party graphics etc.





# Mathematical models of blast-induced TBI: current status, challenges, and prospects

Raj K. Gupta<sup>1\*</sup> and Andrzej Przekwas<sup>2\*</sup>

<sup>1</sup> Department of Defense Blast Injury Research Program Coordinating Office, U.S. Army Medical Research and Materiel Command, Fort Detrick, MD, USA

<sup>2</sup> Computational Medicine and Biology Division, CFD Research Corporation, Huntsville, AL, USA

## Edited by:

Guoqiang Xing, Lotus Biotech.com, USA

## Reviewed by:

Stefania Mondello, University of Messina, USA

Karin A. Rafaels, Army Research Laboratory, USA

## \*Correspondence:

Raj K. Gupta, Department of Defense Blast Injury Research Program Coordinating Office, U.S. Army Medical Research and Materiel Command, 504 Scott Street, Fort Detrick, MD 21702, USA  
e-mail: raj.gupta@us.army.mil;  
Andrzej Przekwas, Computational Medicine and Biology Division, CFD Research Corporation, 215 Wynn Drive, Huntsville, AL 35805, USA  
e-mail: ajp@cfdr.com

Blast-induced traumatic brain injury (TBI) has become a signature wound of recent military activities and is the leading cause of death and long-term disability among U.S. soldiers. The current limited understanding of brain injury mechanisms impedes the development of protection, diagnostic, and treatment strategies. We believe mathematical models of blast wave brain injury biomechanics and neurobiology, complemented with *in vitro* and *in vivo* experimental studies, will enable a better understanding of injury mechanisms and accelerate the development of both protective and treatment strategies. The goal of this paper is to review the current state of the art in mathematical and computational modeling of blast-induced TBI, identify research gaps, and recommend future developments. A brief overview of blast wave physics, injury biomechanics, and the neurobiology of brain injury is used as a foundation for a more detailed discussion of multiscale mathematical models of primary biomechanics and secondary injury and repair mechanisms. The paper also presents a discussion of model development strategies, experimental approaches to generate benchmark data for model validation, and potential applications of the model for prevention and protection against blast wave TBI.

**Keywords:** traumatic brain injury, blast injury, mathematical model, biomechanics, neurobiology

## INTRODUCTION

In the current conflicts in Iraq and Afghanistan improvised explosive devices (IEDs) are frequently used weapons of adversary combatants and terrorists against U.S. troops and civilians (Ramasamy et al., 2009; Duckworth et al., 2012; Kang et al., 2012). The blast-induced traumatic brain injury (bTBI) has become a “signature wound of the war on terror” (Bhattacharjee, 2008). Consequently its mitigation, diagnosis, and management are of particular interest to the military. A recent RAND report estimates that 320,000 service members, or 20% of the deployed force, potentially suffer from TBI (Tanielian and Jaycox, 2008). Blast events account for nearly 70% of injuries in wounded service members in both Iraq and Afghanistan, and are the main cause of TBI (Okie, 2005; Heltemes et al., 2012). While penetrating and severe head injuries comprise only 2.8% of injuries, 155,623, or about 80%, were classified as mild TBI (mTBI) (Curley et al., 2011; DePalma et al., 2011). Most mTBI cases result in cognitive deficits immediately after the brain injury and only ~5% report brief loss of consciousness (Hoge et al., 2008; Ling et al., 2009). Although most of mTBI cases are expected to recover, persistent symptoms after injury, such as chronic dizziness, fatigue, headaches, and delayed recall of memory are common (Elder and Cristian, 2009; Warden et al., 2009; Heltemes et al., 2012).

In spite of immense clinical and preclinical research on impact-related brain injury due to vehicle crash and sport injuries in civilian population, current understanding of injury mechanisms is limited, diagnostics and treatment remain controversial, and little is known about the short- and long-term outcomes of

mTBI. Compared to impact-related brain injury, the mechanisms involved in blast-induced mTBI are much less understood. Over the last few decades the Department of Defense (DoD) has performed substantial research on blast trauma to the body, primarily to address injuries seen in previous conflicts, and to improve personal protective equipment (PPE) (Elsayed and Atkins, 2008). The resulting improvements in the PPE and trauma care have mitigated or reduced potential blast and ballistic injury to the thorax but vulnerability to face, ear, brain, groin, and extremity injury still remain (Curley et al., 2011). Protection against blast wave TBI is particularly challenging because, in spite of the protective helmet, a significant part of the soldier's head is still exposed to the blast. Until recently, it was not clear how a blast wave penetrates the cranium and causes brain injury and, if and how military helmets protect against it (Carey et al., 2006; Nyein et al., 2010; Przekwas et al., 2011; Zhang et al., 2011). Military helmets are traditionally designed to protect against ballistic and impact injury and even recent redesign of the sling suspension replaced by foam pads did not completely resolve blast TBI issues.

Given these uncertainties and the continued need to protect U.S. military, the DoD has made substantial research investments in understanding military relevant acute TBI and chronic mTBI (Leggieri, 2009). Several scientific teams are conducting laboratory and clinical studies to elucidate injury mechanisms and to develop protective strategies. The majority of these efforts use an experimental approach of animal testing, *in vitro* study, and analysis of clinical data, all of which are useful and necessary but are slow, expensive, lack injury scaling, and prediction capability.

Better understanding of the blast wave injury mechanisms may be possible with a complementary experimental and computational modeling approach. Validated biomechanics and physiology based mathematical modeling tools of blast head injury may reduce the need for trial-and-error tests involving laboratory animals, yet provide a capability to study brain injury mechanisms, perhaps accelerating the development of neuroprotective strategies and aiding in the development of improved protective armor (Leggieri, 2009; Gupta and Przekwas, 2011).

Mathematical models of brain injury biomechanics have been developed for decades, primarily to study accidental impacts and vehicle crashes (King et al., 1995; Zhang et al., 2001; Takhounts et al., 2003; Brands et al., 2004; Kleiven, 2007). Models of explosive blast TBI are not well established yet because the injury mechanisms are not well understood and the computational methods needed to simulate these fast and multiphysics events are inadequate. The goal of this paper is to review the current state of the art in mathematical modeling of blast wave TBI, identify areas for further developments, model validation strategies, and potential applications in diagnostics, injury prevention, and protection.

## BLAST WAVES AND BRAIN INJURY MECHANISMS

### BLAST WAVES AND BLAST – HUMAN BODY INTERACTION

The first phase of an explosion is the *detonation*, a rapid chemical reaction and energy release generating high pressures and temperatures. The expansion of gases after detonation compresses the surrounding air into a pressure wave, *shock wave*, that propagates at supersonic speed radially in all directions from the explosion site. The front of the shock wave is followed by a high speed *blast wind*. The shock wave generated by an explosion blast is called the *blast wave*. If the explosion of a charge occurs at the ground surface the energy is released into a half hemisphere, so it generates almost two times larger effects as the free air explosion.

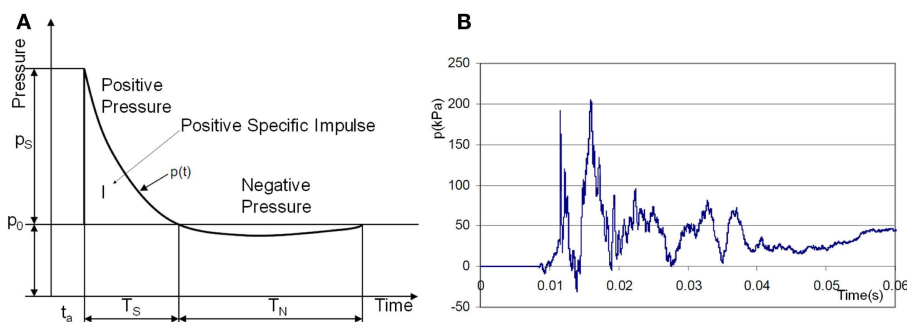
Theoretical and computational models often start with an idealized explosion assuming the instantaneous release of energy from a point source in a free field. In such a case an analytical solution of the Sedov–Taylor problem (Taylor, 1950) provides the pressure-time history in the form of the Friedlander curve, **Figure 1A**. In practice, realistic impulses differ from the ideal Friedlander profile. The effects of reflecting surfaces such as ground or walls of solid objects produce secondary reflected

waves and complex wave patterns. For example, an experimental pressure trace of a blast wave inside of a military vehicle, **Figure 1B** (NATO, 2007), typically exhibits complex patterns with several wave reflections.

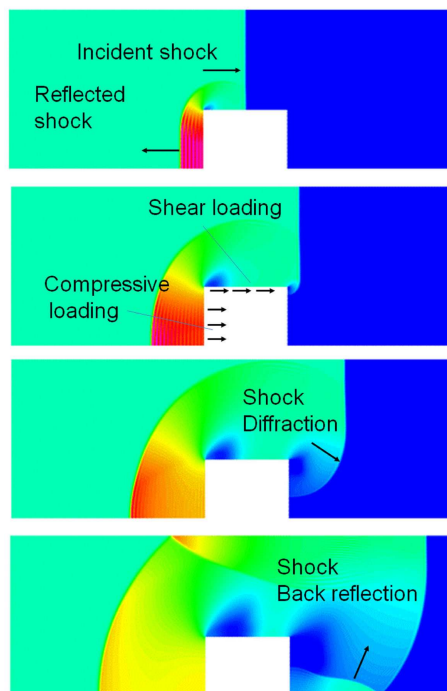
When a blast wave encounters an object of higher density, such as the human body, it reflects off of the object, diffracts around it, and passes through it in the form of elastic and shear waves (Cullis, 2002), **Figure 2**. The reflected wave overpressure significantly exceeds the overpressure of the incident wave. The side walls, parallel to the shock propagation direction, are loaded with the free shock overpressure. The rear side loading begins after the blast wave passes the body and the diffracted waves meet at the center back side. A person next to a solid wall may be exposed to not only the forward shock wave but also to even stronger reflected waves. In addition to the pressure loading, the body will also experience friction drag forces induced by the blast wind. This drag force appears after the primary wave front but its duration is much longer. Furthermore, blast injuries in a confined space may be more severe as the person is exposed to multiple reflected waves coming from various directions.

From the human injury view point, the most important part of the wave energy is the one that is transmitted into the body in the form of both positive (compression) and negative (tension) stress waves as well as shear stress waves. In tissues, the steep gradient pressure waves are absorbed by viscoelastic damping and tissue plastic deformation (tearing, breaking), resulting in mechanical injury. When the pressure wave crosses material interfaces with different densities, large perturbations in stress and deformation take place. A wave impacting a denser material compresses it and when it emerges from denser to lighter material it creates tensile deformations. Therefore in the human body, organs and tissues of different densities are accelerated at different relative rates, resulting in displacement, stretching, and shearing forces (Nakagawa et al., 2011).

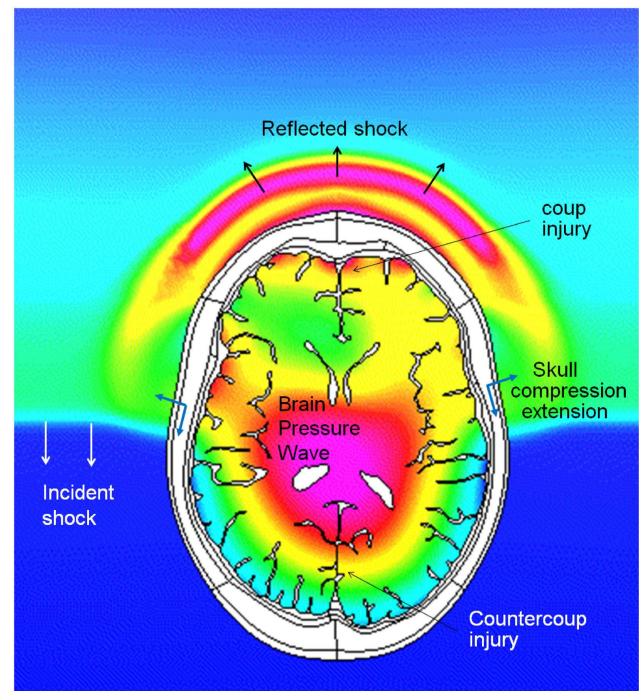
Based on the above physical description of the blast wave events, for the purpose of this article, we classify four potential *insults* caused by blast explosions: *primary blast insult* (PBI) due to the shock wave, *secondary blast insult* due to blast-propelled debris fragments causing blunt or penetrating ballistic trauma, and *tertiary blast insults* due to human body translocation by blast loads and the resulting impact on rigid objects. *Quaternary blast insults*



**FIGURE 1 | (A)** Ideal shock wave pressure profile (Friedlander curve) and **(B)** example of complex overpressure pattern inside a vehicle subjected to a blast mine (NATO, 2007).



**FIGURE 2 |** CFD simulation of a blast wave impacting a solid block; four time instances of pressure fields showing shock reflection from the front face, diffraction around the block, and back reflection behind the block.



**FIGURE 3 |** Coupled simulations of CFD blast wave and FEM biomechanics of a human head. Pressure profiles in the air and in the brain during intracranial pressure wave penetration. Note that the intracranial pressure wave is faster than the incident shock wave in the air.

refer to all other types of injury including burns, environmental wound contamination, etc. Detailed discussion of the injury mechanisms and pathophysiology of trauma for these insult types, particularly lung injury, have been described in military medicine publications and reports (Stuhmiller et al., 1999; DePalma et al., 2005, 2011; Elsayed and Atkins, 2008; Stuhmiller, 2008; Champion et al., 2009).

In the published blast injury literature the expression “primary and secondary injury” is interchangeably used to describe both insults to the body as well as tissue injury and repair mechanisms within the body. For the sake of clarity in this article we define the *insult* to describe external loads to the body and the *injury* to describe the physical, physiological, and biological mechanisms of damage and repair.

### PRIMARY MECHANISMS OF BLAST TBI

There are several potential pathways for the blast wave energy to enter the brain, including: (1) the skull deformation creating a stress wave within the brain, (2) translation/rotation of the head causing compression/shear waves within the brain as well as brain rotation within the skull, (3) the pressure wave directly entering the brain via various foramina (orbital, ethmoidal, vestibulo-cochlear, foramen magnum, and vascular foramina), and (4) an elastic wave propagating along blood vessels from a compressed thorax (Bhattacharjee, 2008; Courtney and Courtney, 2009; Cernak, 2010; Chavko et al., 2011; Bass et al., 2012). Computational and experimental studies show that the cranial bone is a good transmitter

of elastic waves with little attenuation below  $10^4$ – $10^5$  Hz (Stenfelt and Goode, 2005). Cranial deformations are transmitted through the cerebrospinal fluid (CSF) to the brain. In the initial period of skull deformation the compression waves move through the skull and brain tissue faster than the wave in the free air, which is shown in **Figure 3**, presenting predicted pressure profiles in the air and in the brain during a simulated blast load (Przekwas et al., 2011). As in any elastic structure, the impulsively compressed skull, after little delay, will recoil creating a tension wave in the CSF and in the brain. This event may coincide with the arrival of the under-pressure part of the blast wave that may further exacerbate the skull/brain recompression event.

In addition to the compression/tension waves, which propagate in the skull with the speed of sound ( $\sim 1560$  m/s), the geometric/material asymmetries of the skull/brain and non-uniform blast loading will also generate shear waves in the brain. These shear waves are orders of magnitude slower ( $\sim 10$  m/s), persist longer and can be more damaging than compression waves. *In vitro* and *in vivo* experiments show that tension strains are much more damaging to the tissue than compression strains (Xi and Zhong, 2001). Intuitively it can be explained that the surrounding water resists the compression and supports tissue structural components while the tensile force directly disrupts weaker (hydrogen, van der Waals) and stronger (covalent, ionic) bonds at the molecular level.

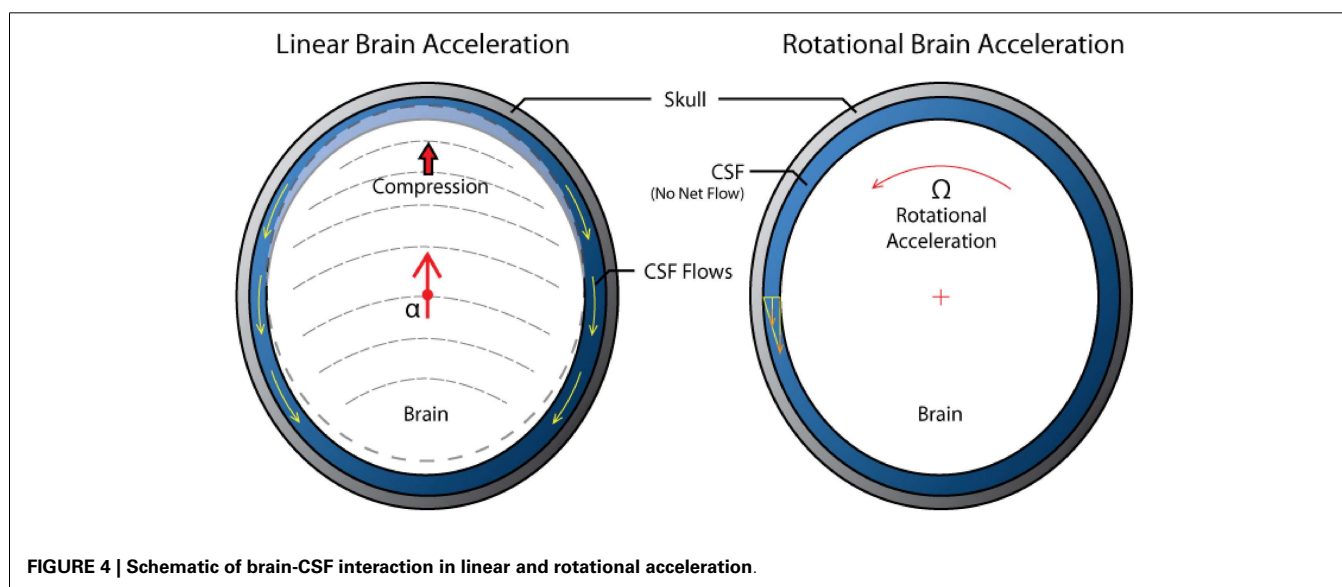
The human brain has several deep sulci filled with CSF separating various gyri, probably to facilitate larger access area for the perfusing blood vessels. We believe that they may also have

an evolutionary biomechanical protective role. As it was mentioned above, the shear waves in brain can be more injurious than compression waves. A fluid filled sulcus between two gyri is a perfect transmitter of a compression wave but it is a very poor transmitter of shear waves. Therefore, sulci may play a protective role in the brain gray matter located close to the surface of gyri during the shear (tangential) motion.

Large, rapidly changing tensions in the brain and in CSF may also cause short living cavitation spots. A collapsing cavitation gas bubble can cause extensive damage to the surrounding tissue. However, the possibility of blast wave induced cavitation in the brain remains controversial. Cavitation has been experimentally observed in laboratory experiments with idealized human head surrogates (cylindrical fluid/gel containers) loaded with high speed impactors (Kurosawa et al., 2009) or exposed to shock tube blasts (Goeller et al., 2012). Recent computational simulations of blast wave head/brain biomechanics predicted unphysical negative absolute pressures in the brain suggesting the presence of cavitation (Moore et al., 2009; Przekwas et al., 2009; Nyein et al., 2010). Others have used “cavitation models” in the form of pressure traps (Ziejewski et al., 2007; Moss et al., 2009; Panzer et al., 2012a). Negative absolute pressures are physically possible in de-gassed or entrapped liquids, e.g., in very tall trees or inside rock formations (Zheng et al., 1991), however they are less likely in the metabolically active brain tissue with relatively large concentrations of  $O_2$  and  $CO_2$  which would act as nuclei spots for cavitation.

The primary compression/tension and shear waves are followed by the macroscopic translational and rotational motion of the brain inside the cranium due to inertial forces. Combination of linear and, more importantly, angular accelerations of the brain often lead to diffuse axonal injury (DAI), contusion, and acute subdural hematoma (Smith and Meaney, 2000; King et al., 2003; Rowson et al., 2012). Experimental tests on human volunteers (Feng et al., 2010) and cadavers (Hardy et al., 2001; Zou et al., 2007) showed that even for low-severity impacts in the sagittal plane, the brain translation has a magnitude of 4–5 mm, and rotation is on the order of  $\pm 5^\circ$  and lasts for almost 300 ms. Due to

the brain's asymmetry and attachment to the brain stem, linear displacement of the skull leads to both linear and angular displacement of the brain relative to the skull. From the hydrodynamic point of view, there is a difference between translational and rotational brain movement in the skull, **Figure 4**. Linear translation of the brain within the skull induces compensatory volumetric flow of the CSF. On the other hand, the rotation of a brain does not involve CSF displacement and the brain rotation is only opposed by the brain surface-CSF shear force. In reality, brain rotations in the horizontal and frontal planes are limited by falx while in the sagittal plane they are limited only by the brain stem anchoring and by bridging veins. As the CSF is almost incompressible any macroscopic brain translation has to be associated with the flow of the displaced surrounding fluid. In fact, the CSF is not only responsible for the well-known neutral buoyancy of the brain, it also provides a “hydrodynamic lubrication” protection of the brain from contact with the cranium. It has been hypothesized that with sufficient forces however, the brain may impact the cranium at the impact point (coup injury) and at the opposite site (contrecoup injury) leading to laceration, contusion, or hemorrhage (Smith and Meaney, 2000). The relative linear inertial acceleration of a floating object in a closed volume is only possible if the density of the suspended object (brain) is different from the surrounding fluid (CSF). The brain-CSF density difference is very small ( $\rho_{\text{Brain}} \sim 1020 \text{ kg/m}^3$ ,  $\rho_{\text{CSF}} \sim 1005 \text{ kg/m}^3$ ) so the relative motion will be slow and it may take a long time for the brain to contact the cranium. This has been experimentally observed in a physical surrogate model of an idealized head (van den Akker, 2010). It should be pointed out that the rotational motion of the brain within the cranium is not constrained by the density difference, it can exhibit much higher velocities and, because of geometrical non-uniformity of the cranium, it may result in a brain-cranium contact. Experimental tests in animal models of TBI have shown that the rotational motion of the brain is much more damaging and can be responsible for focal and diffuse injuries, even in moderate and mild events leading to brain rotation relative to the skull (Margulies, 2000; King et al., 2003; Eucker et al., 2011).





Maintaining the head in a rigid posture allowing linear but no rotational accelerations may explain why race car drivers have survived crashes of 50–80 g; and why woodpeckers can decelerate their brains up to 1200 g during prolonged wood pecking yet can be knocked unconscious by inadvertently flying head first into a window (May et al., 1979; Margulies, 2000).

As the brain is connected to the rest of the body through large blood vessels and the spinal canal, there is a strong possibility of the blast energy to enter the brain in the form of elastic waves propagating along the vessels to the brain (Bhattacharjee, 2008; Courtney and Courtney, 2009; Cernak, 2010). Because the vascular elastic wave speed is very low (10–15 m/s), these waves will arrive at the brain after the initial blast. We define the *primary brain injury* as the mechanical damage to brain structures caused by the initial stress (pressure, shear) waves traversing the brain just after the blast impact and after any mechanical impulse to the head, all lasting tens to hundreds of milliseconds. Accordingly the *secondary brain injury and repair* involves a time evolving myriad of biophysical, neuro-biological, physiological, and potentially cognitive mechanisms, caused by the primary injury, and lasting for hours and, sometimes for life.

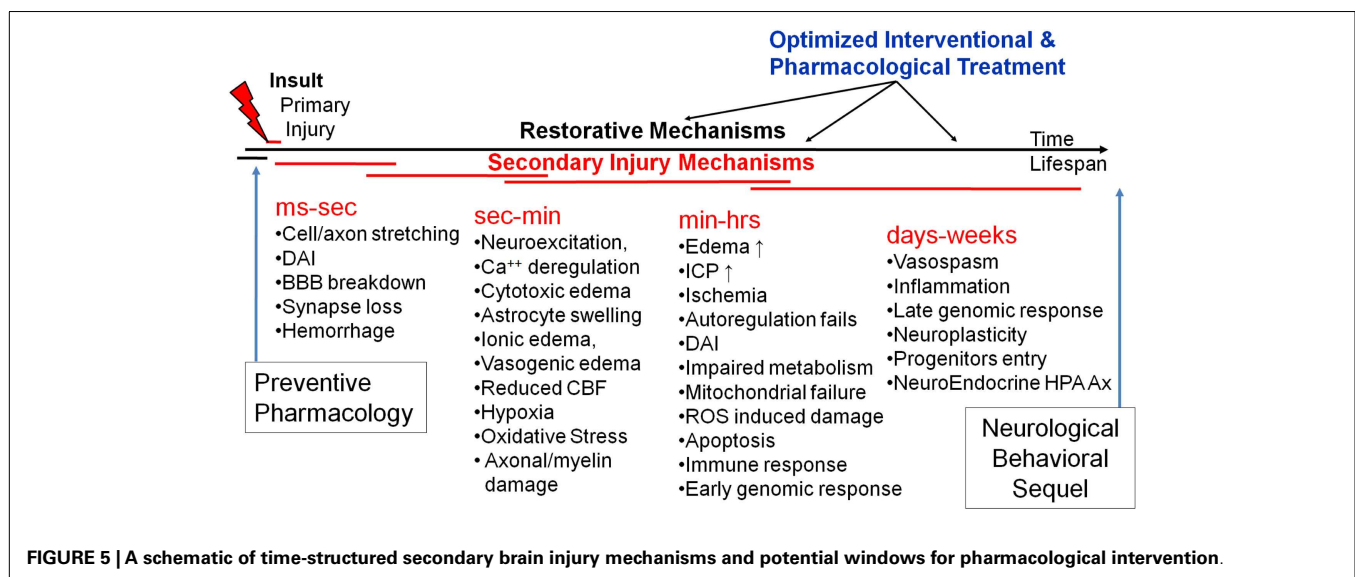
Current understanding of primary injury mechanisms to the brain microstructures is very limited partially because of anatomical heterogeneity of the brain, very short duration of injury events, difficulties in collecting *in vivo* experimental data from animal models, and lack of adequate mathematical models. It is clear, however, that part of the energy in waves traversing the brain is absorbed by various brain structures including vasculature, axonal tracks, neuronal dendrites and synapses, cytoskeleton, and ion channels causing localized and diffuse damage of the primary injury. From the mechanical perspective, macro and micro interfaces between structures with disparate properties (density, elastance) are particularly vulnerable to damage caused by high strain rate loads typically observed in the blast brain injury. These macro and micro interfaces may include the blood brain barrier (BBB), choroid plexus, brain-CSF interface, neuronal/axonal membranes, nodes of Ranvier, dendritic spines,

synaptic clefts, transmembrane structures, and others. These interfaces may be particularly susceptible to mechanical damage if their resonant properties are matched to frequencies of the primary wave. In severe TBI, the primary mechanical damage, e.g., skull fractures or hematomas can be visibly detectable on CT or MRI images. In concussions and mTBI, the primary damage, such as diffuse neuroaxonal injury (Smith and Meaney, 2000; Stys, 2005; Pullarkat et al., 2006; Tsutsui and Stys, 2012), microvascular injury (Dietrich et al., 1994; Readnower et al., 2010; Chodobski et al., 2011), and synaptic injury (Albensi, 2001; Ferenc et al., 2009; Przekwas et al., 2009; Ding et al., 2011) are very difficult to detect, even with high resolution diffusion tensor images (Mac Donald et al., 2011).

## SECONDARY INJURY AND REPAIR MECHANISMS

The primary mechanical insult results in a cascade of secondary injury and repair mechanisms. *In vivo* and *in vitro* experimental models of TBI have begun to unravel the mechanisms producing secondary mechanisms (Kochanek et al., 2000; Smith and Meaney, 2000; Wieloch and Nikolich, 2006; Cernak, 2010; Barkhoudarian et al., 2011; Risling et al., 2011). **Figure 5** schematically illustrates our attempt to establish a timeline of secondary mechanisms as well as windows for optimized pharmacological treatment. In general, they can be classified into several related categories including: biophysical, metabolic, neurochemical, and inflammatory. Each of them includes several mediators involved in a constellation of neuro-biological pathways, most of which are still poorly defined.

Immediately after a mild or moderate primary brain insult, significant electrochemical and hydraulic (osmotic) exchange of ionic, molecular, and fluid constituents occurs between the intracellular and extracellular neuronal and microvascular structures. This exchange generates cytotoxic and ionic swelling (edema) of astrocytes and neurons at the expense of the extracellular space, causing reduction in the diffusive transport of vital metabolites and neurotransmitters. The limited intrinsic energy reserves of the CNS require continuous supply of glucose (Glc) and oxygen for a normal function, most notably for neurotransmission



(predominantly for glutamate (Glu) uptake) and for neuronal ionic repolarization ( $\text{Ca}^{++}$  and  $\text{Na}^+/\text{K}^+$  exchange). Any additional energy requirements needed for structural repair of the injury will have to be facilitated by accelerated supply and utilization of Glc and oxygen to produce ATP. This hypermetabolic state may cause local cerebral ischemia, hypoxia, neuroexcitation, and failure of axonal and neuronal conduction. Because the intra-arterial and capillary blood pressures are much larger than the intracranial pressure (ICP), any mechanical damage to the BBB may cause efflux of water and small molecules (some of them neurotoxic) from the luminal to the interstitial space causing brain swelling, mechanical deformation of the brain tissue and increase of ICP. These in turn may compress the venous and CSF volumes reducing the cerebral blood flow (CBF) rate and causing ischemia. Altered metabolic states may result in further cellular/mitochondrial damage due to oxidative stress, while penetrating blood borne molecules such as cytokines may initiate inflammatory responses (Schmidt et al., 2004; Graber and Dhib-Jalbut, 2009).

Diffuse axonal injuries are the hallmark of mild and moderate TBI and are caused by a combination of rapid tension and shear deformations in the white matter of the brain (Smith and Meaney, 2000; Stys, 2005; Johnson et al., 2012; Tang-Schomer et al., 2012). DAI is believed to be present in all mTBI injuries accompanied with a loss of consciousness (Meythaler et al., 2001), yet each year more than 1.5 million Americans sustain mTBI with no loss of consciousness and no need for hospitalization (DeKosky et al., 2010). The mechano-biological mechanisms of axonal injury are not well understood and are an active research area (Tsutsui and Stys, 2012). Mechanical reasoning indicates that large and rapid forces to an axonal bundle can cause primary axotomy, as in the breaking of a fiber in a rope under large tension, while other axons may only experience partial damage to some of its structures (membrane, cytoskeleton, ion channels). These “partially damaged” axons may further undergo complex and prolonged biophysical and metabolic responses (see secondary injury below) leading to either the axonal repair or cause an irreversible axonal damage, i.e., formation of retraction bulbs. It should be mentioned that secondary effects following non-mechanical injury, e.g., ischemia or neuro-inflammation can display some of the same traits as DAI (Tsutsui and Stys, 2012). The mechanical integrity of the axonal plasma membrane, a critical barrier between intra- and extra-cellular environments, is essential for neuronal function and survival. Even intermittent membrane mechanoporation may result in axonal electrical depolarization which may cause rapid electrochemical and osmotic “fluxing” of ions and water resulting in axonal swelling (Tang-Schomer et al., 2012). Mechanical forces may also disrupt a network of axonal cytoskeleton responsible for structural integrity and intra-axonal two way traffic of various cargo (Fernandez and Pullarkat, 2010). For the neuron to recover from these mechanical derailments it will have to initiate a metabolic “over-drive” (hypermetabolism) needed for electrochemical and osmotic repolarization, and membrane and cytoskeleton repair. Unfortunately, increased hypermetabolism can also be also damaging via oxidative stress.

Primary mechanical damage to axonal tracks, often present in the parasagittal white matter of the cerebral cortex, corpus

callosum, and the brain stem, initiates a cascade of secondary axonal injury and repair mechanisms (Smith and Meaney, 2000; Stys, 2005; Pullarkat et al., 2006; Wieloch and Nikolich, 2006; Tang-Schomer et al., 2012; Tsutsui and Stys, 2012). Axonal fibers with damaged myelin and plasma membrane suffer large current leaks and exhibit increased metabolic requirements to support conduction. Action potential propagation under these conditions exacts a high metabolic price for energy-consuming ion movements, which in turn places increased demands on energy-consuming Na–K ATPase ion exchangers. This, combined with a potentially impaired metabolic ability of mitochondria, may produce a state of chronic axonal hypoxia, deregulation of  $\text{Ca}^{++}$  homeostasis and ultimately structural failure of the fiber, manifested as spheroid formation and finally transection in the form of microbeads, retraction bulb, and axonal transection formation (Stys, 2005; Kilinc et al., 2009; Tang-Schomer et al., 2012).

Diffuse synaptic and dendritic spine injuries are also potentially significant secondary injury and repair sites. These TBI mechanisms have not been reported in the open literature, probably because of lack of viable *in vivo* experimental measurement modalities at such small scales. Synapses are tiny structures ( $\sim 1\ \mu\text{m}$  in diameter and  $\sim 20\text{-nm}$  spacing) precisely packed in the CNS at an incredibly high density (estimates range from  $\sim 2 \times 10^8$  to  $4 \times 10^9$  in rat's brains) (McAllister, 2007). Synaptic terminals are mechanically very dense structures composed of a remarkably large number of proteins, transsynaptic adhesion molecules, and scaffolding. Its proper function strongly depends on its morphology because mechanical deformations may cause malfunction. It is likely that mechanical tension and shear waves cause temporary disconnects and microdamage of synapses and dendritic spines which in turn result in temporary cognitive malfunction (Monnerie et al., 2010; Gao et al., 2011). It is also likely that a large number of deformed synapses in mild injury may be “repaired” by electrokinetic and biomechanical mechanisms – a process of synaptic neuroplasticity and cognitive recovery. The proposed mechanism of synaptic injury has been recently observed in *in vitro* neuronal cultures (Ferenc et al., 2009; Monnerie et al., 2010) exposed to shock waves. These results suggest that shock-waves emanating from explosive devices may specifically affect synaptic plasticity in the brain. Further, *in vitro* and *in vivo* experiments and mathematical modeling studies should be conducted to elucidate these injury mechanisms and to determine whether the diffuse synaptic injury plays a prominent etiological role in mTBI.

## MULTISCALE, MULTI-DISCIPLINE MODELING OF BLAST TBI

### MULTISCALE MODEL OF BLAST TBI – OVERALL APPROACH

A comprehensive computational model of blast TBI should involve several disciplines including: blast wave gas dynamics, human body dynamics, body/head/brain biomechanics, physiological responses, and a host of biophysical and neuro-biological mechanisms of secondary injury and repair. The complexity of a mathematical model of blast wave TBI is magnified by a wide spectrum of length and time scales:

- Length – from meters for a blast scene, to centimeters for the brain, to micrometer for neurons and axons, to nanometer for neuronal synapses

- Time – from microsecond for blast wave transition over the head, to millisecond for brain biomechanical responses, to min/h/days for secondary injury and repair cascade.

To develop such a mathematical model of TBI, a coordinated effort is needed integrating various disciplines including: neuroimaging, neuroanatomy, geometry/mesh generation, computational fluid dynamics (CFD), finite element method (FEM) structures, biomechanics, and computational neurophysiology and neurobiology. A coupling between primary injury models (biomechanical) and the secondary mechanism models (neurobiology) is also required. Development of complex and computationally expensive high-fidelity 3D models for a human and an animal (rat, pig) should be accompanied with the development of “reduced” (compact) but computationally fast models using approximate anatomic/geometric representation, yet affording advanced models of neurobiology. The model development effort should be paralleled with model-guided experiments on neural cells and brain tissue cultures, animal models, physical surrogates, and to some extent on humans to generate benchmark quality data for model validation and scaling.

Computational models of blast wave physics and human body/head/brain biomechanics, have been developed over the last few decades for military/aerospace and automotive safety applications (Takhounts et al., 2003, 2008; Anderson, 2004; Kleiven, 2007; Horgan and Gilchrist, 2008; Needham, 2010; Zhang et al., 2011). For modeling blast TBI, further improvements are needed in: high strain rate tissue material properties, coupled fluid-structures interaction (FSI) of intracranial biomechanics, micromechanics of brain tissue damage, and coupling between the brain macro- and micro-scale biomechanics. Computational models of brain secondary injury and repair mechanisms have not been established yet, mainly because of complexity and incomplete understanding of the processes involved and partially because of lack of supporting benchmark quality *in vitro* and *in vivo* experimental data. There are however, several mathematical models of neurophysiology and neurobiology which could be used as a starting point for the development of a comprehensive model of the secondary mechanisms (Cooley and Dodge, 1966; Koch and Segev, 1998;

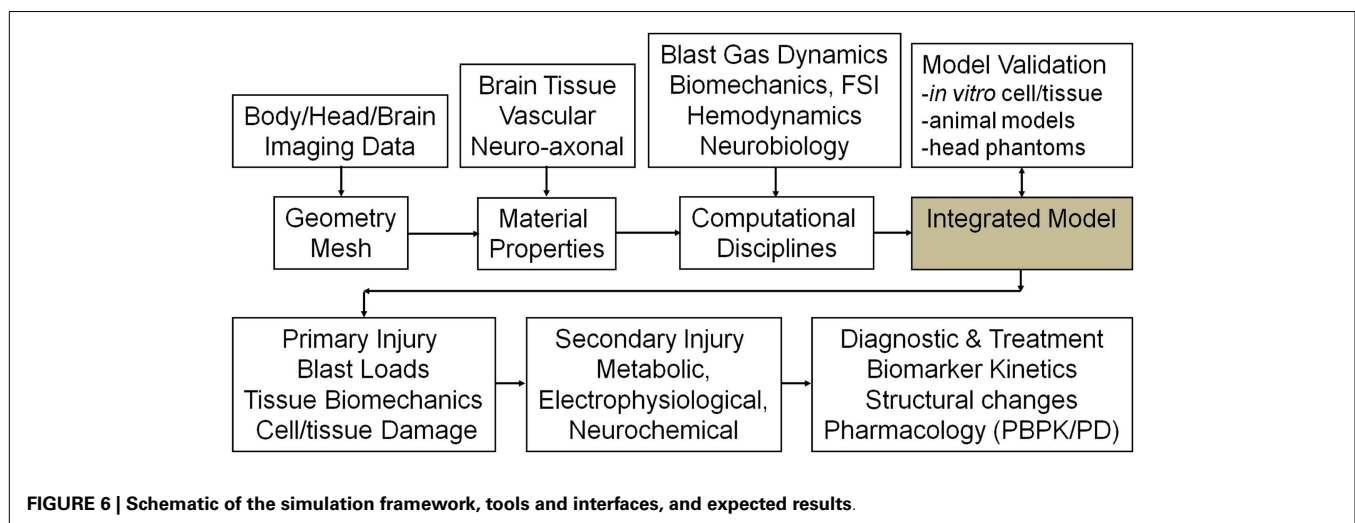
Ursino et al., 2000; Lakin et al., 2003; Wakeland and Goldstein, 2005; Ascoli, 2006; Carnevale and Hines, 2006; Aubert et al., 2007; Gleeson et al., 2007; Humphrey et al., 2007; Savtchenko and Rusakov, 2007; Cloutier et al., 2009; Linninger et al., 2009; Mangia et al., 2009; Kozloski and Wagner, 2011; Liang et al., 2011; Mohan et al., 2011). The schematic in **Figure 6** shows a potential functional layout of such a modeling platform. It could set the standard for comparison of alternative model components and establish a benchmark framework for model calibration and validation against experimental data. Following is a brief overview of key model components, existing models in selected disciplines and suggestions for further development.

## MULTISCALE MODEL OF PRIMARY TBI

### **Anatomy/geometry/mesh**

Accurate simulations of blast wave interaction with a human or animal body requires 3D anatomical/geometric models that could be used to generate computational meshes for CFD and FEM biomechanics models. Anatomical models can be generated using neuroimaging data of brain and skull structures and the whole body imaging data, e.g., “Visible Human” (Spitzer and Whitlock, 1998; Spitzer and Scherzinger, 2006; Tang et al., 2010). Reasonable resolution models of a rat and mouse whole body anatomic geometries are also available (Segars et al., 2004; Bai et al., 2006; Khmelinskii et al., 2011). Improved resolutions of rodent brain functional zones as well as body/cerebral vascular anatomy have to be established. The anatomic geometry models are used to generate computational meshes outside and inside the body for blast and biomechanics simulations. To simulate whole body bio-dynamics (movement in air induced by blast loads) the anatomical/geometric models need to be “articulated,” i.e., individual body parts should be connected by joints to enable their relative motion (Wilkerson and Przekwas, 2007; Arepally et al., 2008; Zhou and Przekwas, 2011; Tan et al., 2012).

Several anatomical/geometry models have been developed to study human body/head impact injury biomechanics (Zhang et al., 2001; Levchakov et al., 2006; Mao et al., 2006, 2010; Kleiven, 2007; Horgan and Gilchrist, 2008; Ramirez, 2010; Gayzik et al., 2011; Yasuki, 2011) and rat head and body injury (Liang et al., 2011;



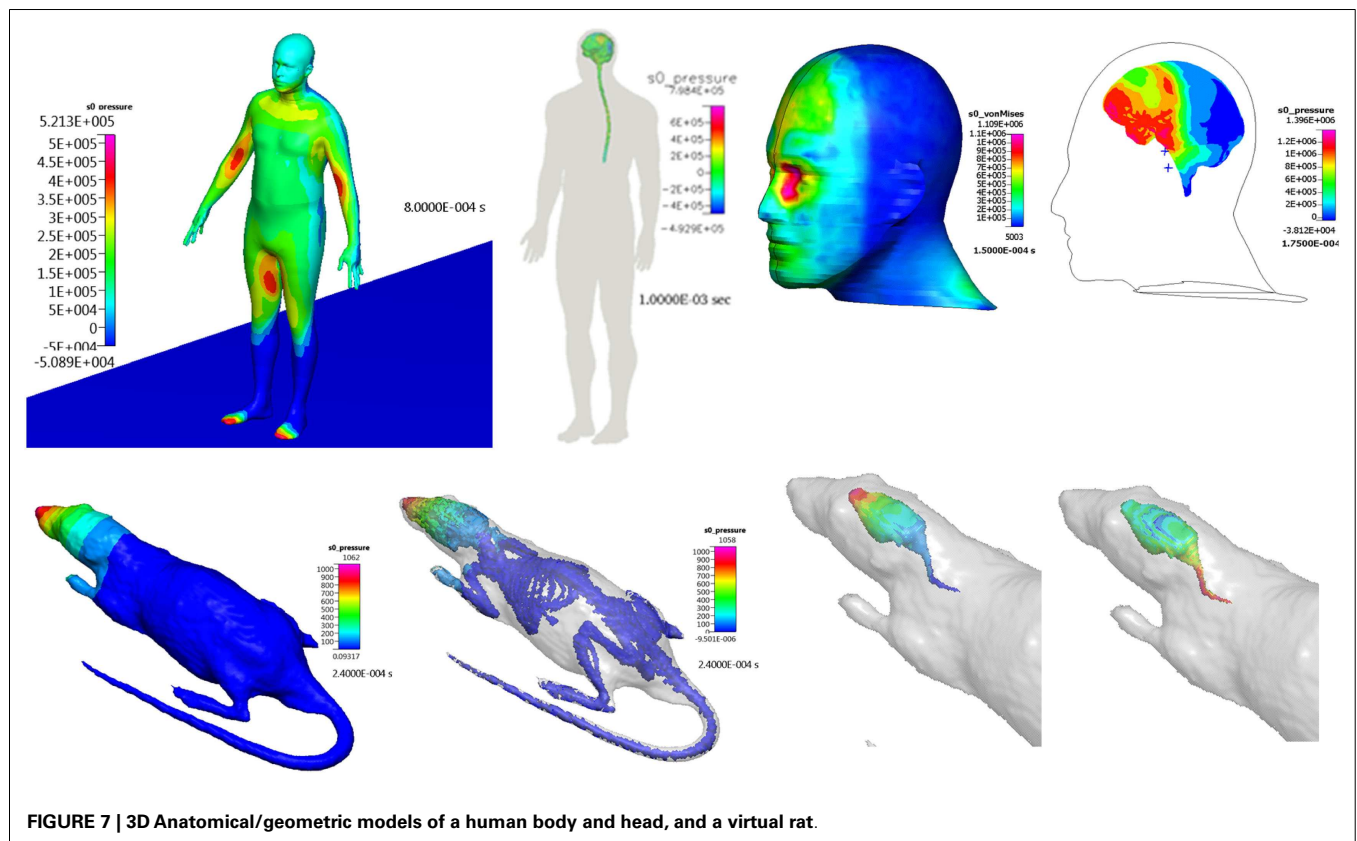
Przekwas et al., 2011). Until recently brain injury models focused on the inertial and impact (crash) injury for which the skull and brain geometry were sufficient. Because the blast loads are spatially and temporally distributed over the entire head and neck, the anatomical model should include the head's skin, facial structures including ocular and nasal cavities, cranium, and neck geometry. Such anatomical geometries are currently being developed (Chafi et al., 2009; Moore et al., 2009; Przekwas et al., 2009, 2011; Nyein et al., 2010; Ortega, 2011; Zhang et al., 2011; Sundaramurthy et al., 2012). Since blast loads occur at very fast rates, the brain injuries tend to be spatially distributed loci of micro-injuries, e.g., DAI. The current models of whole brain biomechanics do not have the proper resolution to model the micro-scale injuries that result from a primary blast exposure. Furthermore, to the best of our knowledge, none of the existing models can properly simulate the physics of the brain-CSF interaction or the head-neck movement.

Experimental *in vitro* tests of brain tissue slices and neuronal cell cultures may enable validation of mathematical models by providing detailed correlation between the primary injury dynamics and the resultant secondary mechanisms (Morrison et al., 2006, 2011; Chen et al., 2009; Frieboes and Gupta, 2009; Yu and Morrison, 2010; Johnson et al., 2012; Tang-Schomer et al., 2012). It is important to develop protocols and tools for the generation of 3D morphological geometries of *in vitro* cell and tissue cultures and their dynamic responses to mechanical or shock wave loads. Ideally, such models should register mechanical, electrokinetic, and biochemical spatiotemporal responses of axonal, synaptic and sub-cellular structures to controlled mechanical insults.

### Blast wave gas dynamics and intracerebral fluid mechanics

Computational fluid dynamics models have been successfully used to simulate blast wave dynamics over a human body and head (Imielinska et al., 2006; Przekwas, 2008; Moore et al., 2009; Taylor and Ford, 2009; Needham et al., 2011) and to calculate pressure and shear forces for subsequent modeling of human body biodynamic and biomechanical responses. **Figure 7** shows examples of CFD model predictions of blast wave interaction with a human body, head, and with a rat body. Reported simulations have shown that such a sequential modeling approach is well justified as the inertial body movement starts well after the blast wave traverses the body (Needham et al., 2011; Tan and Przekwas, 2011). Accurate simulation of moving shock waves and their interaction with solid objects without “smearing” of the shock front discontinuities requires small time steps, very fine computational mesh in the entire flow domain and long computing times. Fine mesh is essentially only needed in the regions of high gradients, e.g., shock front, and much coarser grids could be used elsewhere. One way to solve this problem is to use a solution adaptive mesh refinement.

Computational fluid dynamics models could also be used to simulate the responses of intracranial fluids, including CSF-brain interaction and cerebral blood interaction with brain tissue. Since the movement of intracranial fluids is strongly coupled to mechanical displacements of the skull and the brain, the intracranial fluids should be simulated using a FSI model. Direct numerical simulations of the FSI in a closed intracranial cavity is a non-linear and computationally very challenging problem, as small cranial displacements cause large variations in the ICP. To the best



**FIGURE 7 | 3D Anatomical/geometric models of a human body and head, and a virtual rat.**



of our knowledge, the intracranial FSI problem has not been convincingly solved, yet. Reported simulation results exhibit negative absolute pressures (Moore et al., 2009; Moss et al., 2009; Taylor and Ford, 2009; Przekwas et al., 2011), trap predicted fluid pressures to a prescribed value (e.g., absolute zero or vapor saturation) or show large cavitation volumes (Wardlaw and Goeller, 2010). In most reported models, CSF is treated as compressible deforming “solid” attached to brain and skull, an assumption valid only for the first few milliseconds when there is no significant flow of CSF. However, if longer time scales need to be simulated, such as for shear waves, brain rotation, and brain swelling during edema, a full FSI model may have to be used. Such an approach has been used for high fidelity and reduced order modeling of hydrocephalus (Kurtcuoglu et al., 2007) but has not been well established in 3D TBI models, yet.

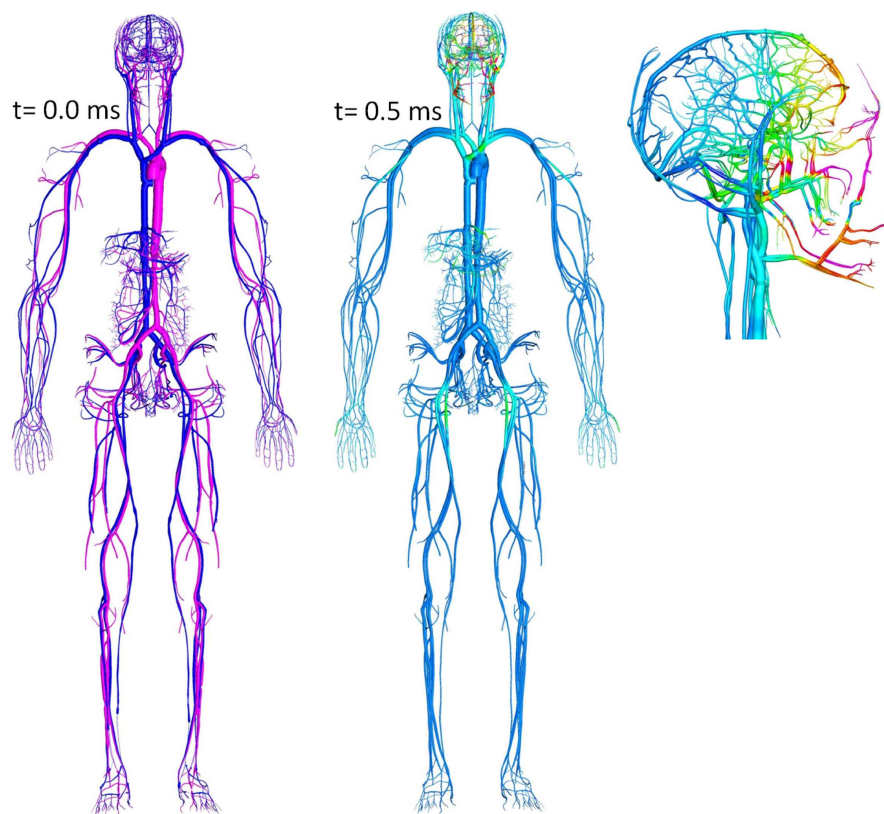
An FSI model, coupling whole body biomechanics, elasto-fluid dynamics of thoracic/cerebral vascular system, and brain biomechanics could be used to evaluate the “thoracic” or “vascular” hypothesis of TBI (Cernak et al., 2001; Chavko et al., 2011). This hypothesis states that a thoracic/abdominal vascular system, compressed by a blast wave, may induce an elastic wave propagation from the thorax along the vascular system to the brain. This may cause brain tissue damage and BBB injury. Since vascular elastic waves propagate relatively slowly (12–15 m/s), these injury events occur much later than primary blast events. **Figure 8** shows a computational model of a human vascular system coupled to

the body/brain biomechanics, currently under development to evaluate the above hypothesis (Przekwas et al., 2011).

An FSI model may be also required to study brain-vascular coupling during vasogenic edema, hemorrhage, and vasospasm, all associated with brain injury (Armonda et al., 2006; Armin et al., 2008; Alford et al., 2012). Mechanical microdamage to the BBB causes an increase of vascular permeability and inflow of osmoles and water to the brain causing volumetric expansion of the brain and increase of the ICP – a consequence of the so-called Monroe–Kellie doctrine. This in turn results in compression of the vascular (venous in particular) system and potentially brain herniation. In such a case, mathematical models of brain poro-visco-elastic biomechanics need to be coupled to CSF flow, vascular fluid mechanics as well as to electrochemistry of solutes and ion transport and osmotic pressure developments.

### Head and brain biomechanics

Computational modeling of human head injury biomechanics has been investigated since the 1970s, first using approximate analytical and spring-mass-damper (SMD) models (Slattenschek and Tauffkirchen, 1970; Alem, 1974) and in 1990s using FEM (Ruan et al., 1993; King et al., 1995). Today FEM tools are routinely used to simulate impact biomechanics and primary brain injury problems, particularly in the automotive occupant safety applications (Miller, 2011). Advanced 3D FEM models of head/brain anatomy and biomechanics and injury have been pioneered at



**FIGURE 8 |** Whole body cardiovascular system model “embedded” in the tissue biomechanics model used to study blast-induced elastic waves.

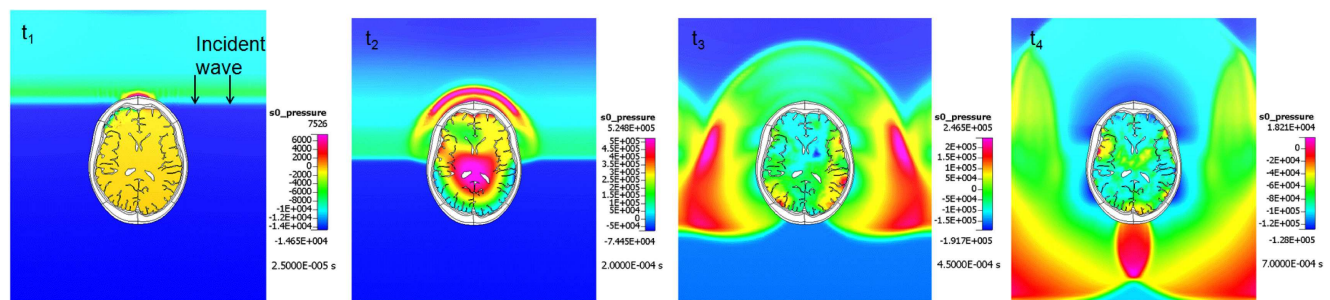
the Wayne State University resulting in the well-known WSUBIM (Wayne State University Brain Injury Model) FEM human head model (Ruan et al., 1993; Zhou et al., 1996; Al-Bsharat et al., 1999). This model of a 50th percentile male human head currently includes scalp, cranium, falx cerebri, tentorium, sagittal sinus, transverse sinus, bridging veins, CSF, and the brain structures as separate anatomical segments (Zhang et al., 2001, 2011; Hu et al., 2007). Svein Kleiven's group at the Royal Institute of Technology in Stockholm, Sweden has developed a human head/neck FEM model with improved resolution of the subarachnoid CSF and 11 pairs of parasagittal bridging veins (Ho and Kleiven, 2007; Kleiven, 2007). A neck model including spinal column, spinal cord, dura mater, and neck muscles was incorporated allowing the brain stem to be extended to the spinal cord. Other FEM head/brain biomechanics and injury models include: Simulated Injury Monitor (SIMon) FEM human head model developed by a team lead by Takhounts at the National Highway Traffic Safety Administration (NHTSA) (Takhounts et al., 2003, 2008), the University College Dublin Brain Trauma Model (UCDBTM) (Horgan and Gilchrist, 2008; Colgan et al., 2010), and the Strasbourg University Finite Element Head Model (SUFEHM) (Willinger et al., 1999; Raul et al., 2008; Meyer et al., 2013) as well as others. All of these models, in spite of successes in modeling head impact and inertial translation/rotation accelerations, still need improvements in anatomical geometry, physics, and numerics, e.g., high strain rate material properties, modeling the CSF flows, accounting for the presence of vasculature, adequately model the micro-scale injuries, addressing numerical stiffness, and long computing times.

In the last few years, FEM head/brain biomechanics models have been adapted for modeling the blast TBI by incorporating head/face anatomical details and by coupling them to the blast physics CFD solvers (Ziejewski et al., 2007; Mott et al., 2008; Przekwas, 2008; Chafi et al., 2009, 2010; Moore et al., 2009; Moss et al., 2009; Przekwas et al., 2009, 2011; Taylor and Ford, 2009; Nyein et al., 2010; Zhang et al., 2011; Panzer et al., 2012a; Zhu et al., 2013). **Figure 9** presents example simulation results of a shock wave reflection from and diffraction around a human head (coronal cross section) and a resultant pressure wave within the brain. In comparison to the blunt brain biomechanics model, the blast injury model has a loading force that is much faster and is spatially and temporally “distributed” over the entire head during the shock wave propagation around the head. Moreover, the intracranial

loads, both compression and tension, and the strain rates are much higher in the blast case. Coupled blast wave gas dynamics and brain biomechanics simulations are needed to compute dynamic response of the head, cranium, and the brain.

The main limitation of all existing FEM models is the treatment of the CSF interaction with the brain and the cranium, particularly modeling the shear waves and brain translation/rotation. Most of the FEM models treat the CSF as a “solid with fluid-like property” allowing a “contact with slip” interfaces between CSF and skull and brain. This approach is inadequate for modeling larger deformations and for modeling brain translation and rotation for longer periods of time. For short duration head/brain primary biomechanical events, lasting only tens of milliseconds, typically the explicit FEM models are used to simulate brain responses. However for longer duration events, such as propagation shear waves, brain rotation, swelling, and CSF displacement, implicit FEM schemes are required. These however require full matrix inversion and are much more difficult to solve for fine meshes, even using parallel computers.

Another very important and challenging problem is the development of material properties for the skull and various anatomical regions of the brain for high strain rates, typical in blast loads. It is clear that different head/brain tissues will require tissue-specific constitutive equations and parameterization. In spite of decades of experimental testing and analytical studies of brain mechanical properties, no universally accepted dataset exists and the material property parameters vary by an order of magnitude (Hrapko et al., 2008). Material models have been extracted from both *in vitro* experimental data (Takhounts et al., 2003; Brands et al., 2004; Miller, 2011; Prevost et al., 2011) as well as from *in vivo* data (Gefen and Margulies, 2004; Atay et al., 2008; Clayton et al., 2011). The results of different studies are difficult to compare, due to the wide range of experimental protocols including the species type/age (human, rodent, porcine), loading configurations (compression, tension, shear, indentation), the loading histories (cyclic, stress relaxation creep), and test regime (levels of strains and strain rates, temperature, tissue hydration). The experimental data have facilitated the development of a large variety of constitutive models ranging from simple linear elastic, hyperelastic, linear viscoelastic to non-linear viscoelastic, yet no consensus exists even on the linear viscoelastic properties. No model has integrated viscoelastic, stress relaxation, and large strain response into one



**FIGURE 9 |** Example coupled CFD-FEM simulation results of a blast wave diffraction around, and transmission through a human head. A sequence of four time instances.

single constitutive framework thus far. Before significant advancements can be made, the modeling and testing communities must come to a consensus on the material model formulations and anatomical/geometric and numerical representations of the FEM head/brain biomechanics and injury model.

Finite element method biomechanics models may also be used to simulate brain tissue/cell damage at the micro-scale. Mathematical models of mechanical damage to neuroaxonal structures may be able to describe damage to cell membranes, cytoskeleton, ion channels, synaptic clefts, dendrites, and axons. These in turn, could provide inputs for the secondary injury and repair models, simulating electrophysiology and ion homeostasis, alterations in metabolism, neuroexcitation, cytotoxic edema, oxidative stress, apoptosis, and other injury and repair mechanisms. In the last few years, the first FEM biomechanics simulations of very simplified axonal structures have been reported (Karami et al., 2009; Cloots et al., 2010; Przekwas et al., 2012). Future advancements in micro-scale FEM can incorporate boundary conditions from macro-scale simulations (Przekwas, 2008; Cloots et al., 2010; LaPlaca and Prado, 2010). *In vivo* micro-imaging may also provide functional response data (electrophysiological, metabolic, and biochemical) needed for the development and validation of mathematical models of secondary brain injury and repair mechanisms. We envision that the next generation of *in vivo* and *in vitro* micro-biomechanics models will be able to elucidate neuroaxonal injury mechanisms and will help establish brain region and insult specific injury criteria.

#### MULTISCALE MODEL OF SECONDARY INJURY AND REPAIR MECHANISMS

The secondary brain injury and repair mechanisms start immediately after the primary insult and, depending on the injury severity, may last for a long period of time (Graham et al., 2000; Margulies, 2000; Cernak et al., 2001; Cernak, 2010; Masel and DeWitt, 2010; Meaney and Smith, 2011). Secondary mechanisms are multiple, interacting cascades of local and systemic responses. Although primary injury comprises the initial tear and shear of neuro-tissue, secondary mechanisms can dramatically exacerbate the initial injury, or conversely, participate in neuro-repair processes.

Development of a mathematical model integrating all secondary mechanisms is a formidable task. A mathematical model of secondary brain injury and repair that couples biomechanics, cerebral perfusion, brain metabolism, and neurobiology does not exist yet. At the same time several components of such a model have been developed and reported including: cerebral perfusion, fluid electrolyte balance, metabolism, cellular signaling pathways, electrophysiology, edema, neuroexcitation, etc. (Yi et al., 2003; Wakeland and Goldstein, 2005; Dronne et al., 2006; Gleeson et al., 2007; Humphrey et al., 2007; Linninger et al., 2009; Østby et al., 2009; Mohan et al., 2011). Traditionally, computational neurophysiology and systems biology have been evolving as separate disciplines and only recently has it become clear that their combination may enable revolutionary progress in neurology (De Schutter, 2008). Cerebral physiology, neurobiology, and secondary injury models are typically formulated using a multi-compartmental modeling approach linking cerebral vascular, interstitial, and intracellular compartments. The next generation secondary brain injury and

repair models will have to combine compartmental or distributed models for the *in vivo* whole brain physiology coupled to neuroaxonal and synaptic biophysics and neurobiology models. From the brain injury modeling perspective it will be essential to combine models of biomechanics and neurobiology, validate them on *in vitro* experiments, and evaluate them on *in vivo* animal/human data.

#### Models of head/brain biomechanics and cerebral hemodynamics

Mathematical modeling of brain biomechanics can be accomplished using both FEM models as well as much simpler but computationally efficient SMD elements. SMDs can be adapted for modeling both macroscopic biomechanical effects of secondary mechanisms, such as cerebral arterial/venous elasticity, hemorrhage, edema and vasospasm, as well as microscopic biomechanics of brain cell/tissue injury, e.g., BBB breakdown, axonal and synaptic injury (Di Bona et al., 2003). The mechanical model will have to be coupled to models of CBF, brain perfusion, and volume shifts between brain compartments. Similar SMD modeling approach has been used for modeling blast lung injury (Przekwas, 2008; Stuhmiller, 2008).

Reduced order fluid-network models have been used for modeling CBF and tissue perfusion, autoregulation, and other aspects of cerebral physiology (Ursino et al., 2000; Wakeland and Goldstein, 2005; Alastruey et al., 2007; Stevens et al., 2008; Linninger et al., 2009; Liang et al., 2011). More elaborate models use networks of blood vessels arranged to represent the topology of the circle of Willis (COW) connected to the whole body circulation (Reymond, 2011). These models solve for time/space resolved intracranial blood flow rate, pressure, and fluid/metabolite exchange between vascular and brain tissue compartments. To simulate brain injury the cerebral hemodynamics model may need to be coupled to a brain biomechanical model via transmural pressure. **Figure 10** shows examples of spatially distributed and multi-compartmental models of the human body, cerebral vascular system, arterial COW and anatomically distributed cerebral perfusion and venous return (Przekwas et al., 2011). In that model, the vascular tree can dynamically adjust its vessel radius to accommodate temporal changes in the perfusion pressure and autoregulation as well as changes in the ICP due to mechanical loads (e.g., blast wave). Ultimately, the cerebral vascular model should provide inputs to several other sub-models such as ischemia, hemorrhage, edema, hypoxia, vasoregulation, vasospasm, and a full range of neurobiology models. Combining a spatially distributed whole body/brain-vascular system model with the FEM body/head biomechanics models may help in elucidating the thoracic/vascular TBI hypothesis.

#### Cerebral metabolism and injury neurobiology models

Secondary brain injury and repair is a multi-factorial process involving a range of bio-electro-chemical events, but two components are of key importance – alterations in metabolism and neurotransmission (Rzigalinski et al., 1998; Magistretti and Pellerin, 1999; Aubert et al., 2007; Payne et al., 2009; Cernak and Noble-Haeusslein, 2010; Peskind et al., 2011). Mathematical models of neurometabolic mechanisms are typically derived from kinetic pathways, involving a large number of kinetic parameters obtained from *in vitro* experiments (Nicholson, 2001; Banaji et al., 2005;





of neurotransmitters outside of the synaptic cleft, synaptic plasticity (LPT, LDT), and other mechanisms. The results of such a model may be able to show that the exacerbated secondary mechanisms, not just the initial mechanical injury, may be responsible for the long-term neurocognitive effects. This in turn could identify targets for neuro-interventions and optimal treatment strategies. The development and validation of such models will require detailed spatiotemporal experimental data from *in vitro* neuroaxonal cell/tissue cultures, *in vivo* animal brain injury models and ultimately *in vivo* conditions in animals and humans.

Mathematical modeling of coupled micro-biomechanics and electrophysiology of neuronal injury has not been reported yet, but has been identified as an important recommendation (LaPlaca and Prado, 2010). Mathematical models of cellular electrophysiology have been developed and used for modeling single neurons and large neuronal networks (Kager et al., 2000; Calvetti and Somersalo, 2011; Kozloski and Wagner, 2011). Typically, mathematical models of neurons, such as neuron and genesis, combine the electrical cable theory for modeling action potential propagation and the Hodgkin–Huxley model to simulate ionic fluxes (Bhalla, 1998; Carnevale and Hines, 2006). Neuron models have been successfully used for a wide range of problems including detailed neurophysiology of complex 3D neurons, propagation of action potentials in myelinated axons and in neuronal synapses (De Schutter and Bower, 1994; Gleeson et al., 2007; Savtchenko and Rusakov, 2007; Lopreore et al., 2008; Brown et al., 2011; Kozloski and Wagner, 2011; Mohan et al., 2011). Significant progress has been achieved in establishing an infrastructure of experimental databanks of 3D neuronal morphologies and neurobiology data that could be used for the development and validation of mathematical models (Ascoli, 2006; Eberhard et al., 2006; Gleeson et al., 2007; Martone et al., 2008; He and Cline, 2011; Halchenko and Hanke, 2012; Leergaard et al., 2012).

An integrated micro-biomechanics and electrophysiology model could be developed based on *in vitro* neuronal cell/tissue cultures with well-defined mechanical loads and spatiotemporal measurements of cellular electrophysiological and biological responses (LaPlaca et al., 1995; Rzigalinski et al., 1998; Morrison et al., 2006, 2011; Lauret et al., 2009). This model could be validated on benchmark quality *in vitro* data, and then used to study *in vivo* neuroaxonal responses to brain injury loads. **Figure 11** presents

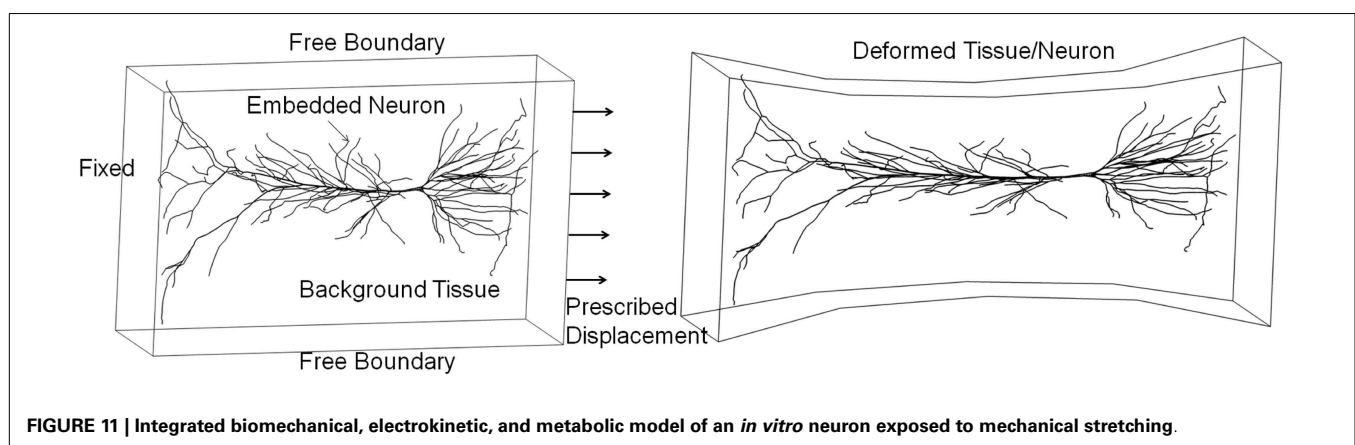
an example of a 3D neuron model “embedded” in a tissue culture exposed to mechanical stretch injury. In this test simulation, the FEM model of the tissue is coupled to a biomechanical-electrokinetic model of a neuron. The model simulates changes in the action potential propagation and metabolic support of axonal repolarization in response to mechanical damage to the neuroaxonal membrane.

## MODEL VALIDATION CHALLENGES AND OPPORTUNITIES

### MODEL VALIDATION AND TESTING APPROACH

The next generation TBI modeling framework will integrate several components, some already well established, e.g., CFD gas dynamics or FEM biomechanics, while others, such as tissue damage and the neurobiology of cellular injury, will have to be developed and validated. Among several challenges impeding the development of such a modeling framework are: incomplete understanding of injury mechanisms, limitations of existing computational tools in solving multiscale/multiphysics problems, and lack of benchmark quality test problems and experimental data for model validation.

In the last few years experimental data directly related to the blast wave head/brain biomechanics and injury have started to emerge and could be used for model validation. To replicate the free-field blast wave loading in laboratory conditions, test articles such as head phantoms, animals (rats, mice, pigs), or cells/tissues have been placed inside or in front of a shock tube (Bayly et al., 2008; Säljö et al., 2008, 2011; Alley et al., 2011; Chavko et al., 2011; Leonardi et al., 2011; Risling et al., 2011; Shoge et al., 2011; Varas et al., 2011; Risling and Davidsson, 2012; Zhu et al., 2013). Shock tubes have been designed to control the pressure-time profile and impulse that replicate desired blast wave parameters (Reneer et al., 2011; Ritzel et al., 2011; Varas et al., 2011). Compared to round shock tubes, newer designs with square cross section allow better visual access to the test article (Sundaramurthy et al., 2012). **Figure 12** shows a round shock tube with a conical exit section for testing a human head phantom with a helmet and hearing protection devices (Przekwas et al., 2012). A conical exit section not only allows more space for the test article, but also allows the formation of a spherical shock wave front resembling a free-field blast wave. It is also important to fully “expand” the wave to ensure a blast wave (Friedlander type) pressure profile.



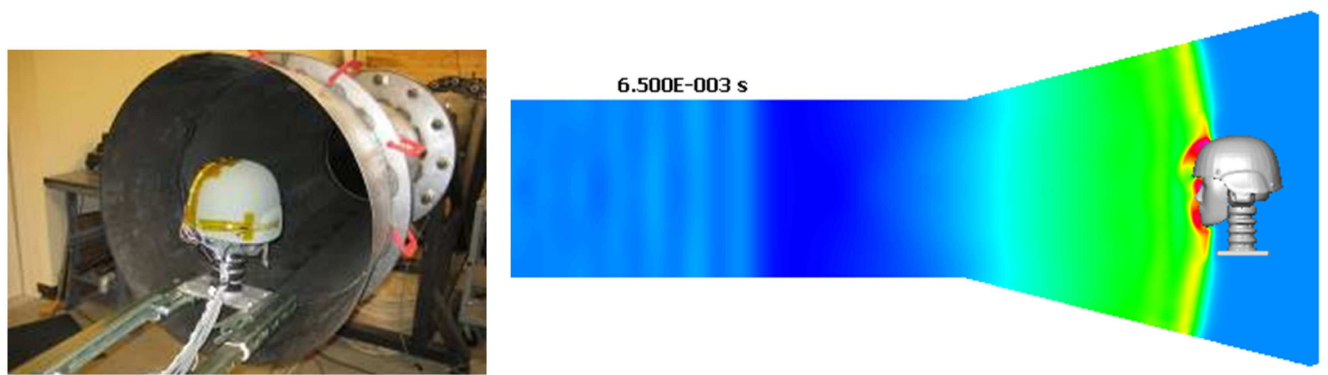


FIGURE 12 | A human head phantom in the shock tube for testing blast wave loading (Przekwas et al., 2011).

### Validation using head phantoms, cadavers, and humans

To validate the primary blast impact model it would be beneficial to establish benchmark anatomic/geometrical and material property models of selected physical phantoms and human (cadaver) heads. Several teams have used the HYBRID III head/neck phantoms as well as custom human head phantoms to evaluate its mechanical responses to shock tube loads (Bir et al., 2011; Leonardi et al., 2011; Qidwai et al., 2011; Varas et al., 2011; Goeller et al., 2012; Przekwas et al., 2012). Shock tube tests on a more anatomically accurate human head/neck phantom with soft skin-like features, cranial bone and brain tissue could become the basic validation test suite. The test procedures and experimental data should be fully documented to ensure proper setup of computational models, e.g., completeness of boundary conditions, locations of instrumentation sensors, etc. From the model development perspective, head phantoms offer several advantages including well-defined anatomical geometry, material properties, and sensor locations as well as reproducibility of tests and modularity of phantom setup, e.g., rigid vs. flexible neck. The benchmark data should include the free stream shock tube pressure traces (total and static) and skin pressures at several locations on the head and neck. If a brain surrogate is used, additional data should include ICPs at selected locations, preferably along three axes relative to the blast direction. Minimally intrusive time-accurate measurements of head and brain displacements at several locations could be used directly to compute strains, strain rates, tissue velocities and accelerations.

Experimental impact tests on human cadaver heads (Nahum et al., 1977; Hardy et al., 2001; Bir et al., 2011) have been used as benchmark data for the validation of FEM models. Cadaver tests are much more challenging since it is difficult to generate precise anatomical head and brain geometry of a specific specimen and to recreate physiological conditions, e.g., vascular perfusion, water-tight CSF space, etc. Compared to a live human, the surrogate models have serious limitations including inadequate anatomy and geometry, reproducibility, inadequate tissue properties, tissue decay in cadavers, and lack of physiology. In the last few years a new imaging technique, tagged MRI synchronized to periodic mechanical excitation has been developed for measuring mechanical deformations of human brain *in vivo* (Bayly et al., 2005; Atay et al., 2008; Sabet et al., 2008; Feng et al., 2010). It has been used

to measure time/space accurate deformations of a human brain in response to rotational and translational deformations as well as loud sound waves in live human volunteers. The spatiotemporal fields of brain deformations and derived strains and strain rates could be used for the validation of a human head/brain biomechanics for non-injurious loads.

### Validation on animal models

Direct experimental evaluation of *in vivo* brain injury is only possible using animal models (Cernak, 2005; Thompson et al., 2005), including rats (Dixon et al., 1987; Marmarou et al., 1994; Bayly et al., 2006; Chavko et al., 2007; Long et al., 2009; Bolander et al., 2011), mice (Carbonell et al., 1998; Cernak and Noble-Haesslein, 2010; Rubovitch et al., 2011), pigs (Smith et al., 1997; Säljö et al., 2008; Bauman et al., 2009), and primates (Lu et al., 2012). Experimental tests on animal models provide a correlation between known insult level to injury response measured by taking samples from the brain for histochemistry analysis or by behavioral tests. Traditionally, animal models of TBI were developed to reproduce impact or acceleration loads such as the controlled cortical impact (CCI), the fluid percussion injury (FPI), and head acceleration and rotational models (Cernak, 2005; Morrison et al., 2011). Because the CCI and LFP require craniotomy and cause focal injury, they are not suitable to study blast brain injury, which typically is a closed head, diffuse type injury. Similar to head models, to better represent the blast brain injury in the open field, several teams have exposed animals, including rats and pigs, to shock waves generated by various types of shock tubes (Chavko et al., 2007; Bauman et al., 2009; Long et al., 2009; Risling et al., 2011; Sundaramurthy et al., 2012). In spite of ongoing challenges with animal position, orientation, and immobilization in the shock tube a method of scaling the shock wave pressure profile to an equivalent human dose needs to be developed. Shock tube animal tests may be able to reproduce DAI representative of human mTBI, reveal the role of head/neck movement in blast brain injury, and provide valuable data for the development and validation of mathematical models of mTBI. Recent experimental tests of mice and primates directly exposed to open field explosives detonation may provide additional information for calibration of shock tube models (Rubovitch et al., 2011; Lu et al., 2012). The shock tube animal tests

provide the intracranial, arterial, venous, and abdominal pressure recordings that could be used for calibration of primary injury (energy deposition) models.

At present, the injury neurobiology data can be collected only from brain tissue necropsies at selected times from several anatomical locations in the brain. The next generation optical imaging with fluorescent labeling and microdialysis methods will enable collection of real time electrophysiology, biochemistry, and physiology injury data within the brain and the body. We believe that correlated experimental and computational animal models of TBI will be able to provide a link between the mechanical models and secondary injury/repair neurobiology models for which human only data will be too limited and too complex. Ultimately they may be able to establish scaling and extrapolation of injury and treatment protocols from animals to humans.

#### **Validation on *in vitro* cell/tissue cultures**

The use of animal models for studying brain injury may be restricted due to ethical and regulatory reasons. Furthermore, while the external mechanical loads in animal models can be well controlled, the internal cell/tissue biomechanics are difficult to monitor and quantify. The analysis of injury outcomes at the tissue/cell level requires animal sacrifices, tissue extraction, and may be affected by animal-to-animal variability. On the other hand, the *in vitro* cell cultures or brain tissue slices enable repeatable, controllable environments with direct access for optical, and electrophysiological measurements. The main requirement for *in vitro* neuro-injury models is that they should replicate the *in vivo* tissue biomechanics and post-injury sequelae. *In vitro* models of TBI have been used to study several aspects of neuronal pathobiology (Geddes and Cargill, 2001; Pfister et al., 2003; Lusardi et al., 2004; LaPlaca et al., 2005; Kumaria and Tolia, 2008; Chen et al., 2009; Lauret et al., 2009; Morrison et al., 2011), including metabolic and signaling events, neuroexcitation, hypoxia, and various targets for pharmacologic intervention (Kochanek, 2011). Conventional experimental *in vitro* models induce the neuronal injury by various methods such as direct deformation of the underlying elastomeric substrate, application of a rapid compression, fluid shear, mechanical transection, or direct micromechanical manipulators. Unfortunately, none of these completely represent the blast-induced biomechanical loads in a living brain, such as propagation of a steep fronted pressure wave which causes compression, tension, and shear waves. One way to achieve such conditions is to place the cell/tissue culture in a shock tube (Sawyer et al., 2011; Panzer et al., 2012b). One must be careful when performing *in vitro* shock tube tests that they are exposing the cell/tissue cultures to the loading that is witnessed inside the head and not in air. Compared to the *in vivo* brain, the *in vitro* neurotrauma models also have other limitations such as considerable variability in cellular morphology, lack of a vascular network, incomplete axonal myelination, low synaptic density, and use of much higher concentration of metabolites (Glc, O<sub>2</sub>) for culture maintenance. Nevertheless, at this time the *in vitro* models are probably the best platform to develop and validate mathematical models of secondary brain injury. To the best of our knowledge, with the exception of the primary biomechanics of the *in vitro* tissue, limited work has been documented on mathematical models of

*in vitro* neurotrauma (LaPlaca et al., 2005; Morrison et al., 2006; Kaster et al., 2011; Prevost et al., 2011). Development of mathematical models of *in vitro* cell/tissue neurotrauma combining primary and secondary injury and repair models should be a priority for future research.

#### **POTENTIAL APPLICATIONS AND FUTURE OPPORTUNITIES**

As in physics and engineering, mathematical modeling could play a major role in advancing our understanding of brain injury mechanisms, and help in neurodiagnostics, treatment, and protection. Development of a comprehensive mathematical model of brain injury, including blast TBI, is certainly feasible and necessary. Current state of the art models of blast waves and head/brain biomechanics provide an excellent foundation for the development of a primary brain injury model. More effort should focus on the development of mathematical models of secondary injury and repair mechanisms and on the link between the two. We also believe that a prototype of an integrated primary-secondary brain injury model can be developed within a few years, but it may require a concerted collaborative effort between biophysicists, neurobiologists, mathematicians, and experimentalists. Existing head anatomical/geometry models and validated CFD tools could be used to evaluate blast wave loading profiles on unprotected and helmeted human heads for various exposures. It would allow detailed analysis of loading pathways through anatomical regions including the eyes, ears, nose, and the role of protective armor (helmet, visors, hearing protection devices, and others). FEM models of primary biomechanics, validated on head phantoms and animal models, could provide a better understanding of how the blast load is transmitted to the brain, where the blast energy is deposited and how to design the protective armor to minimize the blast energy transmission to the brain. Predicted macroscopic tissue strains, strain rates and stresses may provide “initial conditions” for modeling microscopic tissue damage that could be correlated with injury thresholds from *in vitro* and animal experiments. The most challenging step is to link the models of the primary blast event with the resulting brain tissue damage including the secondary mechanobiology of injury and neuro-functional outcome. Such a modeling framework may become a foundation for a rational study of neuroprotection, diagnostics, and treatment. To achieve these goals future computational blast brain injury research should focus on the following aspects:

- High resolution computational models of a human and rat head/neck and articulated whole body models for blast wave and biomechanics simulations, specifically improved morphological resolution of brain structures such as CSF, sulci, gray/white matter, and vascular system
- Anatomic geometry and morphology of selected brain tissue structures such as cortical gray matter, dendritic/synaptic structures, and axonal network in corpus callosum, to support multiscale models of tissue micro-damage
- Benchmark quality, reproducible experimental models replicating blast injury mechanisms in animals, in *in vitro* cell/tissue cultures and human head physical phantoms to provide data for validation of blast biomechanics models

- Constitutive material models of high strain rate brain tissues for macro- and micro-biomechanics analysis of tissue damage and cavitation
- Improved numerical methods for modeling FSI events (e.g., brain-CSF interaction), cavitation, presence of vascular structures and enable long-time simulations
- Calibrated reduced order models for fast simulations of coupled primary injury biomechanics, cerebral hemodynamics, tissue perfusion, secondary injury, and repair mechanisms and structural and functional deficits
- Model based scaling of the injury and repair dynamics from *in vitro* to animals to humans
- Model-guided development of load- and tissue-specific brain injury criteria and thresholds and their effects on the neurological outcome
- Effective use of brain injury models to support diagnostics (e.g., biomarker kinetics), prescribed resting period and return to duty, development of drug targets, exploration of novel protection and treatment methods (e.g., hypothermia), and injury specific optimal pharmacology (pharmacokinetics, pharmacodynamics) and treatment (routes of administration, optimal time window, drug combinations, etc.)
- Support development of novel head (brain, ears, eyes) protective armor.

## DISCLAIMER

The views expressed in this paper are those of the authors and may not necessarily be endorsed by the U.S. Army or U.S. Department of Defense.

## REFERENCES

- Alastruey, J., Parker, K. H., Peiro, J., Byrd, S. M., and Sherwin, J. S. (2007). Modeling the circle of Willis to assess the effects of anatomical variations and occlusions on cerebral flows. *J. Biomech.* 40, 1794–1805. doi:10.1016/j.jbiomech.2006.07.008
- Albensi, B. C. (2001). Models of brain injury and alterations in synaptic plasticity. *J. Neurosci. Res.* 65, 279–283. doi:10.1002/jnr.1151
- Al-Bsharat, A. S., Hardy, W. N., Yang, K., Tashman, C., and King, A. I. (1999). “Brain/skull relative displacement magnitude due to blunt head impact: new experimental data and model,” in *43rd Stapp Car Crash Conference*, SAE Paper No. 99SC22 (Warrendale: Society of Automotive Engineers), 321–332.
- Alem, N. M. (1974). “Simulation of head injury due to combined rotation and translation of the brain,” in *Proceedings of the 18th Stapp Car Crash Conference* (Warrendale: Society of Automotive Engineers), 579–598.
- Alford, P. W., Dabiri, B. E., Goss, J. A., Hemphill, M. A., Brigham, M. D., and Parker, K. K. (2012). Blast-induced phenotypic switching in cerebral vasospasm. *Proc. Natl. Acad. Sci. U.S.A.* 108, 12705–12710. doi:10.1073/pnas.1105860108
- Alley, M. D., Schimzke, B. R., and Son, S. F. (2011). Experimental modeling of explosive blast-related traumatic brain injuries. *Neuroimage* 54, S45–S54. doi:10.1016/j.neuroimage.2010.05.030
- Anderson, J. D. (2004). *Modern Compressible Flow with Historical Perspective*. New York: McGraw-Hill.
- Areppally, S., Gorsich, D., Hope, K., Gentner, S., and Drotleff, K. (2008). “Application of mathematical modeling in potentially survivable blast threats in military vehicles,” in *26th Army Science Conference*, (Orlando, FL: Defense Technical Information Center).
- Armin, S. S., Colohan, A. R. T., and Zhang, J. H. (2008). Vasospasm in traumatic brain injury. *Acta Neurochir. Suppl.* 104, 421–425. doi:10.1007/978-3-211-75718-5\_88
- Armonda, R. A., Bell, R. S., Vo, A. H., Ling, G., DeGarba, T. J., Crandall, B., et al. (2006). Wartime traumatic cerebral vasospasm: recent review of combat casualties. *Neurosurgery* 59, 1215–1225. doi:10.1227/01.NEU.0000249190.46033.94
- Ascoli, G. (2006). Mobilizing the base of neuroscience data: the case of neuronal morphologies. *Nat. Rev. Neurosci.* 7, 319–322. doi:10.1038/nrn1885
- Atay, S. M., Kroenke, C. D., Sabet, A., and Bayly, P. V. (2008). Measurement of the dynamic shear modulus of mouse brain tissue *in vivo* by magnetic resonance elastography. *J. Biomech. Eng.* 130, 021013. doi:10.1115/1.2899575
- Aubert, A., Pellerin, L., Magistretti, P. J., and Costalat, R. (2007). A coherent neurobiological framework for functional neuroimaging provided by a model integrating compartmentalized energy metabolism. *Proc. Natl. Acad. Sci. U.S.A.* 104, 4188–4193. doi:10.1073/pnas.0605864104
- Bai, X., Yu, L., Liu, Q., Zhang, J., Li, A., Han, D., et al. (2006). A high-resolution anatomical rat atlas. *J. Anat.* 209, 707–708. doi:10.1111/j.1469-7580.2006.00645.x
- Banaji, M., Tachtsidis, I., Delpy, D., and Baigent, S. (2005). A physiological model of cerebral blood flow control. *Math. Biosci.* 194, 125–173. doi:10.1016/j.mbs.2004.10.005
- Barkhoudarian, G., Hovda, D. A., and Giza, C. C. (2011). The molecular pathophysiology of concussive brain injury. *Clin. Sports Med.* 30, 33–48. doi:10.1016/j.csm.2010.09.001
- Bass, C. R., Panzer, M. B., Rafaels, K. A., Wood, G. W., and Capehart, B. P. (2012). Brain injuries from blast. *Ann. Biomed. Eng.* 40, 185–202. doi:10.1007/s10439-011-0424-0
- Bauman, R. A., Ling, L., Tong, L., Januszkiewicz, A., Agoston, D., Delanerolle, N., et al. (2009). An introductory characterization of a combat-casualty-care relevant swine model of closed head injury resulting from exposure to explosive blast. *J. Neurotrauma* 26, 841–860. doi:10.1089/neu.2009-0898
- Bayly, P. V., Black, E. E., Pedersen, R. C., Leister, E. P., and Genin, G. M. (2006). *In vivo* imaging of rapid deformation and strain in an animal model of traumatic brain injury. *J. Biomech.* 39, 1086–1095. doi:10.1016/j.jbiomech.2005.02.014
- Bayly, P. V., Cohen, T. S., Leister, E. P., Ajo, D., Leuthardt, E. C., and Genin, G. M. (2005). Deformation of the human brain induced by mild acceleration. *J. Neurotrauma* 22, 845–856. doi:10.1089/neu.2005.22.845
- Bayly, P. V., Massouros, P. G., Christoforou, E., Sabet, A., and Genin, G. M. (2008). Magnetic resonance measurement of transient shear wave propagation in a viscoelastic gel cylinder. *J. Mech. Phys. Solids* 56, 2036–2049. doi:10.1016/j.jmps.2007.10.012
- Bhalla, U. S. (1998). “The network within: signalling pathways,” in *The Book of GENESIS: Exploring Realistic Neural Models with the GENeral Neural Simulation System*, 2nd Edn, eds J. M. Bower and D. Beeman (New York: Springer-Verlag), 169–191.
- Bhattacharjee, Y. (2008). Neuroscience. Shell shock revisited: solving the puzzle of blast trauma. *Science* 319, 406–408. doi:10.1126/science.319.5862.406
- Bir, C., Bolander, R., Leonardi, A., Ritzel, D., VandeVord, P., and Dingell, J. D. (2011). “A biomechanical perspective of blast injury neurotrauma,” in *Proc. HFM-207 NATO Symposium on a Survey of Blast Injury Across the Full Landscape of Military Science* (Halifax, NS).
- Bolander, R., Mathie, B., Bir, C., Ritze, D., and VandeVord, P. (2011). Skull flexure as a contributing factor in the mechanism of injury in the rat when exposed to a shock wave. *Ann. Biomed. Eng.* 39, 2550–2559. doi:10.1007/s10439-011-0343-0
- Brands, D., Peters, G. W. M., and Bovendeerd, P. H. M. (2004). Design and numerical implementation of a 3-D non-linear viscoelastic constitutive model for brain tissue during impact. *J. Biomech.* 37, 127–134. doi:10.1016/S0021-9290(03)00243-4
- Brown, S. A., Moraru, I. I., Schaff, J. C., and Loew, L. M. (2011). Virtual NEURON: a strategy for merged biochemical and electrophysiological modeling. *J. Comput. Neurosci.* 31, 385–400. doi:10.1007/s10827-011-0317-0
- Calvetti, D., and Somersalo, E. (2011). Dynamic activation model for a glutamatergic neuro-vascular unit. *J. Theor. Biol.* 274, 12–29. doi:10.1016/j.jtbi.2010.12.007
- Carbonell, W. S., Maris, D. O., McCall, T., and Grady, M. S. (1998). Adaptation of the fluid percussion injury model to the mouse. *J. Neurotrauma* 15, 217–229. doi:10.1089/neu.1998.15.217
- Carey, M. E., Herz, M., Corner, B., McEntire, J., Malabarba, D., Paquette, S., et al. (2006).



- Ballistic helmets and aspects of their design. *Neurosurgery* 47, 678–689. doi:10.1097/00006123-200009000-00031
- Carnevale, N. T., and Hines, M. L. (2006). *The Neuron Book*. Cambridge: Cambridge University Press.
- Cernak, I. (2005). Animal models of head trauma. *NeuroRx* 2, 410–422. doi:10.1602/neurorx.2.3.410
- Cernak, I. (2010). The importance of systemic response in the pathobiology of blast-induced neurotrauma. *Front. Neurol.* 1:151. doi:10.3389/fneur.2010.00151
- Cernak, I., and Noble-Haesslein, L. J. (2010). Traumatic brain injury: an overview of pathobiology with emphasis on military populations. *J. Cereb. Blood Flow Metab.* 30, 255–266. doi:10.1038/jcbfm.2009.203
- Cernak, I., Wang, Z., Jiang, J., Bian, X., and Savic, J. (2001). Ultrastructural and functional characteristics of blast injury induced neurotrauma. *J. Trauma* 50, 695–706. doi:10.1097/00005373-200104000-00017
- Chafi, M. S., Karami, G., and Ziejewski, M. (2009). Numerical analysis of blast-induced wave propagation using FSI and ALE multi-material formulations. *Int. J. Impact Eng.* 36, 1269–1275. doi:10.1016/j.ijimpeng.2009.03.007
- Chafi, M. S., Karami, G., and Ziejewski, M. (2010). Biomechanical assessment of brain dynamic responses due to blast pressure waves. *Ann. Biomed. Eng.* 38, 490–504. doi:10.1007/s10439-009-9813-z
- Champion, H. R., Holcomb, J. B., and Young, L. A. (2009). Injuries from explosions: physics, biophysics, pathology, and required research focus. *J. Trauma* 66, 1468–1477. doi:10.1097/TA.0b013e3181a27e7f
- Chavko, M., Koller, W. A., Prusaczyk, W. K., and McCarron, R. M. (2007). Measurement of blast wave by a miniature fiber optic pressure transducer in the rat brain. *J. Neurosci. Methods* 159, 277–281. doi:10.1016/j.jneumeth.2006.07.018
- Chavko, M., Watanabe, T., Adeeb, S., Lankasky, J., Ahlers, S., and McCarron, R. (2011). “Transfer of the pressure wave through the body and its impact on the brain,” in *Proc. HFM-207 NATO Symposium on a Survey of Blast Injury Across the Full Landscape of Military Science* (Halifax, NS).
- Chen, Y. C., Smith, D. H., and Meaney, D. F. (2009). In-vitro approaches for studying blast-induced traumatic brain injury. *J. Neurotrauma* 26, 861–876. doi:10.1089/neu.2008.0645
- Chodobski, A., Zink, B. J., and Szmydynger-Chodobska, J. (2011). Blood-brain barrier pathophysiology in traumatic brain injury. *Transl. Stroke Res.* 2, 492–516. doi:10.1007/s12975-011-0125-x
- Clayton, E. H., Garbow, J. R., and Bayly, P. V. (2011). Frequency-dependent viscoelastic parameters of mouse brain tissue estimated by MR elastography. *Phys. Med. Biol.* 56, 2391–2406. doi:10.1088/0031-9155/56/8/005
- Cloots, R. J. H., van Dommelen, J. A. W., Kleiven, S., and Geers, M. G. D. (2010). “Traumatic brain injury at multiple length scales: relating diffuse axonal injury to discrete axonal impairment,” in *IRCOBI Conference* (Hanover).
- Cloutier, M., Bolger, F. B., Lowry, J. P., and Wellstead, P. (2009). An integrative dynamic model of brain energy metabolism using in vivo neurochemical measurements. *J. Comput. Neurosci.* 27, 391–414. doi:10.1007/s10827-009-0152-8
- Colgan, N. C., Gilchrist, M. D., and Curran, K. M. (2010). Applying DTI white matter orientations to finite element head models to examine diffuse TBI under high rotational accelerations. *Prog. Biophys. Mol. Biol.* 103, 304–309. doi:10.1016/j.pbiomolbio.2010.09.008
- Cooley, J. W., and Dodge, F. A. Jr. (1966). Digital computer solutions for excitation and propagation of the nerve impulse. *Biophys. J.* 6, 583–599. doi:10.1016/S0006-3495(66)86679-1
- Courtney, A. C., and Courtney, M. W. (2009). A thoracic mechanism of mild traumatic brain injury due to blast pressure waves. *Med. Hypotheses* 72, 76–83. doi:10.1016/j.mehy.2008.08.015
- Cullis, I. G. (2002). Blast waves and how they interact with structures. *J. R. Army. Med. Corps.* 147, 16–26. doi:10.1136/jramc-147-01-02
- Curley, K. C., Leggieri, M., Jaffee, M. S., and Moore, D. F. (2011). Opening editorial, international state of the science meeting on non-impact blast-induced mild traumatic brain injury. *Neuroimage* 54, S14–S20.
- DeKosky, S. T., Ikonovic, M. D., and Gandy, S. (2010). Traumatic brain injury – football, warfare, and long-term effects. *N. Engl. J. Med.* 363, 1293–1296. doi:10.1056/NEJMp1007051
- DePalma, R., Burris, D. G., Champion, H. R., and Hodgson, M. J. (2005). Blast injuries. *N. Engl. J. Med.* 352, 1335–1342. doi:10.1056/NEJMr042083
- DePalma, R. G., Cross, G. M., Beck, L. B., and Chandler, D. W. (2011). “Epidemiology of mTBI (mild traumatic brain injury) due to blast: history, DOD/VA data bases: challenges and opportunities,” in *Proc NATO RTO-MP-HFM-207 Symposium on A Survey of Blast Injury across the Full Landscape of Military Science* (Halifax).
- De Schutter, E. (2008). Why are computational neuroscience and systems biology so separate? *PLoS Comput. Biol.* 4:e1000078. doi:10.1371/journal.pcbi.1000078
- De Schutter, E., and Bower, J. M. (1994). An active membrane model of the cerebellar Purkinje cell. I. Simulation of current clamps in slice. *J. Neurophysiol.* 71, 375–400.
- Descombes, S., and Dumont, T. (2008). Numerical simulation of a stroke: computational problems and methodology. *Prog. Biophys. Mol. Biol.* 97, 40–53. doi:10.1016/j.pbiomolbio.2007.10.003
- Di Bona, S., Lutzemberger, L., and Salvetti, O. (2003). Simulation model for analysing brain structure deformations. *Phys. Med. Biol.* 48, 4001–4022. doi:10.1088/0031-9155/48/24/002
- Dietrich, W. D., Alonso, O., and Halley, M. (1994). Early microvascular and neuronal consequences of traumatic brain injury: a light and electron microscopic study in rats. *J. Neurotrauma* 11, 289–301. doi:10.1089/neu.1994.11.289
- Ding, M. C., Wang, Q., Lo, E. H., and Stanley, G. B. (2011). Cortical excitation and inhibition following focal traumatic brain injury. *J. Neurosci.* 31, 14085–14094. doi:10.1523/JNEUROSCI.3572-11.2011
- Dixon, C. E., Lyeth, B. G., Povlishock, J. T., Findling, R. L., Hamm, R. J., Marmarou, A., et al. (1987). A fluid percussion model of experimental brain injury in the rat. *J. Neurosurg.* 67, 110–119. doi:10.3171/jns.1987.67.1.0110
- Dronne, M. A., Boissel, J. P., and Grenier, E. (2006). A mathematical model of ion movements in grey matter during a stroke. *J. Theor. Biol.* 240, 599–615. doi:10.1016/j.jtbi.2005.10.023
- Duckworth, J. L., Grimes, J., and Ling, G. S. F. (2012). Pathophysiology of battlefield associated traumatic brain injury. *Pathophysiology*, Available online 14 June 2012. doi:10.1016/j.pathophys.2012.03.001 [Epub ahead of print].
- Eberhard, J. P., Wanner, A., and Witum, G. (2006). NeuGen: a tool for the generation of realistic morphology of cortical neurons and neural networks in 3D. *Neurocomputing* 70, 327–342. doi:10.1016/j.neucom.2006.01.028
- Elder, G. A., and Cristian, A. (2009). Blast-related mild traumatic brain injury: mechanisms of injury and impact on clinical care. *Mt. Sinai J. Med.* 76, 111–118. doi:10.1002/msj.20098
- Elsayed, N. M., and Atkins, J. L. (2008). *Explosion and Blast-Related Injuries: Effects of Explosion and Blast from Military Operations and Acts of Terrorism*. Burlington: Elsevier Academic Press.
- Eucker, S., Smith, C., Ralston, J., Friess, S. H., and Margulies, S. S. (2011). Physiological and histopathological responses following closed rotational head injury depend on direction of head motion. *Exp. Neurol.* 227, 79–88. doi:10.1016/j.expneurol.2010.09.015
- Feng, Y., Abney, T. M., Okamoto, R. J., Pless, R. B., Genin, G. M., and Bayly, P. V. (2010). Relative brain displacement and deformation during constrained mild frontal head impact. *J. R. Soc. Interface* 7, 1677–1688. doi:10.1098/rsif.2010.0210
- Ferenc, M. T., Radovitzky, R., Bass, C. R., Wood, G. P., Panzer, M., Man, H. Y., et al. (2009). *Shockwaves Cause Synaptic Degeneration in Cultured Neurons*. Boston University MA Department of Biology Report for USAARO. Available at: <http://oai.dtic.mil/>
- Fernandez, P., and Pullarkat, P. A. (2010). The Role of the Cytoskeleton in Volume Regulation and Beading Transitions in PC12 Neurites. *Biophys. J.* 99, 3571–3579. doi:10.1016/j.bpj.2010.10.027
- Frieboes, L. R., and Gupta, R. (2009). An in-vitro traumatic model to evaluate the response of myelinated cultures to sustained hydrostatic compression injury. *J. Neurotrauma* 26, 2245–2256. doi:10.1089/neu.2009.0973
- Gao, X., Deng, P., Xu, Z. C., and Chen, J. (2011). Moderate traumatic brain injury causes acute dendritic and synaptic degeneration in the hippocampal dentate gyrus. *PLoS ONE* 6:e24566. doi:10.1371/journal.pone.0024566
- Gayzik, F. S., Moreno, D. P., Geer, C. P., Wuetzer, S. D., Martin, R. S., and Stitzel, J. D. (2011). Development of a full body CAD dataset for computational modeling: a multi-modality approach. *Ann. Biomed. Eng.* 39, 2568–2583. doi:10.1007/s10439-011-0359-5

- Geddes, D. M., and Cargill, R. S. (2001). An in vitro model of neural trauma: device characterization and calcium response to mechanical stretch. *J. Biomech. Eng.* 123, 247–255. doi:10.1115/1.1374201
- Gefen, A., and Margulies, S. S. (2004). Are in vivo and in situ brain tissues mechanically similar? *J. Biomech.* 37, 1339–1352. doi:10.1016/j.jbiomech.2003.12.032
- Gleeson, P., Steuber, V., and Silver, R. A. (2007). neuroConstruct: a tool for modeling networks of neurons in 3D space. *Neuron* 54, 219–235. doi:10.1016/j.neuron.2007.03.025
- Goeller, J., Wardlaw, A., Treichler, D., O'Bruba, J., and Weiss, G. (2012). Investigation of cavitation as a possible damage mechanism in blast-induced traumatic brain injury. *J. Neurotrauma* 29, 1970–1981. doi:10.1089/neu.2011.2224
- Graber, J. J., and Dhibi-Jalbut, S. (2009). Protective autoimmunity in the nervous system. *Pharmacol. Ther.* 121, 147–159.
- Graham, D. I., McIntosh, T. K., Maxwell, W. L., and Nicoll, J. A. (2000). Recent advances in neurotrauma. *J. Neuropathol. Exp. Neurol.* 59, 641–651.
- Gupta, R. K., and Przekwas, A. (2011). "Computational modeling of non-impact, blast induced mild traumatic brain injury," in *Proc. Symp. on Traumatic Brain Injuries in the Nervous System, KTH* (Stockholm).
- Halchenko, Y. O., and Hanke, M. (2012). Open is not enough. Let's take the next step: an integrated, community driven computing platform for neuroscience. *Front. Neuroinformatics* 6:22. doi:10.3389/fninf.2012.00022
- Hardy, W. N., Foster, C. D., Mason, M. J., Yang, K. H., King, A. I., and Tashman, S. (2001). Investigation of head injury mechanism using neutral density technology and high-speed biplanar X-ray. *Stapp Car Crash J.* 45, 337–368.
- He, H. Y., and Cline, H. T. (2011). Diadem X: automated 4 dimensional analysis of morphological data. *Neuroinformatics* 9, 107–112. doi:10.1007/s12021-011-9098-x
- Heltemes, K. J., Holbrook, T. L., MacGregor, A. J., and Galarneau, M. R. (2012). Blast-related mild traumatic brain injury is associated with a decline in self-rated health amongst US military personnel. *Injury* 43, 1990–1995. doi:10.1016/j.injury.2011.07.021
- Ho, J., and Kleiven, H. (2007). Dynamic response of the brain with vasculature: a three-dimensional computational study. *J. Biomech.* 40, 3006–3012. doi:10.1016/j.jbiomech.2007.02.011
- Hoge, C. W., McGurk, D., Thomas, J. L., Cox, A. L., Engel, C. C., and Castro, C. A. (2008). Mild traumatic brain injury in U.S. Soldiers returning from Iraq. *N. Engl. J. Med.* 358, 453–463. doi:10.1056/NEJMoa072972
- Horgan, T. J., and Gilchrist, M. D. (2008). The creation of three-dimensional finite element models for simulating head impact biomechanics. *Int. J. Crashworth.* 8, 1–14.
- Hrapko, M., Van Dommelen, J. A. W., Peters, G. W. M., and Wismans, J. (2008). The influence of test conditions on characterization of the mechanical properties of brain tissue. *J. Biomech. Eng.* 130, 31–38. doi:10.1115/1.2907746
- Hu, J., Jin, X., Lee, J. B., Zhang, L., Chaudhary, V., Guthikonda, M., et al. (2007). Intraoperative brain shift prediction using a 3D inhomogeneous patient-specific finite element model. *J. Neurosurg.* 106, 164–169. doi:10.3171/jns.2007.106.1.164
- Humphrey, J. D., Baek, S., and Niklas, L. E. (2007). Biochemomechanics of cerebral vasospasm and its resolution: I. A new hypothesis and theoretical framework. *Ann. Biomed. Eng.* 35, 1485–1497. doi:10.1007/s10439-007-9321-y
- Imielinska, C., Przekwas, A., and Tan, X. G. (2006). Multi-scale visual analysis of trauma injury. *Inf. Vis.* 5, 279–289. doi:10.1057/palgrave.ivs.9500137
- Johnson, V. E., Stewart, W., and Smith, D. H. (2012). Axonal pathology in traumatic brain injury. *Exp. Neurol.* doi:10.1016/j.expneurol.2012.01.013. [Epub ahead of print].
- Kager, H., Wadman, W. J., and Somjen, G. G. (2000). Simulated seizures and spreading depression in a neuron model incorporating interstitial space and ion concentrations. *J. Neurophysiol.* 84, 495–512.
- Kang, D. G., Lehman, R. A., and Carragee, E. J. (2012). Wartime spine injuries: understanding the improvised explosive device and biophysics of blast trauma. *Spine J.* 12, 849–857. doi:10.1016/j.spinee.2011.11.014
- Karami, G., Grundman, N., Abolfathi, N., Naik, A., and Ziejewski, M. (2009). A micromechanical hyperelastic modeling of brain white matter under large deformation. *J. Mech. Behav. Biomed. Mater.* 2, 243–254. doi:10.1016/j.jmbbm.2008.08.003
- Kaster, T., Sack, I., and Samani, A. (2011). Measurement of the hyperelastic properties of ex vivo brain tissue slices. *J. Biomech.* 44, 1158–1163. doi:10.1016/j.jbiomech.2011.01.019
- Khmelnitskii, A., Baiker, M., Kaijzel, E. L., Chen, J., Reiber, J. H. C., and Lelieveldt, B. P. F. (2011). Articulated whole-body atlases for small animal image analysis: construction and applications. *Mol. Imaging Biol.* 13, 898–910. doi:10.1007/s11307-010-0386-x
- Kilinc, D., Gallo, G., and Barbee, K. A. (2009). Mechanical membrane injury induces axonal beading through localized activation of calpain. *Exp. Neurol.* 219, 553–561. doi:10.1016/j.expneurol.2009.07.014
- King, A. I., Ruan, J. S., Zhou, C., Hardy, W. N., and Khalid, T. B. (1995). Recent advances in biomechanics of brain injury research. A review. *J. Neurotrauma* 12, 651–658. doi:10.1089/neu.1995.12.651
- King, A. I., Yang, K. H., Zhang, L., Hardy, W., and Viano, D. C. (2003). "Is head injury caused by linear or angular acceleration?" in *IRCOBI Conference* (Lisbon).
- Kleiven, S. (2007). Predictors for traumatic brain injuries evaluated through accident reconstructions. *Stapp Car Crash J.* 51, 81–114.
- Koch, C., and Segev, I. (1998). *Methods in Neuronal Modeling: From Ions to Networks*. Cambridge: MIT Press.
- Kochanek, P. (2011). "Operation brain trauma therapy (OBT) project overview – Pittsburgh perspective," in *ATACCC Conference* (Ft. Lauderdale, FL).
- Kochanek, P. M., Clark, R., Ruppel, R. A., Adelson, P. D., Bell, M. J., Whalen, M. J., et al. (2000). Biochemical, cellular, and molecular mechanisms in the evolution of secondary damage after severe traumatic brain injury in infants and children: lessons learned from the bedside. *Pediatr. Crit. Care Med* 1, 4–19. doi:10.1097/00130478-200007000-00003
- Kozloski, J., and Wagner, J. (2011). An ultrascale solution to large-scale neural tissue simulation. *Front. Neuroinformatics* 5:15. doi:10.3389/fninf.2011.00015
- Kumaria, A., and Tolia, C. M. (2008). In vitro models of neurotrauma. *Br. J. Neurosurg.* 22, 200–206. doi:10.1080/02688690701772413
- Kurosawa, Y., Kato, K., Saito, S., Kubo, M., Uzuka, T., Fujii, Y., et al. (2009). "Basic study of brain injury mechanism caused by cavitation," in *31st Annual Intern. Conf. of the IEEE EMBS* (Minneapolis, MN).
- Kurtcuoglu, V., Soellinger, M., Summers, P., Boomsma, K., Poulikakos, D., Boesiger, P., et al. (2007). Computational investigation of subject-specific cerebrospinal fluid flow in the third ventricle and aqueduct of Sylvius. *J. Biomech.* 40, 1235–1245. doi:10.1016/j.jbiomech.2006.05.031
- Lakin, W. D., Stevens, S. A., Tranmer, B. I., and Penar, P. L. (2003). A whole-body mathematical model for intracranial pressure dynamics. *J. Math. Biol.* 46, 347–383. doi:10.1007/s00285-002-0177-3
- LaPlaca, M. C., Cullen, D. K., McLoughlin, J. J., and Cargill, R. S. (2005). High rate shear strain of three-dimensional neural cell cultures: a new in vitro traumatic brain injury model. *J. Biomech.* 38, 1093–1105. doi:10.1016/j.jbiomech.2004.05.032
- LaPlaca, M. C., Cullen, D. C., McLoughlin, J. J., and Cargill II, R. S. (1995). High rate shear strain of three-dimensional neural cell cultures: a new in vitro traumatic brain injury model. *J. Biomech.* 38, 1093–1105. doi:10.1016/j.jbiomech.2004.05.032
- LaPlaca, M. C., and Prado, G. R. (2010). Neural mechanobiology and neural vulnerability to traumatic loading. *J. Biomech.* 43, 71–78. doi:10.1016/j.jbiomech.2009.09.011
- Lauret, C., Hrapko, M., van Dommelen, J. A. W., Peters, G. W. M., and Wismans, J. S. H. M. (2009). Optical characterization of acceleration-induced strain fields in inhomogeneous brain slices. *Med. Eng. Phys.* 31, 392–399. doi:10.1016/j.medengphy.2008.05.004
- Leergaard, T. B., Hilgetag, C. C., and Sporns, O. (2012). Mapping the connectome: multi-level analysis of brain connectivity. *Front. Neuroinformatics* 6:14. doi:10.3389/fninf.2012.00014
- Leggieri, M. J. (2009). "Blast-related traumatic brain injury research gap," in *Proceedings of the Biomedical Science and Engineering Conference* (Oak Ridge: IEEE).
- Leonardi, A. D. C., Bir, C. A., Ritzel, D. V., and VandeVord, P. J. (2011). Intracranial pressure increases during exposure to a shock wave. *J. Neurotrauma* 28, 85–94. doi:10.1089/neu.2010.1324
- Levchakov, A., Linder-Ganz, E., Raghu-pathi, R., Margulies, S. S., and Gefen, A. (2006). Computational studies of strain exposures in neonate and mature rat brains during closed head impact. *J. Neurotrauma* 23, 1570–1580. doi:10.1089/neu.2006.23.1570
- Liang, F., Fukasaku, K., Liu, H., and Takagi, S. (2011). A computational model study of the influence of the anatomy of the circle of Willis on cerebral hyperperfusion following

- carotid artery surgery. *Biomed. Eng.* 10, 84. doi:10.1186/1475-925X-10-84
- Ling, G., Bandak, F., Armonda, R., Grant, G., and Ecklund, J. (2009). Explosive blast neurotrauma. *J. Neurotrauma* 26, 815–825. doi:10.1089/neu.2007.0484
- Linninger, A. A., Xenos, M., Sweetman, B., Ponskhe, S., Guo, X., and Penn, R. (2009). A mathematical model of blood, cerebrospinal fluid and brain dynamics. *J. Math. Biol.* 59, 729–759. doi:10.1007/s00285-009-0250-2
- Long, J. B., Bentley, T. L., Wessner, K. A., Cerone, C., Sweeney, S., and Bauman, R. A. (2009). Blast overpressure in rats: recreating a battlefield injury in the laboratory. *J. Neurotrauma* 26, 827–840. doi:10.1089/neu.2008.0748
- Lopreore, C. L., Bartol, T. M., Coggan, J. S., Keller, D. X., Sosinsky, G. E., Ellisman, M. H., et al. (2008). Computational modeling of three-dimensional electrodiffusion in biological systems: application to the node of Ranvier. *Biophys. J.* 95, 2624–2635. doi:10.1529/biophysj.108.132167
- Lu, J., Ng, K. C., Ling, G., Wu, J., Poon, D. J. F., Kan, E. M., et al. (2012). Effect of blast exposure on the brain structure and cognition in *Macaca fascicularis*. *J. Neurotrauma* 29, 1434–1454. doi:10.1089/neu.2010.1591
- Lusardi, T. A., Rangan, J., Sun, D., Smith, D. H., and Meaney, D. F. (2004). A device to study the initiation and propagation of calcium transients in cultured neurons after mechanical stretch. *Ann. Biomed. Eng.* 32, 1546–1559. doi:10.1114/B:ABME.0000049038.75368.75
- Mac Donald, C. L., Johnson, A. M., Cooper, D., Nelson, E. C., Werner, N. J., Shimony, J. S., et al. (2011). Detection of blast-related traumatic brain injury in U.S. military personnel. *N. Engl. J. Med.* 364, 2091–2100. doi:10.1056/NEJMoa1008069
- Magistretti, P. J., and Pellerin, L. (1999). Cellular mechanisms of brain energy metabolism and their relevance to functional brain imaging. *Philos. Trans. R. Soc. Lond. B Biol. Sci.* 354, 1155–1163. doi:10.1098/rstb.1999.0471
- Mangia, S., Simpson, I. A., Vannucci, S. J., and Carruthers, A. (2009). The in vivo neuron-to-astrocyte lactate shuttle in human brain: evidence from modeling of measured lactate levels during visual stimulation. *J. Neurochem.* 109(Suppl. 1), 55–62. doi:10.1111/j.1471-4159.2009.06003.x
- Mao, H., Yang, K. H., King, A. I., and Yang, K. (2010). Computational neurotrauma – design, simulation, and analysis of controlled cortical impact model. *Biomech. Model. Mechanobiol.* 9, 763–772. doi:10.1007/s10237-010-0212-z
- Mao, H., Zhang, L., Yang, K. H., and King, A. I. (2006). Application of a finite element model of the brain to study traumatic brain injury mechanisms in the rat. *Stapp Car Crash J.* 50, 583–600.
- Margulies, S. (2000). The postconcussion syndrome after mild head trauma: is brain damage overdiagnosed? Part 1. *J. Clin. Neurosci.* 7, 400–408. doi:10.1054/jocn.1999.0681
- Marmarou, A., Foda, M. A., van den Brink, W., Campbell, J., Kita, H., and Demetriadou, K. (1994). A new model of diffuse brain injury in rats. Part I: *pathophysiology and biomechanics*. *J. Neurosurg.* 80, 291–300. doi:10.3171/jns.1994.80.2.0291
- Martone, M. E., Tran, J., Wong, W. W., Sargis, J., Fong, L., Larson, S., et al. (2008). The Cell Centered Database project: an update on building community resources for managing and sharing 3D imaging data. *J. Struct. Biol.* 161, 220–231. doi:10.1016/j.jsb.2007.10.003
- Masel, B. E., and DeWitt, D. S. (2010). Traumatic brain injury: a disease process, not an event. *J. Neurotrauma* 27, 1529–1540. doi:10.1089/neu.2010.1358
- May, P. R., Fuster, J. M., Haber, J., and Hirschman, A. (1979). Woodpecker drilling behaviour: an endorsement of the rotational theory of impact brain injury. *Arch. Neurol.* 36, 370–373. doi:10.1001/archneur.1979.00500420080011
- McAllister, A. K. (2007). Dynamic aspects of CNS synapse formation. *Annu. Rev. Neurosci.* 30, 425–450. doi:10.1146/annurev.neuro.29.051605.112830
- Meaney, D. F., and Smith, D. H. (2011). Biomechanics of concussion. *Clin. Sports Med.* 30, 19–31. doi:10.1016/j.csm.2010.08.009
- Meyer, F., Bourdet, N., Gunzel, K., and Willinger, R. (2013). Development and validation of a coupled head-neck FEM—application to whiplash injury criteria investigation. *Int. J. Crashworth.* 18, 40–63.
- Meythaler, J. M., Peduzzi, J. D., Eleftheriou, E., and Novack, T. A. (2001). Current concepts: diffuse axonal injury-associated traumatic brain injury. *Arch. Phys. Med. Rehabil.* 82, 1461–1471. doi:10.1053/apmr.2001.25137
- Miller, K. (2011). *Biomechanics of the Brain*. New York: Springer.
- Mohan, A., Pendyam, S., Kalivas, P. W., and Nair, S. S. (2011). Molecular diffusion model of neurotransmitter homeostasis around synapses supporting gradients. *Neural Comput.* 23, 984–1014. doi:10.1162/NECO\_a\_00101
- Monnerie, H., Tang-Schomer, M. D., Iwata, A., Smith, D. H., Kim, H. A., and Le Roux, P. D. (2010). Dendritic alterations after dynamic axonal stretch injury in vitro. *Exp. Neurol.* 224, 415–423. doi:10.1016/j.expneurol.2010.05.001
- Moore, D. F., Jérusalem, A., Nyein, M., Noels, L., Jaffee, M. S., and Radovitzky, R. A. (2009). Computational biology – modeling of primary blast effects on the central nervous system. *Neuroimage* 47, T10–T20. doi:10.1016/j.neuroimage.2009.02.019
- Morrison, B. III, Cater, H. L., Benham, C. D., and Sundstrom, L. E. (2006). An in vitro model of traumatic brain injury utilising two-dimensional stretch of organotypic hippocampal slice cultures. *J. Neurosci. Methods* 150, 192–201. doi:10.1016/j.jneumeth.2005.06.014
- Morrison, B. III, Elkin, B. S., Dolle, J. P., and Yarmush, M. L. (2011). In vitro models for traumatic brain injury. *Annu. Rev. Biomed. Eng.* 13, 91–126. doi:10.1146/annurev-bioeng-071910-124706
- Moss, W. C., King, M. J., and Blackman, E. G. (2009). Skull flexure from blast waves: a mechanism for brain injury with implications for helmet design. *Phys. Rev. Lett.* 103, 108702. doi:10.1103/PhysRevLett.103.108702
- Mott, D. R., Schwer, D. A., Young, T. R. Jr., Levine, J., Dionne, J. P., Makris, A., et al. (2008). Blast-Induced Pressure Fields Beneath A Military Helmet. San Antonio: American Physical Society. [Abstract on BAPS].
- Nahum, A. M., Smith, R., and Ward, C. C. (1977). “Intracranial pressure dynamics during head impact,” *Proc. 21st Stapp Car Crash Conference*. New Orleans, SAE Paper No. 770922.
- Nakagawa, A., Manley, G. T., Gean, A. D., Ohtani, K., Armonda, R., Tsukamoto, A., et al. (2011). Mechanisms of primary blast-induced traumatic brain injury: insights from shock-wave research. *J. Neurotrauma* 28, 1101–1119. doi:10.1089/neu.2010.1442
- NATO. (2007). *Test Methodology for Protection of Vehicle Occupants against Anti-Vehicular Landmine Effects*. NATO, RTO, Research and Technology Organization, TR-HFM-090. Neuilly-sur-Seine Cedex: RTO/NATO.
- Needham, C. E. (2010). *Blast Waves Shock Wave and High Pressure Phenomena*. Berlin: Springer.
- Needham, C. E., Rule, G., Weiss, G., Przekwas, A., Tan, X. G., Merkle, A., et al. (2011). “Challenges in measuring and modeling whole body blast effects,” in *Proc. HFM-207 NATO Symposium on a Survey of Blast Injury Across the Full Landscape of Military Science* (Halifax, NS).
- Nicholson, C. (2001). Diffusion and related transport mechanisms in brain tissue. *Rep. Prog. Phys.* 64, 815–884. doi:10.1088/0034-4885/64/7/202
- Nyein, M. K., Jason, A. M., Yua, L., Pita, C. M., Joannopoulos, J. D., Moore, D. F., et al. (2010). In silico investigation of intracranial blast mitigation with relevance to military traumatic brain injury. *Proc. Natl. Acad. Sci. U.S.A.* 107, 20703–20708. doi:10.1073/pnas.1014786107
- Okie, S. (2005). Traumatic brain injury in the war zone. *N. Engl. J. Med.* 352, 2043–2047. doi:10.1056/NEJMp058102
- Orlowski, P., Chappell, M., Park, C. S., Grau, V., and Payne, S. J. (2011). Modelling of pH dynamics in brain cells after stroke. *Interface Focus* 1, 408–416. doi:10.1098/rsfs.2010.0025
- Ortega, J. M. (2011). Non-lethal blast wave interactions with a human head. *Comput. Fluids* 52, 92–103.
- Østby, I., Øyehaug, L., Einevoll, G. T., Nagelhus, E. A., and Plahte, E. (2009). Astrocytic mechanisms explaining neural-activity-induced shrinkage of extraneuronal space. *PLoS Comput. Biol.* 5:e1000272. doi:10.1371/journal.pcbi.1000272
- Panzer, M. B., Myers, B. S., Capehart, B. P., and Bass, C. R. (2012a). Development of a finite element model for blast brain injury and the effects of CSF cavitation. *Ann. Biomed. Eng.* 40, 1530–1544. doi:10.1007/s10439-012-0519-2
- Panzer, M. B., Matthews, K. A., Yu, A. W., Morrison, B., Meaney, D. F., and Bass, C. R. (2012b). A multiscale approach to blast neurotrauma modeling: part I – development of novel test devices for in vivo and in vitro blast injury models. *Front. Neurol.* 3:46. doi:10.3389/fneur.2012.00046
- Payne, S. J., Selb, J., and Boas, D. A. (2009). Effects of autoregulation and CO<sub>2</sub> reactivity on cerebral oxygen transport. *Ann. Biomed. Eng.* 37, 2288–2298. doi:10.1007/s10439-009-9763-5

- Peskind, E. R., Petrie, E. C., Cross, D. J., Pagulayan, K., McCraw, K., Hart, K., et al. (2011). Cerebrocerebellar hypometabolism associated with repetitive blast exposure mild traumatic brain injury in 12 Iraq war Veterans with persistent post-concussive symptoms. *Neuroimage* 54, S76–S82. doi:10.1016/j.neuroimage.2010.04.008
- Pfister, B. J., Weihs, T. P., Betenbaugh, M., and Bao, G. (2003). An in vitro uniaxial stretch model for axonal injury. *Ann. Biomed. Eng.* 31, 589–598. doi:10.1114/1.1566445
- Prevost, T. P., Balakrishnan, A., Suresh, S., and Socrate, S. (2011). Biomechanics of brain tissue. *Acta Biomater.* 7, 83–95. doi:10.1016/j.actbio.2010.06.035
- Przekwas, A. (2008). “Multiscale computational modeling of blast injuries,” in *Explosion and Blast Injuries*, eds E. Elsayed and J. Atkins (Burlington: Elsevier).
- Przekwas, A., Harrand, V. J., Sedberry, K., and Walilko, T. (2012). “Safer Breacher operations derived from field study, shock tube tests, and computational simulations,” in *MHSRS 2012, Military Health System Research Symposium* (Ft Lauderdale, FL).
- Przekwas, A., Somayaji, M., and Chen, Z. J. (2009). “A mathematical model coupling neuroexcitation, astrocyte swelling and perfusion in mild TBI,” in *Int. State-of-the-Science Meeting on Non-Impact, Blast-Induced Mild Traumatic Brain Injury* (Herdon, VA).
- Przekwas, A., Tan, X. G., Harrand, V., Reeves, D., Chen, Z. J., Sedberry, K., et al. (2011). “Integrated experimental and computational framework for the development and validation of blast wave brain biomechanics and helmet protection,” in *Proc. HFM-207 NATO Symposium on a Survey of Blast Injury Across the Full Landscape of Military Science* (Halifax, NS).
- Pullarkat, P. A., Dommersnes, P., Fernández, P., Joanny, J. F., and Ott, A. (2006). Osmotically driven shape transformations in axons. *Phys. Rev. Lett.* 96, 048104. doi:10.1103/PhysRevLett.96.048104
- Qidwai, S. M., Leung, A. C., and Bagchi, A. (2011). “High-fidelity modeling of head under blast and calculation of deformation measures,” in *Proc ASME 2011 Int. Mech. Eng. Congress & Exposition* (Denver, CO).
- Qutub, A. A., and Hunt, C. A. (2005). Glucose transport to the brain: a systems model. *Brain Res. Rev.* 49, 595–617. doi:10.1016/j.brainresrev.2005.03.002
- Ramasamy, A., Hill, A. M., and Clasper, J. C. (2009). Improvised explosive devices: pathophysiology, injury profiles and current medical management. *J. R. Army Med. Corps* 155, 265–272. doi:10.1136/jramc-155-04-05
- Ramirez, G. (2010). *Development of an Animal Brain FE model*. M.Sc. Thesis, Chalmers Univ. of Tech., Göteborg.
- Raul, J. S., Deck, C., Willinger, R., and Ludes, B. (2008). Finite-element models of the human head and their applications in forensic practice. *Int. J. Legal Med.* 122, 359–366. doi:10.1007/s00414-008-0248-0
- Readnower, R. D., Chavko, M., Adeeb, S., Conroy, M. D., Pauly, J. R., McCarron, R. M., et al. (2010). Increase in blood–brain barrier permeability, oxidative stress, and activated microglia in a rat model of blast-induced traumatic brain injury. *J. Neurosci. Res.* 88, 3530–3539. doi:10.1002/jnr.22510
- Reneer, D. V., Hisel, R. D., Hoffman, J. M., Kryscio, R. J., Lusk, B. T., and Geddes, J. W. (2011). A multi-mode shock tube for investigation of blast-induced traumatic brain injury. *J. Neurotrauma* 28, 95–104. doi:10.1089/neu.2010.1513
- Reymond, P. (2011). *Pressure and Flow Wave Propagation in Patient-Specific Models of the Arterial Tree*. Ph.D. Thesis, ETH, Lausanne.
- Risling, M., and Davidsson, J. (2012). Experimental animal models for studies on the mechanisms of blast-induced neurotrauma. *Front. Neurol.* 3:30. doi:10.3389/fneur.2012.00030
- Risling, M., Plantman, S., Angeria, M., Rostami, E., Bellaner, B. M., Kirkegaard, M., et al. (2011). Mechanisms of blast induced brain injuries, experimental studies in rats. *Neuroimage* 54, S89–S97. doi:10.1016/j.neuroimage.2010.05.031
- Ritzel, D. V., Parks, S. A., Roseveare, J., Rude, G., and Sawyer, T. W. (2011). “Experimental blast simulation for injury studies,” in *Proc. HFM-207 NATO Symposium on a Survey of Blast Injury Across the Full Landscape of Military Science* (Halifax, NS).
- Rowson, S., Duma, S. M., Beckwith, J. G., Chu, J. J., Greenwald, R. M., Crisco, J. J., et al. (2012). Rotational head kinematics in football impacts: an injury risk function for concussion. *Ann. Biomed. Eng.* 40, 1–13. doi:10.1007/s10439-011-0392-4
- Ruan, J. S., Khalil, T. B., and King, A. I. (1993). “Finite element modeling of direct head impact,” in *Proceedings of the 37th Stapp Car Crash Conference SAE Paper No. 933114* (Warrendale: Society of Automotive Engineers), 69–81.
- Rubovitch, V., Ten-Bosch, M., Zohar, O., and Harrison, C. R. (2011). A mouse model of blast-induced mild traumatic brain injury. *Exp. Neurol.* 232, 280–289. doi:10.1016/j.expneurol.2011.09.018
- Rzagalinski, B. A., Weber, J. T., Willoughby, K. A., and Ellis, E. F. (1998). Intracellular free calcium dynamics in stretch-injured astrocytes. *J. Neurochem.* 70, 2377–2385. doi:10.1046/j.1471-4159.1998.70062377.x
- Sabet, A. A., Christoforou, E., Zatlin, B., Genin, G. M., and Bayly, P. V. (2008). Deformation of the human brain induced by mild angular head acceleration. *J. Biomech.* 41, 307–315. doi:10.1016/j.jbiomech.2007.09.016
- Säljö, A., Arrhén, F., Bolouri, H., Mayorga, M., and Hamberger, A. (2008). Neuropathology and pressure in the pig brain resulting from low-impulse noise exposure. *J. Neurotrauma* 25, 1397–1406. doi:10.1089/neu.2008.0602
- Säljö, A., Mayorga, M., Bolouri, H., Svensson, B., and Hamberger, A. (2011). Mechanisms and pathophysiology of the low-level blast brain injury in animal models. *Neuroimage* 54(Suppl. 1), S83–S88. doi:10.1016/j.neuroimage.2010.05.050
- Savchenko, L. P., and Rusakov, D. A. (2007). The optimal height of the synaptic cleft. *Proc. Natl. Acad. Sci. U.S.A.* 104, 1823–1828. doi:10.1073/pnas.0606636104
- Sawyer, T. W., Nelson, P., Weiss, T., Villanueva, M., Tenn, C., Wang, Y., et al. (2011). “Development of a novel in vitro approach to assess blast-induced traumatic brain injury,” in *Proc. HFM-207 NATO Symposium on a Survey of Blast Injury Across the Full Landscape of Military Science* (Halifax, NS).
- Schmidt, O. I., Infanger, M., Heyde, C. E., Ertel, F., and Stahel, P. F. (2004). The role of neuroinflammation in traumatic brain injury. *Eur. J. Trauma* 3, 135–149.
- Segars, W. P., Tsui, B. M., Frey, E. C., Johnson, G. A., and Berr, S. S. (2004). Development of a 4-D digital mouse phantom for molecular imaging research. *Mol. Imaging Biol.* 6, 149–159. doi:10.1016/j.mibio.2004.03.002
- Shoge, R. O., Tong, L. C., Riccio, C. A., Atkins, J. L., VanAlburt, S. A., Edwards, A. A., et al. (2011). “Experimental evaluation of blast-induced traumatic brain injury in rats using a cylindrical shock tube,” in *ATACCC Conference*, Frederick.
- Slattenschek, A., and Tauffkirchen, W. (1970). “Critical evaluation of assessment methods for head impact applied in appraisal of brain injury hazard, in particular in head impact on windshield,” in *International Automobile Safety Conference Compendium*, (Warrendale: Society of Automotive Engineers) 1084–1112.
- Smith, D. H., Chen, X. H., Xu, B. N., McIntosh, T. K., Gennarelli, T. A., and Meaney, D. F. (1997). Characterization of diffuse axonal pathology and selective hippocampal damage following inertial brain trauma in the pig. *J. Neuropathol. Exp. Neurol.* 56, 822–834. doi:10.1097/00005072-199707000-00009
- Smith, D. H., and Meaney, D. F. (2000). Axonal damage in traumatic brain injury. *Neuroscientist* 6, 483–495. doi:10.1177/10738584000600611
- Spitzer, V. M., and Scherzinger, A. L. (2006). Virtual anatomy: an anatomist’s playground. *Clin. Anat.* 19, 192–203.
- Spitzer, V. M., and Whitlock, D. G. (1998). The visible human dataset: the anatomical platform for human simulation. *Anat. Rec.* 253, 49–57. doi:10.1002/(SICI)1097-0185(199804)253:2<49::AID-AR8>3.0.CO;2-9
- Stenfelt, S., and Goode, R. (2005). Transmission properties of bone conducted sound: measurements in cadaver heads. *J. Acoust. Soc. Am.* 118, 2373–2391. doi:10.1121/1.2005847
- Stevens, S. A., Stimpson, J., Lakin, W. D., Thakore, N. J., and Penar, P. L. (2008). A model for idiopathic intracranial hypertension and associated pathological ICP wave-forms. *IEEE Trans. Biomed. Eng.* 55, 388–398. doi:10.1109/TBME.2007.900552
- Stuhmiller, J. H. (2008). “Blast injury, translating research into operational medicine,” in *Military Quantitative Physiology: Problems and Concepts in Military Operational Medicine*, Chap. 10, eds W. R. Santee and K. E. Friedl (Fort Detrick: Borden Institute), 267–302.
- Stuhmiller, J. H., Masiello, P. J., Ho, K. H., Mayorga, M. A., Lawless, N., and Argyros, G. (1999). “Biomechanical modeling of injury from blast overpressure,” in *Proceedings of the Specialists’ Meeting of the RTO Human Factors and Medicine Panel, Wright-Patterson Air Force Base*, NATO

- Report RTO-MP-20 (Neuilly-Sur-Seine Cedex: NATO).
- Stys, P. K. (2005). General mechanisms of axonal damage and its prevention. *J. Neurol. Sci.* 233, 3–13. doi:10.1016/j.jns.2005.03.031
- Sundaramurthy, A., Alai, A., Ganpule, S., Holmberg, A., Plougonven, E., and Chandra, N. (2012). Blast-induced biomechanical loading of the rat: experimental and anatomically accurate computational blast injury model. *J. Neurotrauma* 29, 2352–2364. doi:10.1089/neu.2012.2413
- Takhounts, E. G., Eppinger, R. H., Campbell, J. Q., Tannous, R. E., Power, E. D., and Shook, L. S. (2003). On the development of the SIMon finite element head model. *Stapp Car Crash J.* 47, 107–133.
- Takhounts, E. G., Ridella, S. A., Hasija, V., Tannous, R. E., Campbell, J. Q., Malone, D., et al. (2008). Investigation of traumatic brain injuries using the next generation of simulated injury monitor (SIMon) finite element head model. *Stapp Car Crash J.* 52, 1–31.
- Tan, X. G., and Przekwas, A. (2011). A computational model for articulated human body dynamics. *Int. J. Hum. Factors Model. Simulat.* 2, 85–110.
- Tan, X. G., Przekwas, A., Kannan, R., Ott, K., Harrigan, T., Roberts, J., et al. (2012). “A comparative study of the human body model under blast loadings,” in *ASME Int. Mech. Eng. Congress and Exposition* (Houston).
- Tang, T., Chung, M. S., Liu, Q., and Shin, D. S. (2010). Advanced features of whole body sectioned images: virtual Chinese human, 2. *Clin. Anat.* 23, 523–529. doi:10.1002/ca.20975
- Tang-Schomer, M. D., Johnson, V. E., Baas, P. W., Stewart, W., and Smith, D. H. (2012). Partial interruption of axonal transport due to microtubule breakage accounts for the formation of periodic varicosities after traumatic axonal injury. *Exp. Neurol.* 233, 364–372. doi:10.1016/j.expneurol.2011.10.030
- Tanielian, T. L., and Jaycox, L. H. (2008). *Invisible Wounds of War: Psychological and Cognitive Injuries, Their Consequences, and Services to Assist Recovery*. RAND Report. Santa Monica: RAND Corporation.
- Taylor, G. I. (1950). “The formulation of blast wave by a very intense explosion,” in *Proc. of the Royal Society of London, Series A*, 159–186.
- Taylor, P. A., and Ford, C. C. (2009). Simulation of blast-induced early-time intracranial wave physics leading to traumatic brain injury. *J. Biomech. Eng.* 131, 1–11. doi:10.1115/1.3118765
- Thompson, H. J., Lifshitz, J., Marklund, N., Grady, M. S., Graham, D. I., Hovda, D. A., et al. (2005). Lateral fluid percussion brain injury: a 15-year review and evaluation. *J. Neurotrauma* 22, 42–75. doi:10.1089/neu.2005.22.42
- Tsutsui, S., and Stys, P. K. (2012). Metabolic injury to axons and myelin. *Exp. Neurol.* doi:10.1016/j.expneurol.2012.04.016. [Epub ahead of print].
- Ursino, M., Lodi, C. A., and Russo, G. (2000). Cerebral hemodynamic response to CO<sub>2</sub>-tests in patients with internal carotid artery occlusion: modeling study and in vivo validation. *J. Vasc. Res.* 37, 123–133. doi:10.1159/000025723
- van den Akker, R. (2010). *Influence of skull flexibility during closed head impact*, Ph.D. Thesis Chalmers University of Technology, Göteborg.
- Varas, J. M., Philippens, M., Meijer, S. R., van den Berg, A. C., Sibma, P. C., van Bree, J. L. M. J., et al. (2011). Physics of IED blast shock tube simulations form TBI research. *Front. Neurosci.* 2:A58. doi:10.3389/fneur.2011.00058
- Wakeland, W., and Goldstein, B. (2005). A computer model of intracranial pressure dynamics during traumatic brain injury that explicitly models fluid flows and volumes. *Acta Neurochir.* 95(Suppl.), 321–326. doi:10.1007/3-211-32318-X\_66
- Warden, D. L., French, L. M., Shupenko, L., Fargus, J., Riedy, G., Erickson, M. E., et al. (2009). Case report of a soldier with primary blast brain injury. *Neuroimage* 47, T152–T153. doi:10.1016/j.neuroimage.2009.01.060
- Wardlaw, A., and Goeller, J. (2010). “Cavitation as a possible traumatic brain injury (TBI) damage mechanism,” in *IFMBE Proceedings* 32, 26th Southern Biomedical Eng. Conf. eds. K. E. Herold, J. Vossoughi, and W. E. Bentley (Berlin: Springer), 34–37.
- Wieloch, T., and Nikolich, K. (2006). Mechanisms of neural plasticity following brain injury. *Curr. Opin. Neurobiol.* 16, 258–264. doi:10.1016/j.conb.2006.05.011
- Wilkerson, P., and Przekwas, A. (2007). “Integrated modeling framework for anthropometry and physiology virtual body,” in *Oral Presentation at SAE Digital Human Modeling Conf., SAE Paper, 07DHM-49*, Seattle, WA.
- Willinger, R., Kang, H. S., and Diaw, B. (1999). Three-dimensional human head finite-element model validation against two experimental impacts. *Ann. Biomed. Eng.* 27, 403–410. doi:10.1114/1.165
- Xi, X. F., and Zhong, P. (2001). Dynamic photoelastic study of the transient stress field in solids during shock wave lithotripsy. *J. Acoust. Soc. Am.* 109, 1226–1239. doi:10.1121/1.1349183
- Yasuki, T. (2011). “Development of total human model for safety version 4 capable of internal organ injury prediction,” in *Computational Biomechanics for Medicine, Soft Tissues and the Musculoskeletal System*, eds A. Wittek, M. F. Nielsen, and K. Müller (New York: Springer Verlag).
- Yi, C. S., Fogelson, A. L., Keener, J. P., and Peskin, C. S. (2003). A mathematical study of volume shifts and ionic concentration changes during ischemia and hypoxia. *J. Theor. Biol.* 220, 83–106. doi:10.1006/jtbi.2003.3154
- Yu, Z., and Morrison, B. (2010). Experimental mild traumatic brain injury induces functional alteration of the developing hippocampus. *J. Neurophysiol.* 103, 499–510. doi:10.1152/jn.00775.2009
- Zhang, L., Makwana, R., and Sharma, S. (2011). “Comparison of the head response in blast insult with and without combat helmet,” in *Proc. HFM-207 NATO Symp. on a Survey of Blast Injury Across the Full Landscape of Military Science* (Halifax, NS).
- Zhang, L., Yang, K. H., and King, A. I. (2001). Comparison of brain responses between frontal and lateral impacts by finite element modeling. *J. Neurotrauma* 18, 21–30. doi:10.1089/089771501750055749
- Zheng, Q., Durben, D. J., Wolf, G. H., and Angell, C. A. (1991). Liquids at large negative pressures: water at the homogeneous nucleation limit. *Science* 254, 829–832. doi:10.1126/science.254.5033.829
- Zhou, C., Khalil, T., and King, A. (1996). “Viscoelastic response of the human brain to sagittal and lateral rotational acceleration by finite element analysis,” in *Proc. of the 1996 International IRCOBI Conf. on the Biomechanics of Impacts*. Dublin, 35–48.
- Zhou, X., and Przekwas, A. (2011). A fast and robust whole-body control algorithm for running. *Int. J. Hum. Factors Model. Simul.* 2, 127–148.
- Zhu, F., Skelton, P., Chou, C. C., Mao, H., Yang, K. H., and King, A. I. (2013). Biomechanical responses of a pig head under blast loading: a computational simulation. *Int. J. Numer. Method Biomed. Eng.* 29, 392–407. doi:10.1002/cnm.2518
- Ziejewski, M., Karami, G., and Akhatorov, A. (2007). Selected biomechanical issues of brain injury caused by blasts. *Brain Inj. Prof.* 4, 10–15.
- Zou, H., Schmiedeler, J. P., and Hardy, W. N. (2007). Separating brain motion into rigid body displacement and deformation under low-severity impacts. *J. Biomech.* 40, 1183–1191. doi:10.1016/j.jbiomech.2006.06.018

**Conflict of Interest Statement:** The authors declare that the research was conducted in the absence of any commercial or financial relationships that could be construed as a potential conflict of interest.

Received: 23 December 2012; accepted: 09 May 2013; published online: 30 May 2013.

Citation: Gupta RK and Przekwas A (2013) Mathematical models of blast-induced TBI: current status, challenges, and prospects. *Front. Neurol.* 4:59. doi: 10.3389/fneur.2013.00059

This article was submitted to *Frontiers in Neurotrauma*, a specialty of *Frontiers in Neurology*.

Copyright © 2013 Gupta and Przekwas. This is an open-access article distributed under the terms of the Creative Commons Attribution License, which permits use, distribution and reproduction in other forums, provided the original authors and source are credited and subject to any copyright notices concerning any third-party graphics etc.



# Metabolic crisis in severely head-injured patients: is ischemia just the tip of the iceberg?

Emilie Carre<sup>1\*</sup>, Michael Ogier<sup>1</sup>, Henry Boret<sup>2</sup>, Ambroise Montcriol<sup>2</sup>, Lionel Bourdon<sup>1</sup> and Jean-Jacques Risso<sup>1</sup>

<sup>1</sup> Unit of Traumatology, Institut de Recherche Biomedicale des Armees, Bretigny, France

<sup>2</sup> Intensive Care Unit, Hopital d'Instruction des Armees Sainte-Anne, Toulon, France

## Edited by:

Guoqiang Xing, Lotus Biotech.com, USA

## Reviewed by:

Luke R. Johnson, Uniformed Services University of the Health Sciences, USA

Sonia Villapol, Uniformed Services University of the Health Science, USA

## \*Correspondence:

Emilie Carre, Unit of Traumatology, Institut de Recherche Biomedicale des Armees, B.P. 73, 91223 Bretigny-sur-Orge Cedex, France  
e-mail: emilie\_carre@hotmail.com

Ischemia and metabolic crisis are frequent post-traumatic secondary brain insults that negatively influence outcome. Clinicians commonly mix up these two types of insults, mainly because high lactate/pyruvate ratio (LPR) is the common marker for both ischemia and metabolic crisis. However, LPR elevations during ischemia and metabolic crisis reflect two different energetic imbalances: ischemia (Type 1 LPR elevations with low oxygenation) is characterized by a drastic deprivation of energetic substrates, whereas metabolic crisis (Type 2 LPR elevations with normal or high oxygenation) is associated with profound mitochondrial dysfunction but normal supply of energetic substrates. The discrimination between ischemia and metabolic crisis is crucial because conventional recommendations against ischemia may be detrimental for patients with metabolic crisis. Multimodal monitoring, including microdialysis and brain tissue oxygen monitoring, allows such discrimination, but these techniques are not easily accessible to all head-injured patients. Thus, a new “gold standard” and adapted medical education are required to optimize the management of patients with metabolic crisis.

**Keywords: metabolic crisis, ischemia, head injury, multimodal monitoring, intracerebral microdialysis**

Managing traumatic brain injury is like navigating the ocean. Dangers (secondary insults) are everywhere, but, usually, easy to prevent. In this ocean, just imagine cerebral energetic disturbances as an iceberg, where ischemia is the tip (**Figure 1**). All clinicians are aware of what ischemia is and how to prevent/manage ischemic events. However the real danger is the submerged part of the iceberg, the one we cannot even imagine. Metabolic crisis may represent that sneaky part of energetic post-traumatic disturbances: they are still not well understood, difficult to detect and to care.

## CONFUSING DEFINITION OF METABOLIC CRISIS IN THE LITERATURE

In Intensive Care Unit (ICU), cerebral post-traumatic metabolic disturbances have commonly been characterized by an increase of the lactate/pyruvate ratio (LPR) above 40, as measured by clinical intracerebral microdialysis. High LPR has originally been attributed to compromised cerebral perfusion and impaired oxygen delivery. However, high LPR may actually reflect several pathological events or compensatory mechanisms (1). After traumatic brain injury, three different types of metabolic disturbances, all characterized by a LPR > 40, have been reported: hyperglycolysis, ischemia, and a pattern described by Vespa and colleagues initially called “metabolic crisis without brain ischemia” (2). Vespa’s initial study showed a 25% incidence of high LPR, but only a 2.4% incidence of ischemia (measured with positron emission tomography), in 19 brain injury patients. In this study, most of the episodes of high LPR were correlated with non-ischemic reduction in cerebral oxygen metabolism. This metabolic

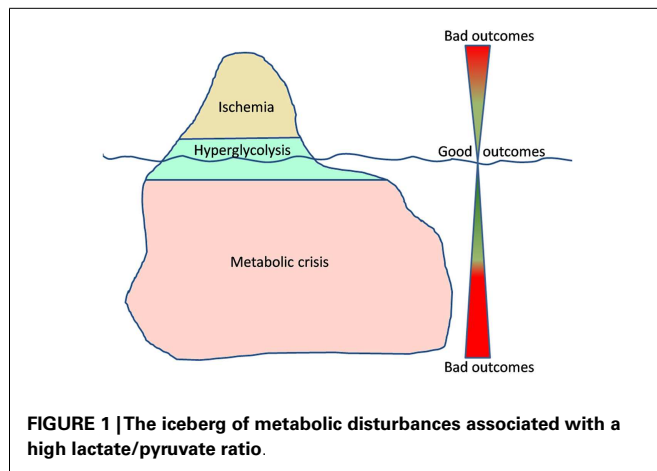
crisis may be the most frequent form of post-traumatic metabolic disturbance (2, 3). Indeed, 74% of head-injured patients may suffer from metabolic crisis in the first days after the initial trauma, despite successful resuscitation and tight control of their intracranial pressure (4). Prolonged state of metabolic crisis is associated with poor outcome at 6 months post-trauma as well as regional chronic brain atrophy (4–6). These metabolic crises have also been observed in patients with terminal herniation (7).

In the literature, confusion persists with articles dealing with metabolic crisis and that potentially refer to any type of metabolic disturbances (hyperglycolysis, ischemia, metabolic crisis . . .). The discrimination between different types of metabolic disturbances is, however, crucial because each type requires an adapted management to avoid deterioration of the patients. In addition, there is currently no consensual terminology for the specific pattern of metabolic disturbance characterized by elevated extracellular LPR and normal oxygenation. Indeed, the original work of Vespa and colleagues referred to this kind of disturbance as “metabolic crisis without brain ischemia” (2), whereas others called it “non-ischemic oxidative metabolic dysfunction” (6), “non-ischemic impairment of oxidative metabolism” (3), or “non-ischemic energy metabolic crisis” (8). Because different terminology could be misleading, we propose the unifying terminology: “metabolic crisis.”

## METABOLIC DISTURBANCES AFTER HEAD INJURY

To understand the singularities of each type of post-traumatic metabolic disturbance (hyperglycolysis, ischemia, and metabolic





crisis), some physiological aspects of the cerebral metabolism need to be considered.

### CEREBRAL METABOLISM IN PHYSIOLOGICAL CONDITIONS

Neurons and astrocytes can efficiently utilize lactate, pyruvate, glutamate, and glutamine as energetic substrates, in addition to glucose (9). Astrocytes play a pivotal role in providing these energetic substrates to neurons (Figure 2A). The astrocyte-neuron lactate shuttle model of Pellerin and Magistretti (10) suggests that neuronal activity is tightly coupled to glucose utilization/glycolysis. Glutamate is released from active synapses and uptaken by astrocytes. Glutamate uptake stimulates the activity of the Na/K-ATPase and subsequently the entry of glucose from the vasculature into astrocytes. A large portion of the glucose entering the astrocytes is then directed to the glycolytic pathway and is metabolized into lactate which is released in the extracellular space. Lactate is then transported to neurons and converted to pyruvate that can be used as an energetic substrate through the tricarboxylic acid (TCA) cycle (10). In addition, part of the neuronal pyruvate is transferred to astrocytes in order to close the redox loop (11). Under certain circumstances, astrocytic glycogen stores may also be metabolized into lactate, which is subsequently released in the extracellular space (12). Astrocytes also play an important role in providing glutamate back to neurons through the glutamate-glutamine cycle. Indeed, glutamate is converted into glutamine in astrocytes; then, glutamine is transported to neurons where it is finally converted into glutamate (10). Glutamate and glutamine can also be metabolized through diverse pathways in astrocytes and neurons, especially through the TCA cycle (9).

### COMPENSATORY HYPERGLYCOLYSIS

An increase in glucose utilization is commonly observed in head-injured patients in the first days after injury. Several roles have been proposed for this post-traumatic hyperglycolysis, including restoration of the ionic balance. This compensatory hyperglycolysis can induce a transient accumulation of lactate in the extracellular compartment of the brain in head-injured patients (2, 7). Under these conditions, lactate is likely to be used by neurons as an additional source of energy. This may explain why cerebral

accumulation of extracellular “good” lactate, in absence of hypoxia, has been associated with good long-term recovery in subarachnoid hemorrhage patients (13). Other mechanisms may participate, in addition to hyperglycolysis, to restore the ionic homeostasis, such as an increase in the glutamate-glutamine cycle turnover (14–16).

### METABOLIC DISTURBANCES DURING ISCHEMIA

It is commonly admitted that ischemia is one of the most deteriorating post-traumatic insults. Experimental studies of traumatic brain injury have shown that cerebral oxidative metabolism is reduced due to ischemia, because of oxygen and glucose deprivation (14, 16). In neurons, as a result of the lack of oxygen, pyruvate no longer enters the TCA cycle and the need for lactate may decrease (Figure 2B). On the other hand, pyruvate and glycogen are heavily metabolized into lactate in astrocytes (12). Therefore, lactate accumulates and pyruvate level decreases in the extracellular space, leading to an increase of the LPR. This pattern is known as “Type I” LPR elevation (8, 17) and has been associated with a poor outcome in head-injured patients (18). Type I LPR elevation can also be associated with high extracellular glutamate, as a consequence of the reversal of neuronal glutamate transporters (19).

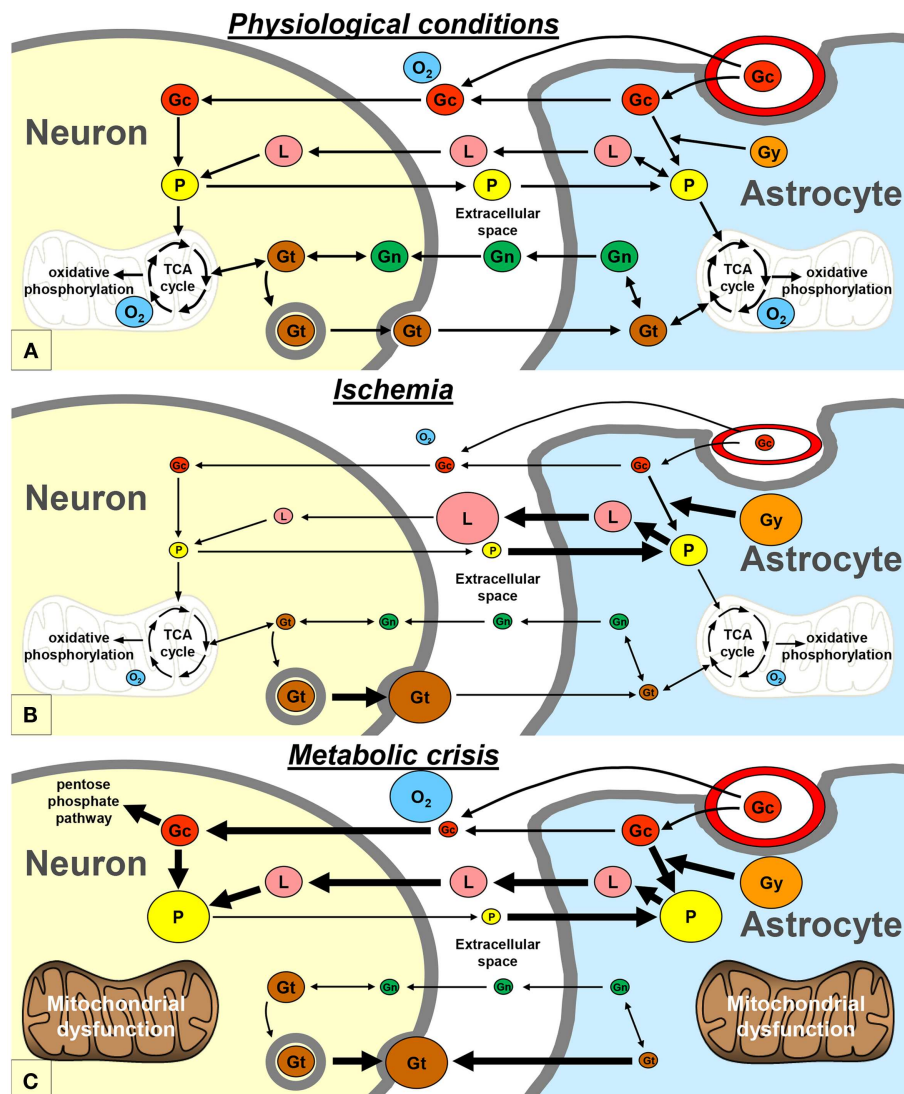
### METABOLIC CRISIS

Vespa’s article published in 2005 may be considered as the principles article introducing the concept of the metabolic crisis (2). Metabolic crisis is characterized by a “Type 2” LPR elevation, which is due to a reduction in extracellular pyruvate level, with normal or elevated tissue oxygen level (Figure 2C) (8, 17). Occurrences of high extracellular glutamate and low glucose have also been reported during metabolic crisis (4, 7). This pattern may appear very similar to that of ischemia; however, the underlying mechanisms are profoundly different (see below).

### SUSPECTED MECHANISMS OF METABOLIC CRISIS

There is a gap of knowledge regarding the exact mechanisms underlying metabolic crisis. Nevertheless, two main hypotheses have been proposed: mitochondrial dysfunction and excessive increase in metabolic demand.

As early as 1942, Lindquist proposed the hypothesis that “some more fundamental factor of disturbed physiology was responsible for the syndrome of head injury, and [...] that the injured nerve cells might be unable to utilize oxygen normally in spite of an adequate oxygen supply” (20). More recently, clinical studies have demonstrated that some head-injured patient have disturbances in oxidative metabolism due to mitochondrial dysfunction, despite good oxygen supply (21, 22), suggesting that mitochondrial dysfunction may be one of the mechanisms underlying metabolic crisis. In experimental settings, however, mitochondrial dysfunction, induced by cyanide poisoning, is associated with an increase in LPR and brain tissue oxygen ( $P_{tiO_2}$ ), but not with a decrease in extracellular pyruvate level (23, 24). Therefore, mitochondrial dysfunction *per se* may be a mechanism involved in metabolic crisis but it is not responsible for the decrease in extracellular pyruvate level. Instead, the low interstitial pyruvate measured during metabolic crisis may be the consequence



**FIGURE 2 | Schematic representation of the proposed exchange of energetic metabolites between neurons and astrocytes, in physiological conditions (A), during ischemia (B), and during metabolic crisis (C).** Gc, glucose; Gy, glycogen; Gn, glutamine; Gt, glutamate; L, lactate; O<sub>2</sub>, oxygen; P, pyruvate; TCA, tricarboxylic acid.

of a shunting of the glycolytic pathway in favor of the pentose phosphate pathway, which plays a protective role in neutralizing oxygen free radicals. This shunting may limit oxidative mitochondrial damage (25). In addition, neuronal pyruvate may not be transferred to astrocytes anymore and might serve as an endogenous free radical scavenger to stabilize neuronal mitochondrial function (26).

Excessive increase in metabolic demand is the other proposed mechanism leading to metabolic crisis. Indeed, post-traumatic seizures and cortical spreading depression both result in excessive increases in metabolic demand (2, 27). Under these circumstances, neuronal and astrocytic hyperglycolysis may not be sufficient to compensate for the deficits in oxidative metabolism. In addition, when astrocytic glycogen stores are depleted, the resulting energetic failure can alter the activity of the Na/K-ATPase and

lead to intracellular accumulation of Na<sup>+</sup>, consecutive astrocytic swelling and subsequent mitochondrial swelling, which may further alter mitochondrial function (28, 29). In response to swelling, astrocytic volume-regulated anion channels can open and allow the efflux of glutamate and other amino acids, as part of an osmoregulation process (30). A reversal of astrocytic glutamate transporters can also be observed (19). The resulting catastrophic surge of extracellular glutamate can lead to excitotoxic NMDA-receptor activation and mitochondrial calcium overload, which result in drastic mitochondrial depolarization and cellular death by apoptosis and/or necrosis (31). Furthermore, as a consequence of intracellular glutamate depletion in astrocytes, the glutamate-glutamine cycle turnover decreases (15), and glutamate and glutamine can no longer be used as energetic substrates.



It is difficult to determine which of mitochondrial dysfunction and excessive energetic demand, if any, is the initial trigger of metabolic crisis but we may assume that mitochondrial impairment enhances excessive energetic demand and that energy failure alters mitochondrial function. Here could be the vicious circle of metabolic crisis.

## DIAGNOSIS AND TREATMENT OF METABOLIC CRISIS

The occurrence of metabolic crisis is associated with poor outcome after brain injury (4, 7, 32). It is therefore important to identify patients with metabolic crisis to optimize their management.

According to us, one of the main problems in the management of head-injured patients is the lack of knowledge about metabolic crisis. Indeed, medical education about metabolic crisis is still very limited. The last Brain Trauma Foundation guidelines, in particular, do not mention metabolic crisis or any similar metabolic pattern (33). Neurointensivists are usually familiar with multimodal monitoring and have consequently at least some knowledge of metabolic crisis. On the other hand, in “general” ICUs, intensivists, and medical staff are well-trained to treat patients with multi-organ failure, but some specificities in the management of neurocritical care patients may sometimes be under-recognized (34). Have all intensivists in “general” ICUs already heard of metabolic crisis? We are not so sure. As only 33% of the US population are within 90 min of a Neurocritical Care Unit (35), the vast majority of head-injured patients may be treated in “general” ICUs, where metabolic crisis is unlikely to be suspected, largely because of unawareness. We believe that an effort should be made in providing medical education about metabolic crisis in all of the ICUs.

Up to now, no therapeutic treatment has shown effectiveness in improving the outcome of patients with metabolic crisis. Indeed, in clinical studies, aggressive maintenance of cerebral perfusion pressure, or decrease of the intracranial pressure (with mannitol, hyperventilation, . . .), have unfortunately failed to improve the oxidative metabolism or normalized the biomarkers of metabolic crisis (4, 36–39). In addition, the treatments used to target ischemia may even be particularly deleterious in patients with metabolic crisis. Hyperoxia, in particular, does not improve cerebral oxygen utilization and may generate free radicals that can exacerbate mitochondrial dysfunction in these patients (40). According to Verweij, “Restoring mitochondrial function might be as important as maintaining oxygen delivery” in patients with severe brain injury (21). Permeabilization of the mitochondrial membrane may therefore represent a particularly interesting target for therapeutic strategies against metabolic crisis (29). Consistent with this hypothesis, recent studies have demonstrated that treatment with Ro5-4864, an inhibitor of mitochondrial membrane permeabilization, decreases intracranial pressure and consequently improves cerebral perfusion in experimental brain injury. This neuroprotective effect has been correlated with normalization of the extracellular markers of metabolic crisis (41). On the other hand, clinical studies have demonstrated that tight glycemic control and intensive insulin therapy result in increased cerebral metabolic crises in patients

with head injury (42, 43). Thus, we may assume that an adapted energetic supply may limit metabolic crisis. This is the strategy chosen by Oddo in his ongoing clinical trials: “Lactate therapy after traumatic brain injury” (ClinicalTrials.gov Identifier: NCT01573507).

Protocol-driven management is currently used to treat most head injuries (44). This approach, which relies on evidence-based recommendations and particularly those collected from clinical trials, has led to improvements in the outcomes of head-injured patients (45). Nevertheless, one main concern regarding these clinical trials is that they are typically conducted on mixed categories of head-injured patients, regardless of their pathological state. As the underlying mechanisms for each type of post-traumatic metabolic disturbance are different, standard therapeutic interventions may not be equally efficient on patients that are (1) stabilized, (2) hyperglycolytic, (3) ischemic, or (4) experiencing metabolic crisis. Thus, there is a real need for clinical trials that would be conducted on homogenous populations of patients with a specific type of post-traumatic metabolic disturbance. As far as we know, no such specific clinical trial has ever been conducted, and especially not in patients with metabolic crisis. In addition to specific clinical trials, there would be clear benefits to shift to an approach targeting the individual needs of the patients (44). Indeed, individualized management may allow the adaptation of the treatment based on the metabolic state of the patient, at any time-point of the pathology. This kind of therapeutic strategy might be particularly helpful in the context of metabolic crisis.

The most important factor to consider in future clinical trials is the segregation of patients with metabolic crisis. To date, in everyday clinical practice, only multimodal monitoring, i.e., microdialysis and brain tissue oxygen ( $P_{ti}O_2$ ) monitoring, has allowed the detection of metabolic crisis. However, these techniques do not meet the requirements for determination of a gold standard: sensitivity and specificity. Indeed, (1) the microdialysis markers of metabolic crisis are not sufficiently specific, and (2)  $P_{ti}O_2$  primarily reflects a compromise between local CBF and oxygen delivery and therefore gives only very indirect information on cerebral oxygen metabolism (46). Moreover, multimodal monitoring generates a lot of data that requires specialized powerful software and adequate training in interpretation (17). So, because its implementation is expensive and time-consuming, not all ICUs are ready to use multimodal monitoring (47). Future research should establish a new gold standard for metabolic crisis that would be easy to deploy in all ICUs.

## CONCLUSION

Although metabolic crises are frequent and deleterious after traumatic brain injury, they have not been much studied so far. The challenge of the coming years will be to clearly define the specific mechanisms underlying metabolic crisis in order to improve its diagnosis and to optimize therapeutic treatment. Medical education about metabolic crisis will be a key factor for optimal management of head-injured patients with metabolic crisis.

## REFERENCES

- Larach DB, Kofke WA, Le Roux P. Potential non-hypoxic/ischemic causes of increased cerebral interstitial fluid lactate/pyruvate ratio: a review of available literature. *Neurocrit Care* (2011) 15:609–22. doi:10.1007/s12028-011-9517-8
- Vespa P, Bergneider M, Hattori N, Wu H-M, Huang S-C, Martin NA, et al. Metabolic crisis without brain ischemia is common after traumatic brain injury: a combined microdialysis and positron emission tomography study. *J Cereb Blood Flow Metab* (2005) 25:763–74. doi:10.1038/sj.jcbfm.9600073
- Soustiel JF, Svirgi GE. Monitoring of cerebral metabolism: non-ischemic impairment of oxidative metabolism following severe traumatic brain injury. *Neurol Res* (2007) 29:654–60. doi:10.1179/016164107X240017
- Stein NR, McArthur DL, Etchepare M, Vespa PM. Early cerebral metabolic crisis after TBI influences outcome despite adequate hemodynamic resuscitation. *Neurocrit Care* (2012) 17:49–57. doi:10.1007/s12028-012-9708-y
- Marcoux J, McArthur DA, Miller C, Glenn TC, Villablanca P, Martin NA, et al. Persistent metabolic crisis as measured by elevated cerebral microdialysis lactate-pyruvate ratio predicts chronic frontal lobe brain atrophy after traumatic brain injury. *Crit Care Med* (2008) 36:2871–7. doi:10.1097/CCM.0b013e3181864a40
- Xu Y, McArthur DL, Alger JR, Etchepare M, Hovda DA, Glenn TC, et al. Early nonischemic oxidative metabolic dysfunction leads to chronic brain atrophy in traumatic brain injury. *J Cereb Blood Flow Metab* (2010) 30:883–94. doi:10.1038/jcbfm.2009.263
- Vespa PM, McArthur D, O'Phelan K, Glenn T, Etchepare M, Kelly D, et al. Persistently low extracellular glucose correlates with poor outcome 6 months after human traumatic brain injury despite a lack of increased lactate: a microdialysis study. *J Cereb Blood Flow Metab* (2003) 23:865–77. doi:10.1097/01.WCB.0000076701.45782.EF
- Hillered L, Enblad P. Non-ischemic energy metabolic crisis in acute brain injury. *Crit Care Med* (2008) 36:2952–3. doi:10.1097/CCM.0b013e3181872178
- Belanger M, Allaman I, Magistretti PJ. Brain energy metabolism: focus on astrocyte-neuron metabolic cooperation. *Cell Metab* (2011) 14:724–38. doi:10.1016/j.cmet.2011.08.016
- Pellerin L, Magistretti PJ. Glutamate uptake into astrocytes stimulates aerobic glycolysis: a mechanism coupling neuronal activity to glucose utilization. *Proc Natl Acad Sci U S A* (1994) 91:10625–9. doi:10.1073/pnas.91.22.10625
- Cerdan S, Rodrigues TB, Sierra A, Benito M, Fonseca LL, Fonseca CP, et al. The redox switch/redox coupling hypothesis. *Neurochem Int* (2006) 48:523–30. doi:10.1016/j.neuint.2005.12.036
- Wender R, Brown AM, Fern R, Swanson RA, Farrell K, Ransom BR. Astrocytic glycogen influences axon function and survival during glucose deprivation in central white matter. *J Neurosci* (2000) 20:6804–10.
- Oddo M, Levine JM, Frangos S, Maloney-Wilensky E, Carrera E, Daniel RT, et al. Brain lactate metabolism in humans with subarachnoid hemorrhage. *Stroke* (2012) 43:1418–21. doi:10.1161/STROKEAHA.111.648568
- Bartnik BL, Sutton RL, Fukushima M, Harris NG, Hovda DA, Lee SM. Upregulation of pentose phosphate pathway and preservation of tricarboxylic acid cycle flux after experimental brain injury. *J Neurotrauma* (2005) 22:1052–65. doi:10.1089/neu.2005.22.1052
- Samuelsson C, Hillered L, Zetterling M, Enblad P, Hesselager G, Ryttefjors M, et al. Cerebral glutamine and glutamate levels in relation to compromised energy metabolism: a microdialysis study in subarachnoid hemorrhage patients. *J Cereb Blood Flow Metab* (2007) 27:1309–17. doi:10.1038/sj.jcbfm.9600433
- Bartnik-Olson BL, Oyoyo U, Hovda DA, Sutton RL. Astrocyte oxidative metabolism and metabolite trafficking after fluid percussion brain injury in adult rats. *J Neurotrauma* (2010) 27:2191–202. doi:10.1089/neu.2010.1508
- Hillered L, Persson L, Nilsson P, Ronne-Engstrom E, Enblad P. Continuous monitoring of cerebral metabolism in traumatic brain injury: a focus on cerebral microdialysis. *Curr Opin Crit Care* (2006) 12:112–8. doi:10.1097/01.ccx.0000216576.11439.df
- Goodman JC, Valadka AB, Gopinath SP, Uzura M, Robertson CS. Extracellular lactate and glucose alterations in the brain after head injury measured by microdialysis. *Crit Care Med* (1999) 27:1965–73. doi:10.1097/00003246-199909000-00041
- Grewer C, Gameiro A, Zhang Z, Tao Z, Braams S, Rauen T. Glutamate forward and reverse transport: from molecular mechanism to transporter-mediated release after ischemia. *IUBMB Life* (2008) 60:609–19. doi:10.1002/iub.98
- Lindquist JL, LeRoy GV. Studies of cerebral oxygen consumption following experimental head injury. *Surg Gynecol Obstet* (1942) 75:28–33.
- Verweij BH, Muizelaar JP, Vinas FC, Peterson PL, Xiong Y, Lee CP. Impaired cerebral mitochondrial function after traumatic brain injury in humans. *J Neurosurg* (2000) 93:815–20. doi:10.3171/jns.2000.93.5.0815
- Verweij BH, Amelink GJ, Muizelaar JP. Current concepts of cerebral oxygen transport and energy metabolism after severe traumatic brain injury. *Prog Brain Res* (2007) 161:111–24. doi:10.1016/S0079-6123(06)61008-X
- Clausen T, Zauner A, Levasseur JE, Rice AC, Bullock R. Induced mitochondrial failure in the feline brain: implications for understanding acute post-traumatic metabolic events. *Brain Res* (2001) 908:35–48. doi:10.1016/S0006-8993(01)02566-5
- Nielsen TH, Olsen NV, Toft P, Nordstrom CH. Cerebral energy metabolism during mitochondrial dysfunction induced by cyanide in piglets. *Acta Anaesthesiol Scand* (2013) 57:793–801. doi:10.1111/aas.12092
- Dusick JR, Glenn TC, Lee WN, Vespa PM, Kelly DF, Lee SM, et al. Increased pentose phosphate pathway flux after clinical traumatic brain injury: a [<sup>1</sup>,<sup>2</sup>-<sup>13</sup>C]glucose labeling study in humans. *J Cereb Blood Flow Metab* (2007) 27:1593–602. doi:10.1038/sj.jcbfm.9600458
- Wang X, Perez E, Liu R, Yan L-J, Mallet RT, Yang S-H. Pyruvate protects mitochondria from oxidative stress in human neuroblastoma SK-N-SH cells. *Brain Res* (2007) 1132:1–9. doi:10.1016/j.brainres.2006.11.032
- Vespa PM, Miller C, McArthur D, Eliseo M, Etchepare M, Hirt D, et al. Nonconvulsive electrographic seizures after traumatic brain injury result in a delayed, prolonged increase in intracranial pressure and metabolic crisis. *Crit Care Med* (2007) 35:2830–6. doi:10.1097/01.CCM.0000295667.66853.BC
- Unterberg AW, Stover J, Kress B, Kiening KL. Edema and brain trauma. *Neuroscience* (2004) 129:1019–27. doi:10.1016/j.neuroscience.2004.06.046
- Soustiel JF, Larisch S. Mitochondrial damage: a target for new therapeutic horizons. *Neurotherapeutics* (2010) 7:13–21. doi:10.1016/j.nurt.2009.11.001
- Rossi DJ, Brady JD, Mohr C. Astrocyte metabolism and signaling during brain ischemia. *Nat Neurosci* (2007) 10:1377–86. doi:10.1038/nn2004
- Hardingham GE, Bading H. The Yin and Yang of NMDA receptor signalling. *Trends Neurosci* (2003) 26:81–9. doi:10.1016/S0166-2236(02)00040-1
- Glenn TC, Kelly DF, Boscardin WJ, McArthur DL, Vespa P, Oertel M, et al. Energy dysfunction as a predictor of outcome after moderate or severe head injury: indices of oxygen, glucose, and lactate metabolism. *J Cereb Blood Flow Metab* (2003) 23:1239–50. doi:10.1097/01.WCB.0000089833.23606.7F
- The Brain Trauma Foundation, American Association of Neurological Surgeons, and Congress of Neurological Surgeons. Guidelines for the management of severe traumatic brain injury. *J Neurotrauma* (2007) 24:S1–106.
- Kramer AH, Zygun DA. Do neurocritical care units save lives? Measuring the impact of specialized ICUs. *Neurocrit Care* (2011) 14:329–33. doi:10.1007/s12028-011-9530-y
- Ward MJ, Shutter LA, Branas CC, Adeoye O, Albright KC, Carr BG. Geographic access to US Neurocritical Care Units registered with the Neurocritical Care Society. *Neurocrit Care* (2012) 16:232–40. doi:10.1007/s12028-011-9644-2
- Johnston AJ, Steiner LA, Coles JP, Chatfield DA, Fryer TD, Smielewski P, et al. Effect of cerebral perfusion pressure augmentation on regional oxygenation and metabolism after head injury. *Crit Care Med* (2005) 33:189–95; discussion 255–7. doi:10.1097/01.CCM.0000149837.09225.BD
- Soustiel JF, Mahamid E, Chistyakov A, Shik V, Benenson R, Zaaroor M. Comparison of moderate hyperventilation and mannitol for control of intracranial pressure control in patients with severe traumatic brain injury – a study of cerebral blood flow and metabolism. *Acta Neurochir (Wien)* (2006) 148:845–51; discussion 851. doi:10.1007/s00701-006-0792-7

38. Vespa PM, O'Phelan K, McArthur D, Miller C, Eliseo M, Hirt D, et al. Pericontusional brain tissue exhibits persistent elevation of lactate/pyruvate ratio independent of cerebral perfusion pressure. *Crit Care Med* (2007) **35**:1153–60. doi:10.1097/01.CCM.0000259466.66310.4F
  39. Bor-Seng-Shu E, De Lima Oliveira M, Teixeira MJ. Traumatic brain injury and metabolism. *J Neurosurg* (2010) **112**:1351–3. doi:10.3171/2009.10.JNS091426
  40. Diringner MN. Hyperoxia: good or bad for the injured brain? *Curr Opin Crit Care* (2008) **14**:167–71. doi:10.1097/MCC.0b013e3282f57552
  41. Soustiel JF, Vlodavsky E, Milman F, Gavish M, Zaaroor M. Improvement of cerebral metabolism mediated by Ro5-4864 is associated with relief of intracranial pressure and mitochondrial protective effect in experimental brain injury. *Pharm Res* (2011) **28**: 2945–53. doi:10.1007/s11095-011-0463-0
  42. Vespa P, Boonyaputthikul R, McArthur DL, Miller C, Etchepare M, Bergsneider M, et al. Intensive insulin therapy reduces microdialysis glucose values without altering glucose utilization or improving the lactate/pyruvate ratio after traumatic brain injury. *Crit Care Med* (2006) **34**: 850–6. doi:10.1097/01.CCM.0000201875.12245.6F
  43. Vespa P, McArthur DL, Stein N, Huang SC, Shao W, Filippou M, et al. Tight glycemic control increases metabolic distress in traumatic brain injury: a randomized controlled within-subjects trial. *Crit Care Med* (2012) **40**:1923–9. doi:10.1097/CCM.0b013e31824e0fcc
  44. Maas AI, Menon DK, Lingsma HF, Pineda JA, Sandel ME, Manley GT. Re-orientation of clinical research in traumatic brain injury: report of an international workshop on comparative effectiveness research. *J Neurotrauma* (2012) **29**:32–46. doi:10.1089/neu.2010.1599
  45. Fakhry SM, Trask AL, Waller MA, Watts DD. Management of brain-injured patients by an evidence-based medicine protocol improves outcomes and decreases hospital charges. *J Trauma* (2004) **56**:492–9; discussion 499–500. doi:10.1097/01.TA.0000115650.07193.66
  46. Rosenthal G, Hemphill JC III, Sorani M, Martin C, Morabito D, Obrist WD, et al. Brain tissue oxygen tension is more indicative of oxygen diffusion than oxygen delivery and metabolism in patients with traumatic brain injury. *Crit Care Med* (2008) **36**:1917–24. doi:10.1097/CCM.0b013e3181743d77
  47. Diedler J, Czosnyka M. Merits and pitfalls of multimodality brain monitoring. *Neurocrit Care* (2010) **12**:313–6. doi:10.1007/s12028-010-9350-5
- Conflict of Interest Statement:** The authors declare that the research was conducted in the absence of any commercial or financial relationships that could be construed as a potential conflict of interest.

Received: 26 April 2013; accepted: 16 September 2013; published online: 11 October 2013.

Citation: Carre E, Ogier M, Boret H, Montcriol A, Bourdon L and Risso J-J (2013) Metabolic crisis in severely head-injured patients: is ischemia just the tip of the iceberg? *Front. Neurol.* **4**:146. doi:10.3389/fneur.2013.00146

This article was submitted to Neurotrauma, a section of the journal *Frontiers in Neurology*.

Copyright © 2013 Carre, Ogier, Boret, Montcriol, Bourdon and Risso. This is an open-access article distributed under the terms of the Creative Commons Attribution License (CC BY). The use, distribution or reproduction in other forums is permitted, provided the original author(s) or licensor are credited and that the original publication in this journal is cited, in accordance with accepted academic practice. No use, distribution or reproduction is permitted which does not comply with these terms.



# Synaptic activity and bioenergy homeostasis: implications in brain trauma and neurodegenerative diseases

Natasha Khatri<sup>1,2</sup> and Heng-Ye Man<sup>1,2\*</sup>

<sup>1</sup> Department of Biology, Boston University, Boston, MA, USA

<sup>2</sup> Department of Pharmacology and Experimental Therapeutics, Boston University School of Medicine, Boston, MA, USA

## Edited by:

Guoqiang Xing, Lotus Biotech.com,  
Gaithersburg, USA

## Reviewed by:

Amade Bregy, University of Miami,  
USA

John Anagli, Banyan Biomarkers Inc.,  
USA

## \*Correspondence:

Heng-Ye Man, Department of Biology,  
Boston University, 5 Cummington  
Mall, Boston, MA 02215, USA  
e-mail: hman@bu.edu

Powered by glucose metabolism, the brain is the most energy-demanding organ in our body. Adequate ATP production and regulation of the metabolic processes are essential for the maintenance of synaptic transmission and neuronal function. Glutamatergic synaptic activity utilizes the largest portion of bioenergy for synaptic events including neurotransmitter synthesis, vesicle recycling, and most importantly, the postsynaptic activities leading to channel activation and rebalancing of ionic gradients. Bioenergy homeostasis is coupled with synaptic function via activities of the sodium pumps, glutamate transporters, glucose transport, and mitochondria translocation. Energy insufficiency is sensed by the AMP-activated protein kinase (AMPK), a master metabolic regulator that stimulates the catalytic process to enhance energy production. A decline in energy supply and a disruption in bioenergy homeostasis play a critical role in multiple neuropathological conditions including ischemia, stroke, and neurodegenerative diseases including Alzheimer's disease and traumatic brain injuries.

**Keywords: glucose metabolism, glutamatergic neurotransmission, AMPK, mitochondria, Alzheimer disease, traumatic brain injury, stroke**

## INTRODUCTION

The brain is the most energy-demanding organ in our body. It consumes 20% oxygen and 25% of total glucose supply, equivalent to approximately 20% of total ATP production (1–5). Given that the brain accounts for only 2% of our body weight, its energy consumption is impressive – 10 times that of other organs on average. The high cost in energy is not solely due to a large number of cells in the brain, with an estimated 100 billion neurons and many fold more glia, because organs with a comparable number of cells such as the liver have a much more modest energy bill (6). In contrast to peripheral tissues, neurons depend almost entirely on glucose for ATP production (1). Notably, the brain lacks cellular mechanisms to store energy or energy-generating sources such as glycogen or fat. Rather, energy must be produced continuously in order to maintain neuronal activity. Therefore, neurons are extremely sensitive to energy decline occurring during hypoxia, ischemia, stroke, and other forms of neurotrauma. Indeed, decreased glucose metabolism and mitochondrial energy production dysfunction have been associated with neurodegenerative diseases such as Alzheimer's, Parkinson's, and Huntington's disease. Alzheimer's and Huntington's patients exhibit reduced glucose energy metabolism even at early stages of disease, possibly caused by reduced glucose uptake through transporters, mitochondrial dysfunction, or changes in mitochondrial motility. Traumatic brain injuries are becoming increasingly concerning in populations due to recent wars and the discovery of Chronic Traumatic Encephalopathy (CTE) in athletes. These conditions also cause rapid declines in neuronal glucose levels and associated long-term damaging effects, such as increased intracellular calcium, production of free radicals, and depolarization of the

mitochondrial membrane. Recent studies have elucidated mechanisms in energy sensing and the role of synaptic events in energy metabolism and neuronal energy homeostasis, which shed light on our understanding of the pathogenesis of neurological diseases. In addition, proteins and pathways involved in neuronal energy metabolism are being investigated as therapeutic targets for neurodegenerative diseases and traumatic brain injuries.

## GLUTAMATERGIC EXCITATORY SYNAPTIC TRANSMISSION IS A PRIMARY ENERGY-CONSUMING EVENT

Although glia outnumber neurons, the latter account for 85% of energy consumption (1). Among many neuronal cellular events, action potential-mediated neuronal communication is believed to be a major process of energy consumption. However, in contrast to a long-held belief, recent studies have revealed that the propagation of action potentials is highly energy efficient (7), consuming only 11% of brain ATP (8). Instead, energy cost mainly comes from synaptic activity, including transmitter release, but primarily postsynaptic receptor activation (9). In the brain, most of the synaptic activity is mediated by glutamate, thus, the excitatory glutamatergic system represents the single largest energy consumer, consuming 50% of ATP in the brain (4, 8, 10, 11). In addition to glutamate receptor channel activity, other glutamate-related events including glutamate synthesis, vesicle filling, release, uptake, and recycling, as well as receptor trafficking and signaling, are also energy consuming.

At the presynaptic terminals, glutamate is enriched in synaptic vesicles (SVs), powered indirectly by a proton pump on the vesicle membrane, at a concentration of 100 mM. During synaptic



transmission, a single vesicle release can cause a rapid rise of glutamate in the synaptic cleft to concentrations as high as 1 mM (12). Under normal conditions, ambient glutamate in the extracellular environment is maintained by the constant activity of glutamate transporters at the plasma membrane of both neurons and glia (12, 13). Glial transporters often surround synapses to ensure an efficient uptake of released transmitter and prevent glutamate spillover.

There are three types of ligand-gated ionotropic glutamate receptors, including AMPA receptors (AMPA), NMDA receptors (NMDARs), and kainate receptors (KRs) (14–16). AMPARs are sodium channels that are the major components responsible for synaptic transmission, whereas NMDARs play an essential role in the formation of synaptic plasticity, mainly via regulation of AMPAR trafficking and synaptic localization. More importantly, the high permeability of NMDARs to calcium enables the receptor to initiate a series of calcium-dependent signaling cascades, including those for energy-dependent protein modification and metabolic regulations (17). Of note, although NMDARs show high permeability to calcium and are often mistakenly considered a calcium channel, more than 80% of NMDA currents are actually carried by sodium (18). Since NMDA synaptic currents have a long-lasting time course compared to that of AMPARs, NMDARs contribute a large amount of sodium influx during synaptic activities.

A large amount of energy consumption results from the maintenance of ionic gradients via the sodium pump. Neuronal activity and synaptic transmission cause rises in intracellular sodium. Compared with the intracellular sodium concentration of about 10 mM at resting conditions, an action potential can increase spine sodium concentrations to 35–40 mM, and tetanus stimulation for the induction of long-term potentiation (100 Hz stimulation for 1 s) leads to sodium levels as high as 100 mM in the spine (19). Inhibition of the sodium pump activity abolishes glutamate-induced ATP reduction (20), indicating the sodium pump as the major cellular machinery attributing to glutamate-related energy spending. Membrane depolarization by glutamate stimulation induces firing of action potentials, which also leads to sodium influx via voltage-gated sodium channels. However, consistent with the notion that action potentials are energy efficient, blockage of sodium channels by tetrodotoxin (TTX) does not affect glutamate-induced ATP reduction, indicating that glutamate receptors are the primary source of intracellular sodium.

### SENSING OF CELLULAR ENERGY BY AMPK SIGNALING

When ATP is hydrolyzed to release energy to enable cellular processes, a rise in the AMP:ATP ratio is sensed by the bioenergy detector AMP-activated protein kinase (AMPK). Once activated, AMPK utilizes its serine/threonine kinase activity to increase the rate of cellular catabolism (glucose utilization, fatty acid oxidation, etc.) while simultaneously inhibiting anabolic processes (cell biosynthesis), resulting in a net increase in ATP production. AMPK is a heterotrimeric protein composed of  $\alpha$ ,  $\beta$ , and  $\gamma$  subunits in equal stoichiometry. The  $\alpha$  subunit constitutes the catalytic domain, conferring kinase activity, while the  $\gamma$  subunit enables AMPK to monitor cellular energy status through two AMP/ATP binding domains, referred to as Bateman domains, that

bind AMP or ATP in a mutually exclusive manner (21–23). An increase in the concentrations of AMP, an indicator of energy insufficiency, will facilitate AMP binding to the AMPK Bateman domains, leading to a change in molecular structure, and exposure of an activation loop in the  $\alpha$  subunit. This conformational alteration allows AMPK to be phosphorylated at the  $\alpha$  subunit Threonine 172 residue by upstream kinases, causing a 50–100-fold increase in the catalytic activity of AMPK (24). Conversely, a high concentration of intracellular ATP promotes ATP/Bateman domain binding and produces an antagonistic effect on AMPK activation. Given that neurons have a high degree of metabolic activity and energy demand, it is expected that AMPK plays a critical role in maintaining energy homeostasis within the brain.

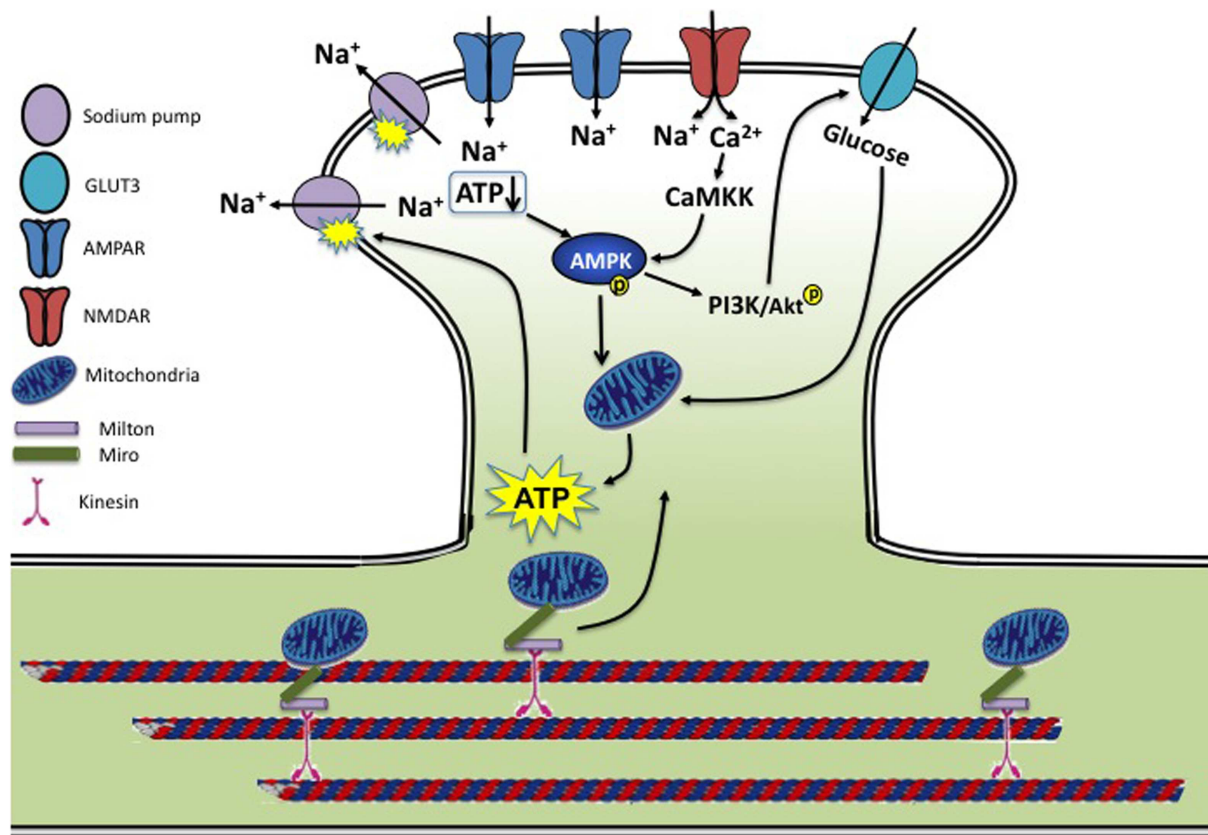
AMPK can be phosphorylated by two upstream kinases including liver kinase B1 (LKB1) and the calmodulin-dependent protein kinase kinases, CaMKK $\alpha$ , and CaMKK $\beta$  (25–28). LKB1 was originally found as the tumor suppressor mutated in the genetically inherited susceptibility to human cancer, coined Peutz–Jeghers Syndrome (PJS) (29). In peripheral tissues, LKB1 has been shown to be necessary for AMPK phosphorylation and activation (30, 31). Despite both LKB1 and AMPK being ubiquitously expressed in mammalian cells, there is evidence to suggest that AMPK may be acted upon by different AMPKKs in a tissue-specific manner. For instance, LKB1 has been demonstrated to be the major upstream activator of AMPK in muscle and liver cells (32, 33), however a study utilizing LKB1 knockouts found that LKB1 deficient neurons had similar levels of phosphorylated AMPK as compared to wild-type cells under normal physiological conditions (34). In neurons, AMPK is more likely to be regulated by calcium-dependent signaling. In rat brain slices, intracellular increases in Ca<sup>2+</sup> results in CaMKK-dependent AMPK phosphorylation. Importantly, membrane depolarization causes AMPK phosphorylation in the absence of an obvious change in cellular AMP:ATP ratio, indicating that AMPK can be regulated in a Ca<sup>2+</sup>-dependent, AMP-independent manner (35). Thus, glutamatergic synaptic activity can signal neurons for energy production via calcium-mediated AMPK activation.

### COUPLING OF SYNAPTIC ACTIVITY AND ENERGY HOMEOSTASIS

In the brain, glutamate is the major neurotransmitter mediating most synaptic transmission. Multiple molecular events occurring during synaptic activation, including sodium pump activity, receptor trafficking, cytoskeletal rearrangements, signaling, and metabolic processes make synaptic activity an energetically costly process (8). Thus, coordinated cellular processes are necessary to convey synaptic signals to bioenergy metabolic activities (Figure 1).

### CO-ORDINATION OF SODIUM PUMP AND GLUTAMATE RECEPTOR LOCALIZATION

The sodium gradient forms the foundation for synaptic transmission and neuronal excitation. Because of the frequent perturbation of ion homeostasis due to constant neuronal activity, the workload of the Na<sup>+</sup>/K<sup>+</sup> ATPase (NKA) is so high that it consumes nearly half of the ATP in the brain. NKA is a heterodimer composed of



**FIGURE 1 | Synaptic activity and energy homeostasis.** During synaptic transmission, activation of glutamate receptors allows influx of a large amount of sodium and calcium. Rises in intracellular sodium are rebalanced by the sodium pump powered by ATP consumption. Cellular energy status is sensed by AMPK via a reduced ATP/AMP ratio and CaMKK-dependent calcium signaling, leading to enhanced mitochondria activity and ATP biogenesis. AMPK activity also activates the PI3K/AKT pathway, leading to enhanced glucose uptake by stimulating glucose transporter membrane expression and transport efficiency. Mitochondria are trafficked on microtubules into metabolically demanding synapses by binding to

Milton/Miro-mediated kinesin motor complex. In conditions of neurotrauma and neurodegenerative diseases, several aspects of this regulation may be disrupted. During hypoxia, ischemia, and stroke, insufficient ATP levels cause dysfunction of the sodium pump, leading to a loss in membrane potential and neuronal function. AD brains show reduced levels of GLUT3, and both AD and HD brains have a reduced rate of neuronal glucose metabolism. Mouse models of AD and PD show mitochondrial dysfunction along with reduced mitochondrial motility, preventing proper mitochondria delivery to the synapse and leading to decreased energy metabolism. Brains of traumatic injuries show reduced ATP levels and suppressed mitochondrial function.

two subunits: the catalytic  $\alpha$  subunit that contains ATPase activity and the regulatory  $\beta$  subunit that is required for the enzymatic activity of NKA. At the single-neuron level, immunostainings have shown widespread localization of NKA in the soma and the dendrites (36, 37). During synaptic transmission, AMPAR-mediated currents are carried by sodium ions that flow into the cytosol of the neuron, typically within a microspace of the spine  $<1\ \mu\text{m}^3$ . In hippocampal neurons, one action potential can cause a several-fold increase in intraspinal sodium. The frequent and often large rises in intraspinal sodium must be exuded efficiently in order to maintain synapse electrophysiology, a task achieved via the activity of NKA. Therefore, there should exist cross-talk between AMPARs and the NKA to coordinate their functions. Indeed, we have shown that sodium pumps are enriched at the synapse and physically associate with AMPARs via interactions between the pump and receptor intracellular C-terminals. AMPAR surface localization and thus activity intensity are controlled to match the functional capacity of the pump. When sodium pump activity

is decreased, AMPARs undergo a translocation from the plasma membrane to intracellular compartments via endocytosis, which are then directed to the proteasome for degradation. Presumably, the adjustment in surface glutamate receptor number can help prevent drastic toxicity caused by sodium and calcium accumulation due to sodium pump insufficiency. It remains unclear whether and how changes in glutamate receptor activity lead to corresponding regulation of NKA. However, changes in sodium pump levels correlating with glutamate receptor density have been documented. In the macaque retina, TTX treatment for 4 weeks caused a significant reduction in NMDARs; this reduction was paralleled by a lower level of NKA, suggesting that glutamate activity regulates NKA levels (38).

#### SYNAPTIC ACTIVATION REGULATES GLUCOSE UPTAKE

Glucose is the sole source for ATP production in neurons (1). Therefore, it is of physiological significance to have synaptic activity coupled with glucose uptake. Both neurons and glia are

equipped with glucose utilization machinery, including glucose transporters and regulators, however higher glucose demands seem to be fulfilled with the assistance from glia. Glucose is first taken up by glia to be converted into lactate via glycolysis, which is then released and retaken by neurons where lactate is used for oxidative ATP genesis in mitochondria. Processes of astrocytes grow in the close proximity to neurons, often wrapping the synaptic cleft, as evidenced by a concentration of the astrocytic glucose transporter GLUT1 around synapses, where glutamate released during synaptic transmission is sensed by the glia and stimulate glial glucose uptake (39, 40).

In addition to the glia-coupled glucose delivery to neurons, synaptic activity can directly stimulate neuronal glucose uptake (41). However, exposure of neurons to glutamate results in a reduction in cellular ATP levels (20) and glucose uptake in neurons (42), indicating distinct signaling and cellular responses to synaptic vs. non-synaptic glutamate receptor activation.

AMPK is implicated in glutamate-induced glucose uptake. In neurons, AMPK signaling leads to activation of the PI3K/Akt pathway. We have shown that in cultured hippocampal neurons application of the AMPK activator AICAR causes a marked increase in phosphorylated Akt (43). This effect results directly from AMPK activation, as introduction of the AMPK antagonist successfully blocks AICAR-induced Akt phosphorylation. Furthermore, addition of a PI3K inhibitor also abolishes AICAR-induced Akt phosphorylation, indicating that the AMPK effect on Akt activation is mediated via PI3K (43). Interestingly, glutamate treatment activates AMPK, and pharmacological activation of AMPK leads to increased amounts of glucose transporters at the cell surface (44). We have recently found that in hippocampal neurons, AMPK activation causes higher levels of membrane GLUT3 and enhances glucose uptake (unpublished data). How AMPK activates PI3K remains unclear. Upon AICAR treatment, AMPK activation has been shown to phosphorylate IRS-1, the upstream component in the PI3K signaling pathway (45), suggesting IRS-1 as the intermediate factor linking AMPK to PI3K/Akt activation. Considering that glutamate-induced ATP reduction is a typical condition for AMPK activation (20, 46), the AMPK-PI3K-mediated enhancement in glucose uptake may function to prevent energy depletion and neuronal excitotoxicity. In addition, phosphorylated Akt may have a stimulatory effect on respiration by translocating to the mitochondria and increasing ATP synthase activity (47).

#### GLUTAMATE TRANSPORTER AND GLUTAMATE RECEPTOR ACTIVITY IN NEURONAL ENERGY CONSUMPTION

Glutamate is an extremely ample neurotransmitter, ranging to levels of 5–10 mmol/kg of brain tissue (48) and reaching millimolar concentrations within the synaptic cleft during synaptic transmission (49). However, glutamate levels are maintained in the micro- to nano-molar concentration in the extracellular milieu (50), many fold against its concentration gradient (12, 51–53). Unlike some neurotransmitters such as acetylcholine, which are efficiently removed by enzymatic digestion at the synaptic cleft, such disposal mechanism for glutamate does not exist. Instead, following release, glutamate is rapidly taken up by glia and neurons via membrane-distributed glutamate transporters (12, 54). By rapidly binding and transporting glutamate from the synaptic cleft, transporters

limit the amount of glutamate receptor-permitted calcium influx and the subsequent excitotoxicity, a principal process involved in neuronal damage and neurodegeneration (55–57).

To date, five excitatory amino acid transporters (EAAT1–5) have been identified in glia and neurons. The glial transporters EAAT1–2 are primarily localized to the plasma membrane of specialized domains in astrocytic processes (58, 59). The distribution of the neuronal transporters shows cell type specificity. EAAT3 is expressed in most neurons, including hippocampal and cortical neurons, whereas EAAT4 is mainly localized in cerebellar Purkinje cells and EAAT5 is restricted to the ribbon synapses of rod bipolar cells in the retina (60, 61). The majority of glutamate re-uptake is conducted by the glial transporters EAAT1 and EAAT2 (62, 63) which are expressed abundantly at the glial plasma membrane (59, 64) located in close proximity to synaptic release sites (65).

Glutamate transport by EAATs is powered indirectly by the sodium gradient across the membrane. During one complete cycle of glutamate transport, an EAAT brings one glutamate molecule against its concentration gradient, together with three Na<sup>+</sup> ions and one H<sup>+</sup> ion into the cell, meanwhile counter-transporting one K<sup>+</sup> ion out of the cell, thereby resetting the transporter to the outward-facing conformation (66, 67). During stroke and brain trauma, a large amount of glutamate release is coupled with elevated activity of EAATs attempting to restore extracellular glutamate concentration. Despite EAAT activity being an ultimately energy consuming event, glutamate removal prevents overexcitation of glutamate receptors including AMPARs and NMDARs, which are ion channels with higher energy cost, and thus reduces net energy consumption. Indeed, inhibition of EAATs results in a decrease in ATP amount, which can be completely blocked by the glutamate receptor antagonists, indicating that local glutamate stimulation at synaptic sites causes ATP reductions similar to that caused by global glutamate application (20). Interestingly, glutamate uptake is powered mainly by glycolytic metabolism both in glia and neurons (68).

An additional layer of co-ordination exists between synaptic activity and glutamate receptor trafficking. In response to glutamate release and binding, glutamate receptors, especially the primary synaptic mediator AMPARs, undergo rapid translocation from the plasma membrane to the cytosolic domain via receptor internalization (69, 70). Elevated neuronal network activity or synaptic glutamate accumulation as a result of transporter suppression lead to AMPAR internalization (71). AMPAR trafficking has been extensively studied as a mechanism for synaptic plasticity and learning, but it may also play a role in energy homeostasis, especially in neurotraumatic conditions to prevent receptor overexcitation and rapid depletion of cellular energy store.

#### SYNAPTIC ACTIVITY AND MITOCHONDRIA FUNCTION AND TRANSLOCATION

Mitochondria are responsible for generating and providing energy in the form of ATP in eukaryotic cells. In addition to converting glucose into ATP, mitochondria are involved in calcium signaling, apoptosis, and the metabolism of reactive oxygen species (ROS). With such high energy demands, neurons rely heavily on the proper functioning of mitochondria. The

significance of this organelle in neurons has been shown by the implication of mitochondrial dysfunction in several neurodegenerative diseases (72). Mitochondria are also involved in other neurobiological processes including neural differentiation, neurite outgrowth, neurotransmitter release, and dendritic remodeling (73).

Because regions of highest energy consumption in the neuron are located at the synapses, mitochondrial transport and distribution are critical, since diffusion of ATP from the center of the neuron would be too slow and inefficient (74). Mitochondrial movement in dendrites is increased in areas with high levels of ATP and decreased in areas containing higher levels of ADP, suggesting that low levels of ATP signal the mitochondria to remain in the area so as to increase local energy supply (75). Dendrites contain a greater proportion of highly charged, more metabolically active mitochondria than axons to match energy demands of local activity. In accordance, axonal mitochondria are more mobile compared to those in the dendrites (76). This activity-dependent mitochondrial stopping results from NMDAR-gated calcium rises, which lead to a recruitment of mitochondria to the synapse (77). Mitochondria use the dynein and kinesin motor complexes to move in the retrograde and anterograde directions, respectively. Specifically, the core of this motor/adaptor complex is made up of kinesin-1, the protein Miro that is anchored to the outer surface of the mitochondria, and Milton, which links kinesin and Miro. A fine balance and regulation of the movements based on these complexes determine where mitochondria will be static or motile to provide adequate ATP for neuronal activity. Elevation of cytosolic  $\text{Ca}^{2+}$ , which arises from activation of glutamate receptors in dendrites, stops both the anterograde and retrograde movement of mitochondria in neurons (77), which may be regulated by a  $\text{Ca}^{2+}$  binding site on Miro (78). How this regulation occurs remains unclear, although proposed mechanisms have included a conformational change in the complex triggered by  $\text{Ca}^{2+}$  (77), and direct binding of  $\text{Ca}^{2+}$  to kinesin, thereby preventing Miro from interacting with microtubules to allow mitochondrial movement (79).

Although less than synapses, axons themselves are also energy-demanding sites, as they are responsible for generating and conducting action potentials along the length of the neuron. In the peripheral nervous system, the nodes of Ranvier harbor the highest density of  $\text{Na}^+$  channels to sustain saltatory conduction (80). During action potentials, mitochondria are recruited to the nodal region and their mobility is reduced to provide more ATP (81). In addition, mitochondria motility seems to be crucial for axon growth and branching. A recent study shows that LKB1-NUAK1 signaling immobilize mitochondria in the axon where locally produced energy presumably supports formation of axon branches (82).

The regulation of mitochondrial function occurs both presynaptically and postsynaptically in the brain. In the presynaptic zone, the cycle of SVs in neuronal synapses involves steps regulated by cytosolic calcium concentrations and dependent on mitochondrial function. Upon the arrival of an action potential at the nerve terminal, voltage-gated  $\text{Ca}^{2+}$  channels open and allow an influx of calcium into the terminals. The elevated cytosolic calcium negatively affects mitochondria transport along microtubules, causing

them to pause, and accumulate close to the active zones where SVs will fuse to the membrane (83). Synapses tend to have an accumulation of mitochondria that have high electrical potential across their inner membranes and are capable of enhanced ATP production (84).

Regulation of mitochondrial function in the postsynaptic region of the dendrite involves responses to glutamate to increase glucose uptake and ATP production. Synaptic activity increases surface expression of GLUT3 leading to an elevation of intracellular glucose (85). This effect is NMDAR-dependent and involves nNOS phosphorylated by Akt. As glutamate itself is utilized by mitochondria to produce ATP, the transport of glutamate into mitochondria is also regulated by activity. Interestingly, EAAT3 (EAAC1) has been shown to be expressed in neuronal and glial mitochondria where it participates in glutamate-stimulated ATP production (86).

### ENERGY DYSREGULATION IN ISCHEMIA AND STROKE

Under normal conditions, high glutamate concentrations only occur at the synaptic cleft; ambient glutamate concentrations are maintained at very low levels (50). However, during traumatic brain injury (TBI) or stroke, massive glutamate release can lead to a marked increase in extracellular glutamate and hyperactivity of the overall glutamate system, causing additional acute and delayed neural pathology. Energy depletion plays a key role in glutamate-induced neurotoxicity (87–90). Glutamate stimulation causes more severe cell death when cellular energy homeostasis is impaired (88). A lack of sufficient ATP undermines a large number of energy-dependent cellular processes including kinase/enzymatic activity, proteasomal protein turnover, transmembrane biochemical gradients, and membrane potentials, all leading to a collapse of cellular functional integrity and deterioration of cell conditions. As the primary energy user consuming half of the ATP in the brain, sodium pump activity is highly sensitive to ATP levels. Under energy deficient conditions such as hypoxia, ischemia, and stroke, NKA dysfunction is often a major early pathological response (91, 92), which leads to a loss in membrane potential and neuronal function.

Ischemic stroke-induced energy depletion is sensed by the master metabolic regulator AMPK. AMPK activation has been observed in glutamate-treated neurons and a variety of ischemia/stroke models both *in vitro* (93) and *in vivo* (94). Because AMPK activation results in enhanced catalytic and suppressed anabolic metabolism, AMPK activity helps to relieve energy stress and is beneficial for neuronal conditions. Studies have shown that in cultured neurons AMPK activation reduces neuronal cell death caused by ischemia/hypoxia (93), whereas AMPK inhibition during energy stress stimulation leads to more severe damage (95). However, there are also studies showing deleterious effects of AMPK. *In vivo* ischemia model shows that blockade of AMPK by Compound C suppressed neural injury (96). Consistently, knock-out of AMPK  $\alpha 2$  results in a reduction of brain damage (97). Mechanisms for the detrimental effects of AMPK are not clear. Possibly, when cells are under conditions of metabolic stress, forced energy production pushes the metabolic machinery over its limits, causing a collapse of the system and irreversible structural and functional failure.



## ALTERATIONS OF BIOENERGY METABOLISM IN NEURODEGENERATIVE DISEASES

Given that the brain is the major energy consumer in the body, and neurons rely heavily on ATP production for development and function, even a slight impairment in energy metabolism can have drastic effects on the brain. In line with this, mitochondria and bioenergy defects have long been proposed as the mechanism underlying chronic neuronal dysfunction and death, and an increasing amount of evidence has been accumulated in support of the hypothesis (**Figure 1**).

Alzheimer's Disease (AD) is a neurodegenerative disease characterized by progressive memory loss and cognitive deficits. Its pathological hallmarks are neuronal loss, extracellular plaques consisting of A $\beta$  aggregates and intracellular neurofibrillary tangles made up of hyperphosphorylated tau. Although the exact cause of neuronal death has not yet been determined, many studies suggest that dysfunction of energy metabolism may be responsible for neuronal deficits contributing to cell death. Indeed, AD patients exhibit reduced glucose energy metabolism, even at an early stage of disease. Positron emission tomography (PET) imaging with the 2-[18F]-fluorodeoxyglucose (FDG) tracer has long been used to track AD-related changes in the brain by estimating the cerebral metabolic rate of glucose (CMR<sub>glc</sub>). FDG-PET studies in AD show consistent and progressive CMR<sub>glc</sub> reductions. Compared to age-matched healthy controls, AD patients show metabolic reductions in the parieto-temporal and posterior cingulate cortices in early and late-onset AD (98, 99), and in the frontal areas in advanced disease (99–102). These changes in glucose metabolism could be caused by a reduction of glucose uptake through glucose transporters, mitochondrial dysfunction, or changes in mitochondrial movement.

The neuronal glucose transporter GLUT3 level is reduced in the AD brain (103). Full-length cAMP response element binding protein (CREB), which is reduced in AD brain along with an increase in the truncated form, regulates the expression of GLUT3. Calpain I proteolyzes CREB at Gln28-Ala29 to generate a 41-kDa truncated CREB, which is less active in promoting GLUT3 expression, supported by the observation that activation of calpain I itself also reduces GLUT3 expression. It has been suggested that overactivation of calpain I by calcium overload proteolyzes CREB, resulting in a reduction of GLUT3 expression, and consequently impairing glucose uptake and metabolism in AD brain (104). AMPK, as a sensor and regulator of cellular energy metabolism, has been shown to decrease with aging, and may contribute to decreased mitochondrial function in AD (105). A study using quercetin, a natural flavonoid and activator of AMPK, showed that activation of AMPK reduces oxidative stress, improves mitochondrial dysfunction and impaired glucose uptake in AD, and slows down A $\beta$  accumulation (106).

Characterization of mitochondrial dynamics and function in three mouse models of familial AD (FAD) (APP, PS1, and APP/PS1) revealed mitochondrial dysfunction before the onset of memory phenotype and the formation of amyloid plaques (107). Movement of mitochondria in both anterograde and retrograde directions in FAD neurons was significantly inhibited compared to wild-type neurons. This reduced motility correlated with increased excitotoxic neuronal cell death by NMDA in all three

FAD mouse models, consistent with the essential role for mitochondrial motility and positioning in proper calcium buffering (83). Additionally, similar effects were seen in mouse hippocampal neurons treated with the A $\beta$ (23–35) peptide. Compared to the control neurons, which showed approximately 35% mobile mitochondria, motile mitochondria in the A $\beta$ -treated neurons were significantly reduced to 20%, suggesting that the A $\beta$ (25–35) peptide impairs axonal transport of mitochondria in AD neurons. This reduction in mitochondrial dynamics also correlated with, and was suggested to be causing, a reduction in synaptic proteins synaptophysin and MAP2. In the Tg2576 AD mouse model, where a significant decrease in mitochondrial movement was also seen (108), the mitochondria-targeted antioxidant SS31, which reduces intracellular free radicals (109), restored mitochondrial transport and synaptic viability, and decreased the percentage of defective mitochondria, implicating the important role of mitochondrial function in the disease. A recent report, however, found no consistent presynaptic bioenergetic deficiencies in three mouse models of AD pathogenesis (J20, Tg2576, and APP/PS1) (110). APP/PS1 cortical synaptosomes showed an increase in respiration associated with proton leak, but calcium handling and membrane potentials of synaptosomes were not consistently impaired. The disparities between these studies may be due to the mouse models used and the age of the animal when mitochondrial dysfunction was examined. In transgenic *Drosophila* expressing human tau, RNAi-mediated knockdown of Milton or Miro enhanced tau-induced neurodegeneration and increased tau phosphorylation at the AD-related site Ser262. Correlated with pathological conditions implicated in AD, a reduction in the number of axonal mitochondria was also observed, and knockdown of Miro alone was sufficient to induce late-onset neurodegeneration in the fly brain (111).

Parkinson's disease (PD) is characterized pathologically by the selective degeneration of dopaminergic neurons in the substantia nigra pars compacta and the presence of Lewy bodies, intraneuronal aggregates comprised primarily of alpha-synuclein ( $\alpha$ -syn). A mutation in  $\alpha$ -syn, A53T, has been identified to cause familial Parkinson's disease (112), and  $\alpha$ -syn transgenic PD models display impaired mitochondrial function and decreased mitochondrial movement (113, 114). In addition, mutations in other Parkinson related proteins, such as PINK1, parkin, and DJ-1, are also believed to be involved in the regulation of mitochondrial function (115–117).

Huntington's disease (HD) is an autosomal dominant neurodegenerative disease characterized by motor and cognitive impairment and caused by a trinucleotide repeat expansion encoding an elongated glutamine tract in the Huntingtin (htt) protein (118). Reduced energy metabolism has been well documented in HD patients. PET scan analysis of HD patients revealed diminished rates of cerebral glucose metabolism in parts of the cortex and throughout the striatum (119). Additionally, HD patient material was found to have significant reductions in the enzymatic activities of complexes II, III, and IV of the mitochondrial oxidative phosphorylation pathway in caudate and putamen (120, 121). BACHD mice of mutant Htt were found to have abnormal mitochondrial dynamics, supposedly due to the interaction of mutant Htt with the mitochondrial protein Drp1, resulting in defective anterograde

movement (122). A major player implicated in mitochondrial dysfunction in Huntington's, as well as Parkinson's, is PPAR $\gamma$  co-activator-1 $\alpha$  (PGC-1 $\alpha$ ). As a transcription co-activator, PGC-1 $\alpha$  regulates the expression of various genes to promote mitochondrial biogenesis and oxidative phosphorylation. Impaired PGC-1 $\alpha$  function is a likely contributor to HD pathology, as demonstrated by reduced PGC-1 $\alpha$  target gene expression in HD transgenic mice (123). PGC-1 $\alpha$  transcriptional activity is also repressed in a conditional knockout model of parkin (124), and activation of PGC-1 $\alpha$  could rescue dopaminergic neuron loss induced by mutant  $\alpha$ -syn (125). Consistently, PGC-1 $\alpha$  has been suggested as a promising therapeutic target for HD and PD, either by boosting PGC-1 $\alpha$  expression by viral delivery, or by modulating the upstream activators of PGC-1 $\alpha$  activity, such as SIRT1 and AMPK (126).

## IMPLICATIONS OF ENERGY HOMEOSTASIS IN TRAUMATIC BRAIN INJURY

Traumatic brain injury (TBI) is a complex brain damage by an external force that causes brain penetrating or closed-head injuries. Recently, TBI has become an increasing concern in the population, as almost 179,000 service members sustained a TBI during the Iraq and Afghanistan wars (127). Additionally, repeated injury to the brain, especially concussions, can lead to CTE, a neurodegenerative disease that has been discovered in brain tissues of athletes who have sustained many close head and concussions injuries over time (128, 129). The complex mechanism by which TBI triggers pathological processes and long-term neurobehavioral abnormalities are still not well understood. Mechanistic investigation is critical to guide the identification of compounds to prevent acute neuronal damage and subsequent effects.

Traumatic brain injuries cause a vast array of primary structural damages that lead to secondary effects including cellular, inflammatory, neurochemical, and metabolic alterations. In the early phases after injury, changes such as metabolic impairment, reductions in cerebral blood flow, low ATP and energy stores, severe ionic shifts, and alterations in the permeability of the blood-brain barrier are seen. Thereafter, brain lactate production increases for the first few days, indicating a shift from aerobic to anaerobic metabolism to maintain ATP production, while glucose levels decline rapidly, as measured by microdialysis in affected patients (130). High levels of lactate in the brain during this period of ischemia may cause additional harmful effects; cerebral acidosis may exacerbate calcium-mediated damage to intracellular pathways and may interfere with ion-channel function (131). ATP levels are decreased following a TBI, along with reduced availability of the nicotinic coenzyme pool, which declines proportionally with the gravity of brain insult (132). The degree of oxidative metabolism depression also correlates with the depth of coma after severe TBI, as indicated by the Glasgow Coma Scale (GSC) (133). In mice, a single blast resulted in a 20% decrease in ATP levels in the cerebral cortex at 6 h after the blast, whereas triple blasts resulted in a similar decrease as early as 1 h (134). A significant, though less severe, decrease remained 24 h after the blast. Energy failure leads to degradation of molecules of key importance to membrane and cytoskeletal integrity. It also causes a disruption in ion homeostasis, especially calcium rises, and an increase in cytosolic acidity. The rise in free cytosolic Ca<sup>2+</sup> is a result of failed calcium

pump function, increased membrane permeability to calcium, and decreased sequestration of intracellular calcium. Elevated calcium levels and oxidative stress lead to the opening of the mitochondrial permeability transition pore (mPTP), which depolarizes the mitochondrial membrane and leads to organelle swelling and subsequent release of cytochrome *c*, leading to caspase-dependent cell death (135, 136). Specific inhibitors of the mPTP are currently under investigation as treatment immediately after TBI to prevent neuronal damage (137).

Mitochondrial dysfunction in TBI may be caused by several mechanisms in addition to the opening of mPTP. Nitric oxide (NO) is believed to cause respiratory chain inhibition in mitochondria after TBI (138), as it has the ability to interfere with energy metabolism by inhibiting the enzymatic activity of complex IV of the electron transport chain. An increase in NO production has been observed in closed-head trauma animal models (139), caused by the increase in the production of inducible NO synthase (iNOS) (140), as indicated by the rapid upregulation of iNOS mRNA at 4 h after injury. The inhibition of pyruvate dehydrogenase (PDH) has also been implicated in causing mitochondrial damage in TBI. PDH is tightly regulated by end-product inhibition and reversible phosphorylation, and a significant decrease in both PDH enzyme levels (141) and PDH phosphorylation (142) was found in rat TBI models. In addition, activation of poly(adenosine diphosphate [ADP]-ribose) polymerase-1 (PARP-1) could be responsible for impaired mitochondrial respiration. PARP-1 senses DNA damage after injury and becomes overactivated, depletes NAD<sup>+</sup>/NADH stores, and impairs the utilization of oxygen for ATP synthesis (143). In support of this mechanism, administration of NAD<sup>+</sup> or the PARP inhibitor GP 6150 was found to be neuroprotective after TBI in rats (144, 145). Similar blockade of mitochondrial damage and metabolic disturbances in the early events occurring immediately after an injury are currently under investigation, which will be advanced following a better understanding of the molecular mechanisms underlying primary TBI impacts.

## CONCLUSION

Excitatory glutamatergic synaptic transmission is the major energy-consuming cellular process in the brain. Therefore, it is critical for neurons to couple synaptic activities with energetic metabolism, and to have adaptive mechanisms in response to metabolic stress and neuronal overexcitation. Dysfunctions in the regulatory system and bioenergy homeostasis can lead to defects in neural development and brain function, and contribute to the pathogenesis of neurodegenerative diseases and traumatic brain injuries. It will be important to further our understandings of how synaptic activity communicates with the metabolic and energetic machineries, including energy sensing, energetic signaling, bioenergy metabolism, and mitochondria dynamics. Age-dependent changes in bioenergy homeostasis, and epigenetic control of the energetic processes are also in need of further investigation.

## ACKNOWLEDGMENTS

We thank Man Lab members for helpful comments on the manuscript. This work was supported by NIH grant MH079407 (Heng-Ye Man).

## REFERENCES

- Attwell D, Laughlin SB. An energy budget for signaling in the grey matter of the brain. *J Cereb Blood Flow Metab* (2001) **21**:1133–45. doi:10.1097/00004647-200110000-00001
- Magistretti PJ, Pellerin L. Metabolic coupling during activation. A cellular view. *Adv Exp Med Biol* (1997) **413**:161–6. doi:10.1007/978-1-4899-0056-2\_18
- Magistretti PJ, Pellerin L, Rothman DL, Shulman RG. Energy on demand. *Science* (1999) **283**:496–7. doi:10.1126/science.283.5401.496
- Raichle ME, Gusnard DA. Appraising the brain's energy budget. *Proc Natl Acad Sci U S A* (2002) **99**:10237–9. doi:10.1073/pnas.172399499
- Rao J, Oz G, Seaquist ER. Regulation of cerebral glucose metabolism. *Minerva Endocrinol* (2006) **31**:149–58.
- Elia M. Organ and tissue contribution to metabolic rate. In: Kinney JM, Tucker HN, editors. *Energ Metabolism: Tissue Determinants and Cellular Corollaries*. New York, NY: Raven Press (1992). p. 61–80.
- Alle H, Roth A, Geiger JR. Energy-efficient action potentials in hippocampal mossy fibers. *Science* (2009) **325**:1405–8. doi:10.1126/science.1174331
- Howarth C, Gleeson P, Attwell D. Updated energy budgets for neural computation in the neocortex and cerebellum. *J Cereb Blood Flow Metab* (2012) **32**:1222–32. doi:10.1038/jcbfm.2012.35
- Jolivet R, Magistretti PJ, Weber B. Deciphering neuron-glia compartmentalization in cortical energy metabolism. *Front Neuroenergetics* (2009) **1**:4. doi:10.3389/fnro.14.004.2009
- Shen J, Petersen KF, Behar KL, Brown P, Nixon TW, Mason GF, et al. Determination of the rate of the glutamate/glutamine cycle in the human brain by in vivo <sup>13</sup>C NMR. *Proc Natl Acad Sci U S A* (1999) **96**:8235–40. doi:10.1073/pnas.96.14.8235
- Sibson NR, Dhankhar A, Mason GF, Rothman DL, Behar KL, Shulman RG. Stoichiometric coupling of brain glucose metabolism and glutamatergic neuronal activity. *Proc Natl Acad Sci U S A* (1998) **95**:316–21. doi:10.1073/pnas.95.1.316
- Danbolt NC. Glutamate uptake. *Prog Neurobiol* (2001) **65**:1–105. doi:10.1016/S0301-0082(00)00067-8
- Tzingounis AV, Wadiche JI. Glutamate transporters: confining runaway excitation by shaping synaptic transmission. *Nat Rev Neurosci* (2007) **8**:935–47. doi:10.1038/nrn2274
- Collingridge GL, Isaac JT, Wang YT. Receptor trafficking and synaptic plasticity. *Nat Rev Neurosci* (2004) **5**:952–62. doi:10.1038/nrn1556
- Man HY, Ju W, Ahmadian G, Wang YT. Intracellular trafficking of AMPA receptors in synaptic plasticity. *Cell Mol Life Sci* (2000) **57**:1526–34. doi:10.1007/PL00000637
- Newpher TM, Ehlers MD. Glutamate receptor dynamics in dendritic microdomains. *Neuron* (2008) **58**:472–97. doi:10.1016/j.neuron.2008.04.030
- Kim MJ, Dunah AW, Wang YT, Sheng M. Differential roles of NR2A- and NR2B-containing NMDA receptors in Ras-ERK signaling and AMPA receptor trafficking. *Neuron* (2005) **46**:745–60. doi:10.1016/j.neuron.2005.04.031
- Skeberdis VA, Chevalyere V, Lau CG, Goldberg JH, Pettit DL, Suadicani SO, et al. Protein kinase A regulates calcium permeability of NMDA receptors. *Nat Neurosci* (2006) **9**:501–10. doi:10.1038/nn1664
- Rose CR, Konnerth A. NMDA receptor-mediated Na<sup>+</sup> signals in spines and dendrites. *J Neurosci* (2001) **21**:4207–14.
- Foo K, Blumenthal L, Man HY. Regulation of neuronal bioenergy homeostasis by glutamate. *Neurochem Int* (2012) **61**:389–96. doi:10.1016/j.neuint.2012.06.003
- Bateman A. The structure of a domain common to archaeobacteria and the homocystinuria disease protein. *Trends Biochem Sci* (1997) **22**:12–3. doi:10.1016/S0968-0004(96)30046-7
- Scott JW, Hawley SA, Green KA, Anis M, Stewart G, Scullion GA, et al. CBS domains form energy-sensing modules whose binding of adenosine ligands is disrupted by disease mutations. *J Clin Invest* (2004) **113**:274–84. doi:10.1172/JCI19874
- Xiao B, Heath R, Saiu P, Leiper FC, Leone P, Jing C, et al. Structural basis for AMP binding to mammalian AMP-activated protein kinase. *Nature* (2007) **449**:496–500. doi:10.1038/nature06161
- Hawley SA, Davison M, Woods A, Davies SP, Beri RK, Carling D, et al. Characterization of the AMP-activated protein kinase kinase from rat liver and identification of threonine 172 as the major site at which it phosphorylates AMP-activated protein kinase. *J Biol Chem* (1996) **271**:27879–87. doi:10.1074/jbc.271.44.27879
- Baron SJ, Li J, Russell RR III, Neumann D, Miller EJ, Tuerk R, et al. Dual mechanisms regulating AMPK kinase action in the ischemic heart. *Circ Res* (2005) **96**:337–45. doi:10.1161/01.RES.0000155723.53868.d2
- Clark SA, Chen ZP, Murphy KT, Aughey RJ, McKenna MJ, Kemp BE, et al. Intensified exercise training does not alter AMPK signaling in human skeletal muscle. *Am J Physiol Endocrinol Metab* (2004) **286**:E737–43. doi:10.1152/ajpendo.00462.2003
- Woods A, Dickerson K, Heath R, Hong SP, Momcilovic M, Johnstone SR, et al. Ca<sup>2+</sup>/calmodulin-dependent protein kinase kinase-beta acts upstream of AMP-activated protein kinase in mammalian cells. *Cell Metab* (2005) **2**:21–33. doi:10.1016/j.cmet.2005.06.005
- Woods A, Vertommen D, Neumann D, Turk R, Bayliss J, Schlattner U, et al. Identification of phosphorylation sites in AMP-activated protein kinase (AMPK) for upstream AMPK kinases and study of their roles by site-directed mutagenesis. *J Biol Chem* (2003) **278**:28434–42. doi:10.1074/jbc.M303946200
- Avizienyte E, Roth S, Loukola A, Hemminki A, Lothe RA, Stenwig AE, et al. Somatic mutations in LKB1 are rare in sporadic colorectal and testicular tumors. *Cancer Res* (1998) **58**:2087–90.
- Hawley SA, Boudeau J, Reid JL, Mustard KJ, Udd L, Makela TP, et al. Complexes between the LKB1 tumor suppressor, STRAD alpha/beta and MO25 alpha/beta are upstream kinases in the AMP-activated protein kinase cascade. *J Biol* (2003) **2**:28. doi:10.1186/1475-4924-2-28
- Shaw RJ, Kosmatka M, Bardeesy N, Hurley RL, Witters LA, DePinho RA, et al. The tumor suppressor LKB1 kinase directly activates AMP-activated kinase and regulates apoptosis in response to energy stress. *Proc Natl Acad Sci U S A* (2004) **101**:3329–35. doi:10.1073/pnas.0308061100
- Sakamoto K, McCarthy A, Smith D, Green KA, Grahame Hardie D, Ashworth A, et al. Deficiency of LKB1 in skeletal muscle prevents AMPK activation and glucose uptake during contraction. *EMBO J* (2005) **24**:1810–20. doi:10.1038/sj.emboj.7600667
- Shaw RJ, Lamia KA, Vasquez D, Koo SH, Bardeesy N, Depinho RA, et al. The kinase LKB1 mediates glucose homeostasis in liver and therapeutic effects of metformin. *Science* (2005) **310**:1642–6. doi:10.1126/science.1120781
- Barnes AP, Lilley BN, Pan YA, Plummer LJ, Powell AW, Raines AN, et al. LKB1 and SAD kinases define a pathway required for the polarization of cortical neurons. *Cell* (2007) **129**:549–63. doi:10.1016/j.cell.2007.03.025
- Hawley SA, Pan DA, Mustard KJ, Ross L, Bain J, Edelman AM, et al. Calmodulin-dependent protein kinase kinase-beta is an alternative upstream kinase for AMP-activated protein kinase. *Cell Metab* (2005) **2**:9–19. doi:10.1016/j.cmet.2005.05.009
- Anupama Adya HV, Mallick BN. Comparison of Na-K ATPase activity in rat brain synaptosome under various conditions. *Neurochem Int* (1998) **33**:283–6. doi:10.1016/S0197-0186(98)00043-6
- Brines ML, Robbins RJ. Cell-type specific expression of Na<sup>+</sup>, K<sup>+</sup>-ATPase catalytic subunits in cultured neurons and glia: evidence for polarized distribution in neurons. *Brain Res* (1993) **631**:1–11. doi:10.1016/0006-8993(93)91179-V
- Wong-Riley MT, Huang Z, Liebl W, Nie F, Xu H, Zhang C. Neurochemical organization of the macaque retina: effect of TTX on levels and gene expression of cytochrome oxidase and nitric oxide synthase and on the immunoreactivity of Na<sup>+</sup> K<sup>+</sup> ATPase and NMDA receptor subunit I. *Vision Res* (1998) **38**:1455–77. doi:10.1016/S0042-6989(98)00001-7
- Loaiza A, Porras OH, Barros LF. Glutamate triggers rapid glucose transport stimulation in astrocytes as evidenced by real-time confocal microscopy. *J Neurosci* (2003) **23**:7337–42.
- Morgello S, Uson RR, Schwartz EJ, Haber RS. The human blood-brain barrier glucose transporter (GLUT1) is a glucose transporter of gray matter astrocytes. *Glia* (1995) **14**:43–54. doi:10.1002/glia.440140107
- Bak LK, Walls AB, Schousboe A, Ring A, Sonnewald U, Waagepetersen HS. Neuronal glucose but not lactate utilization is positively correlated with NMDA-induced neurotransmission and fluctuations in cytosolic Ca<sup>2+</sup> levels. *J Neurochem* (2009) **109**(Suppl 1):87–93. doi:10.1111/j.1471-4159.2009.05943.x
- Porras OH, Loaiza A, Barros LF. Glutamate mediates acute glucose transport inhibition in hippocampal neurons. *J Neurosci* (2004) **24**:9669–73. doi:10.1523/JNEUROSCI.1882-04.2004
- Amato S, Liu X, Zheng B, Cantley L, Rakic P, Man HY. AMP-activated protein kinase regulates neuronal polarization by interfering with PI 3-kinase localization. *Science* (2011) **332**:247–51. doi:10.1126/science.1201678
- Weisova P, Concannon CG, Devocelle M, Prehn JH, Ward MW. Regulation of glucose transporter 3 surface expression by the AMP-activated protein

- kinase mediates tolerance to glutamate excitation in neurons. *J Neurosci* (2009) **29**:2997–3008. doi:10.1523/JNEUROSCI.0354-09.2009
45. Jakobsen SN, Hardie DG, Morrice N, Tornqvist HE. 5'-AMP-activated protein kinase phosphorylates IRS-1 on Ser-789 in mouse C2C12 myotubes in response to 5-aminoimidazole-4-carboxamide riboside. *J Biol Chem* (2001) **276**:46912–6. doi:10.1074/jbc.C100483200
  46. Ioudina M, Uemura E, Greenlee HW. Glucose insufficiency alters neuronal viability and increases susceptibility to glutamate toxicity. *Brain Res* (2004) **1004**:188–92. doi:10.1016/j.brainres.2003.12.046
  47. Li C, Li Y, He L, Agarwal AR, Zeng N, Cadenas E, et al. PI3K/AKT signaling regulates bioenergetics in immortalized hepatocytes. *Free Radic Biol Med* (2013) **60**:29–40. doi:10.1016/j.freeradbiomed.2013.01.013
  48. Butcher SP, Hamberger A. In vivo studies on the extracellular, and veratrine-releasable, pools of endogenous amino acids in the rat striatum: effects of corticostriatal deafferentation and kainic acid lesion. *J Neurochem* (1987) **48**:713–21. doi:10.1111/j.1471-4159.1987.tb05575.x
  49. Clements JD, Lester RA, Tong G, Jahr CE, Westbrook GL. The time course of glutamate in the synaptic cleft. *Science* (1992) **258**:1498–501. doi:10.1126/science.1359647
  50. Herman MA, Jahr CE. Extracellular glutamate concentration in hippocampal slice. *J Neurosci* (2007) **27**:9736–41. doi:10.1523/JNEUROSCI.3009-07.2007
  51. Kanner BI, Schuldiner S. Mechanism of transport and storage of neurotransmitters. *CRC Crit Rev Biochem* (1987) **22**:1–38. doi:10.3109/10409238709082546
  52. Kanner BI, Sharon I. Active transport of L-glutamate by membrane vesicles isolated from rat brain. *Biochemistry* (1978) **17**:3949–53. doi:10.1021/bi00600a011
  53. Stern JR, Eggleston LV. Accumulation of glutamic acid in isolated brain tissue. *Biochem J* (1949) **44**:410–8.
  54. Schousboe A. Transport and metabolism of glutamate and GABA in neurons are glial cells. *Int Rev Neurobiol* (1981) **22**:1–45. doi:10.1016/S0074-7742(08)60289-5
  55. Arundine M, Tymianski M. Molecular mechanisms of calcium-dependent neurodegeneration in excitotoxicity. *Cell Calcium* (2003) **34**:325–37. doi:10.1016/S0143-4160(03)00141-6
  56. Choi DW. Excitotoxic cell death. *J Neurobiol* (1992) **23**:1261–76. doi:10.1002/neu.480230915
  57. Man HY. GluA2-lacking, calcium-permeable AMPA receptors – inducers of plasticity? *Curr Opin Neurobiol* (2011) **21**:291–8. doi:10.1016/j.conb.2011.01.001
  58. Chaudhry FA, Lehre KP, van Lookeren Campagne M, Ottersen OP, Danbolt NC, Storm-Mathisen J. Glutamate transporters in glial plasma membranes: highly differentiated localizations revealed by quantitative ultrastructural immunocytochemistry. *Neuron* (1995) **15**:711–20. doi:10.1016/0896-6273(95)90158-2
  59. Rothstein JD, Martin L, Levey AI, Dykes-Hoberg M, Jin L, Wu D, et al. Localization of neuronal and glial glutamate transporters. *Neuron* (1994) **13**:713–25. doi:10.1016/0896-6273(94)90038-8
  60. Hasegawa J, Obara T, Tanaka K, Tachibana M. High-density presynaptic transporters are required for glutamate removal from the first visual synapse. *Neuron* (2006) **50**:63–74. doi:10.1016/j.neuron.2006.02.022
  61. Wadiche JI, Jahr CE. Patterned expression of Purkinje cell glutamate transporters controls synaptic plasticity. *Nat Neurosci* (2005) **8**:1329–34. doi:10.1038/nn1539
  62. Bergles DE, Jahr CE. Glial contribution to glutamate uptake at Schaffer collateral-commissural synapses in the hippocampus. *J Neurosci* (1998) **18**:7709–16.
  63. Rothstein JD, Dykes-Hoberg M, Pardo CA, Bristol LA, Jin L, Kuncl RW, et al. Knockout of glutamate transporters reveals a major role for astroglial transport in excitotoxicity and clearance of glutamate. *Neuron* (1996) **16**:675–86. doi:10.1016/S0896-6273(00)80086-0
  64. Lehre KP, Danbolt NC. The number of glutamate transporter subtype molecules at glutamatergic synapses: chemical and stereological quantification in young adult rat brain. *J Neurosci* (1998) **18**:8751–7.
  65. Ventura R, Harris KM. Three-dimensional relationships between hippocampal synapses and astrocytes. *J Neurosci* (1999) **19**:6897–906.
  66. Levy LM, Warr O, Attwell D. Stoichiometry of the glial glutamate transporter GLT-1 expressed inducibly in a Chinese hamster ovary cell line selected for low endogenous Na<sup>+</sup>-dependent glutamate uptake. *J Neurosci* (1998) **18**:9620–8.
  67. Zerangue N, Kavanaugh MP. Flux coupling in a neuronal glutamate transporter. *Nature* (1996) **383**:634–7. doi:10.1038/383634a0
  68. Schousboe A, Sickmann HM, Bak LK, Schousboe I, Jajo FS, Faek SA, et al. Neuron-glia interactions in glutamatergic neurotransmission: roles of oxidative and glycolytic adenosine triphosphate as energy source. *J Neurosci Res* (2011) **89**:1926–34. doi:10.1002/jnr.22746
  69. Carroll RC, Beattie EC, von Zastrow M, Malenka RC. Role of AMPA receptor endocytosis in synaptic plasticity. *Nat Rev Neurosci* (2001) **2**:315–24. doi:10.1038/35072500
  70. Lissin DV, Gomperts SN, Carroll RC, Christine CW, Kalman D, Kitamura M, et al. Activity differentially regulates the surface expression of synaptic AMPA and NMDA glutamate receptors. *Proc Natl Acad Sci U S A* (1998) **95**:7097–102. doi:10.1073/pnas.95.12.7097
  71. Jarzylo LA, Man HY. Parasynaptic NMDA receptor signaling couples neuronal glutamate transporter function to AMPA receptor synaptic distribution and stability. *J Neurosci* (2012) **32**:2552–63. doi:10.1523/JNEUROSCI.3237-11.2012
  72. Chen H, Chan DC. Mitochondrial dynamics – fusion, fission, movement, and mitophagy – in neurodegenerative diseases. *Hum Mol Genet* (2009) **18**:R169–76. doi:10.1093/hmg/ddp326
  73. Cheng A, Hou Y, Mattson MP. Mitochondria and neuroplasticity. *ASN Neuro* (2010) **2**:e00045. doi:10.1042/AN20100019
  74. Kuiper JW, Pluk H, Oerlemans F, van Leeuwen FN, de Lange F, Fransen J, et al. Creatine kinase-mediated ATP supply fuels actin-based events in phagocytosis. *PLoS Biol* (2008) **6**:e51. doi:10.1371/journal.pbio.0060051
  75. Macaskill AF, Kittler JT. Control of mitochondrial transport and localization in neurons. *Trends Cell Biol* (2010) **20**:102–12. doi:10.1016/j.tcb.2009.11.002
  76. Overly CC, Rieff HI, Hollenbeck PJ. Organelle motility and metabolism in axons vs dendrites of cultured hippocampal neurons. *J Cell Sci* (1996) **109**(Pt 5):971–80.
  77. Macaskill AF, Rinholm JE, Twelvetrees AE, Arancibia-Carcamo IL, Muir J, Fransson A, et al. Miro1 is a calcium sensor for glutamate receptor-dependent localization of mitochondria at synapses. *Neuron* (2009) **61**:541–55. doi:10.1016/j.neuron.2009.01.030
  78. Fransson S, Ruusala A, Aspenstrom P. The atypical Rho GTPases Miro-1 and Miro-2 have essential roles in mitochondrial trafficking. *Biochem Biophys Res Commun* (2006) **344**:500–10. doi:10.1016/j.bbrc.2006.03.163
  79. Wang X, Schwarz TL. The mechanism of Ca<sup>2+</sup>-dependent regulation of kinesin-mediated mitochondrial motility. *Cell* (2009) **136**:163–74. doi:10.1016/j.cell.2008.11.046
  80. Fabricius C, Berthold CH, Rydmark M. Axoplasmic organelles at nodes of Ranvier. II. Occurrence and distribution in large myelinated spinal cord axons of the adult cat. *J Neurocytol* (1993) **22**:941–54. doi:10.1007/BF01218352
  81. Zhang CL, Ho PL, Kintner DB, Sun D, Chiu SY. Activity-dependent regulation of mitochondrial motility by calcium and Na/K-ATPase at nodes of Ranvier of myelinated nerves. *J Neurosci* (2010) **30**:3555–66. doi:10.1523/JNEUROSCI.4551-09.2010
  82. Courchet J, Lewis TL Jr, Lee S, Courchet V, Liou DY, Aizawa S, et al. Terminal axon branching is regulated by the LKB1-NUAK1 kinase pathway via presynaptic mitochondrial capture. *Cell* (2013) **153**:1510–25. doi:10.1016/j.cell.2013.05.021
  83. Yi M, Weaver D, Hajnoczky G. Control of mitochondrial motility and distribution by the calcium signal: a homeostatic circuit. *J Cell Biol* (2004) **167**:661–72. doi:10.1083/jcb.200406038
  84. Lee CW, Peng HB. Mitochondrial clustering at the vertebrate neuromuscular junction during presynaptic differentiation. *J Neurobiol* (2006) **66**:522–36. doi:10.1002/neu.20245
  85. Ferreira JM, Burnett AL, Rameau GA. Activity-dependent regulation of surface glucose transporter-3. *J Neurosci* (2011) **31**:1991–9. doi:10.1523/JNEUROSCI.1850-09.2011
  86. Magi S, Lariccia V, Castaldo P, Arcangeli S, Nasti AA, Giordano A, et al. Physical and functional interaction of NCX1 and EAAC1 transporters leading to glutamate-enhanced ATP production in brain mitochondria. *PLoS One* (2012) **7**:e34015. doi:10.1371/journal.pone.0034015
  87. Baltan S, Murphy SP, Danilov CA, Bachleda A, Morrison RS. Histone deacetylase inhibitors preserve white matter structure and function during ischemia by conserving ATP and reducing excitotoxicity. *J Neurosci* (2011) **31**:3990–9. doi:10.1523/JNEUROSCI.5379-10.2011



88. Del Rio P, Montiel T, Chagoya V, Massieu L. Exacerbation of excitotoxic neuronal death induced during mitochondrial inhibition in vivo: relation to energy imbalance or ATP depletion? *Neuroscience* (2007) **146**:1561–70. doi:10.1016/j.neuroscience.2007.03.024
89. Nicholls DG, Budd SL. Mitochondria and neuronal glutamate excitotoxicity. *Biochim Biophys Acta* (1998) **1366**:97–112. doi:10.1016/S0005-2728(98)00123-6
90. Nicholls DG, Johnson-Cadwell L, Vesce S, Jakabsons M, Yadava N. Bioenergetics of mitochondria in cultured neurons and their role in glutamate excitotoxicity. *J Neurosci Res* (2007) **85**:3206–12. doi:10.1002/jnr.21290
91. Mahadik SP, Bharucha VA, Stadlin A, Ortiz A, Karpiak SE. Loss and recovery of activities of alpha+ and alpha isozymes of (Na(+)+K(+)-ATPase in cortical focal ischemia: GM1 ganglioside protects plasma membrane structure and function. *J Neurosci Res* (1992) **32**:209–20. doi:10.1002/jnr.490320210
92. Mrcic-Pelcic J, Pelcic G, Vitezic D, Antoncic I, Filipovic T, Simonic A, et al. Hyperbaric oxygen treatment: the influence on the hippocampal superoxide dismutase and Na+,K+-ATPase activities in global cerebral ischemia-exposed rats. *Neurochem Int* (2004) **44**:585–94. doi:10.1016/j.neuint.2003.10.004
93. Culmsee C, Monnig J, Kemp BE, Mattson MP. AMP-activated protein kinase is highly expressed in neurons in the developing rat brain and promotes neuronal survival following glucose deprivation. *J Mol Neurosci* (2001) **17**:45–58. doi:10.1385/JMN:17:1:45
94. Harada S, Fujita-Hamabe W, Tokuyama S. The importance of regulation of blood glucose levels through activation of peripheral 5'-AMP-activated protein kinase on ischemic neuronal damage. *Brain Res* (2010) **1351**:254–63. doi:10.1016/j.brainres.2010.06.052
95. Wang P, Xu TY, Guan YF, Tian WW, Viollet B, Rui YC, et al. Nicotinamide phosphoribosyltransferase protects against ischemic stroke through SIRT1-dependent adenosine monophosphate-activated kinase pathway. *Ann Neurol* (2011) **69**:360–74. doi:10.1002/ana.22236
96. Li J, Zeng Z, Viollet B, Ronnett GV, McCullough LD. Neuroprotective effects of adenosine monophosphate-activated protein kinase inhibition and gene deletion in stroke. *Stroke* (2007) **38**:2992–9. doi:10.1161/STROKEAHA.107.490904
97. McCullough LD, Zeng Z, Li H, Landree LE, McFadden J, Ronnett GV. Pharmacological inhibition of AMP-activated protein kinase provides neuroprotection in stroke. *J Biol Chem* (2005) **280**:20493–502. doi:10.1074/jbc.M409985200
98. Ishii K, Sasaki H, Kono AK, Miyamoto N, Fukuda T, Mori E. Comparison of gray matter and metabolic reduction in mild Alzheimer's disease using FDG-PET and voxel-based morphometric MR studies. *Eur J Nucl Med Mol Imaging* (2005) **32**:959–63. doi:10.1007/s00259-004-1740-5
99. Sakamoto S, Ishii K, Sasaki M, Hosaka K, Mori T, Matsui M, et al. Differences in cerebral metabolic impairment between early and late onset types of Alzheimer's disease. *J Neurol Sci* (2002) **200**:27–32. doi:10.1016/S0022-510X(02)00114-4
100. Foster NL, Chase TN, Mansi L, Brooks R, Fedio P, Patronas NJ, et al. Cortical abnormalities in Alzheimer's disease. *Ann Neurol* (1984) **16**:649–54. doi:10.1002/ana.410160605
101. Friedland RP, Budinger TF, Ganz E, Yano Y, Mathis CA, Koss B, et al. Regional cerebral metabolic alterations in dementia of the Alzheimer type: positron emission tomography with [18F]fluorodeoxyglucose. *J Comput Assist Tomogr* (1983) **7**:590–8. doi:10.1097/00004728-198308000-00003
102. Minoshima S, Giordani B, Berent S, Frey KA, Foster NL, Kuhl DE. Metabolic reduction in the posterior cingulate cortex in very early Alzheimer's disease. *Ann Neurol* (1997) **42**:85–94. doi:10.1002/ana.410420114
103. Simpson IA, Chundu KR, Davies-Hill T, Honer WG, Davies P. Decreased concentrations of GLUT1 and GLUT3 glucose transporters in the brains of patients with Alzheimer's disease. *Ann Neurol* (1994) **35**:546–51. doi:10.1002/ana.410350507
104. Jin N, Qian W, Yin X, Zhang L, Iqbal K, Grundke-Iqbal I, et al. CREB regulates the expression of neuronal glucose transporter 3: a possible mechanism related to impaired brain glucose uptake in Alzheimer's disease. *Nucleic Acids Res* (2013) **41**:3240–56. doi:10.1093/nar/gks1227
105. Jornayvaz FR, Shulman GI. Regulation of mitochondrial biogenesis. *Essays Biochem* (2010) **47**:69–84. doi:10.1042/bse0470069
106. Lu J, Wu DM, Zheng YL, Hu B, Zhang ZF, Shan Q, et al. Quercetin activates AMP-activated protein kinase by reducing PP2C expression protecting old mouse brain against high cholesterol-induced neurotoxicity. *J Pathol* (2010) **222**:199–212. doi:10.1002/path.2754
107. Trushina E, Nemutlu E, Zhang S, Christensen T, Camp J, Mesa J, et al. Defects in mitochondrial dynamics and metabolomic signatures of evolving energetic stress in mouse models of familial Alzheimer's disease. *PLoS One* (2012) **7**:e32737. doi:10.1371/journal.pone.0032737
108. Calkins MJ, Manczak M, Mao P, Shirendeb U, Reddy PH. Impaired mitochondrial biogenesis, defective axonal transport of mitochondria, abnormal mitochondrial dynamics and synaptic degeneration in a mouse model of Alzheimer's disease. *Hum Mol Genet* (2011) **20**:4515–29. doi:10.1093/hmg/ddr381
109. Cho S, Szeto HH, Kim E, Kim H, Tolhurst AT, Pinto JT. A novel cell-permeable antioxidant peptide, SS31, attenuates ischemic brain injury by down-regulating CD36. *J Biol Chem* (2007) **282**:4634–42. doi:10.1074/jbc.M609388200
110. Choi SW, Gerencser AA, Ng R, Flynn JM, Melov S, Danielson SR, et al. No consistent bioenergetic defects in presynaptic nerve terminals isolated from mouse models of Alzheimer's disease. *J Neurosci* (2012) **32**:16775–84. doi:10.1523/JNEUROSCI.2414-12.2012
111. Iijima-Ando K, Sekiya M, Maruko-Otake A, Ohtake Y, Suzuki E, Lu B, et al. Loss of axonal mitochondria promotes tau-mediated neurodegeneration and Alzheimer's disease-related tau phosphorylation via PAR-1. *PLoS Genet* (2012) **8**:e1002918. doi:10.1371/journal.pgen.1002918
112. Polymeropoulos MH, Lavedan C, Leroy E, Ide SE, Dehejia A, Dutra A, et al. Mutation in the alpha-synuclein gene identified in families with Parkinson's disease. *Science* (1997) **276**:2045–7. doi:10.1126/science.276.5321.2045
113. Martin LJ, Pan Y, Price AC, Sterling W, Copeland NG, Jenkins NA, et al. Parkinson's disease alpha-synuclein transgenic mice develop neuronal mitochondrial degeneration and cell death. *J Neurosci* (2006) **26**:41–50. doi:10.1523/JNEUROSCI.4308-05.2006
114. Xie W, Chung KK. Alpha-synuclein impairs normal dynamics of mitochondria in cell and animal models of Parkinson's disease. *J Neurochem* (2012) **122**:404–14. doi:10.1111/j.1471-4159.2012.07769.x
115. Bonifati V, Rizzu P, van Baren MJ, Schaap O, Breedveld GJ, Krieger E, et al. Mutations in the DJ-1 gene associated with autosomal recessive early-onset parkinsonism. *Science* (2003) **299**:256–9. doi:10.1126/science.1077209
116. Kitada T, Asakawa S, Hattori N, Matsumine H, Yamamura Y, Minoshima S, et al. Mutations in the parkin gene cause autosomal recessive juvenile parkinsonism. *Nature* (1998) **392**:605–8. doi:10.1038/33416
117. Valente EM, Abou-Sleiman PM, Caputo V, Muqit MM, Harvey K, Gispert S, et al. Hereditary early-onset Parkinson's disease caused by mutations in PINK1. *Science* (2004) **304**:1158–60. doi:10.1126/science.1096284
118. Norremolle A, Riess O, Epplen JT, Fenger K, Hasholt L, Sorensen SA. Trinucleotide repeat elongation in the Huntingtin gene in Huntington disease patients from 71 Danish families. *Hum Mol Genet* (1993) **2**:1475–6. doi:10.1093/hmg/2.9.1475
119. Stoessl AJ, Martin WR, Clark C, Adam MJ, Ammann W, Beckman JH, et al. PET studies of cerebral glucose metabolism in idiopathic torticollis. *Neurology* (1986) **36**:653–7. doi:10.1212/WNL.36.5.653
120. Browne SE, Bowling AC, MacGarvey U, Baik MJ, Berger SC, Muqit MM, et al. Oxidative damage and metabolic dysfunction in Huntington's disease: selective vulnerability of the basal ganglia. *Ann Neurol* (1997) **41**:646–53. doi:10.1002/ana.410410514
121. Gu M, Gash MT, Mann VM, Javoy-Agid F, Cooper JM, Schapira AH. Mitochondrial defect in Huntington's disease caudate nucleus. *Ann Neurol* (1996) **39**:385–9. doi:10.1002/ana.410390317
122. Shirendeb UP, Calkins MJ, Manczak M, Anekonda V, Dufour B, McBride JL, et al. Mutant Huntingtin's interaction with mitochondrial protein Drp1 impairs mitochondrial biogenesis and causes defective axonal transport and synaptic degeneration in Huntington's disease. *Hum Mol Genet* (2012) **21**:406–20. doi:10.1093/hmg/ddr475
123. Weydt P, Soyak SM, Gellera C, Didonato S, Weidinger C, Oberkofler H, et al. The gene coding for PGC-1alpha modifies age at onset in Huntington's disease. *Mol Neurodegener* (2009) **4**:3. doi:10.1186/1750-1326-4-3
124. Shin JH, Ko HS, Kang H, Lee Y, Lee YI, Pletinkova O, et al. PARIS (ZNF746) repression of PGC-1alpha contributes to neurodegeneration in Parkinson's disease. *Cell* (2011) **144**:689–702. doi:10.1016/j.cell.2011.02.010
125. Zheng B, Liao Z, Locascio JJ, Lesniak KA, Roderick SS, Watt ML, et al. PGC-1alpha, a potential therapeutic target for early intervention in Parkinson's disease. *Sci Transl Med* (2010) **2**:52ra73. doi:10.1126/scitranslmed.3001059

126. Tsunemi T, La Spada AR. PGC-1alpha at the intersection of bioenergetics regulation and neuron function: from Huntington's disease to Parkinson's disease and beyond. *Prog Neurobiol* (2012) **97**:142–51. doi:10.1016/j.pneurobio.2011.10.004
127. Warden D. Military TBI during the Iraq and Afghanistan wars. *J Head Trauma Rehabil* (2006) **21**:398–402. doi:10.1097/00001199-200609000-00004
128. McKee AC, Cantu RC, Nowinski CJ, Hedley-Whyte ET, Gavett BE, Budson AE, et al. Chronic traumatic encephalopathy in athletes: progressive tauopathy after repetitive head injury. *J Neuropathol Exp Neurol* (2009) **68**:709–35. doi:10.1097/NEN.0b013e3181a9d503
129. Omalu BI, DeKosky ST, Minster RL, Kamboh MI, Hamilton RL, Wecht CH. Chronic traumatic encephalopathy in a National Football League player. *Neurosurgery* (2005) **57**:128–34. doi:10.1227/01.NEU.0000163407.92769.ED
130. Goodman JC, Valadka AB, Gopinath SP, Uzura M, Robertson CS. Extracellular lactate and glucose alterations in the brain after head injury measured by microdialysis. *Crit Care Med* (1999) **27**:1965–73. doi:10.1097/00003246-199909000-00041
131. Siesjö BK. Pathophysiology and treatment of focal cerebral ischemia. Part I: pathophysiology. *J Neurosurg* (1992) **77**:169–84. doi:10.3171/jns.1992.77.2.0169
132. Tavazzi B, Signoretti S, Lazzarino G, Amorini AM, Delfini R, Cimatti M, et al. Cerebral oxidative stress and depression of energy metabolism correlate with severity of diffuse brain injury in rats. *Neurosurgery* (2005) **56**:582–9. doi:10.1227/01.NEU.0000156715.04900.E6
133. Obrist WD, Langfitt TW, Jaggi JL, Cruz J, Gennarelli TA. Cerebral blood flow and metabolism in comatose patients with acute head injury. Relationship to intracranial hypertension. *J Neurosurg* (1984) **61**:241–53.
134. Arun P, Abu-Taleb R, Oguntayo S, Wang Y, Valiyaveetil M, Long J, et al. Acute mitochondrial dysfunction after blast exposure: potential role of mitochondrial glutamate oxaloacetate transaminase. *J Neurotrauma* (2013) **30**(19):1645–51. doi:10.1089/neu.2012.2834
135. Singleton RH, Zhu J, Stone JR, Povlishock JT. Traumatically induced axotomy adjacent to the soma does not result in acute neuronal death. *J Neurosci* (2002) **22**:791–802.
136. Young W. Role of calcium in central nervous system injuries. *J Neurotrauma* (1992) **9**(Suppl 1):S9–25.
137. Leung AW, Halestrap AP. Recent progress in elucidating the molecular mechanism of the mitochondrial permeability transition pore. *Biochim Biophys Acta* (2008) **1777**:946–52. doi:10.1016/j.bbabi.2008.03.009
138. Fink MP. Bench-to-bedside review: cytopathic hypoxia. *Crit Care* (2002) **6**:491–9. doi:10.1186/cc1824
139. Wada K, Chatzipanteli K, Kraydieh S, Busto R, Dietrich WD. Inducible nitric oxide synthase expression after traumatic brain injury and neuroprotection with aminoguanidine treatment in rats. *Neurosurgery* (1998) **43**:1427–36. doi:10.1227/00006123-199812000-00096
140. Petrov T, Underwood BD, Braun B, Alousi SS, Rafols JA. Upregulation of iNOS expression and phosphorylation of eIF-2alpha are paralleled by suppression of protein synthesis in rat hypothalamus in a closed head trauma model. *J Neurotrauma* (2001) **18**:799–812. doi:10.1089/089771501316919166
141. Sharma P, Benford B, Li ZZ, Ling GS. Role of pyruvate dehydrogenase complex in traumatic brain injury and Measurement of pyruvate dehydrogenase enzyme by dipstick test. *J Emerg Trauma Shock* (2009) **2**:67–72. doi:10.4103/0974-2700.50739
142. Xing G, Ren M, Watson WD, O'Neill JT, Verma A. Traumatic brain injury-induced expression and phosphorylation of pyruvate dehydrogenase: a mechanism of dysregulated glucose metabolism. *Neurosci Lett* (2009) **454**:38–42. doi:10.1016/j.neulet.2009.01.047
143. Barr TL, Conley YP. Poly(ADP-ribose) polymerase-1 and its clinical applications in brain injury. *J Neurosci Nurs* (2007) **39**:278–84. doi:10.1097/01376517-200710000-00004
144. LaPlaca MC, Zhang J, Raghupathi R, Li JH, Smith F, Bareyre FM, et al. Pharmacologic inhibition of poly(ADP-ribose) polymerase is neuroprotective following traumatic brain injury in rats. *J Neurotrauma* (2001) **18**:369–76. doi:10.1089/089771501750170912
145. Won SJ, Choi BY, Yoo BH, Sohn M, Ying W, Swanson RA, et al. Prevention of traumatic brain injury-induced neuron death by intranasal delivery of nicotinamide adenine dinucleotide. *J Neurotrauma* (2012) **29**:1401–9. doi:10.1089/neu.2011.2228

**Conflict of Interest Statement:** The authors declare that the research was conducted in the absence of any commercial or financial relationships that could be construed as a potential conflict of interest.

Received: 29 August 2013; accepted: 26 November 2013; published online: 11 December 2013.

Citation: Khatri N and Man H-Y (2013) Synaptic activity and bioenergy homeostasis: implications in brain trauma and neurodegenerative diseases. *Front. Neurol.* **4**:199. doi: 10.3389/fneur.2013.00199

This article was submitted to *Neurotrauma*, a section of the journal *Frontiers in Neurology*.

Copyright © 2013 Khatri and Man. This is an open-access article distributed under the terms of the Creative Commons Attribution License (CC BY). The use, distribution or reproduction in other forums is permitted, provided the original author(s) or licensor are credited and that the original publication in this journal is cited, in accordance with accepted academic practice. No use, distribution or reproduction is permitted which does not comply with these terms.



# Impact of repeated stress on traumatic brain injury-induced mitochondrial electron transport chain expression and behavioral responses in rats

Guoqiang Xing<sup>1\*\*†</sup>, Erin S. Barry<sup>2†</sup>, Brandi Benford<sup>1</sup>, Neil E. Grunberg<sup>2</sup>, He Li<sup>3</sup>, William D. Watson<sup>4</sup> and Pushpa Sharma<sup>1\*</sup>

<sup>1</sup> Department of Anesthesiology, Uniformed Services University of the Health Sciences, Bethesda, MD, USA

<sup>2</sup> Department of Medical and Clinical Psychology, Uniformed Services University of the Health Sciences, Bethesda, MD, USA

<sup>3</sup> Department of Psychiatry, Uniformed Services University of the Health Sciences, Bethesda, MD, USA

<sup>4</sup> Department of Neurology, Uniformed Services University of the Health Sciences, Bethesda, MD, USA

## Edited by:

Hengye Man, Boston University, USA

## Reviewed by:

Bridgette D. Semple, University of California San Francisco, USA

Joseph Long, Walter Reed Army Institute of Research, USA

## \*Correspondence:

Pushpa Sharma, Department of Anesthesiology, Uniformed Services University of the Health Sciences, 4301 Jones Bridge Road, Bethesda, MD 20814-4799, USA  
e-mail: pushpa.sharma@usuhs.edu

## \*\*Co-Correspondence:

Guoqiang Xing, Department of Anesthesiology, Uniformed Services University of the Health Sciences, 4301 Jones Bridge Road, Bethesda, MD 20814-4799, USA  
e-mail: gxing99@yahoo.com

<sup>†</sup>Guoqiang Xing and Erin S. Barry have contributed equally to this work.

The views expressed in this article are those of the authors and do not necessarily reflect the official policy or position of the Uniformed Services University, Department of the Navy, Department of Defense, nor the U.S. Government.

A significant proportion of the military personnel returning from Iraq and Afghanistan conflicts have suffered from both mild traumatic brain injury (mTBI) and post-traumatic stress disorder. The mechanisms are unknown. We used a rat model of repeated stress and mTBI to examine brain activity and behavioral function. Adult male Sprague-Dawley rats were divided into four groups: Naïve; 3 days repeated tail-shock stress; lateral fluid percussion mTBI; and repeated stress followed by mTBI (S-mTBI). Open field activity, sensorimotor responses, and acoustic startle responses (ASRs) were measured at various time points after mTBI. The protein expression of mitochondrial electron transport chain (ETC) complex subunits (CI-V) and pyruvate dehydrogenase (PDHE1 $\alpha$ 1) were determined in four brain regions at day 7-post mTBI. Compared to Naïves, repeated stress decreased horizontal activity; repeated stress and mTBI both decreased vertical activity; and the mTBI and S-mTBI groups were impaired in sensorimotor and ASRs. Repeated stress significantly increased CI, CII, and CIII protein levels in the prefrontal cortex (PFC), but decreased PDHE1 $\alpha$ 1 protein in the PFC and cerebellum, and decreased CIV protein in the hippocampus. The mTBI treatment decreased CV protein levels in the ipsilateral hippocampus. The S-mTBI treatment resulted in increased CII, CIII, CIV, and CV protein levels in the PFC, increased CI level in the cerebellum, and increased CIII and CV levels in the cerebral cortex, but decreased CI, CII, CIV, and PDHE1 $\alpha$ 1 protein levels in the hippocampus. Thus, repeated stress or mTBI alone differentially altered ETC expression in heterogeneous brain regions. Repeated stress followed by mTBI had synergistic effects on brain ETC expression, and resulted in more severe behavioral deficits. These results suggest that repeated stress could have contributed to the high incidence of long-term neurologic and neuropsychiatric morbidity in military personnel with or without mTBI.

**Keywords:** oxidative phosphorylation, mitochondria, electron transport chain, behavior change, TBI, PTSD

## INTRODUCTION

Estimates as high as 24% of U.S. military personnel returning from Iraq and Afghanistan battlefields have suffered from a mild traumatic brain injury (mTBI) and/or post-traumatic stress disorder (PTSD) (1–5). Comorbidity of mTBI and PTSD are also high among this sub-population (3). Despite the numbers of cases, dedicated resources and research, and marked concern about these conditions, minimal progress has been made toward understanding the biological mechanisms producing these pathologies.

The brain is the organ of glucose metabolism and adenosine triphosphate (ATP) utilization, which expresses our essence, our nature, and is solely responsible for our behavioral and psychological functions to help define who we are. Dysregulated brain energy metabolism (i.e., acute hyperglycemia during the early phase of TBI and subsequent hypoglycemia during the chronic

phase of TBI) is a metabolic characteristic of TBI that is associated with symptom severity and poor prognosis for functional recovery from TBI (6–9).

Pyruvate dehydrogenase (PDH) is the rate-limiting enzyme that irreversibly transfers the glycolysis product pyruvate into acetyl-coenzyme A (CoA) for efficient production of nicotinamide adenine dinucleotide (NADH) and ATP through mitochondrial tricarboxylic acid (TCA) cycle and oxidative phosphorylation pathway (OXPHOS). OXPHOS is mediated by mitochondrial electron transport chain (ETC) complex subunits (CI, CII, CIII, CIV, and CV).

Mitochondrial ETC generate ATP by coupling electron transfer between electron donors (i.e., NADH) and the electron acceptor (O<sub>2</sub>) with the transfer of protons (H<sup>+</sup>) across the membrane to generate energy in the form of ATP. Complex I (CI, NADH

dehydrogenase) and Complex II (CII, succinate dehydrogenase flavoprotein) accept and transfer electrons to coenzyme Q which sequentially transfers electrons to Complex III (CIII, cytochrome reductase), cytochrome *c*, and Complex IV (CIV, cytochrome oxidase), where oxygen is the terminal acceptor. Complex V (CV) couples proton gradients to ATP synthesis, allowing proton flow from inter-membrane space to the matrix via a special enzyme, converting ADP to ATP.

We previously reported that the PDH pathway is altered in animal models of TBI (10–13). Complex abnormalities in ETC have also been found in many neurological diseases (14–16), yet its potential involvement in combined TBI and stress is unknown. Because aberrant ETC complex activities are the primary source of intracellular reactive oxygen species (ROS), alterations in ETC complexes could lead to increased ROS production, inflammation, impaired signal transduction, mitochondrial damage, and cell death, thus compromising brain vulnerability to subsequent stress and injuries.

Brain energy metabolism is also disrupted during traumatic stress. Under life-threatening situations, energy reserves are intensively mobilized for fight-or-flight response via sympathetic activation and epinephrine/norepinephrine release. This reaction increases cardiovascular output, aerobic supply, fear memory, visual and auditory sensitivity, alertness, vigilance, and selective attention that are essential for survival (17–19). However, potential metabolic over-reactivity meant to increase survivability in an emergent situation has long-lasting deleterious effects that may compromise the brain's response to subsequent injuries.

The main goal of this study was to determine if prior repeated stress altered TBI-induced brain ETC expression and behavioral functions. We hypothesized that the combination of repeated stress followed by mTBI could affect brain ETC complex expression in a way that is different from repeated stress or mTBI alone. We included measures of behavioral and psychological unconditioned responses (i.e., activity, sensorimotor responses, acoustic startle reflexes, and measures of depression-related behavior) to determine whether the repeated stress has functional effects in addition to changes to mitochondrial expression. Rat fluid percussion (FP) was used to create mTBI and repeated stress was used to model PTSD.

## MATERIALS AND METHODS

### ANIMALS AND EXPERIMENTAL GROUPS

Adult, male Sprague-Dawley rats (175–275 g) were obtained from Harlan Laboratories (Indianapolis, IN, USA). All procedures were performed in accordance with guidelines of the National Institutes of Health and were approved by the Institutional Animal Care and Use Committee (IACUC) at the Uniformed Services University of the Health Sciences (USUHS). Rats were pair housed in standard polycarbonate shoebox cages (42.5 cm × 20.5 cm × 20 cm) with hardwood chip bedding (Pine-Dri) and kept on a 12-h reversed light-dark cycle, with food (Harlan Teklad 4% Mouse/Rat Diet 7001) and water continuously available. All animals were weighed just before the experiment (T0) and at the end of the experiment (T7) as a measure of their general health. Rats were given coded tail numbers and assigned randomly to experimental groups after 1 day of acclimation to the environment [Naïve, Stress, mTBI, and

mTBI with prior stress (S-mTBI)]. For behavioral analyses, a total of 54 rats were used in this experiment (Naïve = 16; Stress = 12; mTBI = 16; S-mTBI = 10). In the case of the S-mTBI animals, the stress was given for 3 consecutive days and then mTBI was administered within 24 h. This group originally had 12 animals, but 2 died during the TBI surgery. Necropsies of these animals by Laboratory of Animal Medicine (LAM) personnel found no identifiable cause, including infection, for these deaths. At day 7-post injury, animals were sedated under isoflurane anesthesia, and tissues were collected. Brain tissue from eight animals of each treatment group was dissected for biological analysis.

### INDUCTION OF FLUID PERCUSSION INJURY

Mild traumatic brain injury was induced in rats according to our published procedure (13). In brief, animals were anesthetized with 1–3% isoflurane in oxygen. Under sterile conditions, a 3-cm sagittal incision was made along the midline to expose the cranium. A 5-mm burr hole was placed 2 mm to the right of the sagittal suture halfway between bregma and lambda using a 5-mm trephine drill bit exposing the dura. A Luer-Lock needle hub was placed into the burr hole and cemented to the cranium using cyanoacrylate. The glue was allowed to completely dry, and the empty Luer-Lock hub was filled with normal saline before being connected to the TBI device. A FP pulse of 2.5 atm was administered by an injury cannula positioned parasagittally over the right cerebral cortex. The FP pulse was administered by a pendulum modulated FP biomechanical device (Richmond, VA, USA). The Luer-Lock hub was removed and defects in the cranium were repaired with bone wax. The skin was closed with a surgical skin stapler. Animals were allowed to stabilize in the warm blanket before returned to their home cages. At 7 days post mTBI, animals were sacrificed under anesthetization, and brains were removed followed by the dissection of prefrontal cortex (PFC), cerebellum, and the ipsilateral and contralateral of mTBI hippocampus and cerebral cortex.

### REPEATED TAIL-SHOCK STRESS PROCEDURE

This paradigm was chosen because it has previously demonstrated that repeated immobilization and tail-shock stress sessions are more effective than a single stress session in producing physiological and behavioral abnormalities, such as elevations in basal plasma corticosterone levels and delayed exaggerated acoustic startle responses (ASRs) are similar to symptoms observed in PTSD patients (20–25). This restraint tail-shock model of stress in rats is adapted from the “learned helplessness” paradigm in which animals undergo an aversive experience under conditions in which they cannot perform any adaptive response (26). The stress procedure consisted of a 2-h per day session of immobilization and tail shocks over 3 consecutive days. Stressed animals were restrained in a Plexiglas tube and given 40 electric tail shocks (2 mA, 3 s duration) at varying intervals (140–180 s). Animals were returned to their home cages immediately after exposure to the stress procedure.

### ANIMAL BEHAVIORAL MEASURES

Behavior was observed during the animals' dark cycle (i.e., during their active period). All animals underwent behavioral evaluation prior to stress and/or injury (baseline), and at two other



time points during the week after injury. Behavioral measures included: open field activity (OFA) to measure general health and depression-related behaviors; neurobehavioral testing [revised neurobehavioral severity scale (NSS-R)] to measure sensory-motor functioning; and ASR with and without pre-pulse to measure startle and attention.

### OPEN FIELD ACTIVITY

Open field activity was measured using Accuscan Superflex Sensor Version 2.2 infrared photocell system in the Accuscan Instruments testing chamber (measuring 40 cm × 40 cm × 30 cm; Accuscan Instruments Incorporated, Columbus, OH, USA) located in a dedicated room designed to minimize acoustic interruptions. The testing chamber was constructed of Plexiglas with a ventilated, removable Plexiglas lid that prevents the animal's escape during the trial but allows adequate airflow. The animal's locomotion was captured by three, paired 16-photocell Superflex Sensors, which transmit the location data to the Accuscan Superflex Node which was processed and aggregated by Accuscan Fusion Software (Version 3.4). Animals were acclimated to the chambers prior to the beginning of the experiment. They then received a baseline measurement prior to injury and/or stress and were measured at days 3 and 5 post injury. The OFA of each rat was measured for 1 h during its active period (dark cycle).

### REVISED NEUROBEHAVIORAL SEVERITY SCALE

The NSS-R is a specific, continuous sequence of behavioral tests and observations that is a sensitive and reliable measure in rodents (27, 28). This measure was originally designed to model a clinical neurological exam conducted in patients. This particular sensory-motor assessment scale was based on several previous reports (29–32) and has been modified to increase standardization. The tests assess reflex suppression, general movement, and postural adjustments in response to a challenge. The NSS-R uses a three-point Likert scale, in which a normal, healthy response is assigned a “0,” a partial or compromised response is assigned a “1,” and the absence of a response is assigned a “2.” This three-point scale is clear and reliable and allows for greater discrimination based on sensory-motor responses than do previous scales that used two-point ratings of each response. The NSS-R has a scoring range of 0–20 with higher scores reflecting greater extent of injury. Three NSS-R sessions were conducted in this experiment as a within-subject measure: one before stress/injury (baseline) and two after injury (days 3 and 5).

### ACOUSTIC STARTLE RESPONSE WITH AND WITHOUT PRE-PULSE

Acoustic startle responses with and without pre-pulse were measured in a Med Associates Acoustic Response Test System (Med Associates, Georgia, VT, USA). The Test System consists of weight-sensitive platforms inside individual sound-attenuated chambers. Responses were recorded by an interfaced Nexlink computer. Each rat was placed individually in a ventilated holding cage (small enough to restrict extensive locomotion but large enough to allow the subject to turn around and make other small movements) on the weight-sensitive platform. Following placement of animals in the chambers, a 3-min acclimation period was conducted, in which no startle stimuli were presented. Startle stimuli consisted of 110

or 120 dB noise bursts of 20 ms duration sometimes preceded by a 100-ms, 68 or 82 dB, 1 kHz pure tones (pre-pulses). Intensity of sound in decibel was verified by a Larson-Davis Sound Pressure Machine Model 2800 (unweighted scale; re: 0.0002 dyn/cm<sup>2</sup>). Each startle stimulus had a 0-ms rise and decay time so that onset and offset were abrupt. There were multiple types of stimulus trials, and each trial type was presented six times and averaged. Trial types were presented in random order to avoid order effects and habituation. Animals' movements in response to stimuli were measured as a voltage change by a strain gage inside each platform. Animals were acclimated to the chambers twice prior to the beginning of the experiment. They then received a baseline measurement prior to injury/stress and were measured at days 4 and 6 post injury.

### WESTERN BLOT

Brain tissue homogenates from four brain regions (prefrontal cortex, cerebellum, hippocampus, and cerebral cortex) were homogenized and sonicated in the T-Per tissue lysis buffer (Pierce, IL) in the presence of protease inhibitor cocktail (Sigma, St. Louis). For the mTBI and S-mTBI animals, ipsilateral and contralateral hippocampus, and cerebral cortex were dissected and processed respectively. Protein concentrations were determined using a Bradford assay (BioRad, CA, USA). Aliquots of 20 µg proteins were separated by electrophoresis on NuPage Novex Midi Bis-Tris gels (4–12%) and transferred to a polyvinylidene difluoride membrane (PVDF), Millipore. The membranes were rinsed in a 0.01-M Tris-buffered saline (TBS) solution (pH 7.4, 0.1% Triton X-100) for 30 min, blocked in 5% bovine serum albumin for 30 min, and incubated overnight at 4°C with the primary mouse monoclonal antibodies for ETC complex subunits CI-V and PDHE1α1 (Abcam, UK) at a dilution of 1:200, each in a TBS solution containing 3% bovine serum albumin. The membranes were then washed three times with TBS solution for 30 min and incubated at room temperature with a horseradish peroxidase-conjugated secondary anti-mouse antibody (1:5000 dilution) in TBS solution for 60 min.

Due to the lack of an appropriate housekeeping mitochondrial protein (33, 34), WB band intensity was expressed as fold change relative to naïves, but was not normalized to an internal control. However, we took extra steps to normalize our data by (1) loading the equal amount of protein for each sample; (2) all samples were processed, loaded, and run in parallel, and (3) transfer efficiency of proteins to the PVDF membrane was confirmed by staining with Ponceau solution. Immunoreactive bands were visualized using enhanced chemiluminescence Western blotting detection reagents (GE Healthcare Bio-Sciences Corp, Piscataway, NJ, USA). The western blots were captured with a digital camera and the intensities of protein bands were quantified with NIH Image 1.62.

### STATISTICAL ANALYSIS

For behavioral data, repeated measures analyses of variance (rANOVA; to assess for overall main effects for Time, Group, Injury, Drug, and any interactions) and analysis of variance (ANOVA; to assess for main effects of Group, Injury, Drug, and any interactions at each time point) were conducted for each of the dependent variables. Baseline measurements were used as a covariate to account for any baseline differences. Pairwise

comparisons were performed where appropriate. OFA scores were separated into two subscales: horizontal activity (HA) and vertical activity (VA). Analyses for all measures except for OFA included data for all subjects ( $N = 54$ ). The OFA included a subset of the subjects ( $N = 46$ ) because of an equipment malfunction during one cohort of eight subjects. Cohorts were similar among experimental groups; therefore, the remaining data are representative of all experimental conditions. All tests were two tailed using  $\alpha = 0.05$ . Data analyses were performed at the conclusion of the project, after all measurements were collected.

Mitochondrial complex I-V and PDHE1 $\alpha$ 1 protein expression levels were analyzed for each brain region (prefrontal cortex, cerebellum, and contralateral and ipsilateral hippocampus and cerebral cortex) using a one-way ANOVA followed by LSD multiple comparison. A  $p$ -value  $< 0.05$  was considered statistically significant.

## RESULTS

In reference to the weight gain in the groups the following was observed. The mTBI animals gained only 2.7% of the baseline weight ( $p < 0.05$ ), while the stressed animals gained significantly more both with mTBI at 10.8% and without mTBI at 11.9% ( $p < 0.001$ ). Naïve animals also gained a significant amount of weight at 7.5% in comparison to the baseline, but less than the stressed rats. The behavioral and western blot analysis quantification was not conducted in a blinded fashion.

### BEHAVIORAL FUNCTIONAL OUTCOMES

#### Open field activity

Open field activity measures naturally occurring behaviors exhibited when an animal explores and interacts with its surroundings. These measures provide reliable and valuable data about gross motor and specific movements related to psychological conditions such as anxiety-related and depressive-related behaviors (35–38). For the purposes of this experiment, two variables were extracted from the animal's movement within the chambers: HA and VA. **Figure 1A** presents HA (an index of general health and movement) of the animals. Overall, there was a main effect for Group,  $F(3,40) = 6.00$ ,  $p < 0.01$ ,  $\eta^2 = 0.31$ , such that Naïve animals had significantly more activity overall than did the S-mTBI animals. There was a main effect for Stress,  $F(1,40) = 16.25$ ,  $p < 0.001$ ,  $\eta^2 = 0.29$ , such that the non-stressed animals had significantly more activity overall than did the stressed animals. There also was a significant Time  $\times$  Stress Interaction,  $F(1,40) = 4.13$ ,  $p < 0.05$ ,  $\eta^2 = 0.09$ . At 3 days post injury, there was a main effect for Group,  $F(3,40) = 5.83$ ,  $p < 0.01$ ,  $\eta^2 = 0.30$ , such that the Naïve animals had significantly more activity than did the Stress animals and the S-mTBI animals. There also was a main effect for Stress,  $F(1,40) = 16.38$ ,  $p < 0.001$ ,  $\eta^2 = 0.29$ , such that the non-stressed animals had significantly more activity than did the stressed animals. At day 5 post injury, there was a main effect for Group,  $F(3,40) = 4.38$ ,  $p < 0.01$ ,  $\eta^2 = 0.25$ , such that Naïve animals had significantly more activity than did S-mTBI animals. There also was a main effect for Stress,  $F(1,40) = 10.58$ ,  $p < 0.01$ ,  $\eta^2 = 0.21$ , such that the non-stressed animals had significantly more activity than did the stressed animals.

**Figure 1B** presents VA (an index of depression-related behaviors; where less VA indicates more depression-related behaviors)

of the animals. Overall, there was a main effect for Group,  $F(3,40) = 6.46$ ,  $p < 0.001$ ,  $\eta^2 = 0.32$ , such that Naïve animals had significantly more VA than did S-mTBI animals and Stress animals. There was a main effect for Injury,  $F(1,40) = 7.91$ ,  $p < 0.01$ ,  $\eta^2 = 0.16$ , such that non-injured animals had significantly more VA than did the TBI animals. There was a main effect for Stress,  $F(1,40) = 13.18$ ,  $p < 0.001$ ,  $\eta^2 = 0.25$ , such that non-stressed animals had significantly more VA than did the stressed animals. There also was a significant Time  $\times$  Group Interaction,  $F(3,40) = 6.73$ ,  $p < 0.001$ ,  $\eta^2 = 0.33$ , a Time  $\times$  Injury Interaction,  $F(1,40) = 9.08$ ,  $p < 0.01$ ,  $\eta^2 = 0.19$ , and a Time  $\times$  Injury  $\times$  Stress Interaction,  $F(1,40) = 10.17$ ,  $p < 0.01$ ,  $\eta^2 = 0.20$ . At day 3 post injury, there was a main effect for Group,  $F(3,40) = 7.61$ ,  $p < 0.001$ ,  $\eta^2 = 0.36$ , such that Naïve animals had significantly more VA than did mTBI animals, Stress animals, and the S-mTBI animals. There was a main effect for Injury,  $F(1,40) = 11.81$ ,  $p = 0.001$ ,  $\eta^2 = 0.23$ , such that non-injured animals had significantly more VA than did the TBI animals. There also was a main effect for Stress,  $F(1,40) = 13.34$ ,  $p < 0.001$ ,  $\eta^2 = 0.25$ , such that non-stressed animals had significantly more VA than did stressed animals. At 5 days post injury, there was a main effect for Group,  $F(3,40) = 5.07$ ,  $p < 0.01$ ,  $\eta^2 = 0.27$ , such that Naïve animals had significantly more VA than did S-mTBI animals. There also was a main effect for Stress,  $F(1,40) = 10.54$ ,  $p < 0.01$ ,  $\eta^2 = 0.21$ , such that non-stressed animals had significantly more VA than did stressed animals.

#### Revised neurobehavioral severity scale

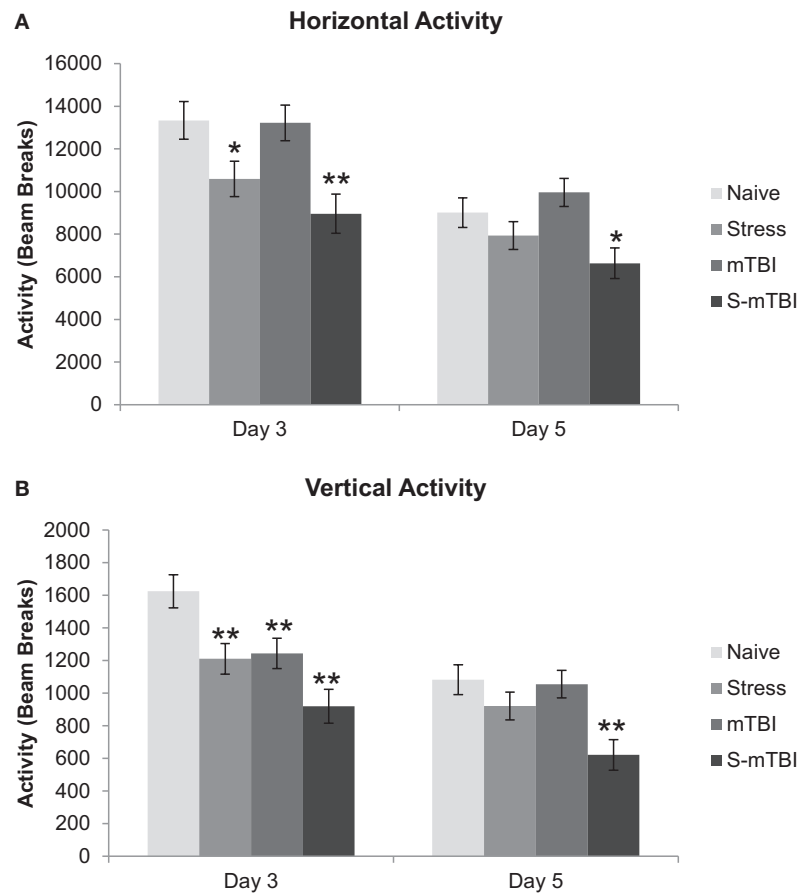
The NSS-R is a sensitive and reliable measure of sensory-motor responses in rodents (27, 28, 39). This measure models a clinical neurological exam of human patients and was based on several previous reports (29–32).

**Figure 2** presents the neurobehavioral severity data (NSS-R; where higher scores indicate more sensorimotor functional impairment) of the animals. Overall, there was a main effect for Group,  $F(3,49) = 5.99$ ,  $p < 0.001$ ,  $\eta^2 = 0.27$ , such that Naïve animals had significantly lower NSS-R scores than did mTBI animals. There also was a main effect for Injury,  $F(1,49) = 14.97$ ,  $p < 0.001$ ,  $\eta^2 = 0.23$ , such that non-injured animals had significantly lower NSS-R scores than did TBI animals. Similarly, at 3 days post injury, there was a main effect for Group,  $F(3,49) = 4.23$ ,  $p < 0.01$ ,  $\eta^2 = 0.21$ , such that Naïve animals had significantly lower NSS-R scores than did mTBI animals. There also was a main effect for Injury,  $F(1,49) = 10.53$ ,  $p < 0.01$ ,  $\eta^2 = 0.18$ , such that non-injured animals had significantly lower NSS-R scores than did TBI animals. At 5 days post injury, there was a main effect for Group,  $F(3,49) = 4.72$ ,  $p < 0.01$ ,  $\eta^2 = 0.22$ , such that Naïve animals had significantly lower NSS-R scores than did mTBI animals and S-mTBI animals. There also was a main effect for Injury,  $F(1,49) = 10.09$ ,  $p < 0.01$ ,  $\eta^2 = 0.17$ , such that non-injured animals had significantly lower NSS-R scores than did TBI animals.

#### Acoustic startle response with and without pre-pulse

The ASR with and without pre-pulse are whole body behavioral responses believed to index information processing (40) and possibly attention (41–43).

**Figure 3A** presents the ASR data with a tone of 110 dB. Overall, there was a main effect for Time,  $F(1,49) = 9.41$ ,  $p < 0.01$ ,



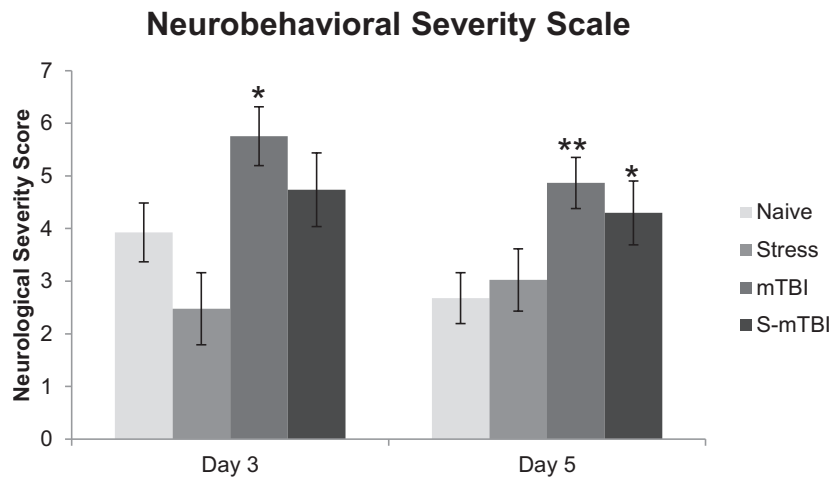
**FIGURE 1 | Effects of stress, mTBI, or the combination on open field activity.** Activity was measured for 60 min at baseline (BL), and 3 and 5 days post injury and the number of beam breaks was collected. **(A)** Horizontal activity (measure of general health and movement) of the animals throughout

the experiment. **(B)** Vertical activity (measure of depression-related behavior) of the animals throughout the experiment. Vertical activity measurement post injury was covaried for baseline measurements due to differences at baseline between groups. \* $p < 0.05$ , \*\* $p < 0.01$  vs. Naïves, respectively.

$\eta^2 = 0.16$ , such that animals 4 days post injury had significantly lower startle to the tone than did animals at 6 days post injury. There also was a main effect for Group,  $F(3,49) = 9.21$ ,  $p < 0.001$ ,  $\eta^2 = 0.36$ , such that Naïve animals had significantly higher startle to the tone than did mTBI animals and S-mTBI animals. There was a main effect for Injury,  $F(1,49) = 23.29$ ,  $p < 0.001$ ,  $\eta^2 = 0.32$ , such that non-injured animals had higher startle responses than did TBI animals. There also was a significant Time  $\times$  Stress Interaction,  $F(1,49) = 6.88$ ,  $p < 0.050$ ,  $\eta^2 = 0.12$ . At 4 days post injury, there was a main effect for Group,  $F(3,49) = 7.25$ ,  $p < 0.001$ ,  $\eta^2 = 0.31$ , such that Naïve animals had significantly more startle to the tone than did mTBI animals and S-mTBI animals. There also was a main effect for Injury,  $F(1,49) = 20.00$ ,  $p < 0.001$ ,  $\eta^2 = 0.29$ , such that non-injured animals had significantly higher startle to the tone than did TBI animals. At 6 days post injury, there was a main effect for Group,  $F(3,49) = 8.42$ ,  $p < 0.001$ ,  $\eta^2 = 0.34$ , such that Naïve animals had significantly higher startle to the tone than did Stress animals, mTBI animals, and S-mTBI animals. There was a main effect for Injury,  $F(1,49) = 18.25$ ,  $p < 0.001$ ,  $\eta^2 = 0.27$ , such that non-injured animals had more startle to the tone than did TBI animals. There also was a main effect for Stress,  $F(1,49) = 6.40$ ,

$p < 0.050$ ,  $\eta^2 = 0.12$ , such that non-stressed animals had more startle to the tone than stressed animals.

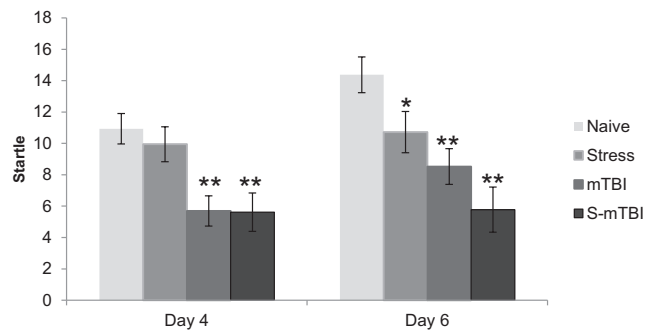
**Figure 3B** represents the ASR data with a tone of 110 dB and a pre-pulse of 68 dB (heard 100 ms before the tone). Similar results were found here as with the 110-dB tone alone. Overall, there was a main effect for Time,  $F(1,49) = 4.66$ ,  $p < 0.05$ ,  $\eta^2 = 0.09$ , such that animals at 4 days post injury had significantly less startle than animals at 6 days post injury. There was a main effect for Group,  $F(3,49) = 15.15$ ,  $p < 0.001$ ,  $\eta^2 = 0.48$ , such that Naïve animals had significantly more startle than did Stress animals, mTBI animals, and S-mTBI animals. There was a main effect for Injury,  $F(1,49) = 37.79$ ,  $p < 0.001$ ,  $\eta^2 = 0.44$ , such that non-injured animals had significantly more startle than did TBI animals. There was a main effect for Stress,  $F(1,49) = 5.77$ ,  $p < 0.050$ ,  $\eta^2 = 0.11$ , such that non-stressed animals had significantly more startle than did stressed animals. There also was a significant Time  $\times$  Stress Interaction,  $F(1,49) = 6.99$ ,  $p < 0.050$ ,  $\eta^2 = 0.13$ . At 4 days post injury, there was a main effect for Group,  $F(3,49) = 11.85$ ,  $p < 0.001$ ,  $\eta^2 = 0.42$ , such that Naïve animals had significantly more startle than did mTBI animals and S-mTBI animals. There also was a main effect for Injury,  $F(1,49) = 32.73$ ,  $p < 0.001$ ,  $\eta^2 = 0.40$ , such



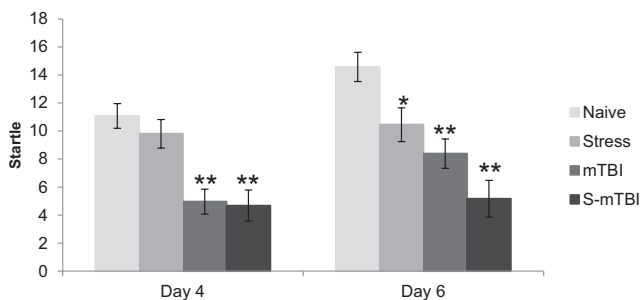
**FIGURE 2 | Effects of stress, mTBI, or the combination on neurobehavioral function.** Neurobehavioral severity was determined by using a 10-item test with a score of 0, 1, 2, on each given task. Higher scores indicate more neurobehavioral impairment. Animals were tested

at baseline (BL), and 3 and 5 days post injury. Neurobehavioral assessment post injury was covaried for baseline measurements due to differences at baseline between groups. \* $p < 0.05$ , \*\* $p < 0.01$  vs. Naïves, respectively.

### A Acoustic Startle Response (110 dB)

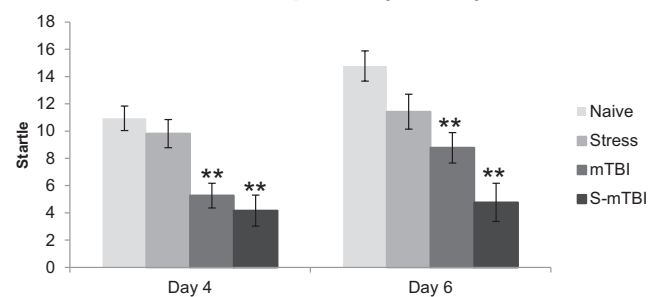


### B Acoustic Startle Response (110 dB) with Prepulse (68 dB)



**FIGURE 3 | Effects of stress, mTBI, or the combination on acoustic startle response (ASR) with and without pre-pulse (a measure of attention).** (A) ASR at 110 dB alone throughout the experiment. (B) ASR at 110 dB with a 68-dB pre-pulse throughout

### C Acoustic Startle Response (110 dB) with Prepulse (82 dB)



the experiment. (C) ASR at 110 dB with an 82-dB pre-pulse throughout the experiment. Animals were measured at baseline (BL), and at 4 and 6 days post injury. \* $p < 0.05$ , \*\* $p < 0.01$  vs. Naïves, respectively.

that non-injured animals had significantly more startle than did TBI animals. At 6 days post injury, there was a main effect for group,  $F(3,49) = 11.81$ ,  $p < 0.001$ ,  $\eta^2 = 0.42$ , such that Naïve animals had significantly more startle than did stress animals, mTBI animals, and S-mTBI animals. There was a main effect for Injury,  $F(1,49) = 24.59$ ,  $p < 0.001$ ,  $\eta^2 = 0.33$ , such that non-injured animals had significantly more startle than did TBI animals. There also was a main effect for Stress,  $F(1,49) = 10.02$ ,  $p < 0.01$ ,  $\eta^2 = 0.17$ , such that non-stressed animals had significantly more startle than did stressed animals.

**Figure 3C** represents the ASR data with a tone of 110 dB and a pre-pulse of 82 dB (heard 100 ms before the tone). Similar results were found here as with the 110-dB tone alone. Overall, there was a main effect for Time,  $F(1,49) = 7.18$ ,  $p < 0.01$ ,  $\eta^2 = 0.13$ , such that animals at 4 days post injury had significantly less startle than animals at 6 days post injury. There was a main effect for Group,  $F(3,49) = 15.03$ ,  $p < 0.001$ ,  $\eta^2 = 0.48$ , such that Naïve animals had significantly more startle than did mTBI animals and S-mTBI animals. There was a main effect for Injury,  $F(1,49) = 39.10$ ,  $p < 0.001$ ,  $\eta^2 = 0.44$ , such that non-injured animals had significantly more startle than did TBI animals. There was a main effect for Stress,  $F(1,49) = 6.27$ ,  $p < 0.05$ ,  $\eta^2 = 0.11$ , such that non-stressed animals had significantly more startle than did stressed animals. There also was a significant Time  $\times$  Stress Interaction,  $F(1,49) = 4.80$ ,  $p < 0.05$ ,  $\eta^2 = 0.090$ . At 4 days post injury, there was a main effect for Group,  $F(3,49) = 11.31$ ,  $p < 0.001$ ,  $\eta^2 = 0.41$ , such that Naïve animals had significantly more startle than did mTBI animals and S-mTBI animals. There also was a main effect for Injury,  $F(1,49) = 32.01$ ,  $p < 0.001$ ,  $\eta^2 = 0.40$ , such that non-injured animals had significantly more startle than did TBI animals. At 6 days post injury, there was a main effect for Group,  $F(3,49) = 11.42$ ,  $p < 0.001$ ,  $\eta^2 = 0.41$ , such that Naïve animals had significantly more startle than did mTBI animals and S-mTBI animals. There was a main effect for Injury,  $F(1,49) = 26.17$ ,  $p < 0.001$ ,  $\eta^2 = 0.35$ , such that non-injured animals had significantly more startle than did TBI animals. There also was a main effect for Stress,  $F(1,49) = 8.90$ ,  $p < 0.01$ ,  $\eta^2 = 0.15$ , such that non-stressed animals had significantly more startle than did stressed animals. Similar results were found with 120 dB with and without pre-pulses (data not shown).

## WESTERN BLOT DATA

### Prefrontal cortex

Expression levels of mitochondrial proteins in Stress and mTBI groups was reduced, whereas S-mTBI increased PDHE1 $\alpha$ 1 protein level in the prefrontal cortex (**Figure 4**). One-way ANOVA revealed significant effects of repeated stress and mTBI treatment on ETC CI ( $p < 0.05$ ), CII ( $p < 0.05$ ), CIII ( $p < 0.05$ ), CIV ( $p < 0.01$ ), CV ( $p < 0.05$ ), and PDHE1 $\alpha$ 1 ( $p < 0.05$ ) protein levels (**Figure 5**). LSD *post hoc* showed that when compared with Naïves, Stress, and S-mTBI animals had significant enhancing effects on CI, CII, and CIII. S-mTBI animals also had enhancing effects on CIV and CV protein levels. In contrast, mTBI treatment alone did not affect ETC subunit expression in the prefrontal cortex.

### Cerebellum

One-way ANOVA showed significant effects of Stress and S-mTBI on cerebellar CI ( $p < 0.05$ ), CV ( $p < 0.05$ ) and PDHE1 $\alpha$ 1

( $p < 0.05$ ) expression in rat cerebellum (**Figures 4 and 6**). LSD *post hoc* showed that when compared with Naïves, cerebellar CI protein level increased significantly ( $p < 0.05$ ) whereas CV protein level decreased at a trend level ( $p < 0.01$ ) in S-mTBI-treated animals. Cerebellar PDHE1 $\alpha$ 1 protein level decreased in the Stress and mTBI groups compared to the Naïve group.

### Hippocampus

One-way ANOVA showed significant effects of Stress, mTBI, and S-mTBI on CI ( $p < 0.05$ ), CII ( $p < 0.05$ ), CIV ( $p < 0.05$ ), CV ( $p < 0.01$ ), and PDHE1 $\alpha$ 1 ( $p < 0.05$ ) protein levels in the hippocampus. LSD *post hoc* showed that, when compared with the Naïve hippocampus, CI and CII proteins in the contralateral and ipsilateral hippocampus of the S-mTBI animals decreased significantly. Complex IV protein levels in the hippocampus of Stress animals and contralateral hippocampus of S-mTBI animals, as well as CV protein level in the ipsilateral hippocampus of mTBI animals also decreased significantly. PDHE1 $\alpha$ 1 protein level in the ipsilateral hippocampus of S-mTBI animals also decreased significantly ( $p < 0.01$ ) (**Figures 4 and 7**).

### Cerebral cortex

One-way ANOVA showed significant effects of TBI treatment on CIII ( $p < 0.05$ ), CIV ( $p < 0.05$ ), CV ( $p < 0.01$ ), and PDHE1 $\alpha$ 1 ( $p < 0.01$ ) protein expression in the cerebral cortex (**Figures 4 and 8**). LSD *post hoc* revealed that when compared with the Naïve group, CIII protein level was significantly higher in the contralateral and ipsilateral cortex of S-mTBI animals ( $p < 0.05$ ), CIV protein level was significantly lower in the ipsilateral cortex of mTBI animals ( $p < 0.05$ ), and CV protein level was significantly higher in the cortex of S-mTBI animals ( $p < 0.05$ ). PDHE1 $\alpha$ 1 was significantly higher in the contralateral cortex of mTBI animals ( $p < 0.05$ ) but lower in the ipsilateral cortex of mTBI ( $p < 0.05$ ) and S-mTBI animals ( $p < 0.01$ ).

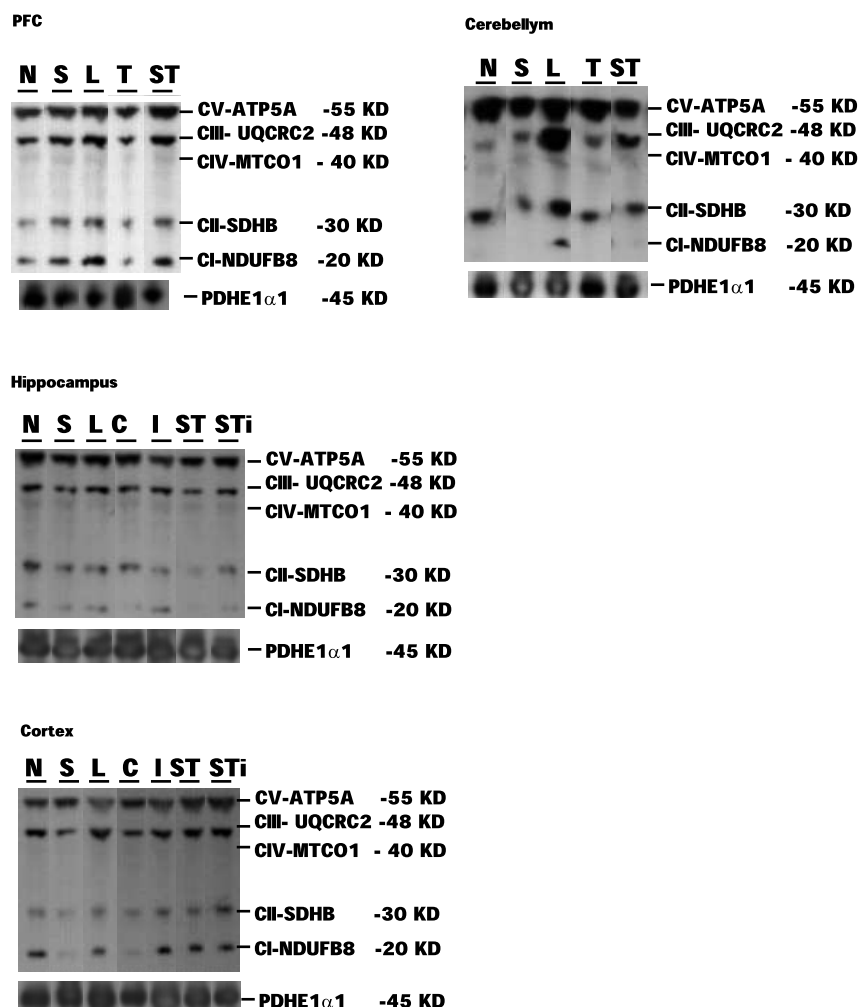
## DISCUSSION

The prevalence of post-concussive syndrome associated with increased anxiety and memory deficit are particularly high among military casualties of the Iraq and Afghanistan wars (5). The role of psychological stress in the battlefield is very important on the outcome of TBI. Currently, the overlapping depressive symptomatology of PTSD and mTBI present a major diagnostic challenge and dilemma for clinicians. In this study, we have dissected the neurobehavioral symptoms and altered brain metabolic pathways following stress or mTBI alone, and combined effect of stress and mTBI in rats. The key findings of this study are (1) animal exposure to the repeated stress or mTBI alone resulted in an early and short term increase in anxiety and impaired memory, (2) these symptoms persisted for a long time in animals with combined stress and mTBI, and (3) abnormal mitochondrial ETC and PDH enzyme expressions in different parts of the brain were seen in all animals with stress with or without brain injury confirming the altered cellular metabolic pathways due to stress or mTBI (44, 45).

### BEHAVIORAL EFFECTS OF STRESS, mTBI, OR STRESS WITH mTBI

The presence of repeat stress in our rat model had little effect on sensorimotor responses, but significant decrease in startle





**FIGURE 4 | Representative samples of Western blotting of CI, CII, CIII, CIV, CV, and PDHE1 $\alpha$ 1 protein bands in the tissue homogenates of rat prefrontal cortex (PFC), cerebellum, hippocampus, and cerebral cortex collected at 7 days post mTBI. Contralateral and ipsilateral hippocampus and cerebral cortex were collected for mTBI and**

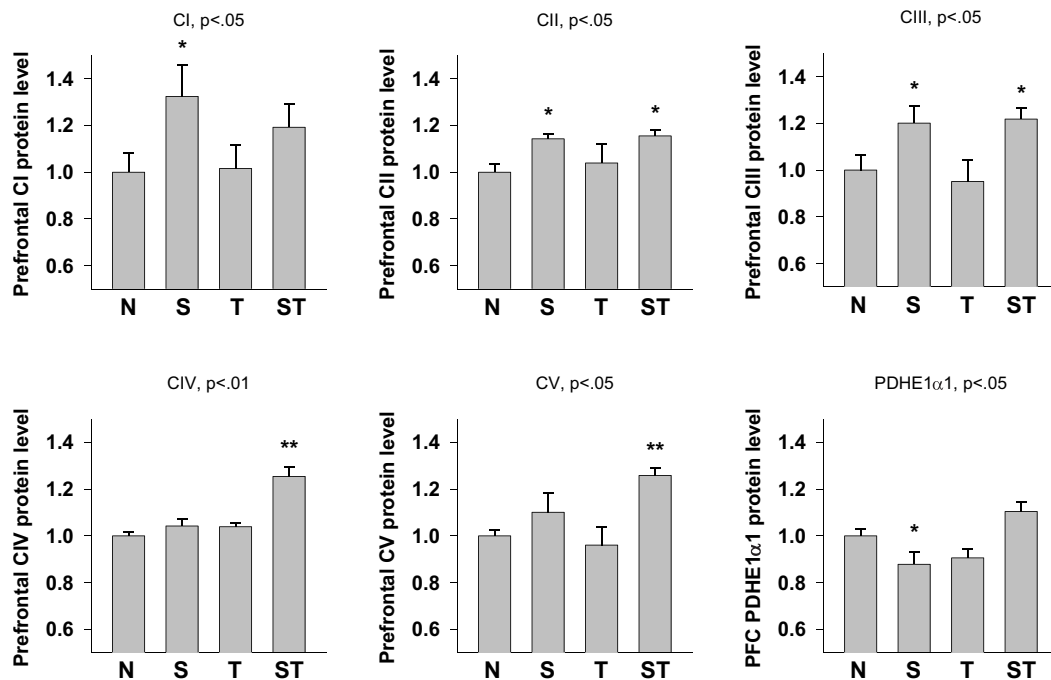
S-mTBI animals. Twenty micrograms of total proteins were resolved on SDS-PAGE gel and incubated with the primary antibodies against each protein. N, Naïves; S, Stress; T, mTBI; ST, stress followed by mTBI; C, contralateral mTBI; I, ipsilateral mTBI; ST, contralateral S-mTBI; STi, ipsilateral S-mTBI.

responses, with and without pre-pulse at day 6. These findings suggest that stress initially decrease movement and temporary increase in depression-related behaviors. These findings are similar to the previous published report in which rat exposure to fear only caused temporary increased in anxiety and impaired memory (46). In contrast, our startle data reveals that information processing was not immediately affected by stress, but became abnormal over time suggesting the progression of secondary brain injury in our rat model of repeat stress. Similarly, patients with PTSD also frequently display increased arousal, which is manifested by irritability, attention deficit, and disturbed sleep (3, 47). These observations confirm the similarities of depression like symptoms in our rat repeat stress model and patients with PTSD.

Brain injury alone caused a significant decline in sensorimotor function and startle responses throughout the experiment when compared with naïves animals. These observations indicate that

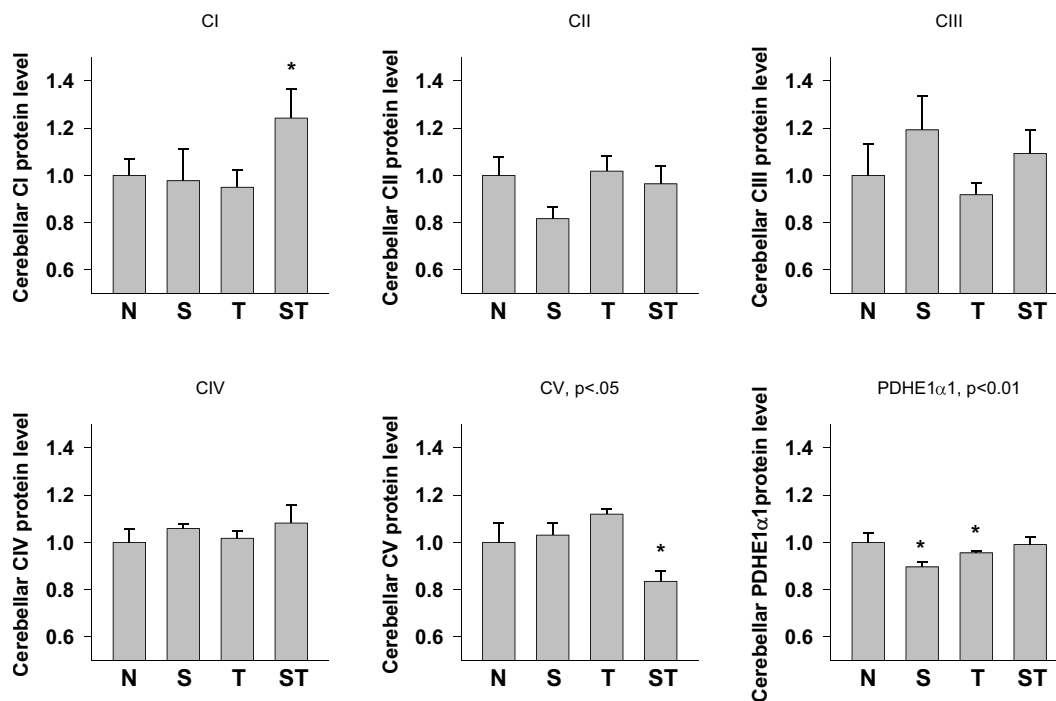
even mTBI initially triggers the depression like behaviors that recovered within 6 days following injury, but the poor sensorimotor function persisted. Similar cognitive dysfunctions have also been published in rat models with controlled cortical impact injury, lateral and midline FP injury, and blast (48). In humans also, cognitive dysfunctions and impaired memory are the common clinical manifestations of mTBI that have not been widely studied in animal models (49). Therefore, functional neurobehavioral responses to mTBI in this study are important for future diagnosis and treatment of mTBI.

The combination of stress and brain injury appeared to produce an additive effect on activity, sensorimotor function, and startle responses. A significant decreased the horizontal and VA, sensorimotor functions and startle responses were noted throughout the experiment in animals with combined stress and mTBI. The additional behavioral findings in our study



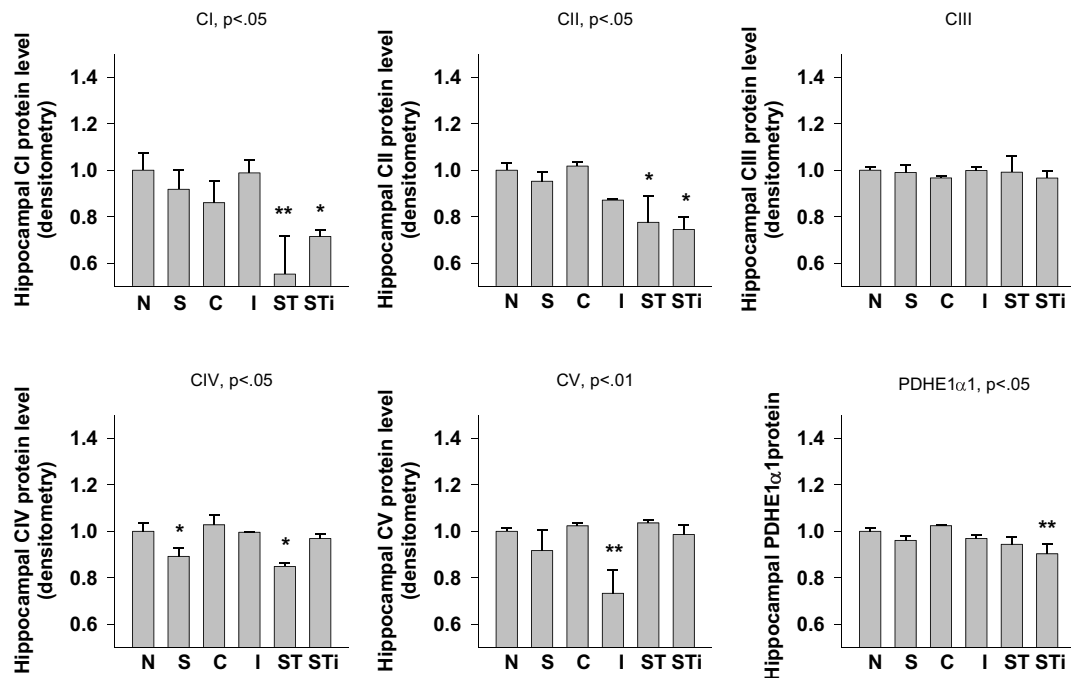
**FIGURE 5 | Semi-quantitative determination of the Western blotting protein bands density of ETC subunits CI, CII, CIII, CIV, CV proteins, and PDHE1 $\alpha$ 1 protein expressed in rat prefrontal cortex (PFC) 7 days post**

**mTBI.** N, Naïves; S, Stress; T, mTBI; ST, stress followed by mTBI. Results are presented as the fold change relative to the Naïves (=1). \* $p$  < 0.05, \*\* $p$  < 0.01 vs. Naïves, respectively.



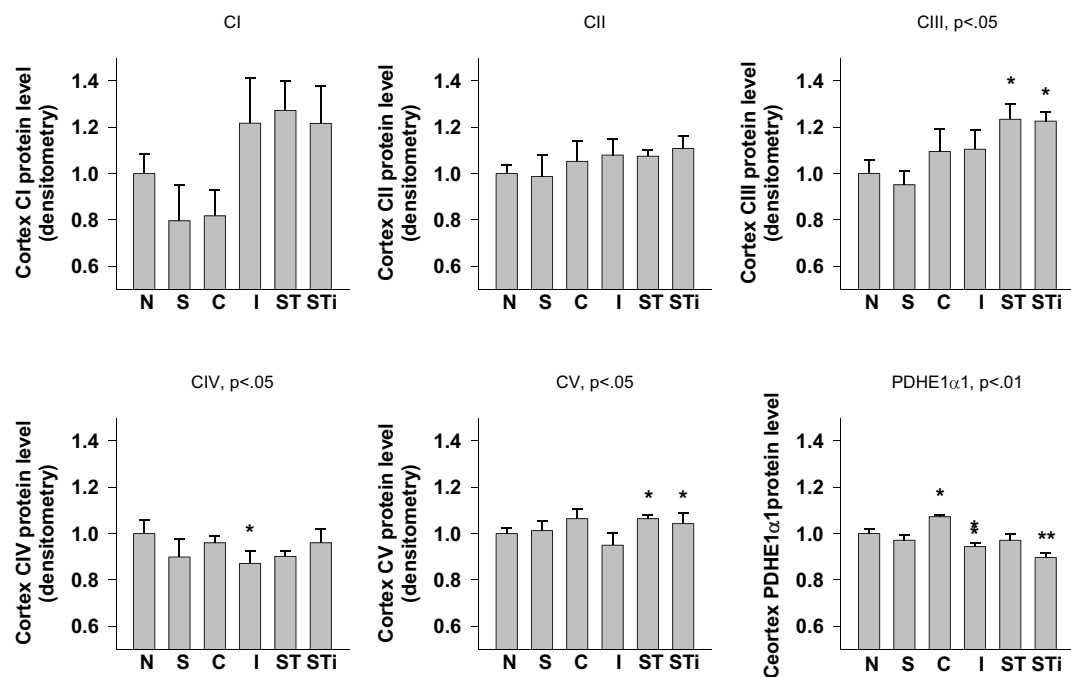
**FIGURE 6 | Semi-quantitative determination of the Western blotting protein bands density of ETC subunits CI, CII, CIII, CIV, CV proteins, and PDHE1 $\alpha$ 1 protein expressed in rat cerebellum 7 days post mTBI.**

N, Naïves; S, 3 days repeated stress; T, mTBI; ST, stress followed by mTBI. Results are presented as the fold change relative to the Naïves (=1). \* $p$  < 0.05, \*\* $p$  < 0.01 vs. Naïves, respectively.



**FIGURE 7 | Semi-quantitative determination of the Western blotting protein bands density of ETC subunits CI, CII, CIII, CIV, CV proteins, and PDHE1 $\alpha$ 1 protein expressed in rat hippocampus 7 days post mTBI.** N, Naïves; S, 3 days repeated stress; T, mTBI; ST,

stress followed by mTBI; C, contralateral mTBI; I, ipsilateral mTBI; ST, contralateral S-mTBI; STi, ipsilateral S-mTBI. Results are presented as the fold change relative to the Naïves (=1). \* $p$  < 0.05, \*\* $p$  < 0.01 vs. Naïves, respectively.



**FIGURE 8 | Semi-quantitative determination of the Western blotting protein bands density of ETC subunits CI, CII, CIII, CIV, CV proteins, and PDHE1 $\alpha$ 1 protein expressed in rat cerebral cortex 7 days post mTBI.** N, Naïves; S, 3 days repeated stress; T, mTBI; ST,

stress followed by mTBI; C, contralateral mTBI; I, ipsilateral mTBI; ST, contralateral S-mTBI; STi, ipsilateral S-mTBI. Results are presented as the fold change relative to the Naïves (=1). \* $p$  < 0.05, \*\* $p$  < 0.01 vs. Naïves, respectively.

confirms that the combination of injury and repeated stress were particularly disruptive. Naïve animals showed the appropriate habituation expected over the course of the experiment with regards to OFA and NSS-R (i.e., the animals' activity or score decreased over time). It is also worth noting that animals were also tested using the rotarod (data not shown), to test for motor deficits, and while TBI decreased the time the animals were able to balance, stress improved the animals' balance. This finding helps in the interpretation of the OFA results, indicating that the combination of stress and mTBI did not cause any motor deficits, therefore the decrease in horizontal and VA can be interpreted as deteriorated general health and depressive-related behaviors.

#### MITOCHONDRIAL EFFECTS OF STRESS, mTBI, OR STRESS WITH mTBI

The specific role of primary mechanisms in stress, mTBI, or combined effects of stress with mTBI is difficult to assess in clinical cases. However, postmortem analysis of brain tissue from patients with PTSD and/or TBI indicated the involvement of mitochondria in neuronal cell death and hippocampus atrophy (44, 45). We believe this is the first study to examine the proteins responsible for mitochondrial energy producing pathways in response to stress, mTBI, or stress with mTBI.

As with the behavioral effects, the stress and injury manipulations have significant measureable effects on PDH and ETC expression in different parts of the brain. These findings extend our previous findings of altered mitochondrial PDH expression and activity after TBI (12, 13). Similar to our findings of neurobehavioral effects of combined stress and mTBI, present experiment indicate that the combination of repeated stress and mTBI had the most effects on mitochondrial PDH and ETC subunit expression compared with stress or mTBI alone. Therefore, the parallel effects of combined stress and injury on behavioral and brain ETC activity are noteworthy and merits further investigation.

The PFC is known to exert a powerful inhibitory effect on amygdala activity and plays an important role in fear extinction (50, 51). The increased ETC subunit expression in the PFC of stressed animals (especially in the stress plus injury animals) could be associated with increased inhibition of amygdala activation, altered fear memory and affect the reorganization of interconnection and inter-regulation between the PFC and limbic circuits to alter endurance and resistance from further stress (52). The region-specific increase of ETC subunits expression in the PFC of Stress and S-mTBI animals is also in agreement with the recent report that chronic stress sensitizes the frontal cortex to the release of cytochrome *c* (CIV) from the mitochondria of male rats. While the relevance of increased PFC in ETC expression in an animal model of repeated stress with brain injury (that may model PTSD with mTBI) remains to be validated. Recent brain imaging studies indicate that combat-exposed war veterans with PTSD and mTBI with high risk for suicide also had hyperactivation of the PFC and anterior cingulate during error processing compared to non-suicidal PTSD with mTBI veterans (53).

Although the mechanism and biological significance of pre-existing stress on the severity of brain injury remains obscure, the

enhanced ETC expression may also reflect a compensatory mechanism for increased energy demand of the injured brain due to increased neuronal activity in several brain regions. This data is also in line with the reported up-regulation of cannabinoid receptor (CBR) expression, an important mediator of energy metabolism in the PFC of juvenile male rats after repeated stress (54). In contrast to the increase ETC complexes in the PFC, the expression of CI, CII, CIV, and PDHE1 $\alpha$ 1 were significantly reduced in the hippocampus of the stress plus injury animals. CV also was decreased in the cerebellum of the stress plus injury animals. These results suggest an increased vulnerability of a repeatedly stressed hippocampus to the detrimental effects of mTBI in terms of ETC complex expression and activity. Reduced ETC and PDHE1 $\alpha$ 1 expression are consistent with reports that inhibition or deficits of mitochondrial ETC complexes are associated with increased ROS production, increased oxidative damage, and apoptotic cell death in the hippocampus after TBI (55–61). These findings corroborate the observations of Opii et al. (62) indicating that, following TBI, several mitochondrial proteins involved in energy producing pathways are modified or oxidatively damaged in different parts of the brain, which may eventually cause cell death and brain atrophy (45). Therefore, the identification of these proteins in response to stress alone or stress followed by mTBI may provide new insights into the brain cell metabolic mechanisms and possible therapeutic interventions after mTBI.

The hippocampus is highly vulnerable to brain injury in both animal models of TBI and humans with TBI, and the hippocampus volume is also reduced in patients with PTSD (63–65). The hippocampus undergoes atrophy and contributes to the chronic memory deficits in the weeks to months following a mTBI (66, 67). Other studies reported that alterations in hippocampus ETC level is associated with aging and increased oxidative damage in mice brains (68) and with Alzheimer's disease (69), a neurodegenerative disorder common among TBI patients (70, 71).

#### Summary

The behavioral and brain protein data support a greater impact of combined stress plus brain injury than mTBI or stress alone on neurobehavioral function and brain mitochondrial ETC expression. Repeated stress exposure prior to TBI potentiated mitochondrial ETC subunit expression in the various brain regions and also potentiated several behavioral effects in rats. These results may explain the relationship between altered regional brain mitochondrial activity and functional outcomes in people with PTSD and mTBI. Repeated stress could have contributed to the high incidence of long-term neurologic and neuropsychiatric morbidity in military personnel with mTBI.

#### ACKNOWLEDGMENTS

This research was supported by DARPA award W911NF 111005 and USAMRMC award W81XWH-10-1-0507 (Pushpa Sharma), and by the Comprehensive National Neuroscience Program (CNNP) award W81XWH-10-2-0198 (William D. Watson). We would like to thank Dr. Min Jia for her contribution with the stress procedure, Mr. Kevin Cravedi for his excellent help in collecting behavioral data and Dr. Prasanth S. Ariyannur for dissecting the brain tissue.

## REFERENCES

- Brenner LA, Vanderploeg RD, Terrio H. Assessment and diagnosis of mild traumatic brain injury, posttraumatic stress disorder, and other polytrauma conditions: burden of adversity hypothesis. *Rehabil Psychol* (2009) **54**(3):239–46. doi:10.1037/a0016908
- Carlson KF, Nelson D, Orazem RJ, Nugent S, Cifu DX, Sayer NA. Psychiatric diagnoses among Iraq and Afghanistan war veterans screened for deployment-related traumatic brain injury. *J Trauma Stress* (2010) **23**(1):17–24. doi:10.1002/jts.20483
- Dolan S, Martindale S, Robinson J, Kimbrel NA, Meyer EC, Kruse MI, et al. Neuropsychological sequelae of PTSD and TBI following war deployment among OEF/OIF veterans. *Neuropsychol Rev* (2012) **22**(1):21–34. doi:10.1007/s11065-012-9190-5
- Schneiderman AI, Braver ER, Kang HK. Understanding sequelae of injury mechanisms and mild traumatic brain injury incurred during the conflicts in Iraq and Afghanistan: persistent postconcussive symptoms and posttraumatic stress disorder. *Am J Epidemiol* (2008) **167**(12):1446–52. doi:10.1093/aje/kwn068
- Hoge CW, McGurk D, Thomas JL, Cox AL, Engel CC, Castro CA. Mild traumatic brain injury in U.S. Soldiers returning from Iraq. *N Engl J Med* (2008) **358**(5):453–63. doi:10.1056/NEJMoa072972
- Hattori N, Huang SC, Wu HM, Liao W, Glenn TC, Vespa PM, et al. Acute changes in regional cerebral (18)F-FDG kinetics in patients with traumatic brain injury. *J Nucl Med* (2004) **45**(5):775–83.
- Hattori N, Huang SC, Wu HM, Yeh E, Glenn TC, Vespa PM, et al. Correlation of regional metabolic rates of glucose with glasgow coma scale after traumatic brain injury. *J Nucl Med* (2003) **44**(11):1709–16.
- Liu-DeRyke X, Collingridge DS, Orme J, Roller D, Zurasky J, Rhoney DH. Clinical impact of early hyperglycemia during acute phase of traumatic brain injury. *Neurocrit Care* (2009) **11**(2):151–7. doi:10.1007/s12028-009-9228-6
- Nakayama N, Okumura A, Shinoda J, Nakashima T, Iwama T. Relationship between regional cerebral metabolism and consciousness disturbance in traumatic diffuse brain injury without large focal lesions: an FDG-PET study with statistical parametric mapping analysis. *J Neurol Neurosurg Psychiatry* (2006) **77**(7):856–62. doi:10.1136/jnnp.2005.080523
- Xing G, Ren M, O'Neill JT, Sharma P, Verma A, Watson WD. Pyruvate dehydrogenase phosphatase1 mRNA expression is divergently and dynamically regulated between rat cerebral cortex, hippocampus and thalamus after traumatic brain injury: a potential biomarker of TBI-induced hyper- and hypo-glycaemia and neuronal vulnerability. *Neurosci Lett* (2012) **525**(2):140–5. doi:10.1016/j.neulet.2012.07.055
- Xing G, Ren M, O'Neill JT, Verma A, Watson WD. Controlled cortical impact injury and craniotomy result in divergent alterations of pyruvate metabolizing enzymes in rat brain. *Exp Neurol* (2012) **234**(1):31–8. doi:10.1016/j.expneurol.2011.12.007
- Xing G, Ren M, Watson WD, O'Neill JT, Verma A. Traumatic brain injury-induced expression and phosphorylation of pyruvate dehydrogenase: a mechanism of dysregulated glucose metabolism. *Neurosci Lett* (2009) **454**(1):38–42. doi:10.1016/j.neulet.2009.01.047
- Sharma P, Benford B, Li ZZ, Ling GS. Role of pyruvate dehydrogenase complex in traumatic brain injury and Measurement of pyruvate dehydrogenase enzyme by dipstick test. *J Emerg Trauma Shock* (2009) **2**(2):67–72. doi:10.4103/0974-2700.50739
- Tretter L, Sipos I, Adam-Vizi V. Initiation of neuronal damage by complex I deficiency and oxidative stress in Parkinson's disease. *Neurochem Res* (2004) **29**(3):569–77. doi:10.1023/B:NERE.0000014827.94562.4b
- Blin O, Desnuelle C, Rascol O, Borg M, Peyro Saint Paul H, Azulay JP, et al. Mitochondrial respiratory failure in skeletal muscle from patients with Parkinson's disease and multiple system atrophy. *J Neurol Sci* (1994) **125**(1):95–101. doi:10.1016/0022-510X(94)90248-8
- Valenti D, Manente GA, Moro L, Marra E, Vacca RA. Deficit of complex I activity in human skin fibroblasts with chromosome 21 trisomy and overproduction of reactive oxygen species by mitochondria: involvement of the cAMP/PKA signalling pathway. *Biochem J* (2011) **435**(3):679–88. doi:10.1042/BJ20101908
- Aston-Jones G, Rajkowski J, Kubiak P, Alexinsky T. Locus coeruleus neurons in monkey are selectively activated by attended cues in a vigilance task. *J Neurosci* (1994) **14**(7):4467–80.
- Seematter G, Binnert C, Martin JL, Tappy L. Relationship between stress, inflammation and metabolism. *Curr Opin Clin Nutr Metab Care* (2004) **7**(2):169–73. doi:10.1097/00075197-200403000-00011
- Lazzeri C, Tarquini R, Giunta F, Gensini GF. Glucose dysmetabolism and prognosis in critical illness. *Intern Emerg Med* (2009) **4**(2):147–56. doi:10.1007/s11739-008-0206-3
- Servatius RJ, Ottenweller JE, Natelson BH. Delayed startle sensitization distinguishes rats exposed to one or three stress sessions: further evidence toward an animal model of PTSD. *Biol Psychiatry* (1995) **38**(8):539–46. doi:10.1016/0006-3223(94)00369-E
- Nutt DJ, Malizia AL. Structural and functional brain changes in posttraumatic stress disorder. *J Clin Psychiatry* (2004) **65**(Suppl 1):11–7.
- Manion ST, Gamble EH, Li H. Prazosin administered prior to inescapable stressor blocks subsequent exaggeration of acoustic startle response in rats. *Pharmacol Biochem Behav* (2007) **86**(3):559–65. doi:10.1016/j.pbb.2007.01.019
- Jiang X, Xing G, Yang C, Verma A, Zhang L, Li H. Stress impairs 5-HT<sub>2A</sub> receptor-mediated serotonergic facilitation of GABA release in juvenile rat basolateral amygdala. *Neuropsychopharmacology* (2009) **34**(2):410–23. doi:10.1038/npp.2008.71
- Jiang X, Zhang ZJ, Zhang S, Gamble EH, Jia M, Ursano RJ, et al. 5-HT<sub>2A</sub> receptor antagonism by MDL 11,939 during inescapable stress prevents subsequent exaggeration of acoustic startle response and reduced body weight in rats. *J Psychopharmacol* (2011) **25**(2):289–97. doi:10.1177/0269881109106911
- Jia M, Meng F, Smerin SE, Xing G, Zhang L, Su DM, et al. Biomarkers in an animal model for revealing neural, hematologic, and behavioral correlates of PTSD. *J Vis Exp* (2012) (68):e3361. doi:10.3791/3361
- Seligman ME, Maier SF. Failure to escape traumatic shock. *J Exp Psychol* (1967) **74**(1):1–9. doi:10.1037/h0024514
- Grunberg NE, Yarnell AM, Hamilton KR, Starosciak AK, Chwa A, Hutchison ES, et al., editors. *A Revised Neurological Severity Scale for Rodents*. Washington, DC: Society for Neuroscience (2011).
- Sharma P, Su YA, Barry ES, Grunberg NE, Lei Z. Mitochondrial targeted neuron focused genes in hippocampus of rats with traumatic brain injury. *Int J Crit Illn Inj Sci* (2012) **2**(3):172–9. doi:10.4103/2229-5151.100931
- Shohami E, Novikov M, Bass R. Long-term effect of HU-211, a novel non-competitive NMDA antagonist, on motor and memory functions after closed head injury in the rat. *Brain Res* (1995) **674**(1):55–62. doi:10.1016/0006-8993(94)01433-1
- Mahmood A, Lu D, Wang L, Li Y, Lu M, Chopp M. Treatment of traumatic brain injury in female rats with intravenous administration of bone marrow stromal cells. *Neurosurgery* (2001) **49**(5):1196–203. doi:10.1097/00006123-200111000-00031 discussion 1203–194.
- Hamm RJ. Neurobehavioral assessment of outcome following traumatic brain injury in rats: an evaluation of selected measures. *J Neurotrauma* (2001) **18**(11):1207–16. doi:10.1089/089771501317095241
- Marti M, Mela F, Fantin M, Zucchini S, Brown JM, Witta J, et al. Blockade of nociceptin/orphanin FQ transmission attenuates symptoms and neurodegeneration associated with Parkinson's disease. *J Neurosci* (2005) **25**(42):9591–601. doi:10.1523/JNEUROSCI.2546-05.2005
- Li R, Shen Y. An old method facing a new challenge: re-visiting housekeeping proteins as internal reference control for neuroscience research. *Life Sci* (2013) **92**(13):747–51. doi:10.1016/j.lfs.2013.02.014
- Ferguson RE, Carroll HP, Harris A, Maher ER, Selby PJ, Banks RE. House-keeping proteins: a preliminary study illustrating some limitations as useful references in protein expression studies. *Proteomics* (2005) **5**(2):566–71. doi:10.1002/pmic.200400941
- Grunberg NE, Bowen DJ. The role of physical activity in nicotine's effects on body weight. *Pharmacol Biochem Behav* (1985) **23**(5):851–4. doi:10.1016/0091-3057(85)90081-4
- Morse DE, Davis HD, Popke EJ, Brown KJ, O'Donoghue VA, Grunberg NE. Effects of ddC and AZT on locomotion and acoustic startle. I: acute effects in female rats. *Pharmacol Biochem Behav* (1997) **56**(2):221–8. doi:10.1016/S0091-3057(96)00214-6
- Faraday MM, O'Donoghue VA, Grunberg NE. Effects of nicotine and stress on locomotion in Sprague-Dawley and Long-Evans male and female rats. *Pharmacol Biochem Behav* (2003) **74**(2):325–33. doi:10.1016/S0091-3057(02)00999-1
- Elliott BM, Faraday MM, Phillips JM, Grunberg NE. Effects of nicotine on elevated plus maze and locomotor activity in male and female adolescent and adult rats. *Pharmacol Biochem Behav* (2004) **77**(1):21–8. doi:10.1016/j.pbb.2003.09.016



39. Cole JT, Yarnell A, Kean WS, Gold E, Lewis B, Ren M, et al. Craniotomy: true sham for traumatic brain injury, or a sham of a sham? *J Neurotrauma* (2011) **28**(3):359–69. doi:10.1089/neu.2010.1427
40. Swerdlow NR, Caine SB, Braff DL, Geyer MA. The neural substrates of sensorimotor gating of the startle reflex: a review of recent findings and their implications. *J Psychopharmacol* (1992) **6**(2):176–90. doi:10.1177/026988119200600210
41. Aciri JB, Grunberg NE, Morse DE. Effects of nicotine on the acoustic startle reflex amplitude in rats. *Psychopharmacology (Berl)* (1991) **104**(2):244–8. doi:10.1007/BF02244186
42. Aciri JB, Morse DE, Popke EJ, Grunberg NE. Nicotine increases sensory gating measured as inhibition of the acoustic startle reflex in rats. *Psychopharmacology (Berl)* (1994) **114**(2):369–74. doi:10.1007/BF02244861
43. Faraday MM, Rahman MA, Scheufele PM, Grunberg NE. Nicotine administration impairs sensory gating in Long-Evans rats. *Pharmacol Biochem Behav* (1998) **61**(3):281–9. doi:10.1016/S0091-3057(98)00094-X
44. Su YA, Wu J, Zhang L, Zhang Q, Su DM, He P, et al. Dysregulated mitochondrial genes and networks with drug targets in postmortem brain of patients with posttraumatic stress disorder (PTSD) revealed by human mitochondria-focused cDNA microarrays. *Int J Biol Sci* (2008) **4**(4):223–35. doi:10.7150/ijbs.4.223
45. Cernak I, Wang Z, Jiang J, Bian X, Savic J. Ultrastructural and functional characteristics of blast injury-induced neurotrauma. *J Trauma* (2001) **50**(4):695–706. doi:10.1097/00005373-200104000-00017
46. Pynoos RS, Ritzmann RE, Steinberg AM, Goenjian A, Prisecaru I. A behavioral animal model of posttraumatic stress disorder featuring repeated exposure to situational reminders. *Biol Psychiatry* (1996) **39**(2):129–34. doi:10.1016/0006-3223(95)00088-7
47. Hoge CW, Castro CA, Messer SC, McGurk D, Cotting DI, Koffman RL. Combat duty in Iraq and Afghanistan, mental health problems and barriers to care. *US Army Med Dep J* (2008). 7–17.
48. Xiong Y, Mahmood A, Chopp M. Animal models of traumatic brain injury. *Nat Rev Neurosci* (2013) **14**(2):128–42. doi:10.1038/nrn3407
49. Masel BE, DeWitt DS. Traumatic brain injury: a disease process, not an event. *J Neurotrauma* (2010) **27**(8):1529–40. doi:10.1089/neu.2010.1358
50. Li CS, Sinha R. Inhibitory control and emotional stress regulation: neuroimaging evidence for frontal-limbic dysfunction in psycho-stimulant addiction. *Neurosci Biobehav Rev* (2008) **32**(3):581–97. doi:10.1016/j.neubiorev.2007.10.003
51. Vlachos I, Herry C, Luthi A, Aertsen A, Kumar A. Context-dependent encoding of fear and extinction memories in a large-scale network model of the basal amygdala. *PLoS Comput Biol* (2011) **7**(3):e1001104. doi:10.1371/journal.pcbi.1001104
52. Zelikowsky M, Bissiere S, Hast TA, Bennett RZ, Abdipranoto A, Vissel B, et al. Prefrontal microcircuit underlies contextual learning after hippocampal loss. *Proc Natl Acad Sci U S A* (2013) **110**(24):9938–43. doi:10.1073/pnas.1301691110
53. Matthews S, Spadoni A, Knox K, Strigo I, Simmons A. Combat-exposed war veterans at risk for suicide show hyperactivation of prefrontal cortex and anterior cingulate during error processing. *Psychosom Med* (2012) **74**(5):471–5. doi:10.1097/PSY.0b013e31824f888f
54. Xing G, Carlton J, Jiang X, Jia M, Sharma P, Li H. Delayed effects of repeated inescapable severe stress on brain cannabinoid receptor expression and acoustic startle response in adolescent male rats: relevance to the development of post-traumatic stress disorder and stress-related brain atrophy. In: Edward Foreman JF, editor. *Posttraumatic Stress Disorder: New Research*. New York: NOVA Science Publisher (2013). p. 83–107.
55. Adam-Vizi V. Production of reactive oxygen species in brain mitochondria: contribution by electron transport chain and non-electron transport chain sources. *Antioxid Redox Signal* (2005) **7**(9–10):1140–9. doi:10.1089/ars.2005.7.1140
56. Lannuzel A, Michel PP, Hoglinger GU, Champy P, Jousset A, Medja F, et al. The mitochondrial complex I inhibitor annonacin is toxic to mesencephalic dopaminergic neurons by impairment of energy metabolism. *Neuroscience* (2003) **121**(2):287–96. doi:10.1016/S0306-4522(03)00441-X
57. Colicos MA, Dash PK. Apoptotic morphology of dentate gyrus granule cells following experimental cortical impact injury in rats: possible role in spatial memory deficits. *Brain Res* (1996) **739**(1–2):120–31. doi:10.1016/S0006-8993(96)00824-4
58. Kirby DM, Crawford M, Cleary MA, Dahl HH, Dennett X, Thorburn DR. Respiratory chain complex I deficiency: an underdiagnosed energy generation disorder. *Neurology* (1999) **52**(6):1255–64. doi:10.1212/WNL.52.6.1255
59. Srinivasan S, Avadhani NG. Cytochrome c oxidase dysfunction in oxidative stress. *Free Radic Biol Med* (2012) **53**(6):1252–63. doi:10.1016/j.freeradbiomed.2012.07.021
60. Murphy MP. How mitochondria produce reactive oxygen species. *Biochem J* (2009) **417**(1):1–13. doi:10.1042/BJ20081386
61. McIntosh TK, Saatman KE, Raghupathi R, Graham DI, Smith DH, Lee VM, et al. The Dorothy Russell Memorial Lecture. The molecular and cellular sequelae of experimental traumatic brain injury: pathogenetic mechanisms. *Neuropathol Appl Neurobiol* (1998) **24**(4):251–67. doi:10.1046/j.1365-2990.1998.00121.x
62. Opii WO, Nukala VN, Sultana R, Pandya JD, Day KM, Merchant ML, et al. Proteomic identification of oxidized mitochondrial proteins following experimental traumatic brain injury. *J Neurotrauma* (2007) **24**(5):772–89. doi:10.1089/neu.2006.0229
63. Villarreal G, Hamilton DA, Petropoulos H, Driscoll I, Rowland LM, Griego JA, et al. Reduced hippocampal volume and total white matter volume in posttraumatic stress disorder. *Biol Psychiatry* (2002) **52**(2):119–25. doi:10.1016/S0006-3223(02)01359-8
64. Felmingham K, Williams LM, Whitford TJ, Falconer E, Kemp AH, Peduto A, et al. Duration of posttraumatic stress disorder predicts hippocampal grey matter loss. *Neuroreport* (2009) **20**(16):1402–6. doi:10.1097/WNR.0b013e3283300fbc
65. Zhang J, Tan Q, Yin H, Zhang X, Huan Y, Tang L, et al. Decreased gray matter volume in the left hippocampus and bilateral calcarine cortex in coal mine flood disaster survivors with recent onset PTSD. *Psychiatry Res* (2011) **192**(2):84–90. doi:10.1016/j.psychres.2010.09.001
66. Ariza M, Serra-Grabulosa JM, Junque C, Ramirez B, Mataro M, Poca A, et al. Hippocampal head atrophy after traumatic brain injury. *Neuropsychologia* (2006) **44**(10):1956–61. doi:10.1016/j.neuropsychologia.2005.11.007
67. Bramlett HM, Green EJ, Dietrich WD. Hippocampally dependent and independent chronic spatial navigational deficits following parasagittal fluid percussion brain injury in the rat. *Brain Res* (1997) **762**(1–2):195–202. doi:10.1016/S0006-8993(97)00387-9
68. Manczak M, Jung Y, Park BS, Partovi D, Reddy PH. Time-course of mitochondrial gene expressions in mice brains: implications for mitochondrial dysfunction, oxidative damage, and cytochrome c in aging. *J Neurochem* (2005) **92**(3):494–504. doi:10.1111/j.1471-4159.2004.02884.x
69. Kim SH, Vlkolinsky R, Cairns N, Lubec G. Decreased levels of complex III core protein 1 and complex V beta chain in brains from patients with Alzheimer's disease and Down syndrome. *Cell Mol Life Sci* (2000) **57**(12):1810–6. doi:10.1007/PL00000661
70. Hasegawa T. Prolonged stress will induce Alzheimer's disease in elderly people by increased release of homocysteic acid. *Med Hypotheses* (2007) **69**(5):1135–9. doi:10.1016/j.mehy.2007.02.034
71. Tsolaki M, Eleftheriou M, Karavida N. Alzheimer's dementia and post-traumatic stress disorder differences and similarities in neuroimaging. *Hell J Nucl Med* (2009) **12**(1):41–6.

**Conflict of Interest Statement:** The authors declare that the research was conducted in the absence of any commercial or financial relationships that could be construed as a potential conflict of interest.

Received: 15 July 2013; accepted: 19 November 2013; published online: 12 December 2013.

Citation: Xing G, Barry ES, Benford B, Grunberg NE, Li H, Watson WD and Sharma P (2013) Impact of repeated stress on traumatic brain injury-induced mitochondrial electron transport chain expression and behavioral responses in rats. *Front. Neurol.* **4**:196. doi: 10.3389/fneur.2013.00196

This article was submitted to *Neurotrauma*, a section of the journal *Frontiers in Neurology*.

Copyright © 2013 Xing, Barry, Benford, Grunberg, Li, Watson and Sharma. This is an open-access article distributed under the terms of the Creative Commons Attribution License (CC BY). The use, distribution or reproduction in other forums is permitted, provided the original author(s) or licensor are credited and that the original publication in this journal is cited, in accordance with accepted academic practice. No use, distribution or reproduction is permitted which does not comply with these terms.



# Culturing layer-specific neocortical neurons as a cell replacement therapy following traumatic brain injury

Nathan Peter Cramer<sup>1,2</sup>, Mitali Chatterjee<sup>1</sup>, Fritz Walter Lischka<sup>1</sup> and Sharon L. Juliano<sup>1,2,3\*</sup>

<sup>1</sup> Center for Neuroscience and Regenerative Medicine, Uniformed Services University of the Health Sciences, Bethesda, MD, USA

<sup>2</sup> Department of Anatomy, Physiology and Genetics, Uniformed Services University of the Health Sciences, Bethesda, MD, USA

<sup>3</sup> Program in Neuroscience, Uniformed Services University of the Health Sciences, Bethesda, MD, USA

## Edited by:

Guoqiang Xing, Lotus Biotech.com, USA

## Reviewed by:

Zhihui Yang, University of Florida, USA

Bor Luen Tang, National University of Singapore, Singapore

## \*Correspondence:

Sharon L. Juliano, Department of Anatomy, Physiology and Genetics, Uniformed Services University of the Health Sciences, 4301 Jones Bridge Road, Bethesda, MD 20814, USA  
e-mail: sharon.juliano@usuhs.edu

Neurophysiological changes resulting from traumatic brain injury (TBI) can result in adverse changes in behavior including mood instability and cognitive dysfunction. Cell death following TBI likely contributes to these altered behaviors and remains an elusive but attractive target for therapies aiming at functional recovery. Previously we demonstrated that neural progenitor cells derived from embryonic rats can be transplanted into donor neonatal rat brain slices and, over the course of 2 weeks in culture, mature into neurons that express neuronal immunohistochemical markers and develop electrophysiological profiles consistent with excitatory and inhibitory interneurons. Here we examine the potential of generating electrophysiologically mature neurons with a layer-specific phenotype as a next step in developing a therapy designed to rebuild a damaged cortical column with the functionally appropriate neuronal subtypes. Preliminary results suggest that neurons derived from passaged neurospheres and grown in dissociated cell culture develop GABAergic and presumed glutamatergic phenotypes and that the percentage of GABAergic cells increases as a function of passage. After 2 weeks in culture, the neurons have a mix of immature and mature neuronal electrophysiological profiles and receive synaptic inputs from surrounding neurons. Subsets of cells expressing neuron specific markers also express layer-specific markers such as Cux1, ER81, and ROR $\beta$ . Future studies will investigate the potential of transplanting layer-specific neurons generated and isolated *in vitro* into the neocortex of neonatal brain slices and their potential to maintain their phenotype and integrate into the host tissue.

**Keywords:** traumatic brain injury, transplantation, neocortex, neuroprogenitor, therapy

## INTRODUCTION

Traumatic brain injury (TBI) results in a host of adverse changes within the central nervous system that can have profound adverse functional and behavioral changes. While the underlying pathology of these deficits is still under investigation, the loss of neural tissue from initial impact or secondary injury mechanisms contributes to these deficits (1). The use of stem cells to replace lost neurons or rebuild missing networks holds great promise for reversing TBI-induced neurological deficits (2, 3). However, our ability to rebuild damaged neuronal networks is limited in part by our capacity to generate specific types of neurons in a controlled fashion. *In vitro* methods that successfully generate neurons phenotypic of the different neocortical layers may help bring viable cell replacement therapies closer to reality.

Within the neocortex, neurons that ultimately reside within a particular cortical layer are born in the ventricular and subventricular zones (VZ and SVZ) arising from neural progenitor cells in both these regions (4–8). Neurons of the deeper cortical layers are born first and subsequent superficial layers arise from later born neurons resulting in an inside-out construction pattern (9). Thus, neurons of the different cortical layers are generated from different cell division cycles of progenitor cells in the VZ and SVZ. These observations suggest that the number of cell division cycles

could be a contributing factor to the final neuronal subtype (10–12) and replication of this process *in vitro* might be capable of generating neurons phenotypic of specific cortical layers. Shen et al. (13) on the other hand, demonstrated that neural progenitor cells harvested from embryonic mice at the onset of corticogenesis (E10.5) contain the machinery for producing multiple neocortical cell types when grown in culture.

As a potential source for a viable mixed population of neurons capable of transplantation we investigated the capacity for neuroprogenitor cells (NPC) harvested from the neocortex of later stage mouse embryos (embryonic days 14–16) to generate neurons characteristic of different cortical layers when grown in culture long enough to become electrophysiologically mature. Furthermore, we investigated whether propagation of these cells through repeated passaging as neurospheres affected the overall composition of subsequent cultures once allowed to differentiate for multiple weeks. Finally, we investigated the ability of later stage embryonic neurons to maintain neuronal identities and integrate with host tissue when transplanted into injured slices of neonatal mouse cortex. We find that this approach successfully generates electrophysiologically mature neurons that express markers characteristic of different neocortical layers and that acutely isolated cells successfully integrate into neuronal networks upon transplantation.

These studies help further our understanding of the potential for NPC to serve as a therapeutic source for treating TBI.

## MATERIALS AND METHODS

### HARVESTING OF EMBRYONIC CORTICAL CELLS

Pregnant wild type C57Bl/6 or C57Bl/6-Tg(UBC-GFP)30Scha/J mouse dams from Jackson Laboratories were injected with euthasol ( $\sim 0.1 \text{ cm}^3$  per 15 g body weight, IP) and embryos (E14–16) removed under sterile surgical conditions. The developing sensory cortex was isolated from each embryo while submerged in sterile ice-cold artificial cerebrospinal fluid continuously bubbled with 95/5%  $\text{O}_2/\text{CO}_2$ . Single cell suspensions were generated by mechanical trituration. Cells were then either used for neurosphere/cell culture experiments or injection into neonatal mouse slice cultures as outlined below.

### GENERATION OF CORTICAL SLICES FROM NEONATAL MICE

WT mouse pups (P1–P3) were heavily anesthetized with isoflurane and decapitated with sharp scissors. The brains were removed and 400  $\mu\text{m}$  thick coronal hemi-sections were cut in sterile filtered ice-cold artificial cerebrospinal fluid continuously bubbled with 95/5%  $\text{O}_2/\text{CO}_2$ . Sections were transferred to sterile tissue culture inserts in a six well plate (one to four sections per well) and washed twice with sterile MEM containing 10% normal horse serum and 4% G:1:2. TBIs were simulated by making a fine incision in the cortex with a 22 gauge needle. A total of 30,000 harvested GFP<sup>+</sup> embryonic cells were injected into each incision in a volume of 10 nl culture medium. Slices were incubated for 1–2 weeks prior to immunohistochemistry or electrophysiology experiments.

### NEUROSPHERE PASSAGING AND DIFFERENTIATION

Harvested embryonic neurons not used for injection were maintained in proliferation media (NeuroCult NSC Basal Medium Mouse, STEMCELL Technologies Inc., Vancouver, BC, Canada) until neurospheres formed. Upon reaching sufficient size, neurospheres were partially dissociated with brief treatment of trypsin (Gibco 0.05% Trypsin EDTA), washed, and divided into two groups. One group was placed in new proliferation media for a subsequent passage and the other used for cell culture experiments. For cell cultures, dissociated neurospheres were plated on coverslips at a density of 6e10 cells per milliliter and maintained in differentiation media (NeuroCult NSC Basal medium Mouse with Proliferation supplement, STEMCELL Technologies Inc., Vancouver, BC, Canada) media for 1–2 weeks prior to use for immunohistochemistry or electrophysiological experiments.

### ELECTROPHYSIOLOGY

Slices with GFP<sup>+</sup> transplanted cells or coverslips with cultured cells were transferred to a submersion style chamber attached to a Zeiss Axioskop; individual neurons were visualized with DIC optics. GFP<sup>+</sup> transplanted neurons were identified by their fluorescence. Slices and cover slips were continuously perfused with ACSF composed of (in millimolar) NaCl 126, KCl 3,  $\text{CaCl}_2$  2,  $\text{NaH}_2\text{PO}_4$  1.25,  $\text{MgSO}_4$  2,  $\text{NaHCO}_3$  26, D-glucose 10, bubbled with a mixture of 95%  $\text{O}_2$ /5%  $\text{CO}_2$  at room temperature. Whole cell recordings were obtained with borosilicate pipettes containing (in millimolar): K-gluconate 130, KCl 15, HEPES 5, EGTA 1, Mg-ATP

4, Na-GTP 0.3 with pH adjusted to  $\sim 7.3$  with KOH. In a subset of recordings, 0.2% Neurobiotin was included in the intracellular solution to enable *post hoc* visualization of recorded cells (Vector Laboratories, Burlingame, CA, USA). Analysis of active and passive membrane properties was performed offline using ClampFit software (Molecular Devices, LLC, Sunnyvale, CA, USA) and custom written routines in Igor Pro (WaveMetrics, Portland, OR, USA). Spontaneous synaptic activity was analyzed by isolating individual synaptic events in MiniAnalysis (SynaptoSoft, Decatur, GA, USA).

### IMMUNOHISTOCHEMISTRY

Coverslips with dissociated cell cultures were fixed with 4% paraformaldehyde followed by four washes with PBS. After a 1 h incubation in blocking buffer at room temperature, coverslips were incubated in blocking buffer plus either mouse monoclonal anti- $\beta$ -tubulin (1:500), rabbit polyclonal anti-MAP-2 (1:200, Sigma Aldrich, St. Louis, MO, USA), or mouse monoclonal anti-NeuN (1:100, EMD Millipore, Billerica, MA, USA) and a layer-specific (rabbit anti-ER81, 1:1000; mouse anti-CUX1, 1:1000; rabbit anti-ROR $\beta$ , 1:500; abcam, Cambridge, MA, USA) or rabbit anti-GABA (Sigma Aldrich, St. Louis, MO, USA) overnight at 4°C. Coverslips were washed in PBS and a secondary antibody (Alexa Fluor 488 or 546, 1:200; Life Technologies, Grand Island, NY, USA) applied for 90 min followed by a final rinse in PBS and application of bisbenz-imide to label cell nuclei. Finally coverslips were mounted on glass slides using Mowiol or Vectashield. Slice cultures were fixed in 4% paraformaldehyde for 20 min followed by overnight incubation in a 30% sucrose/PBS (wt/vol) solution. Slices were sub-sectioned into 20–40  $\mu\text{m}$  thick sections for subsequent immunohistochemistry that proceeded as above following permeabilization with 0.1% Triton X-100 in PBS. All antibody concentrations were the same except anti- $\beta$ -tubulin (1:1000) and secondary antibodies (1:1000). Neurobiotin filled cells were visualized by incubating either cell or tissue cultures with NeutrAvidin-488 (Life Technologies Corporation) diluted 1:200 in PBS for 2 h following primary and secondary antibody reactions.

Images were imported into Fiji (14) and each acquisition channel separated into individual images. The channel containing data from a neuronal marker (NeuN,  $\beta$ -tubulin, or MAP-2) was thresholded using Otsu or Maximum Entropy auto-thresholding. These parameters reliably isolated cell bodies from the background. Regions of interest (ROIs) were drawn around individual neurons and the resulting series of ROIs overlaid on the similarly thresholded image containing a layer-specific marker (Cux1, ER81, or ROR $\beta$ ) or GABA imaging data. The percentage of the neuronal marker ROI filled with a layer-specific or GABA pixels was calculated and a value of greater than 30% of the neuronal ROI was considered co-labeled. DAPI stained nuclei were hand counted using the Cell Counter plugin.

## RESULTS

### NEUROGENIC POTENTIAL AND EXPRESSION OF LAYER-SPECIFIC MARKERS

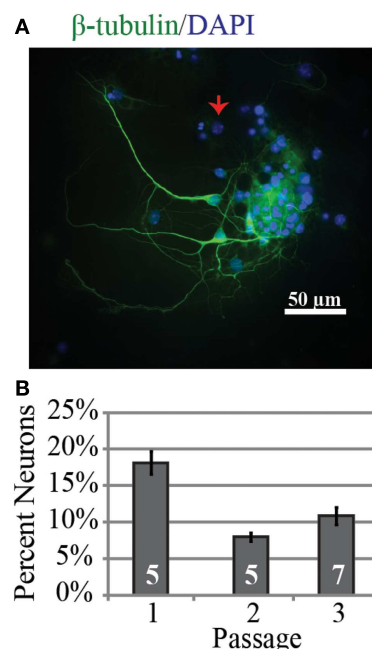
Neuroprogenitor cells capable of generating multiple subtypes of neurons are a potential source for restorative therapies following TBI. We investigated whether cells isolated from the neocortex of embryonic mice during the peak period of corticogenesis [E14–16

(15, 16)] could produce and sustain neurons when cultured as neurospheres and whether the composition of neuronal subtypes changed over repeated passages. After ~7 days in culture, neurospheres were either placed in differentiation media (see Materials and Methods) and allowed to differentiate for at least 2 weeks or back in proliferation media. This was repeated for up to 3 passages. When neurons were differentiated, they were immunoreacted for neuronal markers, laminar markers, and GABA. Results were similar across embryonic ages and were consequently combined.

Investigation of the neurogenic potential of cells following passaging revealed that each passage was capable of generating neurons (**Figure 1**). Passage 1 generated the highest percentage of neurons ( $18 \pm 6\%$ ;  $n = 723$  cells, five experiments) compared to  $9 \pm 2\%$  ( $n = 301$  cells, five experiments) and  $11 \pm 4\%$  ( $n = 294$  cells, seven experiments) for passages 2 and 3 respectively. This pattern is similar to that reported for NPC harvested from e10 embryos (13). In addition to the development of presumed glutamatergic projection neurons we examined the development profile of GABAergic neurons across passages (**Figure 2**). The percentage of neurons immunopositive for GABA in passage 1 was  $24 \pm 6\%$  ( $n = 240$  neurons from four experiments) compared to  $40 \pm 10\%$  ( $n = 102$  neurons from three experiments) and  $47 \pm 3\%$  ( $n = 59$  neurons from two experiments) in passages 2 and 3 respectively (**Figure 2B**). Thus the percentage of inhibitory neurons tended to increase as a function of passage number although the difference was not significant ( $P = 0.34$ , ANOVA).

Examination of the layer specificity of neurons derived from passaged neurospheres and allowed to differentiate for multiple weeks *in vitro* revealed a diverse set of neuronal phenotypes. **Figures 3A–C** shows representative examples of neurons differentiated from neurospheres. In this example, a marker for upper layer neurons, Cux1 (**Figure 3A**), colocalizes with a subset of cells immunopositive for a neuron specific marker ( $\beta$ -tubulin, green). In passage 1, expression of Cux1 was highest (**Figure 3D**,  $89 \pm 4\%$ ,  $n = 161$  cells from four experiments) while the fraction of neurons expressing Er81, a marker of earlier born deeper layer neurons (17, 18), was lowest (**Figures 3E**,  $40 \pm 10\%$ ,  $n = 100$  cells from three experiments). ROR $\beta$  expression levels, a marker of layer IV neurons (18), was in between these two levels at  $56 \pm 4\%$  (**Figure 3F**,  $n = 212$  cells from three experiments). Thus, neurons characteristic of multiple layers of the neocortex were present but upper layer neurons were dominant.

We also investigated whether repeated passaging of neurospheres derived from E14 to E16 embryos altered the neuronal composition of cultures following differentiation. In general, there was variability between passages, but markers for all layers were present in each passage. The distributions did not follow a specific pattern, but markers for all layers were substantially represented after each passage. The persistence of neurons immunoreactive for Er81 suggests that these cells may survive better than those expressing markers for layer 4 (ROR $\beta$ ) or the upper layers (Cux1) (**Figures 3D–E**). These findings suggest that NPCs obtained from proliferative regions at E14–16 are capable of generating neurons intended to reside in multiple layers; this is not surprising given what is known about the dates of generation of mouse neocortical neurons (10–12). Cells expressing GABA also increased in percentage with passage number. This suggests that GABAergic cells may



**FIGURE 1 | Neurons can be successfully generated from passaged neurospheres even after multiple passages. (A)** Representative example of neurons from passage 3 after 9 days *in vitro* immunopositive for the neuronal marker  $\beta$ -tubulin (green) and DAPI labeled cell nuclei (blue). The red arrow indicates a nucleus from a  $\beta$ -tubulin negative cell. **(B)** Group data for percentage of neurons identified as a function of neurosphere passage number. The percentage was highest in passage 1.

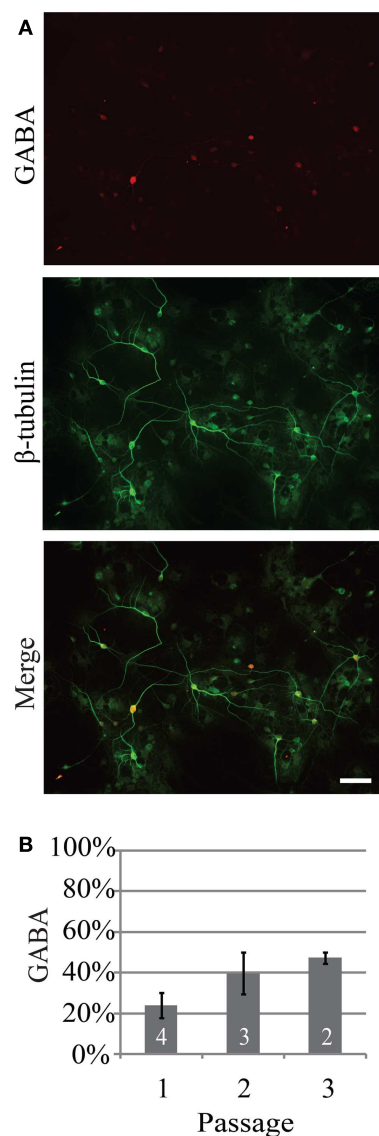
also be more likely to survive over a series of passages in culture perhaps through reduced induction of apoptotic mechanisms as seen in neonatal rat cerebellar cultures (19).

#### ELECTROPHYSIOLOGICAL PROPERTIES OF CULTURED NEURONS

We examined the electrophysiological properties of the cultured neurons using whole cell recordings. Neurons from passage 2 tended to have higher membrane resistances compared to the other passages ( $757 \pm 108$ ,  $985 \pm 169$ ,  $798 \pm 105$  M $\Omega$  for passages 1, 2, and 3 respectively, **Table 1**) however the difference was not significant ( $P = 0.83$ ). There was no significant difference in either the membrane capacitance or resting potential across passages (**Table 1**). Passage 1 cells had a higher current threshold for initiation of action potentials ( $85 \pm 10$  pA) compared to passage 2 and 3 ( $51 \pm 7$  and  $61 \pm 10$  pF respectively). This difference was significant for passage 2 ( $P < 0.03$ , ANOVA with Tukey's *post hoc* comparison, **Table 2**).

Spontaneous synaptic activity between neurons tended to decline as a function of passage number. The number of quiet cells was lowest in passage 1 (4 out of 28, 14%) and highest in passage 3 (7 out of 12, 58%). In passage 2, 4 out of 20 cells were silent (20%). The frequency of synaptic inputs tended to be higher in passage 2 ( $0.5 \pm 0.2$  Hz vs.  $0.32 \pm 0.07$  and  $0.3 \pm 0.2$  Hz for passages 1 and 3 respectively) but the difference was not significant ( $P = 0.19$ ). Examples of evoked and spontaneous synaptic activity are shown in **Figures 4A,B** respectively. In **Figure 4A** simultaneous





**FIGURE 2 | The percentage of neurons generated from neurospheres that are GABAergic increases as a function of passage.**

**(A)** Representative example of GABAergic immunoreactivity (red) in neurons from passage 2, 14 days *in vitro*. Neurons were identified by expression of β-tubulin (green). **(B)** Percentage of neurons that were GABAergic following three consecutive passages. Scale bar equals 50 μm.

whole cell recordings were used to evoke action potentials in one cell (square steps in the blue command traces) while recording the resulting synaptic activity in the other cell. In contrast to action potential mediated responses, hyperpolarizing each cell did not produce a change in the opposite cell suggesting the absence of gap junctions between the two cells. Voltage clamp recordings of spontaneous postsynaptic currents (PSC) activity for these cells is shown in **Figure 4B** and is representative of activity observed in all neurons with active inputs. Bath application of 500 nM gabazine, a GABA<sub>A</sub> receptor antagonist, changed the frequency of synaptic activity but in a variable manner between cells (data not shown)

suggesting the presence of functional GABAergic synapses within the cultured network.

In a subset of recordings, Neurobiotin was included in the intracellular solution. **Figure 5** shows two examples of Neurobiotin labeled cells following immunohistochemistry for GABA. The cell in **Figure 5A** was positive for GABA (upper left) and had smooth processes relatively free of spines, a morphology consistent with neocortical inhibitory neurons (20). Conversely, the neuron depicted in the **Figure 5B** was immuno-negative for GABA (lower left) and, like excitatory neurons of the neocortex (21), had many visible spinous processes when visualized with NeutrAvidin-Alexa488 (lower middle panel; inset shows closer view of dendritic tree). Although neurons across passages were capable of firing multiple action potentials, we did not observe the distinct fast-spiking firing pattern of GABAergic neurons observed in slices of the neocortex or *in vivo* (22–24).

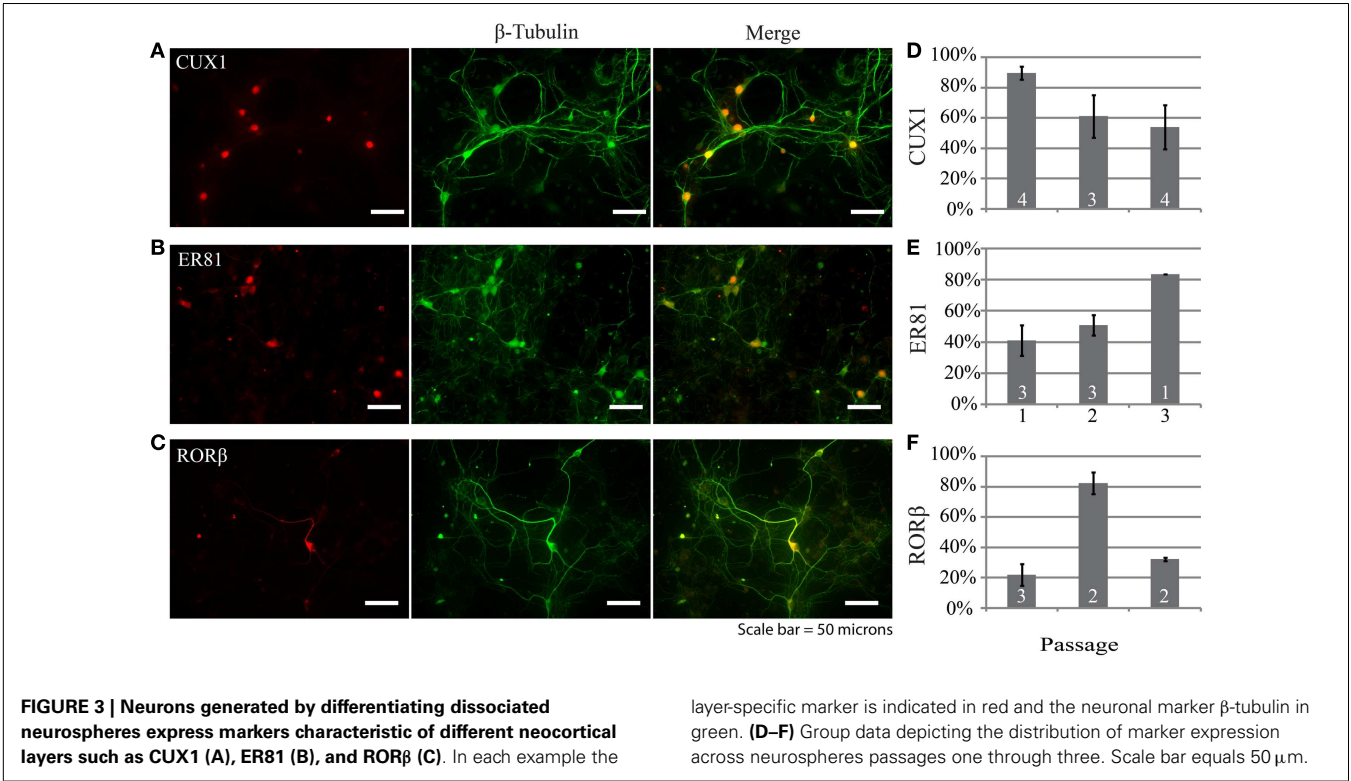
### TRANSPLANTATION OF EMBRYONIC NEURONS

To investigate the regenerative potential of NPC we harvested cells from the neocortex of embryonic GFP-expressing mice and transplanted them into an injured region in the neocortex of brain slices obtained from neonatal mice. GFP-expressing cells remained largely confined to the injury site and frequently retained or established morphologies consistent with neurons. The transplanted cells were also capable of generating long range neurite projections that presumably consisted of axons (representative examples in **Figure 6**). These projections tended to be most dense and focused when projecting away from the cortex (red arrows in **Figures 6A,B**) and more diffuse within the neocortex (**Figure 6A'**). Electrophysiological recordings from GFP<sup>+</sup> cells 4–7 days after transplantation displayed neuronal phenotypes with spontaneous synaptic inputs present in four out of eight cells (representative example in **Figure 6C**, mean frequency of  $0.12 \pm 0.4$  Hz). GFP<sup>+</sup> neurons also exhibited firing patterns typical of fast spiking and regular-spiking neurons in response to depolarizing current steps (presumed inhibitory and excitatory neurons respectively, **Figure 6D**). The electrophysiological properties of the transplanted neurons did not differ over the time points examined.

### DISCUSSION

Damage to the neocortex either through TBI or focal hypoxia can lead to destruction of impacted regions of the neocortex and can result in behavioral deficits. These deficits can be severe and significantly impact the quality of life in affected individuals. With the increased use of improvised explosive devices in the wars in Afghanistan and Iraq there has been a sharp rise in individuals suffering from the effects of TBI (25, 26). However, our ability to treat and reverse the behavioral deficits resulting from brain trauma remains limited. The ability to replace lost or damaged neocortical networks through transplantation of NPC may result in functional recovery from the injury (27). The goal of our present study was to investigate how donor NPC could be guided toward becoming neurons phenotypic of a specific cortical layer as part of a targeted cell replacement therapy. Specifically, we hypothesized that reproducing *in vitro* the iterative cell division cycle that occurs in the developing neocortex during embryogenesis *in vivo* would generate specific neuronal subtypes.





**Table 1 |** Passive membrane properties of neurons differentiated from neurospheres.

	Psg	Mean	SEM	N	P
Membrane resistance (MΩ)	1	757	108	30	0.83
	2	985	169	20	
	3	798	105	12	
Membrane capacitance (pF)	1	39	3	30	0.82
	2	34	3	20	
	3	36	5	12	
Resting potential (mV)	1	−56	1	30	0.85
	2	−58	2	20	
	3	−57	2	12	

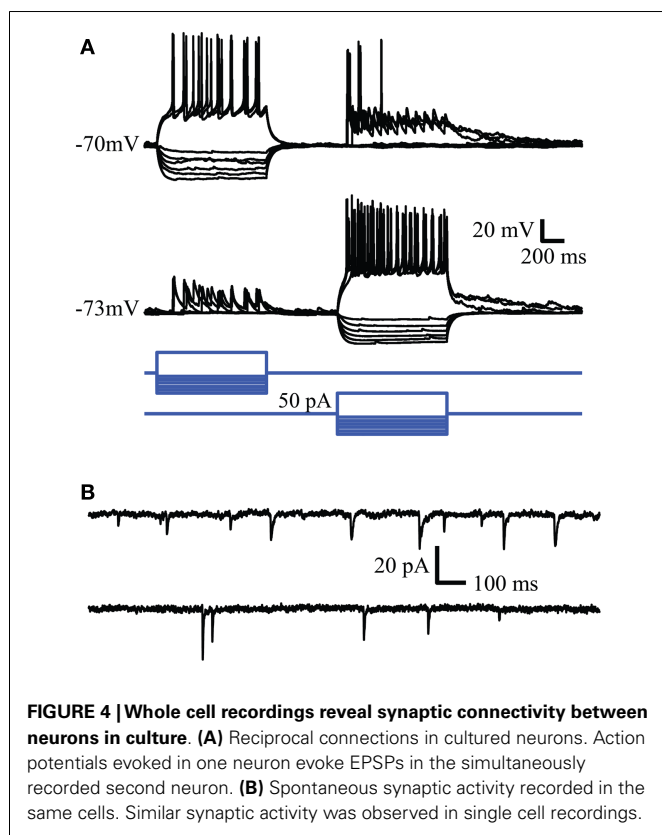
In mice, the neurons populating the neocortex are generated during embryonic days 11 through 17 (E11 and E17 respectively) from the ventricular and subventricular zone (11). Located on the ventricular walls of the developing cortex, NPC repeatedly divide giving rise to neurons that migrate dorsally through previously populated layers of the neocortex resulting in an inside-out manner of construction [e.g., (4, 28–30) for reviews]. NPCs undergo 11 cycles of division with a duration that increases with subsequent divisions (11). Thus, in addition to other trophic signaling factors in the extracellular milieu, the duration and number of cell division cycles appears to play a role in determining the final fate of newly born neurons during embryonic development (12). Upon completion of neocortical development, neurogenesis in the proliferative regions of the cerebral cortex largely ceases (31) while patterning of neuronal connectivity continues. Although

**Table 2 |** Active membrane properties of neurons differentiated from neurospheres.

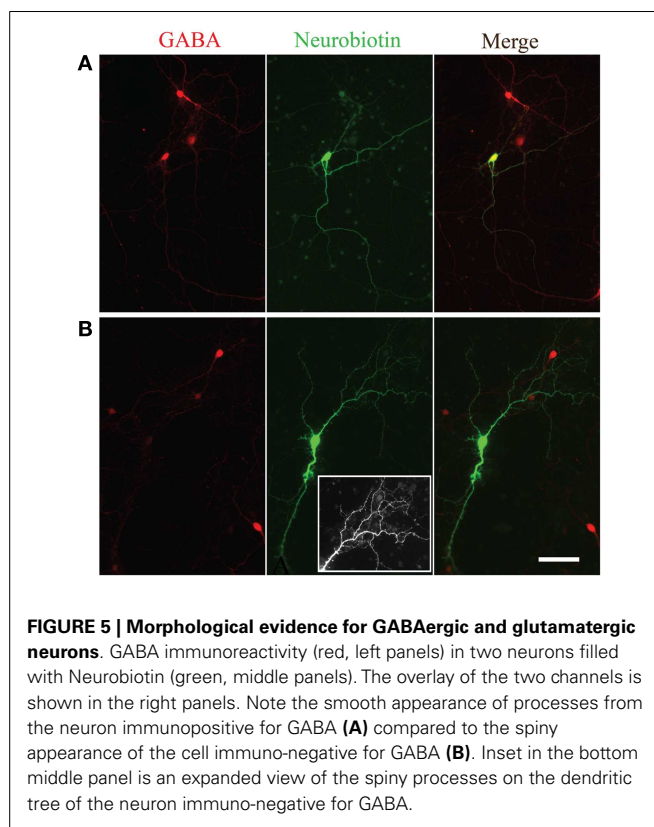
	Psg	Mean	SEM	N	P
Rheobase (pA)	1	85	10	27	0.03
	2	51	7	16	
	3	61	10	12	
Threshold (mV)	1	−32	1	27	0.77
	2	−32	2	16	
	3	−33	1	12	
HWHM (ms)	1	1.6	0.1	27	0.78
	2	1.5	0.1	16	
	3	1.6	0.2	12	
Peak rise rate (mV/s)	1	55	6	27	0.83
	2	58	7	16	
	3	52	5	12	
Peak decay rate (mV/s)	1	−21	2	27	0.78
	2	−22	2	16	
	3	−23	2	12	

Neurons from passage 2 had a lower action potential threshold than those from passage 1 ( $P = 0.03$  ANOVA with Tukey's post hoc comparison).

injury to the brain can stimulate some degree of neurogenesis from NPCs present in the mature brain (32–35), this apparent attempt at circuit repair is insufficient for restoring damaged networks. As a potential avenue for overcoming the limitations to repair damaged neocortical networks, we sought to proliferate layer-specific neurons *in vitro* using relatively developed embryonic mouse neocortex as a tissue source. We found neurons expressing



**FIGURE 4 | Whole cell recordings reveal synaptic connectivity between neurons in culture. (A)** Reciprocal connections in cultured neurons. Action potentials evoked in one neuron evoke EPSPs in the simultaneously recorded second neuron. **(B)** Spontaneous synaptic activity recorded in the same cells. Similar synaptic activity was observed in single cell recordings.



**FIGURE 5 | Morphological evidence for GABAergic and glutamatergic neurons.** GABA immunoreactivity (red, left panels) in two neurons filled with Neurobiotin (green, middle panels). The overlay of the two channels is shown in the right panels. Note the smooth appearance of processes from the neuron immunopositive for GABA **(A)** compared to the spiny appearance of the cell immuno-negative for GABA **(B)**. Inset in the bottom middle panel is an expanded view of the spiny processes on the dendritic tree of the neuron immuno-negative for GABA.

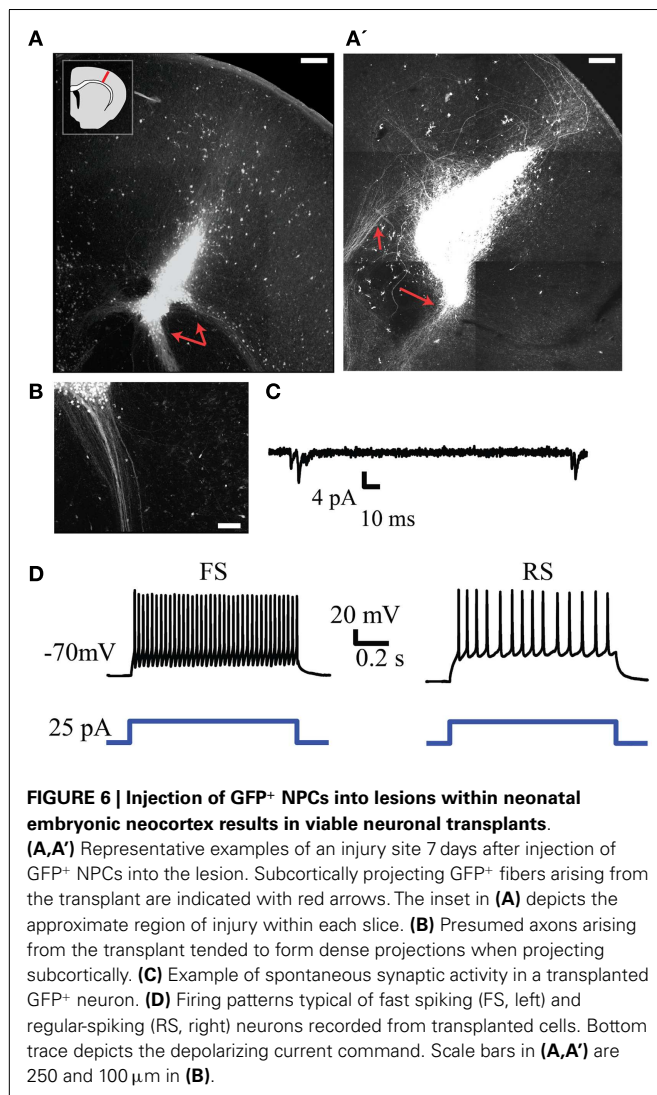
layer-specific markers (Cux1, RoR $\beta$ , and Er81) were present following a single cycle of neurosphere proliferation and differentiation. Additionally, although the relative composition changed, neurons with these markers remained present through the last passage examined, passage 3. Thus this process is capable of producing neurons phenotypic of upper, middle, and deep cortical lamina (17, 18, 36). Our results also support the hypothesis that the mechanisms required to guide neuronal fates are at least partially intrinsic to the cells themselves (13).

In addition to presumed excitatory layer-specific neurons we found that repeated passaging of neurospheres generated from embryonic mouse neocortex also produced GABAergic neurons. The percentage of cells immunopositive for GABA increased as a function of passage. The ability to generate GABAergic neurons is essential for maintaining the proper balance between excitation and inhibition with any putative transplant. Excessive excitatory drive within a cortical network may lead to seizure activity and exacerbation of damage to the neocortex.

Electrophysiological recordings from cells differentiated from neurospheres revealed active and passive membrane properties consistent with neurons. Recorded cells had hyperpolarized resting potentials and membrane resistances and capacitances consistent with neurons. The individual values varied widely between different neurons representing a range of maturity similar to those observed in neurons generated from an mouse ES cell line (37, 38). These differences likely reflect a lower density of ion channels in the cell membrane and a less expansive dendritic tree compared to more mature neurons. Both mature and immature-like neurons

were present in all three passages examined suggesting similar maturation rates of neurons from each passage. When acutely isolated cells from embryonic mouse neocortex were transplanted into neonatal brain slices we observed a similar development and maturation of neurons from the transplant. Although the phenotype of the neurons was not examined immunohistochemically after transplantation into a slice, we observed neurons with fast- and regular-spiking activity characteristic of inhibitory and excitatory neurons respectively. We also observed that neurons grown either in dissociated cell cultures from neurospheres or in brain slices developed functional synaptic contacts. These results suggest that transplanted neurons can indeed develop and maintain neuronal properties and successfully integrate with surrounding neurons.

As these and similar studies progress it will be important to consider the role of glial cells that develop from the transplanted population. The formation of glial scars following CNS injury are associated with a diminished capacity for endogenous rebuilding of damaged neuronal networks (39, 40). Thus, although we have previously demonstrated that glia are rare in similar neural progenitor cell cultures (41), glia arising from transplanted cells may potentially contribute to scar formation and or, conversely, they may produce supportive substances (42–44) that encourage the health of transplanted cells. Although we did not directly investigate whether the presumed axons we observed following transplantation were myelinated, similar studies have found that oligodendrocytes arise from grafted neural stem or progenitor cells (45, 46). Thus transplanted NPCs that become glia may contribute to the overall health of the transplant and its functional



integration with the host networks. Isolating layer-specific neurons generated *in vitro* either through successive passaging as we and others describe (13), or actively through the regulation of cell signaling pathways (47–49) could help achieve the ideal balance between neurons and supportive glia within the transplant. An additional challenge will be successfully transplanting cells into adult tissue where the environment is less conducive to transplant survival.

In this work we investigated the potential of generating layer-specific neurons *in vitro* for potential transplantation into damaged regions of the neocortex. We found that repeatedly passaging neurospheres and differentiating the resulting cells can produce a range of neurons characteristic of those found in the mature neocortex both in electrophysiological characteristics and in the expression of layer-specific markers. Acutely isolated NPCs transplanted into neonatal brain slices could develop into electrophysiologically mature neurons and form functional synaptic connections with the surrounding neurons. Together, our results suggest that generation of specific neocortical neurons *in vitro* may

lead to viable network reconstruction therapies to restore lost or damaged neuronal networks.

## AUTHOR CONTRIBUTIONS

Nathan Peter Cramer designed the experiments and performed cell transplants, slice cultures, electrophysiological recordings, collected and analyzed the data, and prepared the manuscript. Mitali Chatterjee harvested embryonic tissue, maintained neurosphere cultures, performed immunohistochemistry, and assisted with image collection. Fritz Lischka performed electrophysiological recordings. Sharon L. Juliano designed the experiments, oversaw all aspects of data collection and analysis and prepared the manuscript.

## ACKNOWLEDGMENTS

This work was supported by the Center for Neuroscience and Regenerative Medicine (CNR) Neuroregeneration grant number G1703K.

## REFERENCES

1. Blennow K, Hardy J, Zetterberg H. The neuropathology and neurobiology of traumatic brain injury. *Neuron* (2012) **76**:886–99. doi:10.1016/j.neuron.2012.11.021
2. Reekmans K, Praet J, Daans J, Reumers V, Pauwels P, Linden AV, et al. Current challenges for the advancement of neural stem cell biology and transplantation research. *Stem Cell Rev* (2012) **8**:262–78. doi:10.1007/s12015-011-9266-2
3. Ugoya SO, Tu J. Bench to bedside of neural stem cell in traumatic brain injury. *Stem Cells Int* (2012) 2012. [cited 2013 Jun 6]. Available from: <http://www.hindawi.com/journals/sci/2012/141624/abs/>
4. Kriegstein AR, Noctor SC. Patterns of neuronal migration in the embryonic cortex. *Trends Neurosci* (2004) **27**:392–9. doi:10.1016/j.tins.2004.05.001
5. Hansen DV, Lui JH, Parker PRL, Kriegstein AR. Neurogenic radial glia in the outer subventricular zone of human neocortex. *Nature* (2010) **464**:554–61. doi:10.1038/nature08845
6. Martínez-Cerdeño V, Cunningham CL, Camacho J, Antczak JL, Prakash AN, Cziep ME, et al. Comparative analysis of the subventricular zone in rat, ferret and macaque: evidence for an outer subventricular zone in rodents. *PLoS One* (2012) **7**:e30178. doi:10.1371/journal.pone.0030178
7. Tabata H, Yoshinaga S, Nakajima K. Cytoarchitecture of mouse and human subventricular zone in developing cerebral neocortex. *Exp Brain Res* (2012) **216**:161–8. doi:10.1007/s00221-011-2933-3
8. Poluch S, Juliano SL. Fine-tuning of neurogenesis is essential for the evolutionary expansion of the cerebral cortex. *Cereb Cortex* (2013). doi:10.1093/cercor/bht232. [Epub ahead of print].
9. Angevine JB Jr, Sidman RL. Autoradiographic study of cell migration during histogenesis of cerebral cortex in the mouse. *Nature* (1961) **192**:766–8. doi:10.1038/192766b0
10. McConnell SK, Kaznowski CE. Cell cycle dependence of laminar determination in developing neocortex. *Science* (1991) **254**:282–5. doi:10.1126/science.1925583
11. Takahashi T, Nowakowski RS, Caviness VS. The cell cycle of the pseudostratified ventricular epithelium of the embryonic murine cerebral wall. *J Neurosci* (1995) **15**:6046–57.
12. Takahashi T, Goto T, Miyama S, Nowakowski RS, Caviness VS. Sequence of neuron origin and neocortical laminar fate: relation to cell cycle of origin in the developing murine cerebral wall. *J Neurosci* (1999) **19**:10357–71.
13. Shen Q, Wang Y, Dimos JT, Fasano CA, Phoenix TN, Lemischka IR, et al. The timing of cortical neurogenesis is encoded within lineages of individual progenitor cells. *Nat Neurosci* (2006) **9**:743–51. doi:10.1038/nn1694
14. Schindelin J, Arganda-Carreras I, Frise E, Kaynig V, Longair M, Pietzsch T, et al. Fiji: an open-source platform for biological-image analysis. *Nat Methods* (2012) **9**:676–82. doi:10.1038/nmeth.2019
15. Caviness VS Jr, Sidman RL. Time of origin or corresponding cell classes in the cerebral cortex of normal and reeler mutant mice: an autoradiographic analysis. *J Comp Neurol* (1973) **148**:141–51. doi:10.1002/cne.901480202

16. Caviness VS Jr. Neocortical histogenesis in normal and reeler mice: a developmental study based upon [3H]thymidine autoradiography. *Brain Res* (1982) 4:293–302. doi:10.1016/0165-3806(82)90141-9
17. Hevner RF, Daza RAM, Rubenstein JLR, Stunnenberg H, Olavarria JF, Englund C. Beyond laminar fate: toward a molecular classification of cortical projection/pyramidal neurons. *Dev Neurosci* (2003) 25:139–51. doi:10.1159/000072263
18. Hirokawa J, Watakabe A, Ohsawa S, Yamamori T. Analysis of area-specific expression patterns of RORBeta, ER81 and Nurr1 mRNAs in rat neocortex by double in situ hybridization and cortical box method. *PLoS One* (2008) 3:e3266. doi:10.1371/journal.pone.0003266
19. Catania MV, Copani A, Calogero A, Ragonese GI, Condorelli DF, Nicoletti F. An enhanced expression of the immediate early gene, Egr-1, is associated with neuronal apoptosis in culture. *Neuroscience* (1999) 91:1529–38. doi:10.1016/S0306-4522(98)00544-2
20. Gibson JR, Beierlein M, Connors BW. Two networks of electrically coupled inhibitory neurons in neocortex. *Nature* (1999) 402:75–9. doi:10.1038/47035
21. Peters A, Jones E. *Cerebral Cortex. Cellular Components of the Cerebral Cortex*. New York: Plenum (1985).
22. McCormick DA, Connors BW, Lighthall JW, Prince DA. Comparative electrophysiology of pyramidal and sparsely spiny stellate neurons of the neocortex. *J Neurophysiol* (1985) 54:782–806.
23. Kawaguchi Y, Kubota Y. GABAergic cell subtypes and their synaptic connections in rat frontal cortex. *Cereb Cortex* (1997) 1991(7):476–86. doi:10.1093/cercor/7.6.476
24. Puig MV, Ushimaru M, Kawaguchi Y. Two distinct activity patterns of fast-spiking interneurons during neocortical UP states. *Proc Natl Acad Sci U S A* (2008) 105:8428–33. doi:10.1073/pnas.0712219105
25. Warden D. Military TBI during the Iraq and Afghanistan wars. *J Head Trauma Rehabil* (2006) 21(5):398–402. doi:10.1097/00001199-200609000-00004
26. Tanielian T, Jaycox LH. *Invisible Wounds of War: Psychological and Cognitive Injuries, their Consequences, and Services to Assist Recovery*. Santa Monica, CA: RAND (2008).
27. Shear DA, Tate MC, Archer DR, Hoffman SW, Hulce VD, Laplace MC, et al. Neural progenitor cell transplants promote long-term functional recovery after traumatic brain injury. *Brain Res* (2004) 1026:11–22. doi:10.1016/j.brainres.2004.07.087
28. Rakic P, Caviness VS Jr. Cortical development: view from neurological mutants two decades later. *Neuron* (1995) 14:1101–4. doi:10.1016/0896-6273(95)90258-9
29. Noctor SC, Martínez-Cerdeño V, Ivic L, Kriegstein AR. Cortical neurons arise in symmetric and asymmetric division zones and migrate through specific phases. *Nat Neurosci* (2004) 7:136–44. doi:10.1038/nn1172
30. Cooper JA. A mechanism for inside-out lamination in the neocortex. *Trends Neurosci* (2008) 31:113–9. doi:10.1016/j.tins.2007.12.003
31. Gould E, Reeves AJ, Graziano MS, Gross CG. Neurogenesis in the neocortex of adult primates. *Science* (1999) 286:548–52. doi:10.1126/science.286.5439.548
32. Dash PK, Mach SA, Moore AN. Enhanced neurogenesis in the rodent hippocampus following traumatic brain injury. *J Neurosci Res* (2001) 63:313–9. doi:10.1002/1097-4547(20010215)63:4<313::AID-JNR1025>3.0.CO;2-4
33. Jin K, Minami M, Lan JQ, Mao XO, Bateur S, Simon RP, et al. Neurogenesis in dentate subgranular zone and rostral subventricular zone after focal cerebral ischemia in the rat. *Proc Natl Acad Sci U S A* (2001) 98:4710–5. doi:10.1073/pnas.081011098
34. Thored P, Arvidsson A, Cacci E, Ahlenius H, Kallur T, Darsalia V, et al. Persistent production of neurons from adult brain stem cells during recovery after stroke. *Stem Cells* (2006) 24:739–47. doi:10.1634/stemcells.2005-0281
35. Ohira K. Injury-induced neurogenesis in the mammalian forebrain. *Cell Mol Life Sci* (2011) 68:1645–56. doi:10.1007/s00018-010-0552-y
36. Nieto M, Monuki ES, Tang H, Imitola J, Haubst N, Khoury SJ, et al. Expression of Cux-1 and Cux-2 in the subventricular zone and upper layers II–IV of the cerebral cortex. *J Comp Neurol* (2004) 479:168–80. doi:10.1002/cne.20322
37. Benninger F, Beck H, Wernig M, Tucker KL, Brüstle O, Scheffler B. Functional integration of embryonic stem cell-derived neurons in hippocampal slice cultures. *J Neurosci* (2003) 23(18):7075–83.
38. Risner-Janiczek JR, Ungless MA, Li M. Electrophysiological properties of embryonic stem cell-derived neurons. *PLoS One* (2011) 6:e24169. doi:10.1371/journal.pone.0024169
39. Giovanni SD, Movsesyan V, Ahmed F, Cernak I, Schinelli S, Stoica B, et al. Cell cycle inhibition provides neuroprotection and reduces glial proliferation and scar formation after traumatic brain injury. *Proc Natl Acad Sci U S A* (2005) 102:8333–8. doi:10.1073/pnas.0500989102
40. Wang Y, Moges H, Bharucha Y, Symes A. Smad3 null mice display more rapid wound closure and reduced scar formation after a stab wound to the cerebral cortex. *Exp Neurol* (2007) 203:168–84. doi:10.1016/j.expneurol.2006.08.006
41. Schaefer AW, Juliano SL. Migration of transplanted neural progenitor cells in a ferret model of cortical dysplasia. *Exp Neurol* (2008) 210:67–82. doi:10.1016/j.expneurol.2007.10.005
42. Schwartz JP, Nishiyama N. Neurotrophic factor gene expression in astrocytes during development and following injury. *Brain Res Bull* (1994) 35:403–7. doi:10.1016/0361-9230(94)90151-1
43. do Carmo Cunha J, de Freitas Azevedo Levy B, de Luca BA, de Andrade MSR, Gomide VC, Chadi G. Responses of reactive astrocytes containing S100 $\beta$  protein and fibroblast growth factor-2 in the border and in the adjacent preserved tissue after a contusion injury of the spinal cord in rats: implications for wound repair and neuroregeneration. *Wound Repair Regen* (2007) 15:134–46. doi:10.1111/j.1524-475X.2006.00194.x
44. White RE, Yin FQ, Jakeman LB. TGF- $\alpha$  increases astrocyte invasion and promotes axonal growth into the lesion following spinal cord injury in mice. *Exp Neurol* (2008) 214:10–24. doi:10.1016/j.expneurol.2008.06.012
45. Shetty AK, Rao MS, Hattiangady B. Behavior of hippocampal stem/progenitor cells following grafting into the injured aged hippocampus. *J Neurosci Res* (2008) 86:3062–74. doi:10.1002/jnr.21764
46. Chaubey S, Wolfe JH. Transplantation of CD15-enriched murine neural stem cells increases total engraftment and shifts differentiation toward the oligodendrocyte lineage. *Stem Cells Transl Med* (2013) 2:444–54. doi:10.5966/sctm.2012-0105
47. Eiraku M, Watanabe K, Matsuo-Takasaki M, Kawada M, Yonemura S, Matsumura M, et al. Self-organized formation of polarized cortical tissues from ESCs and its active manipulation by extrinsic signals. *Cell Stem Cell* (2008) 3:519–32. doi:10.1016/j.stem.2008.09.002
48. Mutch CA, Funatsu N, Monuki ES, Chenn A.  $\beta$ -catenin signaling levels in progenitors influence the laminar cell fates of projection neurons. *J Neurosci* (2009) 29:13710–9. doi:10.1523/JNEUROSCI.3022-09.2009
49. Hansen DV, Rubenstein JLR, Kriegstein AR. Deriving excitatory neurons of the neocortex from pluripotent stem cells. *Neuron* (2011) 70:645–60. doi:10.1016/j.neuron.2011.05.006

**Conflict of Interest Statement:** The authors declare that the research was conducted in the absence of any commercial or financial relationships that could be construed as a potential conflict of interest.

Received: 11 September 2013; accepted: 18 December 2013; published online: 07 January 2014.

Citation: Cramer NP, Chatterjee M, Lischka FW and Juliano SL (2014) Culturing layer-specific neocortical neurons as a cell replacement therapy following traumatic brain injury. *Front. Neurol.* 4:213. doi: 10.3389/fneur.2013.00213

This article was submitted to *Neurotrauma*, a section of the journal *Frontiers in Neurology*.

Copyright © 2014 Cramer, Chatterjee, Lischka and Juliano. This is an open-access article distributed under the terms of the Creative Commons Attribution License (CC BY). The use, distribution or reproduction in other forums is permitted, provided the original author(s) or licensor are credited and that the original publication in this journal is cited, in accordance with accepted academic practice. No use, distribution or reproduction is permitted which does not comply with these terms.





# Temporal dynamics of cerebral blood flow, cortical damage, apoptosis, astrocyte–vasculature interaction and astrogliosis in the pericontusional region after traumatic brain injury

Sonia Villapol<sup>1,2\*</sup>, Kimberly R. Byrnes<sup>1,3</sup> and Aviva J. Symes<sup>1,2\*</sup>

<sup>1</sup> Center for Neuroscience and Regenerative Medicine, Uniformed Services University of the Health Sciences, Bethesda, MD, USA

<sup>2</sup> Department of Pharmacology, Uniformed Services University of the Health Sciences, Bethesda, MD, USA

<sup>3</sup> Department of Anatomy, Physiology and Genetics, Uniformed Services University of the Health Sciences, Bethesda, MD, USA

## Edited by:

Guoqiang Xing, Lotus Biotech.com, USA

## Reviewed by:

Bruce P. Capehart, Duke University, USA

Zhihui Yang, University of Florida, USA

## \*Correspondence:

Sonia Villapol and Aviva J. Symes, Center for Neuroscience and Regenerative Medicine, Uniformed Services University of the Health Sciences, 4301 Jones Bridge Road, Bethesda, MD 20814, USA  
e-mail: svillapol@gmail.com; aviva.symes@usuhs.edu

Traumatic brain injury (TBI) results in a loss of brain tissue at the moment of impact in the cerebral cortex. Subsequent secondary injury involves the release of molecular signals with dramatic consequences for the integrity of damaged tissue, leading to the evolution of a pericontusional-damaged area minutes to days after in the initial injury. The mechanisms behind the progression of tissue loss remain under investigation. In this study, we analyzed the spatial–temporal profile of blood flow, apoptotic, and astrocytic–vascular events in the cortical regions around the impact site at time points ranging from 5 h to 2 months after TBI. We performed a mild–moderate controlled cortical impact injury in young adult mice and analyzed the glial and vascular response to injury. We observed a dramatic decrease in perilesional cerebral blood flow (CBF) immediately following the cortical impact that lasted until days later. CBF finally returned to baseline levels by 30 days post-injury (dpi). The initial impact also resulted in an immediate loss of tissue and cavity formation that gradually increased in size until 3 dpi. An increase in dying cells localized in the pericontusional region and a robust astrogliosis were also observed at 3 dpi. A strong vasculature interaction with astrocytes was established at 7 dpi. Glial scar formation began at 7 dpi and seemed to be compact by 60 dpi. Altogether, these results suggest that TBI results in a progression from acute neurodegeneration that precedes astrocytic activation, reformation of the neurovascular unit to glial scar formation. Understanding the multiple processes occurring after TBI is critical to the ability to develop neuroprotective therapeutics to ameliorate the short and long-term consequences of brain injury.

**Keywords:** astrogliosis, cell death, cerebral blood flow, vasculature, glial scar

## INTRODUCTION

Traumatic brain injury (TBI) can result in significant impairment of function, if the patient survives the initial impact. TBI induces a series of events in the brain that trigger an instantaneous loss of tissue and damaged area around the impact site (1). Repair of the damaged brain may result from avoiding or reducing secondary neuronal degeneration and decreasing glial activation that leads to the deterioration of the neurological state.

Excessive glutamate stimulation induces excitotoxicity predominantly in neurons and has been linked to the pathological process of various chronic CNS diseases and TBI (2). Under this pathological environment within the injured cortex, apoptosis, inflammation, gliosis, and a reduction in regional cerebral blood flow (CBF), all play a role in secondary cell injury (3). This secondary reaction is predominately located in the primary cortical lesion and around the core impact zone, referred to as the perilesional or pericontused regions (4). A collection of detrimental mechanisms contributes to this secondary injury, including edema, decreased CBF, disruption of the blood–brain barrier

(BBB), necrosis, apoptosis, gliosis, excitotoxicity and energy depletion. These dynamic processes, involving glial cells and vessels, are becoming the target of potential therapeutics to treat brain trauma.

The neurovascular unit is also altered after TBI, although much less is known about this process (5). The neurovascular system is composed of a complex network of neurons, astrocytes, and cerebral blood vessels (endothelium, smooth muscle cells, and perivascular matrix) (6). Cerebrovascular dysfunction is observed after TBI with a decrease in CBF, glucose consumption, and oxygen extraction (7). However, the temporal pattern of disruption and the underlying mechanisms remain poorly understood.

Astrocytes are thought to play a crucial role in response to injury; they are important in neuronal antioxidant defense, secreting neuroprotective factors, and in maintaining the homeostasis of the extracellular environment after brain injury (8, 9). Astrocytes also provide neurons with energy from metabolic substrates and the precursors of neurotransmitters. On the other hand, astrocytes can contribute to neuronal damage by releasing glutamate in glutamate- and calcium-dependent manners



and thus, support lesion progression (10–12). Further, astrocytic hypertrophy, hyperplasia, and glial scar formation have negative effects on axonal regeneration (13).

The present study reports on the patterns of neurodegeneration, astrogliosis, and neurovascular interactions from 5 h to 2 months after TBI. We examine the short and long-term relationships between vascular changes and astrocytes and their possible involvement in neuronal cell damage after adult brain injury. Collectively, our results indicate an interplay between astrocytes, blood flow, and neurodegeneration that may guide future therapeutic intervention for specific cell types at specific times after TBI.

## MATERIALS AND METHODS

### ANIMALS AND CONTROLLED CORTICAL IMPACT INJURY

The experiments were performed on 75 9-week-old male C57BL/6 mice weighing 21–25 g, which were kept under 12:12 light and dark cycle with access to food and water *ad libitum*. Surgery was performed 1 week after recovery from transportation-related stress. Mice were anesthetized with isoflurane (3% induction, 2% maintained). The skull was fixed in a stereotactic frame and a 5-mm craniotomy was performed above the left parietal cortex. We performed mild–moderate controlled cortical impact (CCI) injury (coordinates: 2 mm lateral, 2 mm posterior to Bregma) at an impact depth of 1 mm, with a 2 mm diameter round impact tip (speed 3.6 m/s, dwell time 100 ms) and a 12° angle, using an electromagnetically driven CCI injury device (Impact One stereotaxic impactor CCI, Leica Microsystems GmbH, Wetzlar, Germany). The bone flap was replaced but not sealed, the skin was sutured, and the mice were allowed to recover fully from anesthesia before transfer to their home cages. The mice were sacrificed at 5 h, 1, 3, 7, 14, 30, and 60 days after CCI injury. The control group for all comparisons was comprised of age-matched uninjured naïve mice ( $n = 4–5$ ). All animal studies were approved by the USUHS Institutional Animal Care and Use Committee and were conducted in accordance with the NRC guide to the Care and Use of Laboratory Animals.

### DETERMINATION OF CEREBRAL BLOOD FLOW

Cerebral blood flow was measured in the pericontusional region using a laser-Doppler flowmeter (PeriFlux System 5000 LDPM, Perimed). Changes in CBF were taken using a flexible fiber optic extension to the LDPM probe tip 404 as described previously (14). Baseline values were recorded after positioning the fiber optic extension on the skull at the –2 mm posterior, and 2 mm lateral from Bregma. After CCI injury, to record CBF, animals were anesthetized with isoflurane, the fiber optic extension was positioned on the skull around the craniotomy site, 5–10 measurements were taken at each time point for each animal and averaged. CBF was recorded starting at 15 s after cortical impact, and subsequently at 2 h, and 1, 3, and 30 days after CCI injury. Changes in CBF were expressed as the percentage of the baseline value recorded before CCI injury.

### Nissl STAINING AND LESION VOLUME MEASUREMENTS

Mice were sacrificed at 5 h, 1, 3, 7, 14, 30, and 60 days post-injury (dpi) by transcardial perfusion with 4% paraformaldehyde (PFA) in phosphate buffer. Brains were removed and placed in 4% PFA overnight, then transferred to 30% sucrose solution and stored at

4°C. Brains were cut in 30  $\mu$ m-thick sections using a microtome and were stored in cryoprotectant solution. Every third section was chosen for Nissl staining to reveal histology of the cortical lesion area. Brain slices were mounted on polylysine-coated slides and stained for 20 min with 0.1% cresyl-violet (Sigma) dissolved in distilled water and filtered. Slides stained were dehydrated for 2 min using 100, 95, 70, and 50% ethanol, cleared in xylene for another 2 min, covered with DPX, and coverslipped. Lesion volume was obtained by multiplying the sum of the lesion areas by the distance between 9 and 15 brain sections. Percent lesion volume was calculated by dividing each lesion volume by the total ipsilateral hemisphere volume (similarly obtained by multiplying the sum of the areas of the ipsilateral hemispheres by the distance between sections).

### IMMUNOFLOUORESCENCE ANALYSIS

Sections were blocked with 10% normal goat serum (NGS) in PBS with 0.1% Triton X-100 (PBS-T) for 1 h. The following primary antibodies were incubated at 4°C overnight in PBS-T and 5% NGS: anti-glial fibrillary acidic protein (GFAP), either mouse monoclonal (1:2000, Millipore) or chicken polyclonal (1:400, abcam) for astrocytes; anti-vimentin, mouse monoclonal (1:200, Sigma) for reactive astrocytes; anti-NeuN, mouse monoclonal (1:200, Chemicon) for mature neurons; anti-Iba-1 rabbit polyclonal (1:750, Wako) for microglia; and anti-collagen IV rabbit polyclonal (1:3000, Chemicon) a component of the basal lamina that is used as a specific marker for cerebral microvessels (15). Sections were washed in PBS-T three times and incubated with the corresponding Alexa Fluor 568-conjugated (red) and Alexa Fluor 488-conjugated (green) IgG secondary antibodies (all 1:1000, Invitrogen) for 2 h at room temperature. Sections were rinsed with PBS and distilled water and coverslipped with ProLong Gold antifade reagent with DAPI (Invitrogen).

### CELL DEATH ASSAY

Sections were processed for DNA strand breaks (TUNEL assay, labeling of fragmented DNA) using the Fluorescence *In situ* Cell Death Detection Kit (Roche, IL, USA), according to the manufacturer's instructions. TUNEL-positive nuclei were counted in cortical regions in three to five coronal sections for each animal, with five animals per group.

### QUANTITATIVE AND DENSITOMETRY ANALYSIS

Quantitative image analysis of the immunoreactive areas for GFAP, Iba-1, and collagen IV clusters positive cells were performed on five cortical sections per brain through the level of impact site (AP: 2.0 mm) taken with the  $\times 20$  objective and using the same densitometric analysis method as previously described (16). Immunofluorescence intensity was calculated using the threshold method and defined as the number of pixels, divided by the total area (square millimeter) in the imaged field with the average background subtracted. The grade of astrogliosis was calculated by GFAP immunoreactivity values (IR-GFAP) multiplied by the number of GFAP-positive astrocytes. To assess astrocytic interaction with microvessels, we co-stained brain sections with GFAP and collagen IV; colocalization clusters were determined by pixel-by-pixel quantification of both markers that connected astrocytes

and vessels. Images were acquired on an Olympus BX61 with attached qImaging Retiga EXi Aqua CCD camera, and iVision software (BioVision Technologies, Exton, PA, USA). For colocalized images, double-stained cells were analyzed with a Zeiss confocal-laser scanning microscope (LSM 510) equipped with argon and He/Ne 488 and 568 nm laser. Images were taken at 20 $\times$ , 40 $\times$ , and 63 $\times$  magnification, and cropped and adjusted using Adobe Photoshop CS5.

### STATISTICAL ANALYSES

Data were analyzed using one-way analysis of variance (ANOVA) for comparison of measurements at different time points after CCI injury with those of naïve control brains. Quantitative data for all figures and tables are expressed as mean  $\pm$  SEM, except for CBF measurements that are expressed as mean  $\pm$  SD. All statistics were analyzed using Prism software (Graphpad).

## RESULTS

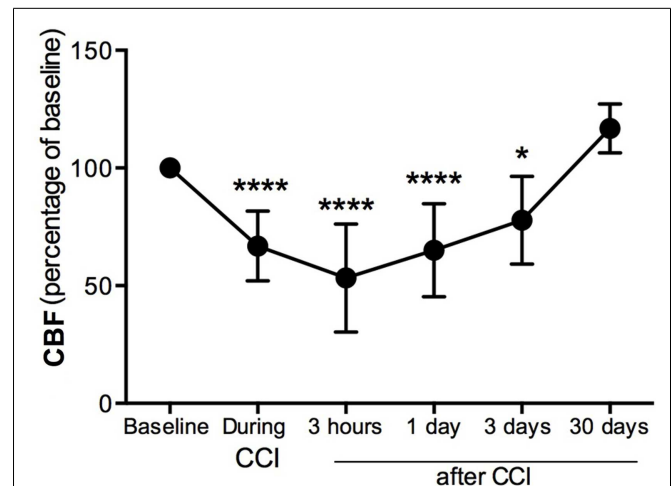
In this study we determined, in the pericontusional cortical region, the temporal progression of post-injury alterations in CBF, cell death, and the vascular–astroglial response in the mouse after mild–moderate CCI injury. The study of these perilesional phenomena is essential to understanding the metabolic equilibrium between glial cells, vasculature, and dying cells. We chose to use naïve mice as our controls rather than those with craniotomy as we have previously shown with an identical injury, the mice subject to craniotomy had equivalent numbers of GFAP-positive proliferative astrocytes as those undergoing CCI (17). Our experience is consistent with that of others who have shown that craniotomy alone is equivalent to a minor injury in terms of the acute inflammatory response (18). As we wanted to compare injured mice with uninjured, we used naïve mice as controls in all our experiments.

### DECREASE OF CEREBRAL BLOOD FLOW IN THE PERICONTUSIONAL AREA AFTER CCI INJURY

Cerebral blood flow was measured in the pericontusional region around the impact site where a hole was perforated in the skull. CBF was decreased 34% immediately (seconds) after the impact contusion (“during CCI”) (Figure 1) compared to baseline levels. Three hours after injury, we found the CBF to be 53% of baseline levels, the lowest CBF measured. CBF increased at 1 and 3 dpi, reaching 35 and 23%, respectively, of the baseline levels initially obtained before CCI injury (Figure 1). By 30 dpi, CBF was restored to baseline.

### PERICONTUSIONAL-DAMAGED AREAS AND CORTICAL CAVITY GENERATED AFTER CCI INJURY

We assessed the pattern of cortical lesion volume at 5 h and 1, 3, 7, 14, 30, and 60 dpi (Figure 2), dividing tissue damage into lesion cavity and pericontusional area (Figure 2C). Nissl staining revealed an immediate loss of cortical tissue after the impact–rounded tip entered the sensorimotor cortex. As early as 5 h post-injury, neocortical Nissl staining diminished in intensity, and scattered cell loss and shrinkage was evident through all neocortical layers (Figure 2). A damaged region around the contusion site was also generated early. Damaged tissue was evident via

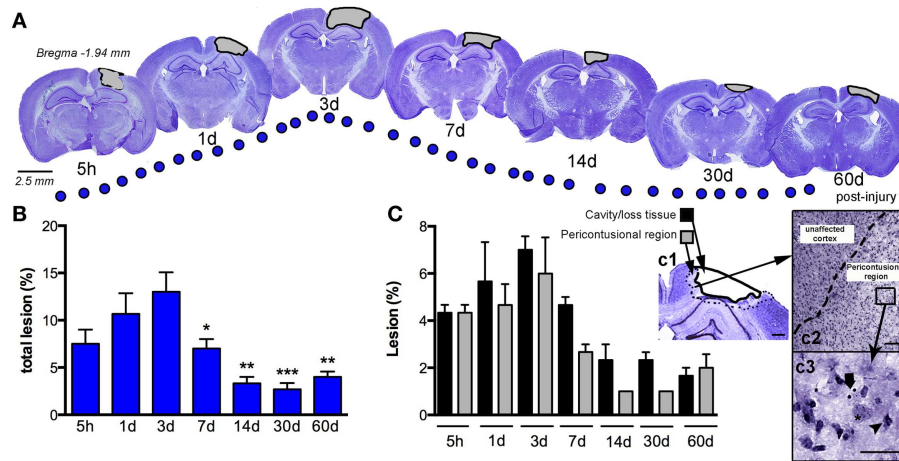


**FIGURE 1 | Cerebral blood flow decreases in the pericontusional region after CCI injury.** Cerebral blood flow (CBF) measurements were expressed as percentage of baseline levels before injury. CBF was reduced in the injured cerebral cortex during CCI injury, and at 3 h, 1 dpi, and 3 dpi; it increased at 4 weeks after CCI injury. Values are expressed as the mean  $\pm$  SD,  $n = 8$ –10 per group, \* $p < 0.05$ , \*\*\*\* $p < 0.0001$  compared to baseline.

a loss of Nissl intensity with the pyknotic and apoptotic neurons delimiting the pericontusional region (Figures 2c1–c3). At 1 dpi, the injury cavity increased despite a loss of necrotic tissue, while the pericontusional region remained unchanged. At 3 dpi, the cavity expanded further, contributing to the peak volume of both lesioned cortex and damaged pericontusional regions (Figures 2B,C). This cortical lesion volume decreased at 7, 14, 30, and 60 dpi.

### BIPHASIC PEAK OF CELL DEATH IN THE PERICONTUSIONAL REGION

Quantification of cell death (by TUNEL-positive cells) within the ipsilateral sensorimotor cortex following injury revealed marked loss overtime during the evolution of cortical damage. By 5 h after injury, we observed a significant increase in the number of apoptotic cells that were diffusely distributed throughout the pericontusional region (Figure 3A). At 1 dpi, there was a reduction in dying cells; however, at 3 dpi there was a secondary peak in apoptosis around the lesioned area, which correlated with increased astroglial reactivity (Figure 4). TUNEL labeled morphologically distinct cells were principally neurons with apoptotic bodies and chromatin condensation (Figure 3Aa). Dying astrocytes were also identified at 1 and 3 dpi with double staining via vimentin and GFAP (Figure 3Ab). Additionally, Iba-1-positive microglial cells with TUNEL-positive nuclei (Figure 3Ac) showing typical phagocytic morphology were observed at 3 dpi (Figure 3Ad). At 7 dpi, we occasionally observed dying neurons and sporadic Iba-1/TUNEL-positive cells. At longer time points (14, 30, and 60 dpi), rare cases of dying neurons were observed (Figure 3C). Combined, these findings suggest that neurons are the main cell population susceptible to death, especially at early time points after TBI.



**FIGURE 2 | Temporal progression of the cortical lesion.**

(A) Representative drawings of Nissl staining from coronal sections at 5 h, and 1, 3, 7, 14, 30, and 60 days post-CCI injury (dpi). Black lines delimit the lesioned cortex (gray). (B) Graph shows the percent lesioned area relative to the area of the whole ipsilateral hemisphere, starting at 5 h after injury, with a peak at 3 days and remaining up to 60 days after injury. (C) Graph illustrates the composition of the total lesion that is either cavity (or lost tissue) versus the damaged pericontusional region as a percentage of the area of the total

ipsilateral hemisphere at different times post-injury. (c1) Representative images showing the delimited damaged cortical regions corresponding to cavity or tissue loss or the pericontusional region. High magnification image of the unaffected cortex and pericontusional region (c2) containing apoptotic cells (c3, arrow) and chromatin condensate (c3, arrowhead). Scale bar; 100  $\mu$ m (c1), 50  $\mu$ m (c2), and 20  $\mu$ m (c3). Values are expressed as the mean  $\pm$  SEM,  $n = 3$ –5 per group, \* $p < 0.05$ , \*\* $p < 0.01$ , \*\*\* $p < 0.0001$  compared to 3 dpi.

## DYNAMIC OF ASTROCYTIC ACTIVATION IN RESPONSE TO CORTICAL DAMAGED

Astrogliosis, observed by GFAP staining, was not apparent at early time points (5 h post-injury and 1 dpi) but appeared in the pericontusional region at 3 dpi (Figure 4). Activated astrocytes possessed thick, labeled processes, and hypertrophic astrocytic bodies (Figure 4c2). Reactive astrocytes occupied an extended region corresponding to cortical layers II through VI at 3 dpi, mainly around the impact site and near the lesion border. GFAP/vimentin double-labeled cells identified astrocytic activation that was extended to the peripheral cortical regions near the lesion core. At 3 dpi, vimentin expressing astrocytes were distributed around the impact site, mainly associated with reactive astrocytes in the gliotic tissue (Figures 4a–c). At 7 dpi, the branches of vimentin/GFAP-positive cells were arranged parallel to each other and perpendicularly to the border of the lesion starting to form the glial scar (Figures 4d–f). GFAP-positive astrocytes were observed at 14 dpi bordering the lesion near the formation of a glial scar (Figures 4g–i). This chronic astrogliosis persisted up until 60 dpi with a notable involvement in maintaining the glial scar, defining the border of the cavity (Figures 4m–o). Quantitative analysis revealed that the grade of astrogliosis had a peak at 3 dpi (Figure 4p). No changes in GFAP upregulation in undamaged areas of the contralateral or naïve control cortex were observed (data not shown).

## ASTROCYTIC–VASCULATURE INTERACTION AFTER INJURY

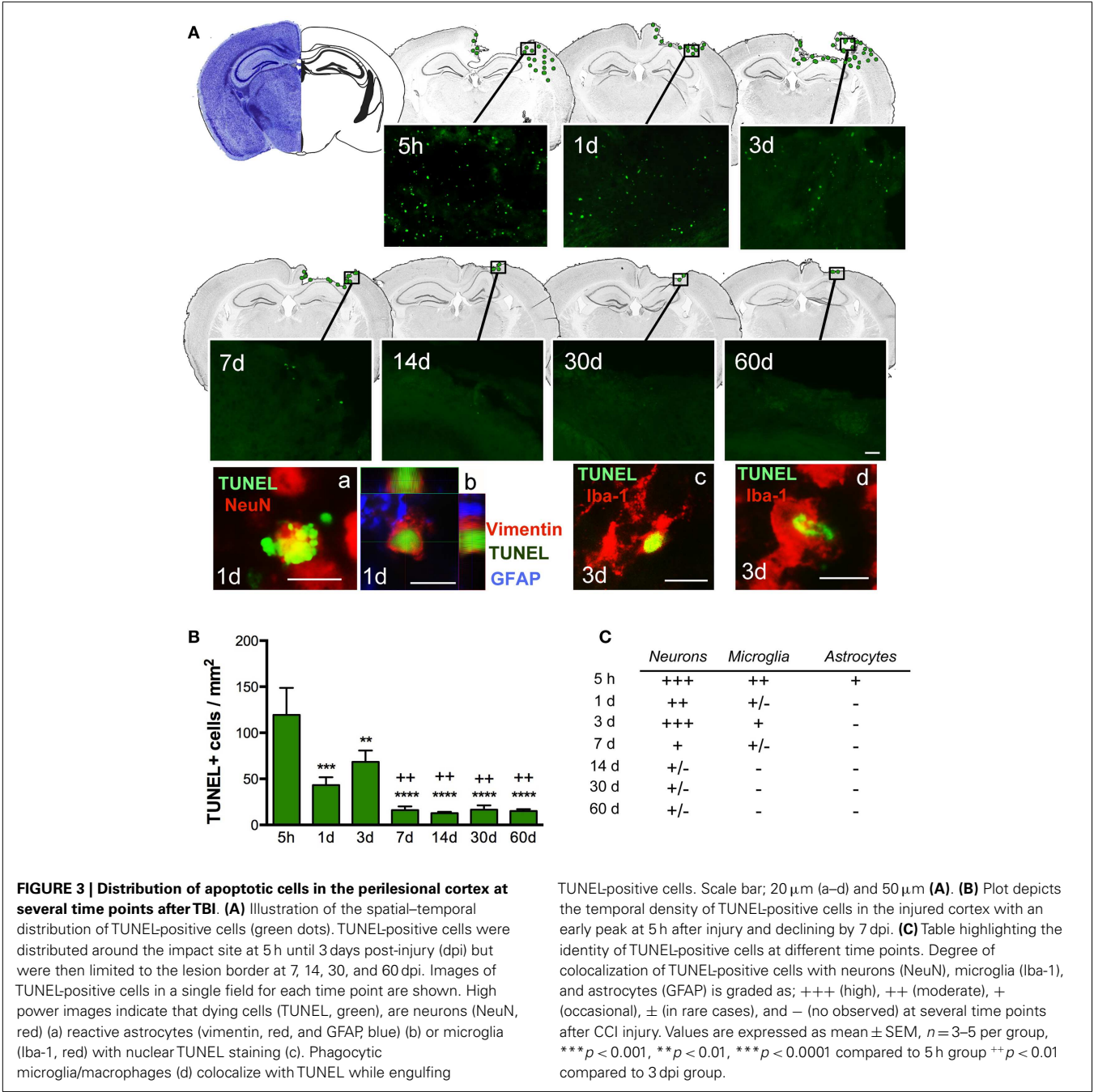
Cerebral vasculature within the pericontusional region was stained with the collagen IV antibody; we observed varying distribution of immunoreactivity after injury (Figures 5a–f). Distribution of cortical microvessels in the perilesional region at 5 h post-injury

(Figure 5a) and 1 dpi (Figure 5b) was similar to uninjured control brains (Figure 5g). After 3 dpi, vessels increased in thickness (Figures 5c–f). Interactions between astrocytes and vessels were detectable at 7 dpi, and this interaction peaked at 14 dpi (Figure 5e). Initial formation of the glial scar was detected at 7 dpi (Figures 5d,d1). Interactions between astrocytes and thick-walled blood vessels remained detectable until 30 dpi (Figures 5f,h). Astrocytic-vessel contacts with the cavity border were maintained until 60 dpi (Figure 5i).

## DISCUSSION

In this study, we have characterized the pattern of neurodegeneration and astrogliosis occurring in the cortex, in conjunction with glial–vascular interactions and alterations of regional CBF, at multiple times points after CCI injury. Our regional analysis of neurovascular interaction provides further understanding of the different responses of astrocytes and vasculature after brain injury.

Our results suggest that a chronically progressive degenerative process in the pericontusional-injured region is initiated hours after CCI injury, but persists for weeks after impact. Thus, there seems to be a relatively broad therapeutic window for drug administration to exert maximum efficacy and ameliorate the short and long-term consequences of TBI. The cascade of events that lead to the initial response could correspond with the rapid release of glutamate and excitotoxic metabolites that subsequently induce cell death (19). This phenomenon has been observed in several models of brain injury, mainly after ischemia, where necrotic cell death has been observed to have a quick yet extended response in the ipsilateral hemisphere (20). We have shown here that a cortical cavity, generated via an impact tip, had maximal extension at 3 days after CCI injury. However, other studies in different brain

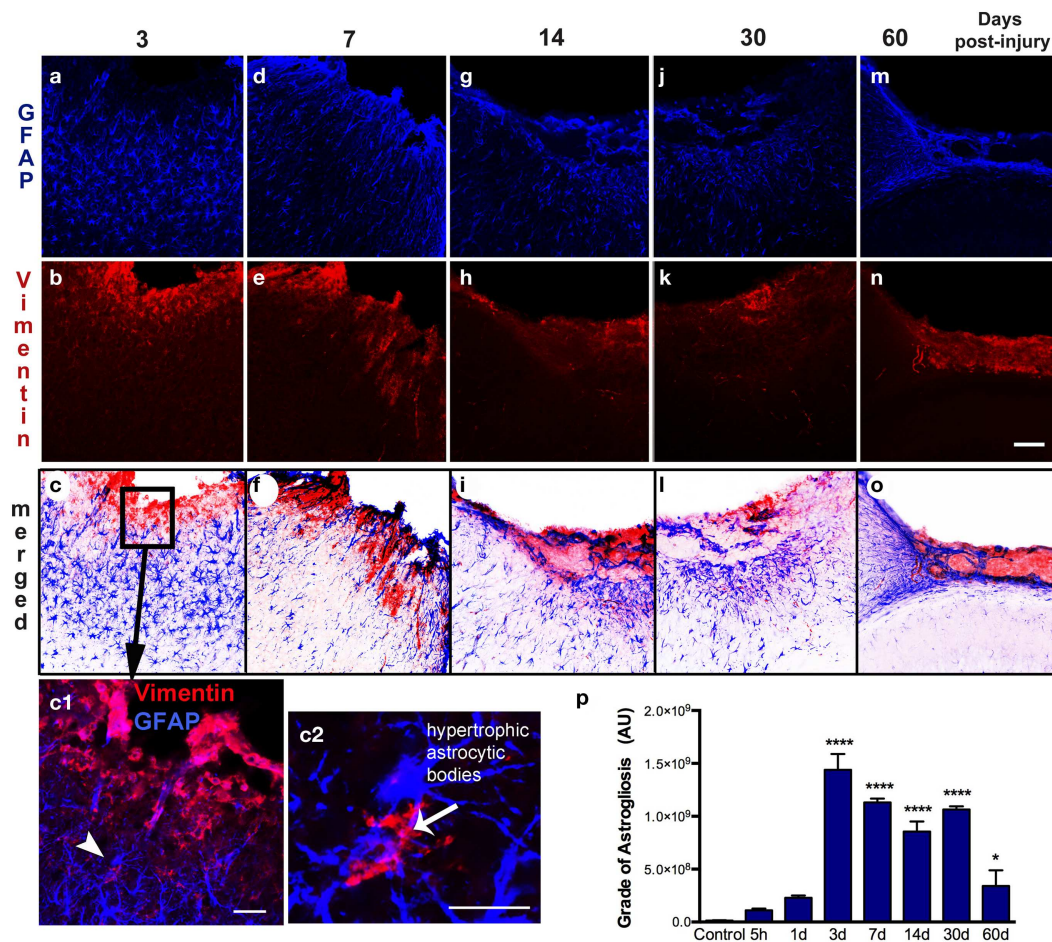


injury models have shown that the size of the cortical cavity was fully developed as early as 6 h after TBI (21). At 3 dpi, we identified apoptotic cell death located in the lesion periphery, limited to the lesion border and mainly corresponding to neuronal death. This results from neurons being more susceptible to CNS insults than astrocytes, as they have limited antioxidant capacity and rely on their metabolic coupling with astrocytes to combat oxidative stress (20, 22, 23).

Astrocytes become reactive after trauma, ischemia, or neurodegenerative diseases (astrogliosis). Hypertrophy of astrocytic processes is accompanied by the upregulation of GFAP

and vimentin, two intermediate filaments that are abundantly expressed in immature and reactive astrocytes (24, 25). Reactive astrocytes can form GFAP positive filaments in vimentin-deficient mice, but with more compact bundles than in wild-type astrocytes, showing that both vimentin and GFAP normally contribute to the cytoskeletal structure of astrocytes (26). Other studies have suggested that GFAP-positive reactive astrocytes contribute to the resistance of CNS tissue to specific types of severe mechanical stress (27), taking up excess glutamate (10), rebuilding the blood-brain barrier (28, 29), and production of growth factors (30).





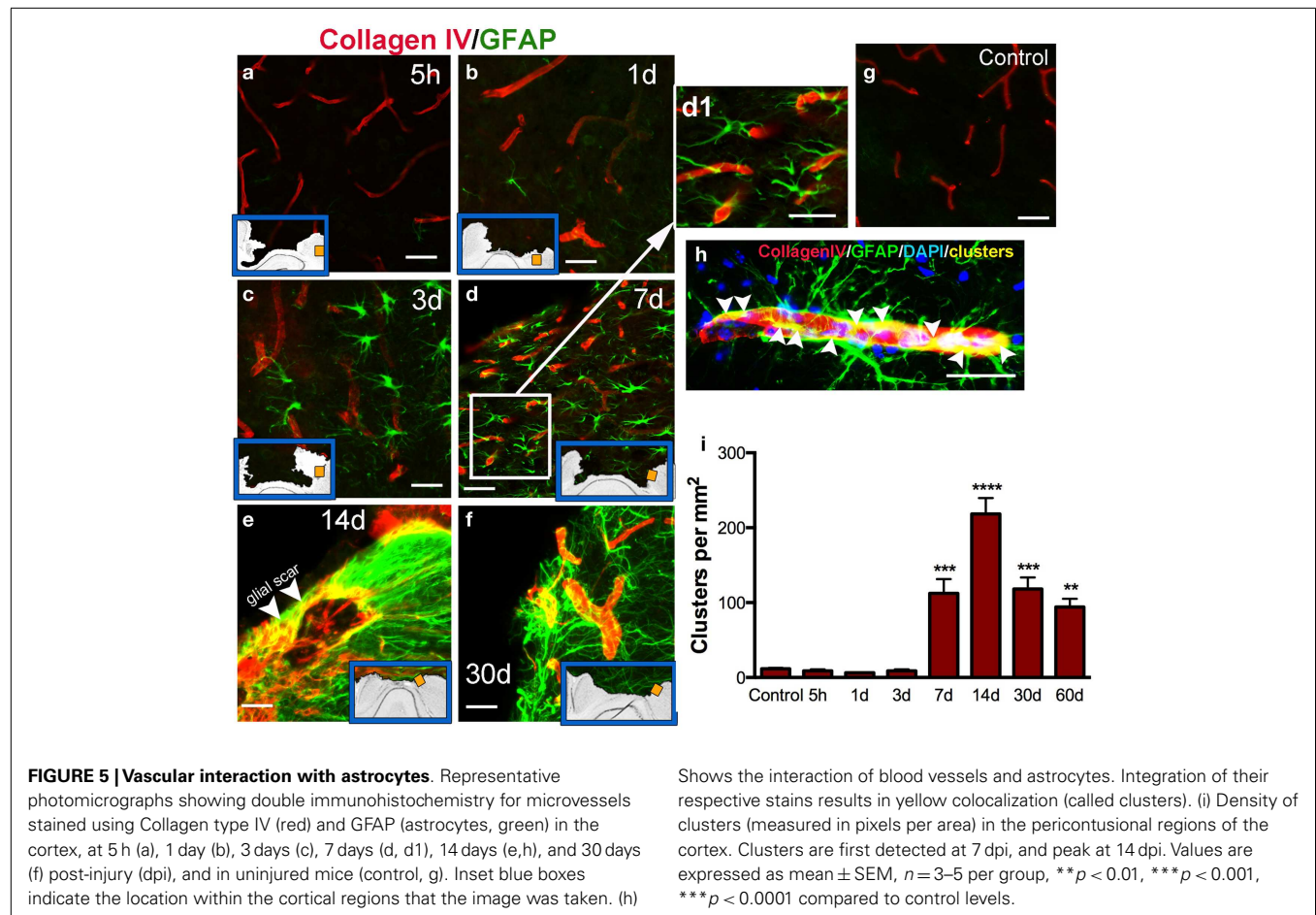
**FIGURE 4 | Spatial-temporal pattern of astroglial reactivity.** GFAP (a–m) and vimentin (b–n) immunoreactivity in the ipsilateral cortex of lesioned mice at 3, 7, 14, 30, and 60 days post-injury (dpi). The sensorimotor cortex lesion of the young adult mouse brain evoked extensive reactive astroglial reactivity at 3 dpi, as shown by upregulation of GFAP and vimentin expression, surrounding the lesion site (a–c). Enlarged detail of the lesion site (box in c) shows that reactive astrocytes are vimentin-positive (arrowhead in c1) have large hypertrophic astrocytic bodies and an increased number of short processes (arrow in c2). These reactive astrocytes have an enlarged body with an

increased number of short, thick processes that are directed towards the border of the lesion at 7 dpi (d–f). Extensive reactive astroglial reactivity was primarily detected in the border of the damaged cortex at 14 dpi (g–i). Once the glial scar has formed, both GFAP and vimentin expression is weak and restricted to the superficial part of the injured cortex at 30 and 60 dpi (m–o). Quantification of the grade of astroglial reactivity (p) showed a peak at 3 dpi that decreases overtime. Scale bar; 100  $\mu$ m (a–o), 50  $\mu$ m (c1), and 20  $\mu$ m (c2). Values are expressed as mean  $\pm$  SEM,  $n = 3–5$  per group, \*\*\*\* $p < 0.0001$ , \* $p < 0.05$  compared to control.

Interestingly, we found that the pericontusional region at early time points after injury is devoid of GFAP-positive astrocytes. Further, we found that some astrocytes are TUNEL-positive 5 h after injury (Figure 3) illustrating that astrocytes are vulnerable in the acute phase of injury. This early astrocytic demise has been previously demonstrated in ischemic animal models (31). Previous studies have also suggested that there is an immense variability in the subpopulation structure of astrocytes, characterized by several grades of susceptibility in their response to brain injury (25, 32). We show that, in the vicinity of the lesion, reactive astrocytes on day 3 increase the thickness of their main cellular processes and convert to a hypertrophic morphology. We also identified a strong astroglial reactivity from 7 days after injury until 2 months after injury, where astrocytes contribute to the formation of the glial scar.

Astrocytic hypertrophy, hyperplasia, and glial scar formation all have negative effects on regeneration, although some evidence favors a positive role for astrocytes in brain injury as they have phagocytic capabilities and are partially responsible for clean up of the lesion site in the acute stages after trauma (33). While, at later stages they facilitate the formation of a post-traumatic glial scar (25, 34). Formation of the glial scar, a barrier composed of extracellular matrix, where collagen IV is a major constituent of basement membranes, has been considered a major factor involved in inhibition of neurite outgrowth and repair after CNS injuries (15). Thus, some treatments under development seek to limit the formation of the astroglial scar in order to repair the injured CNS. Some studies have shown how the inhibition of collagen IV synthesis enhances regeneration of axons that become remyelinated with compact myelin after brain injury (35, 36). Spatial-temporal





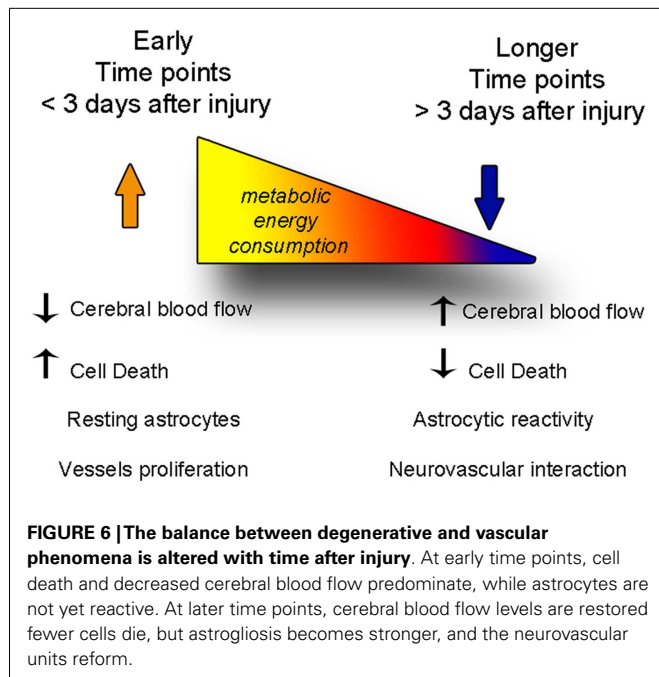
analysis of reactive astrocytes in the injured cortex may help to provide a better understanding on the role of diverse astrocytes, and accordingly, the distinct glial responses, depending on the distance from the injury core and the time point studied.

Astrocytes, as a result of their close relationships with neurons, microglial cells, and blood vessels have long been hypothesized to be involved in cerebrovascular regulation (1, 37). The terminal processes or “endfeet” of astrocytes cover the majority of the albuminal vascular surface of microvessels, intracerebral arterioles, and venules (38). Glutamate released during synaptic transmission stimulates astrocytic calcium signaling, which in turn induces vasodilatation (39). Other agents released from neurons or vessels participate in the increase in CBF induced by neural activity, such as nitric oxide, ATP, or calcium (40–42). While the interaction between adjacent reactive astrocytes and vasculature in the pericontusional-injured cortex remains minimal at early stages, it becomes densely packed near the lesion borders at later times after trauma. Our immunohistological analysis highlighted the link between astrocytes and large vessels in the border of the lesion starting at 7 days after injury when the surfaces of large to medium-size vessels were densely covered by GFAP astrocytic endfeet (Figure 5).

The structural and functional integrity of the brain depends on a continuous vascular supply of oxygen and glucose, and

if CBF is interrupted or unable to meet an increased metabolic demand, neurons cease to function, and reduced thresholds for activation of pathways leading to delayed neuronal death (1, 8, 43). A phasic elevation in CBF after acute head injury is a necessary condition for achieving functional recovery (44). Lower levels of blood flow further contribute to an excitotoxic cascade explosion with the release of glutamate to the extracellular space, as well as other toxic metabolites that induce a rapid expansion of cell death surrounded by an intense astrocytic reaction (33, 45). Mean arterial pressure (MAP), intracranial pressure, and other physiological variables also influence CBF (46).

Cerebral blood flow has been measured following experimental TBI (41, 47, 48) and an increase in CBF has a neuroprotective role after brain injury (8). Our results demonstrate a sudden decrease in CBF after traumatic impact within the cerebral cortex, from the first seconds after the impact tip was removed from the brain, and persisting for several days. Coinciding with a decrease of CBF in the pericontusional cortical regions, a massive astrocytic response, cell death, and an increase in perilesional vasculature all occur after mild–moderate TBI in mice. Astrocytes have processes in direct contact with blood vessels, which has long indicated that they may be involved in neurovascular regulation. These cells have the ability to dilate and constrict blood vessels and finely modulate



the distribution of CBF changes during neuronal activation (49, 50) and energy metabolism (7). We show that CBF was restored to baseline values by 30 dpi (Figure 1) but did not determine at which point between 3 and 30 dpi, the CBF normalized. However, we also show increased formation of astrocytic–vascular clusters starting at 7 dpi and continuing until 60 dpi. Thus, it is possible that the formation of these clusters could help restore the CBF to baseline levels, even though these structures are not found in naïve mouse brain.

The pathological disruption of vessel interactions with astrocytes may be involved in neurovascular regulation, glial scar formation, and CBF. However, despite intense research in neurovascular interactions, the role that astrocyte–vasculature interaction may play in neuronal survival remains poorly understood. Modulating the energy demands or interacting with microvessels to influence the vascular flow in the pericontusional cortex may be one mechanism by which astrocytes contribute to neuronal recovery.

## CONCLUSION

In this study, we determined the spatial–temporal course of the astrocytic–vascular reaction, in parallel with apoptotic cell death, after mild–moderate brain injury in mice. We focused on assessing changes detected in the pericontusional cortical regions, targeting the possible involvement of astrocytes with cerebrovascular dysfunction and neurodegeneration.

A clear understanding of the molecular regulation of cellular damage including the neurovascular unit will be crucial for the design of new treatments for brain injury. Further elucidation of the temporal response of the astroglial–vasculature complex after brain injury should indicate potential critical points for intervention to increase CBF after injury that should have clinical relevance.

## ACKNOWLEDGMENTS

The authors thank M. Balarezo for her excellent technical assistance. This work was supported by grants from the Center for Neuroscience and Regenerative Medicine (CNRM). Sonia Villapol is supported by a CNRM post-doctoral fellowship. The opinions and assertions contained herein are the private opinions of the authors and are not to be construed as reflecting the views of the Uniformed Services University of the Health Sciences, the US Department of Defense or the Government of the United States.

## REFERENCES

- Ragaisis V. Brain contusion: morphology, pathogenesis and treatment. *Medicina* (2002) **38**:243–9; quiz 354.
- Obrenovitch TP, Urenjak J. Is high extracellular glutamate the key to excitotoxicity in traumatic brain injury? *J Neurotrauma* (1997) **14**:677–98. doi:10.1089/neu.1997.14.677
- Smith DH, Chen XH, Pierce JE, Wolf JA, Trojanowski JQ, Graham DI, et al. Progressive atrophy and neuron death for one year following brain trauma in the rat. *J Neurotrauma* (1997) **14**:715–27. doi:10.1089/neu.1997.14.715
- Harris NG, Mironova YA, Hovda DA, Sutton RL. Chondroitinase ABC enhances pericontusion axonal sprouting but does not confer robust improvements in behavioral recovery. *J Neurotrauma* (2010) **27**:1971–82. doi:10.1089/neu.2010.1470
- Martin-Lopez E, Garcia-Marques J, Nunez-Llaves R, Lopez-Mascaraque L. Clonal astrocytic response to cortical injury. *PLoS One* (2013) **8**:e74039. doi:10.1371/journal.pone.0074039
- Badaut J, Bix GJ. Vascular neural network phenotypic transformation after traumatic injury: potential role in long-term sequelae. *Transl Stroke Res* (2014) **5**:394–406. doi:10.1007/s12975-013-0304-z
- Iadecola C, Nedergaard M. Glial regulation of the cerebral microvasculature. *Nat Neurosci* (2007) **10**:1369–76. doi:10.1038/nn2003
- Alessandri B, Schwandt E, Kamada Y, Nagata M, Heimann A, Kempinski O. The neuroprotective effect of lactate is not due to improved glutamate uptake after controlled cortical impact in rats. *J Neurotrauma* (2012) **29**:2181–91. doi:10.1089/neu.2011.2067
- Massucci FA, Dinuzzo M, Giove F, Maraviglia B, Castillo IP, Marinari E, et al. Energy metabolism and glutamate–glutamine cycle in the brain: a stoichiometric modeling perspective. *BMC Syst Biol* (2013) **7**:103. doi:10.1186/1752-0509-7-103
- Zou J, Wang YX, Dou FF, Lu HZ, Ma ZW, Lu PH, et al. Glutamine synthetase down-regulation reduces astrocyte protection against glutamate excitotoxicity to neurons. *Neurochem Int* (2010) **56**:577–84. doi:10.1016/j.neuint.2009.12.021
- Barreto GE, Gonzalez J, Torres Y, Morales L. Astrocytic–neuronal crosstalk: implications for neuroprotection from brain injury. *Neurosci Res* (2011) **71**:107–13. doi:10.1016/j.neures.2011.06.004
- Katsel P, Byrne W, Roussos P, Tan W, Siever L, Haroutunian V. Astrocyte and glutamate markers in the superficial, deep, and white matter layers of the anterior cingulate gyrus in schizophrenia. *Neuropsychopharmacology* (2011) **36**:1171–7. doi:10.1038/npp.2010.252
- Chen S, Pickard JD, Harris NG. Time course of cellular pathology after controlled cortical impact injury. *Exp Neurol* (2003) **182**:87–102. doi:10.1016/S0014-4886(03)00002-5
- Villapol S, Bonnin P, Fau S, Baud O, Renolleau S, Charriat-Marlangue C. Unilateral blood flow decrease induces bilateral and symmetric responses in the immature brain. *Am J Pathol* (2009) **175**:2111–20. doi:10.2353/ajpath.2009.090257
- Muellner A, Benz M, Kloss CU, Mautes A, Burggraf D, Hamann GF. Microvascular basal lamina antigen loss after traumatic brain injury in the rat. *J Neurotrauma* (2003) **20**:745–54. doi:10.1089/089771503767869971
- Villapol S, Fau S, Renolleau S, Biran V, Charriat-Marlangue C, Baud O. Melatonin promotes myelination by decreasing white matter inflammation after neonatal stroke. *Pediatr Res* (2011) **69**:51–55. doi:10.1203/PDR.0b013e3181fcb40b
- Susarla BT, Villapol S, Yi JH, Geller HM, Symes AJ. Temporal patterns of cortical proliferation of glial cell populations after traumatic brain injury in mice. *ASN Neuro* (2014) **6**:e00143. doi:10.1042/AN20130034

18. Cole JT, Yarnell A, Kean WS, Gold E, Lewis B, Ren M, et al. Craniotomy: true sham for traumatic brain injury, or a sham of a sham? *J Neurotrauma* (2011) **28**:359–69. doi:10.1089/neu.2010.1427
19. Bazan NG, Rodriguez de Turco EB, Allan G. Mediators of injury in neuro-trauma: intracellular signal transduction and gene expression. *J Neurotrauma* (1995) **12**:791–814. doi:10.1089/neu.1995.12.791
20. Walton M, Connor B, Lawlor P, Young D, Sirimanne E, Gluckman P, et al. Neuronal death and survival in two models of hypoxic-ischemic brain damage. *Brain Res Brain Res Rev* (1999) **29**:137–68. doi:10.1016/S0165-0173(98)00053-8
21. Thompson HJ, Marklund N, Lebold DG, Morales DM, Keck CA, Vinson M, et al. Tissue sparing and functional recovery following experimental traumatic brain injury is provided by treatment with an anti-myelin-associated glycoprotein antibody. *Eur J Neurosci* (2006) **24**:3063–72. doi:10.1111/j.1460-9568.2006.05197.x
22. Shih AY, Johnson DA, Wong G, Kraft AD, Jiang L, Erb H, et al. Coordinate regulation of glutathione biosynthesis and release by Nrf2-expressing glia potently protects neurons from oxidative stress. *J Neurosci* (2003) **23**:3394–406.
23. Wang JY, Wen LL, Huang YN, Chen YT, Ku MC. Dual effects of antioxidants in neurodegeneration: direct neuroprotection against oxidative stress and indirect protection via suppression of glia-mediated inflammation. *Curr Pharm Des* (2006) **12**:3521–33. doi:10.2174/138161206778343109
24. Hernandez MR, Agapova OA, Yang P, Salvador-Silva M, Ricard CS, Aoi S. Differential gene expression in astrocytes from human normal and glaucomatous optic nerve head analyzed by cDNA microarray. *Glia* (2002) **38**:45–64. doi:10.1002/glia.10051
25. Pekny M, Wilhelmsson U, Bogestal YR, Pekna M. The role of astrocytes and complement system in neural plasticity. *Int Rev Neurobiol* (2007) **82**:95–111. doi:10.1016/S0074-7742(07)82005-8
26. Eliasson C, Sahlgren C, Berthold CH, Stakeberg J, Celis JE, Betsholtz C, et al. Intermediate filament protein partnership in astrocytes. *J Biol Chem* (1999) **274**:23996–4006. doi:10.1074/jbc.274.34.23996
27. Nawashiro H, Messing A, Azzam N, Brenner M. Mice lacking GFAP are hypersensitive to traumatic cerebrospinal injury. *Neuroreport* (1998) **9**:1691–6. doi:10.1097/00001756-199806010-00004
28. Nordal RA, Wong CS. Molecular targets in radiation-induced blood-brain barrier disruption. *Int J Radiat Oncol Biol Phys* (2005) **62**:279–87. doi:10.1016/j.ijrobp.2005.01.039
29. Mitra S, Gera R, Siddiqui WA, Khandelwal S. Tributyltin induces oxidative damage, inflammation and apoptosis via disturbance in blood-brain barrier and metal homeostasis in cerebral cortex of rat brain: an in vivo and in vitro study. *Toxicology* (2013) **310**:39–52. doi:10.1016/j.tox.2013.05.011
30. Karki P, Smith K, Johnson J Jr, Lee E. Astrocyte-derived growth factors and estrogen neuroprotection: role of transforming growth factor- $\alpha$  in estrogen-induced upregulation of glutamate transporters in astrocytes. *Mol Cell Endocrinol* (2014). doi:10.1016/j.mce.2014.01.010
31. Villapol S, Gelot A, Renolleau S, Charriaud-Marlangue C. Astrocyte responses after neonatal ischemia: the Yin and the Yang. *Neuroscientist* (2008) **14**:339–44. doi:10.1177/1073858408316003
32. Hinkle DA, Baldwin SA, Scheff SW, Wise PM. GFAP and S100 $\beta$  expression in the cortex and hippocampus in response to mild cortical contusion. *J Neurotrauma* (1997) **14**:729–38. doi:10.1089/neu.1997.14.729
33. Schwab JM, Beschorn R, Nguyen TD, Meyermann R, Schluesener HJ. Differential cellular accumulation of connective tissue growth factor defines a subset of reactive astrocytes, invading fibroblasts, and endothelial cells following central nervous system injury in rats and humans. *J Neurotrauma* (2001) **18**:377–88. doi:10.1089/089771501750170930
34. Fawcett JW, Asher RA. The glial scar and central nervous system repair. *Brain Res Bull* (1999) **49**:377–91. doi:10.1016/S0361-9230(99)00072-6
35. Stichel CC, Hermanns S, Luhmann HJ, Lausberg F, Niermann H, D'Urso D, et al. Inhibition of collagen IV deposition promotes regeneration of injured CNS axons. *Eur J Neurosci* (1999) **11**:632–46. doi:10.1046/j.1460-9568.1999.00466.x
36. Stichel CC, Lausberg F, Hermanns S, Muller HW. Scar modulation in subacute and chronic CNS lesions: effects on axonal regeneration. *Restor Neurol Neurosci* (1999) **15**:1–15.
37. Sochocka M, Koutsouraki ES, Gasiorowski K, Leszek J. Vascular oxidative stress and mitochondrial failure in the pathobiology of Alzheimer's disease: a new approach to therapy. *CNS Neurol Disord Drug Targets* (2013) **12**:870–81. doi:10.2174/18715273113129990072
38. Simard M, Arcuino G, Takano T, Liu QS, Nedergaard M. Signaling at the glio-vascular interface. *J Neurosci* (2003) **23**:9254–62.
39. Leffler CW, Parfenova H, Fedinec AL, Basuroy S, Tcheranova D. Contributions of astrocytes and CO to pial arteriolar dilation to glutamate in newborn pigs. *Am J Physiol Heart Circ Physiol* (2006) **291**:H2897–904. doi:10.1152/ajpheart.00722.2006
40. Armstead WM. NMDA and age dependent cerebral hemodynamics after traumatic brain injury. *Exp Toxicol Pathol* (2004) **56**:75–81. doi:10.1016/j.etp.2004.04.003
41. Engel DC, Mies G, Terpolilli NA, Trabold R, Loch A, De Zeeuw CI, et al. Changes of cerebral blood flow during the secondary expansion of a cortical contusion assessed by 14C-iodoantipyrine autoradiography in mice using a non-invasive protocol. *J Neurotrauma* (2008) **25**:739–53. doi:10.1089/neu.2007.0480
42. Li AL, Zhi DS, Wang Q, Huang HL. Extracellular glycerol in patients with severe traumatic brain injury. *Chin J Traumatol* (2008) **11**:84–8.
43. Longhi L, Roncati Zanier E, Valeriani V, Ghisoni L, Besozzi A, Ferrari C, et al. Brain vulnerability and its modulation. *Minerva Anestesiol* (2003) **69**:227–31.
44. Westergren H, Ryding E, Zbornickova V, Hillman J. Traumatic occlusion of the internal carotid artery in a healthy young male: effects on the regional cerebral blood flow. *Acta Neurochir* (1991) **113**:91–5. doi:10.1007/BF01402121
45. Yi JH, Hazell AS. Excitotoxic mechanisms and the role of astrocytic glutamate transporters in traumatic brain injury. *Neurochem Int* (2006) **48**:394–403. doi:10.1016/j.neuint.2005.12.001
46. Bragin DE, Bush RC, Muller WS, Nemoto EM. High intracranial pressure effects on cerebral cortical microvascular flow in rats. *J Neurotrauma* (2011) **28**:775–85. doi:10.1089/neu.2010.1692
47. Lewelt W, Jenkins LW, Miller JD. Autoregulation of cerebral blood flow after experimental fluid percussion injury of the brain. *J Neurosurg* (1980) **53**:500–11. doi:10.3171/jns.1980.53.4.0500
48. DeWitt DS, Jenkins LW, Wei EP, Lutz H, Becker DP, Kontos HA. Effects of fluid-percussion brain injury on regional cerebral blood flow and pial arteriolar diameter. *J Neurosurg* (1986) **64**:787–94. doi:10.3171/jns.1986.64.5.0787
49. Haydon PG, Carmignoto G. Astrocyte control of synaptic transmission and neurovascular coupling. *Physiol Rev* (2006) **86**:1009–31. doi:10.1152/physrev.00049.2005
50. Jakovcic D, Harder DR. Role of astrocytes in matching blood flow to neuronal activity. *Curr Top Dev Biol* (2007) **79**:75–97. doi:10.1016/S0070-2153(06)79004-4

**Conflict of Interest Statement:** The authors declare that the research was conducted in the absence of any commercial or financial relationships that could be construed as a potential conflict of interest.

Received: 26 March 2014; accepted: 14 May 2014; published online: 04 June 2014.

Citation: Villapol S, Byrnes KR and Symes AJ (2014) Temporal dynamics of cerebral blood flow, cortical damage, apoptosis, astrocyte–vasculature interaction and astrogliosis in the pericontusional region after traumatic brain injury. *Front. Neurol.* **5**:82. doi: 10.3389/fneur.2014.00082

This article was submitted to *Neurotrauma*, a section of the journal *Frontiers in Neurology*.

Copyright © 2014 Villapol, Byrnes and Symes. This is an open-access article distributed under the terms of the Creative Commons Attribution License (CC BY). The use, distribution or reproduction in other forums is permitted, provided the original author(s) or licensor are credited and that the original publication in this journal is cited, in accordance with accepted academic practice. No use, distribution or reproduction is permitted which does not comply with these terms.



# Differential expression of brain cannabinoid receptors between repeatedly stressed males and females may play a role in age and gender-related difference in traumatic brain injury: implications from animal studies

Guoqiang Xing\*, Janis Carlton, Xiaolong Jiang, Jillian Wen, Min Jia and He Li\*

Department of Psychiatry, Uniformed Services University of the Health Sciences, Bethesda, MD, USA

## Edited by:

Yumin Zhang, Uniformed Services University of the Health Sciences, USA

## Reviewed by:

Gina Signoracci, Eastern Colorado Health Care System, USA  
Jinhui Chen, Indiana University School of Medicine, USA

## \*Correspondence:

Guoqiang Xing, Johns Hopkins University-MCC, 9601 Medical Center Drive, Suite 227, Rockville, MD 20850, USA

e-mail: gxing99@yahoo.com;

He Li, Department of Psychiatry, Uniformed Services University of the Health Sciences, 4301 Jones Bridge Road, Bethesda, MD 20814-4799, USA

e-mail: he.li@usuhs.edu

The views expressed in this article are those of the authors and do not necessarily reflect the official policy or position of the Department of the Navy, Department of Defense, nor the U.S. Government.

Inconsistent gender differences in the outcome of TBI have been reported. The mechanism is unknown. In a recent male animal study, repeated stress followed by TBI had synergistic effects on brain gene expression and caused greater behavioral deficits. Because females are more likely to develop anxiety after stress and because anxiety is mediated by cannabinoid receptors (CBRs) (CB<sub>1</sub> and CB<sub>2</sub>), there is a need to compare CB<sub>1</sub> and CB<sub>2</sub> expression in stressed males and females. CB<sub>1</sub> and CB<sub>2</sub> mRNA expression was determined in the amygdala, hippocampus, prefrontal cortex (PFC), and hypothalamus of adolescent male and female rats after 3 days of repeated tail-shock stress using qPCR. PFC CB<sub>1</sub> and CB<sub>2</sub> protein levels were determined using Western blot techniques. Both gender and stress had significant effects on brain CB<sub>1</sub> mRNA expression levels. Overall, females showed significantly higher CB<sub>1</sub> and CB<sub>2</sub> mRNA levels in all brain regions than males ( $p < 0.01$ ). Repeated stress reduced CB<sub>1</sub> mRNA levels in the amygdala, hippocampus, and PFC ( $p < 0.01$ , each). A gender  $\times$  stress interaction was found in CB<sub>1</sub> mRNA level in the hippocampus ( $p < 0.05$ ), hypothalamus ( $p < 0.01$ ), and PFC ( $p < 0.01$ ). Within-sex one-way ANOVA analysis showed decreased CB<sub>1</sub> mRNA in the hippocampus, hypothalamus, and PFC of stressed females ( $p < 0.01$ , each) but increased CB<sub>1</sub> mRNA levels in the hypothalamus of stressed males ( $p < 0.01$ ). There was a gender and stress interaction in prefrontal CB<sub>1</sub> receptor protein levels ( $p < 0.05$ ), which were decreased in stressed females only ( $p < 0.05$ ). Prefrontal CB<sub>2</sub> protein levels were decreased in both male and female animals after repeated stress ( $p < 0.05$ , each). High basal levels of CBR expression in young naïve females could protect against TBI damage whereas stress-induced CBR deficits could predict a poor outcome of TBI in repeatedly stressed females. Further animal studies could help evaluate this possibility.

**Keywords:** stress, anxiety, brain cannabinoid receptors, sex dimorphism, TBI outcome

## INTRODUCTION

There is a growing body of literature supporting a gender effect on the acute response and long-term outcomes of TBI, yet the findings are inconsistent (1–5). Several studies suggest that gender differences in TBI outcome may be age-dependent. In a recent retrospective mortality study, involving 10,135 prepubescent (0–12 years), and 10,145 pubescent (12–18 years) hospitalized patients who sustained isolated moderate-to-severe TBI (defined as a head Abbreviated Injury Scale (AIS) score of 3 or greater). Ley et al. (6) found a significantly reduced mortality rate in prepubescent patients than in pubescent patients (5.2 vs. 8.6%,  $p < 0.0001$ ). Additionally, females in the pubescent but not in the prepubescent age group showed a significantly greater decrease in mortality than males. Groswasser et al. (7) also reported a significantly better predicted-outcome for young females than for males under the age of 18 with comparable levels of TBI severity. Barr (8) reported that high school girls with TBI outperform boys of the same age on selected measures of processing speed and executive

functions. Similar gender specific findings have been reported by others (9–12). However, other studies demonstrated that older women took significantly longer time than men to recover from TBI, after controlling for age, injury severity, mechanism of injury, and comorbidities (13–15). The mechanism for the inconsistent gender effect across different age groups is unknown.

Both genetic and epigenetic/environmental factors could be involved (16–19). Early stress exposure has been recognized as an important mechanism for neuropsychiatric disorders (20–22). Stress and stress-related anxiety could also influence TBI outcome as people who exhibited high levels of acute stress symptoms and anxiety had poor TBI outcome (23). A significant portion of the US military personnel returning from Iraq and Afghanistan battlefields have experienced persistent somatic pain, as well as comorbidity of mild traumatic brain injury (mTBI) and post-traumatic stress disorder (PTSD) (24–30). In a logistic regressions study of 2,348 veterans of Operation Enduring Freedom (OEF) and Operation Iraqi Freedom (OIF) (51% female), Iverson et al. (31)



reported significant associations between probable TBI, symptomatic anxiety, and symptomatic physical health in both genders. Additionally, TBI is more strongly associated with all health symptoms for females and symptomatic anxiety and physical health for male veterans without probable PTSD (31). To examine the potential influence of repeated stress on the outcome of TBI, we recently reported that repeated stress followed by TBI had synergistic effects on the expression of brain mitochondrial electron transport chain complex subunits, and caused more severe behavioral deficits in male animals (females were not examined in that study) (32).

It is not clear if stress could have an equal influence on the outcome of TBI in males and females, although a greater impact of stress on the psychological outcome of females is well known. Our recent animal model studies of PTSD have shown that brain cannabinoid receptors (CBRs) are more rapidly depleted in the cerebellum and brain stems of stressed female adolescent rats than in males (32, 33). Other studies suggest that endocannabinoids (eCBs) and CBR activity are involved in the functional recovery of animal experiencing repeated stress and TBI (32–37).

From the results of these studies and other evidence, we hypothesized that CBR-mediated activity may be a critical mechanism linking PTSD and TBI and is responsible for gender difference in PTSD and TBI. We are intent on investigating neuroprotective factors in male and female rats to evaluate how this may relate to recovery following TBI. While actual TBI procedure was not part of the current study design, the findings may translate to issues regarding TBI and co-occurring stress as evidenced in diagnoses such as PTSD.

Anandamide and 2-arachidonoylglycerol (2-AG) are the main components of brain eCBs. eCBs are synthesized upon demand through enzymatic cleavage of membrane lipid precursors and immediately released into the synaptic space. Anandamide has a higher affinity for the CB<sub>1</sub> than for CB<sub>2</sub> receptors (38), which are highly expressed in the hippocampus, striatum, cerebellum, and cortex (39). 2-AG has a low affinity for CB<sub>1</sub> but is more abundant than anandamide (>200-fold) in the brain.

Endocannabinoids are synthesized upon demand through enzymatic cleavage of membrane lipid precursors and are immediately released into the synaptic space. They induce complex neuroprotective, anxiolytic, and modulator effects on brain structure and function via the activation of CBRs (mainly CB<sub>1</sub> and CB<sub>2</sub>). Anandamide and 2-arachidonoylglycerol (2-AG) are the main brain eCBs and can alleviate blood–brain barrier dysfunction, brain edema, lesion volume, neuronal death, and improve behavioral performance in rodent models of TBI through multiple mechanisms (40–45). Anandamide has a higher affinity for CB<sub>1</sub> receptors than for CB<sub>2</sub> receptors (38), which are highly expressed in the hippocampus, striatum, cerebellum, and cortex (39). 2-AG, on the other hand, has a low affinity for CB<sub>1</sub> but is more abundant than anandamide (by >200-fold) in the brain. The neuroprotective effects of eCBs in TBI could also be mediated by CB<sub>1</sub> receptor activation, which can inhibit anxiety, stress response, and the retention of aversive memories (46). Animals lacking CB<sub>1</sub> receptors show hypersensitivity to stressful stimuli, increased anxiety-like behaviors, and higher mortality (reduced lifespan) (47–50). CB<sub>2</sub> receptors are primarily expressed in peripheral immune cells; however, recent studies show that they are also

expressed in microglia, dendritic cells, brain endothelial cells, and the subgroups of neurons in several brain regions (51–55).

Evidence supporting a role of eCBs in TBI-induced injury and/or neuroprotection includes the significantly elevated levels of 2-AG following TBI (41). When administered to mice with TBI, 2-AG decreased brain edema, inflammation and infarct volume, and improved clinical recovery (42–44). 2-AG also suppressed inflammation, tumor necrosis factor- $\alpha$  (TNF- $\alpha$ ), and reactive oxygen species (ROS) in LPS-stimulated macrophages and LPS-stimulated mice (56).

In this study, we examined CB<sub>1</sub> and CB<sub>2</sub> receptor expression after repeated tail-shock stress in the amygdala, hypothalamus, hippocampus, and prefrontal cortex (PFC) of adolescent male and female rats to determine how the base-line CBR can be affected by chronic stress. These brain regions play key roles in stress response and emotional memory. Adolescent animals were studied because they are more sensitive to stress than adult, a trait that could have a significant influence on disease development in adulthood (57–60). Furthermore, a gender difference in TBI outcome has been shown for pubescent animals, but not for prepubescent ones (6).

## MATERIALS AND METHODS

### ANIMALS

Male and female Sprague–Dawley rats ( $n = 16$ , each) (Taconic Farms, Germantown, NY, USA) weighing 120–150 g (5–6 weeks old) were used in this study. Animals of the same sex were housed two per cage and raised at room temperature ( $22 \pm 2^\circ\text{C}$ ) on a 12 h light–dark schedule (lights on 1800 h). Animals had *ad libitum* access to food and water. All experimental procedures were approved by the Institutional Animal Care and Use Committee of the Uniformed Services University of the Health Sciences, and were carried out in accordance with the NIH Guidelines for the Care and Use of Laboratory Animals.

### STRESS PROTOCOL

Animals were left undisturbed for 7-day after arrival. The stress procedure consisted of a 2-h per day session of immobilization and tail-shocks over three consecutive days as reported previously (61). In brief, half of the animals (eight per sex group) were restrained in individual Plexiglas tube and given 40 electric shocks (2 mA, 3 s duration) at varying intervals (140–180 s). The control animals were handled daily for the same time period but were not subjected to the immobilization and tail-shock stress procedures. All animals were returned to their home cages immediately after exposure to the stress or control conditions.

### TISSUE DISSECTION

Following the last stress session on day 3, both the control animals and the stressed animals were decapitated after light anesthesia with halothane. The brains were rapidly removed. A Vibratome (Technical Products International, St. Louis, MO, USA) was used to cut 1.6 mm-thick transverse slices containing the whole amygdala region (Bregma  $-3.60$  to  $-2.00$  mm) from tissue blocks. The basolateral complex, composed mainly of the lateral and basolateral nuclei, was dissected from this slice laterally, as outlined, by the white matter tract of the external capsule (corpus callosum) and medially by the white matter tract of the longitudinal association



bundle. This transverse slice (Bregma  $-3.60$  to  $-2.00$  mm) also contained the hippocampal dentate gyrus and CA1–CA3 regions as well as part of the hypothalamus. The PFC was similarly dissected. All tissue samples were immediately stored in pre-cooled isopentane ( $-40^{\circ}\text{C}$ ).

### REVERSE TRANSCRIPTION AND QUANTITATIVE REAL-TIME PCR

Dissected brain tissue samples were homogenized and total RNA was extracted using an RNeasy kit (Qiagen, Germany) according to the manufacturer's protocol. One microgram of total RNA was reverse transcribed into first-strand cDNA using the RETROscript reverse transcriptase kit (Ambion, TX, USA) according to the manufacturer's recommendations.

Fifty nanograms of the reverse transcribed RNA from the RT-reaction was used as the template for quantitative real-time PCR reaction with a final PCR reaction volume of  $25\ \mu\text{l}$  and a final concentration of the 5' and 3' PCR primers at  $100\ \text{nM}$  each. CB1 (TTTCCCACTCATTTGACGAGAC, GTGAGCCTTCCAGAGAATGT) and CB2 (AAAGCACACCAACATGTAGCC, GGAACCAGCATATGAGCAGAA) qPCR primers were designed using Primer3 software (MIT, MA, USA) with the size of amplified cDNA ranging between 90 and 150 bp (34). Quantification of CB<sub>1</sub> and CB<sub>2</sub> mRNA expression was performed (in triplicate) using a two-step PCR reaction procedure on an iQ5 Real-Time PCR System (BioRad, CA, USA) using the SYBR Green SuperMix (BioRad, CA, USA). After initial denaturation at  $95^{\circ}\text{C}$  for 3 min, 40 cycles of primer annealing and elongation were conducted at  $60^{\circ}\text{C}$  for 45 s, followed by denaturation at  $95^{\circ}\text{C}$  for 10 s. Fluorescent emission data were captured, and mRNA levels were quantified using the threshold cycle value (Ct).

Fold change in mRNA expression was calculated using the following equation:  $\text{Fold} = 2^{(\text{Ct}_{\text{control}} - \text{Ct}_{\text{stress}})}$ . To compensate for potential variations in input RNA amounts and the efficiency of reverse transcription, data for CB<sub>1</sub> and CB<sub>2</sub> mRNA of each sample were additionally normalized by reference to the data obtained from house keeping genes  $\beta$ -actin (GenBank accession no. X62085) determined from the same sample. The fold change in the compensated mRNA expression data was calculated using the equation:  $\text{fold change} = 2^{-\Delta\Delta\text{Ct}}$ , where  $\Delta\text{Ct} = \text{target gene Ct} - \text{housekeeping gene } (\beta\text{-actin}) \text{ Ct}$ , and  $\Delta\Delta\text{Ct} = \Delta\text{Ct}_{\text{control}} - \Delta\text{Ct}_{\text{stress}}$  (or fold change)  $= 2^{(\Delta\text{Ct}_{\text{control}} - \Delta\text{Ct}_{\text{stress}})}$ .

### WESTERN BLOT

Prefrontal cortex tissues from the stressed and control animals were homogenized and sonicated for 40 s in the T-Per tissue lysis buffer for western blot analysis (Pierce, IL, USA). Amygdala, hypothalamus, and hippocampus tissue proteins were not examined due to the limited amount of these tissues that were dissected. Protein concentrations were determined using a Bradford assay (BioRad, CA, USA). Aliquots of  $20\ \mu\text{g}$  proteins were separated by electrophoresis on NuPage gels (10%) and transferred to a polyvinylidene difluoride membrane before being incubated with the primary antibodies of CB<sub>1</sub>, phosphorylated-CB<sub>1</sub>, glycosylated-CB<sub>1</sub>, and CB<sub>2</sub>, diluted at 1:500 each (Santa Cruz Biotechnologies, CA, USA). The membranes were rinsed in a 0.01 M Tris-buffered saline solution (pH 7.4) containing 0.1% Triton X-100 for 30 min, blocked in 5% non-fat dry milk

for 30 min and incubated overnight at  $4^{\circ}\text{C}$  with the primary antibody in a Tris-buffered saline solution containing 3% non-fat dry milk. Membranes were washed three-times with the Tris-buffered saline solution and incubated overnight at  $4^{\circ}\text{C}$  with a horseradish peroxidase-conjugated secondary antibody in the Tris-buffered saline solution containing 3% non-fat dry milk. Immunoreactive bands were visualized using horseradish peroxidase-conjugated anti-rabbit antibodies in a 1:3000 ratio, and ECL Western blotting detection reagents (GE Healthcare Bio-Sciences Corp., Piscataway, NJ, USA). The western blots were captured with a digital camera and the intensities quantified with NIH Image 1.62.

### STATISTICS

Data regarding the effects of gender and stress on CB<sub>1</sub> and CB<sub>2</sub> receptors for individual brain regions were analyzed using two-way ANOVA analyses. Because of the significant gender and stress interactions found in brain CB<sub>1</sub> receptor expression, within-sex one-way ANOVA analyses were also conducted. A  $p$ -value of  $<0.05$  was considered statistically significant.

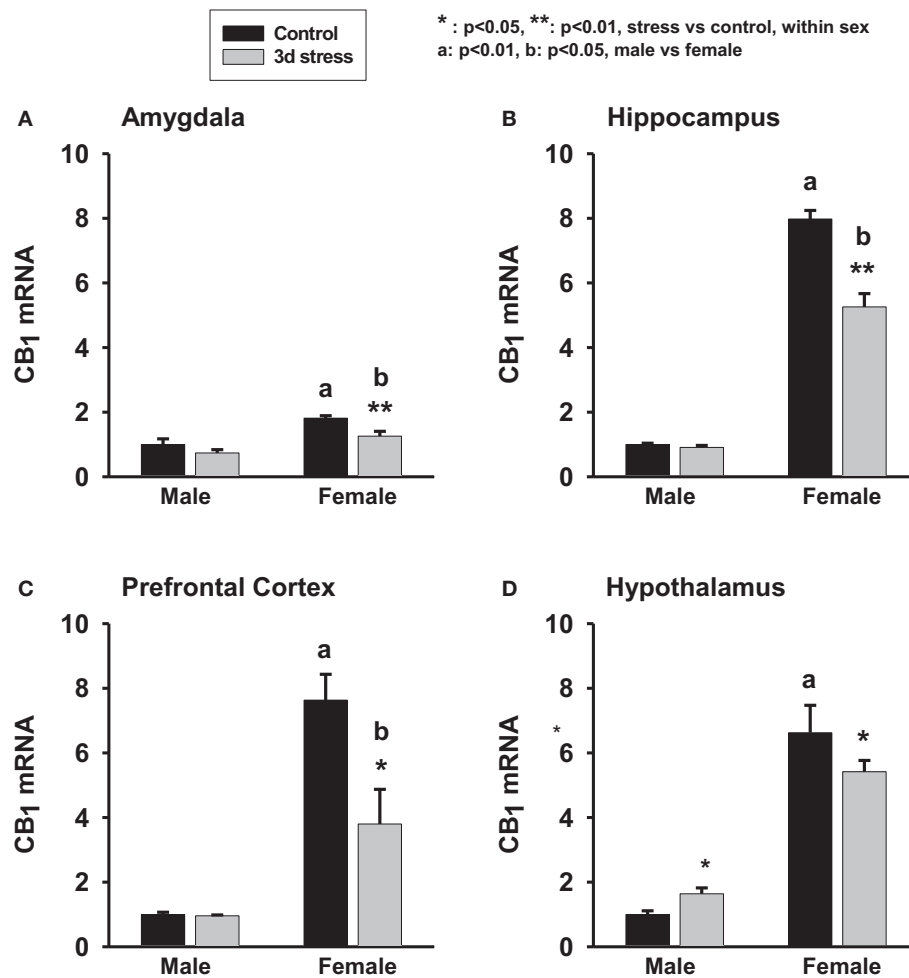
### RESULTS

Two-way ANOVA analyses revealed significant gender and stress effects on CB<sub>1</sub> mRNA levels in the amygdala, hippocampus, and the PFC ( $p < 0.01$ , each). Overall, female animals exhibited higher basal levels of CB<sub>1</sub> mRNA expression in the amygdala, hippocampus, and the PFC than male animals ( $p < 0.01$ , each) (Figure 1; Table 1). Stressed animals exhibited reduced CB<sub>1</sub> mRNA levels in the amygdala, hippocampus, and the PFC when compared to those brain regions of the control animals ( $p < 0.01$ , each) (Figure 1). However, in the hypothalamus there was no significant difference between the CB<sub>1</sub> mRNA levels in the stress and control groups ( $p > 0.05$ ). A significant interaction between gender and stress on CB<sub>1</sub> mRNA levels was found in the hippocampus ( $p < 0.05$ ), hypothalamus ( $p < 0.01$ ), and PFC ( $p < 0.01$ ). Within-sex one-way ANOVA revealed decreased CB<sub>1</sub> mRNA levels in the hippocampus, hypothalamus, and PFC of female animals ( $p < 0.01$ , each) but increased CB<sub>1</sub> mRNA level in the hypothalamus of male animals after the stress ( $p < 0.05$ ) (Figures 1A–D).

Base-line CB<sub>2</sub> mRNA levels were significantly higher in the hippocampus, hypothalamus, and PFC of female animals than in male animals ( $p < 0.01$ , each) (Figures 2A–D). CB<sub>2</sub> mRNA levels, however, remained unchanged following stress.

Two-way ANOVA analyses showed no significant gender or stress effects on total CB<sub>1</sub> proteins, phosphorylated (p-CB<sub>1</sub>), or glycosylated-CB<sub>1</sub> (g-CB<sub>1</sub>) proteins in the PFC (Figure 3; Table 2). There were, however, significant gender-by-stress interactions in total proteins and glycosylated-CB<sub>1</sub> proteins ( $p < 0.05$ , each). Within-sex one-way ANOVA analyses showed significantly decreased total CB<sub>1</sub> protein levels ( $p < 0.05$ ) and glycosylated-CB<sub>1</sub> protein levels ( $p < 0.05$ ) in the PFC of stressed female rats but not in stressed males.

Two-way ANOVA analyses showed that prefrontal CB<sub>2</sub> protein levels were greater in males than in females ( $p < 0.01$ ) and were significantly suppressed in both sexes after repeated stress ( $p < 0.05$ ). There was no significant gender-by-stress interaction in prefrontal CB<sub>2</sub> protein levels.



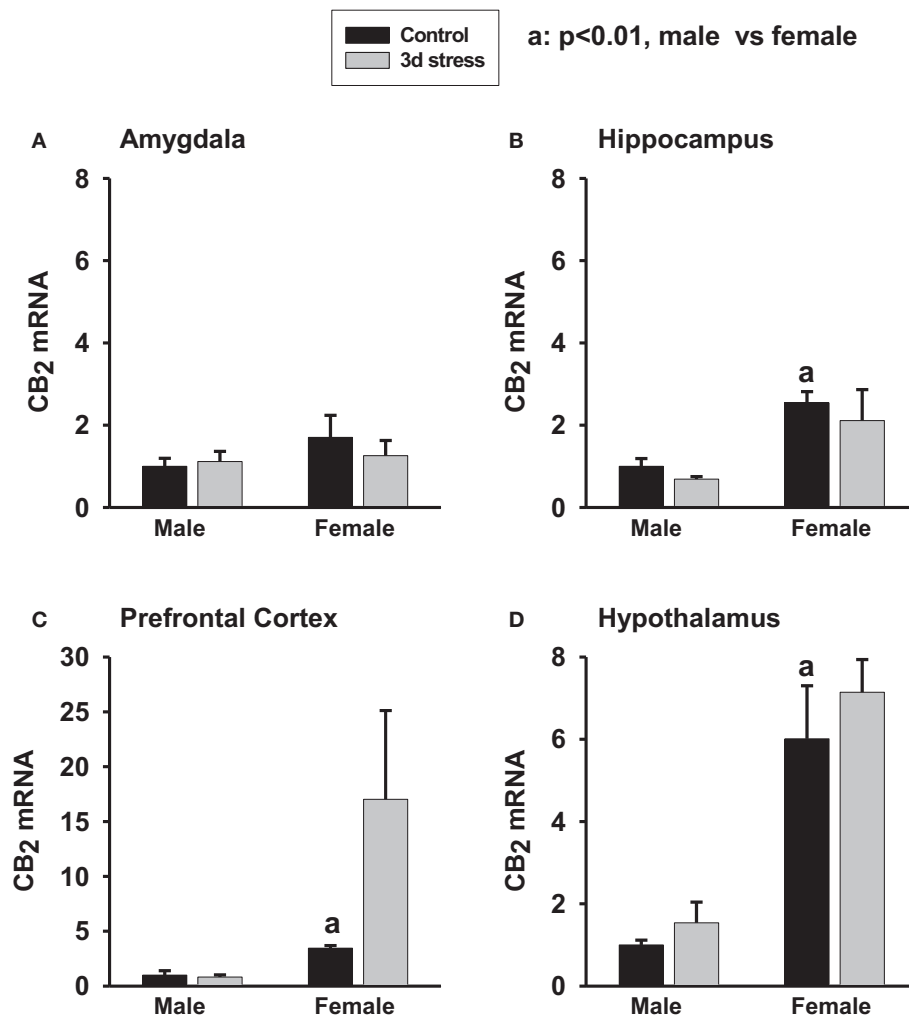
**FIGURE 1 | Two-way ANOVA show significant effects of gender and stress.** Female adolescent rats show a greater baseline of CB<sub>1</sub> mRNA expression in the amygdala, hippocampus, hypothalamus and prefrontal cortex than the males ( $p < 0.01$ , each). Three days repeated tail-shock stress significantly down-regulated CB<sub>1</sub> mRNA levels in rat

amygdala (A), hippocampus (B), prefrontal cortex (C) and hypothalamus (D), especially in the female rats. Black column: control; gray column, stressed group, a,  $p < 0.01$ , male vs. female; b,  $p < 0.01$ : control group vs. stress group; \*  $p < 0.05$ ; \*\*  $p < 0.01$ , control vs. stress within sex comparison.

**Table 1 | Relative fold change (mean  $\pm$  SD) in CB<sub>1</sub> and CB<sub>2</sub> mRNA expression levels in the amygdala, hippocampus, prefrontal cortex (PFC) and hypothalamus of male and female adolescent rats after 3 days repeated (2 h/day) tail-shock stress.**

	Amygdala			Hippocampus			PFC			Hypothalamus		
	Baseline	3d Stress	Fold change	Baseline	3d Stress	Fold change	Baseline	3d Stress	Fold change	Baseline	3d Stress	Fold change
<b>CB<sub>1</sub> mRNA</b>												
Male (n = 16)	1 $\pm$ 0.17	0.74 $\pm$ 0.1	0.74	1 $\pm$ 0.1	0.9 $\pm$ 0.1	0.9	1 $\pm$ 0.1	0.96 $\pm$ 0.03	0.96	1 $\pm$ 0.11	1.65 $\pm$ 0.18	1.65*
Female (n = 16)	1.8 $\pm$ 0.1	1.30 $\pm$ 0.14	0.69**	7.9 $\pm$ 0.26	5.3 $\pm$ 0.4	0.66**	7.6 $\pm$ 0.8	4.0 $\pm$ 1.1	0.5*	6.6 $\pm$ 0.8	5.4 $\pm$ 0.4	0.81*
<b>CB<sub>2</sub> mRNA</b>												
Male (n = 16)	1.0 $\pm$ 0.19	1.1 $\pm$ 0.25	1.1	1 $\pm$ 0.2	0.69 $\pm$ 0.1	0.69	1 $\pm$ 0.4	0.8 $\pm$ 0.2	0.8	1 $\pm$ 0.1	1.5 $\pm$ 0.5	1.5
Female (n = 16)	1.7 $\pm$ 0.53	1.26 $\pm$ 0.37	0.59	2.5 $\pm$ 0.27	2.1 $\pm$ 0.75	0.83	3.4 $\pm$ 0.25	17.0 $\pm$ 8	4.9	6.0 $\pm$ 1.3	7.1 $\pm$ 0.8	1.2

The baseline mRNA level of control male group in each region was used as the arbitrary reference (=1) for the males and females. \* $p < 0.05$ ; \*\* $p < 0.01$ , control vs. stress within sex comparison.



**FIGURE 2 | Two-way ANOVA show that female rats exhibited greater CB<sub>2</sub> mRNA expression in the amygdala (A) ( $p < 0.1$ ), hippocampus (B) ( $p < 0.01$ ), prefrontal cortex (C) ( $p < 0.01$ ) and hypothalamus (D) ( $p < 0.01$ ) than male rats. Within-sex one-way ANOVA show that CB<sub>2</sub>**

mRNA levels were significantly increased in the prefrontal cortex of female rats after the stress exposure ( $p < 0.05$ ). Black column: control; gray column, stressed group, a,  $p < 0.01$ , male control vs. female control; \* $p < 0.05$ ; \*\* $p < 0.01$ , control vs. stress within sex comparison.

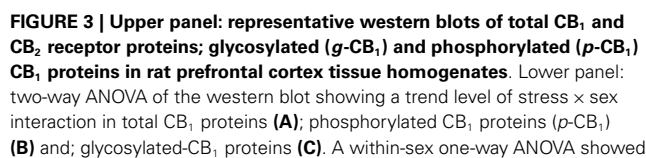
## DISCUSSION

A recent retrospective mortality study of TBI, involving more than 20,200 prepubescent and pubescent patients with moderate-to-severe TBI, showed that mortality rates were significantly lower in the prepubescent patients than in pubescent patients ( $p < 0.0001$ ) (6). Within the pubescent group, it was further found that females had a significantly lower mortality rate than males. The mechanism underlying the age-dependent gender differences in TBI outcome is unknown. Besides a potential role of female sex hormones that may have protected the pubescent females, our studies as well as others suggest that brain CBR-mediated activity could play a critical role in the age-related gender difference in TBI outcome through at least two mechanisms: anxiolytic activity and neuroprotection.

In our study, female adolescent animals showed higher base-line CB<sub>1</sub> and CB<sub>2</sub> mRNA expression levels in the amygdala,

hippocampus, hypothalamus, and PFC than the male adolescents (Figures 1 and 2; Table 1). That difference, however, disappeared rapidly after the repeated stress induced a larger reduction in CB<sub>1</sub> mRNA levels in the female brain. Furthermore, although repeated stress down-regulated CB<sub>1</sub> mRNA expression in the hypothalamus of female rats, caused the up-regulation of CB<sub>1</sub> mRNA expression in the hypothalamus of male rats. This divergent result is consistent with the selective inhibition of hypothalamic neuronal activity by CB<sub>1</sub> agonists in female but not in male guinea pigs (62), and the observation of a greater elevation of corticosterone in females than in males after stress (63). A reduction in CB<sub>1</sub> protein and glycosylated-CB<sub>1</sub> protein levels was also found in the PFC of the stressed female rats whereas a trend of increased CB<sub>1</sub> protein was found in the male animals.

The higher base-line CB<sub>1</sub> mRNA expression in the adolescent female rat brain when compared to their male counterparts is



significantly reduced total CB<sub>1</sub> proteins and glycosylated-CB<sub>1</sub> proteins in female prefrontal cortex (mean  $\pm$  SD); CB<sub>2</sub> protein levels were significantly reduced in the prefrontal cortex of both female and male rats after repeated stress (**D**). The mean value of the male control group was used as the arbitrary reference = 1, \* $p$  < 0.05, control vs. stress within sex comparison, black column, control group; blank column, stressed group.

such female-specific neuroprotection is present only in the pubescent but not in the pre- or post-pubescent populations, recent studies suggest that chronic stress when combined with high levels of stress hormone production but lower levels of female sex hormones production may deplete brain CBRs more rapidly, which could result in a large eCB/CBR deficit in the affected females.

To support this, Reich et al. (68) reported a lower level of CB<sub>1</sub> expression in the hippocampus of socially isolated adult female rats than in their male counterparts. It should be noted that Reich et al.'s study differs from this study in many aspects including:

**Table 2 | Relative fold change (mean  $\pm$  SD) in CB<sub>1</sub> and CB<sub>2</sub> protein expression levels in the prefrontal cortex of male adolescent rats after 3 days repeated inescapable repeated tail-shock stress and female.**

	CB <sub>1</sub> protein			p-CB <sub>1</sub> protein			Glycosyl-CB <sub>1</sub>			CB <sub>2</sub> protein		
	Baseline	3d Stress	Fold change	Baseline	3d Stress	Fold change	Baseline	3d Stress	Fold change	Baseline	3d Stress	Fold change
Male (n = 16)	1 $\pm$ 0.11	1.09 $\pm$ 0.05	1.09	1 $\pm$ 0.03	0.94 $\pm$ 0.02	0.94	1 $\pm$ 0.16	1.16 $\pm$ 0.07	1.16	1 $\pm$ 0.1	0.85 $\pm$ 0.05	0.85*
Female (n = 16)	1.04 $\pm$ 0.03	0.9 $\pm$ 0.03	0.87*	1.03 $\pm$ 0.1	1.02 $\pm$ 0.05	0.98	1.02 $\pm$ 0.08	0.88 $\pm$ 0.05	0.87*	0.74 $\pm$ 0.1	0.55 $\pm$ 0.11	0.74*

The baseline CB protein value of the control male group was used as the arbitrary reference (=1) for the males and females. \* $p < 0.05$ , control vs. stress within sex comparison.

(1) differences in stress paradigms (i.e., 3 days of repeated intense stress in our study vs. 3 weeks of chronic mild heterotypic stressors); (2) controls (naïve normal controls in this study vs. socially isolated controls); (3) feeding regimes (*ad libitum* feeding in this study vs. a frequent 14 h food/water deprivation); (4) housing environments (same sex pair-housing in this study vs. trio-housing with frequent wet cage rotation); (5) study times (acute phase of stress in this study vs. 3 weeks after chronic stress), and (6) hormone statuses (adolescent in our study vs. adult).

Increased crowding of unisex housing has been found to be stressful for female rats but anxiolytic for males and the opposite is true under isolated rearing (69). The unisex pair-housing in our study may be more stressful for the females than for the males and thus potentiating a greater loss of base-line CB<sub>1</sub> receptors in the females after repeated stress. In contrast, chronic mild heterotypic stressors were more stressful for male rats but anxiolytic for females reared in isolation (69).

Gender-related differences in fasting-induced lipid catabolism also exist. It has been reported that females mobilize more fat reserve and thus catabolize more lipophilic eCBs than males during short-term fasting (70, 71). Animals in this study were fed *ad libitum* without fasting whereas the stressed animals in the Reich's study experienced multiple episodes of food and water deprivation (>6 times in 14 h) that may have potentiated greater eCB release and CB<sub>1</sub> receptor depletion in the stressed adult female brain of that study.

In this study, repeated stress caused a divergent pattern of prefrontal CB<sub>1</sub> receptor expression between the males and females. Adolescent female rats displayed a significant reduction in prefrontal CB<sub>1</sub> receptor expression. However, prefrontal CB<sub>1</sub> receptor expression followed a positive trend in adolescent male rats, which became significant seven afterwards (33), reinforcing the findings of the divergent CB<sub>1</sub> gene expression patterns after stress. This increased CB<sub>1</sub> expression in male PFC is consistent with the increased mitochondrial electron transport chain complex subunit expression in the PFC of stressed male animals (32). Because of the known anxiolytic and analgesic effects of eCBs and CB<sub>1</sub> activation, the more-rapid loss of CB<sub>1</sub> in stressed adolescent female brains is consistent with the clinical observations of a greater prevalence and higher severity of anxiety symptoms such as increased sensitivity to fear signals, emotional disturbance, and pain in females after chronic stress exposure (72–76).

Ley et al. (6) showed that human prepubescent, regardless of sex, are better protected against TBI-caused mortality than human

pubescent (and possibly the adults as well). Although the mechanism is unknown, developmental studies have shown that the level of CB<sub>1</sub> expression in the human PFC is highest after birth but declines rapidly during the postnatal and prepubescent periods and with age (77). Thus, potentially high levels of CB<sub>1</sub> expression and activity during the prepubescent periods of development may have provided equally strong neuroprotection against TBI-induced brain damage and mortality in both naïve prepubescent males and females (6). While developmentally regulated decline in brain CB<sub>1</sub> expression and CB<sub>1</sub>-associated neuroprotection may be partially compensated by increased sex hormone in naïve pubescent and young adult females, this compensation may be adversely affected in stressed females.

The mechanisms for the poor reported long-term poor outcome of TBI in the older female population could be more complex (78). Again, deficient brain CB<sub>1</sub> activity, due to chronic stress, elevated stress hormone levels, and reduced sex hormone levels could all play a role in the female brain, leaving it more vulnerable to TBI damage.

It is possible that the neuroprotective effects of sex steroids in TBI (79) may act partially by upregulating brain eCB activity and CB receptor expression (77). Sex hormones during the estrous cycle have been linked with brain CB<sub>1</sub> receptor density, which is reduced in the limbic forebrain and hypothalamus after ovariectomy and castration but can be restored after estradiol, progesterone, and testosterone administration in intact and ovariectomized/castrated rats (80–84). High levels of stress-induced corticosteroid secretion and base-line corticosteroids as well as slow clearance of corticosteroids could lead to reduced CB<sub>1</sub> receptor levels in stressed females (85, 86). Chronic exposure to high level of corticosterone, CB<sub>1</sub> agonists, and cannabinoids have been reported to downregulate CB<sub>1</sub> receptor density, CB<sub>1</sub> receptor binding, and CB<sub>1</sub> mRNA expression in various brain regions of male and female animals (87–91).

It is noted that although a reduction in prefrontal CB<sub>1</sub> and CB<sub>2</sub> mRNA expression was not immediately observed in the male animals after 3 days of repeated stress, the expression was significantly decreased in the stressed male animals 7 days following the stress (33), suggesting a delayed pattern of CBR reduction in male adolescents after repeated stress when compared to the females. Other studies showed that 10 days of mild chronic stress (30 min restraint stress per day) upregulated CB<sub>1</sub> binding in the PFC of adolescent and adult male rats that was resolved after 40 days recovery period. Furthermore, adolescents exposed to stress were found to have a



sustained downregulation of prefrontocortical CB<sub>1</sub> receptors in adulthood (92).

CB<sub>1</sub> receptor activation in the forebrain and amygdala is anxiolytic (46, 93, 94). The loss of CB<sub>1</sub>-mediated anxiolytic and neuroprotective activity in these brain regions of both female and males could predict enhanced amygdala-mediated fear memory, especially in the females due to a greater propensity for CB<sub>1</sub> reduction. Indeed, loss or inhibition of CB<sub>1</sub> receptors in the amygdala, hippocampus, and PFC have been associated with the impaired ability to extinguish fear memories (50, 95, 96). PFC is known to exert a powerful inhibitory effect on amygdala activity and on fear extinction (97, 98) and it has been observed that the amygdala and hippocampus interact to mediate emotional memories (99).

Stress-induced reduction of brain CB<sub>1</sub> and CB<sub>2</sub> protein expression may also contribute to a more vulnerable brain structure and function (100–111) through multiple mechanisms in response to TBI, including increased microglia activation, inflammation and apoptosis, impaired blood–brain barrier integrity, compromised neuroprotection, and neuroregeneration in response to TBI (42, 112, 113). Activation of CB<sub>1</sub> and CB<sub>2</sub> receptors may minimize brain damage and promote tissue repair after TBI through the attenuation of injury-stimulated inducible nitric oxide (iNOS) and ROS in microglia (114), promoting neural progenitor (NP) proliferation, and neurosphere generation (115–118). These actions are abrogated when there is a deficit of brain CB<sub>1</sub> receptors (119–121). Altered expression levels of brain and peripheral CB<sub>1</sub> and CB<sub>2</sub> receptors could also underlie changes in energy metabolism and body weight loss, both of which are common phenomena resulting from TBI, due to their direct influence on feeding, glucose uptake, fatty acid synthesis and triglyceride accumulation, energy expenditure, and metabolic homeostasis (122–127).

It is tempting to speculate that brain CBR deficit, associated with stress, age, gender, and anxiety/agitation, could play a central role in the individual variations in the outcome of TBI (128). While TBI is not part of the current study, the findings of stress-induced CBR deficits may translate to issues regarding TBI and co-occurring stress as evidenced in diagnoses of comorbidity of PTSD and mTBI in military personnel returned from Iraq and Afghanistan war zone that could advance our understanding of the neuroprotection of the consequences of TBI. Strategies to reduce gender and stress-related brain CBR deficit and agents to restore CBR activity could become potentially effective therapies for TBI. Indeed, treatment with synthetic 2-AG resulted in attenuated edema formation, infarct volume, and blood–brain barrier permeability in a mouse model of TBI, an effect dose-dependently attenuated by a CB<sub>1</sub> antagonist (41). And partial inhibition of 2-AG degradation, improved motor coordination, and working memory performance in mice model of TBI (37). Selective and highly potent cannabinoid CB<sub>1</sub> and CB<sub>2</sub> receptor agonist showed a pronounced neuroprotective effect in a rat TBI model (129). A potent and CB<sub>1</sub> and CB<sub>2</sub> receptor agonist, when applied before, during, and after transient occlusion of the middle cerebral artery, significantly and dose-dependently reduced cortical lesion sizes and motor deficits (130).

In summary, we found a higher basal value of CBRs in the forebrain of adolescent female animals, which was significantly

reduced after repeated stress. Because of the known anxiolytic and neuroprotective effect of eCB and CBR activities, this high base-line CBR may provide a neuroprotective mechanism for the improved outcome of prepubescent and pubescent females with TBI. The stress-induced reduction of CBR may underlie the poor long-term outcome of older female TBI patients who may also be experiencing postmenopause-related reductions in reproductive hormones. As brain eCBs and CBR activity is implicated in age and gender-dependent difference in the outcome of TBI and PTSD, further studies in this direction are required.

## ACKNOWLEDGMENTS

This work was supported, in part, by Lotus Biotech.com and the Center for the Study of Traumatic Stress, Uniformed Services University of the Health Sciences. Daniel Xing proofread this manuscript.

## REFERENCES

- Berry C, Ley EJ, Tillou A, Cryer G, Margulies DR, Salim A. The effect of gender on patients with moderate to severe head injuries. *J Trauma* (2009) **67**:950–3. doi:10.1097/TA.0b013e3181ba3354
- Aaro Jonsson C, Catroppa C, Godfrey C, Smedler AC, Anderson V. Individual profiles of predictors and their relations to 10 years outcome after childhood traumatic brain injury. *Brain Inj* (2013) **27**:831–8. doi:10.3109/02699052.2013.775493
- Anderson V, Catroppa C, Godfrey C, Rosenfeld JV. Intellectual ability 10 years after traumatic brain injury in infancy and childhood: what predicts outcome? *J Neurotrauma* (2012) **29**:143–53. doi:10.1089/neu.2011.2012
- McIntyre A, Mehta S, Aubut J, Dijkers M, Teasell RW. Mortality among older adults after a traumatic brain injury: a meta-analysis. *Brain Inj* (2013) **27**:31–40. doi:10.3109/02699052.2012.700086
- King N. A systematic review of age and gender factors in prolonged post concussion symptoms after mild head injury. *NeuroRehabilitation* (2014) **34**(4):741–8. doi:10.3233/NRE-141072
- Ley EJ, Short SS, Liou DZ, Singer MB, Mirocha J, Melo N, et al. Gender impacts mortality after traumatic brain injury in teenagers. *J Trauma Acute Care Surg* (2013) **75**:682–6. doi:10.1097/TA.0b013e31829d024f
- Groszasser Z, Cohen M, Keren O. Female TBI patients recover better than males. *Brain Inj* (1998) **12**:805–8. doi:10.1080/026990598122197
- Barr WB. Neuropsychological testing of high school athletes. Preliminary norms and test-retest indices. *Arch Clin Neuropsychol* (2003) **18**:91–101. doi:10.1093/arclin/18.1.91
- Xiong Y, Mahmood A, Lu D, Qu C, Goussev A, Schallert T, et al. Role of gender in outcome after traumatic brain injury and therapeutic effect of erythropoietin in mice. *Brain Res* (2007) **1185**:301–12. doi:10.1016/j.brainres.2007.09.052
- Ratcliff JJ, Greenspan AI, Goldstein FC, Stringer AY, Bushnik T, Hammond FM, et al. Gender and traumatic brain injury: do the sexes fare differently? *Brain Inj* (2007) **21**:1023–30. doi:10.1080/02699050701633072
- Wagner AK, Kline AE, Ren D, Willard LA, Wenger MK, Zafonte RD, et al. Gender associations with chronic methylphenidate treatment and behavioral performance following experimental traumatic brain injury. *Behav Brain Res* (2007) **181**:200–9. doi:10.1016/j.bbr.2007.04.006
- Niemeier JP, Marwitz JH, Leshner K, Walker WC, Bushnik T. Gender differences in executive functions following traumatic brain injury. *Neuropsychol Rehabil* (2007) **17**:293–313. doi:10.1080/09602010600814729
- Brown SB, Colantonio A, Kim H. Gender differences in discharge destination among older adults following traumatic brain injury. *Health Care Women Int* (2012) **33**:896–904. doi:10.1080/07399332.2012.673654
- Renner C, Hummelsheim H, Kopczak A, Steube D, Schneider HJ, Schneider M, et al. The influence of gender on the injury severity, course and outcome of traumatic brain injury. *Brain Inj* (2012) **26**:1360–71. doi:10.3109/02699052.2012.667592
- Schmidt AT, Hanten GR, Li X, Vasquez AC, Wilde EA, Chapman SB, et al. Decision making after pediatric traumatic brain injury: trajectory of recovery and relationship to age and gender. *Int J Dev Neurosci* (2012) **30**:225–30. doi:10.1016/j.ijdevneu.2011.11.003

16. Conley YP, Okonkwo DO, Deslouches S, Alexander S, Puccio AM, Beers SR, et al. Mitochondrial polymorphisms impact outcomes after severe traumatic brain injury. *J Neurotrauma* (2014) **31**:34–41. doi:10.1089/neu.2013.2855
17. Bulstrode H, Nicoll JA, Hudson G, Chinnery PF, Di Pietro V, Belli A. Mitochondrial DNA and traumatic brain injury. *Ann Neurol* (2014) **75**(2):186–95. doi:10.1002/ana.24116
18. Bigler ED, Abildskov TJ, Petrie J, Farrer TJ, Dennis M, Simic N, et al. Heterogeneity of brain lesions in pediatric traumatic brain injury. *Neuropsychology* (2013) **27**:438–51. doi:10.1037/a0032837
19. Ponsford J. Factors contributing to outcome following traumatic brain injury. *NeuroRehabilitation* (2013) **32**(4):803–15. doi:10.3233/NRE-130904
20. Schmitt A, Malchow B, Hasan A, Falkai P. The impact of environmental factors in severe psychiatric disorders. *Front Neurosci* (2014) **8**:19. doi:10.3389/fnins.2014.00019
21. Karsten CA, Baram TZ. How does a neuron “know” to modulate its epigenetic machinery in response to early-life environment/experience? *Front Psychiatry* (2013) **4**:89. doi:10.3389/fpsyt.2013.00089
22. Gudsnuik KM, Champagne FA. Epigenetic effects of early developmental experiences. *Clin Perinatol* (2011) **38**:703–17. doi:10.1016/j.clp.2011.08.005
23. Broomhall LG, Clark CR, McFarlane AC, O'Donnell M, Bryant R, Creamer M, et al. Early stage assessment and course of acute stress disorder after mild traumatic brain injury. *J Nerv Ment Dis* (2009) **197**:178–81. doi:10.1097/NMD.0b013e318199fe7f
24. Higgins DM, Kerns RD, Brandt CA, Haskell SG, Bathulapalli H, Gilliam W, et al. Persistent pain and comorbidity among operation enduring freedom/operation Iraqi freedom/operation new dawn veterans. *Pain Med* (2014) **15**(5):782–90. doi:10.1111/pme.12388
25. Schneiderman AI, Braver ER, Kang HK. Understanding sequelae of injury mechanisms and mild traumatic brain injury incurred during the conflicts in Iraq and Afghanistan: persistent postconcussive symptoms and posttraumatic stress disorder. *Am J Epidemiol* (2008) **167**:1446–52. doi:10.1093/aje/kwn068
26. Hoge CW, Castro CA, Messer SC, McGurk D, Cotting DI, Koffman RL. Combat duty in Iraq and Afghanistan, mental health problems and barriers to care. *US Army Med Dep J* (2008):7–17; republished from *New Engl J Med* (2004) **351**:13–22. doi:10.1056/NEJMoa040603
27. Hoge CW, McGurk D, Thomas JL, Cox AL, Engel CC, Castro CA. Mild traumatic brain injury in U.S. soldiers returning from Iraq. *N Engl J Med* (2008) **358**:453–63. doi:10.1056/NEJMoa072972
28. Carlson KF, Nelson D, Orazem RJ, Nugent S, Cifu DX, Sayer NA. Psychiatric diagnoses among Iraq and Afghanistan war veterans screened for deployment-related traumatic brain injury. *J Trauma Stress* (2010) **23**:17–24. doi:10.1002/jts.20483
29. Carlson KF, Barnes JE, Hagel EM, Taylor BC, Cifu DX, Sayer NA. Sensitivity and specificity of traumatic brain injury diagnosis codes in United States Department of Veterans Affairs administrative data. *Brain Inj* (2013) **27**:640–50. doi:10.3109/02699052.2013.771795
30. Brenner LA, Vanderploeg RD, Terrio H. Assessment and diagnosis of mild traumatic brain injury, posttraumatic stress disorder, and other polytrauma conditions: burden of adversity hypothesis. *Rehabil Psychol* (2009) **54**:239–46. doi:10.1037/a0016908
31. Iverson KM, Pogoda TK, Gradus JL, Street AE. Deployment-related traumatic brain injury among operation enduring freedom/operation Iraqi freedom veterans: associations with mental and physical health by gender. *J Womens Health (Larchmt)* (2013) **22**:267–75. doi:10.1089/jwh.2012.3755
32. Xing G, Barry ES, Benford B, Grunberg NE, Li H, Watson WD, et al. Impact of repeated stress on traumatic brain injury-induced mitochondrial electron transport chain expression and behavioral responses in rats. *Front Neurol* (2013) **4**:196. doi:10.3389/fneur.2013.00196
33. Xing G, Carlton J, Jiang X, Jia M, Sharma P, Li H. Delayed effects of repeated inescapable severe stress on brain cannabinoid receptor expression and acoustic startle response in adolescent male rats: relevance to the development of post-traumatic stress disorder and stress-related brain atrophy. In: Forman E, Fuller J, editors. *PTSD: The New Research*. New York, NY: Nova (2013). p. 83–108.
34. Xing G, Carlton J, Zhang L, Jiang X, Fullerton C, Li H, et al. Cannabinoid receptor expression and phosphorylation are differentially regulated between male and female cerebellum and brain stem after repeated stress: implication for PTSD and drug abuse. *Neurosci Lett* (2011) **502**:5–9. doi:10.1016/j.neulet.2011.05.013
35. Martinez-Vargas M, Morales-Gomez J, Gonzalez-Rivera R, Hernandez-Enriquez C, Perez-Arredondo A, Estrada-Rojas F, et al. Does the neuroprotective role of anandamide display diurnal variations? *Int J Mol Sci* (2013) **14**:23341–55. doi:10.3390/ijms141223341
36. Amenta PS, Jallo JI, Tuma RF, Elliott MB. A cannabinoid type 2 receptor agonist attenuates blood-brain barrier damage and neurodegeneration in a murine model of traumatic brain injury. *J Neurosci Res* (2012) **90**:2293–305. doi:10.1002/jnr.23114
37. Tchantchou F, Zhang Y. Selective inhibition of alpha/beta-hydrolase domain 6 attenuates neurodegeneration, alleviates blood brain barrier breakdown, and improves functional recovery in a mouse model of traumatic brain injury. *J Neurotrauma* (2013) **30**:565–79. doi:10.1089/neu.2012.2647
38. Felder CC, Joyce KE, Briley EM, Mansouri J, Mackie K, Blond O, et al. Comparison of the pharmacology and signal transduction of the human cannabinoid CB1 and CB2 receptors. *Mol Pharmacol* (1995) **48**:443–50.
39. Egertova M, Elphick MR. Localisation of cannabinoid receptors in the rat brain using antibodies to the intracellular C-terminal tail of CB. *J Comp Neurol* (2000) **422**:159–71. doi:10.1002/(SICI)1096-9861(20000626)422:2<159::AID-CNE1>3.0.CO;2-1
40. van der Stelt M, Veldhuis WB, van Haaften GW, Fezza F, Bisogno T, Bar PR, et al. Exogenous anandamide protects rat brain against acute neuronal injury in vivo. *J Neurosci* (2001) **21**:8765–71.
41. Panikashvili D, Simeonidou C, Ben-Shabat S, Hanus L, Breuer A, Mechoulam R, et al. An endogenous cannabinoid (2-AG) is neuroprotective after brain injury. *Nature* (2001) **413**:527–31. doi:10.1038/35097089
42. Panikashvili D, Mechoulam R, Beni SM, Alexandrovich A, Shohami E. CB1 cannabinoid receptors are involved in neuroprotection via NF-kappa B inhibition. *J Cereb Blood Flow Metab* (2005) **25**:477–84. doi:10.1038/sj.jcbfm.9600047
43. Panikashvili D, Shein NA, Mechoulam R, Trembovler V, Kohen R, Alexandrovich A, et al. The endocannabinoid 2-AG protects the blood-brain barrier after closed head injury and inhibits mRNA expression of proinflammatory cytokines. *Neurobiol Dis* (2006) **22**:257–64. doi:10.1016/j.nbd.2005.11.004
44. Shohami E, Cohen-Yeshurun A, Magid L, Algali M, Mechoulam R. Endocannabinoids and traumatic brain injury. *Br J Pharmacol* (2011) **163**:1402–10. doi:10.1111/j.1476-5381.2011.01343.x
45. Cohen-Yeshurun A, Willner D, Trembovler V, Alexandrovich A, Mechoulam R, Shohami E, et al. N-arachidonoyl-L-serine (AraS) possesses proneurogenic properties in vitro and in vivo after traumatic brain injury. *J Cereb Blood Flow Metab* (2013) **33**:1242–50. doi:10.1038/jcbfm.2013.75
46. Chhatwal JP, Davis M, Maguschak KA, Ressler KJ. Enhancing cannabinoid neurotransmission augments the extinction of conditioned fear. *Neuropsychopharmacology* (2005) **30**:516–24. doi:10.1038/sj.npp.1300655
47. Haller J, Bakos N, Szirmay M, Ledent C, Freund TF. The effects of genetic and pharmacological blockade of the CB1 cannabinoid receptor on anxiety. *Eur J Neurosci* (2002) **16**:1395–8. doi:10.1046/j.1460-9568.2002.02192.x
48. Martin M, Ledent C, Parmentier M, Maldonado R, Valverde O. Involvement of CB1 cannabinoid receptors in emotional behaviour. *Psychopharmacology (Berl)* (2002) **159**:379–87. doi:10.1007/s00213-001-0946-5
49. Urquien L, Perez-Rial S, Ledent C, Palomo T, Manzanares J. Impaired action of anxiolytic drugs in mice deficient in cannabinoid CB1 receptors. *Neuropharmacology* (2004) **46**:966–73. doi:10.1016/j.neuropharm.2004.01.003
50. Marsicano G, Wotjak CT, Azad SC, Bisogno T, Rammes G, Cascio MG, et al. The endogenous cannabinoid system controls extinction of aversive memories. *Nature* (2002) **418**:530–4. doi:10.1038/nature00839
51. Pertwee RG. Ligands that target cannabinoid receptors in the brain: from THC to anandamide and beyond. *Addict Biol* (2008) **13**:147–59. doi:10.1111/j.1369-1600.2008.00108.x
52. Maresz K, Carrier EJ, Ponomarev ED, Hillard CJ, Dittel BN. Modulation of the cannabinoid CB2 receptor in microglial cells in response to inflammatory stimuli. *J Neurochem* (2005) **95**:437–45. doi:10.1111/j.1471-4159.2005.03380.x
53. Golech SA, McCarron RM, Chen Y, Bembry J, Lenz F, Mechoulam R, et al. Human brain endothelium: coexpression and function of vanilloid and endocannabinoid receptors. *Brain Res Mol Brain Res* (2004) **132**:87–92. doi:10.1016/j.molbrainres.2004.08.025
54. Van Sickle MD, Duncan M, Kingsley PJ, Mouhate A, Urbani P, Mackie K, et al. Identification and functional characterization of brainstem cannabinoid CB2 receptors. *Science* (2005) **310**:329–32. doi:10.1126/science.1115740

55. Mackie K. Distribution of cannabinoid receptors in the central and peripheral nervous system. *Handb Exp Pharmacol* (2005) **168**:299–325. doi:10.1007/3-540-26573-2\_10
56. Gallily R, Breuer A, Mechoulam R. 2-Arachidonylglycerol, an endogenous cannabinoid, inhibits tumor necrosis factor- $\alpha$  production in murine macrophages, and in mice. *Eur J Pharmacol* (2000) **406**:R5–7. doi:10.1016/S0014-2999(00)00653-1
57. Romeo RD. Pubertal maturation and programming of hypothalamic-pituitary-adrenal reactivity. *Front Neuroendocrinol* (2010) **31**:232–40. doi:10.1016/j.yfrne.2010.02.004
58. Widom CS, Czaja SJ, Dutton MA. Childhood victimization and lifetime revictimization. *Child Abuse Negl* (2008) **32**:785–96. doi:10.1016/j.chiabu.2007.12.006
59. Weber K, Rockstroh B, Borgelt J, Awiszus B, Popov T, Hoffmann K, et al. Stress load during childhood affects psychopathology in psychiatric patients. *BMC Psychiatry* (2008) **8**:63. doi:10.1186/1471-244X-8-63
60. Wainwright NW, Surtees PG. Childhood adversity, gender and depression over the life-course. *J Affect Disord* (2002) **72**:33–44. doi:10.1016/S0165-0327(01)00420-7
61. Jiang X, Xing G, Yang C, Verma A, Zhang L, Li H. Stress impairs 5-HT<sub>2A</sub> receptor-mediated serotonergic facilitation of GABA release in juvenile rat basolateral amygdala. *Neuropsychopharmacology* (2009) **34**:410–23. doi:10.1038/npp.2008.71
62. Tang SL, Tran V, Wagner EJ. Sex differences in the cannabinoid modulation of an A-type K<sup>+</sup> current in neurons of the mammalian hypothalamus. *J Neurophysiol* (2005) **94**:2983–6. doi:10.1152/jn.01187.2004
63. Malcher-Lopes R, Di S, Marcheselli VS, Weng FJ, Stuart CT, Bazan NG, et al. Opposing crosstalk between leptin and glucocorticoids rapidly modulates synaptic excitation via endocannabinoid release. *J Neurosci* (2006) **26**:6643–50. doi:10.1523/JNEUROSCI.5126-05.2006
64. Nong L, Newton C, Cheng Q, Friedman H, Roth MD, Klein TW. Altered cannabinoid receptor mRNA expression in peripheral blood mononuclear cells from marijuana smokers. *J Neuroimmunol* (2002) **127**:169–76. doi:10.1016/S0165-5728(02)00113-3
65. Onaivi ES, Chaudhuri G, Abaci AS, Parker M, Manier DH, Martin PR, et al. Expression of cannabinoid receptors and their gene transcripts in human blood cells. *Prog Neuropsychopharmacol Biol Psychiatry* (1999) **23**:1063–77. doi:10.1016/S0278-5846(99)00052-4
66. Bradshaw HB, Rimmerman N, Krey JF, Walker JM. Sex and hormonal cycle differences in rat brain levels of pain-related cannabimimetic lipid mediators. *Am J Physiol Regul Integr Comp Physiol* (2006) **291**:R349–58. doi:10.1152/ajpregu.00933.2005
67. Zimmer A, Zimmer AM, Hohmann AG, Herkenham M, Bonner TI. Increased mortality, hypoactivity, and hypoalgesia in cannabinoid CB<sub>1</sub> receptor knockout mice. *Proc Natl Acad Sci U S A* (1999) **96**:5780–5. doi:10.1073/pnas.96.10.5780
68. Reich CG, Taylor ME, McCarthy MM. Differential effects of chronic unpredictable stress on hippocampal CB<sub>1</sub> receptors in male and female rats. *Behav Brain Res* (2009) **203**:264–9. doi:10.1016/j.bbr.2009.05.013
69. Westenbroek C, Snijders TA, den Boer JA, Gerrits M, Fokkema DS, Ter Horst GJ. Pair-housing of male and female rats during chronic stress exposure results in gender-specific behavioral responses. *Horm Behav* (2005) **47**:620–8. doi:10.1016/j.yhbeh.2005.01.004
70. Hill JO, Talano CM, Nickel M, DiGirolamo M. Energy utilization in food-restricted female rats. *J Nutr* (1986) **116**:2000–12.
71. Mittendorfer B, Horowitz JF, Klein S. Gender differences in lipid and glucose kinetics during short-term fasting. *Am J Physiol Endocrinol Metab* (2001) **281**:E1333–9.
72. Canli T, Desmond JE, Zhao Z, Gabrieli JD. Sex differences in the neural basis of emotional memories. *Proc Natl Acad Sci U S A* (2002) **99**:10789–94. doi:10.1073/pnas.162356599
73. Marumo K, Takizawa R, Kawakubo Y, Onitsuka T, Kasai K. Gender difference in right lateral prefrontal hemodynamic response while viewing fearful faces: a multi-channel near-infrared spectroscopy study. *Neurosci Res* (2009) **63**:89–94. doi:10.1016/j.neures.2008.10.012
74. Pratchett LC, Pelcovitz MR, Yehuda R. Trauma and violence: are women the weaker sex? *Psychiatr Clin North Am* (2010) **33**:465–74. doi:10.1016/j.psc.2010.01.010
75. Meulders A, Vansteenwegen D, Vlaeyen JW. Women, but not men, report increasingly more pain during repeated (un)predictable painful electrocutaneous stimulation: evidence for mediation by fear of pain. *Pain* (2012) **153**(5):1030–41. doi:10.1016/j.pain.2012.02.005
76. Stevens JS, Hamann S. Sex differences in brain activation to emotional stimuli: a meta-analysis of neuroimaging studies. *Neuropsychologia* (2012) **50**(7):1578–93. doi:10.1016/j.neuropsychologia.2012.03.011
77. Choi K, Le T, McGuire J, Xing G, Zhang L, Li H, et al. Expression pattern of the cannabinoid receptor genes in the frontal cortex of mood disorder patients and mice selectively bred for high and low fear. *J Psychiatr Res* (2012) **46**:882–9. doi:10.1016/j.jpsychires.2012.03.021
78. Ng I, Lee KK, Lim JH, Wong HB, Yan XY. Investigating gender differences in outcome following severe traumatic brain injury in a predominantly Asian population. *Br J Neurosurg* (2006) **20**:73–8. doi:10.1080/02688690600682259
79. Stein DG. Progesterone in the treatment of acute traumatic brain injury: a clinical perspective and update. *Neuroscience* (2011) **191**:101–6. doi:10.1016/j.neuroscience.2011.04.013
80. Busch L, Sterin-Borda L, Borda E. Effects of castration on cannabinoid cb receptor expression and on the biological actions of cannabinoid in the parotid gland. *Clin Exp Pharmacol Physiol* (2006) **33**:258–63. doi:10.1111/j.1440-1681.2006.04355.x
81. Craft RM. Sex differences in behavioral effects of cannabinoids. *Life Sci* (2005) **77**:2471–8. doi:10.1016/j.lfs.2005.04.019
82. Fattore L, Fratta W. How important are sex differences in cannabinoid action? *Br J Pharmacol* (2010) **160**:544–8. doi:10.1111/j.1476-5381.2010.00776.x
83. González S, Bisogno T, Wenger T, Manzanera J, Milone A, Berrendero F, et al. Sex steroid influence on cannabinoid CB<sub>1</sub> receptor mRNA and endocannabinoid levels in the anterior pituitary gland. *Biochem Biophys Res Commun* (2000) **270**:260–6. doi:10.1006/bbrc.2000.2406
84. Rodriguez de Fonseca F, Cebeira M, Ramos JA, Martin M, Fernandez-Ruiz JJ. Cannabinoid receptors in rat brain areas: sexual differences, fluctuations during estrous cycle and changes after gonadectomy and sex steroid replacement. *Life Sci* (1994) **54**:159–70. doi:10.1016/0024-3205(94)00585-0
85. Butkevich I, Mikhailenko V, Semionov V, Bagaeva T, Otellin V, Aloisi AM. Effects of maternal corticosterone and stress on behavioral and hormonal indices of formalin pain in male and female offspring of different ages. *Horm Behav* (2009) **55**:149–57. doi:10.1016/j.yhbeh.2008.09.008
86. Caudell KA, Gallucci BB. Neuroendocrine and immunological responses of women to stress. *West J Nurs Res* (1995) **17**:672–92. doi:10.1177/019394599501700607
87. Fan F, Tao Q, Abood M, Martin BR. Cannabinoid receptor down-regulation without alteration of the inhibitory effect of CP 55,940 on adenylyl cyclase in the cerebellum of CP 55,940-tolerant mice. *Brain Res* (1996) **706**:13–20. doi:10.1016/0006-8993(95)01113-7
88. Hill MN, Carrier EJ, Ho WS, Shi L, Patel S, Gorzalka BB, et al. Prolonged glucocorticoid treatment decreases cannabinoid CB<sub>1</sub> receptor density in the hippocampus. *Hippocampus* (2008) **18**:221–6. doi:10.1002/hipo.20386
89. Malcher-Lopes R, Franco A, Tasker JG. Glucocorticoids shift arachidonic acid metabolism toward endocannabinoid synthesis: a non-genomic anti-inflammatory switch. *Eur J Pharmacol* (2008) **583**:322–39. doi:10.1016/j.ejphar.2007.12.033
90. Oviedo A, Glowa J, Herkenham M. Chronic cannabinoid administration alters cannabinoid receptor binding in rat brain: a quantitative autoradiographic study. *Brain Res* (1993) **616**:293–302. doi:10.1016/0006-8993(93)90220-H
91. Romero J, Garcia-Palomero E, Castro JG, Garcia-Gil L, Ramos JA, Fernandez-Ruiz JJ. Effects of chronic exposure to delta-9-tetrahydrocannabinol on cannabinoid receptor binding and mRNA levels in several rat brain regions. *Brain Res Mol Brain Res* (1997) **46**:100–8.
92. Lee TT, Hill MN. Age of stress exposure modulates the immediate and sustained effects of repeated stress on corticolimbic cannabinoid CB<sub>1</sub> receptor binding in male rats. *Neuroscience* (2013) **249**:106–14. doi:10.1016/j.neuroscience.2012.11.017
93. Patel S, Hillard CJ. Pharmacological evaluation of cannabinoid receptor ligands in a mouse model of anxiety: further evidence for an anxiolytic role for endogenous cannabinoid signaling. *J Pharmacol Exp Ther* (2006) **318**:304–11. doi:10.1124/jpet.106.101287
94. Pamplona FA, Bitencourt RM, Takahashi RN. Short- and long-term effects of cannabinoids on the extinction of contextual fear memory in rats. *Neurobiol Learn Mem* (2008) **90**:290–3. doi:10.1016/j.nlm.2008.04.003

95. Roche M, O'Connor E, Diskin C, Finn DP. The effect of CB(1) receptor antagonism in the right basolateral amygdala on conditioned fear and associated analgesia in rats. *Eur J Neurosci* (2007) **26**:2643–53. doi:10.1111/j.1460-9568.2007.05861.x
96. De Oliveira Alvares L, Genro BP, Diehl F, Quilfeldt JA. Differential role of the hippocampal endocannabinoid system in the memory consolidation and retrieval mechanisms. *Neurobiol Learn Mem* (2008) **90**:1–9. doi:10.1016/j.nlm.2008.01.009
97. Li CS, Sinha R. Inhibitory control and emotional stress regulation: neuroimaging evidence for frontal-limbic dysfunction in psycho-stimulant addiction. *Neurosci Biobehav Rev* (2008) **32**:581–97. doi:10.1016/j.neubiorev.2007.10.003
98. Vlachos I, Herry C, Luthi A, Aertsen A, Kumar A. Context-dependent encoding of fear and extinction memories in a large-scale network model of the basal amygdala. *PLoS Comput Biol* (2011) **7**:e1001104. doi:10.1371/journal.pcbi.1001104
99. Maren S, Hobin JA. Hippocampal regulation of context-dependent neuronal activity in the lateral amygdala. *Learn Mem* (2007) **14**:318–24. doi:10.1101/lm.477007
100. Villarreal G, Hamilton DA, Petropoulos H, Driscoll I, Rowland LM, Griego JA, et al. Reduced hippocampal volume and total white matter volume in posttraumatic stress disorder. *Biol Psychiatry* (2002) **52**:119–25. doi:10.1016/S0006-3223(02)01359-8
101. De Bellis MD, Kuchibhatla M. Cerebellar volumes in pediatric maltreatment-related posttraumatic stress disorder. *Biol Psychiatry* (2006) **60**:697–703. doi:10.1016/j.biopsych.2006.04.035
102. Felmingham K, Williams LM, Whitford TJ, Falconer E, Kemp AH, Peduto A, et al. Duration of posttraumatic stress disorder predicts hippocampal grey matter loss. *Neuroreport* (2009) **20**:1402–6. doi:10.1097/WNR.0b013e3283300fbc
103. Zhang J, Tan Q, Yin H, Zhang X, Huan Y, Tang L, et al. Decreased gray matter volume in the left hippocampus and bilateral calcarine cortex in coal mine flood disaster survivors with recent onset PTSD. *Psychiatry Res* (2011) **192**:84–90. doi:10.1016/j.psychres.2010.09.001
104. Morey RA, Haswell CC, Selgrade ES, Massoglia D, Liu C, Weiner J, et al. Effects of chronic mild traumatic brain injury on white matter integrity in Iraq and Afghanistan war veterans. *Hum Brain Mapp* (2012) **34**(11):2986–99. doi:10.1002/hbm.22117
105. Liu Y, Li YJ, Luo EP, Lu HB, Yin H. Cortical thinning in patients with recent onset post-traumatic stress disorder after a single prolonged trauma exposure. *PLoS One* (2012) **7**:e39025. doi:10.1371/journal.pone.0039025
106. Cardenas VA, Samuelson K, Lenoci M, Studholme C, Neylan TC, Marmar CR, et al. Changes in brain anatomy during the course of post-traumatic stress disorder. *Psychiatry Res* (2011) **193**:93–100. doi:10.1016/j.psychres.2011.01.013
107. Thomaes K, Dorrepaal E, Draijer N, de Ruiter MB, van Balkom AJ, Smit JH, et al. Reduced anterior cingulate and orbitofrontal volumes in child abuse-related complex PTSD. *J Clin Psychiatry* (2010) **71**:1636–44. doi:10.4088/JCP.08m04754blu
108. Woon FL, Sood S, Hedges DW. Hippocampal volume deficits associated with exposure to psychological trauma and posttraumatic stress disorder in adults: a meta-analysis. *Prog Neuropsychopharmacol Biol Psychiatry* (2010) **34**:1181–8. doi:10.1016/j.pnpbp.2010.06.016
109. Hedges DW, Woon FL. Premorbid brain volume estimates and reduced total brain volume in adults exposed to trauma with or without posttraumatic stress disorder: a meta-analysis. *Cogn Behav Neurol* (2010) **23**:124–9. doi:10.1097/WNN.0b013e328181e1cbe1
110. Woodward SH, Schaefer M, Kaloupek DG, Cediell L, Eliez S. Smaller global and regional cortical volume in combat-related posttraumatic stress disorder. *Arch Gen Psychiatry* (2009) **66**:1373–82. doi:10.1001/archgenpsychiatry.2009.160
111. Rogers MA, Yamasue H, Abe O, Yamada H, Ohtani T, Iwanami A, et al. Smaller amygdala volume and reduced anterior cingulate gray matter density associated with history of post-traumatic stress disorder. *Psychiatry Res* (2009) **174**:210–6. doi:10.1016/j.psychres.2009.06.001
112. Marchalant Y, Brothers HM, Norman GJ, Karelina K, DeVries AC, Wenk GL. Cannabinoids attenuate the effects of aging upon neuroinflammation and neurogenesis. *Neurobiol Dis* (2009) **34**:300–7. doi:10.1016/j.nbd.2009.01.014
113. Bolognini D, Costa B, Maione S, Comelli F, Marini P, Di Marzo V, et al. The plant cannabinoid Delta9-tetrahydrocannabinol can decrease signs of inflammation and inflammatory pain in mice. *Br J Pharmacol* (2010) **160**:677–87. doi:10.1111/j.1476-5381.2010.00756.x
114. Ribeiro R, Wen J, Li S, Zhang Y. Involvement of ERK1/2, cPLA2 and NF-kappaB in microglia suppression by cannabinoid receptor agonists and antagonists. *Prostaglandins Other Lipid Mediat* (2013) **10**(0–101):1–14. doi:10.1016/j.prostaglandins.2012.11.003
115. McLaughlin CR, Abood ME. Developmental expression of cannabinoid receptor mRNA. *Brain Res Dev Brain Res* (1993) **76**:75–8.
116. Aguado T, Monory K, Palazuelos J, Stella N, Cravatt B, Lutz B, et al. The endocannabinoid system drives neural progenitor proliferation. *FASEB J* (2005) **19**:1704–6. doi:10.1096/fj.05-3995fje
117. Aguado T, Palazuelos J, Monory K, Stella N, Cravatt B, Lutz B, et al. The endocannabinoid system promotes astroglial differentiation by acting on neural progenitor cells. *J Neurosci* (2006) **26**:1551–61. doi:10.1523/JNEUROSCI.3101-05.2006
118. Palazuelos J, Ortega Z, Diaz-Alonso J, Guzman M, Galve-Roperh I. CB2 cannabinoid receptors promote neural progenitor cell proliferation via mTORC1 signaling. *J Biol Chem* (2012) **287**:1198–209. doi:10.1074/jbc.M111.291294
119. Czéh B, Müller-Keuker JI, Rygula R, Abumaria N, Hiemke C, Domenici E, et al. Chronic social stress inhibits cell proliferation in the adult medial prefrontal cortex: hemispheric asymmetry and reversal by fluoxetine treatment. *Neuropsychopharmacology* (2007) **32**:1490–503. doi:10.1038/sj.npp.1301275
120. Tishkina AO, Levshina IP, Lazareva NA, Passikova NV, Stepanichev MY, Ajrapetyanz MG, et al. Chronic stress induces nonapoptotic neuronal death in the rat hippocampus. *Dokl Biol Sci* (2009) **428**:403–6. doi:10.1134/S0012496609050032
121. Yun J, Koike H, Ibi D, Toth E, Mizoguchi H, Nitta A, et al. Chronic restraint stress impairs neurogenesis and hippocampus-dependent fear memory in mice: possible involvement of a brain-specific transcription factor Npas4. *J Neurochem* (2010) **114**:1840–51. doi:10.1111/j.1471-4159.2010.06893.x
122. Richard D, Guesdon B, Timofeeva E. The brain endocannabinoid system in the regulation of energy balance. *Best Pract Res Clin Endocrinol Metab* (2009) **23**:17–32. doi:10.1016/j.beem.2008.10.007
123. Bajzer M, Olivieri M, Haas MK, Pfluger PT, Magrisso IJ, Foster MT, et al. Cannabinoid receptor 1 (CB1) antagonism enhances glucose utilisation and activates brown adipose tissue in diet-induced obese mice. *Diabetologia* (2011) **54**:3121–31. doi:10.1007/s00125-011-2302-6
124. Silvestri C, Di Marzo V. The endocannabinoid system in energy homeostasis and the etiology of metabolic disorders. *Cell Metab* (2013) **17**:475–90. doi:10.1016/j.cmet.2013.03.001
125. Vettor R, Pagano C. The role of the endocannabinoid system in lipogenesis and fatty acid metabolism. *Best Pract Res Clin Endocrinol Metab* (2009) **23**:51–63. doi:10.1016/j.beem.2008.10.002
126. Silvestri C, Ligresti A, Di Marzo V. Peripheral effects of the endocannabinoid system in energy homeostasis: adipose tissue, liver and skeletal muscle. *Rev Endocr Metab Disord* (2011) **12**:153–62. doi:10.1007/s11154-011-9167-3
127. Di Marzo V, Capasso R, Matias I, Aviello G, Petrosino S, Borrelli F, et al. The role of endocannabinoids in the regulation of gastric emptying: alterations in mice fed a high-fat diet. *Br J Pharmacol* (2008) **153**:1272–80. doi:10.1038/sj.bjp.0707682
128. Jonsson CA, Catroppa C, Godfrey C, Smedler AC, Anderson V. Cognitive recovery and development after traumatic brain injury in childhood: a person-oriented, longitudinal study. *J Neurotrauma* (2013) **30**:76–83. doi:10.1089/neu.2012.2592
129. Mauler F, Horváth E, De Vry J, Jäger R, Schwarz T, Sandmann S, et al. BAY 38-7271: a novel highly selective and highly potent cannabinoid receptor agonist for the treatment of traumatic brain injury. *CNS Drug Rev* (2003) **9**:343–58. doi:10.1111/j.1527-3458.2003.tb00259.x
130. Schmidt W, Schafer F, Striggow V, Frohlich K, Striggow F. Cannabinoid receptor subtypes 1 and 2 mediate long-lasting neuroprotection and improve motor behavior deficits after transient focal cerebral ischemia. *Neuroscience* (2012) **227**:313–26. doi:10.1016/j.neuroscience.2012.09.080

**Conflict of Interest Statement:** The Guest Associate Editor Yumin Zhang declares that, despite being affiliated to the same institution as authors Guoqiang Xing, Janis Carlton, Xiaolong Jiang, Jilian Wen, Min Jia and He Li, the review process was handled objectively and no conflict of interest exists. The authors declare that the research was conducted in the absence of any commercial or financial relationships that could be construed as a potential conflict of interest.

Received: 15 March 2014; accepted: 12 August 2014; published online: 28 August 2014.

Citation: Xing G, Carlton J, Jiang X, Wen J, Jia M and Li H (2014) Differential expression of brain cannabinoid receptors between repeatedly stressed males and females may

play a role in age and gender-related difference in traumatic brain injury: implications from animal studies. *Front. Neurol.* 5:161. doi: 10.3389/fneur.2014.00161

This article was submitted to *Neurotrauma*, a section of the journal *Frontiers in Neurology*.

Copyright © 2014 Xing, Carlton, Jiang, Wen, Jia and Li. This is an open-access article distributed under the terms of the Creative Commons Attribution License (CC BY). The use, distribution or reproduction in other forums is permitted, provided the original author(s) or licensor are credited and that the original publication in this journal is cited, in accordance with accepted academic practice. No use, distribution or reproduction is permitted which does not comply with these terms.





# Divergent temporal expression of hyaluronan metabolizing enzymes and receptors with craniotomy vs. controlled-cortical impact injury in rat brain: a pilot study

Guoqiang Xing\*, Ming Ren and Ajay Verma

Department of Neurology, Uniformed Services University of the Health Sciences, Bethesda, MD, USA

## Edited by:

Yumin Zhang, Uniformed Services University of the Health Sciences, USA

## Reviewed by:

Sonia Villapol, Georgetown University, USA

Zhihui Yang, University of Florida, USA

## \*Correspondence:

Guoqiang Xing, Lotus Biotech.com, John Hopkins University-MCC, 9601 Medical Center Drive, Suite 227, Rockville, MD 20850, USA  
e-mail: gxing99@yahoo.com

The views expressed in this article are those of the authors and do not necessarily reflect the official policy or position of the Department of the Navy, Department of Defense, nor the U.S. Government.

Traumatic brain injury (TBI) triggers many secondary changes in tissue biology, which ultimately determine the extent of injury and clinical outcome. Hyaluronan [hyaluronic acid (HA)] is a protective cementing gel present in the intercellular spaces whose degradation has been reported as a causative factor in tissue damage. Yet little is known about the expression and activities of genes involved in HA catabolism after TBI. Young adult male Sprague-Dawley rats were assigned to three groups: naïve control, craniotomy, and controlled-cortical impact-induced TBI (CCI-TBI). Four animals per group were sacrificed at 4 h, 1, 3, and 7 days post-CCI. The mRNA expression of hyaluronan synthases (HAS1–3), hyaluronidases (enzymes for HA degradation, HYAL 1–4, and PH20), and CD44 and RHAMM (membrane receptors for HA signaling and removal) were determined using real-time PCR. Compared to the naïve controls, expression of HAS1 and HAS2 mRNA, but not HAS3 mRNA increased significantly following craniotomy alone and following CCI with differential kinetics. Expression of HAS2 mRNA increased significantly in the ipsilateral brain at 1 and 3 days post-CCI. HYAL1 mRNA expression also increased significantly in the craniotomy group and in the contralateral CCI at 1 and 3 days post-CCI. CD44 mRNA expression increased significantly in the ipsilateral CCI at 4 h, 1, 3, and 7 days post-CCI (up to 25-fold increase). These data suggest a dynamic regulation and role for HA metabolism in secondary responses to TBI.

**Keywords:** TBI, secondary injury factors, hyaluronic acid, receptor, synthesis, degradation, hyaluronidase, rat brain

## INTRODUCTION

Traumatic brain injury (TBI) is the leading cause of mortality in children and young adult under 44 years of age in the USA. Brain tissues that are not destroyed immediately following the primary injury may undergo sub-acute injury or delayed death caused by secondarily generated auto-destructive factors (1, 2). Despite extensive research, the mechanism underlying TBI-induced secondary injury remains to be fully elucidated.

Hyaluronan [hyaluronic acid (HA)] is a stable sulfate-free mucopolysaccharide (glycosaminoglycan) containing about 2,500 repeating acetylglucosamine and glucuronic acid disaccharide units and is synthesized by a class of integral membrane proteins, i.e., hyaluronan synthases (HAS1, HAS2, and HAS3). The three HAS genes show distinct patterns of expression during development and their protein products play significantly different roles in the formation of the HA matrix and in response to different stimuli (3–5).

Both HAS1 and HAS2 synthesize high-molecular-weight HA, whereas HAS3 produces lower molecular weight HA (3). The expression of the three HAS isoforms is more prominent in growing cells than in resting cells and is differentially regulated by various stimuli, suggesting distinct functional roles of the three proteins. HAS lengthens hyaluronan by repeatedly adding glucuronic acid and *N*-acetylglucosamine to the nascent polysaccharide. HA is extruded via ABC-transporter through the cell

membrane into the extracellular space (6). Hyaluronan forms a protective cementing gel in intercellular spaces throughout the body and acts as a binding and lubricating agent as well as antioxidant (7, 8). Hyaluronan also modulates cell migration, adhesion, wound healing, and tumor invasion (9, 10). The concentration of high-molecular-weight hyaluronan is high in the brains of young rats, but it decreases with aging whereas the low molecular weight hyaluronan increases with aging (11, 12).

As the HAS enzymes are important in cell development and proliferation, they must be strictly regulated. This regulation may occur transcriptionally and post-transcriptionally by naturally occurring anti-sense HAS2 (13–17), by changes in the levels of the sugar substrates needed for HA production, and by modification of the enzymes through HAS dimerization or monoubiquitination (18, 19).

Recent studies in peripheral tissues have implicated a critical role of altered hyaluronan (HA) metabolism in the pathophysiology and healing process of injured tissues. Significantly increased HA production (by 32-fold in the circulation) has been found as a characteristic of patients with acute peripheral lung injury (20) and block HA production by hyaluronan synthase inhibitors effectively suppressed staphylococcal enterotoxin-induced inflammation (21).

The high-molecular-weight hyaluronan is readily degraded into small molecules after tissue injury (22), primarily by increased

levels of hyaluronidases (HYALs) and reactive oxygen species (ROS) (23). The degraded hyaluronan fragments play important roles in inflammation, innate immunity, cell proliferation, and wound healing through its antioxidant properties and through interacting with its primary cell surface receptors, CD44, RHAMM, and toll-like receptor 4 (TLR-4) (24–26). The increased fragmentation of HA in the early stages of injury could exert antioxidant effect against ROS and stimulate white blood cells-mediated immune response by up-regulating CD44 (27, 28). Increased levels of hyaluronan and CD44 could also stimulate cell proliferation and migration as found in cancer malignancy (29–31).

Hyaluronidases are a family of lysosomal enzymes that are crucial for the spread of bacterial infections and venoms toxins and the progression of cancer (32–34). Six HYAL genes have been identified [HYAL1, HYAL2, HYAL3, HYAL4, PH20, and HYAL-like pseudogene (HYALP1)] (35–38). Hyal-1 and Hyal-2 are the major mammalian HYALs in somatic tissues, and that they act in concert to degrade high-molecular-weight hyaluronan to the tetrasaccharide (37). HYAL1 is highly expressed in the serum too. HYAL2 enzymes have an acidic pH-optimum with an activity that is considerably lower than for other types of HYALs. HYAL3 is highly expressed in testis and bone marrow but low in other tissues. HYAL4 is expressed in placenta and skeletal muscle and it may form a complex with HYALP1 and PH-20. Human HYALP1 is a pseudogene with mutation in genomic DNA and cDNA (36). HYALs are absent or lowly expressed in normal adult brain. However, injury-induced HYAL expression and HA degradation may alter brain tissue hydration and osmotic balance resulting in edema, and promotes cell proliferation and migration.

Altered HA metabolism has been reported at protracted periods following stroke in human (39) and following middle cerebral artery occlusion (MCAO) in the rat (40). In the human study, the production of total HA and low molecular mass 3–10 disaccharides of HA (o-HA) was increased in post-mortem tissue and in the serum of patients at 1, 3, 7, and 14 days (peaking at 7 days) after ischemic stroke. Hyaluronidase activity was also increased in serum samples (peaking after 3 days) that may underlie the subsequent increase in o-HA (39). Moreover, HA synthases (HAS1 and 2) and HYALs (HYAL1 and 2) protein expression was increased in inflammatory cells from both stroke and peri-infarcted regions of the brain, with HYAL1 upregulated in microvessels and intracellularly in neurons, while HAS2 became translocated into the nuclei of neurons in peri-infarcted areas (39). And the HA receptor CD44 was increased in infiltrating mononuclear cells in the inflammatory regions. Similar results were found in the rat model of stroke (40).

Hyaluronic acid effects are mediated through two receptors, CD44 and the receptor of HA mediated motility (RHAMM). CD44 is a member of the closely related cell surface glycoproteins [cell adhesion molecules (CAMs)]. CD44 is a 742 amino acid single-pass type I membrane protein that is involved in hematopoiesis, lymphocyte activation, and tumor metastasis (41). CD44 mediates both cell–cell and cell–matrix interactions and plays an essential role in cell adhesion and cell migration. CD44 is expressed as multiple isoforms in normal and cancer tissues throughout the body due to alternative splicing events (42, 43). CD44 deficiency is associated with decreased *Cryptococcus neoformans* brain infection

(44). When compared to wild type animals, mice deficient in CD44 show significant reduction in ischemic infarct size and in the expression of soluble interleukin-1 $\beta$  following transient (30 min ischemia) and permanent (24 h) occlusion of the middle cerebral artery (45). RHAMM, also known as CD168, is a matrix receptor, which is linked to the plasma membrane by a GPI anchor and regulates cell motility. RHAMM is involved in glial cell locomotion and may play a role in the motile behavior of glial cells *in vivo* after CNS injury (46).

So far, no study has examined changes in the hyaluronan pathway after TBI. Considering the importance of hyaluronan metabolism in maintaining the integrity of tissue structure and function and tissue repair, we determined the mRNA expression of hyaluronan receptors (CD44, RHAMM), hyaluronan synthases (HAS1, HAS2, and HAS3), and HYALs (HYAL1, HYAL2, HYAL3, HYAL4, and PH20) in rat brains after controlled-cortical impact-induced TBI (CCI-TBI).

## MATERIALS AND METHODS

### ANIMALS AND CONTROLLED-CORTICAL IMPACT-INDUCED TBI

Forty-eight male Sprague-Dawley rats (170–200 g) (Taconic Farm, NY, USA) were randomly assigned to three different groups: (1) naïve control; (2) craniotomy (sham CCI); and (3) CCI. Four animals per group were sacrificed at 4 h, 24 h, 3 days and 7 days post-CCI.

For the craniotomy-only and the CCI groups, animals were initially anesthetized with 4% isoflurane in O<sub>2</sub> with a vented anesthesia chamber connected to an isoflurane scrubber. The rats were mounted in the injury device, secured by ear bars and incisor bar and spontaneously anesthetized with a 1–2% isoflurane in O<sub>2</sub> via blow-by nose cone connected to a charcoal canister passive isoflurane scavenger. An incision and a 10-mm craniotomy are made over the left primary and secondary motor cortex (bregma 3.70 mm, interaural 12.70 mm). After removal of the bone flap, cortical injury was induced with a CCI device (47), with a penetration depth of 1.5 mm, a velocity of 5 m/s, and a duration of 50 ms over the cortex. The bone scalp was replaced and sealed with dental cement, and the scalp incision was closed with staples following the injury. For the craniotomy alone group, only the cortical injury was excluded from the above animal procedures. Animals were observed after the surgery till they recovered from anesthesia. The animal body temperature was maintained at between 35 and 37°C during the surgery by a warming lamp. All CCI animals looked healthy before and after the CCI injury. All CCI and sham CCI animals recovered from isoflurane anesthesia and became mobile within 5 min after isoflurane discontinuation. Although most CCI animal reassumed some exploratory behavior 30 min after CCI, they did not regain full motor activity till 3 days post-CCI. Animals were sacrificed and transverse (i.e., contralateral and ipsilateral CCI) hemispheres were collected at 4 h, 24 h, 3 days, and 7 days post-CCI ( $N = 4/\text{group}/\text{time}$ ). For mRNA analysis, the contralateral and ipsilateral hemispheres (coronal sections containing the epicenter of the injury) of the CCI, and the corresponding ipsilateral hemispheres of the naïve and sham rats were separated, rapidly frozen in pre-cooled isopentane (on dry-ice) and stored at  $-80^{\circ}\text{C}$ . All animal procedures were approved by the IACUC of the Uniformed Services University of the Health Sciences (USUHS).

## RNA EXTRACTION, REVERSE TRANSCRIPTION, AND QUANTITATIVE REAL-TIME PCR

Frozen transverse brain hemispheres were homogenized and total RNA was extracted using RNeasy kit (Qiagen, Germany). Total RNA was reverse transcribed into first-strand cDNA in a total volume of 20  $\mu$ l using the M-MLV reverse transcriptase kit (Promega, Madison, WI, USA). Quantification of mRNA expression was performed in triplicate using the SYBR Green SuperMix (BioRad, CA, USA) in a two-step PCR reaction procedure, performed on the MyiQ single color real-time PCR detection system (BioRad, CA, USA). One microliter cDNA from the RT-reaction was used as the template for quantitative real-time PCR reaction with a final PCR reaction volume of 25  $\mu$ l, with the 5' and 3' gene-specific PCR primer concentrations at 200 nM each. Real-time PCR primers were designed using Primer3 software (Whitehead Institute, MIT, MA, USA) according to the coding sequences of each gene (Table 1). After the initial denaturation at 95°C for 3 min, 40 cycles of primer annealing and elongation were conducted at 60°C for 45 s, followed by denaturation at 95°C for 10 s. Fluorescent emission data were captured, and mRNA levels were quantified using the threshold cycle value (Ct). To compensate for variations in input RNA amounts and efficiency of reverse transcription, qPCR data for mRNA for each sample were normalized by reference to the data obtained for the house keeping beta-actin (GenBank#. BC063166) determined from the same sample. Fold change in mRNA expression was calculated using the equation: fold change =  $2^{-\Delta\Delta Ct}$ , where  $\Delta Ct$  = target gene Ct – house

keeping gene ( $\beta$ -actin) Ct, and  $\Delta\Delta Ct$  is  $\Delta Ct$  control –  $\Delta Ct$  CCI-TBI (or fold change) =  $2^{(\Delta Ct \text{ control} - \Delta Ct \text{ CCI-TBI})}$ .

## STATISTICAL ANALYSIS

Data were expressed as mean  $\pm$  SD. Differences in CD44/HAS/HYAL mRNA expression among the naïve controls, craniotomy, and contralateral and ipsilateral CCI-TBI brains at each time point post-CCI were examined for statistical significance using one-way ANOVA analysis followed by *post hoc* LSD test (two-tailed). A difference with a *p*-value <0.05 was considered statistically significant.

## RESULTS

Fold change in mRNA expression between the control and CCI/Craniotomy groups was calculated using the qPCR equation: fold change =  $2^{-\Delta\Delta Ct}$ , where  $\Delta Ct$  = target gene Ct – house keeping gene ( $\beta$ -actin) Ct, and  $\Delta\Delta Ct$  is  $\Delta Ct$  control –  $\Delta Ct$  CCI-TBI (or fold change). One-way ANOVA showed significant effect of CCI/Craniotomy on HAS1 mRNA expression at 4 h, 24 h, and 3 days after the injury (*p* < 0.01, respectively). *Post hoc* test (two-tailed) showed that compared to that of the naïve control animals, HA synthase 1 (HAS1) mRNA increased significantly (by twofold) in the craniotomy (sham CCI-TBI) at 4 and 24 h post-CCI (*p* < 0.01 and *p* < 0.05, respectively) before returning to the control level 3 days after the craniotomy surgery. HAS1 mRNA expression also increased markedly (two to threefold) in the contralateral and ipsilateral CCI hemispheres at 4, 24, and 72 h post-CCI. And the increase was significance in the contralateral CCI (*p* < 0.05) and ipsilateral CCI (*p* < 0.01) hemispheres at 3 days post-CCI. Thereafter, HAS1 mRNA level returned to control level 7 days post the surgery (Figure 1A).

One-way ANOVA showed significant effect of CCI on HAS2 mRNA expression at 24 h and 3 days post-CCI (*p* < 0.01, respectively). *Post hoc* test showed that compared to the naïve controls, HAS2 mRNA expression increased significantly (>twofold) in the ipsilateral CCI hemisphere at 24 h and 3 days post-CCI (*p* < 0.01, each) (Figure 1B). Thereafter, HAS2 mRNA level returned to basal level 7 days post the injury. Although HAS2 mRNA also increased considerably in the contralateral CCI at 4, 24, and 72 h post the injury, the increase was not significant due to great within-group variation.

No significant effect of craniotomy or CCI-TBI in HAS3 mRNA or in PH20 mRNA expression level was found at anytime after craniotomy and CCI-TBI (Figures 1C,D).

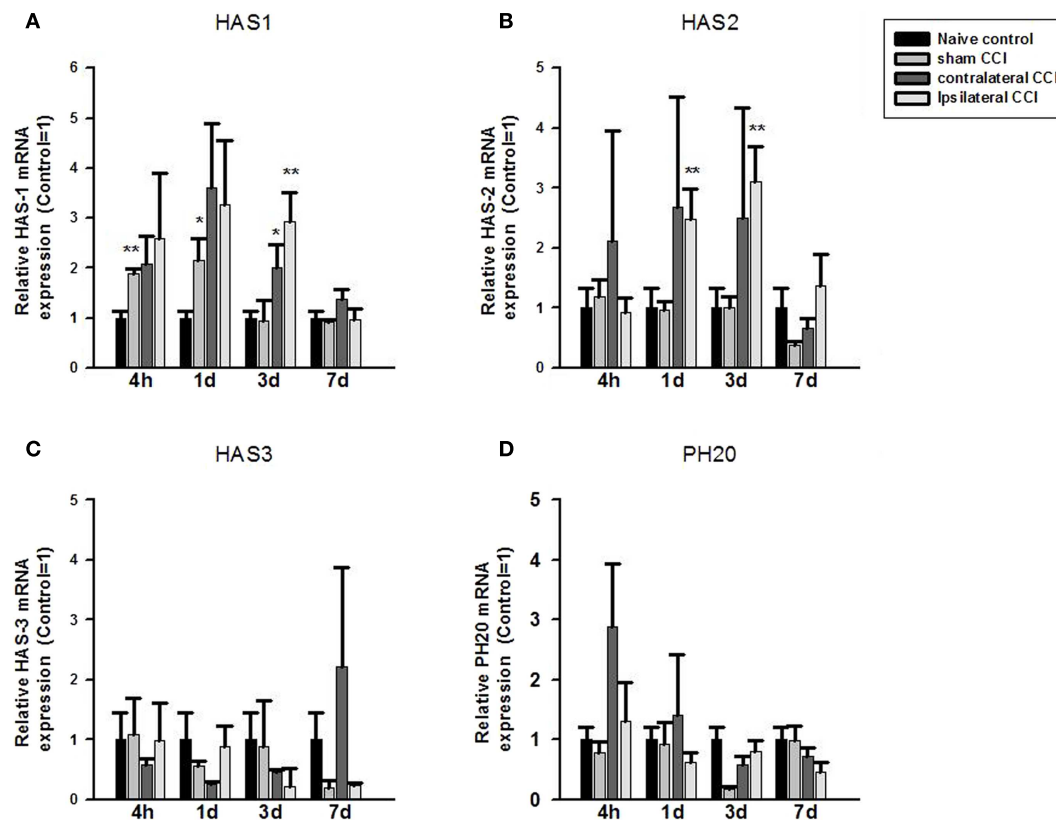
Compared to the naïve groups, hyaluronidase 1 (HYAL1) mRNA expression level increased markedly but non-significantly in the craniotomy group and in the contralateral CCI hemisphere 4 h after craniotomy or CCI (Figure 2A). That increase in HYAL1 mRNA level expression became significant in the craniotomy group at 24 h post the surgery (*p* < 0.05), and in the contralateral CCI hemisphere 72 h after CCI-TBI (*p* < 0.05), respectively (Figure 2A). No significant change in HYAL1 mRNA was found in the ipsilateral CCI hemisphere after CCI-TBI.

No significant change was found in HYAL2, HYAL3, and HYAL4 mRNA expression in the craniotomy and CCI animals after the surgeries (Figures 2B–D).

**Table 1 | Primer sequences for real-time qPCR.**

cDNA bp	Sense primer (5')	Anti-sense primer (3')
HAS1 (120)	AGTATACCTCGCGCTCCAGA	ACCACAGGGCGTTGTATAGC
HAS2 (124)	ATAAGCGGTCTCTGGGAAT	CCCTGTTGGTAAGGTGCCTA
HAS3 (130)	AGCAGCGTGAGGTACTGGAT	AGTCCTCCAGGAAGTCTGA
PH20 (117)	TGGTGAAACAGTTGCTCTGG	GGATTCAGGGTGGTCTTCAA
HYLA1 (107)	ATGACCAGCTAGGGTGGTTG	CTCTGCACACGGTATCGAA
HYLA2 (107)	AGGCCTGTATCCACGTTTTG	GTTCCACAGCTTCCTTCAGC
HYLA3 (145)	CACCAGATCCTCCACAACCT	GAGGCTGCCTGGTAGACTTG
HYLA4 (133)	ACCCATCAATGGTGGTCTTC	GCGCCAATATCCAGTCTA
CD44 (102)	GCTATCTGTGCAGCCAACAA	AAGAGGAGCTGAGGCATTGA
RHAMM (101)	TGCAAAGCCAGTCACTTCTG	GACATTCCTCTCGGAGGTCA

Oligonucleotide sequences of qPCR primers.



**FIGURE 1 |** Quantitative real-time PCR determination of HAS1 (A), HAS2 (B), HAS3 (C), and PH20 (D) mRNA expression in brain homogenates of the control, craniotomy (sham CCI), contralateral

CCI, and ipsilateral CCI hemisphere at 4 h, 24 h, 3 days, and 7 days post-CCI. Results are presented as the fold change relative to the control group (=1). \* $p < 0.05$ ; \*\* $p < 0.01$ .

One-way ANOVA showed significant effect of CCI-TBI on brain CD44 mRNA expression at all four observation time points after CCI. *Post hoc* test showed that compared to that of the naïve controls, CD44 mRNA expression level increased significantly in the ipsilateral CCI hemisphere (>twofold) 4 h, 24 h (by 25-fold), 3 days (23-fold) post-CCI, and 7 days post-CCI (sevenfold) ( $p < 0.01$ , each) (Figure 3A). CD44 mRNA also increased significantly in the contralateral CCI hemisphere at 24 h (20-fold) and 3 days (twofold) post-CCI (Figure 3A).

In contrast to CD44, RHAMM mRNA level only increased briefly and significantly in the ipsilateral CCI (threefold) ( $p < 0.05$ ) 3 days post-CCI (Figure 3B).

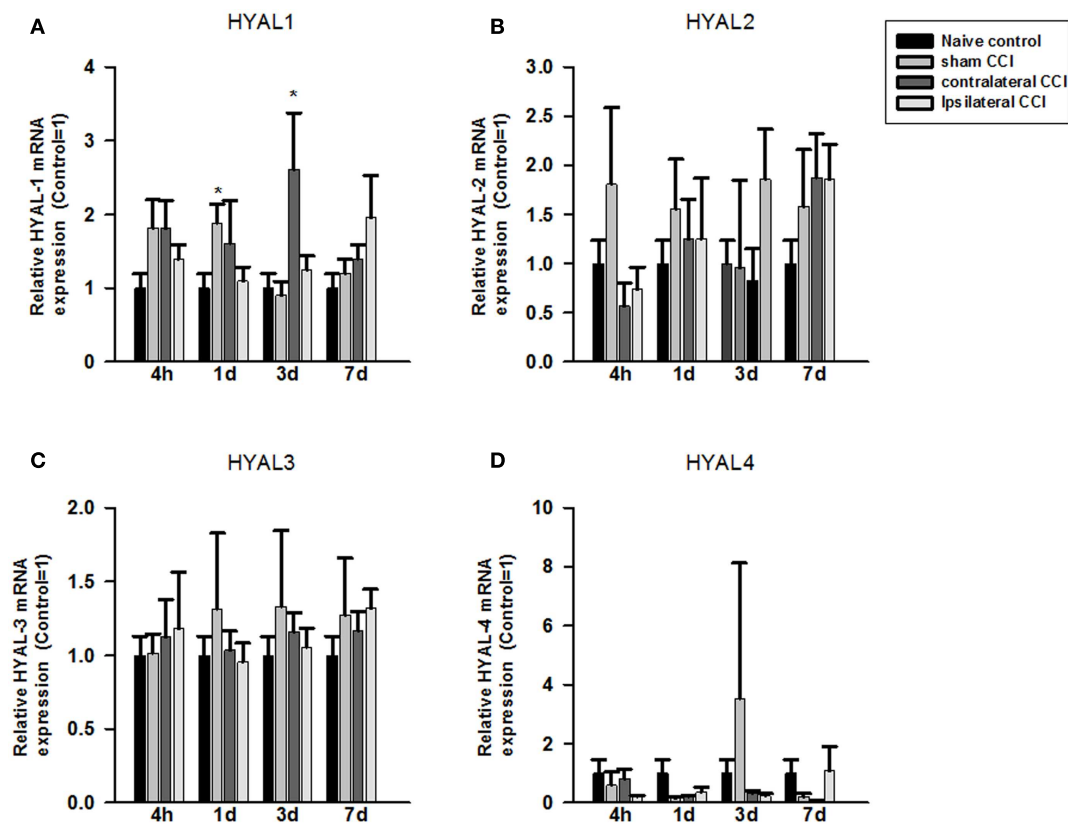
## DISCUSSION

In this study, we found significant sub-acute increases in brain hyaluronan synthases (HAS1 and HAS2) mRNA and in CD44 mRNA expression after CCI-TBI and, to a lesser extent, after craniotomy alone. Although the biological relevance of the increased expression of HAS and CD44 remains to be fully understood, the results suggest that brain HA metabolism could have been altered and may represent a potentially important mechanism of secondary injury and/or repair in TBI. So far there is a lack of information about the regulation of brain HA metabolism after TBI, but recent findings in stroke and in the peripheral tissues could

serve as the valuable guide for understanding HA metabolism in injured brain (20, 39).

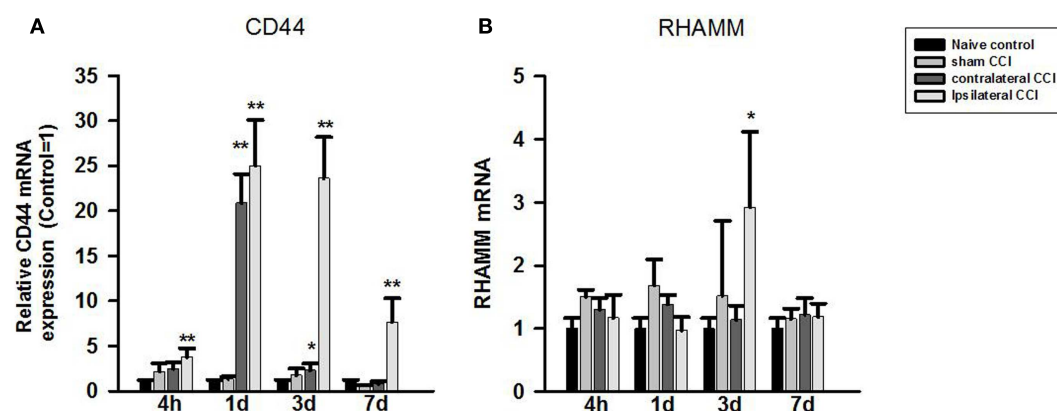
Altered HA metabolism has been reported at protracted periods following stroke in human (39) and following MCAO in the rat (40). Recent studies in peripheral tissues have implicated a role of altered hyaluronan metabolism in the pathophysiology and healing process of injured peripheral tissues. Significantly increased HA production (by 32-fold in the circulation) has been reported in the acute phase of patients with direct lung injury (20) and blocking HA production by hyaluronan synthase inhibitors effectively suppressed staphylococcal enterotoxin-induced inflammation (21), suggesting increased HA production is potentially involved in the inflammatory or healing process after acute injury or infection.

Studies of organ/tissue during development suggest that intact high-molecular-weight HA is essential for normal vascular development, tissue/organ structure, and functional integrity as absence of HA in HAS2 knockout animal results in reduced HA production and embryonic lethality due to severe cardiac and vascular abnormalities (48). Under physiologic conditions, HA is present as high-molecular-weight (HMW) polymers with an average molecular weight between 3,000 and 4,000 kDa. HMW HA but not low molecular weight HA is suggested to be able to modulate cytoskeleton regulation, signal transduction, biosynthesis, redox



**FIGURE 2 |** Quantitative real-time PCR determination of HYAL1 (A), HYAL2 (B), HYAL3 (C), and HYAL4 (D) mRNA expression in brain homogenates of the control, craniotomy (sham CCI), contralateral CCI,

and ipsilateral CCI hemisphere at 4 h, 24 h, 3 days, and 7 days post-CCI. Results are presented as the fold change relative to the control group (=1). \* $p < 0.05$ ; \*\* $p < 0.01$



**FIGURE 3 |** Quantitative real-time PCR determination of CD44 (A) and RHAMM (B) mRNA expression in brain homogenates of the control, craniotomy (sham CCI), contralateral CCI, and ipsilateral CCI

hemisphere at 4 h, 24 h, 3 days, and 7 days post-CCI. Results are presented as the fold change relative to the control group (=1). \* $p < 0.05$ ; \*\* $p < 0.01$ .

regulation, and protein folding, and act as antioxidant to prevent oxidative stress and cell death after UV-induced injury and to stimulate wound healing (49, 50). However, naïve HA can undergo rapid degradation after tissue injury resulting in accumulation of degraded lower molecular weight species (51, 52) that can induce

the expression of a variety of inflammatory factors, including chemokines, cytokines, growth factors, and adhesion molecules in various cell types, indicating an important role of HA in inflammatory processes (26). Studies also showed that degraded hyaluronan products may have biological functions distinct from the native



high-molecular-weight polymer. For instance, HA oligomers of 8–16 disaccharides have been found to induce angiogenesis (53, 54), and HA with low to intermediate molecular weight HA (20–450 kDa) have been found to induce the expression of inflammatory genes in macrophages, endothelial cells, eosinophils, and epithelial cells (51, 52, 55–60).

Recent studies showed that treatment with the tetrasaccharide of HA (HA4), significantly enhanced axonal regeneration/sprouting and improved motor function recovery after spinal cord injury in rats and blocked NMDA-induced neuronal cell death *in vitro* (61). Studies also showed that the hyaluronan receptor RHAMM is required for neurite extension and motility in primary neurons and neuronal cell lines (62). And disruption of the hyaluronan-based extracellular matrix in spinal cord promotes astrocyte proliferation (63) whereas HA coating onto the cortical brain after brain damage significantly reduced gliosis, GFAP positive cells, and the thickness of scar formation in the injured brain region at 8 and 12 weeks after the injury in rats (64). Brain tissue scarring (gliosis) is believed to be the major cause of epileptic focus after brain injury, and prevention of scarring could reduce the incidence of seizure.

Several mechanisms have been identified for HA depolymerizing (and thus for CD44 induction) in injured tissues, including HYALs-mediated and ROS-mediated HA depolymerizing processes (65–71). TBI-induced ROS, due to the release of cellular debris of damaged/dead cells (72) and activation of microglia, macrophages, and neutrophils, could directly fragment HA randomly at internal glycoside linkages into smaller fragments (73) and contribute to inflammation (74, 75). ROS-induced Hyal2 expression and the sustained HA fragmentation have been reported in the inflammatory airway lumen of smokers (76). The increased fragmentation of HA in the early stages of injury could exert antioxidant effect against ROS and stimulate white blood cells-mediated immune response by up-regulating CD44 (27, 28).

It has been reported that HYAL2 generates HA fragments of 1–2 kDa (77) that contribute to fibrosis of injured lung tissue (78, 79). Inhibition of hyaluronidase expression and hyaluronan degradation with specific HYAL1, HYAL2, and HYAL3 small interference RNA (siRNAs) significantly reduced CD44 mRNA and protein expression and pro-inflammatory cytokines in mouse synovial fibroblasts after collagen-induced arthritis (80).

In this study, HYAL1 mRNA expression only increased briefly in craniotomy and contralateral CCI-TBI 24 h and 3 days post-CCI. The signaling pathways activating the expression of these genes in TBI are unclear.

The marked induction of CD44 mRNA expression after CCI-TBI suggests that CD44 is critically involved in TBI-induced HA catabolism. It is known that CD44-mediated binding, endocytosis, and intracellular degradation of HA are an important mechanism for the removal of local degraded HA within the injured tissues (81–84). The acute and prolonged increase in CD44 mRNA expression is likely paralleled by a change in CD44 protein expression that could reflect an increased production, binding, internalization, and turnover rate of lower molecular weight HA after TBI (85). Hyaluronans bound to CD44 are catabolized in lysosomes (86). Although the mechanism of CD44 turnover in TBI has yet to be

fully understood, cytokines, CD44 phosphorylation and induction of alternatively spliced isoforms of CD44 could be involved in the removal of degraded hyaluronan products (39, 40, 64, 85, 87–93).

The increased HA synthases (HAS1 and HAS2) mRNA expression in the acute phase of TBI suggests that synthesis of new HA may be critical for tissue/vascular repair and remodeling after TBI (94, 95). This is supported by the experimental evidence that absence of HA in HAS2 knockout animal causes vascular abnormalities (48), while overexpression of HAS2 promotes neointimal formation after vascular injury (96).

An interaction between fragmented HA and CD44 could stimulate T-cell recruitment (to the sites of inflammation), macrophage activation, neutrophil migration, endothelial cell activation, and the expression of inflammatory genes by activated glial (immune) cells in the injured tissue that could protect against further tissue damage (94, 95, 97). CD44 activation has been shown to protect against hyperoxia-induced lung injury and mortality by a mechanism related to its ability to clear HA from the bronchoalveolar space (98). Failure to clear hyaluronan fragments after the injury may lead to unremitting inflammation. Study show that in the absence of CD44, alveolar macrophages continue to produce chemokines in response to hyaluronan fragments (99).

In this study, we observed parallel change in HAS1, HAS2, and CD44 mRNA expression in the ipsilateral CCI and contralateral CCI hemispheres, and to a lesser extent, in the craniotomy-only group. Although craniotomy has long been used as a control of TBI, it is itself a significant form of injury and can cause morphological damage and functional change as revealed by recent brain imaging and behavioral tests (100). Skull bone removal with high-speed drilling during the craniotomy procedure may not only induce persistent pathological changes in the affected adjacent cortical tissues including altered blood flow, inflammation, and neural cell atrophy but may also cause severe and persistent pain that could trigger HA degradation and systemic inflammatory responses (100). Recent imaging studies have demonstrated a close metabolic connectivity between brain hemispheres and between anatomically separated brain regions (101–105). Although it is not clear yet if this connectivity could have facilitated the transfer of the degraded HA molecules from the ipsilateral hemisphere to the contralateral side, significantly increased HA production (32-fold increase in the circulation) has been reported in patients with acute peripheral lung injury (20). Our observations and other studies also suggest that brain edema can develop and spread to other brain regions rapidly following TBI that may involve altered HA metabolism. The parallel induction of HAS and CD44 mRNA expression between the ipsilateral and contralateral CCI is consistent with the recent reports of rapid and significant global reduction in cerebral blood flow (CBF), cerebral oxygen, and glucose metabolic rate in craniotomized cats (106, 107) and alterations in pyruvate metabolizing enzymes in rats with ipsilateral and contralateral CCI and craniotomy (108). Thus, the synergistic changes in HAS/HYAL/CD44 expression between the ipsilateral, contralateral, and craniotomy could reflect differential brain lesions and blood vessel damage between the ipsilateral/contralateral CCI group and the craniotomy group. Further experiment is needed to firmly establish a close relationship between HA catabolism and HAS/HYAL/CD44 expression in TBI.

There are limitations of the study. The protein expression level for the HAS, HYAL HA-metabolizing isoenzymes, and CD44 receptors were not determined due to the lack of suitable specific antibodies. Nor was the change in HA precursors (i.e., acetylglucosamine and glucuronic acid) and the degraded HA products determined after the CCI-TBI. Further study is warranted for these measurements and to determine whether HA metabolism (synthesis and degradation) is associated with the severity and outcome of patients with severe TBI.

In summary, our study provides preliminary molecular evidence of altered gene expression for HA-metabolizing enzymes and receptors in animal model of TBI. Further study of HA metabolism could help us better understanding of the role of HA in the inflammatory responses, secondary injury, and healing process after TBI.

## ACKNOWLEDGMENTS

This work was supported in part by, Lotus Biotech.com, GEMI Fund and Henry Jackson Foundation DBSCIP. Daniel Xing proofread the manuscript.

## REFERENCES

1. Flaada JT, Leibson CL, Mandrekar JN, Diehl N, Perkins PK, Brown AW, et al. Relative risk of mortality after traumatic brain injury: a population-based study of the role of age and injury severity. *J Neurotrauma* (2007) **24**:435–45. doi:10.1089/neu.2006.0119
2. Moppett IK. Traumatic brain injury: assessment, resuscitation and early management. *Br J Anaesth* (2007) **99**:18–31. doi:10.1093/bja/aem128
3. Itano N, Sawai T, Yoshida M, Lenas P, Yamada Y, Imagawa M, et al. Three isoforms of mammalian hyaluronan synthases have distinct enzymatic properties. *J Biol Chem* (1999) **274**:25085–92. doi:10.1074/jbc.274.35.25085
4. Jacobson A, Brinck J, Briskin MJ, Spicer AP, Heldin P. Expression of human hyaluronan synthases in response to external stimuli. *Biochem J* (2000) **348**(Pt 1):29–35. doi:10.1042/0264-6021:3480029
5. Temiz A, Kazikdas KC, Ergur B, Tugyan K, Bozok S, Kaya D, et al. Esterified hyaluronic acid improves cartilage viability in experimental tracheal reconstruction with an auricular graft. *Otolaryngol Head Neck Surg* (2010) **143**:772–8. doi:10.1016/j.otohns.2010.07.007
6. Schulz T, Schumacher U, Prehm P. Hyaluronan export by the ABC transporter MRP5 and its modulation by intracellular cGMP. *J Biol Chem* (2007) **282**:20999–1004. doi:10.1074/jbc.M700915200
7. Fukuda K, Oh M, Asada S, Hara F, Matsukawa M, Otani K, et al. Sodium hyaluronate inhibits interleukin-1-evoked reactive oxygen species of bovine articular chondrocytes. *Osteoarthritis Cartilage* (2001) **9**:390–2. doi:10.1053/joca.2000.0400
8. Cortivo R, Brun P, Cardarelli L, O'Regan M, Radice M, Abatangelo G. Antioxidant effects of hyaluronan and its alpha-methyl-prednisolone derivative in chondrocyte and cartilage cultures. *Semin Arthritis Rheum* (1996) **26**:492–501. doi:10.1016/S0049-0172(96)80030-8
9. Sironen RK, Tammi M, Tammi R, Auvinen PK, Anttila M, Kosma VM. Hyaluronan in human malignancies. *Exp Cell Res* (2011) **317**:383–91. doi:10.1016/j.yexcr.2010.11.017
10. Aya KL, Stern R. Hyaluronan in wound healing: rediscovering a major player. *Wound Repair Regen* (2014). doi:10.1111/wrr.12214
11. Margolis RU, Margolis RK, Chang LB, Preti C. Glycosaminoglycans of brain during development. *Biochemistry* (1975) **14**:85–8. doi:10.1021/bi00672a014
12. Holmes MW, Bayliss MT, Muir H. Hyaluronic acid in human articular cartilage. Age-related changes in content and size. *Biochem J* (1988) **250**:435–41.
13. Recklies AD, White C, Melching L, Roughley PJ. Differential regulation and expression of hyaluronan synthases in human articular chondrocytes, synovial cells and osteosarcoma cells. *Biochem J* (2001) **354**:17–24. doi:10.1042/0264-6021:3540017
14. Nishida Y, Knudson CB, Nietfeld JJ, Margulis A, Knudson W. Antisense inhibition of hyaluronan synthase-2 in human articular chondrocytes inhibits proteoglycan retention and matrix assembly. *J Biol Chem* (1999) **274**:21893–9. doi:10.1074/jbc.274.31.21893
15. Nishida Y, Knudson CB, Nietfeld JJ, Margulis A, Knudson W. Antisense inhibition of hyaluronan synthase-2 in human articular chondrocytes inhibits proteoglycan retention and matrix assembly. *J Biol Chem* (2014) **289**:18121. doi:10.1074/jbc.A114.021893
16. Nishida Y, Knudson W, Knudson CB, Ishiguro N. Antisense inhibition of hyaluronan synthase-2 in human osteosarcoma cells inhibits hyaluronan retention and tumorigenicity. *Exp Cell Res* (2005) **307**:194–203. doi:10.1016/j.yexcr.2005.03.026
17. Michael DR, Phillips AO, Krupa A, Martin J, Redman JE, Altaf A, et al. The human hyaluronan synthase 2 (HAS2) gene and its natural antisense RNA exhibit coordinated expression in the renal proximal tubular epithelial cell. *J Biol Chem* (2011) **286**:19523–32. doi:10.1074/jbc.M111.233916
18. Karousou E, Kamiryo M, Skandalis SS, Ruusala A, Asteriou T, Passi A, et al. The activity of hyaluronan synthase 2 is regulated by dimerization and ubiquitination. *J Biol Chem* (2010) **285**:23647–54. doi:10.1074/jbc.M110.127050
19. Ventura CL, Cartee RT, Forsee WT, Yother J. Control of capsular polysaccharide chain length by UDP-sugar substrate concentrations in *Streptococcus pneumoniae*. *Mol Microbiol* (2006) **61**:723–33. doi:10.1111/j.1365-2958.2006.05259.x
20. Schmidt EP, Li G, Li L, Fu L, Yang Y, Overdier KH, et al. The circulating glycosaminoglycan signature of respiratory failure in critically ill adults. *J Biol Chem* (2014) **289**:8194–202. doi:10.1074/jbc.M113.539452
21. McKallip RJ, Hagele HF, Uchakina ON. Treatment with the hyaluronic acid synthesis inhibitor 4-methylumbelliferone suppresses SEB-induced lung inflammation. *Toxins (Basel)* (2013) **5**:1814–26. doi:10.3390/toxins5101814
22. Averbeck M, Gebhardt CA, Voigt S, Beilharz S, Anderegg U, Termeer CC, et al. Differential regulation of hyaluronan metabolism in the epidermal and dermal compartments of human skin by UVB irradiation. *J Invest Dermatol* (2007) **127**:687–97. doi:10.1038/sj.jid.5700614
23. Soltes L, Mendichi R, Kogan G, Schiller J, Stankovska M, Arnhold J. Degradative action of reactive oxygen species on hyaluronan. *Biomacromolecules* (2006) **7**:659–68. doi:10.1021/bm050867v
24. Trabucchi E, Pallotta S, Morini M, Corsi F, Franceschini R, Casiraghi A, et al. Low molecular weight hyaluronic acid prevents oxygen free radical damage to granulation tissue during wound healing. *Int J Tissue React* (2002) **24**:65–71.
25. Moseley R, Leaver M, Walker M, Waddington RJ, Parsons D, Chen WY, et al. Comparison of the antioxidant properties of HYAFF-11p75, AQUACEL and hyaluronan towards reactive oxygen species in vitro. *Biomaterials* (2002) **23**:2255–64. doi:10.1016/S0142-9612(01)00360-X
26. Jiang D, Liang J, Noble PW. Hyaluronan as an immune regulator in human diseases. *Physiol Rev* (2011) **91**:221–64. doi:10.1152/physrev.00052.2009
27. Krasinski R, Tchorzewski H, Lewkowicz P. Antioxidant effect of hyaluronan on polymorphonuclear leukocyte-derived reactive oxygen species is dependent on its molecular weight and concentration and mainly involves the extracellular space. *Postepy Hig Med Dosw (Online)* (2009) **63**:205–12.
28. Krasinski R, Tchorzewski H. Hyaluronan-mediated regulation of inflammation. *Postepy Hig Med Dosw (Online)* (2007) **61**:683–9.
29. Ekici S, Cerwinka WH, Duncan R, Gomez P, Civantos F, Soloway MS, et al. Comparison of the prognostic potential of hyaluronic acid, hyaluronidase (HYAL-1), CD44v6 and microvessel density for prostate cancer. *Int J Cancer* (2004) **112**:121–9. doi:10.1002/ijc.20368
30. Josefsson A, Adamo H, Hammarsten P, Granfors T, Stattin P, Egevad L, et al. Prostate cancer increases hyaluronan in surrounding nonmalignant stroma, and this response is associated with tumor growth and an unfavorable outcome. *Am J Pathol* (2011) **179**:1961–8. doi:10.1016/j.ajpath.2011.06.005
31. Gritsenko PG, Ilna O, Friedl P. Interstitial guidance of cancer invasion. *J Pathol* (2012) **226**:185–99. doi:10.1002/path.3031
32. Fox JW. A brief review of the scientific history of several lesser-known snake venom proteins: L-amino acid oxidases, hyaluronidases and phosphodiesterases. *Toxicon* (2013) **62**:75–82. doi:10.1016/j.toxicon.2012.09.009
33. Berg S, Brodin B, Hesselvik F, Laurent TC, Maller R. Elevated levels of plasma hyaluronan in septicemia. *Scand J Clin Lab Invest* (1988) **48**:727–32. doi:10.3109/0036518809088752
34. Bertrand P, Courel MN, Maingonnat C, Jardin F, Tilly H, Bastard C. Expression of HYAL2 mRNA, hyaluronan and hyaluronidase in B-cell non-Hodgkin lymphoma: relationship with tumor aggressiveness. *Int J Cancer* (2005) **113**:207–12. doi:10.1002/ijc.20562

35. Kim E, Baba D, Kimura M, Yamashita M, Kashiwabara S, Baba T. Identification of a hyaluronidase, Hyal5, involved in penetration of mouse sperm through cumulus mass. *Proc Natl Acad Sci U S A* (2005) **102**:18028–33. doi:10.1073/pnas.0506825102
36. Csoka AB, Scherer SW, Stern R. Expression analysis of six paralogous human hyaluronidase genes clustered on chromosomes 3p21 and 7q31. *Genomics* (1999) **60**:356–61. doi:10.1006/geno.1999.5876
37. Csoka AB, Frost GI, Stern R. The six hyaluronidase-like genes in the human and mouse genomes. *Matrix Biol* (2001) **20**:499–508. doi:10.1016/S0945-053X(01)00172-X
38. Triggs-Raine B, Salo TJ, Zhang H, Wicklow BA, Natowicz MR. Mutations in HYAL1, a member of a tandemly distributed multigene family encoding disparate hyaluronidase activities, cause a newly described lysosomal disorder, mucopolysaccharidosis IX. *Proc Natl Acad Sci U S A* (1999) **96**:6296–300. doi:10.1073/pnas.96.11.6296
39. Al'Qteishat A, Gaffney J, Krupinski J, Rubio F, West D, Kumar S, et al. Changes in hyaluronan production and metabolism following ischaemic stroke in man. *Brain* (2006) **129**:2158–76. doi:10.1093/brain/awl139
40. Al'Qteishat A, Gaffney JJ, Krupinski J, Slevin M. Hyaluronan expression following middle cerebral artery occlusion in the rat. *Neuroreport* (2006) **17**:1111–4. doi:10.1097/01.wnr.0000227986.69680.20
41. Zhuo L, Kanamori A, Kannagi R, Itano N, Wu J, Hamaguchi M, et al. SHAP potentiates the CD44-mediated leukocyte adhesion to the hyaluronan substratum. *J Biol Chem* (2006) **281**:20303–14. doi:10.1074/jbc.M506703200
42. Hanley WD, Napier SL, Burdick MM, Schnaar RL, Sackstein R, Konstantopoulos K. Variant isoforms of CD44 are P- and L-selectin ligands on colon carcinoma cells. *FASEB J* (2006) **20**:337–9. doi:10.1096/fj.05-4574fje
43. Sugahara KN, Hirata T, Hayasaka H, Stern R, Murai T, Miyasaka M. Tumor cells enhance their own CD44 cleavage and motility by generating hyaluronan fragments. *J Biol Chem* (2006) **281**:5861–8. doi:10.1074/jbc.M506740200
44. Jong A, Wu CH, Gonzales-Gomez I, Kwon-Chung KJ, Chang YC, Tseng HK, et al. Hyaluronic acid receptor CD44 deficiency is associated with decreased Cryptococcus neoformans brain infection. *J Biol Chem* (2012) **287**:15298–306. doi:10.1074/jbc.M112.353375
45. Cabrera PV, Blanco G, Argibay P, Hajos SE. Isoforms modulation of CD44 adhesion molecule in a murine model of ischemia and intestinal reperfusion. *Medicina (B Aires)* (2000) **60**:940–6.
46. Turley EA, Hossain MZ, Sorokan T, Jordan LM, Nagy JL. Astrocyte and microglial motility in vitro is functionally dependent on the hyaluronan receptor RHAMM. *Glia* (1994) **12**:68–80. doi:10.1002/glia.440120109
47. Dixon CE, Ma X, Marion DW. Effects of CDP-choline treatment on neurobehavioral deficits after TBI and on hippocampal and neocortical acetylcholine release. *J Neurotrauma* (1997) **14**:161–9. doi:10.1089/neu.1997.14.161
48. Camenisch TD, Spicer AP, Brehm-Gibson T, Biesterfeldt J, Augustine ML, Calabro A Jr, et al. Disruption of hyaluronan synthase-2 abrogates normal cardiac morphogenesis and hyaluronan-mediated transformation of epithelium to mesenchyme. *J Clin Invest* (2000) **106**:349–60. doi:10.1172/JCI10272
49. Miki Y, Teramura T, Tomiyama T, Onodera Y, Matsuoka T, Fukuda K, et al. Hyaluronan reversed proteoglycan synthesis inhibited by mechanical stress: possible involvement of antioxidant effect. *Inflamm Res* (2010) **59**:471–7. doi:10.1007/s00011-009-0147-y
50. Li JM, Chou HC, Wang SH, Wu CL, Chen YW, Lin ST, et al. Hyaluronic acid-dependent protection against UVB-damaged human corneal cells. *Environ Mol Mutagen* (2013) **54**:429–49. doi:10.1002/em.21794
51. Noble PW. Hyaluronan and its catabolic products in tissue injury and repair. *Matrix Biol* (2002) **21**:25–9. doi:10.1016/S0945-053X(01)00184-6
52. Horton MR, Olman MA, Noble PW. Hyaluronan fragments induce plasminogen activator inhibitor-1 and inhibit urokinase activity in mouse alveolar macrophages: a potential mechanism for impaired fibrinolytic activity in acute lung injury. *Chest* (1999) **116**:17S.
53. West DC, Hampson IN, Arnold F, Kumar S. Angiogenesis induced by degradation products of hyaluronic acid. *Science* (1985) **228**:1324–6. doi:10.1126/science.2408340
54. West DC, Kumar S. The effect of hyaluronate and its oligosaccharides on endothelial cell proliferation and monolayer integrity. *Exp Cell Res* (1989) **183**:179–96. doi:10.1016/0014-4827(89)90428-X
55. Hodge-Dufour J, Noble PW, Horton MR, Bao C, Wysoka M, Burdick MD, et al. Induction of IL-12 and chemokines by hyaluronan requires adhesion-dependent priming of resident but not elicited macrophages. *J Immunol* (1997) **159**:2492–500.
56. Horton MR, McKee CM, Bao C, Liao F, Farber JM, Hodge-DuFour J, et al. Hyaluronan fragments synergize with interferon-gamma to induce the C-X-C chemokines mig and interferon-inducible protein-10 in mouse macrophages. *J Biol Chem* (1998) **273**:35088–94. doi:10.1074/jbc.273.52.35088
57. Scheibner KA, Lutz MA, Boodoo S, Fenton MJ, Powell JD, Horton MR. Hyaluronan fragments act as an endogenous danger signal by engaging TLR2. *J Immunol* (2006) **177**:1272–81. doi:10.4049/jimmunol.177.2.1272
58. McKee CM, Lowenstein CJ, Horton MR, Wu J, Bao C, Chin BY, et al. Hyaluronan fragments induce nitric-oxide synthase in murine macrophages through a nuclear factor kappaB-dependent mechanism. *J Biol Chem* (1997) **272**:8013–8. doi:10.1074/jbc.272.12.8013
59. Noble PW, Lake FR, Henson PM, Riches DW. Hyaluronate activation of CD44 induces insulin-like growth factor-1 expression by a tumor necrosis factor-alpha-dependent mechanism in murine macrophages. *J Clin Invest* (1993) **91**:2368–77. doi:10.1172/JCI116469
60. Noble PW, McKee CM, Cowman M, Shin HS. Hyaluronan fragments activate an NF-kappa B/I-kappa B alpha autoregulatory loop in murine macrophages. *J Exp Med* (1996) **183**:2373–8. doi:10.1084/jem.183.5.2373
61. Wakao N, Imagama S, Zhang H, Tauchi R, Muramoto A, Natori T, et al. Hyaluronan oligosaccharides promote functional recovery after spinal cord injury in rats. *Neurosci Lett* (2011) **488**:299–304. doi:10.1016/j.neulet.2010.11.051
62. Nagy JL, Hacking J, Frankenstein UN, Turley EA. Requirement of the hyaluronan receptor RHAMM in neurite extension and motility as demonstrated in primary neurons and neuronal cell lines. *J Neurosci* (1995) **15**:241–52.
63. Struve J, Maher PC, Li YQ, Kinney S, Fehlings MG, Kuntz C4th, et al. Disruption of the hyaluronan-based extracellular matrix in spinal cord promotes astrocyte proliferation. *Glia* (2005) **52**:16–24. doi:10.1002/glia.20215
64. Andhare RA, Takahashi N, Knudson W, Knudson CB. Hyaluronan promotes the chondrocyte response to BMP-7. *Osteoarthritis Cartilage* (2009) **17**:906–16. doi:10.1016/j.joca.2008.12.007
65. Monzon ME, Fregien N, Schmid N, Falcon NS, Campos M, Casalino-Matsuda SM, et al. Reactive oxygen species and hyaluronidase 2 regulate airway epithelial hyaluronan fragmentation. *J Biol Chem* (2010) **285**:26126–34. doi:10.1074/jbc.M110.135194
66. Grootveld M, Henderson EB, Farrell A, Blake DR, Parkes HG, Haycock P. Oxidative damage to hyaluronate and glucose in synovial fluid during exercise of the inflamed rheumatoid joint. Detection of abnormal low-molecular-mass metabolites by proton-n.m.r. spectroscopy. *Biochem J* (1991) **273**(Pt 2):459–67.
67. Konttinen YT, Saari H, Honkanen VE, Szocsik K, Mussalo-Rauhamaa H, Tulensalo R, et al. Serum baseline hyaluronate and disease activity in rheumatoid arthritis. *Clin Chim Acta* (1990) **193**:39–47. doi:10.1016/0009-8981(90)90005-D
68. Laurent UB, Fraser JR, Engstrom-Laurent A, Reed RK, Dahl LB, Laurent TC. Catabolism of hyaluronan in the knee joint of the rabbit. *Matrix* (1992) **12**:130–6. doi:10.1016/S0934-8832(11)80054-5
69. Moseley R, Waddington RJ, Embery G. Degradation of glycosaminoglycans by reactive oxygen species derived from stimulated polymorphonuclear leukocytes. *Biochim Biophys Acta* (1997) **1362**:221–31. doi:10.1016/S0925-4439(97)00083-5
70. Agren UM, Tammi RH, Tammi ML. Reactive oxygen species contribute to epidermal hyaluronan catabolism in human skin organ culture. *Free Radic Biol Med* (1997) **23**:996–1001. doi:10.1016/S0891-5849(97)00098-1
71. Yamazaki K, Fukuda K, Matsukawa M, Hara F, Yoshida K, Akagi M, et al. Reactive oxygen species depolymerize hyaluronan: involvement of the hydroxyl radical. *Pathophysiology* (2003) **9**:215–20. doi:10.1016/S0928-4680(03)00024-5
72. Kehrer JP. Free radicals as mediators of tissue injury and disease. *Crit Rev Toxicol* (1993) **23**:21–48. doi:10.3109/10408449309104073
73. Deguine V, Menasche M, Ferrari P, Fraisse L, Pouliquen Y, Robert L. Free radical depolymerization of hyaluronan by Maillard reaction products: role in liquefaction of aging vitreous. *Int J Biol Macromol* (1998) **22**:17–22. doi:10.1016/S0141-8130(97)00084-6
74. Saari H. Oxygen derived free radicals and synovial fluid hyaluronate. *Ann Rheum Dis* (1991) **50**:389–92. doi:10.1136/ard.50.6.389

75. Flugge LA, Miller-Deist LA, Petillo PA. Towards a molecular understanding of arthritis. *Chem Biol* (1999) **6**:R157–66. doi:10.1016/S1074-5521(99)80068-4
76. Forteza RM, Casalino-Matsuda SM, Falcon NS, Valencia Gattas M, Monzon ME. Hyaluronan and layilin mediate loss of airway epithelial barrier function induced by cigarette smoke by decreasing E-cadherin. *J Biol Chem* (2012) **287**:42288–98. doi:10.1074/jbc.M112.387795
77. Lepperdinger G, Mullegger J, Kreil G. Hyal2 – less active, but more versatile? *Matrix Biol* (2001) **20**:509–14. doi:10.1016/S0945-053X(01)00170-6
78. Lepperdinger G, Strobl B, Kreil G. HYAL2, a human gene expressed in many cells, encodes a lysosomal hyaluronidase with a novel type of specificity. *J Biol Chem* (1998) **273**:22466–70. doi:10.1074/jbc.273.35.22466
79. Li Y, Rahmanian M, Widstrom C, Lepperdinger G, Frost GI, Heldin P. Irradiation-induced expression of hyaluronan (HA) synthase 2 and hyaluronidase 2 genes in rat lung tissue accompanies active turnover of HA and induction of types I and III collagen gene expression. *Am J Respir Cell Mol Biol* (2000) **23**:411–8. doi:10.1165/ajrcmb.23.3.4102
80. Campo GM, Avenoso A, D'Ascola A, Scuruchi M, Prestipino V, Nastasi G, et al. The inhibition of hyaluronan degradation reduced pro-inflammatory cytokines in mouse synovial fibroblasts subjected to collagen-induced arthritis. *J Cell Biochem* (2012) **113**:1852–67. doi:10.1002/jcb.24054
81. Kaya G, Rodriguez I, Jorcano JL, Vassalli P, Stamenkovic I. Selective suppression of CD44 in keratinocytes of mice bearing an antisense CD44 transgene driven by a tissue-specific promoter disrupts hyaluronate metabolism in the skin and impairs keratinocyte proliferation. *Genes Dev* (1997) **11**:996–1007. doi:10.1101/gad.11.8.996
82. Morales TI, Hascall VC. Correlated metabolism of proteoglycans and hyaluronic acid in bovine cartilage organ cultures. *J Biol Chem* (1988) **263**:3632–8.
83. Ng CK, Handley CJ, Preston BN, Robinson HC. The extracellular processing and catabolism of hyaluronan in cultured adult articular cartilage explants. *Arch Biochem Biophys* (1992) **298**:70–9. doi:10.1016/0003-9861(92)90095-E
84. Casalino-Matsuda SM, Monzon ME, Day AJ, Forteza RM. Hyaluronan fragments/CD44 mediate oxidative stress-induced MUC5B up-regulation in airway epithelium. *Am J Respir Cell Mol Biol* (2009) **40**:277–85. doi:10.1165/rcmb.2008-0073OC
85. Takahashi N, Knudson CB, Thankamony S, Ariyoshi W, Mellor L, Im HJ, et al. Induction of CD44 cleavage in articular chondrocytes. *Arthritis Rheum* (2010) **62**:1338–48. doi:10.1002/art.27410
86. Culty M, Nguyen HA, Underhill CB. The hyaluronan receptor (CD44) participates in the uptake and degradation of hyaluronan. *J Cell Biol* (1992) **116**:1055–62. doi:10.1083/jcb.116.4.1055
87. Fang XJ, Jiang H, Zhao XP, Jiang WM. The role of a new CD44st in increasing the invasion capability of the human breast cancer cell line MCF-7. *BMC Cancer* (2011) **11**:290. doi:10.1186/1471-2407-11-290
88. Knepper PA, Miller AM, Choi J, Wertz RD, Nolan MJ, Goossens W, et al. Hypophosphorylation of aqueous humor sCD44 and primary open-angle glaucoma. *Invest Ophthalmol Vis Sci* (2005) **46**:2829–37. doi:10.1167/iovs.04-1472
89. Knudson W, Chow G, Knudson CB. CD44-mediated uptake and degradation of hyaluronan. *Matrix Biol* (2002) **21**:15–23. doi:10.1016/S0945-053X(01)00186-X
90. Bugiani M, Postma N, Polder E, Dieleman N, Scheffer PG, Sim FJ, et al. Hyaluronan accumulation and arrested oligodendrocyte progenitor maturation in vanishing white matter disease. *Brain* (2013) **136**:209–22. doi:10.1093/brain/awt320
91. Piao JH, Wang Y, Duncan ID. CD44 is required for the migration of transplanted oligodendrocyte progenitor cells to focal inflammatory demyelinating lesions in the spinal cord. *Glia* (2013) **61**:361–7. doi:10.1002/glia.22438
92. Ariyoshi W, Takahashi N, Hida D, Knudson CB, Knudson W. Mechanisms involved in enhancement of the expression and function of aggrecanases by hyaluronan oligosaccharides. *Arthritis Rheum* (2012) **64**:187–97. doi:10.1002/art.33329
93. Matsumoto T, Imagama S, Hirano K, Ohgomori T, Natori T, Kobayashi K, et al. CD44 expression in astrocytes and microglia is associated with ALS progression in a mouse model. *Neurosci Lett* (2012) **520**:115–20. doi:10.1016/j.neulet.2012.05.048
94. Jiang D, Liang J, Noble PW. Hyaluronan in tissue injury and repair. *Annu Rev Cell Dev Biol* (2007) **23**:435–61. doi:10.1146/annurev.cellbio.23.090506.123337
95. Jiang D, Liang J, Noble PW. Regulation of non-infectious lung injury, inflammation, and repair by the extracellular matrix glycosaminoglycan hyaluronan. *Anat Rec (Hoboken)* (2010) **293**:982–5. doi:10.1002/ar.21102
96. Kashima Y, Takahashi M, Shiba Y, Itano N, Izawa A, Koyama J, et al. Crucial role of hyaluronan in neointimal formation after vascular injury. *PLoS One* (2013) **8**:e58760. doi:10.1371/journal.pone.0058760
97. Yu H, Li Q, Zhou X, Kolosov VP, Perelman JM. Role of hyaluronan and CD44 in reactive oxygen species-induced mucus hypersecretion. *Mol Cell Biochem* (2011) **352**:65–75. doi:10.1007/s11010-011-0740-6
98. van der Windt GJ, Schouten M, Zeerleder S, Florquin S, van der Poll T. CD44 is protective during hyperoxia-induced lung injury. *Am J Respir Cell Mol Biol* (2011) **44**:377–83. doi:10.1165/rcmb.2010-0158OC
99. Noble PW, Jiang D. Matrix regulation of lung injury, inflammation, and repair: the role of innate immunity. *Proc Am Thorac Soc* (2006) **3**:401–4. doi:10.1513/pats.200604-097AW
100. Cole JT, Yarnell A, Kean WS, Gold E, Lewis B, Ren M, et al. Craniotomy: true sham for traumatic brain injury, or a sham of a sham? *J Neurotrauma* (2011) **28**:359–69. doi:10.1089/neu.2010.1427
101. Zhang N, Rane P, Huang W, Liang Z, Kennedy D, Frazier JA, et al. Mapping resting-state brain networks in conscious animals. *J Neurosci Methods* (2010) **189**:186–96. doi:10.1016/j.jneumeth.2010.04.001
102. Bifone A, Gozzi A, Schwarz AJ. Functional connectivity in the rat brain: a complex network approach. *Magn Reson Imaging* (2010) **28**:1200–9. doi:10.1016/j.mri.2010.07.001
103. Sokoloff L. Relationships among local functional activity, energy metabolism, and blood flow in the central nervous system. *Fed Proc* (1981) **40**:2311–6.
104. Sokoloff L. The physiological and biochemical bases of functional brain imaging. *Cogn Neurodyn* (2008) **2**:1–5. doi:10.1007/s11571-007-9033-x
105. Ramnani N, Behrens TE, Penny W, Matthews PM. New approaches for exploring anatomical and functional connectivity in the human brain. *Biol Psychiatry* (2004) **56**:613–9. doi:10.1016/j.biopsych.2004.02.004
106. Schaller B, Graf R, Sanada Y, Rosner G, Wienhard K, Heiss WD. Hemodynamic and metabolic effects of decompressive hemicraniectomy in normal brain. An experimental PET-study in cats. *Brain Res* (2003) **982**:31–7. doi:10.1016/S0006-8993(03)02900-7
107. Schaller B, Graf R, Sanada Y, Wienhard K, Heiss WD. Decompressive hemicraniectomy in a new cat model. Methodological description of the PET study protocol. *Brain Res Brain Res Protoc* (2004) **12**:125–31. doi:10.1016/j.brainresprot.2003.09.003
108. Xing G, Ren M, O'Neill JT, Verma A, Watson WD. Controlled cortical impact injury and craniotomy result in divergent alterations of pyruvate metabolizing enzymes in rat brain. *Exp Neurol* (2012) **234**:31–8. doi:10.1016/j.expneurol.2011.12.007

**Conflict of Interest Statement:** The Guest Associate Editor Yumin Zhang declares that despite being affiliated to the same institution as authors Guoqiang Xing, Ming Ren, and Ajay Verma, the review process was handled objectively and no conflict of interest exists. The authors declare that the research was conducted in the absence of any commercial or financial relationships that could be construed as a potential conflict of interest.

Received: 17 November 2013; accepted: 26 August 2014; published online: 11 September 2014.

Citation: Xing G, Ren M and Verma A (2014) Divergent temporal expression of hyaluronan metabolizing enzymes and receptors with craniotomy vs. controlled-cortical impact injury in rat brain: a pilot study. *Front. Neurol.* 5:173. doi: 10.3389/fneur.2014.00173

This article was submitted to *Neurotrauma*, a section of the journal *Frontiers in Neurology*.

Copyright © 2014 Xing, Ren and Verma. This is an open-access article distributed under the terms of the Creative Commons Attribution License (CC BY). The use, distribution or reproduction in other forums is permitted, provided the original author(s) or licensor are credited and that the original publication in this journal is cited, in accordance with accepted academic practice. No use, distribution or reproduction is permitted which does not comply with these terms.



# Mitochondrial gene expression profiles and metabolic pathways in the amygdala associated with exaggerated fear in an animal model of PTSD

He Li<sup>1\*</sup>, Xin Li<sup>2</sup>, Stanley E. Smerin<sup>1</sup>, Lei Zhang<sup>1</sup>, Min Jia<sup>1</sup>, Guoqiang Xing<sup>1</sup>, Yan A. Su<sup>3</sup>, Jillian Wen<sup>1</sup>, David Benedek<sup>1</sup> and Robert Ursano<sup>1</sup>

<sup>1</sup> Department of Psychiatry, Center for the Study of Traumatic Stress, Uniformed Services University of the Health Sciences, Bethesda, MD, USA

<sup>2</sup> Department of Biostatistics, Bioinformatics, and Biomathematics, Georgetown University Medical Center, Washington, DC, USA

<sup>3</sup> Department of Gene and Protein Biomarkers, GenProMarkers, Rockville, MD, USA

## Edited by:

Yumin Zhang, Uniformed Services University of the Health Sciences, USA

## Reviewed by:

Namas Chandra, New Jersey Institute of Technology, USA

Firas H. Kobeissy, University of Florida, USA

## \*Correspondence:

He Li, Department of Psychiatry, Center for the Study of Traumatic Stress, Uniformed Services University of the Health Sciences, Building B, Room B3060, 4301 Jones Bridge Road, Bethesda, MD 20814, USA  
e-mail: he.li@usuhs.edu

The views expressed in this article are those of the authors and do not necessarily reflect the official policy or position of the Uniformed Services University, Department of the Navy, Department of Defense, nor the U.S. Government.

The metabolic mechanisms underlying the development of exaggerated fear in post-traumatic stress disorder (PTSD) are not well defined. In the present study, alteration in the expression of genes associated with mitochondrial function in the amygdala of an animal model of PTSD was determined. Amygdala tissue samples were excised from 10 non-stressed control rats and 10 stressed rats, 14 days post-stress treatment. Total RNA was isolated, cDNA was synthesized, and gene expression levels were determined using a cDNA microarray. During the development of the exaggerated fear associated with PTSD, 48 genes were found to be significantly upregulated and 37 were significantly downregulated in the amygdala complex based on stringent criteria ( $p < 0.01$ ). Ingenuity pathway analysis revealed up- or downregulation in the amygdala complex of four signaling networks – one associated with inflammatory and apoptotic pathways, one with immune mediators and metabolism, one with transcriptional factors, and one with chromatin remodeling. Thus, informatics of a neuronal gene array allowed us to determine the expression profile of mitochondrial genes in the amygdala complex of an animal model of PTSD. The result is a further understanding of the metabolic and neuronal signaling mechanisms associated with delayed and exaggerated fear.

**Keywords:** PTSD, amygdala, mitochondrial genes, stress, fear, Bcl-2, microarray

## INTRODUCTION

The neurobiology of exaggerated fear is important in understanding traumatic stress and post-traumatic stress disorder (PTSD). Decades of animal studies have shown that the amygdala is key in the neuronal system that orchestrates the fear memory and exaggerated fear evoked by stress. In PTSD patients exposed to an aversive visual stimulus or a fear inducing pulse of sound, fMRI shows an increased blood flow and metabolic rate in the amygdala, indicating a prolonged dysregulation of metabolism and an altered neuronal transmitter system in the amygdala circuitry (1–3). Dysregulation appears to persist throughout life, at least in the frontal cortex, as we found by analyzing a mitochondria gene array from post-mortem frontal cortex samples of PTSD patients. Genes and signaling pathways, as well as pharmacological targets, were significantly dysregulated (4).

Mitochondria are targets for stress hormones such as corticosterone (CORT) and are increasingly recognized as key components in stress-related mental disorders (5, 6). Prolonged and repetitive psychological stress can induce long-lasting neurobiological consequences. However, the exact subcellular mechanisms involved in such long-term neuronal and hormonal impairment remain elusive. The current study used a rat model of PTSD

to further examine amygdala function and traumatic stress. In this study, we examined the relationship of altered amygdala mitochondrial-function genes and the molecular signaling pathways associated with a key symptom of PTSD: delayed and exaggerated fear. Amygdala tissues were collected from rats 14 days after stress, a time point at which exaggerated fear manifests. We then screened for 1500 mitochondrial-function-associated genes, including 37 mitochondrial DNA (mtDNA)-encoded genes, 1,098 nuclear DNA (nDNA)-encoded and mitochondria-focused genes, and 365 neuron-related genes (7, 8).

Up until now, the altered subcellular and metabolic molecular markers associated with delayed and exaggerated fear in the amygdala were unknown. Thus, this research was carried out in an attempt to determine whether traumatic stress alters the expression profiles of mitochondrial genes in association with the pathogenesis of delayed and exaggerated fear. A mitochondrial microarray technique was used to examine all mitochondrial-function-associated transcriptomes and to map the susceptible gene clusters in the amygdala complex associated with delayed and exaggerated fear. Our results indicate that signaling pathways, including pre-inflammatory, apoptotic, metabolic, neuronal transmitter system, and genes of G-protein-coupled receptors are up- or



downregulated 14 days after the stress paradigm. The impacts of alteration in regulation of these molecular mechanisms are discussed below.

## MATERIALS AND METHODS

### ANIMAL MODEL OF PTSD

The animal model of PTSD employs restraint and tail shocks on three consecutive days. This inescapable tail-shock model (ITS) in rats mimics in many ways the pathophysiology of PTSD (9–13). In our model, stress exposure consists of a daily 2-h session of immobilization and tail-shocks for three consecutive days. The animals are restrained in Plexiglas tubes, and 40 electric shocks (2 mA, 3 s duration) are applied at varying intervals (140–180 s). Animals thereby undergo an aversive experience under conditions in which they cannot adaptively respond. We and others have verified that the ITS model induces behavioral and neurobiological alterations similar to those found in PTSD subjects (9–12). Specifically, these stressed rats exhibit (1) a delayed and exaggerated startle response appearing several days after stressor cessation which, given the compressed time scale of the rat's life compared to a humans, corresponds to the 1–3 months delay of symptoms in PTSD patients (14, 15), (2) enhanced plasma CORT for several days, indicating a compromised hypothalamopituitary axis (HPA), and (3) retarded body weight gain after stressor cessation, indicating dysfunction of gene expression. The gene expression microarray used in this experiment, dubbed the rat mitochondrion-neuron focused microarray (rMNChip), focuses on mitochondrial and mitochondria-related nuclear genes in the rat so as to specifically address the neuronal bioenergetics hypothesized to be involved in arousal, CORT, and growth as addressed in our model of PTSD (13).

Male albino Sprague Dawley rats were used (Taconic Farms, Derwood, MD, USA), weighing 150–200 g at the time of administration of the stress protocol. Two groups of animals ( $n = 20$ ) were studied. Twenty animals were assigned to each group based on their body weight and baseline startle response. Group 1 received the stress protocol, and Group 2 was the control. Stress exposure consisted of a daily 2-h session of restraint by immobilization in ventilated Plexiglas tubes (“inescapable”) and tail shocks for three consecutive days. Stressing was performed in the morning (between 08:00 and 12:00 hours).

Forty electric shocks (2 mA, 3 s duration; Animal Test Cage Grid Floor Shocker, Coulbourn Instruments, USA) were delivered to the tail of Group 1 rats at semi-random intervals of 150–210 s (Graphic State Notation Software, Habitest Universal Link, Coulbourn Instruments, USA). Electrode gel was applied using Q-tips to form a thin layer of conducting gel between the electrode and the skin of the rat's tail. The electrode clips were adjusted and connected to the tail to ensure a good connection without affecting the blood circulation of the tail. Amygdala dissection was performed as previously described (13).

### RAT MITOCHONDRIA NEURONAL CHIP

The rMNChip was designed and fabricated by GenProMarkers, Inc. (Rockville, MD, USA) using published methods (8). Briefly, the rMNChip contains 1,500 genes, including 37 mtDNA-encoded genes, 1,098 nDNA-encoded and mitochondria-focused genes,

and 365 genes associated with neuronal functions, including fear response, circadian rhythms, intraneuronal signal transduction, and neurotransmitters. The oligonucleotides used were designed with the software MacVector v10.6.0 (MacVector) using full-length mRNA sequences as the templates according to published criteria. An amino-C6 modifier was added to the 5'-end of each oligonucleotide probe to enhance the binding of the DNA to glass slides and the accessibility of hybridization with target DNA. The 1,500 test genes (including 80 “housekeeping” genes as positive controls) and 36 negative controls (non-rat DNA) were printed, each in triplicates, onto the *N*-hydroxysuccinimide ester reactive group-coated glass slides (CodeLink Activated Slide, SurModics, Eden Prairie, MI, USA). DNA probes in the print buffer (50 mM sodium phosphate), at a final concentration of 20  $\mu$ M of 5'-amino-C6 modified 50-mers, were printed in the Class 100 super-clean environment as described previously (7, 16, 17), using 100  $\mu$ M pins and the GeneMachine OmniGrid 100 Microarrayer (Genomic Solutions, Ann Arbor, MI, USA).

### RNA PURIFICATION

Total cellular RNA was purified from rat brain tissues by using a PAXgene RNA Kit (QIAGEN Inc., Valencia, CA, USA) following the manufacturer's instructions. The amygdalas of rats from both the stress and control groups were dissected immediately after euthanasia (13).

### MICROARRAY HYBRIDIZATION

One microgram of RNA per sample was used for Cy5dUTP labeling of cDNA by use of the express array detection kit (3DNA Array 900, Genisphere, Hatfield, PA, USA) following the manufacturer's instructions. Slides were scanned using 5  $\mu$ M resolution and the LOWESS method with a ScanArray Microarray Scanner (PerkinElmer). Triplicate microarray experiments were performed for each RNA sample purified from the amygdala. The background-subtracted mean values of the measured gene expression signal intensities were used for microarray data analysis. All microarray experiments were performed in the same laboratory as GenProMarkers, Inc. (8).

### MICROARRAY DATABASE, BIOINFORMATICS, AND SYSTEMS BIOLOGY

A gene expression database was constructed using FileMaker software (FileMaker Pro, Inc., Santa Clara, CA, USA). Database construction, data filtering, selection, exclusion and inclusion procedures, and criteria were performed as described previously (7, 8). The quantile normalization method (18) in software R version 2.15.1 (The R Foundation for Statistical Computing) was used to normalize background-subtracted mean intensities across all intra- and inter-slides of informative microarray data. Correlation and Single linkage methods were used to cluster and to make the heatmap using Cluster version 3.0 and MapleTree softwares<sup>1</sup>. The normalized data were also used for the calculation of means, SD, fold changes, moderated *p*-values, and false discovery rates (FDR). Gene IDs, official symbols, and official full names were updated using the NCBI database<sup>2</sup>. Kyoto Encyclopedia of

<sup>1</sup><http://rana.lbl.gov/EisenSoftware.htm>

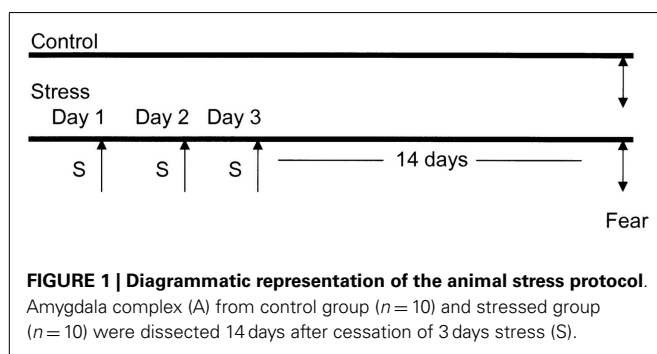
<sup>2</sup>[www.ncbi.nlm.nih.gov/gene](http://www.ncbi.nlm.nih.gov/gene)

Genes and Genomes (KEGG) pathways and Online Mendelian Inheritance in Man (OMIM) were from DAVID Bioinformatics Resources<sup>3</sup>.

### STATISTICS

The quantile normalization method (18) in software R/Bioconductor version 2.15.1 (The R Foundation for Statistical Computing) was used to normalize data. Means, SDs, and fold changes were calculated from triplicate spots (Amygdala complex) and triplicate experiments using XLSTAT 2006 (XLSTAT, New York, NY, USA). Differentially expressed genes were identified arbitrarily as having a greater than twofold change in the average expression of the background-subtracted mean intensity ratios of a gene between comparisons (19). The moderated *p*-values and FDR for multiple statistical testing with Benjamini and Hochberg methods (20) were calculated with the software R/Bioconductor version 2.15.1 (The R Foundation for Statistical Computing). The level of statistical significance was set at a *p*-value <0.01 with a specific FDR indicated. The error bar and plot were generated using Origin Lab version 8.5.

### EXPERIMENTAL PARADIGM (FIGURE 1)



## RESULTS

### HEATMAP PRESENTATION FOLLOWING MICROARRAY DATA COLLECTION AND ANALYSIS

The amygdala tissues were dissected from the rat brain 14 days after the cessation of the 3 days of stress. Total RNA samples were extracted from the amygdala complex of stressed rats (*n* = 10), and controls (*n* = 10) (13). Microarray experiments were triplicated using our recently developed fourth generation rat mitochondria-focused cDNA chip rMitChip3. With three spots in one cDNA microarray chip and three chips per each amygdala sample, the resulting analysis of nine data values from each single specimen greatly reduces misclassification rates (8). The measurement of expression of individual genes on the rMitChip3 (rMNChip) in one group was analyzed using 90 values (3 identical probes per microarray, 3 microarray experiments per specimen, and 10 specimens per gene), which generated reliable expression data for further pathway analysis. In this present study, the mitochondria-focused gene expression profilings in the amygdala

complex 14 days after traumatic stress were analyzed using the cDNA microarray chip containing 1500 genes associated with mitochondria functions. Based on the unsupervised cluster results, we calculated the average expression level of each gene in the stressed group (*n* = 10) and in the non-stressed control group (*n* = 10). The microarray data of 270,000 spots across all 60 microarray chips used for 20 RNA samples were filtered by uniform statistic and bioinformatic criteria (7), which generated 85 genes with informative expression profiles.

We identified a cluster and heatmap of 85 genes with significantly expressed RNA derived from the amygdala complex of the 10 control rats and the 10 stressed rats (Figure 2). The resultant dendrograms for all of these 85 genes and 20 amygdala complex specimens are classified as control group from CON-01 to CON-10 and stressed group from STR-1 to STR-10 in Figure 2; these analyses separated the stressed amygdala from those of the controls by their gene expression profiles. Figure 2A reveals 37 downregulated gene profiles and Figure 2B reveals 48 upregulated gene profiles.

### PATHWAY ANALYSIS OF UP- AND DOWNREGULATED GENES

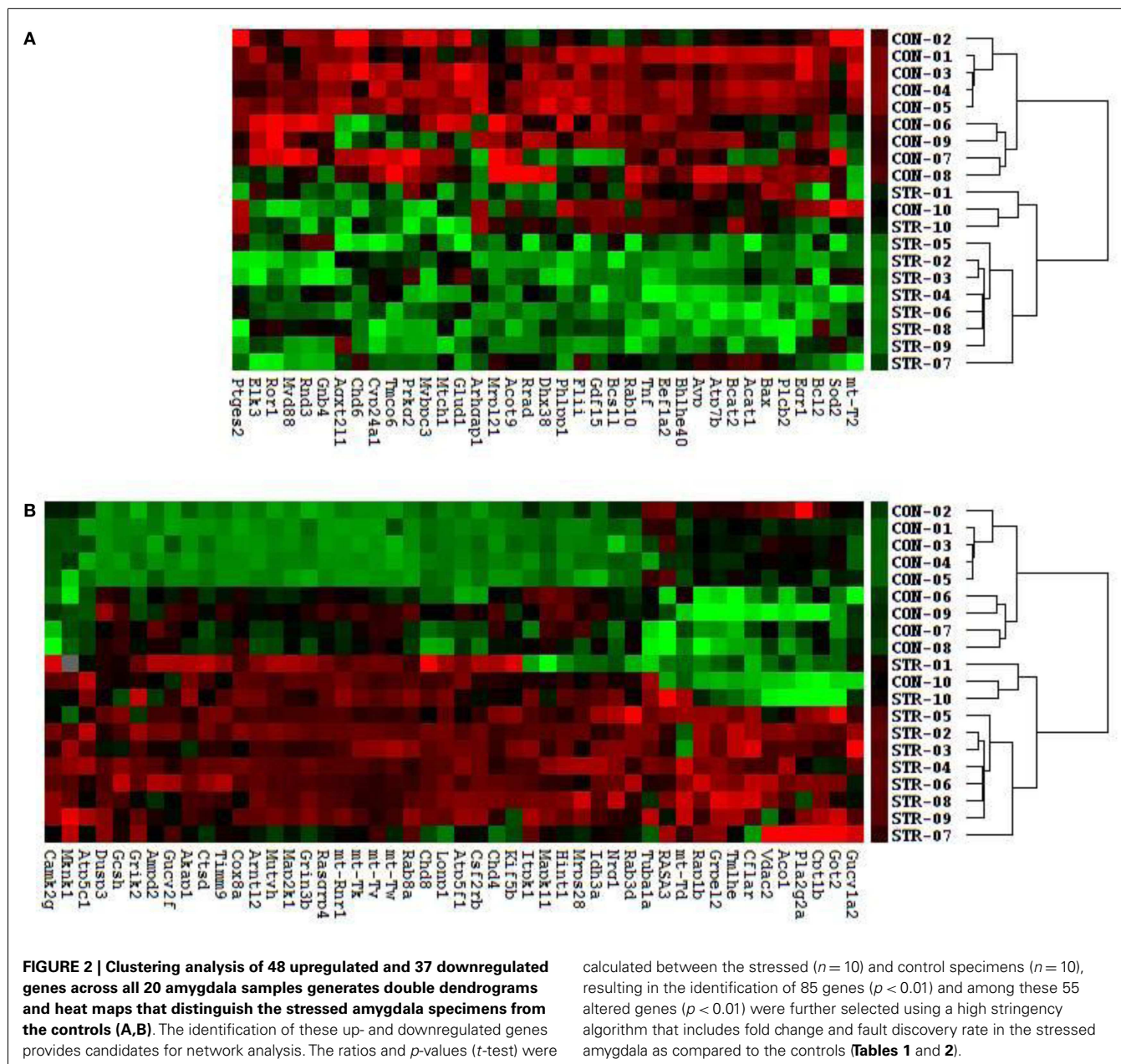
Pathways containing protein products of the up- and downregulated genes were determined using the Ingenuity Pathway Analysis (IPA) program. Table 1 illustrates the 34 upregulated genes and 21 downregulated genes in the amygdala after stress. A high stringency algorithm was used, including fold changes and FDR comparing stressed to controls (Tables 1 and 2). The tables include gene symbols, full names of genes listed in Genecards, fold change [ratio of stress and control, log(2) of the ratio], *p*-value, and false discover rate (FDR).

Molecular networks associated with mitochondrial functions were constructed based on up- and downregulated genes from the amygdala complex associated with exaggerated fear (13). Network analysis indicated that four reregulated molecular networks were associated with metabolic molecules and neurotransmitter systems, as well as with translational factors in the amygdala complex (Figure 2). Mitochondrial dysfunction involved in endocrine and neuronal signaling was evident in the amygdala. Detailed molecular correlations of these reregulated molecular pathways and the symptoms of PTSD such as exaggerated fear are noted (Figure 2). The results also suggest possible molecular targets for pharmacological intervention following exposure to traumatic stress.

In the network analysis, the networks identified are presented as graphs indicating the molecular relationships between gene products. Gene products are represented as nodes, and a biological relationship between two nodes is indicated by a line. The intensity of the node color indicates the degree of upregulation (red) or downregulation (green). Gene products in uncolored nodes were not identified as differentially expressed in our experiment, but were integrated into the computationally generated networks on the basis of the evidence stored in the IPA knowledge base indicating a relevance to this network.

The node shapes denote enzymes, phosphates, transmembrane receptors, cytokines, channels, transcription factors, G-protein-coupled receptors, growth factors, or nuclear receptor, as shown in Figure 3. Canonical pathway analysis identified the canonical pathways from the IPA library that were most significantly related

<sup>3</sup><http://david.abcc.ncifcrf.gov>



calculated between the stressed ( $n = 10$ ) and control specimens ( $n = 10$ ), resulting in the identification of 85 genes ( $p < 0.01$ ) and among these 55 altered genes ( $p < 0.01$ ) were further selected using a high stringency algorithm that includes fold change and false discovery rate in the stressed amygdala as compared to the controls (Tables 1 and 2).

to the input data set. The significance of the association between the data set and the canonical pathway was determined based on two parameters: (1) a ratio of the number of genes from the data set that map to the pathway divided by the total number of genes that map to the canonical pathway and (2) a *p*-value calculated using Fischer's exact test determining the probability that the association between the genes in the data set, and the canonical pathway is due to chance alone.

To reveal specific and detailed interactions among up- and downregulated genes in the amygdala, and to further identify gene targets for pharmacological agents, four molecular networks were delineated: (1) Bcl-2 and TNF centered inflammatory and apoptotic signaling networks as shown in Figure 4; (2) energy

production and neurotransmitter-mediated signaling pathways as shown in Figure 5; (3) transcriptional factor and chromatin remodeling pathways as shown in Figure 6; (4) immune mediator-related pathways as shown in Figure 7. The genes in the pathways were selected based on recent literature in the IPA database and relevance to neurological dysfunction, psychiatric disorders, and exaggerated fear response associated with amygdala functions as addressed in the Section "Discussion." Within these networks, 34 (62%) of the genes were significantly upregulated (Table 2; Figure 2B) and 21 (38%) of the genes were significantly downregulated (Table 1; Figure 2A). In the network analysis, these genes display particular relevance to the symptoms of PTSD.



**Table 1 | Downregulated genes in amygdala (14 days after stress).**

No	Gene symbols	Names of genes listed in Genecards	Fold change		Significance	
			Stress/CON	Log(2)	p	FDR
1	Eef1a2	Eukaryotic translation elongation factor 1 alpha 2	0.22	-2.20	0.0007	0.0044
2	Atp7b	ATPase, Cu++ transporting, beta polypeptide	0.31	-1.69	0.0062	0.0129
3	mt-Tl2	Mitochondrially encoded tRNA leucine 2 (CUN)	0.31	-1.68	0.0035	0.0088
4	Bhlhe40	Basic helix-loop-helix family, member e40	0.34	-1.58	0.0006	0.0044
5	Mtch1	Mitochondrial carrier 1	0.35	-1.53	0.0012	0.0047
6	Cyp24a1	Cytochrome P450, family 24, subfamily A, polypeptide 1	0.35	-1.52	0.0145	0.0199
7	Bcl-2	B-cell CLL/lymphoma 2	0.37	-1.42	0.0000	0.0014
8	Bcs1l	Mitochondrial chaperone BCS1	0.41	-1.30	0.0079	0.0134
9	Tnf	Tumor necrosis factor-alpha	0.42	-1.25	0.0005	0.0044
10	Acot9	Acyl-CoA thioesterase 9	0.44	-1.20	0.0024	0.0071
11	Rnd3	RND3 Rho family GTPase 3	0.44	-1.20	0.0056	0.0122
12	Dhx38	DEAH (Asp-Glu-Ala-His) box polypeptide 38	0.46	-1.13	0.0075	0.0133
13	Bcat2	Branched chain amino-acid transaminase 2, mitochondrial	0.47	-1.09	0.0097	0.0155
14	GDF-15	Growth differentiation factor 15	0.47	-1.08	0.0039	0.0091
15	Flii	Flightless I homolog	0.48	-1.06	0.0039	0.0091
16	Gnb4	Guanine nucleotide binding protein (G-protein), beta polypeptide 4	0.48	-1.05	0.0069	0.0133
17	Rrad	Ras-related associated with diabetes	0.49	-1.04	0.0041	0.0091
18	Acat1	Acetyl-CoA acetyltransferase 1	0.49	-1.03	0.0146	0.0199
19	Elk3	ETS-domain protein (SRF accessory protein 2)	0.50	-0.99	0.0073	0.0133
20	Phlpp1	PH domain and leucine rich repeat protein phosphatase 1	0.51	-0.97	0.0012	0.0047
21	Plcb2	Phospholipase C, beta 2	0.54	-0.90	0.0103	0.0159

Approved symbol from the HUGO Gene Nomenclature Committee (HGNC) database.

### VALIDATION OF THE Rap1b AND Arhgap1 GENE EXPRESSIONS IN THE AMYGDALA (MICROARRAY) AND BLOOD (qRT-PCR)

Quantitative real-time PCR (qRT-PCR) was used to validate and to confirm gene expression results obtained from microarray analysis in our previous published results (4). The relative mRNA levels of identified genes measure by qRT-PCR were in agreement with the data detected by microarray from 92 to 67% on five genes examined (4). In an attempt to correlate biomarkers in peripheral tissue (blood) with the profile of dysregulated genes in the amygdala, Rap1b and Arhgap1 were chosen in the current study because of upregulation of (Rap1b) and downregulation of (Arhgap1) expressions observed in stressed amygdala and blood as well as because Rap1b is of known relevance to abnormal fear response (21). The results show that the relative mRNA levels of these genes measured by qRT-PCR (blood,  $n = 8$ ,  $p < 0.01$ ) were in agreement with the data detected by microarray (amygdala,  $n = 10$ ,  $p < 0.01$ ) experiments (shown in Figures 1A,B in Supplementary Material).

### DISCUSSION

Animal models of PTSD offer opportunities to identify mechanisms, potential biomarkers, and treatment targets for this disorder. In this study, we have shown that a substantial number of up- and downregulated genes related to mitochondrial function in the amygdala are associated with an animal model of PTSD based on exaggerated startle and retardation of growth (9, 13). These mitochondrial-function genes have been previously

related to neurological dysfunction, psychiatric disorders, and stress response (4, 6). In addition, we have identified novel mitochondrial-function-related genes associated with endocrine and neuronal signaling (4, 5, 22).

Traumatic stress up- or downregulation of anti-inflammatory and anti-apoptotic cellular pathways are evidenced in the amygdala 14 days after stress, as indicated in **Figure 4** and **Tables 1** and **2**. Seven genes, including RAP1B, Cathepsin D (CTSD), MKNK1, RASGRP, CSF2RB, GMCSF, and CFLAR are upregulated and nine genes, including tumor necrosis factor (TNF), Bcl-2, GDF-15, early growth response (Egr1), GNB, FLII, BHLHE40, RND3, and GNB4 are downregulated in the inflammatory and apoptotic signaling networks in the amygdala.

Levels of inflammatory cytokines in blood samples have been used as biomarkers of PTSD vulnerability and resilience in traumatized individuals (23–26). TNF- $\alpha$  and related anti-inflammatory cytokines in the peripheral blood have been correlated with symptoms of PTSD, including re-experiencing, avoidance, and hyperarousal, and with PTSD total symptom score (23, 24, 26). In a single stress rat model, increased neuronal apoptosis has been observed in the medial prefrontal cortex (mPFC) 7 days after stress exposure indicating that apoptotic-related molecules are sensitive to traumatic stress (27). Emerging data indicate that TNF and the anti-apoptotic protein Bcl-2 exert a neuroprotective effect in the brain against traumatic stress (28–30).

Using network analysis, current results reveal for the first time that the 15 genes of the inflammatory pathway in the amygdala

**Table 2 | Upregulated genes in amygdala (14 days after stress).**

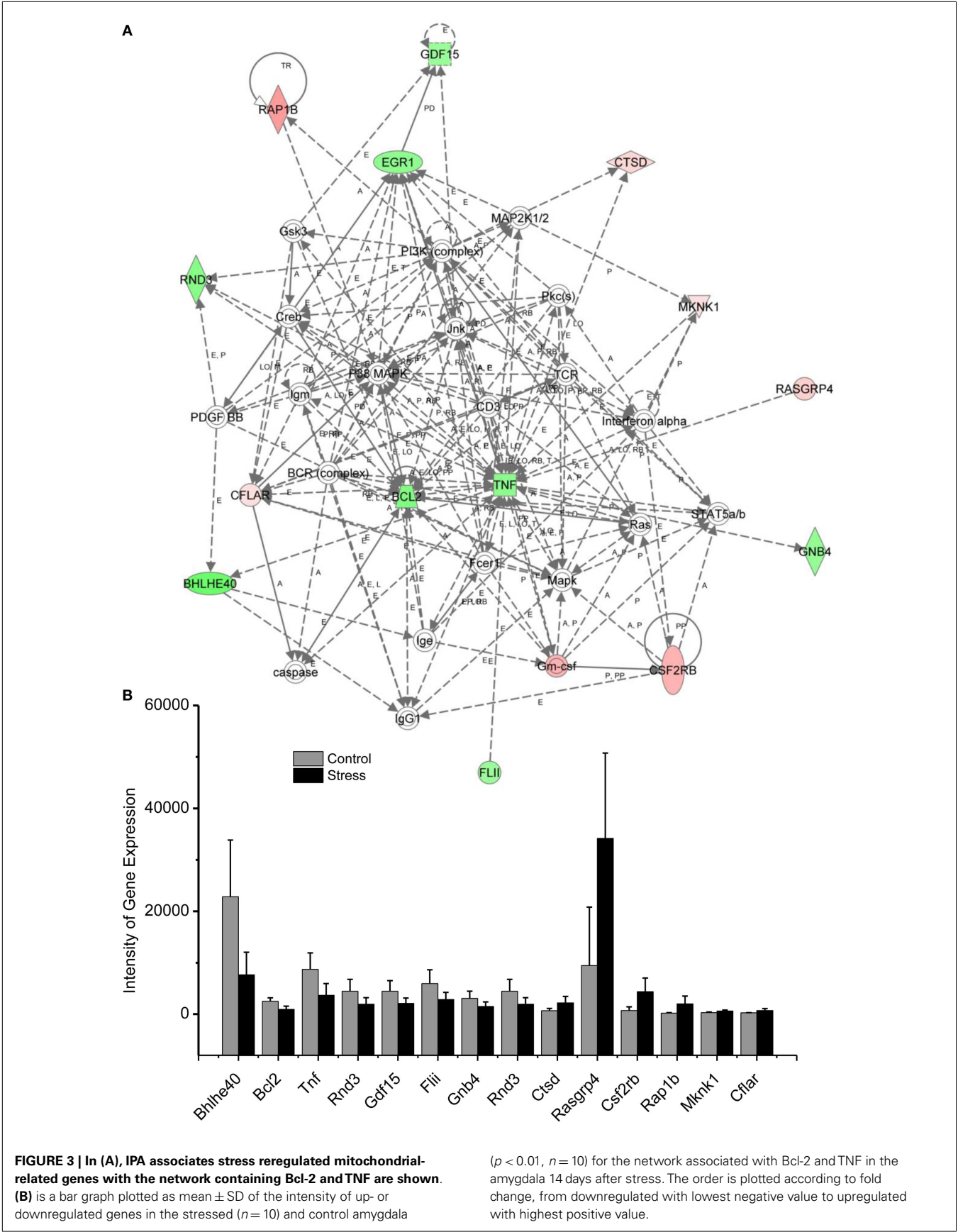
No	Gene	Names of genes listed in Genecards	Fold change		Significance	
			Stress/CON	Log(2)	p	FDR
1	RASA3	Ras GTPase-activating protein 3	2.02	1.01	0.0040	0.0091
2	Dusp3	Dual specificity protein phosphatase 3	2.03	1.02	0.0107	0.0163
3	Gucy1a2	Guanylate cyclase 1, soluble, alpha 2	2.05	1.03	0.0023	0.0071
4	Grik2	Glutamate receptor, ionotropic, kainate 2	2.06	1.04	0.0012	0.0047
5	Mrps28	Mitochondrial ribosomal protein S28	2.21	1.14	0.0143	0.0199
6	Got2	Glutamic-oxaloacetic transaminase 2	2.27	1.18	0.0077	0.0133
7	Gucy2f	Guanylate cyclase 2F, retinal	2.34	1.23	0.0075	0.0133
8	Atp5c1	ATP synthase, H <sup>+</sup> transporting, mitochondrial F1 complex, gamma polypeptide 11	2.36	1.24	0.0111	0.0165
9	Akap1	A-kinase anchor protein 1	2.39	1.25	0.0098	0.0155
10	Idh3a	Isocitrate dehydrogenase 3 (NAD <sup>+</sup> ) alpha	2.57	1.36	0.0034	0.0088
11	Cox8a	Cytochrome c oxidase subunit VIIIA (ubiquitous)	2.61	1.38	0.0024	0.0071
12	Cpt1b	Carnitine palmitoyltransferase 1B (muscle)	2.80	1.49	0.0074	0.0133
13	Atp5f1	ATP synthase, H <sup>+</sup> transporting, mitochondrial Fo complex, subunit B1	3.02	1.59	0.0002	0.0029
14	mt-Tw	Mitochondrially encoded tRNA tryptophan	3.18	1.67	0.0011	0.0047
15	Kif5b	Kinesin family member 5B	3.21	1.68	0.0147	0.0199
16	CTSD	Cathepsin D	3.30	1.72	0.0017	0.0055
17	Nrg1	Neuregulin 1	3.34	1.74	0.0006	0.0044
18	mt-Ty	Mitochondrially encoded tRNA tyrosine	3.44	1.78	0.0011	0.0047
19	Timm9	Translocase of inner mitochondrial membrane 9 homolog	3.49	1.80	0.0011	0.0047
20	Rab8a	Member RAS oncogene family	3.54	1.82	0.0000	0.0014
21	Rasgrp4	RAS guanyl releasing protein 4	3.62	1.86	0.0008	0.0047
22	mt-Tk	Mitochondrially encoded tRNA lysine	3.69	1.88	0.0006	0.0044
23	mt-Rnr1	Mitochondrially encoded 12S RNA1	4.05	2.02	0.0001	0.0024
24	Camk2g	Calcium/calmodulin-dependent protein kinase II gamma	4.13	2.05	0.0032	0.0086
25	Grin3b	Glutamate receptor, ionotropic, N-methyl-D-aspartate 3B protein	4.77	2.25	0.0016	0.0055
26	Itpk1	Inositol 1,3,4-trisphosphate 5/6 kinase2	5.59	2.48	0.0006	0.0044
27	Csf2rb	Colony stimulating factor 2 receptor, beta, low-affinity (granulocyte-macrophage)	6.11	2.61	0.0005	0.0044
28	Tmlhe	Trimethyllysine hydroxylase, epsilon	6.71	2.75	0.0007	0.0045
29	Arntl2	Aryl hydrocarbon receptor nuclear translocator-like 2	7.86	2.97	0.0001	0.0028
30	Mutyh	mutY homolog ( <i>E. coli</i> )	7.92	2.99	0.0141	0.0199
31	Rap1b	Ras family small GTP binding protein RAP1B2	10.13	3.34	0.0014	0.0053
32	Lonp1	Lon peptidase 1, mitochondrial	12.04	3.59	0.0016	0.0055
33	Grpel2	GrpE-like 2, mitochondrial ( <i>E. coli</i> )	13.49	3.75	0.0009	0.0047
34	mt-Td	Mitochondrially encoded tRNA aspartic acid	14.17	3.82	0.0032	0.0086

complex are up- or downregulated in the exaggerated fear response (Figure 4). These inflammatory signaling molecules may participate in the evolution of PTSD to a chronic disorder because they remain up- or downregulated 14 days after the stress protocol. Bcl-2, an integral outer mitochondrial membrane protein, was initially found to block the apoptotic death of lymphocytes, and over expression of Bcl-2 in transgenic mice reduced the fear response (31, 32). In the current stress model of PTSD, the expression of Bcl-2 is downregulated in the amygdala, indicating that both neuronal inflammatory and cellular apoptosis signaling pathways contribute to the exaggeration of fear following traumatic stress. The network analysis encourages future studies to detail the cellular mechanisms that are evidenced to underlie PTSD (4, 5, 27, 33). For example, the Bcl-2 mediated apoptotic cellular process may contribute not only to the degenerated amygdala structure in PTSD patients but also to the impairment of the controlling

function of the amygdala in the fear response of PTSD patients. This process may also be observable in animal models of PTSD (27, 34–36).








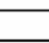









Among the downregulated genes, the basic helix–loop–helix transcription genes, BHLHE, have been associated with symptoms of PTSD such as sleep disturbance. For example, BHLHE40 and BHLHE41 are mainly expressed in the suprachiasmatic nucleus of the hypothalamus, which governs circadian rhythm (37). BHLHE40 synchronizes the circadian rhythm at the intracellular level with the external light–dark cycle. The current study demonstrates for the first time that downregulated BHLHE40 expression in the amygdala is associated with exaggerated fear following traumatic stress. Thus BHLHE40 may be a target for treatment of the disruption of sleep associated with PTSD, a symptom that is often resistant to present pharmacotherapy. Changes in the light/dark cycle have also been shown to disrupt memory of conditioned





## Molecule Shapes

### Network Shapes

-  Cytokine
-  Growth Factor
-  Chemical / Drug/ Toxicant
-  Enzyme
-  G-protein Coupled Receptor
-  Ion Channel
-  Kinase
-  Ligand-dependent Nuclear Receptor
-  Peptidase
-  Phosphatase
-  Transcription Regulator
-  Translation Regulator
-  Transmembrane Receptor
-  Transporter
-  microRNA
-  Complex / Group
-  Other

**FIGURE 4 | Node (gene) and edge (gene relationship) symbols are described in the figure.** The intensity of the node color-(red) indicates the degree of upregulation. Genes in uncolored nodes are not identified as differentially expressed genes in our experiment and are integrated into the computationally generated networks on the basis of the evidence stored in the IPA knowledge memory indicating a relevance to this network. The node shapes denote enzymes, phosphatases, kinases, peptidases, G-protein-coupled receptors, transmembrane receptors, cytokines, growth factors, ion channels, transporters, translation factors, nuclear receptors, and transcription factors.

fear (38–40). Thus, the circadian system may relate to anxiety and altered cognition following traumatic stress.

In addition to the Hub molecules such as Bcl-2 and TNF in the inflammatory and apoptotic pathways, other up- or down-regulated gene products in the pathways could contribute to the exaggerated fear response. Although little has been published associating these molecules with exaggerated fear or other PTSD symptoms, they have been related to neuronal regulation. For example, GDF-15 is a potent trophic factor in the recovery of 6-OHDA-lesioned midbrain dopaminergic neurons (41). Downregulation of GDF-15 may jeopardize neuronal survival in the amygdala following traumatic stress. Mitochondrial carrier homolog 1 (Mtch1) is an outer mitochondrial membrane protein and overexpression of Mtch1 causes mitochondrial depolarization and apoptosis, likely via the permeability transition pore (42). Egr transcriptional regulators such as Egr1 have been widely recognized as molecules essential for emotional learning and memory (43, 44). Moreover, Egr1-deficient mice have impairments in late phase hippocampal LTP and consolidation of some forms of amygdala-dependent memory through a protein phosphatase calcineurin-mediated mechanism (43, 44). Thus, downregulated Egr1 following traumatic stress may impair cellular processes associated with emotional learning.

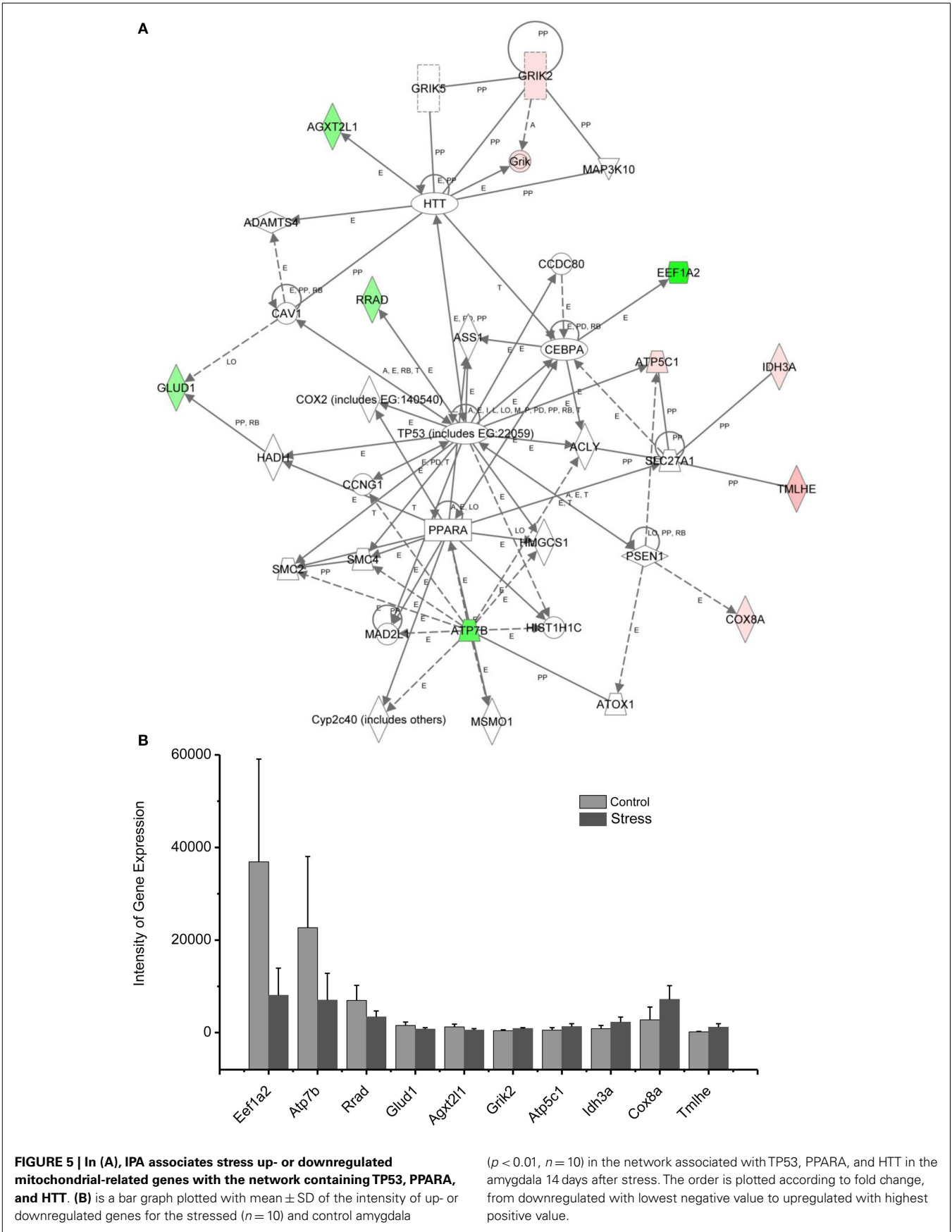
### TRAUMATIC STRESS UP- AND DOWNREGULATED GENES IN THE AMYGDALA ASSOCIATED WITH SUICIDE

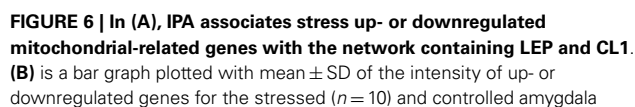
Post-traumatic stress disorder significantly increases risk for suicide, even after adjusting for depression, which is often comorbid. Therefore, it appears that traumatic stress exposure and its consequences are risk factors for suicide in some people (45, 46). Correlation of mechanisms underlying suicide anxiety can help in understanding the cellular and molecular connections between these two mental disorders. Using molecular network analysis of genes up- or downregulated by traumatic stress, as shown in **Figure 2** and **Tables 1** and **2**, genes including TUBA1, CTSD, and Grik2 have been associated with suicidal events (47, 48). Dysregulation of each of these genes produces profound damage to the brain.

Mutations of TUBA1A in this gene cause lissencephaly type 3 (LIS3), a neurological condition characterized by microcephaly, mental retardation, early-onset epilepsy, and defective neuronal migration (49). TUBA1 is also an interacting cytoskeleton protein that has a functional connection to glutamate, GABA, and serotonin receptors (48). Mutations in the CTSD gene are involved in the pathogenesis of AD and Niemann–Pick disease (50–53).

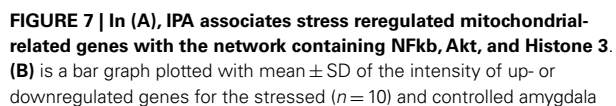
A recent proteomic study on post mortem brains of suicide victims shows that both TUBA1A and CTSD are highly expressed in the prefrontal cortex and amygdala of suicide victims, suggesting that these genes may be a risk biomarker for suicide (48). As shown in **Figure 4**, S100 Calcium Binding Protein A1 (S100A1; one of the proteins in the super family of S100, also called P11) interacts with TUBA1A and may regulate the function of TUBA1 under stressful conditions (54). In fact, in a recent clinical study, the mRNA level of S100A10 was found to be a potential adjunctive biomarker for the assessment of suicide risk in anxiety disorders (55).

Kainate receptors are members of the ionotropic class of glutamate receptors and are highly expressed in the amygdala neuronal





( $p < 0.01$ ,  $n = 10$ ) in the network associated with LEP and CL1 in the amygdala 14 days after stress. The order is plotted according to fold change, from downregulated with lowest negative value to upregulated with highest positive value.



( $p < 0.01$ ,  $n = 10$ ) in the network associated with NF $\kappa$ B, AKT, and Histone 3 in the amygdala 14 days after stress. The order is plotted according to fold change, from downregulated with lowest negative value to upregulated with highest positive value.



circuitry (56–60). These kainate receptors have been identified both pre- and post-synaptically. They modulate inhibitory and excitatory postsynaptic currents in the basolateral amygdala circuitry and play a role in synaptic plasticity associated with emotional learning and memory (56–60). Thus upregulated *Grik2* and *Grik* genes, as found in the current study, may participate in the emotional hyperarousal following traumatic stress. In addition, recent pharmacogenomic studies of antidepressant treatment-emergent suicidal events report associations with polymorphisms of *Grik2* receptor genes in depressed patients (47). The network analysis from the present results suggests that the pharmacologic agents that target specific subtypes of kainate receptors may be therapeutic medications for the treatment of PTSD with suicidal ideation.

In summary, network analysis reveals that signaling pathways associated with *TUBA1A*, *CTSD*, and *Grik2* are potential biomarkers and therapeutic targets for PTSD with suicidal ideation.

#### UP/DOWNREGULATION OF GENES IN THE AMYGDALA SUBSERVING ENERGY PRODUCTION AND NEUROTRANSMITTER SYNTHESIS

Diminished interest and participation in activities along with detachment and lack of positive emotions may be seen in PTSD as energy loss or mental fatigue. This decreased energy is a common complaint of service members after repetitive traumatic stress, including PTSD and TBI (61). While the mechanisms underlying the mental fatigue are speculated to be due to a shortage of energetic molecules in the brain, the detailed mechanism remains elusive. The relationship between mitochondrial gene expression in the amygdala and exaggerated fear provides an approach to the cellular and molecular basis of mental fatigue after trauma. As shown in **Figure 5**, two citrate cycle genes, *Idh3a* and *Cpt1b*, were upregulated. *Idh3a* promotes ATP production by catalyzing the oxidative decarboxylation of isocitrate to 2-oxoglutarate. *Cpt1b* generates ATP from lipids via beta-oxidation of fatty acids (62–64). Expression of *ATP5C1* is enhanced. *ATP5C1* is the mitochondrial membrane ATP synthase. Suppression of the *ATP5C1* gene caused a decrease in cell proliferation and ATP production (65). Enhanced expression of *ATP5C1* may suggest an enhanced demand for energy in the amygdala in response to traumatic stress associated with exaggerated fear. Indeed, enhanced expression of *ATP5C1* was also found in the prefrontal cortex of PTSD postmortem brains, indicating that the *ATP5C1* gene could be a biomarker for the diagnosis of PTSD (4).

Mitochondrial genes supporting biosynthesis are differentially regulated under conditions of stress. *Got2*, which is involved in arginine, tyrosine, and tryptophan biosynthesis, is upregulated; *Acot1* and *Bcat2*, two enzymes involved in fatty acid metabolism, as well as synthesis of valine, leucine, and isoleucine, and degradation of lysine, are downregulated. Tryptophan is a precursor of serotonin, which is thought to contribute to emotional well-being and is related to depression, which is highly comorbid with PTSD (66, 67). In addition, selective serotonin reuptake inhibitors (SSRIs) are a first line treatment for PTSD.

These results indicate that altered regulation of expression of genes involved with energy production and biosynthesis in the

amygdala may be associated with the diminished interest, overall mental fatigue, and comorbid symptoms of depression in PTSD.

#### UP/DOWNREGULATION OF GENES IN THE AMYGDALA ASSOCIATED WITH IMMUNE MEDIATORS AND ENERGY EXPENDITURE

Proinflammatory chemokines have been suggested to be involved in chronic stress, major depressive disorder, panic disorder, and PTSD (68–73). The chemokines *IL4* and *CCL13* are interconnected with the up- and downregulated genes shown in the network 3, including *Lonp1*, *ATP5F1*, *Rab8A*, and *Gucy2F*. Levels of chemokines including *IL4*, *IL2*, and *TNF alpha* in the plasma have been found to be significantly altered in some patients suffering from traumatic stress, including those with PTSD and those suffering from child abuse (74). *CCL13* is a chemotactic cytokine that regulates leukocyte migration through interactions with G-protein-coupled receptors (75, 76).

The up- and downregulated genes shown in the network (**Figure 6**) are connected with *Leptin* (*LEP*), which is a key mediator in the regulation of food intake, body weight, and possibly memory. Dysregulation of *LEP* could be involved in the weight loss resulting from chronic and repetitive stress in our rat model of PTSD (11, 13, 77). Weight loss is a common symptom of depression, highly comorbid with PTSD. Indeed, elevated serum *LEP* levels were found in PTSD patients suffering from depressive symptoms caused by earthquakes and myocardial infarctions (78, 79). In addition, intraperitoneal injection of *LEP* mitigated the impairment of fear memory in the mouse deprived of rapid eye movement sleep (80). Thus, it appears that the elevation of *LEP* in patients with PTSD may be associated with elevated fear, similar to an observation made in the current rat model of PTSD.

#### UP/DOWNREGULATION OF GENES IN THE AMYGDALA ASSOCIATED TRANSCRIPTION FACTORS AND CHROMATIN REMODELING

As indicated in the signaling pathway shown in **Figure 7**, four genes, including *neuregulin 1* (*Nrg1*), *calmodulin-dependent kinases 2 gamma* (*Camk2g*), *tubuline* (*Tuba1A*), and the *A-kinase anchor protein 1* (*AKAP1*), are upregulated in the amygdala 14 days after stress, and *E-twenty six* (*ETS*) domain-containing transcription factor (*ELK3*) is downregulated. In addition to the functions of the individual up- or downregulated genes in **Figure 7**, these genes are interconnected with *histone 3* and *histone 4*. *Histone H3* and *histone H4* are two of the five main histone proteins involved in the structure of chromatin in eukaryotic cells. Thus, the up- or downregulated genes in the network appear to affect transcription and chromatin remodeling.

Regulation of chromatin structure through post-translational modification of histone proteins is a critical step in the formation of long-term memory (81). As revealed in the network analysis, traumatic and repetitive stress leads to altered regulation of chromatin-related genes in the amygdala, including the upregulation of *Nrg1*, *CamK2g*, *Tuba1A*, and *AKAP1*, as well as the downregulation of *ELK3* interacting with *NF-kappa B*, *histone 3*, and *histone 4*. *Histone 3* and *histone 4* drive epigenetic modifications and conformational changes in chromatin, stimulating the expression of neuroplasticity-related genes involved in traumatic memory and fear learning (82, 83). *Histone acetylation* mediated by *BDNF* gene transcription is involved in the consolidation of

fear memory associated with an animal model of PTSD (84). This modulation could promote chromatin remodeling in the amygdala induced by glucocorticoids following traumatic stress. Indeed, activation of the glucocorticoid receptor (GR) under stress has also been shown to modify chromatin structure by post-translational modifications of histones and is considered to be a new therapeutic target for PTSD (85, 86).

Nuclear factor kappa-light-chain-enhancer of activated B cells (NF- $\kappa$ B), a protein complex that controls the transcription of DNA, interacts with up- or downregulated genes in network 4. Inhibition of NF- $\kappa$ B in the basolateral amygdala impairs the memory reconsolidation associated with auditory fear conditioning (87).

## SUMMARY

The current study reveals that multiple signaling networks are up- or downregulated in the amygdala circuitry 14 days after traumatic stress. Traumatic stress significantly alters at least 55 genes associated with at least four pathways related to mitochondria functions in the stressed amygdala. These molecules include well-studied and -documented networks as well as novel networks that have not been well documented in previous literature. These findings provide a guide for further studies associated with diagnostic biomarkers, therapeutic molecular targets, and identification of optimal strategies for fostering resilience before and after traumatic stress. In addition, current analyses suggest new targets for pharmacological intervention to treat PTSD and suicide. Suicide-related genes revealed in the stressed amygdala indicate that dysregulated signaling pathways interweave suicide and fear. These results elucidate the molecular pathways underlying PTSD as a road to diagnosis and treatment.

## ACKNOWLEDGMENTS

This research was supported by CSTS and CDMRP grant W81XWH-08-2-006 to He Li.

## SUPPLEMENTARY MATERIAL

The Supplementary Material for this article can be found online at <http://www.frontiersin.org/Journal/10.3389/fneur.2014.00164/abstract>

## REFERENCES

- Rabinak CA, Angstadt M, Welsh RC, Kenndy AE, Lyubkin M, Martis B, et al. Altered amygdala resting-state functional connectivity in post-traumatic stress disorder. *Front Psychiatry* (2011) 2:62. doi:10.3389/fpsy.2011.00062
- Bryant RA, Kemp AH, Felmingham KL, Liddell B, Olivieri G, Peduto A, et al. Enhanced amygdala and medial prefrontal activation during nonconscious processing of fear in posttraumatic stress disorder: an fMRI study. *Hum Brain Mapp* (2008) 29:517–23. doi:10.1002/hbm.20415
- Stein MB, Simmons AN, Feinstein JS, Paulus MP. Increased amygdala and insula activation during emotion processing in anxiety-prone subjects. *Am J Psychiatry* (2007) 164:318–27. doi:10.1176/appi.ajp.164.2.318
- Su YA, Wu J, Zhang L, Zhang Q, Su DM, He P, et al. Dysregulated mitochondrial genes and networks with drug targets in postmortem brain of patients with posttraumatic stress disorder (PTSD) revealed by human mitochondria-focused cDNA microarrays. *Int J Biol Sci* (2008) 4:223–35. doi:10.7150/ijbs.4.223
- Zhang L, Zhou R, Li X, Ursano RJ, Li H. Stress-induced change of mitochondria membrane potential regulated by genomic and non-genomic GR signaling: a possible mechanism for hippocampus atrophy in PTSD. *Med Hypotheses* (2006) 66:1205–8. doi:10.1016/j.mehy.2005.11.041
- Manoli I, Alesci S, Blackman MR, Su YA, Rennert OM, Chrousos GP. Mitochondria as key components of the stress response. *Trends Endocrinol Metab* (2007) 18:190–8. doi:10.1016/j.tem.2007.04.004
- Bai X, Wu J, Zhang Q, Alesci S, Manoli I, Blackman MR, et al. Third-generation human mitochondria-focused cDNA microarray and its bioinformatic tools for analysis of gene expression. *Biotechniques* (2007) 42:365375. doi:10.2144/000112388
- Su YA, Zhang Q, Su DM, Tang MX. Rat mitochondrion-neuron focused microarray (rMNCChip) and bioinformatics tools for rapid identification of differential pathways in brain tissues. *Int J Biol Sci* (2011) 7:308–22. doi:10.7150/ijbs.7.308
- Servatius RJ, Ottenweller JE, Natelson BH. Delayed startle sensitization distinguishes rats exposed to one or three stress sessions: further evidence toward an animal model of PTSD. *Biol Psychiatry* (1995) 38:539–46. doi:10.1016/0006-3223(94)00369-E
- Braga MF, roniadou-Anderjaska V, Post RM, Li H. Lamotrigine reduces spontaneous and evoked GABAA receptor-mediated synaptic transmission in the basolateral amygdala: implications for its effects in seizure and affective disorders. *Neuropharmacology* (2002) 42:522–9. doi:10.1016/S0028-3908(01)00198-8
- Jiang X, Xing G, Yang C, Verma A, Zhang L, Li H. Stress impairs 5-HT<sub>2A</sub> receptor mediated serotonergic facilitation of GABA release in juvenile rat basolateral amygdala. *Neuropsychopharmacology* (2009) 34:410–23. doi:10.1038/npp.2008.71
- Garrick T, Morrow N, Shalev AY, Eth S. Stress-induced enhancement of auditory startle: an animal model of posttraumatic stress disorder. *Psychiatry* (2001) 64:346–54.
- Jia M, Meng F, Smerin SE, Xing G, Zhang L, Su DM, et al. Biomarkers in an animal model for revealing neural, hematologic, and behavioral correlates of PTSD. *J Vis Exp* (2012) 68:e3361. doi:10.3791/3361
- Dunleavy K, Kubo SA. Emergence of delayed posttraumatic stress disorder symptoms related to sexual trauma: patient-centered and trauma-cognizant management by physical therapists. *Phys Ther* (2012) 92:339–51. doi:10.2522/ptj.20100344
- Tomb DA. The phenomenology of post-traumatic stress disorder. *Psychiatr Clin North Am* (1994) 17:237–50.
- Su YA, Bittner ML, Chen Y, Tao L, Jiang Y, Zhang Y, et al. Identification of tumor-suppressor genes using human melanoma cell lines UACC903, UACC903(+6), and SRS3 by comparison of expression profiles. *Mol Carcinog* (2000) 28:119–27. doi:10.1002/1098-2744(200006)28:2<119::AID-MC8>3.0.CO;2-N
- Su YA, Trent JM. Isolation of tumor suppressor genes in melanoma by cDNA microarray. *Methods Mol Med* (2001) 61:15–29. doi:10.1385/1-59259-145-0:15
- Bolstad BM, Irizarry RA, Astrand M, Speed TP. A comparison of normalization methods for high density oligonucleotide array data based on variance and bias. *Bioinformatics* (2003) 19:185–93. doi:10.1093/bioinformatics/19.2.185
- Tarca AL, Romero R, Draghici S. Analysis of microarray experiments of gene expression profiling. *Am J Obstet Gynecol* (2006) 195:373–88. doi:10.1016/j.ajog.2006.07.001
- Benjamini Y, Drai D, Elmer G, Kafkafi N, Golani I. Controlling the false discovery rate in behavior genetics research. *Behav Brain Res* (2001) 125:279–84. doi:10.1016/S0166-4328(01)00297-2
- Pan BX, Vautier F, Ito W, Bolshakov VY, Morozov A. Enhanced cortico-amygdala efficacy and suppressed fear in absence of Rap1. *J Neurosci* (2008) 28:2089–98. doi:10.1523/JNEUROSCI.5156-07.2008
- Choi KH, Le T, McGuire J, Coyner J, Higgs BW, Diglisic S, et al. Expression profiles of mitochondrial genes in the frontal cortex and the caudate nucleus of developing humans and mice selectively bred for high and low fear. *PLoS One* (2012) 7:e49183. doi:10.1371/journal.pone.0049183
- Gill J, Vythilingam M, Page GG. Low cortisol, high DHEA, and high levels of stimulated TNF- $\alpha$ , and IL-6 in women with PTSD. *J Trauma Stress* (2008) 21:530–9. doi:10.1002/jts.20372
- Gola H, Engler H, Sommershof A, Adenauer H, Kolassa S, Schedlowski M, et al. Posttraumatic stress disorder is associated with an enhanced spontaneous production of pro-inflammatory cytokines by peripheral blood mononuclear cells. *BMC Psychiatry* (2013) 13:40. doi:10.1186/1471-244X-13-40
- Guo M, Liu T, Guo JC, Jiang XL, Chen F, Gao YS. Study on serum cytokine levels in posttraumatic stress disorder patients. *Asian Pac J Trop Med* (2012) 5:323–5. doi:10.1016/S1995-7645(12)60048-0
- von KR, Hepp U, Kraemer B, Traber R, Keel M, Mica L, et al. Evidence for lowgrade systemic proinflammatory activity in patients with posttraumatic

- stress disorder. *J Psychiatr Res* (2007) **41**:744–52. doi:10.1016/j.jpsychires.2006.06.009
27. Li XM, Han F, Liu DJ, Shi YX. Single-prolonged stress induced mitochondrial dependent apoptosis in hippocampus in the rat model of post-traumatic stress disorder. *J Chem Neuroanat* (2010) **40**:248–55. doi:10.1016/j.jchemneu.2010.07.001
  28. Della FP, Abelaira HM, Reus GZ, Antunes AR, Dos Santos MA, Zappellini G, et al. Tianeptine exerts neuroprotective effects in the brain tissue of rats exposed to the chronic stress model. *Pharmacol Biochem Behav* (2012) **103**:395–402. doi:10.1016/j.pbb.2012.09.018
  29. Rossi-George A, Urbach D, Colas D, Goldfarb Y, Kusnecov AW. Neuronal, endocrine, and anorexic responses to the T-cell superantigen staphylococcal enterotoxin A: dependence on tumor necrosis factor- $\alpha$ . *J Neurosci* (2005) **25**:5314–22. doi:10.1523/JNEUROSCI.0687-05.2005
  30. Salim S, Asghar M, Taneja M, Hovatta I, Chugh G, Vollert C, et al. Potential contribution of oxidative stress and inflammation to anxiety and hypertension. *Brain Res* (2011) **1404**:63–71. doi:10.1016/j.brainres.2011.06.024
  31. Rondi-Reig L, Lemaigre DY, Martinou JC, haye-Bouchaud N, Caston J, Mariani J. Fear decrease in transgenic mice overexpressing bcl-2 in neurons. *Neuroreport* (1997) **8**:24292432. doi:10.1097/00001756-199707280-00004
  32. Pinkoski MJ, Green DR. Lymphocyte apoptosis: refining the paths to perdition. *Curr Opin Hematol* (2002) **9**:43–9. doi:10.1097/00062752-200201000-00008
  33. Ding J, Han F, Shi Y. Single-prolonged stress induces apoptosis in the amygdala in a rat model of post-traumatic stress disorder. *J Psychiatr Res* (2010) **44**:48–55. doi:10.1016/j.jpsychires.2009.06.001
  34. Shucard JL, Cox J, Shucard DW, Fetter H, Chung C, Ramasamy D, et al. Symptoms of posttraumatic stress disorder and exposure to traumatic stressors are related to brain structural volumes and behavioral measures of affective stimulus processing in police officers. *Psychiatry Res* (2012) **204**:25–31. doi:10.1016/j.pscychres.2012.04.006
  35. Majewska MD. Cocaine addiction as a neurological disorder: implications for treatment. *NIDA Res Monogr* (1996) **163**:1–26.
  36. Karl A, Malta LS, Maercker A. Meta-analytic review of event-related potential studies in post-traumatic stress disorder. *Biol Psychol* (2006) **71**:123–47. doi:10.1016/j.biopsycho.2005.03.004
  37. Honma S, Kawamoto T, Takagi Y, Fujimoto K, Sato F, Noshiro M, et al. Dec1 and Dec2 are regulators of the mammalian molecular clock. *Nature* (2002) **419**:841844. doi:10.1038/nature01123
  38. Amir S, Stewart J. Conditioned fear suppresses light-induced resetting of the circadian clock. *Neuroscience* (1998) **86**:345–51. doi:10.1016/S0306-4522(98)00172-9
  39. Loh DH, Navarro J, Hagopian A, Wang LM, Deboer T, Colwell CS. Rapid changes in the light/dark cycle disrupt memory of conditioned fear in mice. *PLoS One* (2010) **5**(9):e12546. doi:10.1371/journal.pone.0012546
  40. Chaudhury D, Colwell CS. Circadian modulation of learning and memory in fear conditioned mice. *Behav Brain Res* (2002) **133**:95–108. doi:10.1016/S0166-4328(01)00471-5
  41. Kriegstein K, Strelau J, Schober A, Sullivan A, Unsicker K. TGF- $\beta$  and the regulation of neuron survival and death. *J Physiol Paris* (2002) **96**:25–30. doi:10.1016/S0928-4257(01)00077-8
  42. Lamarca V, Marzo I, Sanz-Clemente A, Carrodeguas JA. Exposure of any of two proapoptotic domains of presenilin 1-associated protein/mitochondrial carrier homolog 1 on the surface of mitochondria is sufficient for induction of apoptosis in a Bax/Bak-independent manner. *Eur J Cell Biol* (2008) **87**:325–34. doi:10.1016/j.ejcb.2008.02.004
  43. Baumgartel K, Genoux D, Welzl H, Tweedie-Cullen RY, Koshibu K, Livingstone Zatchej M, et al. Control of the establishment of aversive memory by calcineurin and Zif268. *Nat Neurosci* (2008) **11**:572–8. doi:10.1038/nn.2113
  44. Li L, Yun SH, Keblesh J, Trommer BL, Xiong H, Radulovic J, et al. Egr3, a synaptic activity regulated transcription factor that is essential for learning and memory. *Mol Cell Neurosci* (2007) **35**:76–88. doi:10.1016/j.mcn.2007.02.004
  45. Capron DW, Cogle JR, Ribeiro JD, Joiner TE, Schmidt NB. An interactive model of anxiety sensitivity relevant to suicide attempt history and future suicidal ideation. *J Psychiatr Res* (2012) **46**:174–80. doi:10.1016/j.jpsychires.2011.10.009
  46. Hendin H, Haas AP. Suicide and guilt as manifestations of PTSD in Vietnam combat veterans. *Am J Psychiatry* (1991) **148**:586–91.
  47. Brent D, Melhem N, Turecki G. Pharmacogenomics of suicidal events. *Pharmacogenomics* (2010) **11**:793–807. doi:10.2217/pgs.10.64
  48. Kekesi KA, Juhasz G, Simor A, Gulyassy P, Szego EM, Hunyadi-Gulyas E, et al. Altered functional protein networks in the prefrontal cortex and amygdala of victims of suicide. *PLoS One* (2012) **7**:e50532. doi:10.1371/journal.pone.0050532
  49. Sohal AP, Montgomery T, Mitra D, Ramesh V. TUBA1A mutation-associated lissencephaly: case report and review of the literature. *Pediatr Neurol* (2012) **46**:127–31. doi:10.1016/j.pediatrneurol.2011.11.017
  50. Cluzeau CV, Watkins-Chow DE, Fu R, Borate B, Yanjanin N, Dail MK, et al. Microarray expression analysis and identification of serum biomarkers for Niemann-Pick disease, type C1. *Hum Mol Genet* (2012) **21**:3632–46. doi:10.1093/hmg/dds193
  51. Li XQ, Chen D, Zhang ZX, Qu QM, Zhang JW. Association between cathepsin D polymorphism and Alzheimer's disease in a Chinese Han population. *Dement Geriatr Cogn Disord* (2004) **18**:115–9. doi:10.1159/000079189
  52. Lloyd-Evans E, Morgan AJ, He X, Smith DA, Elliot-Smith E, Sillence DJ, et al. Niemann-Pick disease type C1 is a sphingosine storage disease that causes deregulation of lysosomal calcium. *Nat Med* (2008) **14**:12471255. doi:10.1038/nm.1876
  53. May FE, Smith DJ, Westley BR. The human cathepsin D-encoding gene is transcribed from an estrogen-regulated and a constitutive start point. *Gene* (1993) **134**:277–82. doi:10.1016/0378-1119(93)90107-E
  54. Hong D, Chen HX, Yu HQ, Wang C, Deng HT, Lian QQ, et al. Quantitative proteomic analysis of dexamethasone-induced effects on osteoblast differentiation, proliferation, and apoptosis in MC3T3-E1 cells using SILAC. *Osteoporos Int* (2011) **22**:2175–86. doi:10.1007/s00198-010-1434-8
  55. Zhang L, Su TP, Choi K, Maree W, Li CT, Chung MY, et al. P11 (S100A10) as a potential biomarker of psychiatric patients at risk of suicide. *J Psychiatr Res* (2011) **45**:435–41. doi:10.1016/j.jpsychires.2010.08.012
  56. Braga MF, roniadou-Anderjaska V, Li H. The physiological role of kainate receptors in the amygdala. *Mol Neurobiol* (2004) **30**:127–41. doi:10.1385/MN:30:2:127
  57. Rogawski MA, Gryder D, Castaneda D, Yonekawa W, Banks MK, Li H. GluR5 kainate receptors, seizures, and the amygdala. *Ann N Y Acad Sci* (2003) **985**:150–62. doi:10.1111/j.1749-6632.2003.tb07079.x
  58. Braga MF, Roniadiou-Anderjaska V, Xie J, Li H. Bidirectional modulation of GABA release by presynaptic glutamate receptor 5 kainate receptors in the basolateral amygdala. *J Neurosci* (2003) **23**:442–52. doi:10.1385/MN:30:2:127
  59. Li H, Chen A, Xing G, Wei ML, Rogawski MA. Kainate receptor-mediated heterosynaptic facilitation in the amygdala. *Nat Neurosci* (2001) **4**:612–20. doi:10.1038/88432
  60. Li H, Rogawski MA. GluR5 kainate receptor mediated synaptic transmission in rat basolateral amygdala in vitro. *Neuropharmacology* (1998) **37**:1279–86. doi:10.1016/S0028-3908(98)00109-9
  61. Weeks SR, McAuliffe CL, Durussel D, Pasquina PF. Physiological and psychological fatigue in extreme conditions: the military example. *PMR* (2010) **2**:438–41. doi:10.1016/j.pmrj.2010.03.023
  62. Dunning KR, Cashman K, Russell DL, Thompson JG, Norman RJ, Robker RL. Betaoxidation is essential for mouse oocyte developmental competence and early embryo development. *Biol Reprod* (2010) **83**:909–18. doi:10.1095/biolreprod.110.084145
  63. Zhang HN, Wu J, Jin T, Chang M, Sun L. Transient elevation of synaptosomal mitochondrial proteins and Hsp70 early in a rat model of chronic cerebrovascular hypoperfusion. *Neurol Sci* (2013) **34**:471–7. doi:10.1007/s10072-012-1063-4
  64. Huh TL, Kim YO, Oh IU, Song BJ, Inazawa J. Assignment of the human mitochondrial NAD $^{+}$ -specific isocitrate dehydrogenase  $\alpha$  subunit (IDH3A) gene to 15q25.1->q25.2 by in situ hybridization. *Genomics* (1996) **32**:295–6. doi:10.1006/geno.1996.0120
  65. Lwin WW, Park K, Wauson M, Gao Q, Finn PW, Perkins D, et al. Systems biology approach to transplant tolerance: proof of concept experiments using RNA interference (RNAi) to knock down hub genes in Jurkat and HeLa cells in vitro. *J Surg Res* (2012) **176**:e41–6. doi:10.1016/j.jss.2011.12.002
  66. Arun P, bu-Taleb R, Oguntayo S, Wang Y, Valiyaveetil M, Long J, et al. Acute mitochondrial dysfunction after blast exposure: potential role of mitochondrial glutamate oxaloacetate transaminase. *J Neurotrauma* (2013) **30**:1645–51. doi:10.1089/neu.2012.2834
  67. Young SN. The effect of raising and lowering tryptophan levels on human mood and social behaviour. *Philos Trans R Soc Lond B Biol Sci* (2013) **368**:20110375. doi:10.1098/rstb.2011.0375

68. Hoge EA, Brandstetter K, Moshier S, Pollack MH, Wong KK, Simon NM. Broad spectrum of cytokine abnormalities in panic disorder and posttraumatic stress disorder. *Depress Anxiety* (2009) **26**:447–55. doi:10.1002/da.20564
69. Mommersteeg PM, Vermetten E, Kavelaars A, Geuze E, Heijnen CJ. Hostility is related to clusters of T-cell cytokines and chemokines in healthy men. *Psychoneuroendocrinology* (2008) **33**:1041–50. doi:10.1016/j.psyneuen.2008.05.007
70. Song Y, Zhou D, Guan Z, Wang X. Disturbance of serum interleukin-2 and interleukin-8 levels in posttraumatic and non-posttraumatic stress disorder earthquake survivors in northern China. *Neuroimmunomodulation* (2007) **14**:248–54. doi:10.1159/000112050
71. Meucci O, Fatatis A, Simen AA, Bushell TJ, Gray PW, Miller RJ. Chemokines regulate hippocampal neuronal signaling and gp120 neurotoxicity. *Proc Natl Acad Sci U S A* (1998) **95**:14500–5. doi:10.1073/pnas.95.24.14500
72. Haroon E, Raison CL, Miller AH. Psychoneuroimmunology meets neuropsychopharmacology: translational implications of the impact of inflammation on behavior. *Neuropsychopharmacology* (2012) **37**:137–62. doi:10.1038/npp.2011.205
73. Raison CL, Capuron L, Miller AH. Cytokines sing the blues: inflammation and the pathogenesis of depression. *Trends Immunol* (2006) **27**:24–31. doi:10.1016/j.it.2005.11.006
74. Smith AK, Conneely KN, Kilaru V, Mercer KB, Weiss TE, Bradley B, et al. Differential immune system DNA methylation and cytokine regulation in post-traumatic stress disorder. *Am J Med Genet B Neuropsychiatr Genet* (2011) **156B**:700–8. doi:10.1002/ajmg.b.31212
75. Zlotnik A, Yoshie O. The chemokine superfamily revisited. *Immunity* (2012) **36**:705–16. doi:10.1016/j.immuni.2012.05.008
76. O'Boyle G, Brain JG, Kirby JA, Ali S. Chemokine-mediated inflammation: identification of a possible regulatory role for CCR2. *Mol Immunol* (2007) **44**:1944–53. doi:10.1016/j.molimm.2006.09.033
77. Harris RB, Mitchell TD, Simpson J, Redmann SM Jr., Youngblood BD, Ryan DH. Weight loss in rats exposed to repeated acute restraint stress is independent of energy or leptin status. *Am J Physiol Regul Integr Comp Physiol* (2002) **282**:R77–88.
78. Liao SC, Lee MB, Lee YJ, Huang TS. Hyperleptinemia in subjects with persistent partial posttraumatic stress disorder after a major earthquake. *Psychosom Med* (2004) **66**:23–8. doi:10.1097/01.PSY.0000106880.22867.0E
79. von KR, Begre S, Abbas CC, Saner H, Gander ML, Schmid JP. Inflammatory biomarkers in patients with posttraumatic stress disorder caused by myocardial infarction and the role of depressive symptoms. *Neuroimmunomodulation* (2010) **17**:39–46. doi:10.1159/000243084
80. Chang HF, Su CL, Chang CH, Chen YW, Gean PW. The beneficial effects of leptin on REM sleep deprivation-induced cognitive deficits in mice. *Learn Mem* (2013) **20**:328335. doi:10.1101/lm.030775.113
81. Gupta S, Kim SY, Artis S, Molfese DL, Schumacher A, Sweatt JD, et al. Histone methylation regulates memory formation. *J Neurosci* (2010) **30**:3589–99. doi:10.1523/JNEUROSCI.3732-09.2010
82. Moriya T, Kouzu Y, Shibata S, Kadohara H, Fukunaga K, Miyamoto E, et al. Close linkage between calcium/calmodulin kinase II alpha/beta and NMDA-2A receptors in the lateral amygdala and significance for retrieval of auditory fear conditioning. *Eur J Neurosci* (2000) **12**:3307–14. doi:10.1046/j.1460-9568.2000.00203.x
83. Trollope AF, Gutierrez-Mecinas M, Mifsud KR, Collins A, Saunderson EA, Reul JM. Stress, epigenetic control of gene expression and memory formation. *Exp Neurol* (2012) **233**:3–11. doi:10.1016/j.expneurol.2011.03.022
84. Takei S, Morinobu S, Yamamoto S, Fuchikami M, Matsumoto T, Yamawaki S. Enhanced hippocampal BDNF/TrkB signaling in response to fear conditioning in an animal model of posttraumatic stress disorder. *J Psychiatr Res* (2011) **45**:460–8. doi:10.1016/j.jpsychires.2010.08.009
85. Zhang L, Li H, Hu X, Li XX, Smerin S, Ursano R. Glucocorticoid-induced p11 overexpression and chromatin remodeling: a novel molecular mechanism of traumatic stress? *Med Hypotheses* (2011) **76**:774–7. doi:10.1016/j.mehy.2011.02.015
86. Deroo BJ, Archer TK. Glucocorticoid receptor-mediated chromatin remodeling in vivo. *Oncogene* (2001) **20**:3039–46. doi:10.1038/sj.onc.1204328
87. Si J, Yang J, Xue L, Yang C, Luo Y, Shi H, et al. Activation of NF-kappaB in basolateral amygdala is required for memory reconsolidation in auditory fear conditioning. *PLoS One* (2012) **7**:e43973. doi:10.1371/journal.pone.0043973

**Conflict of Interest Statement:** The Guest Associate Editor Yumin Zhang declares that, despite being affiliated to the same institution as authors He Li, Stanley E. Smerin, Lei Zhang, Min Jia, Guoqiang Xing, Jillian Wen, David Benedek, and Robert Ursano, the review process was handled objectively and no conflict of interest exists. The authors declare that the research was conducted in the absence of any commercial or financial relationships that could be construed as a potential conflict of interest.

Received: 03 December 2013; accepted: 15 August 2014; published online: 23 September 2014.

Citation: Li H, Li X, Smerin SE, Zhang L, Jia M, Xing G, Su YA, Wen J, Benedek D and Ursano R (2014) Mitochondrial gene expression profiles and metabolic pathways in the amygdala associated with exaggerated fear in an animal model of PTSD. *Front. Neurol.* 5:164. doi: 10.3389/fneur.2014.00164

This article was submitted to Neurotrauma, a section of the journal *Frontiers in Neurology*.

Copyright © 2014 Li, Li, Smerin, Zhang, Jia, Xing, Su, Wen, Benedek and Ursano. This is an open-access article distributed under the terms of the Creative Commons Attribution License (CC BY). The use, distribution or reproduction in other forums is permitted, provided the original author(s) or licensor are credited and that the original publication in this journal is cited, in accordance with accepted academic practice. No use, distribution or reproduction is permitted which does not comply with these terms.



# Efficacy and safety of *Panax notoginseng* saponin therapy for acute intracerebral hemorrhage, meta-analysis, and mini review of potential mechanisms of action

Dongying Xu<sup>1\*</sup>, Ping Huang<sup>1</sup>, Zhaosheng Yu<sup>2</sup>, Daniel H. Xing<sup>3</sup>, Shuai Ouyang<sup>4</sup> and Guoqiang Xing<sup>5\*</sup>

<sup>1</sup> Faculty of Nursing, Guangxi University of Chinese Medicine, Nanning, China

<sup>2</sup> Department of Oncology, Huanggang Hospital of Traditional Chinese Medicine, Huanggang, China

<sup>3</sup> Thomas Wootton High School, Rockville, MD, USA

<sup>4</sup> School of Business, University of Alberta, Edmonton, AB, Canada

<sup>5</sup> Lotus Biotech.com LLC, Rockville, MD, USA

## Edited by:

Yumin Zhang, Uniformed Services  
University of the Health Sciences,  
USA

## Reviewed by:

Stefan Plantman, Karolinska  
Institutet, Sweden  
Zhengtao Wang, Shanghai University  
of Traditional Chinese Medicine, China

## \*Correspondence:

Dongying Xu, Faculty of Nursing,  
Guangxi University of Chinese  
Medicine, 61 Dongge Road, Nanning  
530022, Guangxi, China  
e-mail: donnaxu\_cn@hotmail.com;  
Guoqiang Xing, Lotus Biotech.com  
LLC, John Hopkins University-MCC,  
9601 Medical Center Drive, Suite 227,  
Rockville, MD 20850, USA  
e-mail: gxing99@yahoo.com

Intracranial/intracerebral hemorrhage (ICH) is a leading cause of death and disability in people with traumatic brain injury (TBI) and stroke. No proven drug is available for ICH. *Panax notoginseng* (total saponin extraction, PNS) is one of the most valuable herb medicines for stroke and cerebrovascular disorders in China. We searched for randomized controlled clinical trials (RCTs) involving PNS injection to treat cerebral hemorrhage for meta-analysis from various databases including the Chinese Stroke Trials Register, the trials register of the Cochrane Complementary Medicine Field, the Cochrane Central Register of Controlled Trials, MEDLINE, Chinese BioMedical disk, and China Doctorate/Master Dissertations Databases. The quality of the eligible trials was assessed by Jadad's scale. Twenty (20) of the 24 identified randomized controlled trials matched the inclusive criteria including 984 ICH patients with PNS injection and 907 ICH patients with current treatment (CT). Compared to the CT groups, PNS-treated patients showed better outcomes in the effectiveness rate (ER), neurological deficit score, intracranial hematoma volume, intracerebral edema volume, Barthel index, the number of patients died, and incidence of adverse events. **Conclusion:** PNS injection is superior to CT for acute ICH. A review of the literature shows that PNS may exert multiple protective mechanisms against ICH-induced brain damage including hemostasis, anti-coagulation, anti-thromboembolism, cerebral vasodilation, invigorated blood dynamics, anti-inflammation, antioxidation, and anti-hyperglycemic effects. Since vitamin C and other brain cell activators (BCA) that are not considered common practice were also used as parts of the CT in several trials, potential PNS and BCA interactions could exist that may have made the effect of PNS therapy less or more impressive than by PNS therapy alone. Future PNS trials with and without the inclusion of such controversial BCAs as part of the CT could clarify the situation. As PNS has a long clinical track record in Asia, it could potentially become a therapy option to treat ICH in the US and Europe. Further clinical trials with better experimental design could determine the long-term effects of PNS treatment for TBI and stroke.

**Keywords:** notoginsenosides, botanical medicine, nutraceuticals, TBI and stroke recovery, randomized controlled clinical trials, hemostasis, anti-coagulation, pharmacological mechanisms

## INTRODUCTION

Traumatic brain injury (TBI) is a leading cause of death and disability in young people (1). Every year approximately 1.5 million people die and at least 10 million people are hospitalized after TBI (2). The incidence of TBI fatality and disability rates are higher in developing countries than in developed countries (3).

Secondary brain damage due to continued intracranial and intracerebral bleeding and hemorrhage swelling is a common cause of morbidity and mortality (4, 5). In one clinical trial, 56% of the patients with mild, moderate and severe TBI developed intracranial hemorrhage (6). Another study showed that 51% of TBI patients developed progressive intracranial/intracerebral

hemorrhage (ICH), and hemorrhage expansion during the first 24–48 h after hospital admission (7). Prognostic studies have shown that ICH is associated with increased mortality and disability 6 months after injury (8, 9). One recent survey reported that TBI patients who developed ICH showed a 10-fold increase in stroke incidence 3 months after the injury when compared to TBI patients without ICH (10).

Acute intracerebral hemorrhage (AICH) accounts for only about 10% of the people with stroke, and is the most lethal form of stroke compared to the ischemic stroke. Thus, ICH is among the most devastating disorders and a leading cause of disability and mortality of people with severe stroke, hypertension,



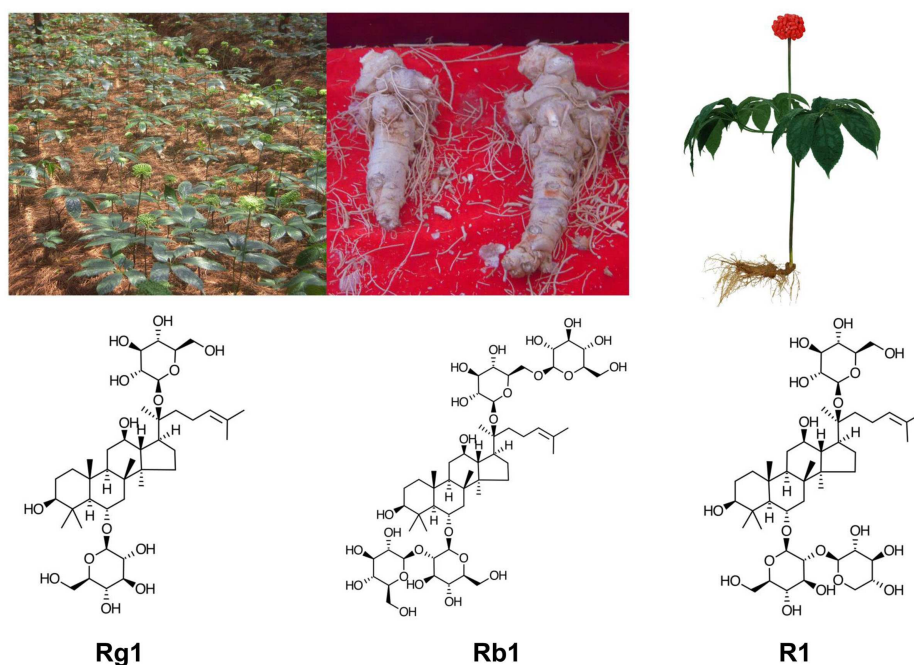
and TBI (11). During the last decade, the incidence of ICH has increased steadily in Asian countries (12) and it accounts for ~20% and ~10% of strokes in low-middle and high income countries, respectively (13).

So far, few proven therapies exist for ICH. Hematoma expansion, perihematomal edema with increased intracranial pressure, intraventricular extension of hemorrhage with hydrocephalus, seizures, venous thrombotic events, hyperglycemia, increased blood pressure, fever, and infections are among the complications of ICH as recently reviewed by Balami and Buchan (14). Current treatment of ICH is supportive and life-sustaining rather than a complete cure that aims to limit secondary brain damage and associated complications (15, 16). Considering the very limited therapeutic options for patients with ICH, recent studies suggest that evidence-based alternative and complimentary medicines could be effective in reducing the adverse effects early in the course of ICH and in improving its prognosis as found in the treatment of cerebral ischemia (17).

*Panax notoginseng* [(Burk.) F.H. Chen] (also called Sanqi in Chinese), is one of the most valuable Chinese herbal medicine. *P. notoginseng* is a perennial plant, mainly grown in the high mountain areas of Southwest China. Its roots are harvested after 3–5 years of growth (Figure 1). *P. notoginseng* has numerous hematological and pharmacological effects, which include regulation of platelet aggregation and platelet free calcium levels, reducing blood viscosity, improving local blood supply and circulation to end stasis, cerebral vasodilation, analgesic, hypolipidemic, hemostatic, anti-edema, anti-hyperglycemia, antioxidation, anti-inflammation, and anti-apoptosis (18, 19).

*P. notoginseng* saponins extract (PNS) ameliorate learning and memory deficits in animals (20–26), probably by inhibiting oxidative stress and apoptosis and by stimulating neurogenesis (21, 22, 27–33). PNS is effective against ICH, transient focal ischemia, and cerebral infarction probably in part through improved brain blood circulation and energy metabolism (34–38). *P. notoginseng* has been used alone and as a key tonic ingredient in many other patent Chinese medicine for treatment of a variety of health conditions and has been proved to be effective in animal models of cerebral ischemia/reperfusion injury, arterial thrombosis, cardiovascular disorders, Alzheimer disease, diabetes and obesity, erectile dysfunction, neurodegeneration, neuroinflammation, oxidative stress, neurotoxicity, organ injury, and cancer (38–47).

The ability of notoginseng to normalize hemorheological parameters is due to the presence of multiple active compounds including different ginsenosides and notoginsenosides, some of which appear to have similar yet differential effects. Ginsenosides Rg1 and Rb1, and notoginsenoside R1 are the main active ingredients present in high concentrations in PNS, which contains more than 20 different ginsenosides and notoginsenosides (48–55). Purified and patented PNS under different trade names, i.e., Xuesaitong (51, 56–59), Xueshuantong (60), and Lulutong have been approved for treatment of stroke and other cerebral disorders in China. Intravenous injection of PNS has been developed for critical care because orally administered PNS has a low permeability, poor intestinal absorption, and bioavailability (51, 61, 62) due to the relative large sugar molecular mass (> 500 Da), high molecular flexibility, high hydrogen binding capacity, and low lipophilicity.



**FIGURE 1 |** *Panax notoginseng* (*P. notoginseng*, Sanqi): clockwise from top left: in cultivation, the roots, artistic drawing a Sanqi plant, the main chemical ingredients of PNC: notoginsenoside R1, ginsenosides Rb1, and Rg1.

*In vivo* studies showed marked variability of Rb1 bioavailability among different administration routes to rats: i.v. (intravenous) (100%) > p.v. (portal venous) (59.49%) > i.d. (intra-duodenal) (2.46%) > p.o. (peroral) (0.64%) (63). After absorption, PNS has a long residual time, but individual ginsenosides and notoginsenosides vary in their elimination rate. For example, the half-life is much longer and peak concentration higher for ginsenoside Rb1 than that for ginsenoside Rg1 and notoginsenoside R1, due to the slower clearance and longer residence time of Rb1 (61, 63–67). In fact, ginsenoside Rb1 is considered a pharmacokinetic marker of PNS (67).

Multiple clinical studies have been conducted in China in recent years to explore the use of PNS injection in the treatment of cerebral hemorrhage and ICH. These studies have yet to be systematically evaluated for the efficacy and safety to provide evidence and guidance for further clinical application of PNS for cerebral hemorrhage. Because many of these trials were reported in un-indexed Chinese medical journals, the international research community may not have access to these findings. In this study, we reviewed randomized controlled clinical trials (RCTs) published in Chinese journals that involved PNS injection treatment for ICH. The results suggest that PNS injection has a wide range of different protective mechanisms and is a better treatment than current treatments for ICH.

## MATERIALS AND METHODS

### INCLUSIVE AND EXCLUSIVE CRITERIA

Only RCTs that included a comparison of the efficacy and safety of *P. notoginseng* saponin (PNS) injection treatment with that of current treatment (CT) in patients with AICH resulted from hypertension or wind stroke were included. The diagnostic criteria of acute ICH in trials were in accordance with the criteria of diagnosis of various types of cerebrovascular disease updated at the 4th Annual Conferences of Chinese Society of Neurology (68): subjects should not suffer from secondary AICH or other diseases such as hematologic diseases, intracranial aneurysms, intracranial tumors, cerebral arteries, venous malformations, severe comas, and cardiac, hepatic, or renal diseases. There was no restriction on race, but the majority of patients were thought to be of the Chinese Han ethnic group. The PNS intervention is defined as intravenous drip of the commercially available PNS preparations that are approved by Chinese Food and Drug Administration (CFDA) for clinical use alone, or in combination with other routine therapies for subjects in the treatment groups. The control ICH subjects received current treatment other than PNS treatment. The outcome measures included the effectiveness rate (ER), neurological deficit score (NDS), intracerebral hematoma volume (IHV), intracerebral edema volume (IEV), Barthel index (BI), and number of patients died (NDP), as well as incidence of adverse events after treatments with PNS or CT, respectively. The BI is an interviewer-based disability profile scale developed by D.W. Barthel in 1965 to assess physical functions, specifically self-care abilities and ambulation (e.g., stair climbing) in 10 areas, including bowel and bladder control. The patient is scored from 0 to 15 points in various categories, depending on his or her need for help, such as in feeding, bathing, dressing, and walking.

### SEARCH STRATEGY

The search strategy was developed by modifying the reported strategies used for herbal medicines in a Cochrane review (69). We retrieved the literatures of relevant clinical trials by electronic searching and by hand searching, regardless of language or publication status. Many electronic databases were searched, including the Chinese Stroke Trials Register, the trials register of the Cochrane Complementary Medicine Field, the Cochrane Central Register of Controlled Trials, MEDLINE, CINAHL, AMED, Chinese BioMedical disk, Wanfang Chinese Scientific Journal Database, VIP, China National Knowledge Infrastructure, Traditional Chinese Medicine Database, Chinese Medical Current Contents, China Doctorate/Master Dissertations Full-Text Databases, and China Proceedings of Conference Databases. The reference lists of retrieved papers were further scanned for any possible titles matching the inclusive criteria. A hand search with an emphasis on relevant journals pertaining to stroke, senile disease, neurology, complementary, and alternative medicine was carried out to explore entities matching the inclusive criteria among periodicals, journals, and symposium abstracts found in libraries of Guangxi Chinese Medical University (date of last search: December, 2013).

### DATA EXTRACTION

Full-text articles of each potential eligible trial were retrieved and assessed by two independent reviewers (Dongying Xu and Ping Huang) to determine if the articles should be recruited and further analyzed according to the inclusive and exclusive criteria. Missing information was sought by contacting the article authors. A data abstraction form was used to summarize key information from included trials, and key information was extracted by one reviewer and confirmed by the other. Any disagreements were resolved by discussion.

### DATA ANALYSIS

The meta-analysis was carried out by using Revman 5.3 software (Cochrane Collaboration) to combine and analyze the data from the individual trials. The statistical validity of combining various trials was assessed by examining the homogeneity of outcomes from trials using a Q-test (Mantel–Haenszel Chi-square test). The results of the combined trials were calculated with random or fixed-effect models. The measurements of each category's data were evaluated by a weighted mean difference (WMD) or odd ratio (OR), and by 95% confidence intervals (95% CI). The methodological quality of all included trials was assessed by Jadad's scale that evaluated randomization, double blinding, and dropout rate of the trials by ranking them with 1–5 points. The trials that scored with 1 or 2 points were considered low-quality trials, while those that scored with 3–5 points were considered high-quality trials (70).

## RESULTS

### EXCLUDED AND INCLUDED TRIAL

The literature search yielded a total of 24 RCTs conducted in China that treated acute intracerebral hemorrhagic patients with intravenous drip of PNS. However, four of these trials were excluded as they did not match the inclusive criteria. Specifically, they are (1) no-comparison made between PNS and RT in trials (two trials)

and (2) no or unclear measurement report in trials (two trials). Therefore, only 20 trials published in Chinese medical journals, with 1,891 ICH patients that met the study criteria, were included for analysis (71–90).

The characteristics of the patients are shown in **Table 1**. The trials' size varied from 24 to 200 participants, with an average of 46 patients per trial. All of the patients are adults ranged from 24 to 92 years old with more males than females included (62% males vs. 38% females). Hemorrhage/ICH duration was reported in 13 trials, ranging from 4 h to 20 days. The main causes of intracerebral hemorrhage were wind stroke (15 trials) and hypertension (2 trials) (**Table 1**).

The classification of the patients (sites of bleeding) is shown in **Table 2**. Of these, 984 ICH patients received PNS injection treatments that lasted between 10 and 70 days, and 907 patients received current treatments (**Table 2**). Of the PNS injection treatments, 6 trials used Xuesaitong PNS freeze-dry powder injections (72, 73, 77–79, 85), 7 trials used Xuesaitong injections (74, 75, 84, 86–88, 90), 5 trials used Xueshuantong injections (76, 80, 81, 83, 89), one trial used Lulutong injections (71), and one trial used Sanqi Zaogan injection powder (82). For the CT control groups, dehydration, control of intracranial pressure, anti-hypertensive treatment, symptomatic treatment, neurotrophyl medicine, and brain cell activators (BCA) were used. Mannitol, glycerol, and/or ructose injection was used for dehydration (**Table 2**).

## OUTCOME MEASUREMENT

For evaluating the therapeutic and adverse effects of the PNS treatment and the control groups, the outcome assessment of this study was focused on the ER, NDS, intracerebral hematoma volume (IHV), IEV, BI, and the NDP. The incidence of adverse events after treatments was also evaluated. Thirteen trials reported the number of improved patients. Six trials reported NDS. Eight trials reported intracerebral hematoma volume. Three trials reported intracranial edema volume. Two trials reported BI, and six trials reported the NDP.

## META-ANALYSIS ON PNS EFFICACY

### Sites of bleeding

There were 15 trials involving 687 ICH patients in the PNS group and 583 patients in the CT group (total of 1,270 ICH patients) that provided detailed descriptions of the bleeding sites including (unilateral and/or bilateral) the basal ganglia, external capsule, internal capsule, frontal lobe, medial occipital lobe, arietal lobe, cerebellum, brainstem, ventricles, and supratentorial hemorrhage (**Table 3**). Among them, the basal ganglia region was the most common site of hemorrhage, accounting for 45.85% (315/687) of patients in the PNS group, and 41.51% (242/583) of patients in the CT group.

### Effectiveness rate

By using the fixed-effect model, **Figure 2** shows the results of meta-analyses on the ER, comparing the therapeutic effect of PNS injection with that of the CT. A total of 13 trials reported the effect rate, which was categorized into three subgroups by the evaluating time: (1) 7 trials assessed the ER at the end of 2 weeks of treatment, (2) 2 trials assessed the rate at the end of 3 weeks, and (3) 5 trials assessed

the rate at the end of 4 weeks. There was no significant heterogeneity among these three subgroups ( $P = 0.47$ ). The total overall effect showed significant statistical difference in ER between the PNS and CT groups ( $OR = 2.70$ ; 95%  $CI = 2.16, 3.38$ ;  $P < 0.00001$ ). There were significant differences in ER between PNS and CT groups assessed at 2 weeks ( $OR = 2.73$ ; 95%  $CI = 1.92, 3.88$ ;  $P < 0.00001$ ), 3 weeks ( $OR = 2.43$ ; 95%  $CI = 1.54, 3.83$ ;  $P = 0.0001$ ), and 4 weeks ( $OR = 2.87$ ; 95%  $CI = 1.97, 4.18$ ;  $P < 0.00001$ ) after the start of treatment. No significant heterogeneity was presented in the analyses of the data ( $P = 0.55, 0.61$ , and  $0.13$ ) in the three subgroups, respectively. Thus, ICH patients with PNS treatment showed a better therapeutic ER than those in the CT group.

### Neurological deficit score

Neurological deficit score is an important index for the diagnosis of symptom severity and functional recovery of the patients (91). Six of the selected trials reported NDS in this study, with three of them showing NDS (74, 77, 86) at 7, 15, 21, 28, and 30 days after PNS treatment (**Figure 3**). No significant differences in NDS were found between the PNS and CT groups at 7 (77) and 15 days (86). The results of 21 days are controversial, since one trial showed no difference between the PNS and CT groups (74), whereas the other showed a better NDS in the PNS group than in the CT group (77). The NDS was significantly lower in PNS group than that in CT group at 28 days (86) and 40 days (74) after the treatment ( $P < 0.05, P < 0.01$ , respectively). No heterogeneity ( $P = 0.48$ ) was found in the NDS. When all data were combined, the results showed significantly reduced NDS in PNS-treated ICH patients than in ICH patients of the CT group ( $MD = 4.36$ ; 95%  $CI = 3.07, 5.65$ ;  $P < 0.00001$ ) (**Figure 3**).

### Intracerebral hematoma volume

Of the 8 trials that reported IHV, 6 trials showed no differences in IHV between the PNS and CT groups after 4–7 days of treatment (82, 84, 85, 88, 89) ( $MD = -0.37$ ; 95%  $CI = -1.60, 0.87$ ;  $P = 0.58$ ) (**Figure 4**). Three trials (82, 84, 87) showed significant improvement in IHV in the PNS group (about 25% less IHV) than in the CT group at 10–14 days after the treatment ( $MD = -3.80$ ; 95%  $CI = -5.87, -1.74$ ;  $P = 0.0003$ ). Four trials showed significantly smaller IHV values in the PNS group (about 40% less) than in the CT group at 20–21 days after the treatment (74, 81, 84, 89) ( $MD = -4.82$ ; 95%  $CI = -8.32, -1.33$ ;  $P = 0.007$ ). Another 4 trials showed significantly smaller IHV values in the PNS group (about 50% less) than in the CT group at 28–40 days after the treatment (74, 82, 85, 88) ( $MD = -5.15$ ; 95%  $CI = -5.98, -4.33$ ;  $P < 0.00001$ ). These results show a time-dependent effect of PNS treatment on ICH, i.e., significant improvement in IHV occurs after 21 days or more of PNS treatment, but not in the 1st week of treatment (10–14 days,  $MD = -3.8$ ; 20–21 days,  $MD = -4.82$ ; 28–40 days,  $MD = -5.15$ ).

### Intracerebral edema volume

**Figure 5** shows the results of meta-analyses on IEV. Only three trials (82, 85, 89) assessed IEV in ICH patients with PNS/CT treatment 7 days after ICH onset. Two of the trials with a duration of 3–4 weeks showed significant differences in IEV between the PNS and CT groups (65, 68). The other trial showed no significant difference between the two groups after 14 days of PNS injection due

**Table 1 | Baseline characteristics of each trial used in the meta-analysis.**

Authors	Sample size (F/M) Average age (range)	Disease duration	Cause	Authors	Sample size (F/M) Average age (range)	Disease duration	Cause
Guo et al. (90)	PNS: $n = 100$ (40/60) 57.4 (30–70) CT: $n = 100$ (38/62) 57.2 (31–69.5)	$\geq 3D$	WS WS	Gao et al. (86)	PNS: $n = 28$ (12/16) 65.68 $\pm$ 9.55 CT: $n = 24$ (11/13) 65.88 $\pm$ 9.47	$\leq 24H$	WS WS
He et al. (89)	PNS: $n = 12$ (5/7) 69.20 $\pm$ 14.32 CT: $n = 12$ (4/8) 67.22 $\pm$ 13.83	$\leq 48H$	WS WS	Chen (87)	PNS: $n = 61$ (23/38) 60.7 $\pm$ 7.7 (38–74) CT: $n = 60$ (19/41) 61.3 $\pm$ 8.0 (36–75)	$\geq 7D$	WS WS
Xu and Dong (72)	PNS: $n = 42$ (17/25) 60.63 (33–80) RT: $n = 40$ (17/23) 58.30 (34–79)	NR	WS WS	<i>CT, current treatment; D, day; H, hour; HYTN, hypertension; N/A, not applicable; NR, not reported; PNS, Panax notoginseng saponin; WS, wind stroke [Stroke including hemorrhagic cerebrovascular accident (CVA), ischemic infarction CVA and subarachnoid hemorrhage, etc. is often collectively referred to as wind stroke in traditional Chinese medicine because of its sudden and acute onset, sudden loss of consciousness with unilateral weakness, numbness, paralysis and dysphasia with or without experiencing unconsciousness, multiple symptoms and rapid alterations in manifestations that are similar to the natural characteristics of wind, which is changing rapidly].</i>			
Li et al. (88)	A:PNS: $n = 60$ (25/35) (24–78) B:PNS: $n = 55$ (22/33) (31–75) C:CT: $n = 60$ (26/34) (40–82)	$< 24H$	WS WS WS	to a small sample size (89) (MD = 14.87; 95% CI = –0.37, 30.11). Analysis of the combined data showed significant statistical difference in IEV values between the PNS and CT groups (MD = 10.78; 95% CI = 9.07, 12.49; $P < 0.00001$ ) (Figure 5). On average, PNS treatment reduced IEV value by about 50%.			
Li and Yang (73)	PNS: $n = 48$ (13/35) 57.2 $\pm$ 9.6 (45–75) CT: $n = 44$ (12/32) 56.8 $\pm$ 9.4 (43–74)	$> 20D$	WS WS	<b>Barthel index</b>			
Tian et al. (74)	PNS: $n = 36$ (16/20) 60.32 $\pm$ 5.14 CT: $n = 30$ (16/14) 58.41 $\pm$ 6.33	NR	WS WS	The BI is a measure of functional disability and represents the current quality of life (92). Only 2 trials of the 20 trials examined in this study reported BI (76, 83). The results showed that PNS treatment significantly increased BI when compared to the CT (MD = –11.73; 95% CI = –19.31, –4.16; $P = 0.002$ ) (Figure 6). One trial involved 10 weeks of PNS treatment after ICH and the result showed no significant difference in BI at 14 days after PNS treatment ( $P > 0.05$ ), but significant differences were observed at 28 days ( $P < 0.05$ ) and 90 days after the treatment ( $P < 0.01$ ), suggesting that a relatively long course of PNS treatment is necessary for significant improvement in functional recovery (76).			
Li and Sun (75)	PNS: $n = 29$ (9/20) 58.5 $\pm$ 10.8 (31–82) CT: $n = 31$ (9/22) 57.5 $\pm$ 11.2 (33–81)	NR	NR NR	<b>Mortality rate</b>			
Xie et al. (76)	PNS: $n = 24$ (6/18) 61.1 (34–89) CT: $n = 22$ (6/16) 61.2 (35–92)	NR	NR NR	Figure 7 shows the results of meta-analyses on the NDP. Six trials reported mortality data, showing that 48 of the 715 patients across the six trials died (6.7%). The mortality of ICH patients was significantly lower in the PNS group (13/361, or 3.6%) than in the CT group (35/354, or 9.9%) (Peto OR = 2.78; 95% CI = 1.52, 5.08; $P = 0.0009$ ). The trials were further divided into two subgroups depending on the time of PNS intervention: (1) three trials that started PNS treatment within 48 h of ICH onset (74, 84, 88) and (2) four trials that started PNS treatment at or after 7 days of ICH onset (72, 78, 87). One trial evaluated PNS intervention at both 48 h and 7 days after ICH onset (88). All trials assessed the mortality at the end of the treatment course. The duration of PNS treatment was 4 (72) and 6 (74) weeks, respectively, for 2 of the trials, and was 2 weeks for the other trials. The results showed significant reduction in the mortality of ICH patients treated with			
Chen et al. (77)	PNS: $n = 22$ (7/15) N/A CT: $n = 21$ (7/14) N/A	4H–12H	WS WS				
Dong and Wang (78)	PNS: $n = 40$ (16/24) 60.63 (33–80) CT: $n = 38$ (16/22) 58.3 (34–79)	NR	HYTN HYTN				
Zhang et al. (71)	PNS: $n = 65$ (N/A) 57.6 (35–69) CT: $n = 65$ (N/A) 58.2 (36–70)	NR	WS WS				
Zhou et al. (79)	PNS: $n = 70$ (24/46) 56.8 $\pm$ 10.4 (35–78) CT: $n = 70$ (27/43) 55.6 $\pm$ 10.1 (33–79)	$\leq 7D$	WS WS				
Zheng (80)	PNS: $n = 22$ (N/A) N/A CT: $n = 19$ (N/A) N/A	$< 72H$	N/A N/A				
Tang et al. (81)	PNS: $n = 63$ (25/38) 62.2 $\pm$ 14.6 CT: $n = 63$ (23/40) 62.5 $\pm$ 15.2	3rd	WS WS				
Song (82)	PNS: $n = 39$ (12/27) N/A CT: $n = 39$ (15/24) N/A	$\leq 48H$	WS WS				
Ding et al. (83)	PNS: $n = 15$ (6/9) 55.1 (35–74) CT: $n = 17$ (4/13) 57.7 (44–72)	$< 48H$	WS WS				
Yuan et al. (84)	PNS: $n = 67$ (26/41) 59.2 (39–75) CT: $n = 66$ (27/39) 61.3 (41–75)	NR	WS WS				
Ding and Geng (85)	PNS: $n = 86$ (34/52) 60.2 $\pm$ 8.5 CT: $n = 86$ (37/49) 61.4 $\pm$ 8.2	$\geq 7D$	HYTN HYTN				

(Continued)

**Table 2 | PNS treatment information of the 20 trials included in the meta-analyses.**

Authors	Interventions (sample size) Dosage	Durations	Observations	Adverse incidences (%)
Guo et al. (90)	PNS( <i>n</i> = 100): XST Inj 200 mg/day CT( <i>n</i> = 100): MNT,ST	3 weeks	ER	NO NR
He et al. (89)	PNS( <i>n</i> = 12): XSHT Inj 140 mg/day CT( <i>n</i> = 12): MNT,VC,KCI	2 weeks	IHV,IEV	NR
Xu and Dong (72)	PNS( <i>n</i> = 42): XST FDP 400 mg/day CT( <i>n</i> = 40): DH,ICP,ST	4 weeks	ER,NDP	NR
Li et al. (88)	PNS( <i>n</i> = 55): XST Inj 600 mg/day CT( <i>n</i> = 60): AHT,CICP,ST	2 weeks	ER,NDP,IHV	Sr (5%) NO
Li and Yang (73)	PNS( <i>n</i> = 48): XST FDPI 400 mg/day CT( <i>n</i> = 44): CAS	2 weeks	ER,NDS	NO NR
Tian et al. (74)	PNS( <i>n</i> = 36): XST Inj 200 mg/day CT( <i>n</i> = 30): MNT,FRS,ST	6 weeks	ER,NDP,NDS,IHV	NR
Li and Sun (75)	PNS( <i>n</i> = 29): XST Inj 500 mg/day CT( <i>n</i> = 31): DH,NTM,BCA,ST	4 weeks	ER	NR
Xie et al. (76)	PNS( <i>n</i> = 24): XSHT Inj 400 mg/day CT( <i>n</i> = 22): DH,CICP,ST	10 weeks	ER,BI	NO
Chen et al. (77)	PNS( <i>n</i> = 22): XST FDPI 800 mg/day CT( <i>n</i> = 21): DH,CICP,AHT,ST	2 weeks	NDS	NO
Dong and Wang (78)	PNS( <i>n</i> = 40): XST FDPI 400 mg/day	2 weeks	ER,NDP	NR
Zhang et al. (71)	CT( <i>n</i> = 38): DH,CICP,ST PNS( <i>n</i> = 65): LLT Inj 250 mg/day CT( <i>n</i> = 65): MNT, MGSO <sub>4</sub> ,KCL, INS, Aceglutamide Inj	2 weeks	ER	NO
Zhou et al. (79)	PNS( <i>n</i> = 70): XST FDPI 400 mg/day CT( <i>n</i> = 70): CICP,MNT,FRS Inj, GFI,BCA,AHT,ST	2 weeks	ER,NDS	NR
Zheng (80)	PNS( <i>n</i> = 22): XSHT Inj 300 mg/day CT( <i>n</i> = 19): ST	3 weeks	NDS	NR
Tang et al. (81)	PNS( <i>n</i> = 63): XSHT Inj 300 mg/day CT( <i>n</i> = 63): MNT,VC,ST	3 weeks	IHV	NR
Song (82)	PNS( <i>n</i> = 39): XSHT Inj powder 450 mg/day CT( <i>n</i> = 39): CICP, AHT,ST	4 weeks	IHV,IEV	NR
Ding HY 2008 (83)	PNS( <i>n</i> = 15): XST FDPI 200 mg/day CT( <i>n</i> = 17):AHT, MNT,CICP, ST	2 weeks	BI	NR
Yuan HY 2008 (84)	PNS( <i>n</i> = 67): XST Inj 750 mg/day CT( <i>n</i> = 66): MNT,GFI	2 weeks	ER,NDP	NO NR
Ding and Geng (85)	PNS( <i>n</i> = 86): XSHT Inj 175 mg/day CT( <i>n</i> = 86): CICP, AHT,ST	3 weeks	ER,IHV,IEV	NO
Gao HY 2008 (86)	PNS( <i>n</i> = 28): XST Inj 250 mg/day CT( <i>n</i> = 24): MNT,CICP, AHT,ST	2 weeks	NDS	NR
Chen (87)	PNS( <i>n</i> = 61): SQZG 350 mg/day CT( <i>n</i> = 60): CICP, AHT,ST	2 weeks	ER,NDP,IHV	NR

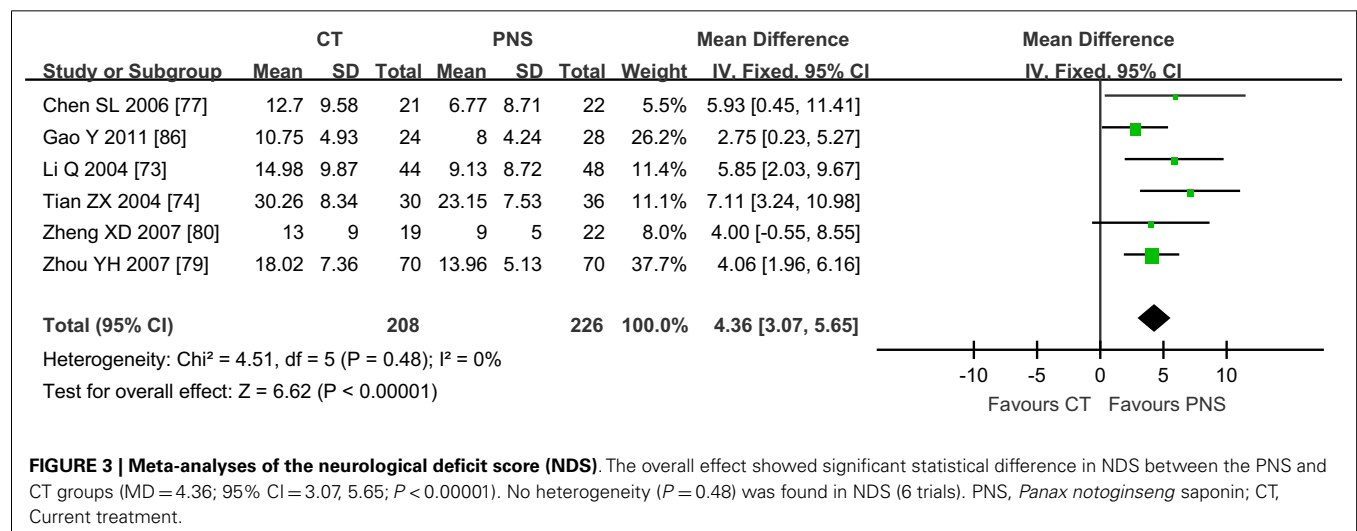
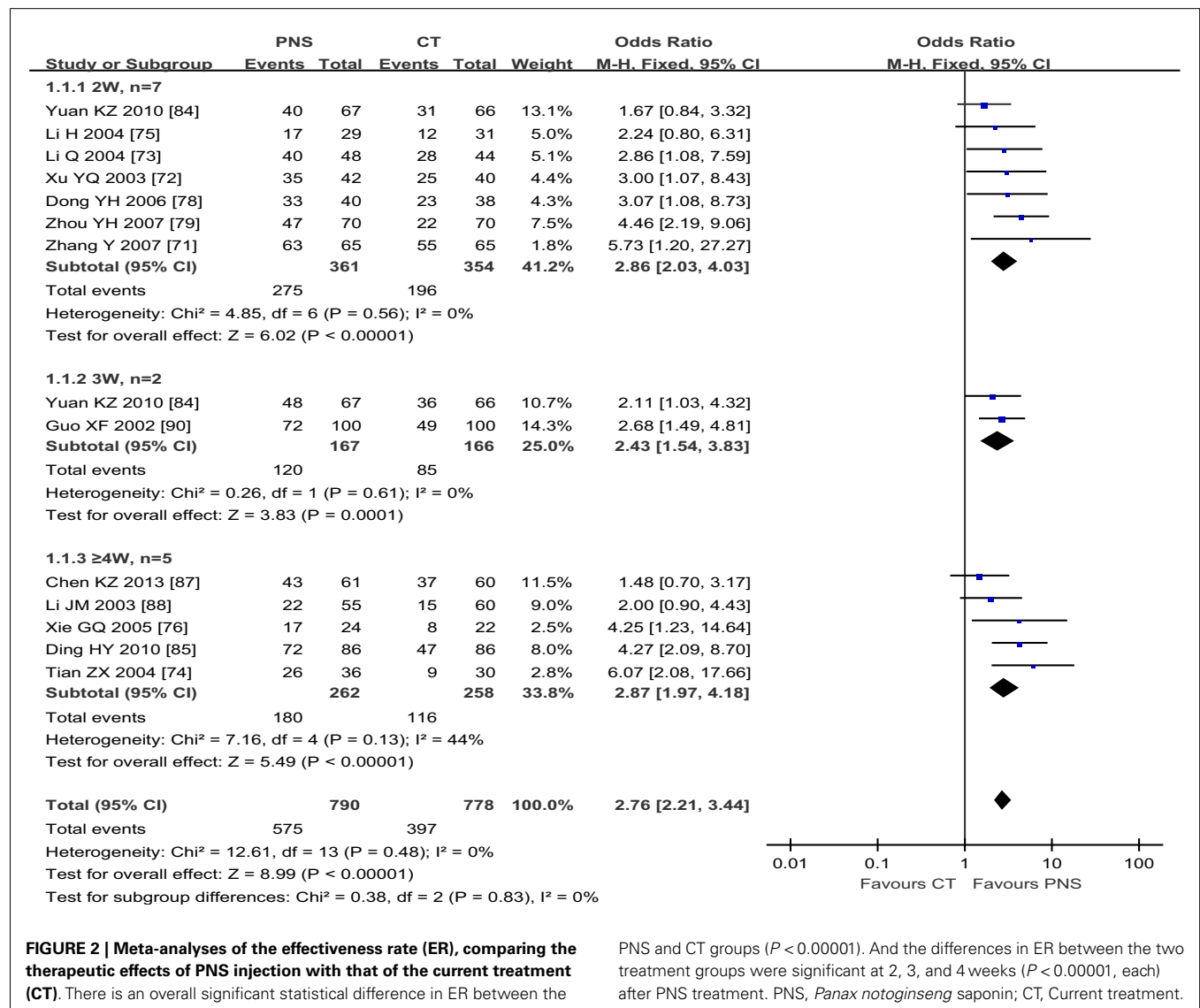
AHT, anti-hypertensive treatment; BCA, brain cell activators; BI, Barthel index; CAS, citicoline sodium; CICP, control of intracerebral pressure; DH, dehydration; ER, effectiveness rate; DPI, freeze-dry powder injector; FRS, furosemide; GFI, glycerol and fructose injection; IEV, intracerebral edema volume; IHV, intracerebral hematoma volume; Inj, injection; INS, insulin; KCl, potassium chloride; MGSO<sub>4</sub>, magnesium sulfate; MNT, mannitol; NDP, number of death patients; NDS, neurological deficit score; NR, not reported; NTM, neurotrophyl medicine; PNS, Panax notoginseng saponin; CT, current treatment; SQZG, sanqi zaogan; Sr, skin rashes; ST, symptomatic treatment; VC, vitamin C; XSHT, Xue Shuan Tong; XST, Xue Sai Tong (Xuesaitong).

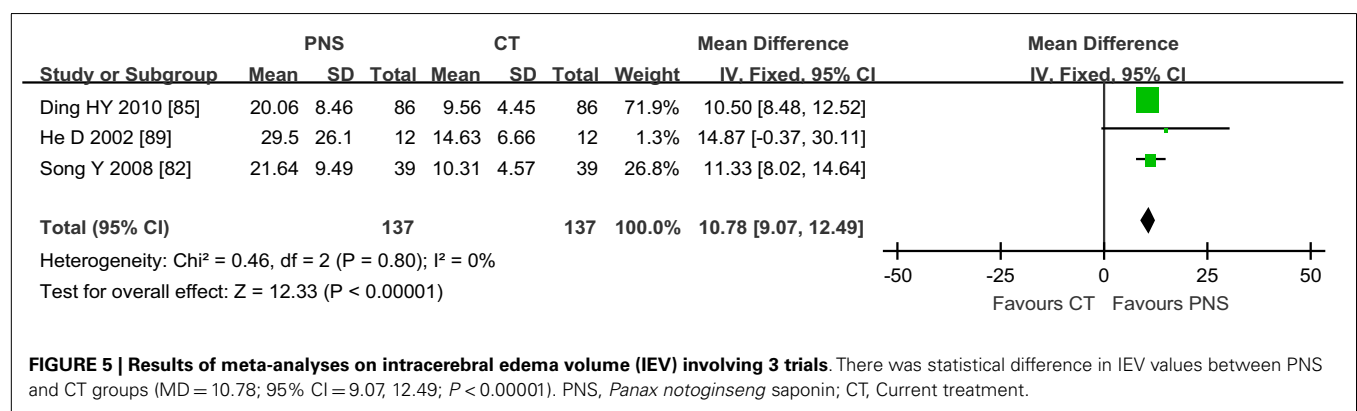
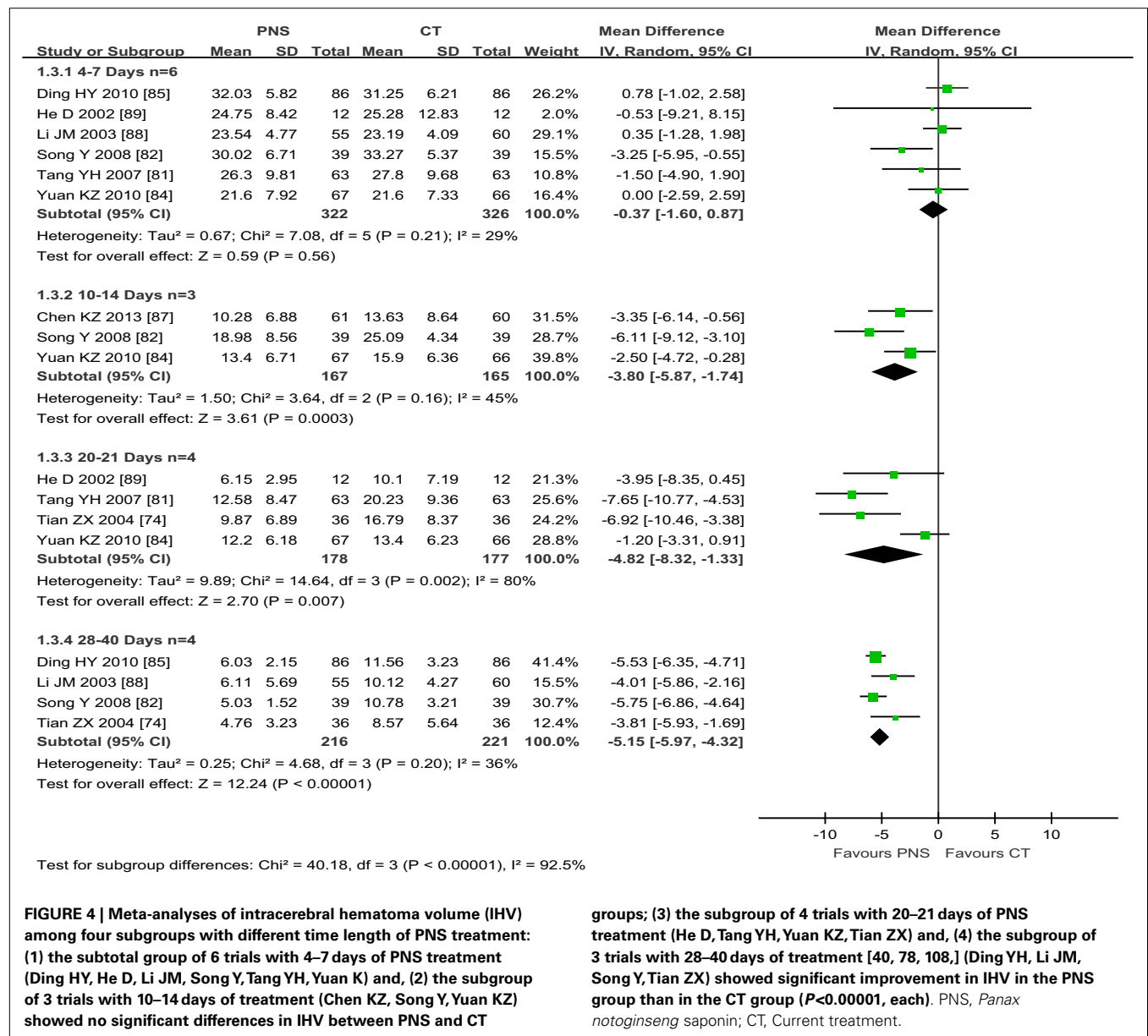


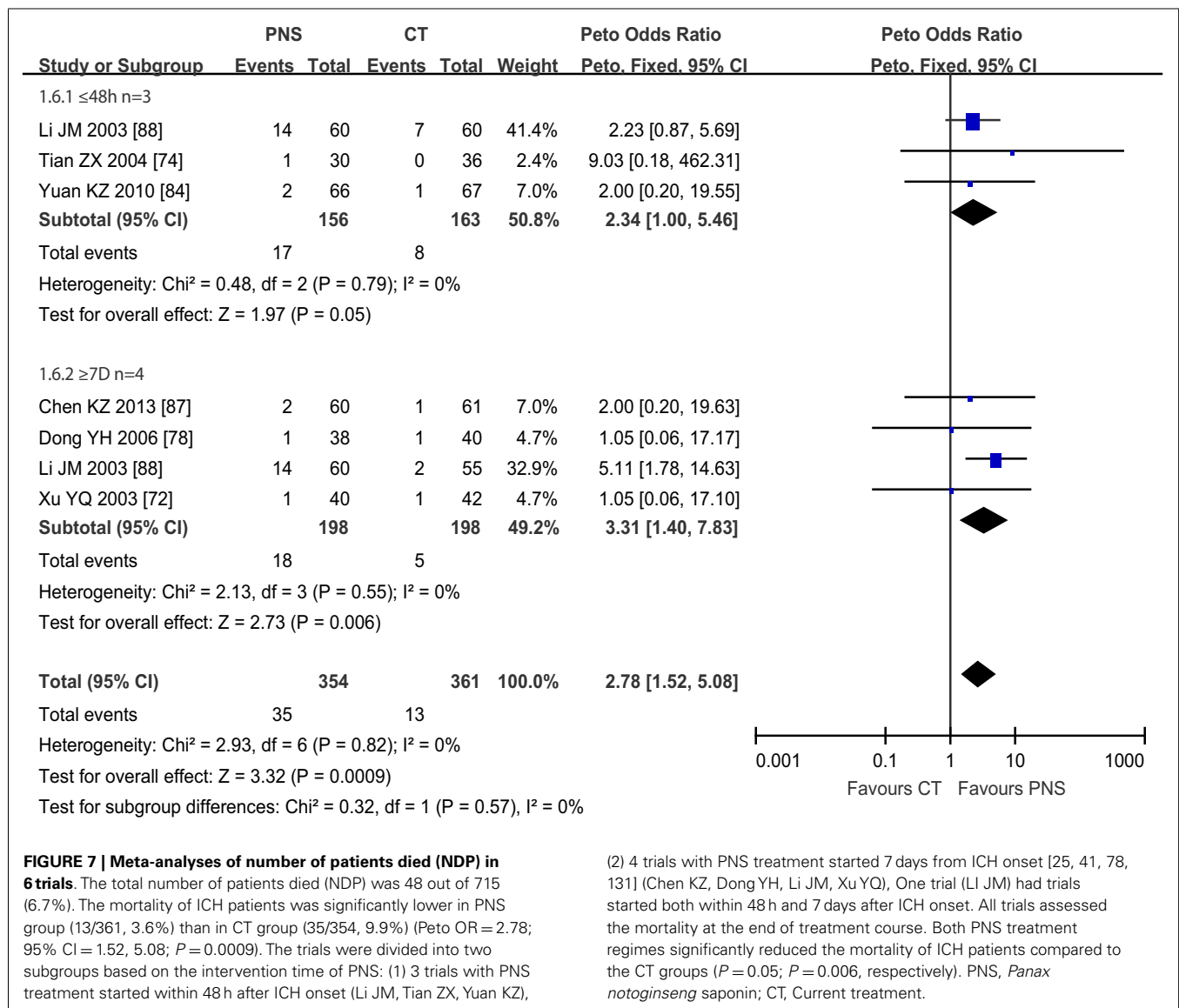
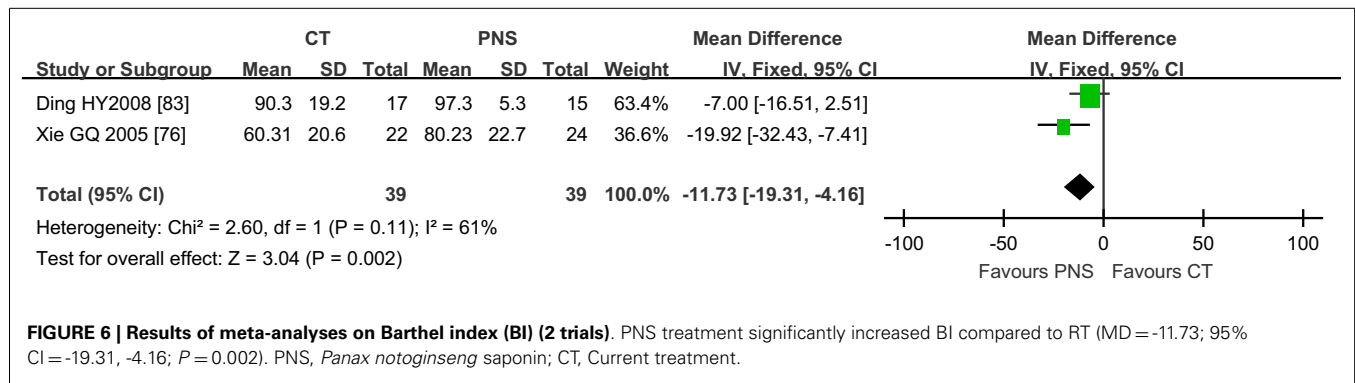
**Table 3 | Detailed information of the hemorrhage sites of the 20 trials included in the meta-analyses.**

Authors	Sample size	Intervention time	Hematoma volume	Sites of bleeding (cases)
Guo et al. (90)	PNS( <i>n</i> = 100) CT( <i>n</i> = 100)	3rd D	10–60 ml	BGR (40),thalamus (20),lobar (33),cerebellar (7) BGR (42),thalamus (16),lobar (36),cerebellar (6)
He et al. (89)	PNS( <i>n</i> = 12) CT( <i>n</i> = 12)	5th D	10–30 ml	UBG (12) UBG (12)
Xu and Dong (72)	PNS( <i>n</i> = 42) CT( <i>n</i> = 40)	10th–15th D	<30 ml, 30–50 ml, >50 ml	Putamen (18),thalamus (9), lobar (6),brainstem (6),cerebellar (3) Putamen (17),thalamus (8), lobar (7),brainstem (6),cerebellar (2)
Li et al. (88)	A:PNS( <i>n</i> = 60)  B:PNS( <i>n</i> = 55)  C:CT( <i>n</i> = 60)	≤ 48H, ≥ 7 D	<42 ml	A:BGR (46),FL (3),EC (1),IC (2),brainstem (3), Ventricle (2), thalamus (1),cerebellar (2) B:BGR (43),FL (2),EC (2),IC (3),brainstem (2), Ventricle (1), cerebellar (2) C:BGR (45),FL (2),EC (2),IC (3),brainstem (3), Ventricle (2), thalamus (1),cerebellar (2)
Li and Yang (73)	PNS( <i>n</i> = 48) CT( <i>n</i> = 44)	20th–22nd D	<40 ml	Lobar (12), EC or BG region (21), IC (9), ventricle (2), cerebellar (4) Lobar (10), EC or BG region (22), IC (8), ventricle (1), cerebellar (3)
Tian et al. (74)	PNS( <i>n</i> = 36) CT( <i>n</i> = 30)	≤ 48H	≤30 ml	BGR (16), thalamus (11), lobar (9) BGR (13), thalamus (10), lobar (7)
Li and Sun (75)	PNS( <i>n</i> = 29) CT( <i>n</i> = 31)	1st–15th D	6–58 ml	MBG (15), BGR (10), parietal lobe (2), FL (1),temporal (1) NR
Xie et al. (76)	PNS( <i>n</i> = 24)  CT( <i>n</i> = 22)	3rd W	SH ≤ 30 ml, cerebellar ≤ 15 ml, Brainstem ≤ 5 ml	SH (20) cerebellar (3), brainstem (1)  SH (17) cerebellar (4), brainstem (1)
Chen et al. (77)	PNS( <i>n</i> = 22) CT( <i>n</i> = 21)	2nd W	≤ 25 ml	SH (22) SH (21)
Dong and Wang (78)	PNS( <i>n</i> = 40) CT( <i>n</i> = 38)	10th–15th D	<30 ml, 30–50 ml, >50 ml	Putamen (18),thalamus (8),lobar (5),brainstem (6),cerebellar (3) Putamen (17),thalamus (8),lobar (6),brainstem (5),cerebellar (2)
Zhang et al. (71)	PNS( <i>n</i> = 65) CT( <i>n</i> = 65)	3rd–8th D	30–50 ml	NR
Zhou et al. (79)	PNS( <i>n</i> = 70) CT( <i>n</i> = 70)	4th–7th D	6–40 ml	BG (48), lobar (17), cerebellar (5) BG (44), lobar (20), cerebellar (6)
Zheng (80)	PNS( <i>n</i> = 22) CT( <i>n</i> = 19)	≤ 48H	<30 ml	NR
Tang et al. (81)	PNS( <i>n</i> = 63) CT( <i>n</i> = 63)	≥ 3 D	10–40 ml	NR
Song (82)	PNS( <i>n</i> = 39) CT( <i>n</i> = 39)	≤ 48H	Low to medium	SH 39 SH 39
Ding et al. (83)	PNS( <i>n</i> = 15) CT( <i>n</i> = 17)	≤ 48H	≤30 ml	BGR (15) BGR (17)
Yuan et al. (84)	PNS( <i>n</i> = 67) CT( <i>n</i> = 66)	≤ 48H	10–30 ml	BGR (49), temporal (5),FL (7), OL (5), cerebellar (<5 ml) (1) BGR (47), temporal (6), FL (7), OL (3), cerebellar (<5 ml) (3)
Ding and Geng (85)	PNS( <i>n</i> = 86) CT( <i>n</i> = 86)	≥ 7 D	Low to medium	NR
Gao et al. (86)	PNS( <i>n</i> = 28) CT( <i>n</i> = 24)	≤ 48H	<30 ml	Thalamus (7),putamen (15),caudate nucleus (2),lobar (4) Thalamus (7),putamen (13),caudate nucleus (2),lobar (2)
Chen (87)	PNS( <i>n</i> = 61) CT( <i>n</i> = 60)	≥ 7 D	≤ 40 ml	NR

BG, basal ganglia; BGR, basal ganglia region; CT, current treatment; EC, external capsule; FL, frontal lobe; IC, internal capsule; MBG, medial basal ganglia; OL, occipital lobe; PNS, *Panax notoginseng* saponin; PL, parietal lobe; SH, supratentorial hemorrhage; UBG, unilateral basal ganglia.







PNS within 48 h of ICH onset (Peto OR = 3.31; 95% CI = 1.40, 7.83;  $P = 0.006$ ), but no significant differences between the PNS and CT groups when PNS treatment started more than 48 h after

ICH onset (Peto OR = 2.34; 95% CI = 1.00, 5.46;  $P = 0.05$ ), suggesting that early PNS intervention is critical in reducing ICH mortality.

## META-ANALYSIS ON SAFETY

Seven trials reported incidences of adverse events (73, 76, 77, 84, 85, 88, 90). Only one trial reported three cases of skin rashes related to PNS injection (56). No severe side effects were reported in the other six trials.

## QUALITY ASSESSMENT

The quality assessment of the 20 included trials was evaluated in accordance with Jadad's scale. Four trials were assessed as high-quality trials (scoring 3–5 marks) (76, 80, 88, 89), and the rest were assessed as low-quality trials (scoring 1–2 marks) owing to poor description on randomization and blindness in the papers. All trials mentioned randomization and dropout rate but only three of them described randomization methods (76, 80, 88) and one trial mentioned single blinding in their methodological design (89).

## FUNNEL PLOTS

To determine potential publication bias, funnel plot based on the effective rate was elaborated (Figure 8). A total of 13 trials reported the effect rate, which was categorized into three subgroups by the treatment outcome evaluating time: (1) 7 trials assessed the ER at the end of 2 weeks of treatment, (2) 2 trials assessed the ER at the end of 3 weeks, and (3) 5 trials assessed the ER at the end of 4 weeks.

## DISCUSSION

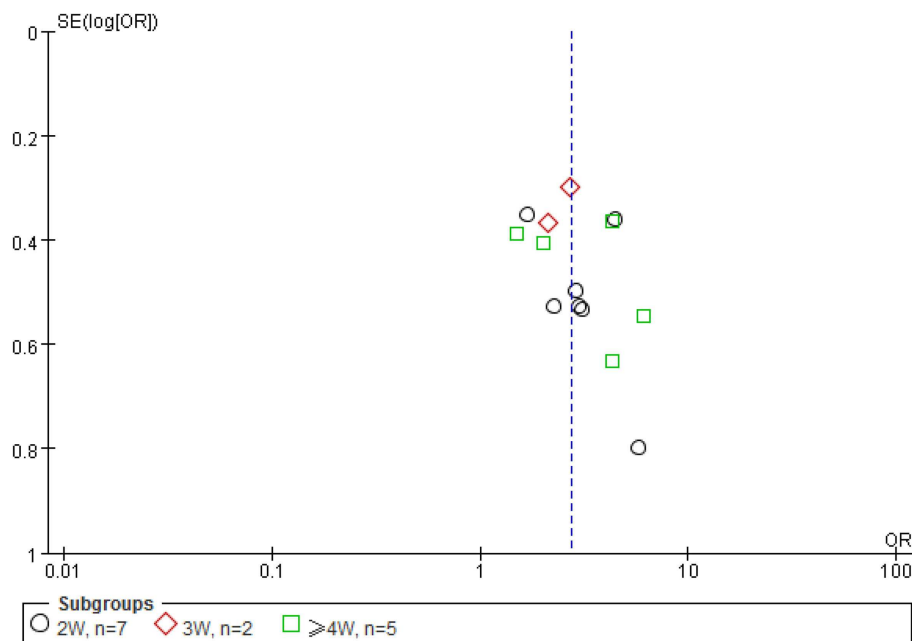
Intracerebral hemorrhage is the leading cause of death and disability in people with TBI and stroke. So far, no proven drug is available for ICH. From the meta-analysis of multiple clinical trials involving PNS treatment for intracerebral hemorrhage (ICH), we found

that ICH patients treated with PNS exhibited better outcomes than ICH patients that received current treatments in all aspects examined including the ER, the NDS, intracranial hematoma volume (IHV), intracranial edema volume (IEV), BI, and NDP. This finding is consistent with the knowledge that *P. notoginseng* is an effective medical herb for wound healing and bleeding.

## INTERVENTION TIME

Because intracerebral bleeding is a major cause of mortality and morbidity in ICH patients, timely intervention is critical for saving lives and for better outcomes of the patients. *P. notoginseng* is a hemostatic drug that has been used to stop bleeding after gunshots and traumatic injuries since the Ming Dynasty (93). The non-protein amino acid dencichine and notoginsenoside Ft1 of PNS have been identified as the active hemostatic components of *P. notoginseng* (17).

The timing of PNS intervention varied among the 20 clinical trials examined. The earliest PNS intervention was given within 48 h of ICH onset (74, 80, 82, 84–86). These early treated patients had the following common characteristics: hemorrhaging of less than 30 ml, diagnosis of the precise bleeding site, no comas, and stable vital signs. The last PNS intervention began 3 weeks after ICH onset (73, 76). The majority of the patients, however, received PNS between 1 and 2 weeks after ICH onset. Only one trial examined the timing effect of PNS intervention on the outcome of ICH (88). In that trial, 60 ICH patients received 600 mg/day of PNS within 24 h after ICH onset, and 55 ICH patients received 600 mg/day of PNS injection 7 days after ICH onset. Both treatments lasted 14 days and both treatments improved the outcome



**FIGURE 8 | A funnel plot was made using the data of effectiveness rate (ER).** A total of 13 trials reported the effect rate, which was categorized into three subgroups by the evaluating time: (1) 7 trials assessed the ER at the end of 2 weeks of treatment, (2) 2 trials assessed

the ER at the end of 3 weeks, and (3) 5 trials assessed the ER at the end of 4 weeks. Because of the small number of trials involved, the imperfect or asymmetrical funnel plot is not a reliable indication of potential publication bias in this case.



of the ICH patients compared to the CT groups. No difference was found in the ER between the two PNS treatment groups ( $P > 0.5$ ).

The results show that the death rate was two- to threefold lower in ICH patients that received PNS treatment within 48 h of ICH onset than those in the CT group ( $P = 0.05$ , **Figure 6**), suggesting early PNS intervention can be critical for saving the lives of ICH patients at risk of death.

Animal studies showed that PNS given at the third day of acute cerebral hemorrhage produced the best effects in reducing cerebral edema and hematoma volume in rats when compared to PNS administration given at other times (94). These authors reported up regulation of Bcl-2 expression in cerebral tissue after PNS treatment. Another animal model study showed that early PNS treatment after ICH onset can significantly suppress brain inflammation as reflected in reduced level of CAM-1 and TNF- $\alpha$  expression in PNS-treated rats (95). Thus early PNS intervention could minimize ICH-induced brain inflammation and neuronal apoptosis, and facilitate the restoration of normal brain function.

#### ADVERSE EVENTS, DOSAGE, AND ROUTE OF ADMINISTRATION

Seven clinical trials included in this study reported the observation of adverse events (73, 76, 77, 84, 85, 88, 90). Only three cases of skin rash were reported after PNS (XST) injection in one trial (56), accounting for 5.5% of the 55 PNS-treated patients of that trial (**Table 1**). This finding is in agreement with our previous study that the side effects of PNS use are relatively rare, with skin rash being the most common side effect of PNS use, accounting for more than 52% of all its adverse reactions (96).

There were considerable variations in the daily dose and total dose of PNS administration among the 20 clinical trials included in this study, with the lowest dose at 140 mg/day, the highest dose at 800 mg/day, and the average dose at  $373.25 \pm 181.57$  mg/day. Most of the trials administered PNS at a dose range between 300 and 400 mg/day, with 12 trials at a dose greater than 300 mg/day. So far, there is no consensus about the ideal daily dose and total dose of PNS for ICH although 200–300 mg/day for 2–4 weeks are usually recommended by the manufacturers of medical PNS.

For the treatment duration and the total dose, some studies recommend a treatment course of 14 days (78), but others propose a 30–40-day treatment regime for achieving a better outcome (74, 97). Of the 20 clinical trials included in this study, 1 trial treated the ICH patients for 1 week, 2 trials for 11 weeks, 4 trials for 3 weeks, 3 trials for 4 weeks, and 1 trial for 6 weeks (**Table 1**). Our analysis shows that an increased duration of PNS treatment is linked to a better outcome of the intracerebral hematoma volume (**Figure 4**). Significant improvement in IHV was found only after 10 or more days of PNS treatment. It appears that a minimum of 2–4 weeks of treatment is required to achieve significant improvement in the outcome of patients with acute ICH. A longer treatment could bring additional benefit but with an additional medical cost.

#### MORTALITY

Significantly reduced morbidity and mortality are the key indexes of successful treatment of intracerebral hemorrhage. Of the 20 clinical trials, 3 trials reported short-term mortality in ICH patients who received PNS treatment within 48 h after ICH onset

(74, 84, 88) (**Figure 7**), and 4 trials reported short-term mortality in ICH patients who received PNS treatment 7 days after ICH onset (**Figure 7**). Both treatment regimens exhibited a more significantly reduced the death rate in the PNS group than in the CT group (by  $>2$ ,  $P < 0.05$ , and  $>3$ -fold,  $P < 0.01$ , respectively). This is consistent with a recent report that certain herbal ingredients of traditional Chinese medicine (TCM) could stimulate the activation of blood, resolve hemostasis, and reduce acute ICH-induced short-term mortality (10).

#### QUALITY OF LIFE

The quality of life of the ICH patients is closely associated with the severity of the disease and the efficacy of the treatment (98, 99) and is often assessed using the NDS and the BI. Of the 20 trials included in the present study (with a total of 1,891 ICH patients), only 2 trials measured BI (**Figure 4**) and reported improved activities of daily living in the PNS-treated ICH patients compared to the patients in the CT group.

Neurological deficit score is an important index for the diagnosis of symptom severity and functional recovery of the patients. Three of the trials included in this study reported NDS at 7, 15, 21, 28, and 30 days after PNS treatment (74, 77, 86) (**Figure 2**). The results showed that it took at least 21 days for the PNS treatment to produce noticeable improvements in ICH patients when compared with the CT groups (74, 77, 86). That improvement in terms of NDS, however, became significant at 28 days in one study (86) and 40 days in another (74) after the start of PNS treatment ( $P < 0.05$ ,  $P < 0.01$ , respectively).

#### FUNNEL PLOTS

The funnel plot is often used to check for the existence of publication bias in meta-analyses, assuming that the largest studies will be plotted near the average, and smaller studies will be spread evenly on both sides of the average, creating a roughly funnel-shaped distribution. Deviation from this shape can indicate publication bias. Although the funnel plot appeared asymmetrical in this study, it may reflect the fact of unbalanced and very limited data of each group (2W  $n = 7$ , 3W,  $n = 2$ , 4W,  $n = 5$ ) (**Figure 8**) used for the plot rather than a true publication bias as eight samples from each group is considered minimal (while more than 20 is preferred) number required for a meaningful funnel plot, and a less funnel plot may give a wrong impression of publication bias if high precision studies are different from low precision studies with respect to effect size (e.g., due to different populations examined) (100). The appearance of the funnel plot can also alter substantially depending on the scale on the y-axis (101).

#### MECHANISM OF PNS ACTION

Intracerebral hemorrhage can disrupt cerebral blood flow, energy metabolism, and the integrity of the blood–brain barrier (BBB), resulting in edema, inflammation, apoptosis, neurological dysfunction, and often death. Acute and chronic macro- and micro-bleeding and thrombosis are the primary determinants of hematoma and edema development. Agents that can effectively control the bleeding and reduce hematoma and edema hold the promise to become effective therapies for ICH and have been the major treatment targets of multiple international ongoing randomized control trials of ICH (102).

Our meta-analysis shows that total *P. notoginseng* saponin extract (PNS) could be a therapeutic agent for ICH because it can significantly attenuate edema and hematoma in ICH patients. This is in line with recent reports that PNS (XST) injection treatment (175 mg/day) for 2 weeks significantly improved hematoma absorption and neurological function in 32 acute ICH patients compared to 29 RT controls (103). PNS has also been shown to improve microcirculation around the hematoma ischemic area, promote the absorption of hematoma, slow down and inhibit brain edema development, and significantly shorten the time for the edema to disappear (104).

The mechanism of PNS' neuroprotection against ICH injury remains to be fully understood. It may involve differential protective activities of various ginsenosides and notoginsenosides on hemostasis, anti-coagulant, anti-thrombotic, platelet aggregation and complement activation, hemorheology, blood viscosity and hematocrit, vasodilation, microcirculation, energy metabolism, oxidative stress, inflammation, and immune function. Some of the recently published PNS actions are presented below as they may be relevant or potential mechanisms of PNS in ICH.

### HEMOSTATIC EFFECTS OF PNS

Spontaneous acute and chronic macro- and micro-bleeding contribute directly to hematoma growth in TBI and ICH patients and are linked with symptom severity, recurrence, and poor outcome (105, 106). Preclinical TBI studies showed that the extent of ICH acquired during acute and subacute phases (3 h, 3, 9, and 23 days) post-ICH can predict the functional and histopathological outcome in rats 6–12 months later and is correlated with the final cortical atrophy ( $P < 0.05$ ), hippocampal atrophy ( $P < 0.01$ ), and memory deficits ( $P < 0.01$ ) (107).

At least two PNS components, i.e., dencichine and notoginsenoside Ft1 have been identified to possess hemostatic properties that could block or minimize bleeding and hematoma expansion after ICH onset (17, 108). Dencichine is a bioactive non-protein therapeutic amino acid found in *P. notoginseng*. At low concentrations, dencichine has hemostatic and platelet-enhancing activity, but at high concentrations, it is neurotoxic (108). Dencichine enhances hemostasis of activated platelets via AMPA receptors (109). Notoginsenoside Ft1 is a potent procoagulant that can induce dose-dependent and ADP-induced platelet aggregation, increase plasma coagulation indexes, decrease tail-bleeding time, and increase thrombogenesis and cytosolic Ca (2+) accumulation. Dencichine and notoginsenoside Ft1 may underlie the hemostatic mechanism of PNS during the acute and subacute phases of ICH.

### ANTI-THROMBOSIS, FIBRINOLYSIS, AND ANTI-COAGULATION MECHANISM: ROLE OF NITRIC OXIDE

Patients with TBI and resultant intracranial hemorrhage (ICH) are at high risk for developing venous thromboembolism (VTE) (110). Intrahematoma blood clotting is also a pathogenetic factor in hyperacute perihematoma edema formation (111). There is an increasing use of anti-platelets and/or anti-coagulants in the treatment of blood clotting and hyperviscosity in ICH and there is some evidence of therapeutic effects in animal models of ICH

(112–115). Several compounds of PNS including adenosine and guanosine, ginsenoside Rh1, F1, Rg1, and Rg2 have anti-platelet and anti-coagulant activities, with adenosine and guanosine and the ginsenosides as the main anti-platelet aggregation compounds of PNS (116–118).

One study showed that sanchinoside Rg1 markedly inhibited experimental thrombosis formation by enhancing the function of fibrinolysis system and stimulating vascular endothelial cells to release nitric oxide (NO) (119). Ginsenoside Rb1 can also reverse oxidative stress- and ischemia-related umbilical endothelial dysfunction and myocardial injury through upregulation of the endothelial NO synthase (eNOS) pathway in diabetes rat model (120, 121).

### PNS HAS ANTI-HYPERTENSION ACTIVITY

Hypertension is a critical pathological factor in triggering ICH onset. Notoginsenoside Ft1 activates both glucocorticoid and estrogen receptors to induce endothelium-dependent, NO-mediated relaxations in rat mesenteric arteries (122).

### PNS INHIBITS COMPLEMENT ACTIVATION

PNS could improve the outcome of acute ICH by suppressing the complement 3 (C3)-mediated pathway. Activation of complement cascades plays an important role in anaphylatoxin-mediated inflammation, secondary toxicity, and brain damage after ICH (24, 123). Studies have shown that PNS (co-)therapy inhibited the enhancement of blood complement C3 levels in experimental ICH (86). Significant reduction in circulation complement (C3) was found in 43 rheumatoid arthritis patients treated with PNS for 28 days, and which was associated with improved clinical symptoms such as joint swelling index when compared to the control subjects (50). This could be a potential mechanism underlying the decreased volume of intracerebral edema in the patients receiving PNS treatment group reported in the three clinical trials (Figure 5). In ICH-induced local tissue inflammation, C3 promotes the adhesion, exudation and translocation of inflammatory cells, and stimulates the secretion of large amounts of inflammatory mediators such as TNF- $\alpha$  and IL-1 $\beta$ , resulting in an increased inflammatory response and brain damage. These responses are absent in mice deficient in C3 activity and show reduced inflammatory cell infiltration, brain edema formation, and improved neurologic outcome after experimental ICH (124, 125).

### PNS PROTECTS BBB INTEGRATION

Blood-brain barrier disruption is a hallmark of ICH-induced brain injury and contributes to edema formation, the influx of leukocytes, and the entry of potentially neuroactive agents into the perihematoma brain, all of which can contribute to brain injury. Factors implicated in BBB disruption include: inflammatory mediators (e.g., cytokines and chemokines), thrombin, hemoglobin breakdown products, oxidative stress, complement proteins, and matrix metalloproteinases, etc. (126, 127). Two studies have shown that ginsenoside Rg1 provides neuroprotection against BBB disruption, edema formation, and neurological injury in rat models of cerebral ischemia/reperfusion through the downregulation of aquaporin 4 expression and anti-apoptosis pathways (38, 128).

### PNS PROTECTS AGAINST ISCHEMIA/REPERFUSION, AND STIMULATES ANGIOGENESIS

Neurons are oxygen sensitive and are vulnerable to ischemic-reperfusion injury after ICH. Experimental studies have shown that PNS and ginsenosides Rb1 and Rb3 can provide significant protection against ischemia/reperfusion injury in rodent brains (36, 129), cardiomyocytes (130, 131), and kidneys (132). Ginsenoside Rb1 prevents homocysteine-induced endothelial dysfunction via PI3K/Akt activation and PKC inhibition (133). Ginsenoside Rg1 enhances angiogenesis after hypoxia ischemia brain damage in neonatal rats and in diabetic mice, in part through hypoxia-inducible factor (HIF-1 $\alpha$ ), glucocorticoid receptor (GR), and fibroblast growth factor receptor (VEGFR)-mediated pathways (134–138), and enhances the resistance of hematopoietic stem/progenitor cells to radiation-induced aging in mice (38). Notoginsenoside Ft1 promotes angiogenesis via HIF-1 $\alpha$  mediated VEGF secretion and the regulation of PI3K/AKT and Raf/MEK/ERK signaling pathways (139). PNS also enhances VEGF signals and promotes angiogenesis derived from rat bone marrow and mesenchymal stem cells (140) as well as inhibit ischemia-induced apoptosis by activating the PI3K/Akt pathway in cardiomyocytes (141).

### PNS STIMULATES STEM CELL PROLIFERATION AND DIFFERENTIATION

Cognitive impairment is common and is linked to neuronal cell loss after ICH (92). PNS could promote functional recovery of ICH patients through stimulating stem cell proliferation and differentiation. Studies have shown that ginsenoside Rb1 can improve spatial learning and memory by stimulating neurogenesis in the hippocampal subregions of rats (22) and that ginsenoside Rd can stimulate the proliferation of rat neural stem cells *in vivo* and *in vitro* (28). Ginsenoside Rg1 stimulates the proliferation and differentiation of human dental pulp stem cells and facilitates neural differentiation of mouse embryonic stem cells via the GR-dependent signaling pathway (31, 32), which promotes peripheral nerve regeneration in the rat model of nerve crush injury (142) and improves spatial learning-memory in dementia rats after bone marrow mesenchymal stem cell transplant (21). Ginsenoside Rg1 mediates microenvironment-dependent endothelial differentiation of human mesenchymal stem cells (143).

### PNS PROTECTS MICROCIRCULATION FROM ISCHEMIA/REPERFUSION-INDUCED INJURY

PNS treatment improved microcirculation around the hematoma ischemic area, promoted the absorption of hematoma, slowed down and inhibited brain edema development, and significantly shortened the time for the edema to disappear (104). Notoginsenoside R1 can attenuate ischemia/reperfusion (I/R)-induced microvascular hyperpermeability, inflammatory cytokine production, NF- $\kappa$ B activation, leukocyte rolling and adhesion, the expression of E-selectin in endothelium and CD18 in neutrophils, loss of tight junction proteins, and deficit in energy metabolism during I/R in rats (144, 145). Ginsenosides Rb1 and Rg1, and notoginsenoside R1 have been shown to protect lipopolysaccharide-induced microcirculatory disturbance in rat mesentery (146).

### PNS HAS ROS-SCAVENGER, ANTIOXIDATION, AND ANTI-APOPTOSIS PROPERTIES

PNS has been shown to be a potent antioxidant in various experimental models. PNS induces thioredoxin-1 expression and prevents 1-methyl-4-phenylpyridinium ion-induced neurotoxicity (147). Ginsenoside Rb1 directly scavenges hydroxyl radicals and hypochlorous acid (103) and inhibits apoptosis in hydrogen peroxide-treated chondrocytes by stabilizing mitochondria and inhibiting Caspase-3 (148). Ginsenoside Rb1 also prevented MPP(+)-induced apoptosis in PC12 cells by activating estrogen receptors and ERK1/2/Akt pathways, and inhibiting SAPK/JNK/p38 MAPK pathways (149). Ginsenoside Rb1 protects against oxidative damage and renal interstitial fibrosis in rats with unilateral ureteral obstruction (150), and against beta-amyloid protein(1-42)-induced neurotoxicity in cortical neurons and in PC12 cells (30, 33) as well as against hypoxia and oxidative stress in rat retinal ganglion cells (29).

Ginsenoside Rd appears to be a superior neuroprotector with a wide therapeutic window in experimental stroke (151). Ginsenoside Rd attenuates redox imbalance, improves stroke outcome following focal cerebral ischemia in aged mice (152), and attenuates early oxidative damage and sequential inflammatory responses after transient focal ischemia in rats (153). Ginsenoside Rd prevents glutamate-induced apoptosis in rat cortical neurons (154), and promotes glutamate clearance by up-regulating the expression of glial glutamate transporter proteins (155). Ginsenoside-Rd exhibits anti-inflammatory activities through the enhancement of antioxidant enzyme activities and the inhibition of JNK and ERK activation *in vivo* (156).

Ginsenoside Rg1 protects against hydrogen peroxide-induced cell death in PC12 cells via the inhibition of NF- $\kappa$ B activation (157), reduction of nigral iron levels in MPTP-treated C57BL6 mice by regulation of iron transport proteins (158), and protection against beta-amyloid peptide-induced human endothelial cell apoptosis by activation of the GR-ERK signaling pathway (159). Oral Rg1 supplementation strengthens the antioxidant defense system against exercise-induced oxidative stress (160) and protects the liver against exhaustive exercise-induced oxidative stress in rats (161).

### PNS HAS ANTI-INFLAMMATION PROPERTIES

Ginsenoside Rb1 shows anti-neuroinflammation effects in rat models of Alzheimer's disease (20) and prevents interleukin-1 $\beta$ -induced inflammation and apoptosis in human articular chondrocytes (162). Ginsenoside Rd inhibits the expression of iNOS and COX-2 by suppressing NF- $\kappa$ B in LPS-stimulated RAW264.7 cells and in mouse livers (163), and attenuates neuroinflammation in cultured dopaminergic neurons (164). Ginsenoside Re ameliorates inflammation by inhibiting the binding of lipopolysaccharides to TLR4 on macrophages (165). Ginsenoside Rg1 improves survival in a murine model of polymicrobial sepsis by suppressing the inflammatory response and apoptosis of lymphocytes (166). Ginsenoside Rg1 improves streptozocin (STZ)-induced diabetic nephropathy in rats by suppressing inflammatory reactions and expression of ectodermal dysplasia and TGF- $\beta$  (167). PNS also suppresses inflammation in a collagen-induced arthritis model (146).

## ANTI-HYPERGLYCEMIA AND ANTI-HYPERLIPIDEMIC EFFECTS OF PNS

Hyperglycemia is associated with poor outcome in patients with TBI and ICH and in experimental models of ICH (93, 168, 169). PNS has hypolipidemic and antioxidant activities in rats with high-fat diets (170). Ginsenoside Rb1 has antiobesity and anti-hyperglycemic effects in rats (171). Ginsenoside Rb2 exerts its antidiabetic effects via activation of AMPK (172). Ginsenoside Rb2 lowers cholesterol and triacylglycerol levels in 3T3-L1 adipocytes under high cholesterol or fatty acids culture conditions (173). Ginsenoside Re reverses insulin resistance in muscles of high-fat diet rats (174). Ginsenoside Rg1 promotes glucose uptake through the activated AMPK pathway in insulin-resistant muscle cells (175).

## MANY COMPONENTS AND MANY MECHANISMS

Cerebral hemorrhage causes brain damage through multiple mechanisms, with spontaneous bleeding, hematoma development and perihematoma edema formation as the main factors contributing to the poor outcome of ICH. Effective therapies for ICH should be able to target all these factors. Our meta-analysis and literature review suggest that PNS is an effective therapy for acute ICH, and potentially functions through multiple mechanisms. Its most notable effects include hemostatic and anti-thrombotic effects, hemodynamic and hemorheological effects, angiogenesis and stem cell promoting effects, anti-hyperglycemia and anti-hyperlipidemia effects, and antioxidant and anti-inflammation effects, etc. Additionally, the strong tonic effects of PNS (176) could be beneficial to ICH patients, who are often weak and fragile during the recovery phase. A double-blind, double-dummy, randomized, and parallel-controlled study showed that 8 weeks after the onset of cerebral infarction, treatment of PNS tablets for 4 weeks significantly improved the outcome of the patients compared to the control treatments (177).

There are limitations to this research. Not all of the clinical trials analyzed were of high quality nor did they all include each desirable outcome evaluation. The number of ICH patients in each trial was often less than 100 and no long-term outcome data of the ICH patients were available. These and other factors should be controlled in further large scale studies so that the therapeutic effect of PNS can be better evaluated.

In conclusion, meta-analysis of the clinical trials suggests that PNS is superior to current treatment for acute ICH with minimal side effects. PNS could be an alternative therapy for acute ICH patients with a hemorrhagic volume of less than 30 ml. More clinical trials with better experimental designs could be conducted in the US and Europe to verify and extend the current findings and to determine the long-term effects of *P. notoginseng* on the recovery and recurrence of ICH patients.

## ACKNOWLEDGMENTS

Ms. Jillian W. Wen edited the manuscript. Mr. Zhongjian Chen of Panax Notoginseng Research Institute of Wenshan State/Region, Yunnan Province, China provided the artistic drawing of notoginseng. This study is supported, in part, by a grant from the Department of Education, Guangxi Zhuang Autonomous Region, P.R. China (New Century Higher Education Reform program in Guangxi: Research and Practice of English Curriculum System in Nursing at Guangxi Traditional Chinese Medicine College) (2011JGZD. 014) (to Dongying Xu).

## SUPPLEMENTARY MATERIAL

The Supplementary Material for this article can be found online at <http://www.frontiersin.org/Journal/10.3389/fneur.2014.00274/abstract>

## REFERENCES

- Ghajar J. Traumatic brain injury. *Lancet* (2000) **356**:923–9. doi:10.1016/S0140-6736(00)02689-1
- Langlois JA, Rutland-Brown W, Thomas KE. *Traumatic Brain Injury in the United States: Emergency Department Visits, Hospitalizations, and Deaths*. Atlanta (GA): Centers for Disease Control and Prevention, National Center for Injury Prevention and Control (2006).
- Hyder AA, Wunderlich CA, Puvanachandra P, Gururaj G, Kobusingye OC. The impact of traumatic brain injuries: a global perspective. *NeuroRehabilitation* (2007) **22**(5):341–53.
- Hanlon RE, Demery JA, Kuczen C, Kelly JP. Effect of traumatic subarachnoid haemorrhage on neuropsychological profiles and vocational outcome following moderate or severe traumatic brain injury. *Brain Inj* (2005) **19**:257–62. doi:10.1080/02699050400004955
- Harvey LA, Close JC. Traumatic brain injury in older adults: characteristics, causes and consequences. *Injury* (2012) **43**:1821–6. doi:10.1016/j.injury.2012.07.188
- Edwards P, Arango M, Balica L, Cottingham R, El-Sayed H, Farrell B, et al. Final results of MRC CRASH, a randomised placebo-controlled trial of intravenous corticosteroid in adults with head injury—outcomes at 6 months. *Lancet* (2005) **365**:1957–9. doi:10.1016/S0140-6736(05)66552-X
- Vogel T, Ockert B, Krötz M, Linsenmaier U, Kirchhoff C, Pfeifer KJ, et al. [Progression of intracranial bleeding after traumatic brain injury. When is a control CCT necessary?]. *Unfallchirurg* (2008) **111**:898–904. doi:10.1007/s00113-008-1502-0
- Maas AI, Marmarou A, Murray GD, Teasdale SG, Steyerberg EW. Prognosis and clinical trial design in traumatic brain injury: the IMPACT study. *J Neurotrauma* (2007) **24**:232–8. doi:10.1089/neu.2006.0024
- MRC CRASH Trial Collaborators, Perel P, Arango M, Clayton T, Edwards P, Komolafe E, et al. Predicting outcome after traumatic brain injury: practical prognostic models based on large cohort of international patients. *BMJ* (2008) **336**:425–9. doi:10.1136/bmj.39461.643438.25
- Chen J, Zhang XY. Systematic evaluation of activating blood to resolve stasis for acute intracerebral hemorrhage mortality. *Tradit Chin Emerg Med* (2011) **20**:1273–5.
- Murray CJ, Lopez AD. Global mortality, disability, and the contribution of risk factors: global burden of disease study. *Lancet* (1997) **349**:1436–42. doi:10.1016/S0140-6736(96)07495-8
- van Asch CJ, Luitse MJ, Rinkel GJ, van der Tweel I, Algra A, Klijn CJ. Incidence, case fatality, and functional outcome of intracerebral haemorrhage over time, according to age, sex, and ethnic origin: a systematic review and meta-analysis. *Lancet Neurol* (2010) **9**:167–76. doi:10.1016/S1474-4422(09)70340-0
- Feigin VL, Lawes CM, Bennett DA, Barker-Collo SL, Parag V. Worldwide stroke incidence and early case fatality reported in 56 population-based studies: a systematic review. *Lancet Neurol* (2009) **8**:355–69. doi:10.1016/S1474-4422(09)70025-0
- Balami JS, Buchan AM. Complications of intracerebral haemorrhage. *Lancet Neurol* (2012) **11**:101–18. doi:10.1016/S1474-4422(11)70264-2
- Skolarus LE, Morgenstern LB, Zahuranec DB, Burke JF, Langa KM, Iwashyna TJ. Acute care and long-term mortality among elderly patients with intracerebral hemorrhage who undergo chronic life-sustaining procedures. *J Stroke Cerebrovasc Dis* (2013) **22**:15–21. doi:10.1016/j.jstrokecerebrovasdis.2011.05.025
- Rodríguez-Yáñez M, Castellanos M, Freijo MM, López Fernández JC, Martí-Fàbregas J, Nombela F, et al. Clinical practice guidelines in intracerebral haemorrhage. *Neurologia* (2013) **28**:236–49. doi:10.1016/j.nrl.2011.03.010
- Gao B, Huang L, Liu H, Wu H, Zhang E, Yang L, et al. Platelet P2Y12 receptors are involved in the haemostatic effect of notoginsenoside Ft1, a saponin isolated from *Panax notoginseng*. *Br J Pharmacol* (2014) **171**:214–23. doi:10.1111/bph.12435
- Liang XH, Yong J, Man R. Notoginsenoside Rg1 on experimental thrombosis, platelet aggregation and platelet free calcium levels affect. *Chin J Pharmacol Toxicol* (1998) **12**:40–2.

19. Liu HZ, Pang J, Wang ZL, Ying GH, Li SR. [Studies of the effects of *Gynura segetum* and *Panax notoginseng* on the ultrastructure of platelets in guinea-pigs]. *Yao Xue Xue Bao* (1982) **17**:801–8.
20. Wang Y, Liu J, Zhang Z, Bi P, Qi Z, Zhang C. Anti-neuroinflammation effect of ginsenoside Rb1 in a rat model of Alzheimer disease. *Neurosci Lett* (2011) **487**:70–2. doi:10.1016/j.neulet.2010.09.076
21. Wu W, Yang JQ, He ZY. [Effect of ginsenoside Rg1 on the spatial learning-memory ability in dementia rats after transplanted with bone marrow mesenchymal stem cells]. *Zhongguo Zhong Xi Yi Jie He Za Zhi* (2011) **31**:799–802.
22. Liu L, Hoang-Gia T, Wu H, Lee MR, Gu L, Wang C, et al. Ginsenoside Rb1 improves spatial learning and memory by regulation of cell genesis in the hippocampal subregions of rats. *Brain Res* (2011) **1382**:147–54. doi:10.1016/j.brainres.2011.01.051
23. An DS, Wang L, Kim MS, Bae HM, Lee ST, Im WT. Solirubrobacter ginsenosidimutans sp. nov., isolated from soil of a ginseng field. *Int J Syst Evol Microbiol* (2011) **61**:2606–9. doi:10.1099/ijs.0.028431-0
24. Bai Y, Hu Y, Wu Y, Zhu Y, He Q, Jiang C, et al. A prospective, randomized, single-blinded trial on the effect of early rehabilitation on daily activities and motor function of patients with hemorrhagic stroke. *J Clin Neurosci* (2012) **19**:1376–9. doi:10.1016/j.jocn.2011.10.021
25. Liu YW, Zhu X, Li W, Lu Q, Wang JY, Wei YQ, et al. Ginsenoside Re attenuates diabetes-associated cognitive deficits in rats. *Pharmacol Biochem Behav* (2012) **101**:93–8. doi:10.1016/j.pbb.2011.12.003
26. Liu J, Yan X, Li L, Zhu Y, Qin K, Zhou L, et al. Ginsenoside Rd attenuates cognitive dysfunction in a rat model of Alzheimer's disease. *Neurochem Res* (2012) **37**:2738–47. doi:10.1007/s11064-012-0866-2
27. Cheng Y, Shen LH, Zhang JT. Anti-amnesic and anti-aging effects of ginsenoside Rg1 and Rb1 and its mechanism of action. *Acta Pharmacol Sin* (2005) **26**:143–9. doi:10.1111/j.1745-7254.2005.00034.x
28. Lin T, Liu Y, Shi M, Liu X, Li L, Zhao G. Promotive effect of ginsenoside Rd on proliferation of neural stem cells in vivo and in vitro. *J Ethnopharmacol* (2012) **142**:754–61. doi:10.1016/j.jep.2012.05.057
29. Liu Z, Chen J, Huang W, Zeng Z, Yang Y, Zhu B. Ginsenoside Rb1 protects rat retinal ganglion cells against hypoxia and oxidative stress. *Mol Med Rep* (2013) **8**:1397–403. doi:10.3892/mmr.2013.1658
30. Qian YH, Han H, Hu XD, Shi LL. Protective effect of ginsenoside Rb1 on beta-amyloid protein(1-42)-induced neurotoxicity in cortical neurons. *Neurol Res* (2009) **31**:663–7. doi:10.1179/174313209X385572
31. Wang P, Wei X, Zhang F, Yang K, Qu C, Luo H, et al. Ginsenoside Rg1 of Panax ginseng stimulates the proliferation, odontogenic/osteogenic differentiation and gene expression profiles of human dental pulp stem cells. *Phytomedicine* (2014) **21**:177–83. doi:10.1016/j.phymed.2013.08.021
32. Wu J, Pan Z, Cheng M, Shen Y, Yu H, Wang Q, et al. Ginsenoside Rg1 facilitates neural differentiation of mouse embryonic stem cells via GR-dependent signaling pathway. *Neurochem Int* (2013) **62**:92–102. doi:10.1016/j.neuint.2012.09.016
33. Xie X, Wang HT, Li CL, Gao XH, Ding JL, Zhao HH, et al. Ginsenoside Rb1 protects PC12 cells against beta-amyloid-induced cell injury. *Mol Med Rep* (2010) **3**:635–9. doi:10.3892/mmr\_00000308
34. Ma LY, Wang CL, Zhang Q, Du LJ, Chen JM, Xiao PG. Effects of PNS on cerebral blood supply and energy metabolism in mice. *Chin Pharmacol Bull* (1998) **14**:27–9.
35. Gu P, Zhang Y. Effect of Sanqi PNS on Bcl-2 expression and neural cell apoptosis in rats with intracerebral hemorrhage. *J Chin Clin Med* (2006) **13**:527–9.
36. Jia D, Deng Y, Gao J, Liu X, Chu J, Shu Y. Neuroprotective effect of *Panax notoginseng* polysaccharides against focal cerebral ischemia reperfusion injury in rats. *Int J Biol Macromol* (2014) **63**:177–80. doi:10.1016/j.ijbiomac.2013.10.034
37. Zhou Y, Wang JW, Jiang R, Yao X, Yang B, Cai SZ, et al. [Study on anti-aging effect of ginsenoside Rg1 in serial transplantation of hematopoietic stem cells and progenitor cells]. *Zhongguo Zhong Yao Za Zhi* (2013) **38**:2848–53.
38. Chen C, Mu XY, Zhou Y, Shun K, Geng S, Liu J, et al. Ginsenoside Rg1 enhances the resistance of hematopoietic stem/progenitor cells to radiation-induced aging in mice. *Acta Pharmacol Sin* (2014) **35**:143–50. doi:10.1038/aps.2013.136
39. Li C, Li Q, Liu YY, Wang MX, Pan CS, Yan L, et al. Protective effects of notoginsenoside R1 on intestinal ischemia-reperfusion injury in rats. *Am J Physiol Gastrointest Liver Physiol* (2014) **306**:G111–22. doi:10.1152/ajpgi.00123.2013
40. Li H, He WY, Lin F, Gou X. *Panax notoginseng* saponins improve erectile function through attenuation of oxidative stress, restoration of Akt activity and protection of endothelial and smooth muscle cells in diabetic rats with erectile dysfunction. *Urol Int* (2014) **93**(1):92–9. doi:10.1159/000354878
41. Li W, Li P, Liu Z, Du Q, Steinmetz A, Wang N, et al. A Chinese medicine preparation induces neuroprotection by regulating paracrine signaling of brain microvascular endothelial cells. *J Ethnopharmacol* (2014) **151**:686–93. doi:10.1016/j.jep.2013.11.035
42. Lin N, Cai DL, Jin D, Chen Y, Shi JJ. Ginseng panaxoside rb1 reduces body weight in diet-induced obese mice. *Cell Biochem Biophys* (2014) **68**:189–94. doi:10.1007/s12013-013-9688-3
43. Meng X, Sun G, Ye J, Xu H, Wang H, Sun X. Notoginsenoside R1-mediated neuroprotection involves estrogen receptor-dependent crosstalk between Akt and ERK1/2 pathways: a novel mechanism of Nrf2/ARE signaling activation. *Free Radic Res* (2014) **48**:445–60. doi:10.3109/10715762.2014.885117
44. Shen K, Leung SW, Ji L, Huang Y, Hou M, Xu A, et al. Notoginsenoside Ft1 activates both glucocorticoid and estrogen receptors to induce endothelium-dependent, nitric oxide-mediated relaxations in rat mesenteric arteries. *Biochem Pharmacol* (2014) **88**(1):66–74. doi:10.1016/j.bcp.2014.01.007
45. Zhang ZG, Niu XY, He XJ, Shu J. Ginsenoside Rg1 reduces toxicity of fine particulate matter on human alveolar epithelial cells: a preliminary observation. *Mol Med Rep* (2014) **9**:989–92. doi:10.3892/mmr.2013.1870
46. Zhou Q, Jiang L, Xu C, Luo D, Zeng C, Liu P, et al. Ginsenoside Rg1 inhibits platelet activation and arterial thrombosis. *Thromb Res* (2014) **133**:57–65. doi:10.1016/j.thromres.2013.10.032
47. Gao B, Shi HL, Li X, Qiu SP, Wu H, Zhang BB, et al. p38 MAPK and ERK1/2 pathways are involved in the pro-apoptotic effect of notoginsenoside Ft1 on human neuroblastoma SH-SY5Y cells. *Life Sci* (2014) **108**:63–70. doi:10.1016/j.lfs.2014.05.010
48. Cui HM, Zhang CG, Lin H, Lu WL, Cheng HP, Wang J. [Determination of effective components in different positions of *Panax notoginseng* by HPLC]. *Zhong Yao Cai* (2009) **32**:1810–3.
49. Anderson CS, Huang Y, Arima H, Heeley E, Skulina C, Parsons MW, et al. Effects of early intensive blood pressure-lowering treatment on the growth of hematoma and perihematomal edema in acute intracerebral hemorrhage: the Intensive Blood Pressure Reduction in Acute Cerebral Haemorrhage Trial (INTERACT). *Stroke* (2010) **41**:307–12. doi:10.1161/STROKEAHA.109.561795
50. Chen G, Yang M, Lu Z, Zhang J, Huang H, Liang Y, et al. Microbial transformation of 20(S)-protopanaxatriol-type saponins by *Absidia coerulea*. *J Nat Prod* (2007) **70**:1203–6. doi:10.1021/np070053v
51. Abou-Chebl A, Reginelli J, Bajzer CT, Yadav JS. Intensive treatment of hypertension decreases the risk of hyperperfusion and intracerebral hemorrhage following carotid artery stenting. *Catheter Cardiovasc Interv* (2007) **69**:690–6. doi:10.1002/ccd.20693
52. Aung HH, Mehendale SR, Wang CZ, Xie JT, McEntee E, Yuan CS. Cisplatin's tumoricidal effect on human breast carcinoma MCF-7 cells was not attenuated by American ginseng. *Cancer Chemother Pharmacol* (2007) **59**:369–74. doi:10.1007/s00280-006-0278-6
53. Chen W, Hu GL, Wang YR, Wang XR. [Determination of six ginsenosides in Panax species by high performance liquid chromatography]. *Se Pu* (2000) **18**:439–41.
54. Yoshikawa M, Morikawa T, Yashiro K, Murakami T, Matsuda H. Bioactive saponins and glycosides. XIX. Notoginseng (3): immunological adjuvant activity of notoginsenosides and related saponins: structures of notoginsenosides-L, -M, and -N from the roots of Panax notoginseng (Burk.) F. H. Chen. *Chem Pharm Bull (Tokyo)* (2001) **49**:1452–6. doi:10.1248/cpb.49.1452
55. Yoshikawa M, Murakami T, Ueno T, Yashiro K, Hirokawa N, Murakami N, et al. Bioactive saponins and glycosides. VIII. Notoginseng (1): new dammarane-type triterpene oligoglycosides, notoginsenosides-A, -B, -C, and -D, from the dried root of Panax notoginseng (Burk.) F.H. Chen. *Chem Pharm Bull (Tokyo)* (1997) **45**:1039–45. doi:10.1248/cpb.45.1039
56. Adu-Bonsaffoh K, Samuel OA, Binlinla G. Maternal deaths attributable to hypertensive disorders in a tertiary hospital in Ghana. *Int J Gynaecol Obstet* (2013) **123**:110–3. doi:10.1016/j.ijgo.2013.05.017
57. Cui X, Trinh K, Wang YJ. Chinese herbal medicine for chronic neck pain due to cervical degenerative disc disease. *Cochrane Database Syst Rev* (2010) (1):CD006556. doi:10.1002/14651858.CD006556.pub2
58. Chan EC, Yap SL, Lau AJ, Leow PC, Toh DE, Koh HL. Ultra-performance liquid chromatography/time-of-flight mass spectrometry based metabolomics of



- raw and steamed *Panax notoginseng*. *Rapid Commun Mass Spectrom* (2007) 21:519–28. doi:10.1002/rcm.2864
59. Auriat A, Plakhta WC, McGie SC, Yan R, Colbourne F. 17beta-Estradiol pretreatment reduces bleeding and brain injury after intracerebral hemorrhagic stroke in male rats. *J Cereb Blood Flow Metab* (2005) 25:247–56. doi:10.1038/sj.cbfm.9600026
  60. Abou-Chebl A. Endovascular treatment of acute ischemic stroke may be safely performed with no time window limit in appropriately selected patients. *Stroke* (2010) 41:1996–2000. doi:10.1161/STROKEAHA.110.578997
  61. Liu H, Yang J, Du F, Gao X, Ma X, Huang Y, et al. Absorption and disposition of ginsenosides after oral administration of *Panax notoginseng* extract to rats. *Drug Metab Dispos* (2009) 37:2290–8. doi:10.1124/dmd.109.029819
  62. Tan ZY, Xiong WN, Huang XZ, Liang JQ. [Pharmacokinetics and bioavailability of ginsenoside Rg1 in rats]. *Zhong Yao Cai* (2013) 36:1121–3.
  63. Li X, Sun J, Wang G, Hao H, Liang Y, Zheng Y, et al. Simultaneous determination of panax notoginsenoside R1, ginsenoside Rg1, Rd, Re and Rb1 in rat plasma by HPLC/ESI/MS: platform for the pharmacokinetic evaluation of total panax notoginsenoside, a typical kind of multiple constituent traditional Chinese medicine. *Biomed Chromatogr* (2007) 21:735–46. doi:10.1002/bmc.813
  64. Li L, Sheng Y, Zhang J, Wang C, Guo D. HPLC determination of four active saponins from *Panax notoginseng* in rat serum and its application to pharmacokinetic studies. *Biomed Chromatogr* (2004) 18:849–56. doi:10.1002/bmc.400
  65. Li X, Wang G, Sun J, Hao H, Xiong Y, Yan B, et al. Pharmacokinetic and absolute bioavailability study of total panax notoginsenoside, a typical multiple constituent traditional chinese medicine (TCM) in rats. *Biol Pharm Bull* (2007) 30:847–51. doi:10.1248/bpb.30.847
  66. Xu QF, Fang XL, Chen DF. Pharmacokinetics and bioavailability of ginsenoside Rb1 and Rg1 from *Panax notoginseng* in rats. *J Ethnopharmacol* (2003) 84:187–92. doi:10.1016/S0378-8741(02)00317-3
  67. Lin L, Liu JX, Zhang Y, Duan CL. Pharmacokinetic studies of ginsenoside Rg1, Re, Rb1 and Rd in rats by LC–MS/MS method. *Chin Pharm* (2009) 44:373–7.
  68. CNS TtCNCoN. Criteria for diagnosis of various types of cerebrovascular disease. *Chin J Neurol Sci* (1996) 29:379.
  69. Yuan Y, Zeng X, Luo Y, Li Z, Wu T. Chuanxiong-type preparations for acute ischemic stroke. *Cochrane Database Syst Rev* (2008) (4):CD005569. doi:10.1002/14651858.CD005569.pub2
  70. Jadad AR, Moore RA, Carroll D, Jenkinson C, Reynolds DJ, Gavaghan DJ, et al. Assessing the quality of reports of randomized clinical trials: is blinding necessary? *Control Clin Trials* (1996) 17:1–12. doi:10.1016/0197-2456(95)00134-4
  71. Zhang Y, Yuan F, Zhang X. Clinical study of 130 cases of Lu Lu Tong injection treatment for brain edema after intracerebral hemorrhage (ICH). *JPMPT* (2007) 14:1877–8.
  72. Xu YQ, Dong YH. Clinical application of Luo Tai for patients with intracerebral hemorrhage during the phase of hemorrhage absorption. *Inner Mongol J Tradit Chin Med* (2003) 22:41.
  73. Li Q, Yang XY. Observation on the effect of *Panax notoginseng* saponin for intracerebral hemorrhage in the convalescence phase. *Chin J Misdiagn* (2004) 4:262–3.
  74. Tian ZX, Wang HB, Wei YM. Xue Sai Tong injection applied for the treatment of 36 cases with acute cerebral hemorrhage. *J Pract Tradit Chin Intern Med* (2004) 18:68.
  75. Li H, Sun HH. Clinical observation of cerebral hemorrhage treated by Xuesaitong injection. *Chin J Integr Tradit West Med Intensive Crit Care* (2004) 11:50–2.
  76. Xie GQ, Liu JL, Wang XY, Gao C. Clinical observation of thrombus clear to cerebral hemorrhage. *Chin J Integr Med Cardio/Cerebrovasc Dis* (2005) 3:496–7.
  77. Chen SL, Liang YY, Wang YX. Twenty tow cases of intracerebral hemorrhage in acute phase treated with Xue Sai Tong. *Chin J Integr Med Cardio/Cerebrovasc Dis* (2006) 4:80–1.
  78. Dong YH, Wang XR. The clinical effect of Xue Sai Tong in the treatment of hematoma absorption. *J Med Theory Pract* (2006) 19:253–4.
  79. Zhou YH, Zhang SX, Liu JJ. Observation on the effect of *Panax notoginseng* saponin for intracerebral hemorrhage in acute phase. *Chin J Integr Med Cardio/Cerebrovasc Dis* (2007) 5:69–70.
  80. Zheng XD. Xue Shuan Tong injection used for twenty-two cases with intracerebral hemorrhage. *J Mod Clin Med* (2007) 33:112.
  81. Tang YH, Guo WL, Rao P, Weng TM, Zhou L. Clinical observations on the effects of herbal preparation with the function of promoting blood circulation and removing blood stasis at the acute and sub-acute phases of primary intracerebral hemorrhage. *Mod J Integr Tradit Chin West Med* (2007) 16:4285–6.
  82. Song Y. Observation on the effect of Xue Shuan Tong for hypertensive intracerebral hemorrhage with small or medium volume. *Chin J Misdiagn* (2008) 8:8875–6.
  83. Ding HY, Dong Q, Han X, Shi LF, Lv CZ. Effects of total *Panax notoginseng* saponins on rCBF and neurological function in patients with acute basal ganglia hemorrhage. *Neural Inj Funct Reconstr* (2008) 3:386–98.
  84. Yuan KZ, Zhang F, He HJ. The analysis of the clinical effect of Xue Sai Tong applied for the treatment of patients in the early stage of intracerebral hemorrhage. *Chin Community Doctors* (2010) 12:136–7.
  85. Ding HY, Geng WX. Clinical research on Xue Shuan Tong for the treatment of small volume hypertensive intracerebral hemorrhage in acute phase. *China Mod Med* (2010) 17:56–9.
  86. Gao Y, Dan S, Zhang J, Zhang J, Fan SS, Wang Z. Effects of total *Panax notoginseng* saponins on neurological function and serum complement C3 in patients with acute intracerebral hemorrhage. *Chin Tradit Patent Med* (2011) 33:1851–3.
  87. Chen KZ. Observation on clinical effect of *Panax notoginseng* saponin for the treatment of sixty-one patients with acute intracerebral hemorrhage. *Hunan J Tradit Chin Med* (2013) 29:41–2.
  88. Li JM, Gong NX, Li SG, Hu B, Zhou JQ, Guo YH, et al. Observation on *Panax notoginseng*'s clinical effect of different administrating time for patients with intracerebral hemorrhage. *Chin J Integr Tradit West Med Intens Crit Care* (2003) 23:546–7.
  89. He D, Liu QR, Zhao J, Dong Q, Zhang RL, Han X. Therapeutic efficacy of Xueshuantong on patients with early stage acute intracerebral hemorrhage. *Chin J Integr Tradit West Med Intens Crit Care* (2002) 9:27–9.
  90. Guo XF, Yan YB, Zhao YH, Sun CX, Tan YM, Zhao Q, et al. Clinical research on therapy of invigorating the circulation of blood for the treatment of intracerebral hemorrhage in early stage. *Chin J Misdiagn* (2002) 2:1355–6.
  91. Ogata T, Yasaka M, Wakugawa Y, Inoue T, Ibayashi S, Okada Y. Deep venous thrombosis after acute intracerebral hemorrhage. *J Neurol Sci* (2008) 272:83–6. doi:10.1016/j.jns.2008.04.032
  92. Tveiten A, Ljøstad U, Mygland Å, Naess H. Functioning of long-term survivors of first-ever intracerebral hemorrhage. *Acta Neurol Scand* (2014) 129(4):269–75. doi:10.1111/ane.12185
  93. Frutos Bernal E, Rubio Gil FJ, Martin Corral JC, Marcos Prieto LA, Gonzalez Robledo J. [Prognostic factors in severe traumatic brain injury]. *Med Intensiva* (2013) 37:327–32. doi:10.1016/j.medint.2012.05.015
  94. Chen XF, Song XG. Influence and applied time of *P. notoginseng* on cerebral edema, hematoma volume and Bcl-2 expression in cerebral tissue in rats with acute cerebral hemorrhage. *J Clin Neuro (Chinese)* (2011) 24:191–3.
  95. Zhao XS, Chen ZG, Xu ZF. Effect of early use of *Panax notoginseng* saponins on inflammation in rats with cerebral hemorrhage. *Int Tradit Chin Med* (2013) 8:787–9.
  96. Xu DY, Huang HB. Analysis of the adverse reactions induced by Sanqi and its preparations. *Zhongguo Zhong Yao Za Zhi* (2005) 30:1465–8.
  97. Ning MH, Jiang F, Xu LP. Thirty cases of Xuesaitong injection treatment of acute intracerebral hemorrhage. *J Tradit Chin Med* (2004) 8:592–4.
  98. Cadilhac DA, Dewey HM, Vos T, Carter R, Thrift AG. The health loss from ischemic stroke and intracerebral hemorrhage: evidence from the North East Melbourne Stroke Incidence Study (NEMESIS). *Health Qual Life Outcomes* (2010) 8:49. doi:10.1186/1477-7525-8-49
  99. Revel-Vilk S, Golomb MR, Achonu C, Stain AM, Armstrong D, Barnes MA, et al. Effect of intracranial bleeds on the health and quality of life of boys with hemophilia. *J Pediatr* (2004) 144:490–5. doi:10.1016/j.jpeds.2003.12.016
  100. Lau J, Ioannidis JP, Terrin N, Schmid CH, Olkin I. The case of the misleading funnel plot. *BMJ* (2006) 333:597–600. doi:10.1136/bmj.333.7568.597
  101. Tang JL, Liu JL. Misleading funnel plot for detection of bias in meta-analysis. *J Clin Epidemiol* (2000) 53:477–84. doi:10.1016/S0895-4356(99)00204-8
  102. Davis SM, Broderick J, Hennerici M, Brun NC, Diringer MN, Mayer SA, et al. Hematoma growth is a determinant of mortality and poor outcome after intracerebral hemorrhage. *Neurology* (2006) 66:1175–81. doi:10.1212/01.wnl.0000208408.98482.99
  103. Gao L, Zhao H, Liu Q, Song J, Xu C, Liu P, et al. Improvement of hematoma absorption and neurological function in patients with acute intracerebral hemorrhage treated with Xueshuantong. *J Neurol Sci* (2012) 323:236–40. doi:10.1016/j.jns.2012.09.028

104. Luo PD, Luo Y. Clinical study of notoginsenoside therapy for cerebral hemorrhage. *J Prev Med* (2008) **35**:4307–9.
105. Lays D, Bodenat M, Cordonnier C. [Intra-cerebral haemorrhages in the elderly]. *Rev Prat* (2012) **62**:1239–42.
106. Fujii Y, Takeuchi S, Tanaka R, Koike T, Sasaki O, Minakawa T. Liver dysfunction in spontaneous intracerebral hemorrhage. *Neurosurgery* (1994) **35**:592–6. doi:10.1097/00006123-199410000-00003
107. Immonen RJ, Kharatishvili I, Grohn H, Pitkanen A, Grohn OH. Quantitative MRI predicts long-term structural and functional outcome after experimental traumatic brain injury. *Neuroimage* (2009) **45**:1–9. doi:10.1016/j.neuroimage.2008.11.022
108. Zhao G, Wang X. The hemostatic component of *Panax notoginseng*: dencichine. *Chin Tradit Herb Drugs* (1986) **17**:34–6.
109. Huang LF, Shi HL, Gao B, Wu H, Yang L, Wu XJ, et al. Decichine enhances hemostasis of activated platelets via AMPA receptors. *Thromb Res* (2014) **133**:848–54. doi:10.1016/j.thromres.2014.02.009
110. Chan CM, Zilberberg MD. Preferences in traumatic intracranial hemorrhage: bleeding vs. clotting. *Crit Care* (2010) **14**:153. doi:10.1186/cc8996
111. Gebel JM, Brott TG, Sila CA, Tomsick TA, Jauch E, Salisbury S, et al. Decreased perihematomal edema in thrombolysis-related intracerebral hemorrhage compared with spontaneous intracerebral hemorrhage. *Stroke* (2000) **31**:596–600. doi:10.1161/01.STR.31.3.596
112. Lauer A, Schlunk F, Van Cott EM, Steinmetz H, Lo EH, Foerch C. Antiplatelet pretreatment does not increase hematoma volume in experimental intracerebral hemorrhage. *J Cereb Blood Flow Metab* (2011) **31**:1736–42. doi:10.1038/jcbfm.2011.22
113. Lok J, Leung W, Murphy S, Butler W, Noviski N, Lo EH. Intracranial hemorrhage: mechanisms of secondary brain injury. *Acta Neurochir Suppl* (2011) **111**:63–9. doi:10.1007/978-3-7091-0693-8\_11
114. Chen G, Mu L, Zhang X, Hou S, Nan H. [In vivo distribution and pharmacokinetics of multiple effective components contained in *Panax notoginseng* saponins after intratympanic administration]. *Zhongguo Zhong Yao Za Zhi* (2011) **36**:1815–20.
115. Emiru T, Bershad EM, Zantek ND, Datta YH, Rao GH, Hartley EW, et al. Intracerebral hemorrhage: a review of coagulation function. *Clin Appl Thromb Hemost* (2013) **19**:652–62. doi:10.1177/1076029612454938
116. Allard CB. Retraction note to: ginsenoside-Rg1 enhances angiogenesis and ameliorates ventricular remodeling in a rat model of myocardial infarction. *J Mol Med (Berl)* (2013) **91**:645.
117. Allard CB, Scarpelini S, Rhind SG, Baker AJ, Shek PN, Tien H, et al. Abnormal coagulation tests are associated with progression of traumatic intracranial hemorrhage. *J Trauma* (2009) **67**:959–67. doi:10.1097/TA.0b013e3181ad5d37
118. Chai H, Dong Y, Wang X, Zhou W. Ginsenoside Rb1 attenuates homocysteine-augmented guidewire injury-induced intimal hyperplasia in mice. *J Surg Res* (2009) **157**:193–8. doi:10.1016/j.jss.2008.07.005
119. Xu HL, Liu WB, Rao MR. [Effect of sanchinoside Rg1 on experimental thrombosis and its mechanisms]. *Yao Xue Xue Bao* (1997) **32**:502–5.
120. Liu DH, Chen YM, Liu Y, Hao BS, Zhou B, Wu L, et al. Ginsenoside Rb1 reverses H2O2-induced senescence in human umbilical endothelial cells: involvement of eNOS pathway. *J Cardiovasc Pharmacol* (2012) **59**:222–30. doi:10.1097/FJC.0b013e31823c1d34
121. Xia R, Zhao B, Wu Y, Hou JB, Zhang L, Xu JJ, et al. Ginsenoside Rb1 preconditioning enhances eNOS expression and attenuates myocardial ischemia/reperfusion injury in diabetic rats. *J Biomed Biotechnol* (2011) **2011**:767930. doi:10.1155/2011/767930
122. Chen HZ, Li YF, Zhong JH, Fan XH. [Identification of major components of traditional Chinese medicine Naodesheng tablet by HPLC-DAD-MS(n)]. *Zhejiang Da Xue Xue Bao Yi Xue Ban* (2012) **41**:32–42.
123. Berek L, Szabo D, Petri IB, Shoyama Y, Lin YH, Molnar J. Effects of naturally occurring glucosides, solasodine glucosides, ginsenosides and parishin derivatives on multidrug resistance of lymphoma cells and leukocyte functions. *In vivo* (2001) **15**:151–6.
124. Garrett MC, Otten ML, Starke RM, Komotar RJ, Magotti P, Lambris JD, et al. Synergistic neuroprotective effects of C3a and C5a receptor blockade following intracerebral hemorrhage. *Brain Res* (2009) **1298**:171–7. doi:10.1016/j.brainres.2009.04.047
125. Chang Y, Lai PH, Wang CC, Chen SC, Chang WC, Sung HW. Mesothelium regeneration on acellular bovine pericardia loaded with an angiogenic agent (ginsenoside Rg1) successfully reduces postsurgical pericardial adhesions. *J Thorac Cardiovasc Surg* (2006) **132**:867–74. doi:10.1016/j.jtcvs.2006.06.029
126. Gong Y, Xi G, Wan S, Gu Y, Keep RF, Hua Y. Effects of aging on complement activation and neutrophil infiltration after intracerebral hemorrhage. *Acta Neurochir Suppl* (2008) **105**:67–70. doi:10.1007/978-3-211-09469-3\_14
127. Loftspring MC, McDole J, Lu A, Clark JE, Johnson AJ. Intracerebral hemorrhage leads to infiltration of several leukocyte populations with concomitant pathophysiological changes. *J Cereb Blood Flow Metab* (2009) **29**:137–43. doi:10.1038/jcbfm.2008.114
128. Yao XH, Li XJ. [Protective effects and its mechanism of panaxatriol saponins isolated from *Panax notoginseng* on cerebral ischemia]. *Zhongguo Zhong Yao Za Zhi* (2002) **27**:371–3.
129. Lu T, Jiang Y, Zhou Z, Yue X, Wei N, Chen Z, et al. Intranasal ginsenoside Rb1 targets the brain and ameliorates cerebral ischemia/reperfusion injury in rats. *Biol Pharm Bull* (2011) **34**:1319–24. doi:10.1248/bpb.34.1319
130. Shi Y, Han B, Yu X, Qu S, Sui D. Ginsenoside Rb3 ameliorates myocardial ischemia-reperfusion injury in rats. *Pharm Biol* (2011) **49**:900–6. doi:10.3109/13880209.2011.554845
131. Gong W, Xiao Y, Zhang M, Wang Y. [Synergistic protective effects of salvianolic acids and *Panax notoginseng* saponins on cardiomyocytes with hypoxia-reoxygenation injury]. *Zhongguo Zhong Yao Za Zhi* (2013) **38**:1046–51.
132. Sun Q, Meng QT, Jiang Y, Liu HM, Lei SQ, Su WT, et al. Protective effect of ginsenoside Rb1 against intestinal ischemia-reperfusion induced acute renal injury in mice. *PLoS One* (2013) **8**:e80859. doi:10.1371/journal.pone.0080859
133. Lan TH, Xu ZW, Wang Z, Wu YL, Wu WK, Tan HM. Ginsenoside Rb1 prevents homocysteine-induced endothelial dysfunction via PI3K/Akt activation and PKC inhibition. *Biochem Pharmacol* (2011) **82**:148–55. doi:10.1016/j.bcp.2011.04.001
134. Cheung LW, Leung KW, Wong CK, Wong RN, Wong AS. Ginsenoside-Rg1 induces angiogenesis via non-genomic crosstalk of glucocorticoid receptor and fibroblast growth factor receptor-1. *Cardiovasc Res* (2011) **89**:419–25. doi:10.1093/cvr/cvq300
135. Leung KW, Ng HM, Tang MK, Wong CC, Wong RN, Wong AS. Ginsenoside-Rg1 mediates a hypoxia-independent upregulation of hypoxia-inducible factor-1alpha to promote angiogenesis. *Angiogenesis* (2011) **14**:515–22. doi:10.1007/s10456-011-9235-z
136. Tang B, Qu Y, Wang D, Mu D. Targeting hypoxia inducible factor-1alpha: a novel mechanism of ginsenoside Rg1 for brain repair after hypoxia/ischemia brain damage. *CNS Neurol Disord Drug Targets* (2011) **10**:235–8. doi:10.2174/187152711794480456
137. Wang DJ, Li QY, Xu SJ, Zeng N. [Effect of ginsenoside Rg1 on angiogenesis after neonatal hypoxia ischemia brain damage in rats]. *Sichuan Da Xue Xue Bao Yi Xue Ban* (2011) **42**:503–7.
138. Yang N, Chen P, Tao Z, Zhou N, Gong X, Xu Z, et al. Beneficial effects of ginsenoside-Rg1 on ischemia-induced angiogenesis in diabetic mice. *Acta Biochim Biophys Sin (Shanghai)* (2012) **44**:999–1005. doi:10.1093/abbs/gms092
139. Shen K, Ji L, Gong C, Ma Y, Yang L, Fan Y, et al. Notoginsenoside Ft1 promotes angiogenesis via HIF-1alpha mediated VEGF secretion and the regulation of PI3K/AKT and Raf/MEK/ERK signaling pathways. *Biochem Pharmacol* (2012) **84**:784–92. doi:10.1016/j.bcp.2012.05.024
140. Zheng H, Liu C, Ou Y, Zhang Y, Fu X. Total saponins of *Panax notoginseng* enhance VEGF and relative receptors signals and promote angiogenesis derived from rat bone marrow mesenchymal stem cells. *J Ethnopharmacol* (2013) **147**:595–602. doi:10.1016/j.jep.2013.03.043
141. Chen S, Liu J, Liu X, Fu Y, Zhang M, Lin Q, et al. *Panax notoginseng* saponins inhibit ischemia-induced apoptosis by activating PI3K/Akt pathway in cardiomyocytes. *J Ethnopharmacol* (2011) **137**:263–70. doi:10.1016/j.jep.2011.05.011
142. Ma J, Li W, Tian R, Lei W. Ginsenoside Rg1 promotes peripheral nerve regeneration in rat model of nerve crush injury. *Neurosci Lett* (2010) **478**:66–71. doi:10.1016/j.neulet.2010.04.064
143. He W, Wu WK, Wu YL, Yang XH, Lin QX, Yu WH. Ginsenoside-Rg1 mediates microenvironment-dependent endothelial differentiation of human mesenchymal stem cells in vitro. *J Asian Nat Prod Res* (2011) **13**:1–11. doi:10.1080/10286020.2010.535519
144. Arauz A, Berge E, Sandercock P. Third International Stroke Trial 3: an update. *Curr Opin Neurol* (2014) **27**:8–12. doi:10.1097/WCO.0000000000000045

145. Balsevich JJ, Bishop GG, Deibert LK. Use of digitoxin and digoxin as internal standards in HPLC analysis of triterpene saponin-containing extracts. *Phytochem Anal* (2009) **20**:38–49. doi:10.1002/pca.1095
146. Chang SH, Choi Y, Park JA, Jung DS, Shin J, Yang JH, et al. Anti-inflammatory effects of BT-201, an *n*-butanol extract of *Panax notoginseng*, observed in vitro and in a collagen-induced arthritis model. *Clin Nutr* (2007) **26**:785–91. doi:10.1016/j.clnu.2007.07.008
147. Luo FC, Wang SD, Li K, Nakamura H, Yodoi J, Bai J. Panaxatriol saponins extracted from *Panax notoginseng* induces thioredoxin-1 and prevents 1-methyl-4-phenylpyridinium ion-induced neurotoxicity. *J Ethnopharmacol* (2010) **127**:419–23. doi:10.1016/j.jep.2009.10.023
148. Na JY, Kim S, Song K, Lim KH, Shin GW, Kim JH, et al. Anti-apoptotic activity of ginsenoside Rb1 in hydrogen peroxide-treated chondrocytes: stabilization of mitochondria and the inhibition of caspase-3. *J Ginseng Res* (2012) **36**:242–7. doi:10.5142/jgr.2012.36.3.242
149. Hashimoto R, Yu J, Koizumi H, Ouchi Y, Okabe T. Ginsenoside Rb1 prevents MPP(+)-induced apoptosis in PC12 cells by stimulating estrogen receptors with consequent activation of ERK1/2, Akt and inhibition of SAPK/JNK, p38 MAPK. *Evid Based Complement Alternat Med* (2012) **2012**:693717. doi:10.1155/2012/693717
150. Xie XS, Liu HC, Yang M, Zuo C, Deng Y, Fan JM. Ginsenoside Rb1, a panaxadiol saponin against oxidative damage and renal interstitial fibrosis in rats with unilateral ureteral obstruction. *Chin J Integr Med* (2009) **15**:133–40. doi:10.1007/s11655-009-0133-9
151. Ye R, Kong X, Yang Q, Zhang Y, Han J, Li P, et al. Ginsenoside Rd in experimental stroke: superior neuroprotective efficacy with a wide therapeutic window. *Neurotherapeutics* (2011) **8**:515–25. doi:10.1007/s13311-011-0051-3
152. Ye R, Kong X, Yang Q, Zhang Y, Han J, Zhao G. Ginsenoside Rd attenuates redox imbalance and improves stroke outcome after focal cerebral ischemia in aged mice. *Neuropharmacology* (2011) **61**:815–24. doi:10.1016/j.neuropharm.2011.05.029
153. Ye R, Yang Q, Kong X, Han J, Zhang X, Zhang Y, et al. Ginsenoside Rd attenuates early oxidative damage and sequential inflammatory response after transient focal ischemia in rats. *Neurochem Int* (2011) **58**:391–8. doi:10.1016/j.neuint.2010.12.015
154. Li XY, Liang J, Tang YB, Zhou JG, Guan YY. Ginsenoside Rd prevents glutamate-induced apoptosis in rat cortical neurons. *Clin Exp Pharmacol Physiol* (2010) **37**:199–204. doi:10.1111/j.1440-1681.2009.05286.x
155. Zhang X, Shi M, Björås M, Wang W, Zhang G, Han J, et al. Ginsenoside Rd promotes glutamate clearance by up-regulating glial glutamate transporter GLT-1 via PI3K/AKT and ERK1/2 pathways. *Front Pharmacol* (2013) **4**:152. doi:10.3389/fphar.2013.00152
156. Zhang YX, Wang L, Xiao EL, Li SJ, Chen JJ, Gao B, et al. Ginsenoside-Rd exhibits anti-inflammatory activities through elevation of antioxidant enzyme activities and inhibition of JNK and ERK activation in vivo. *Int Immunopharmacol* (2013) **17**:1094–100. doi:10.1016/j.intimp.2013.10.013
157. Liu Q, Kou JP, Yu BY. Ginsenoside Rg1 protects against hydrogen peroxide-induced cell death in PC12 cells via inhibiting NF-kappaB activation. *Neurochem Int* (2011) **58**:119–25. doi:10.1016/j.neuint.2010.11.004
158. Wang J, Xu HM, Yang HD, Du XX, Jiang H, Xie JX. Rg1 reduces nigral iron levels of MPTP-treated C57BL6 mice by regulating certain iron transport proteins. *Neurochem Int* (2009) **54**:43–8. doi:10.1016/j.neuint.2008.10.003
159. Yan J, Liu Q, Dou Y, Hsieh Y, Liu Y, Tao R, et al. Activating glucocorticoid receptor-ERK signaling pathway contributes to ginsenoside Rg1 protection against beta-amyloid peptide-induced human endothelial cells apoptosis. *J Ethnopharmacol* (2013) **147**:456–66. doi:10.1016/j.jep.2013.03.039
160. Yu SH, Huang HY, Korivi M, Hsu MF, Huang CY, Hou CW, et al. Oral Rg1 supplementation strengthens antioxidant defense system against exercise-induced oxidative stress in rat skeletal muscles. *J Int Soc Sports Nutr* (2012) **9**:23. doi:10.1186/1550-2783-9-23
161. Korivi M, Hou CW, Huang CY, Lee SD, Hsu MF, Yu SH, et al. Ginsenoside-Rg1 protects the liver against exhaustive exercise-induced oxidative stress in rats. *Evid Based Complement Alternat Med* (2012) **2012**:932165. doi:10.1155/2012/932165
162. Cheng W, Wu D, Zuo Q, Wang Z, Fan W. Ginsenoside Rb1 prevents interleukin-1 beta induced inflammation and apoptosis in human articular chondrocytes. *Int Orthop* (2013) **37**:2065–70. doi:10.1007/s00264-013-1990-6
163. Kim DH, Chung JH, Yoon JS, Ha YM, Bae S, Lee EK, et al. Ginsenoside Rd inhibits the expressions of iNOS and COX-2 by suppressing NF-kappaB in LPS-stimulated RAW264.7 cells and mouse liver. *J Ginseng Res* (2013) **37**:54–63. doi:10.5142/jgr.2013.37.54
164. Lin WM, Zhang YM, Moldzio R, Rausch WD. Ginsenoside Rd attenuates neuroinflammation of dopaminergic cells in culture. *J Neural Transm Suppl* (2007):105–12. doi:10.1007/978-3-211-73574-9\_13
165. Lee IA, Hyam SR, Jang SE, Han MJ, Kim DH. Ginsenoside Re ameliorates inflammation by inhibiting the binding of lipopolysaccharide to TLR4 on macrophages. *J Agric Food Chem* (2012) **60**:9595–602. doi:10.1021/jf301372g
166. Zou Y, Tao T, Tian Y, Zhu J, Cao L, Deng X, et al. Ginsenoside Rg1 improves survival in a murine model of polymicrobial sepsis by suppressing the inflammatory response and apoptosis of lymphocytes. *J Surg Res* (2013) **183**:760–6. doi:10.1016/j.jss.2013.01.068
167. Ma X, Xie X, Zuo C, Fan J. [Effects of ginsenoside Rg1 on streptozocin-induced diabetic nephropathy in rats]. *Sheng Wu Yi Xue Gong Cheng Xue Za Zhi* (2010) **27**:342–7.
168. Liu RY, Wang JJ, Qiu X, Wu JM. Acute hyperglycemia together with hematoma of high-glucose blood exacerbates neurological injury in a rat model of intracerebral hemorrhage. *Neurosci Bull* (2014) **30**:90–8. doi:10.1007/s12264-013-1371-6
169. Chiu CD, Chen CC, Shen CC, Chin LT, Ma HI, Chuang HY, et al. Hyperglycemia exacerbates intracerebral hemorrhage via the downregulation of aquaporin-4: temporal assessment with magnetic resonance imaging. *Stroke* (2013) **44**:1682–9. doi:10.1161/STROKEAHA.113.675983
170. Xia W, Sun C, Zhao Y, Wu L. Hypolipidemic and antioxidant activities of sanchi (radix notoginseng) in rats fed with a high fat diet. *Phytomedicine* (2011) **18**:516–20. doi:10.1016/j.phymed.2010.09.007
171. Xiong Y, Shen L, Liu KJ, Tso P, Xiong Y, Wang G, et al. Antiobesity and anti-hyperglycemic effects of ginsenoside Rb1 in rats. *Diabetes* (2010) **59**:2505–12. doi:10.2337/db10-0315
172. Lee KT, Jung TW, Lee HJ, Kim SG, Shin YS, Whang WK. The antidiabetic effect of ginsenoside Rb2 via activation of AMPK. *Arch Pharm Res* (2011) **34**:1201–8. doi:10.1007/s12272-011-0719-6
173. Kim EJ, Lee HI, Chung KJ, Noh YH, Ro Y, Koo JH. The ginsenoside-Rb2 lowers cholesterol and triacylglycerol levels in 3T3-L1 adipocytes cultured under high cholesterol or fatty acids conditions. *BMB Rep* (2009) **42**:194–9. doi:10.5483/BMBRep.2009.42.4.194
174. Han DH, Kim SH, Higashida K, Jung SR, Polonsky KS, Klein S, et al. Ginsenoside Re rapidly reverses insulin resistance in muscles of high-fat diet fed rats. *Metabolism* (2012) **61**:1615–21. doi:10.1016/j.metabol.2012.04.008
175. Lee HM, Lee OH, Kim KJ, Lee BY. Ginsenoside Rg1 promotes glucose uptake through activated AMPK pathway in insulin-resistant muscle cells. *Phytother Res* (2012) **26**:1017–22. doi:10.1002/ptr.3686
176. Yong-Xin X, Jian-Jun Z. Evaluation of anti-fatigue activity of total saponins of Radix notoginseng. *Indian J Med Res* (2013) **137**:151–5. doi:10.4236/wjms.2014.41002
177. Wang JH, Peng L, Wei C, Luo QZ, Cao XJ. Thirty cases of Xuesetong pill treatment of blood stasis syndrome during stroke recovery. *Shaanxi Tradit Chin Med* (2007) **28**:1314–5.

**Conflict of Interest Statement:** The authors declare that the research was conducted in the absence of any commercial or financial relationships that could be construed as a potential conflict of interest.

Received: 25 February 2014; accepted: 03 December 2014; published online: 07 January 2015.

Citation: Xu D, Huang P, Yu Z, Xing DH, Ouyang S and Xing G (2015) Efficacy and safety of *Panax notoginseng* saponin therapy for acute intracerebral hemorrhage, meta-analysis, and mini review of potential mechanisms of action. *Front. Neurol.* 5:274. doi: 10.3389/fneur.2014.00274

This article was submitted to *Neurotrauma*, a section of the journal *Frontiers in Neurology*.

Copyright © 2015 Xu, Huang, Yu, Xing, Ouyang and Xing. This is an open-access article distributed under the terms of the Creative Commons Attribution License (CC BY). The use, distribution or reproduction in other forums is permitted, provided the original author(s) or licensor are credited and that the original publication in this journal is cited, in accordance with accepted academic practice. No use, distribution or reproduction is permitted which does not comply with these terms.

# Advantages of publishing in Frontiers



## OPEN ACCESS

Articles are free to read  
for greatest visibility  
and readership



## FAST PUBLICATION

Around 90 days  
from submission  
to decision



## HIGH QUALITY PEER-REVIEW

Rigorous, collaborative,  
and constructive  
peer-review



## TRANSPARENT PEER-REVIEW

Editors and reviewers  
acknowledged by name  
on published articles

## Frontiers

Avenue du Tribunal-Fédéral 34  
1005 Lausanne | Switzerland

Visit us: [www.frontiersin.org](http://www.frontiersin.org)

Contact us: [frontiersin.org/about/contact](http://frontiersin.org/about/contact)



## REPRODUCIBILITY OF RESEARCH

Support open data  
and methods to enhance  
research reproducibility



## DIGITAL PUBLISHING

Articles designed  
for optimal readership  
across devices



## FOLLOW US

@frontiersin



## IMPACT METRICS

Advanced article metrics  
track visibility across  
digital media



## EXTENSIVE PROMOTION

Marketing  
and promotion  
of impactful research



## LOOP RESEARCH NETWORK

Our network  
increases your  
article's readership